

University of Nebraska - Lincoln

DigitalCommons@University of Nebraska - Lincoln

Civil and Environmental Engineering Theses,
Dissertations, and Student Research

Civil and Environmental Engineering

12-2022

Empirical Fragility Functions and Numerical Parametric Study for Buckling of Steel Grain Bins under High Wind Loads

Andrew Ruder

University of Nebraska-Lincoln, aruder2@huskers.unl.edu

Follow this and additional works at: <https://digitalcommons.unl.edu/civilengdiss>



Part of the [Civil Engineering Commons](#), and the [Other Civil and Environmental Engineering Commons](#)

Ruder, Andrew, "Empirical Fragility Functions and Numerical Parametric Study for Buckling of Steel Grain Bins under High Wind Loads" (2022). *Civil and Environmental Engineering Theses, Dissertations, and Student Research*. 185.

<https://digitalcommons.unl.edu/civilengdiss/185>

This Article is brought to you for free and open access by the Civil and Environmental Engineering at DigitalCommons@University of Nebraska - Lincoln. It has been accepted for inclusion in Civil and Environmental Engineering Theses, Dissertations, and Student Research by an authorized administrator of DigitalCommons@University of Nebraska - Lincoln.

EMPIRICAL FRAGILITY FUNCTIONS AND NUMERICAL PARAMETRIC STUDY
FOR BUCKLING OF STEEL GRAIN BINS UNDER HIGH WIND LOADS

by

Andrew S. Ruder

A THESIS

Presented to the Faculty of
The Graduate College at the University of Nebraska
In Partial Fulfillment of the Requirements
For the Degree of Master of Science

Major: Civil Engineering

Under the Supervision of Professor Christine E. Wittich

Lincoln, Nebraska

December 2022

EMPIRICAL FRAGILITY FUNCTIONS AND NUMERICAL PARAMETRIC STUDY
FOR BUCKLING OF STEEL GRAIN BINS UNDER HIGH WIND LOADS

Andrew S. Ruder, M.S.

University of Nebraska, 2022

Advisor: Christine E. Wittich

While rural infrastructure is critical to the agricultural industry, it has been historically more susceptible to damage and slower to recover following natural disasters than its urban and suburban counterparts. This has been made evident most recently by the events of the August 10, 2020, derecho in which rural regions in Iowa were among the hardest hit areas with sustained windspeeds exceeding 120 mph. Among the most frequently damaged structures in this event were corrugated steel grain bins, which farmers and co-ops use to dry and store certain commodities. Unlike most other critical structures, steel grain bins are not designed and constructed to consistent design standards for wind loads resulting in a wide range of performance and impact to individual farmers and the economy. Therefore, the overarching goal of this thesis is to enhance knowledge of steel grain bin performance under wind loads, which is accomplished by field reconnaissance, empirical fragility analysis, and finite element modeling.

A survey of over 600 standard construction corrugated steel grain bins was carried out over a large area of eastern and central Iowa in the immediate aftermath of the August 2020 storm. Physical characteristics, configuration, construction, and damage severity were observed and recorded. Windspeed data from the National Weather Service and point estimates from observed damage indicators were used to build a more detailed

estimate of peak windspeeds across the region. Empirical fragility curves were developed to relate the probability of various steel grain bin damage states to windspeed. This fragility analysis considered the effects of the physical characteristics, configuration, and construction of the grain bins. The results of this analysis showed that grain bin diameter and exposure of the terrain they are located on are the most significant factors when it comes to their susceptibility to damage.

Finite element modelling was used to carry out a parametric analysis of the effects of a wide range of physical characteristics of empty steel grain bins on their buckling strength under wind loads. The finite element software LS-DYNA was utilized to construct three-dimensional numerical models using shell elements. Critical wind load was determined by a nonlinear buckling analysis by the arc-length method. The parametric analysis was carried out by looking at the effects of diameter, height, number of vertical stiffeners, number of wind rings, presence of wind on the roof of the structure, analysis as vented or unvented, wavelength of the corrugation profile, depth of the corrugation profile, thickness of the cylinder wall, and thickness of vertical stiffeners. The results of this analysis were compared to empirical results from the data collected during the August 2020 derecho in order to confirm the trends observed during the parametric analysis. The conclusions drawn from this were that grain bin height, diameter, and openness of terrain have the greatest influence on susceptibility to damage from high winds regardless of other characteristics. Parameters such as presence of stiffeners, wind rings, and roof vents had more influence on the theoretical buckling wind load than they had on observed performance in the field.

Acknowledgements

This thesis is based upon work supported by the National Science Foundation under Grant No. CMMI-2050152 “RAPID: Performance of Agricultural Storage Silos and Farm Bins in Nebraska and Iowa During the August 2020 Derecho”. This work was completed utilizing the Holland Computing Center of the University of Nebraska, which receives support from the Nebraska Research Initiative.

Thank you to the researchers who worked on this project before me, Evi Troulis of Cal Poly SLO and Bennet Jackson of UNL.

I would also like to sincerely thank my advisor, Dr. Christine Wittich, whose guidance and encouragement has been paramount. Throughout the project, she helped me keep the bigger picture in mind and provided invaluable feedback on approaches to engineering problems and report drafts. It has been a pleasure being a part of your research group.

To Luis Tuarez, thank you for letting me bounce ideas off you. You were always willing to offer your knowledge and experience. Beyond that, your dedication to and love of engineering is inspiring. I appreciated working alongside you. To the rest of the Wittich Research Lab, thank you for making my time here enjoyable.

This thesis, in part, is being finalized for submission as two separate journal articles. The contents of Chapter 3 and Chapter 4 will be submitted to *Natural Hazards Review* as: Ruder, A. S. and Wittich C. E. (202X). “Empirical Fragility Functions of Steel Grain Bins based on August 2020 Iowa Derecho.” The contents of Chapter 5 will be submitted to *Engineering Structures* as: Ruder, A. S. and Wittich C. E. (202X). “Parametric FEM Wind Buckling Analysis of Steel Grain Bins.”

I would also like to thank my friends and family, especially my parents. I would not be where I am today without your love, support, and guidance. Lastly, to Madison, thank you for being there for me every single day. I could not have done it without you by my side.

Table of Contents

Abstract.....	ii
Acknowledgements	iv
List of Figures.....	ix
List of Tables	xiii
Chapter 1: Introduction	1
1.1. Background	1
1.2. Summary of the State-of-the-Art	3
1.3. Problem Statement	6
1.4. Objectives	7
1.5. Scope.....	8
Chapter 2: Literature Review.....	9
2.1. Wind Pressure Distribution.....	9
2.2. Stresses in Cylinders	16
2.3. Numerical Modelling.....	17
2.4. Field Performance	23
2.5. Novelty and Scope	25
Chapter 3: Reconnaissance and Damage Observations	27
3.1. Event Description.....	27
3.2. Reconnaissance and Damage Observations.....	28
3.3. Wind Speed Mapping	34
Chapter 4: Fragility Analysis.....	36
4.1. Abstract	36

4.2. Methodology	36
4.3. Full Set of Bins	39
4.4. Correlation Analysis	43
4.5. Fragility Functions of the Intersection of Parameters	46
4.6. Conclusions.....	53
Chapter 5: Finite Element Modelling	54
5.1. Abstract	54
5.2. Model Development.....	54
5.2.1. Geometry	54
5.2.2. Elements and Material Model.....	57
5.2.3. Wind Loading	57
5.2.4. Arc-Length Method	60
5.2.5. Model Validation.....	62
5.3. Parametric Analysis of Finite Element Model Configurations.....	66
5.3.1. Methodology.....	66
5.3.2. Impact of Bin Geometry and Load Application	67
5.3.3. Impact of Stiffener and Wind Ring Configuration	74
5.3.4. Impact of Corrugation Profile.....	78
5.3.5. Impact of Wall and Stiffener Thickness	81
5.4. Conclusions.....	82
Chapter 6: Comparison of Empirical and Numerical Results.....	85
6.1. Abstract	85
6.2. Comparison	85

6.3. Conclusions..... 89

Chapter 7: Conclusions 90

7.1. Summary 90

7.2. Conclusions..... 91

7.3. Recommendations..... 92

References 94

Appendix A: Empirical Fragility Functions..... 98

Appendix B: Buckling Results of FEA..... 161

List of Figures

Fig. 1.1 Standard Steel Grain Bin	2
Fig. 1.2 Damage mechanisms in steel grain bins.....	3
Fig. 2.1 Wind Load Distribution over Grain Bins (Abdel-Sayed et al. 1985).....	13
Fig. 2.2 Mean wall pressure distribution for silos with an aspect ratio of 1:1 (MacDonald et al. 1988)	14
Fig. 2.3 Mean roof pressure distribution for silo with an aspect ratio of 1:1 (MacDonald et al. 1988)	15
Fig. 2.4 Mean pressure coefficients on tanks with a conical roof obtained for different aspect ratios (Portela and Godoy 2005).....	16
Fig. 2.5 Severe buckling of the cylindrical shells (Kikitsu and Sarkar 2015)	24
Fig. 2.6 Grain Bin Damage from August 10 derecho (Shouse et al. 2021).....	25
Fig. 3.1 Peak winds and tornado paths (NOAA 2021)	28
Fig. 3.2 Classification of damage state a) minor, b) major, and c) severe.....	31
Fig. 3.3 Distribution of damage states	31
Fig. 3.4 Map of regions and structures	31
Fig. 3.5 Distribution of bin diameters.....	32
Fig. 3.6 Wind speed map	35
Fig. 4.1 Fragility functions of all grain bins	41
Fig. 4.2 Fragility functions of a) all diameters, minor damage, b) all diameters, major damage c) all diameters, severe damage.....	43

Fig. 4.3 Fragility functions of a) $D = (7.62,10.7]m$ ((25,35]ft), grouped, minor damage, b) $D = (7.62,10.7]m$ ((25,35]ft), grouped, major damage, and c) $D = (7.62,10.7]m$ ((25,35]ft), grouped, severe damage 48

Fig. 4.4 Fragility functions of a) $D = (10.7,15.2]m$ ((35,50]ft), stiffened, minor damage, b) $D = (10.7,15.2]m$ ((35,50]ft), stiffened, major damage, and c) $D = (10.7,15.2]m$ ((35,50]ft), stiffened, severe damage 49

Fig. 4.5 Fragility functions of a) $D = (10.7,15.2]m$ ((35,50]ft), wind rings, minor damage, b) $D = (10.7,15.2]m$ ((35,50]ft), wind rings, major damage, and c) $D = (10.7,15.2]m$ ((35,50]ft), wind rings, severe damage 49

Fig. 4.6 Fragility Functions of $D = (7.62,10.7]m$ ((25,35]ft), Vented/Unvented Bins, major damage..... 50

Fig. 4.7 Fragility functions of Diameter and Condition..... 51

Fig. 4.8 Fragility functions of Diameter and Terrain..... 52

Fig. 5.1 Grain bin a) in the field b) finite element model c) close-up of wall and stiffener elements 56

Fig. 5.2 Stiffener cross-section 57

Fig. 5.3 Meridional wind pressure distribution..... 59

Fig. 5.4 Circumferential wind pressure distribution for unvented bin..... 60

Fig. 5.5 Circumferential wind pressure distribution for vented bin..... 60

Fig. 5.6 Stiffener cross-sections..... 63

Fig. 5.7 First eigen-frequency mode shape..... 64

Fig. 5.8 Non-linear buckled form with resultant displacement 65

Fig. 5.9 Non-linear buckled form with Von Mises stress distribution..... 66

Fig. 5.10 Critical Buckling Load versus Diameter for unvented bins without wind loads applied to the roof	70
Fig. 5.11 Critical Buckling Load versus Diameter for vented bins with wind loads applied to the roof	70
Fig. 5.12 Load-Displacement Curves for unstiffened bins of varying diameter	71
Fig. 5.13 Von Mises Stress Distribution of 5.49 m (18 ft) Diameter Bin.....	71
Fig. 5.14 Von Mises Stress Distribution of 16.5 m (54 ft) Diameter Bin.....	72
Fig. 5.15 Resultant Displacement of 5.49 m (18 ft) Diameter Bin.....	72
Fig. 5.16 Resultant Displacement of 16.5 m (54 ft) Diameter Bin.....	73
Fig. 5.17 Critical Buckling Load versus Diameter for unstiffened bins	73
Fig. 5.18 Critical Buckling Load versus Diameter for stiffened bins	74
Fig. 5.19 Critical Buckling Load versus Height	74
Fig. 5.20 Critical Buckling Load versus Number of Stiffeners	76
Fig. 5.21 Critical Buckling Load versus Number of Wind Rings	76
Fig. 5.22 Resultant Displacement of Stiffened Bin without Wind Rings.....	77
Fig. 5.23 Resultant Displacement of Stiffened Bin with Two Wind Rings.....	77
Fig. 5.24 Resultant Displacement of Stiffened Bin with Four Wind Rings	78
Fig. 5.25 Critical Buckling Load versus Corrugation Length (unstiffened).....	79
Fig. 5.26 Critical Buckling Load versus Corrugation Depth (unstiffened)	80
Fig. 5.27 Resultant Displacement of Bin with Corrugation Depth of 6.35 mm (0.25 in) ..	80
Fig. 5.28 Resultant Displacement of Bin with Corrugation Depth of 38.1 mm (1.5 in) ..	81
Fig. 5.29 Critical Buckling Load versus Corrugation Depth	81
Fig. 5.30 Critical Buckling Load versus Wall Thickness	82

Fig. 5.31 Critical Buckling Load versus Stiffener Thickness	82
Fig. 6.1 Percent increase in windspeed at 50% rate of exceeding minor damage	88
Fig. 6.2 Percent increase in windspeed at buckling	88
Fig. 6.3. Comparison of percent increase in windspeed	89

List of Tables

Tab. 3.1 Summary of Field Reconnaissance.....	33
Tab. 4.1 Statistical variables for full set of grain bins	39
Tab. 4.2 Windspeed at median for minor damage state.....	42
Tab. 4.3 Cramer's V of select parameters	45
Tab. 4.4 Conditional probabilities of diameter given various parameters	45
Tab. 5.1 Stiffener Variation	64
Tab. 5.2 Variation of parametric analysis.....	67

Chapter 1: Introduction

1.1. Background

Approximately 97 percent of the nation's land area is rural, while being home to 19.3 percent of the population (New Census Data, 2016). The National Oceanic and Atmospheric Administration (NOAA) has been keeping track of billion-dollar natural disasters since 1980. In 2020, NOAA (2022) calculated a total of \$102.0 billion in damages from 22 events. Due to several factors, rural areas are both more susceptible to damage and less resilient to natural disasters. Despite this, agricultural support structures, such as irrigation systems, storage bins and silos, and barns are not designed to the same standards as structures in urban and suburban areas (Loken et al., 2020). One example is grain bins. Modern grain bins are most commonly constructed of corrugated steel plates with a conical sheet metal roof, are anchored to a concrete foundation, and range in diameter from 3.66 meters (12 feet) to 50.29 meters (165 feet). Figure 1.1 depicts a standard steel grain bin with its various components labeled. Grain bins can either be built in isolated locations or in groups. Some bins also feature external vertical stiffeners and/or wind rings.

Due to their lightweight construction and large surface area, steel grain bins are especially susceptible to damage in high wind conditions. Figure 1.2 shows the range of damage that can occur to grain bins, from nonstructural damage to stairs or other attachments (a), to minor buckling of the sidewall or roof (b), to major buckling of the bin side wall or roof or failure of the roof-wall connection (c), to the total anchorage failure of the bin (d). In addition to this, the impacts of grain bin failure can be catastrophic to farmers, co-ops, and rural communities as a whole. In addition to personal

injury that can occur to anyone in the vicinity during a failure, severe economic harm can accompany grain bin failure. When accompanied by the loss of crops, complete monetary loss is incurred since stored commodities cannot be insured.

Despite the vital role they play, grain bin performance suffers from a lack of research compared to other critical structures and a lack of codified design standards. The goal of this thesis is to advance the knowledge of grain bin performance in high wind events.

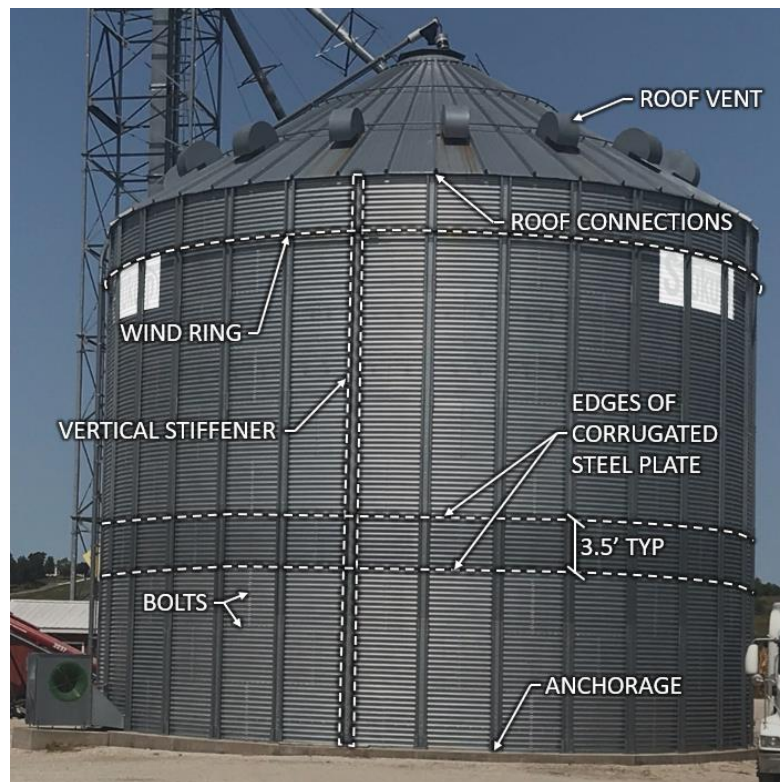


Fig. 1.1 Standard Steel Grain Bin



a)

b)



c)

d)

Fig. 1.2 Damage mechanisms in steel grain bins, a) non-structural b) wall buckling c) wall and roof buckling d) anchorage failure

1.2. Summary of the State-of-the-Art

While a detailed literature review is presented in Chapter 2, this summary provides a synopsis of the current practices in the study of steel grain bins in high wind

conditions. The other prominent loads on these structures include grain pressure on the sidewalls, snow load on the roof, and wind loads. Historically, only empty, or mostly empty, bins are susceptible to severe wind loads (Abdel-Sayed et al. 1985). Despite the size of some of these structures, there has been limited research in the performance of different configurations under wind loads. Macdonald et al. (1988) developed wind pressure coefficients for both the sidewalls and conical roof of grain bins through several wind tunnel experiments. This paper also produced a simple equation for the sidewall pressure distribution based on aspect ratio. Kebeli (2002) went through a more thorough set of wind pressure tests. This report used more sensors on its model, looked at a wider range of groupings, considered vertical stiffeners, and found similar distributions to MacDonald et al. (1988). However, this paper did not provide any new equations for the distribution of pressures. Portela and Godoy (2005) combined wind tunnel testing with numerical analysis. This paper looked at the wind tunnel test of a bin with a lower aspect ratio and found the results agreed with MacDonald et al. (1988) and suggested a new equation for the distribution of wind pressures.

Due to the complexity of the wind pressure distribution and mechanical behavior of grain bins, historically, it has been common practice to model them using Finite Element Method (FEM) software. In one of the earliest papers on modelling wind loads on grain bins, Briassoulis and Pecknold (1986a), commented on the “extreme insensitive” results of analyzing bins as a cantilever structure. In this paper, they went on to develop an equation for anchorage stresses based on adjusted membrane theory that closely matched the results of finite element solutions. In a second paper, Briassoulis and Pecknold (1986b) provide greater detail on their finite element modelling methods, that

has many similarities to how grain bins are currently modelled, such as, how wind loads are applied to wall and roof elements and the constraints of nodes at the base of the bin. Their wind pressure distributions on the bin wall come from older ANSI standards that are similar but not identical to distributions used by later papers based on Eurocode. They also set the standard of applying roof wind loads based on the distribution for a dome roof, due to the lack of research on conical roofs. However, one source of difference arises from the limited computing power of the day. Because of this, Briassoulis and Pecknold modelled their grain bin wall with coarsely meshed shell elements that cannot capture the corrugation profile. To overcome this, they modelled the wall elements as an equivalent orthotropic material. Additionally, they modelled stiffeners and wind rings as beam elements. Whereas later studies model them as finely meshed shells. However, as Briassoulis and Pecknold (1986b) were interested in stress distribution, not critical wind load, their results provided extremely valuable information despite the limitations of the time.

In a later paper, Godoy and Flores (2002), used similar modelling techniques using the commercial finite element software ABAQUS. A difference between this paper and previous ones, is that Godoy and Flores developed their own wind pressure distribution for bins more consistent with those in their local area. Additionally, they were interested in the critical windspeed at which the bin wall lost the ability to take more load and buckled. They used two different methods to calculate critical loads. First, they used an eigenvalue buckling approach. Then they used a more advanced nonlinear buckling analysis based on the Riks method. A very similar approach was used by Raessi et al. (2017). Similar to Godoy and Flores (2002), ABAQUS was used for eigenvalue and

non-linear buckling analysis. However, this study made use of more detailed modeling techniques. For example, they used a much finer mesh for the bin wall that could capture the corrugation profile of the wall panels. Additionally, wall thickness was doubled in areas corresponding to the overlap between consecutive rings of panels. Raessi et al. (2017) also modelled stiffeners and wind rings with shell elements tied to the bin wall. In order to relieve some computational expense, rather than modelling the entire grain bin, they took advantage of the symmetry of the bin and wind loads to model only one half of the bin split bilaterally to the windward direction while imposing the appropriate symmetry boundary conditions. Wind pressure distribution came from EN 1993-4-1. This paper made use of several models to explore the effects of stiffeners, wind rings, and aspect ratio on critical windspeed.

Maleki and Mehretehran (2018) performed a similar study, using many of the same modelling, loading, and analysis techniques. Some differences included a flat roof to prevent out of round deformation at the top of the cylinder, whereas Raessi et al. (2017) modelled a conical roof. In this paper, they analyzed the effects of corrugation profile and behavior of bins with equivalent flat sheets. In a second paper, Maleki and Mehretehran (2019), explored many variables affecting critical windspeed, such as grouped wind loading distribution, presence of wind loads on the roof, and additional internal pressures due to a vented roof.

1.3. Research Gaps and Problem Statement

Due to their large surface area and light-weight construction, steel grain bins are highly susceptible to damage from high winds, particularly when empty. Damage to or

destruction of grain bins can be extremely detrimental to individual farmers, co-ops, and agricultural communities as a whole. Several researchers over many decades have studied the problem of steel grain bins under high wind loads. Through these studies, wind pressure distributions have been proposed and several key variables related to increased strength have been identified. These past studies have primarily leveraged finite element analysis in a deterministic approach, and many have focused on general grain bin design or grain bin designs from outside of the United States. However, steel grain bins in the United States are not held to the same design standards as those in other countries and there is substantial variation in the design and construction among various manufacturers and installers. Therefore, there is a critical need to evaluate the performance of typical steel grain bins in the United States and to do so in a probabilistic approach to account for the variation in design and construction.

1.4. Objectives

The goal of this thesis is to enhance current understanding of the performance of steel grain bins in high wind events by development of empirical fragility functions and conducting a numerical parametric study. Through the fragility analysis, a probabilistic, rather than deterministic, approach is taken towards grain bin performance. This is done to diminish structure-to-structure variation and help present a more realistic expectation of structural performance. The current research focuses on using data collected by field reconnaissance after a significant wind event to establish the maximum windspeed on a large sample of grain bins in order to determine the importance of each of a number of

physical characteristics. It also seeks to provide a physics-based damage interpretation by a parametric numerical analysis to help better understand these observations and trends.

1.5. Scope

The objectives were addressed by:

1. Performing a detailed literature review on wind pressure distribution, stresses, numerical modelling, and performance of grain bins (**Chapter 2**).
2. Using field reconnaissance to develop a detailed windspeed map of the study area during the August 10, 2020, Derecho (**Chapter 3**).
3. Performing a fragility analysis of a set of over 600 effected grain bins in central Iowa (**Chapter 4**).
4. Using the finite element software LS-DYNA to perform a parametric numerical analysis of grain bin buckling strength under wind loads (**Chapter 5**).
5. Comparing the results of the fragility analysis to the results of the parametric numerical analysis (**Chapter 6**).

Chapter 2: Literature Review

A literature review of existing research on steel grain bins under wind loads was conducted with the goal of establishing the current state-of-the-art and determining existing gaps. Due to the complexity of the loading and structural response, most research has revolved around developing accurate wind pressure distributions through wind-tunnel testing and determining responses by finite element analysis. The literature review was structured to explore these aspects individually as well as the performance of grain bins in the field.

2.1. Wind Pressure Distribution

One of the earlier papers on grain bin analysis by Abdel-Sayed et al. (1985) shows that grain bin design classically focused on loads applied to the bin walls by grain pressure. However, they do point out that snow and wind loads may govern for larger bins, over 9.14 m (30 ft) in diameter. In a short passage of the paper, they comment on the application of wind pressures based on an earlier study of “isotropic oil tanks with no or very shallow covers”. This distribution is broken into vertical and circumferential components, as will be seen in later studies. They include figures depicting a uniform vertical distribution and a circumferential distribution of pressure on bin walls that varies with angle from the stagnation zone. Their figure is included as Figure 2.1. In this figure, ϕ is the angle from the windward in degrees. They end their discussion with the acknowledgement that more research is needed.

The additional research mentioned by Abdel-Sayed et al. (1985) came in a series of papers by MacDonald et al. In the first of these papers, MacDonald et al. (1988)

present their results of wind tunnel tests on scale models of circular bins of various aspect ratios and roof profiles. These tests were performed to replicate the effects of straight-line winds and are not applicable to tornadic winds. Surface roughness elements were incorporated in the atmospheric boundary layer wind tunnel testing to reflect expected wind flow at the grain bin as closely as possible. Their tests were performed on grain bin models with aspect ratios (height/diameter, h/D) of 0.5, 1.0, and 2.0. Roof geometries were open, flat, or 25° pitch conical. A number of important observations were made in this study. First, they noted that the pressure varies vertically, with the magnitude of the mean pressures noticeably reduced below 50% of the height. The shape of the circumferential was very similar to that of isotropic oil tanks, with a positive value at the stagnation zone that decreased to a peak negative value on the sides and then fell to a lower fairly constant suction on the back of the bin. Figure 2.2 shows their measured mean wall pressure distribution for a bin with an aspect ratio of 1.0. In this figure, $C_{\bar{p}}$ is the circumferential mean wind pressure coefficient and θ is the angle from windward in degrees. They determined that flat or conical roof geometry had insignificant effect on wall pressure distribution. However, open roof configurations had pressure coefficients that were affected by the negative internal pressure that resulted. MacDonald et al. (1988) demonstrated that the magnitude of maximum suction increased significantly with aspect ratio. Additionally, they tested the pressure distribution on the conical roof and found the whole surface to be in suction, with the highest magnitudes at the leading edge and near the apex as shown in Figure 2.3.

Previous studies looked at wind pressure distributions on isolated bins. However, as bins are often constructed in uniform rows, it was necessary to consider the effects of

this arrangement on wind pressure distribution. In a second paper, MacDonald et al. (1990a) study the effects of grouping grain bins on their wind pressure distribution for various spacings and wind direction relative to the group. Their results showed that pressure distribution varied with spacing, wind direction relative to the group, and position within the group. With respect to spacing, closely spaced bins experience a larger area but lower magnitude of positive mean pressure and a greater magnitude of maximum suction on the sides. At angles up to 20° from perpendicular to the line of bins, interior bins experience their highest negative pressure on the windward side “at the point of shortest distance from the adjacent silo.” For winds parallel to a line of bins, the windward bin experiences a pressure distribution similar to an isolated bin, with slightly lower magnitudes of negative pressure. At the same time, downwind bins are partially shielded, experiencing lower magnitude positive and negative pressures.

A third paper by MacDonald et al. (1990b) investigated fluctuating and peak pressure distributions. This paper differentiates from their previous ones by considering coincident peak pressure distributions as a pseudo-instantaneous peak pressure distribution rather than taking a quasi-steady approach. The results of this paper showed that the quasi-steady approach is unconservative for buckling loads due to too small areas under positive pressure, but conservative for drag coefficients.

Additional research in wind pressure coefficients on grain bins came in a series of papers by Kebeli et al. and a Ph.D. dissertation by Kebeli. In the first paper, Kebeli et al. (2001a) performed numerous wind tunnel tests on wind pressure coefficients of conical roofs on grain bins. The wind tunnel procedures were similar to those carried out in MacDonald et al. (1988). However, a larger number of pressure taps were used, along

with a wider range of roof slopes. The results of the paper showed a similar wind pressure distribution to the past studies. In the second paper, Kebeli et al. (2001b) incorporate the results of their first paper (2001a) with the results of wind pressure distribution on bin walls as well. This study showed that roof angle, surface roughness, wind direction, and bin configuration all affect wind pressure distribution.

In his dissertation, Kebeli (2002) goes into much greater detail of the experiments conducted for the first two papers in addition to conducting a full-scale test. The results of circumferential wind pressure distribution agreed with past literature. An additional parameter considered was to roughen the bin wall to approximate the effects of vertical stiffeners. The results of this test showed a very similar distribution in the positive pressure area, but a lower magnitude for negative pressures on the rough-walled bin. The study also showed that roof pressure distribution varied with roof slope and bin aspect ratio. In the investigation of grouping, Kebeli (2002) found similar results to MacDonald et al. (1990a) but considered more grouping cases, including 2 rows of bins and a set of bins arranged in a circular pattern. It is noted that differences between the two could arise from Kebeli (2002) using rough-walled models and differences in wind tunnel set up. Full scale testing seemed not to agree with wind tunnel testing. For example, wall pressure coefficients were all measured as positive values as opposed to wind tunnel tests, which showed negative pressure regions. In the paper, these discrepancies are attributed to a number of structural (geometrical) and wind flow (laminar versus turbulent) differences.

Previous studies had mostly been concerned with bins with higher aspect ratios, generally greater than 1.0 (h/D). Portela and Godoy (2005a) saw a lack of testing of bins

typical to the Caribbean and the southern-eastern United States, with aspect ratios of 0.25 to 0.60. They performed their own wind tunnel tests on bins with aspect ratios more relevant to that area. Figure 2.4 depicts the results for a range of aspect ratios. They found a lower magnitude of maximum negative pressure than previous studies. They used this data to construct a simplified distribution through Fourier coefficients. Testing of roof wind pressures found similar results to MacDonald et al. (1990a) with the entire roof in suction and maximums at the leading edge and the apex. In a second paper, Portela and Godoy (2005b) conducted similar experiments on bins with domed roofs, rather than conical. They observed similar results on wall pressure. Roof pressure was similar to conical roofs except that it was more uniform and lacked the maximum at the leading edge.

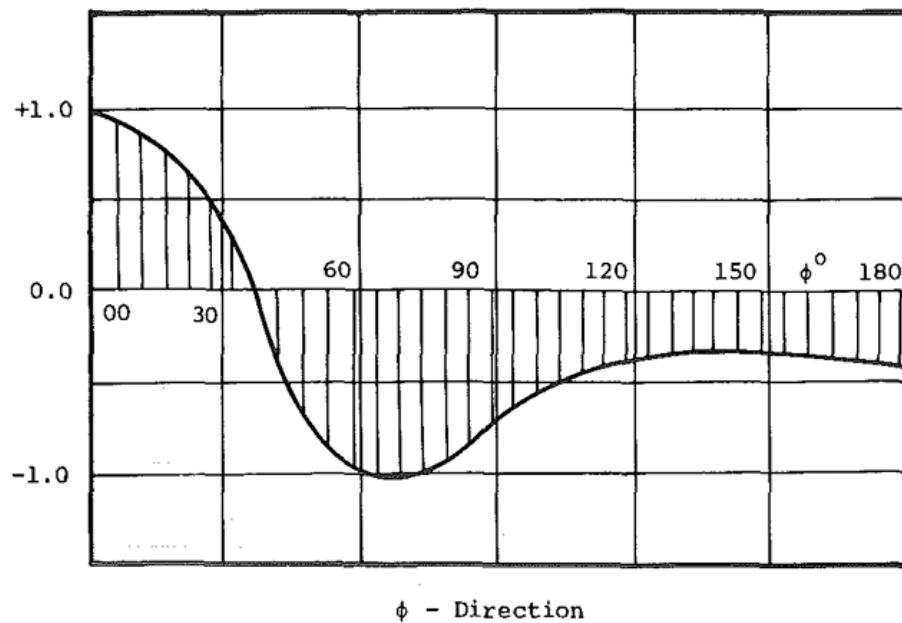


Fig. 2.1 Wind pressure coefficient over grain bin wall with respect to degrees from windward (ϕ) for oil tanks with no or shallow covers (Abdel-Sayed et al. 1985)

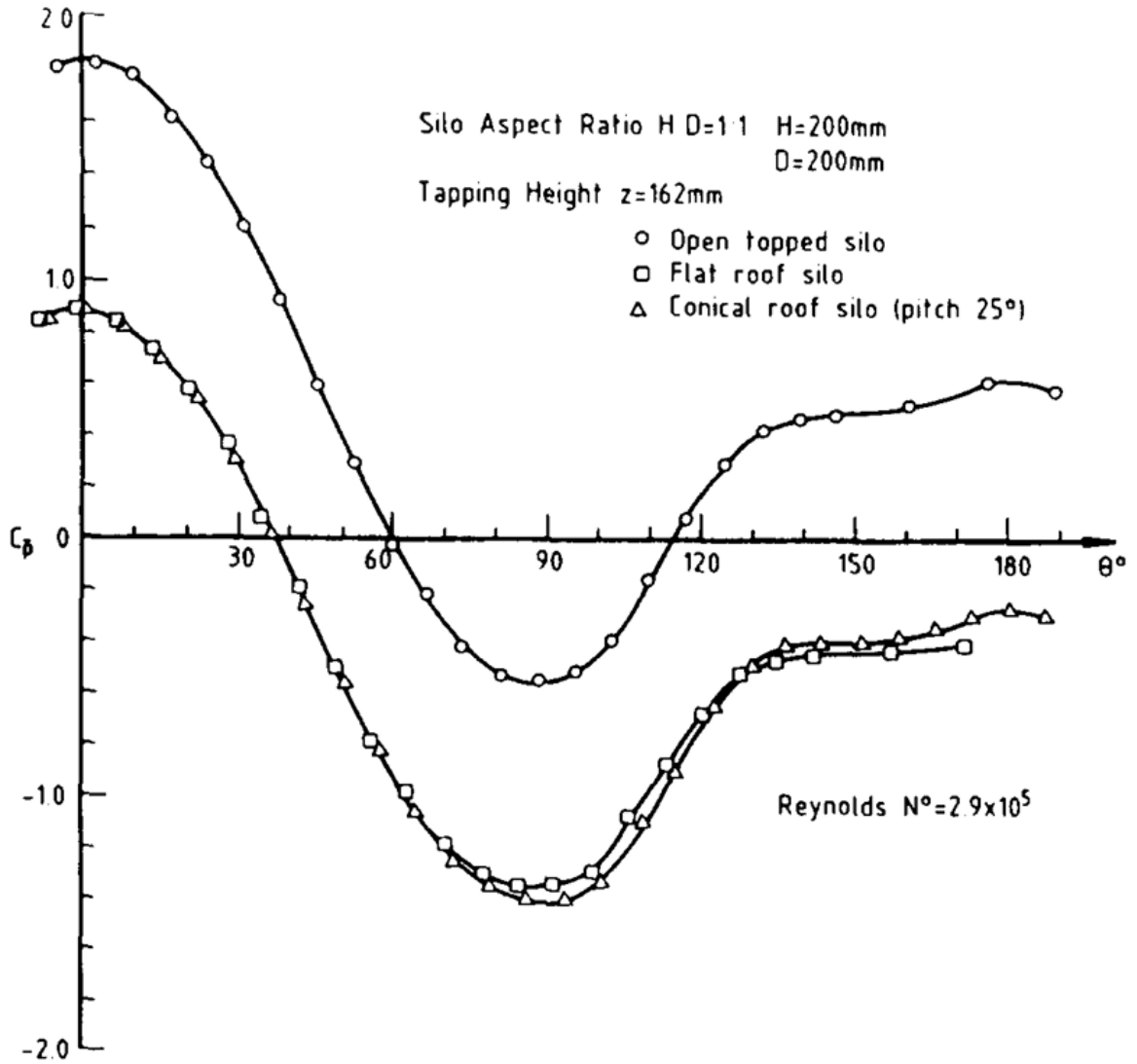


Fig. 2.2 Wind pressure coefficient (C_p) over grain bin wall with respect to degrees from windward (θ) for grain bins with an aspect ratio of 1:1 considering various roof styles

(MacDonald et al. 1988)

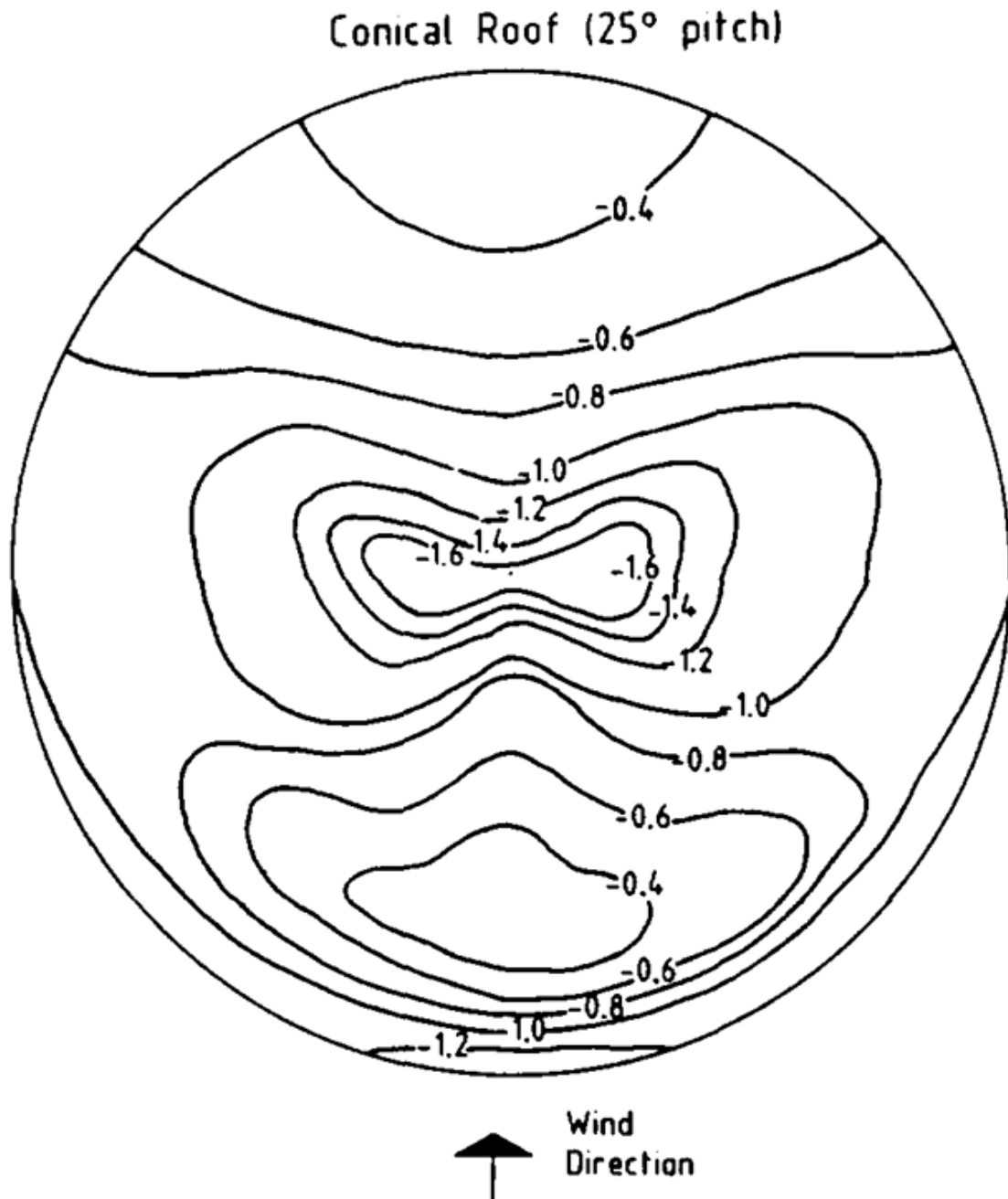


Fig. 2.3 Wind pressure coefficient for grain bin roof for an aspect ratio of 1:1 and a conical roof (MacDonald et al. 1988)

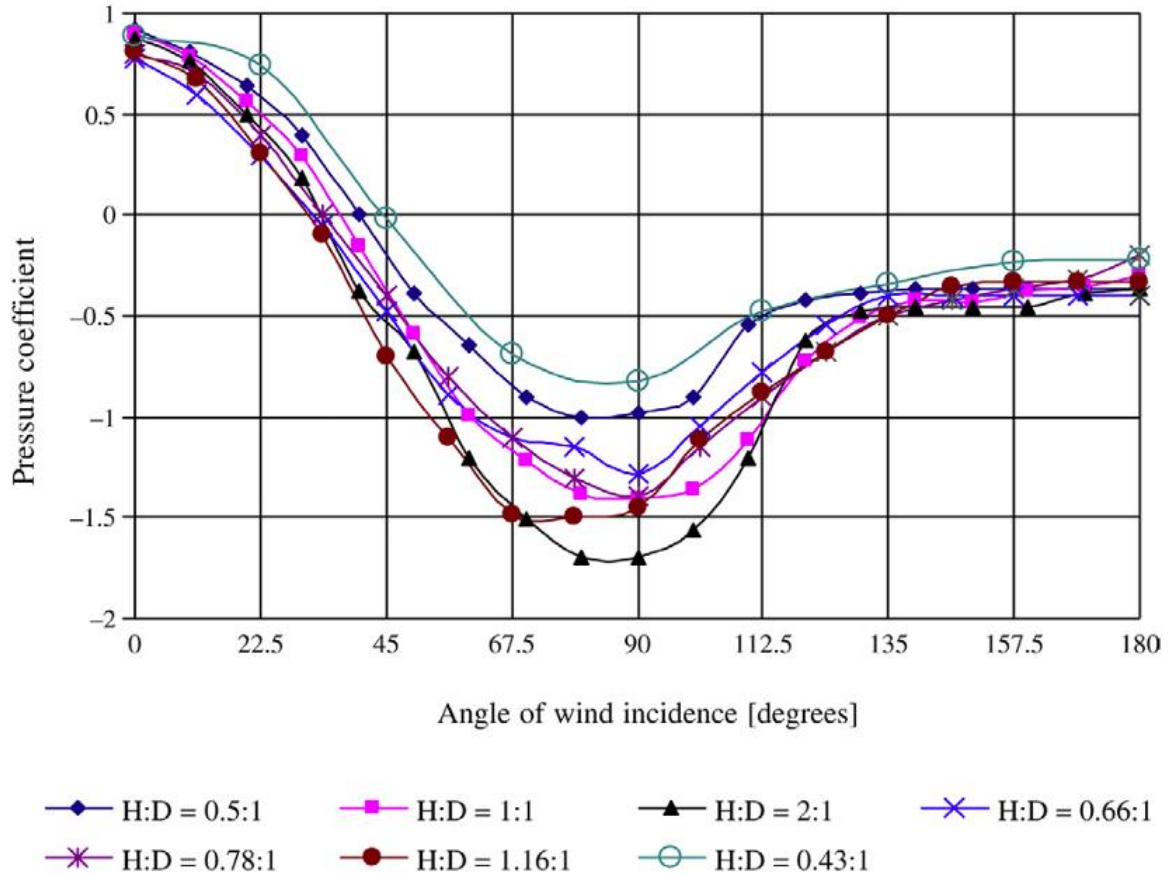


Fig. 2.4 Wind pressure coefficient for walls of tanks with a conical roof obtained for different aspect ratios as a function of angle of wind incidence (degrees from windward)

(Portela and Godoy 2005)

2.2. Stresses in Cylinders

Due to the complexity of behavior in cylindrical bins under wind loading, classical cantilever and membrane theories are inaccurate representations of the system. Several studies have tried different methods of calculating stresses in cylinders. One such paper by Pecknold (1989) uses Vlasov's semi-membrane theory to capture "the most important bending effects in closed thin-walled cylinders." It emphasizes that the purpose of this method is to "aid in understanding behavior," not provide a full bending solution.

This method is used by Pecknold and Raham (1990) to approximate ovaling stresses in ring stiffened cylinders. Similarly, Briassoulis (1992) comments on the inadequacy of cantilever and membrane theories while deeming full shell bending to complicated or impossible to solve. This study considers finite element methods to be the most efficient approach but sees the method of Pecknold (1989) as filling an important gap. The study goes on to propose an integrated physical model for cylindrical shells loaded by nonaxisymmetric pressure. However, it admits that this model is not applicable to regions near boundary constraints. Following a similar procedure Zeybek et al. (2019) developed an algebraic equation for approximating the ring stress in the top of an open cylinder that much more closely matches the finite element results than traditional approaches. While these approaches are useful for determining specific stresses in simple cases, the complexities of full bin response and failure, especially stiffened bins, require finite element analysis.

2.3. Numerical Modelling

Following the discussion of the previous section, and due to the complexities mentioned there, finite element modelling has been the best way to analyze stresses in cylindrical bins under wind loads. The majority of studies of empty grain bins are concerned with wall buckling. However, Briassoulis and Pecknold (1986a) consider anchorage failure instead. In their finite element modelling of grain bins, they apply wind loads to the wall that vary circumferentially and set the precedent of applying wind loads to the conical roof based on the provisions for domed roofs. They analyzed bins with three different aspect ratios (2.40, 0.92, and 0.49 h/D). Due to limited computing power

of the day, Briassoulis and Pecknold (1986a) modelled the wall elements with orthotropic properties equivalent to those of the corrugated shell. In this way, they did not need to refine the mesh to a level that could capture the corrugation profile. Stiffeners and wind rings were modelled as compatible eccentric shell stiffening beam elements. Bolted connections were not explicitly modelled. As they were concerned with anchorage requirements, boundary conditions were applied to the base of stiffeners to approximate the reaction of single bolt at each stiffener. They then used the results of the finite element analysis to determine anchorage requirements that met American Institute of Steel Construction (AISC) standards. Furthermore, they used the results to develop an equation for stress resultants that match the finite element analysis much more closely than cantilever or membrane theory predict.

Using the same modelling techniques, a second study by Briassoulis and Pecknold (1986b) looked at stresses and deflections in the cylinder wall. The deflected shapes of these analyzes showed an inward deformation of the wall at the stagnation zone which was increased by the effects of the wind on the roof pulling the roof upwards and the upper part of the wall inward. They found overturning moment was primarily resisted by axial stress at the base of the bin. They also found the behavior was based on a “rather complicated combination of shell and spaceframe actions.” Furthermore, this study only looked at the linear elastic response of the bin. It did not consider elastic buckling or material failure. An important observation they made was that wind rings should not be overly stiff, so as to cause high localized stresses at their connection to the bin wall.

A third paper, Briassoulis and Pecknold (1988) looked specifically at stresses and deformations in the conical roof. Using the same pressure distribution developed for

domed roofs, they determined that overall downwind deflection of the roof was negligible, but uplift on the roof could have significant effect on stresses in the top of the cylinder wall. They demonstrate that stiffened and unstiffened roof systems behave quite differently. Additionally, purlins could be under high tensile and bending forces depending on the diameter of the bin and rafter experience large moments and axial forces near their junction with the wall.

All these previous papers were concerned with stress distribution but did not take into account elastic buckling or material failure. One paper that does consider elastic buckling is Godoy and Flores (2002). This study uses open cylindrical tanks to investigate the effects of imperfection sensitivity on elastic buckling. They modelled their bins as fixed at the base and free at the top. Wind load was applied according to circumferential distribution. A traditional eigen analysis was performed to determine buckling loads and mode shapes. Then, a static nonlinear analysis was implemented to develop load-displacement curves. The results of this paper showed that short tanks ($0.17 h/D$) are highly sensitive to geometric imperfections, while tall tanks ($1.0 h/D$) are practically insensitive to them.

In a previous section, two papers by Portela and Godoy (2005a and 2005b) were presented for their contributions to the development of wind pressure coefficients on unstiffened grain bins with low aspect ratios. Within those papers, they also performed finite element analyses using the distributions they developed. In these analyses they determined elastic buckling loads by eigen analysis and a nonlinear arc-length analysis using the Riks method, which simultaneously varies load and displacement along the equilibrium path. For their bin with a conical roof, the critical load found by eigen

analysis was found to be 2.39 kPa. Likewise, by the Riks method, critical wind pressure was calculated as 2.48 kPa, showing close agreement. Imperfection analysis showed slight reductions in critical load, but bins experience significant softening. They also showed that decreased wall thickness has a significant reduction on critical buckling load. Additionally, bins with roofs have significantly higher critical loads than open bins. The same results were reached for bins with domed roofs.

A more recent study by Raessi et al. (2017) combines two areas of interest. They perform linear and nonlinear buckling analyses on bins with stiffeners and wind rings using the commercial finite element software ABAQUS. They did not, however, include wind loads on the roof. In their modelling they made use of the symmetry of the bin by modelling half of the bin and applying the necessary symmetry boundary conditions. The bin wall was modelled as fixed at the bottom, with stiffeners tied to the wall panels and likewise fixed at the bottom. They modelled the wall as double thick in areas of panel overlap. The roof was modelled as a flat conical surface. A circular horizontal disc was modeled and tied to the bins walls near the base to approximate the steel floor typically found inside grain bins. Rings were modelled as hollow circular tubes. All components were made of the same galvanized metal. They made use of a fine mesh to capture the behavior of the corrugation. Circumferential distribution of wind loads came from the Fourier series determined by MacDonald et al. (1988) which is the same one used by Eurocode. Wind pressure was applied to wall panels by converting wind velocity to pressure by application of the Bernoulli equation in the form:

$$P = \frac{1}{2} \rho v^2$$

where, ρ is the density of the air and v is wind velocity. They then performed a parametric study on the effects of stiffeners, wind rings, and aspect ratio. Through this parametric analysis, they found an approximately linear direct relationship between windspeed at buckling and number of stiffeners. Likewise, the effects of aspect ratio (H/D) were found to be approximately linear and directly related to critical windspeed. However, it should be noted that aspect ratio was varied by changing diameter while keeping height constant. The results showed that the addition of wind rings had a significant effect on critical wind speed. An optimal height of 87.5% of wall height was determined for the first ring. For nonlinear buckling analysis, the modified Riks method was used in ABAQUS. The critical buckling loads of the nonlinear analysis agreed with those of the linear buckling analysis.

In two papers Maleki and Mehrehtehran (2018 and 2019) performed finite element analyses of grain bins in ABAQUS. In the first paper (2018), they considered a bin with uniform wall thickness from top to bottom. They based the height, diameter, corrugation profile, and stiffener geometry on a physical bin. Some simplifications they made were to model the roof as a flat plate and not to include wind loads on the roof. They performed linear buckling analysis as well as nonlinear buckling analysis by the Riks method. They considered the variables of corrugation depth, corrugation length, and grouping. In varying corrugation depth, they found that deeper corrugations corresponded to higher critical buckling loads while corrugation length (crest-to-crest distance of the corrugated wall panels) had little effect. They found that grouping bins increased critical wind speed for most cases. In the second paper, Maleki and Mehrehtehran (2019) go into greater detail and look at additional variables. They look at bins with three different aspect ratios and

consider wall thickness that varies with height, as opposed to the uniform wall thickness in the first paper. It is important to note that aspect ratio was varied by changing both height and diameter while keeping volume constant. In this paper, wind loads on the roof and effects of venting were considered. For the case of isolated unvented bins, the effects of aspect ratio were small, with the intermediate bin have a slightly higher critical windspeed than either the squat bin or the slender bin. The same was true for grouped bins with unvented roofs. Additionally, the grouped bins generally had lower critical windspeeds than isolated bins, seemingly in disagreement with their previous study. The venting of bins significantly reduced the critical windspeed. The addition of wind pressure on the roof showed negligible effects. Finally, investigation of geometric imperfection returned similar results to Portela and Godoy (2005a).

While each study investigated at most a few variables, the amalgamated data revealed several parameters correlated with increased buckling strength. Of these, increased wall thickness, decreased height while diameter was held constant, decreased diameter while height was held constant, increased number of stiffeners, increased number of wind rings, corrugation depth, and a closed roof pressure distribution have a positive correlation with increased buckling strength. Conversely, aspect ratio with volume held constant shows little correlation with buckling strength. Finally, the effects of grouped versus isolated pressure distributions have conflicting results, even within an individual study.

2.4. Field Performance

Literature on the performance of grain bins in the field under high winds is limited. A paper by Kikitsu and Sarkar (2015) includes some observations on grain bin performance in response to an EF5 tornado that hit Parkersburg, Iowa in 2008. The paper noted that most bins lost their roofs and experienced severe wall buckling, likely due to the loss of reinforcement provided by the roof as seen in Figure 2.5. It was also noted that many smaller bins were simply overturned. The contents of these bins were unknown. They also made the comparison to an F3 tornado that struck Utica, Illinois in 2004. They noted that in the latter case damage ranged from wall buckling just below the roof, partial damage to the roof, total roof loss, and total structural collapse.

Loken et al. (2020) produced a set of fragility functions for steel grain bins in tornados as an important aspect of the performance of rural infrastructure. Fragility functions were built using two separate data sets, one consisting of grain bins subject to two tornados in Iowa and the other set consisting of a full digital reconnaissance database for 2018. In this study, the term *digital reconnaissance* refers to the gathering of observational structural damage data (e.g., photos) through local news, social media, and governmental databases, which is in contrast to *field reconnaissance* where the data is gathered by a structural engineer on site. They returned median probabilities of exceedance for damage state 1 (DS1) as 151 km/h (94 mi/h) and 190 km/h (118 mi/h) for each dataset respectively. Damage state 1 is defined as “moderate damage, such as local buckling of the wall or roof, which does not preclude use of the silo.” The authors attribute the discrepancy to the fact that digital reconnaissance tends to under report damage, therefore making that estimate nonconservative. For comparison the Canadian

Enhanced Fujita scale damage indicators estimate expected windspeeds of 90 km/h (55.9 mi/h) in the case of “anchored grain bin damaged”, 135 km/h (83.9 mi/h) for “anchored grain bin toppled”, and 180km/h (111.8 mi/h) for “anchored grain bin rolled or carried less than 10 m” (Environment Canada, 2013).

A paper by Shouse et al. (2021) dealt with the damage caused by the August 10, 2020, Derecho. They note grain bin failures due to wall buckling, roof tear off and anchorage failure. Figure 2.6 shows the complete anchorage failure of several large grain bins. They note that, in some areas, design windspeeds were exceeded.



Fig. 2.5 Severe buckling of the cylindrical shells (Kikitsu and Sarkar 2015)



Fig. 2.6 Grain Bin Damage from August 10 derecho (Shouse et al. 2021)

2.5. Novelty and Scope

Steel grain bins are a widespread and vital part of rural infrastructure. Despite their importance, their unique construction and lack of codified design standards make them a vulnerable fixture of that infrastructure. The current state of the knowledge shows that wind pressure distributions have been well established and experienced few updates over the last several years. Additionally, some of the more prominent variables affecting buckling strength under wind loads, such as aspect ratio, wall thickness, corrugation length, corrugation depth, vented roofs, and grouping, have been explored by multiple authors using finite element analysis. However, these studies have taken a deterministic

approach to grain bin performance. The few studies that have taken a probabilistic approach based on reconnaissance have been limited by their number of data points and lack of detail on grain bin construction. As a result, the goal of this thesis is to enhance current understanding of the performance of steel grain bins in high wind events by taking a probabilistic approach to grain bin performance in high wind conditions using empirical fragility functions and confirming the results through conducting a numerical parametric study.

Techniques used to develop a detailed windspeed map of the study area during the August 10, 2020, Derecho are described in **Chapter 3**. Empirical fragility functions developed from these estimates of maximum windspeed for a set of over 600 effected grain bins in central Iowa are presented in **Chapter 4**. Then, a parametric numerical analysis of grain bin buckling under wind loads was performed using the finite element software LS-DYNA, as described in **Chapter 5**. This chapter expands on the trends studied in the empirical fragility analysis. Next, **Chapter 6** compares the results of the fragility analysis to the results of the parametric numerical analysis. Finally, **Chapter 7** provides a summary of conclusions of the thesis and recommendations for related future work.

Chapter 3: Reconnaissance and Damage Observations

In order to take a probabilistic approach to grain bin performance, a large amount of field data must be gathered and processed. Most damage to grain bins from high winds is associated with tornadic activity or localized events. However, in August 2020 a widespread straight-line wind event, known as a derecho, swept across the Midwest. While its effects were devastating, it offered a unique opportunity to study a large number of grain bins subjected to the same event. A wide range of grain bins construction, configurations, and damage states were represented in the data collected. Additionally, to build the empirical fragility functions discussed in Chapter 4, maximum windspeed estimates had to be determined for each individual grain bin considered. This was done by combining windspeed estimates from multiple sources and interpolating maximum windspeeds at the location of each bin.

3.1. Event Description

On Monday August 10, 2020, a powerful derecho swept across much of the Midwest causing an estimated \$11.8 billion in damages and 4 deaths (NOAA 2022). A derecho is widespread, long-lived storm associated with a band of rapidly moving showers or thunderstorms with winds exceeding 25.9 m/s (58 mi/h) at numerous locations along a corridor at least 402 kilometers (250 miles) long (NOAA 2021). The highest estimated wind gusts occurred in Iowa, with a maximum estimated wind speed of around 62.6 m/s (140 mi/h) occurring in Cedar Rapids, Iowa. According to the NOAA National Weather Service (2021), these were among the highest known to have occurred

in a derecho and the costliest severe thunderstorm event in United States history. Figure 3.1 depicts the extent and severity of the August 10, 2020, Derecho.

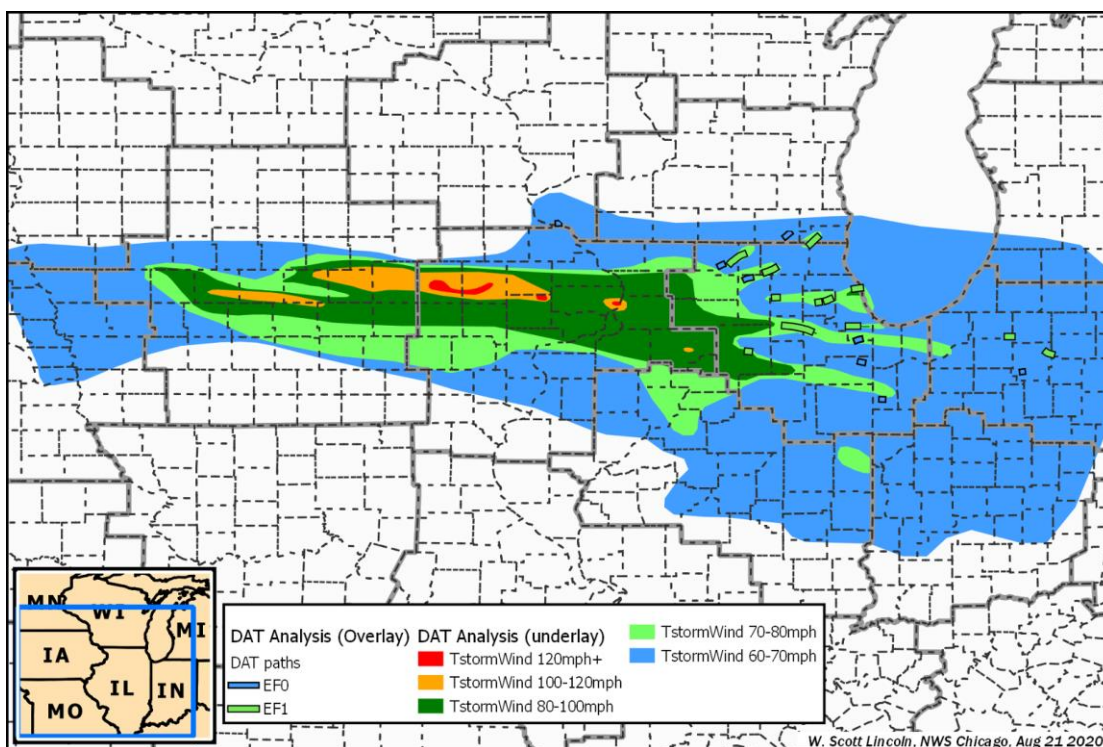


Fig. 3.1 Peak winds and tornado paths (NOAA 2021)

3.2. Reconnaissance and Damage Observations

After the wind event, field reconnaissance was performed throughout the central and eastern Iowa region to document performance of steel grain bins. Regions were pre-selected to span the measured wind speed ranges from mild to severe and to align with other structural reconnaissance initiatives in the area. To limit observer bias, sites within these regions were predetermined using pre-event satellite imagery following drivable paths or loops through the regions. Every other property containing a grain bin along the path or loop was selected to be surveyed in the field. In this way, a representative sample of damaged and undamaged grain bins could be collected. Measurements and audio notes

were collected to be processed later. Photo documentation was captured from the ground and aerial photos and videos were captured using a drone. Data was collected on a total of 728 structures, of which 643 were standard construction corrugated steel grain bins. Grain bins were assigned to sequential damage states of severe, major, minor, or none (Fig. 3.2). Damage states correlate with functionality to align with other resilience and recover-related research efforts (Troulis and Wittich 2022). Severely damaged bins were ones that had suffered complete anchorage failure and were deemed unsalvageable. Major damage was assigned to bins that experienced extreme buckling or roof tear off but were still partially attached to their foundation and were at least partly salvageable. Minor damage was assigned to bins that suffered minor wall or roof buckling or nonstructural damage and were still mostly functional. Most bins were undamaged while the number of bins in each damage state increased with severity (Fig. 3.3).

In addition to the grain bins, damage indicators were recorded at several cases using existing windspeed estimators for damage to buildings, trees, and cornfields. Data was collected across 7 different sites in several counties in central Iowa (Fig. 3.4). Data recorded for bins included damage rating, damage mechanism, silo group, silo type, bin contents, manufacturer, prior condition, diameter, number of corrugated steel plates, steel plate height, wall height, anchorage types. Silo group refers to whether or not bins are closely spaced in an orderly pattern. For prior condition, grain bins were divided into the categories of poor, okay, good, and new condition. One of the parameters of most interest was diameter. Bins ranged from 4.57 to 39.6 meters (15 to 130 feet) in diameter with almost 90% being under 15.2 meters (50 feet) (Fig 3.5). Google Earth aerial imagery and street view were used to fill gaps in the data.

Additional parameters added later were the presence of external vertical stiffeners, ring stiffeners, and roof vents. A parameter of interest was the terrain in the upwind direction. A WbN direction was used to determine the exposure of all bins. This was based on the prevailing wind direction and the direction of fallen corn in nearby fields. Exposure conditions were categorized as in town, behind buildings, behind trees, behind other grain bins, or exposed to open terrain. In this way, terrain categories roughly corresponded to ASCE-7 Surface Roughness Categories, with in town falling into Surface Roughness B, behind buildings, trees, or grain bins falling into Surface Roughness C, and open terrain also falling into Surface Roughness C despite being considered separately here. Bins arranged in a closely spaced orderly pattern were treated as grouped. Bins in a group were assigned the same exposure condition. The condition “behind other grain bins” was assigned to bins whose closest cover was another grain bin but was not close enough to consider grouped. The condition “exposed” was assigned to bins with no obstructions within 304.8 meters (1000 feet) in the upwind direction. For open terrain bins, additional parameters were recorded, such as prominence above the surrounding landscape and slope of the terrain leading towards the grain bin. For these parameters, elevation profiles were taken from path profiles in Google Earth. Table 3.1 summarizes the results of the reconnaissance by indicating the number grain bins characterized by each variable.

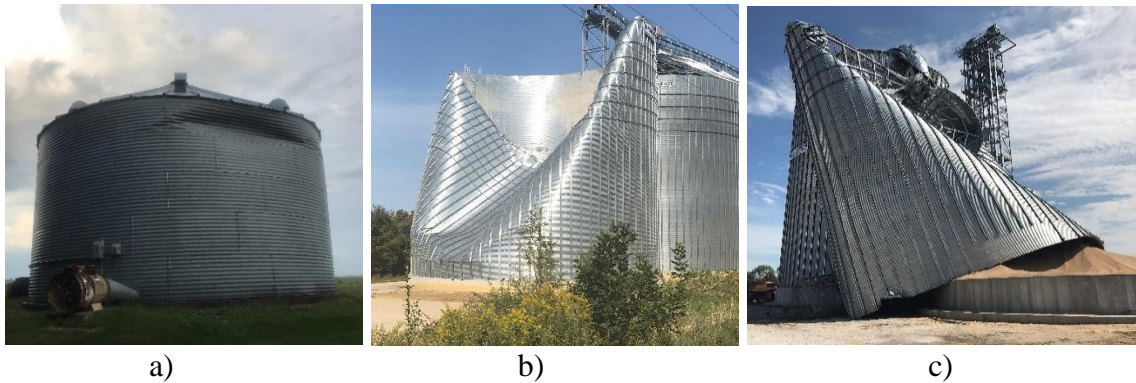


Fig. 3.2 Classification of damage state a) minor, b) major, and c) severe

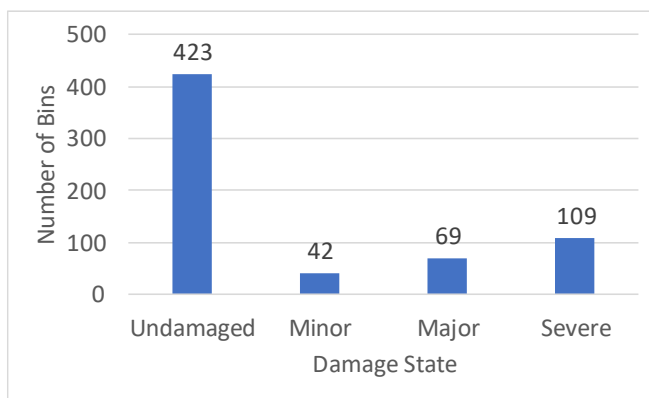


Fig. 3.3 Distribution of damage states

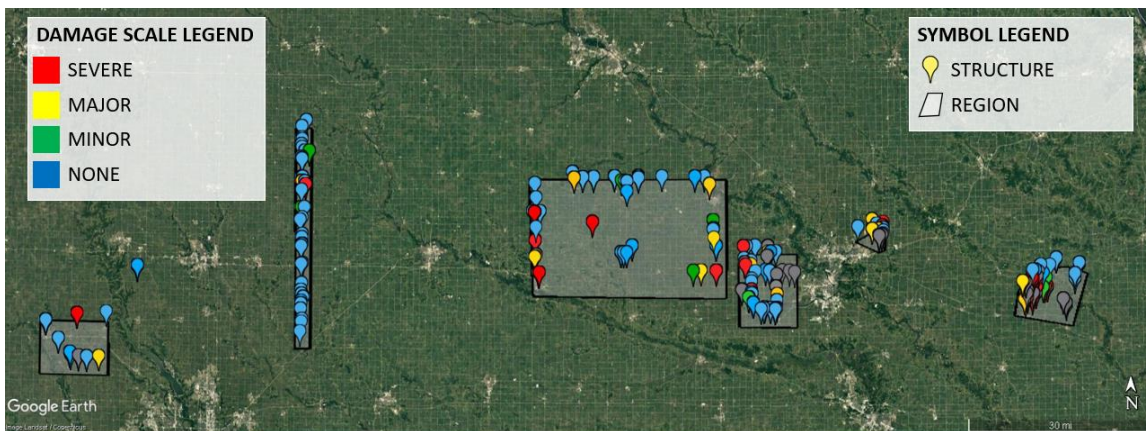


Fig. 3.4 Map of regions and structures

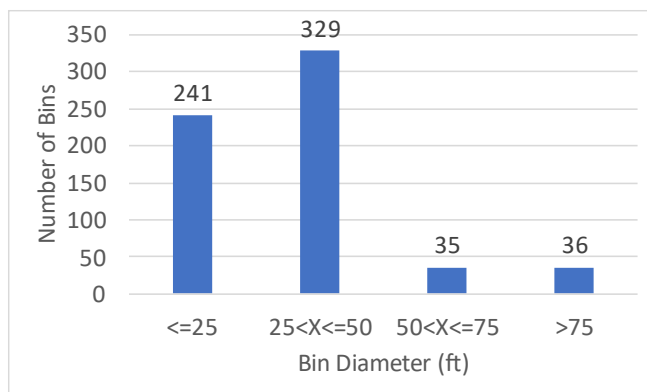


Fig. 3.5 Distribution of bin diameters

Tab. 3.1 Summary of Field Reconnaissance

Variable	Category	Number of Bins
Full Set	All bins	643
Damage State	None	423
	Minor	42
	Major	69
	Severe	109
Grouped/ Ungrouped	Grouped	223
	Ungrouped	420
Manufacturer	Manufacturer 1	46
	Manufacturer 2	22
	Manufacturer 3	40
	Manufacturer 4	31
Condition	Poor	79
	Okay	26
	Good	480
	New	44
Diameter	[0,25] ft	241
	(25,35] ft	228
	(35,130] ft	172
Height	[0,20] ft	142
	(20,35] ft	247
	(35,135] ft	134
Aspect Ratio	[0,0.75]	180
	(0.75,1.0]	208
	(1.0,1.89]	135
Stiffened/ Unstiffened	Stiffened	126
	Unstiffened	476
Wind Rings/No Wind Rings	Wind Rings	79
	No Wind Rings	522
Terrain	In town	109
	Trees/Buildings	216
	Grain Bins	40
	Open Terrain	277
Behind Other Bins/ Not Behind Other Bins	Behind Other Bins	211
	Exposed Bins	432
Distance to Obstruction	[0,50] ft	87
	(50,150] ft	92
	(150,1000] ft	72
Prominence	[-20,-4] ft	66
	(-4,4] ft	97
	(4,30] ft	104
Slope	[-0.07,-0.004]	87
	(-0.004,0.004]	69
	(0.004,0.04]	111
Roof Vents	Roof Vents	359
	No Roof Vents	284

3.3. Wind Speed Mapping

In addition to the wind speed estimates determined from damage indicators recorded in the field, a .kml file was provided by the NOAA National Weather Service (2021), in an online report of the event, with their estimates of windspeeds. NOAA NWS data was provided as a very coarse contour plot. In addition to this, a set of spot estimates of wind speed were obtained from NOAA's Damage Assessment Toolkit (NOAA 2022). More spot estimates were made during the initial field reconnaissance. This was done by making observations of damage to buildings and trees and assigning windspeeds based on the damage descriptions prescribed by the Enhanced Fujita Scale at the sites of the observed grain bins (McDonald et al. 2006). These three sets of data were imported into MATLAB and converted into a structure data type. These two sets of windspeed estimates were combined by creating a linear interpolation of the NWS contours, finding the interpolated windspeed at the locations of point estimates from both NWS and field reconnaissance, and taking a weighted average of the interpolated windspeeds and the spot estimates. Then a second linear interpolation was created using the NWS contours and weighted spot estimates. This was used to find the windspeed at the location of each grain bin. The contour plot of the final interpolation was then exported back to Google Earth (Fig. 3.6).

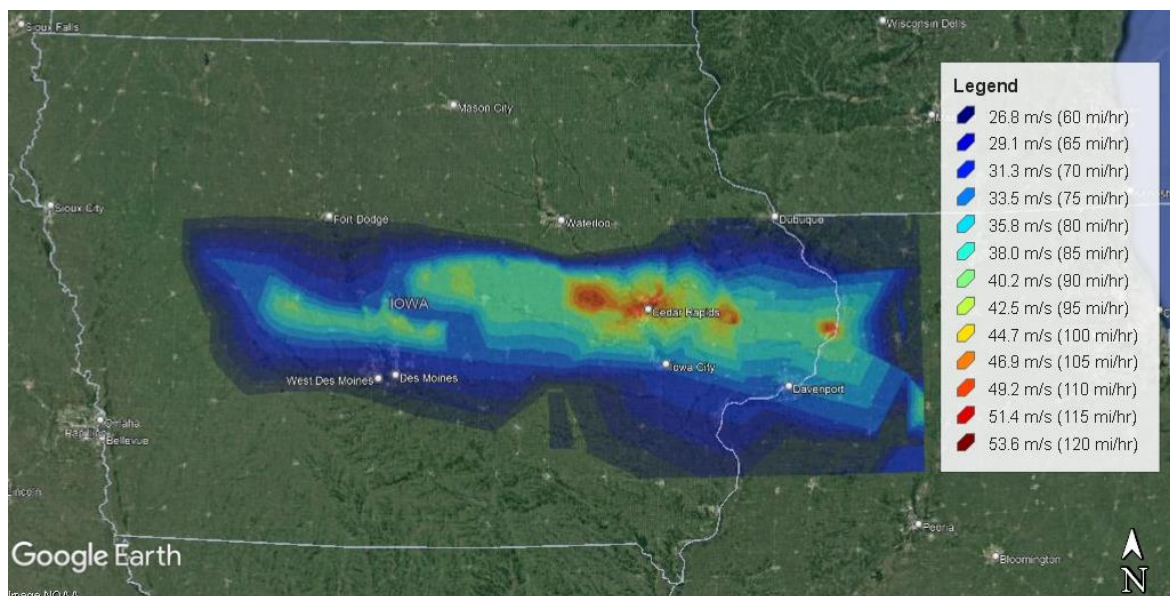


Fig. 3.6 Wind speed map

Chapter 4: Fragility Analysis

4.1. Abstract

Fragility analyses are commonly applied to structure performance in natural disasters. They have often been used in response to seismic events due to the innumerable variables requiring a probabilistic approach. They work just as well in cases of failure in high winds. Lognormal cumulative distribution functions were used to perform a fragility analysis of the grain bins surveyed in response to the August 10, 2020, derecho. The large number of parameters affecting performance made it difficult to identify the contribution of individual variables. By performing a study on conditional probabilities, the effects of individual variables could be identified. The result of this fragility analysis showed that the most relevant variables were grain bin diameter and surrounding terrain.

4.2. Methodology

The empirical fragility functions in this thesis were developed using lognormal cumulative distribution functions (CDF). A lognormal was chosen due to its simplicity, the fact that it must take on a positive value, because it has been shown to adequately represent the performance of a wide variety of structures. Using the interpolated wind speed at the location of each bin, lognormal fragility functions were developed for three sequential damage states as assigned during field reconnaissance. The fragility functions represent the probability of a grain bin being in or above a given damage state. The fragility is represented by a lognormal CDF with the form:

$$F(x) = \Phi\left(\frac{\ln(x) - \mu}{\sigma}\right)$$

where $F(x)$ is the fragility as a function of x (windspeed in mi/h) and the variables of μ and σ are the logarithmic mean and standard deviation of the lognormal distribution. In cases of poor fit or small sample sizes, it is possible for best-fit fragility functions of different damage states to cross. Since the damage states are sequential, meaning there is an ordered pattern to the severity of the damage states, crossing fragility functions would be an inaccurate representation of reality. A way to prevent this is to use the maximum-likelihood method, in which, fragility functions are derived simultaneously with a common β and separate medians θ for each damage state d . The maximum-likelihood method fits the fragility functions to the data by finding the medians θ and β to maximize the objective function, O , which is the intersection of the probabilities of observing y failures for each combination of damage state and level of excitation:

$$O = \prod_{d=1}^m \prod_{i=1}^s P_Y(y)$$

where O is the objective function, d represents the damage state, and i represents the level of excitation. For this analysis, damage states went from 1 to 3 (minor, major, and severe damage), and levels of excitation went from 1 to 5, corresponding to windspeeds of approximately 35.7, 40.2, 44.7, 49.2, and 53.6 m/s (80, 90, 100, 110, and 120 mi/h) respectively. Within each set i , there are n observations, of which y reach or exceed damage state d . $P_Y(y)$ represents the probability of observing y failures and is given by the binomial distribution:

$$P_Y(y) = \frac{n!}{y!(n-y)!} \cdot p^y(1-p)^{n-y}$$

Since lognormal CDFs are being used, the probability p that any specimen reaches or exceeds damage state d is given by:

$$p = \Phi\left(\frac{\ln(x/\theta_a)}{\beta}\right)$$

Starting with the full set of all 643 grain bins, i , x , n , and y for each damage state are shown in Table 4.1. In the calculation of $P_Y(y)$, in some cases, the expressions of $n!$ and $(n - y)!$ could not be computed since they exceed the maximum value that can be stored in the double data type. To remedy this, the basic rules of logarithms were utilized along with natural logarithm of the gamma function:

$$\gamma \ln(n + 1) = \ln(n!)$$

The MATLAB routine `fminsearch` was then used to maximize the value of O .

Fragility functions were built for the thirteen parameters of silo group, manufacturer, prior condition, diameter, wall height, aspect ratio, presence of external vertical stiffeners, presence of ring stiffeners, terrain, exposed or sheltered behind other grain bins, distance from nearest obstruction, prominence above the surrounding landscape, and slope of the terrain in the prevailing wind direction. Continuous data was lumped into groups so that distinct fragility functions could be developed in the same way as the categorical parameters. These categories were divided in a way such that each group had roughly the same number of grain bins. However, some categorical parameters, such as manufacturer, which had several categories and were unable to be determined for many grain bins, had relatively small datasets to build fragility functions from.

Tab. 4.1 Statistical variables for full set of grain bins

Set	Windspeed, m/s (mi/h)	Specimens	Damage State 1	Damage State 2	Damage State 3
i	x	n	y	y	y
1	35.8 (80)	50	4	3	2
2	40.2 (90)	125	14	11	7
3	44.7 (100)	232	73	58	39
4	49.2 (110)	149	72	58	32
5	53.6 (120)	87	57	48	29

4.3. Full Set of Bins

The fragility functions of all three damage states for the full set of grain bins was developed as a base line to compare the rest of the fragility functions to (Fig. 4.1). The horizontal axis shows the peak windspeed in miles per hour. The vertical axis shows the probability of exceeding a certain damage state. The blue line represents the probability that a grain bin received at least minor damage at a given windspeed. Therefore, all grain bins contributing to the major damage line also counted towards the probability of minor damage. Likewise, the red line, representing bins receiving at least major damage, includes bins that were severely damaged. Since severe was the highest damage state, the yellow line represents the probability that a bin was destroyed at a given windspeed. The fragility functions of the three damage states had medians of 50.1, 52.3, and 57.2 m/s (112, 117, and 128 mi/h) for minor, major, and severe damage respectively. Meaning, at these windspeeds half of the grain bins received at least that level of damage. Next, fragility functions of subsets of the data were built to look at the effects on fragility of the numerous parameters recorded during field reconnaissance. Table 4.2 displays the median of the fragility functions for minor damage for each category. Some categories

did not have enough datapoint to build fragility functions. Since there are thirteen parameters being considered, there is not room to include the plots of all fragility functions. Instead, only certain key fragility functions are presented here. The complete list of empirical fragility functions is included in **Appendix A** of this thesis. In addition to Table 4.2, the reconnaissance fragility functions of diameter showed a strong correlation between increasing diameter and susceptibility to damage. The effects of diameter can be seen by looking that the fragility functions of the same damage state for different ranges of diameters (Fig. 4.2). These plots clearly show the greater fragility of bins with larger diameters. This is expected due to the increased surface area exposed to wind pressure. The results of the analysis of wall height yielded similar results. In this case, the effects of stronger winds at greater heights likely contribute as well. The results of aspect ratio (h/D) showed that there is only a slight difference in the windspeed corresponding to a 50% change of failure between squat and intermediate bins. Table 4.2 showed that grouped bins are more susceptible to damage than ungrouped bins, disagreeing with Maleki and Mehrethran (2018). For prior condition, the very small number of data points for okay bins caused fragility functions that did not provide relevant results. The remaining results showed that susceptibility increases as bin condition improves. Bins with external vertical stiffeners showed worse performance than bins without stiffeners, which disagrees with Raeesi et al. (2017). The same results were found in the analysis of bins with wind rings (Tab. 4.2). Grain bins with roof vents performed slightly worse than bins without roof vents, but not to the level suggested by Maleki and Mehrethran (2019). The effects of terrain showed that grain bins on open terrain were the most susceptible to damage and the most sheltered bins, those in town, were the least susceptible. However,

the other parameters showed no strong patterns. Counterintuitively, the parameters of condition, presence of external vertical stiffeners, and presence of ring stiffeners showed that worse condition bins, bins without vertical stiffeners, and bins without ring stiffeners performed better than better condition bins, bins with vertical stiffeners, and bins with ring stiffeners. Due to confounding issues, a parametric evaluation is needed to determine the correlation between each variable to determine the most significant parameters. These causes will also be investigated in the finite element analysis of the subsequent chapter.

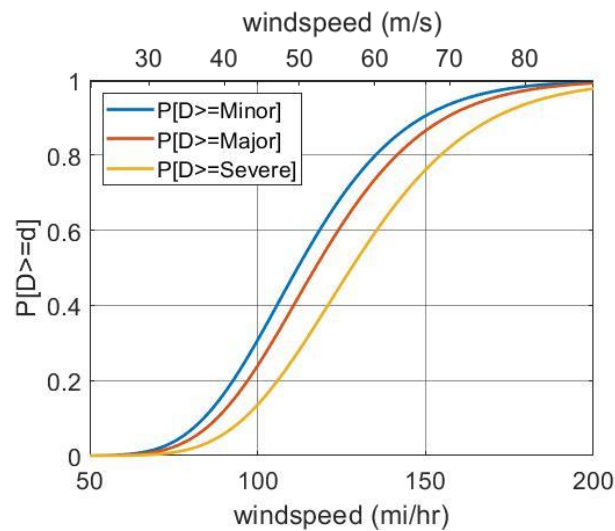


Fig. 4.1 Fragility functions of all grain bins

Tab. 4.2 Windspeed at median for minor damage state

Variable	Category	Windspeed, m/s (mi/h)
Full Set	All bins	50.1 (112)
Grouped/ Ungrouped	Grouped	46.4 (104)
	Ungrouped	51.7 (116)
Manufacturer	Manufacturer 1	47.8 (107)
	Manufacturer 2	46.6 (104)
	Manufacturer 3	53.5 (120)
	Manufacturer 4	-
Condition	Poor	53.4 (120)
	Okay	-
	Good	49.9 (112)
	New	43.5 (97.4)
Diameter	[0,25]ft	54.4 (122)
	(25,35] ft	49.6 (111)
	(35,130] ft	43.6 (97.5)
Height	[0,20] ft	51.5 (115)
	(20,35] ft	51.3 (115)
	(35,135] ft	46.6 (104)
Aspect Ratio	[0,0.75]	48.9 (110)
	(0.75,1.0]	50.4 (113)
	(1.0,1.89]	-
Stiffened/ Unstiffened	Stiffened	46.3 (104)
	Unstiffened	52.2 (117)
Wind Rings/No Wind Rings	Wind Rings	45.8 (103)
	No Wind Rings	51.7 (116)
Terrain	In town	63.7 (143)
	Trees/Buildings	51.4 (115)
	Grain Bins	49.1 (110)
	Open Terrain	47.4 (106)
Behind Other Bins/ Not Behind Other Bins	Behind Other Bins	50.1 (112)
	Exposed Bins	50.1 (112)
Distance to Obstruction	[0,50] ft	53.5 (120)
	(50,150] ft	49.1 (110)
	(150,1000] ft	57.3 (128)
Prominence	[-20,-4] ft	48.9 (109)
	(-4,4] ft	44.2 (98.9)
	(4,30] ft	47.9 (107)
Slope	[-0.07,-0.004]	46.4 (104)
	(-0.004,0.004]	45.4 (102)
	(0.004,0.04]	48.4 (108)
Roof Vents	Roof Vents	46.8 (105)
	No Roof Vents	53.4 (120)

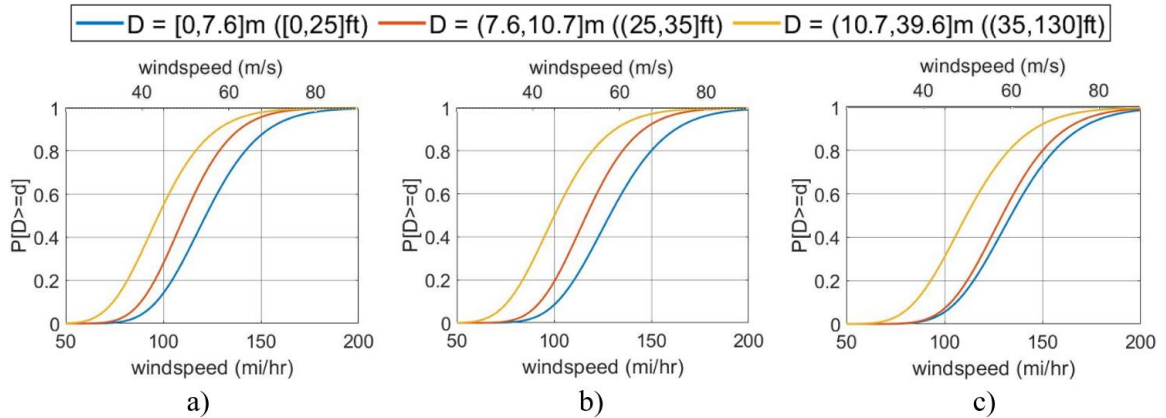


Fig. 4.2 Fragility functions of a) all diameters, minor damage, b) all diameters, major damage c) all diameters, severe damage

4.4. Correlation Analysis

The eight parameters that exhibited a clear trend in their fragility functions were analyzed for their correlation to each other. Since the parameters were categorical or had been lumped into categories for their fragility functions, the statistical method selected for determining correlation had to be able to handle categorical data. Additionally, many of these categories were not binary, further limiting the number of available statistical methods. Two very closely related methods are possible for implementation with this data set: the Cramer's V statistic and the Tschuprow's T statistic. Both are based on the chi-squared statistic and return values ranging from 0 to 1, with 0 corresponding to no association between variables and 1 corresponding to complete association. Tschuprow's T-statistic is equivalent to the Cramer's V statistic when considering correlation between equivalent sets as is the case in this analysis. Therefore, the Cramer's V statistic is used herein. Cramer's V is calculated:

$$V = \sqrt{\frac{\chi^2 / n}{\min(k - 1, r - 1)}}$$

where χ^2 is the chi-squared statistic, n is the total of observations, k is the number of columns, and r is the number of rows. Table 4.3 shows the Cramer's V statistic of the parameters whose row and column intersect at that point in the table. For example, the main diagonal is all 1.0 since each parameter is perfectly correlated with itself. The Cramer's V analysis of the parameters showed a relatively high correlation between all parameters and at least one other, except for terrain, which is relatively independent of the other parameters (Tab. 4.3). A possible reason for this is that, in general, similar sized grain bins tend to share other characteristics as well. Therefore, a point of interest that was looked at was whether size was the controlling factor that made it appear as if other characteristics had a significant effect on a grain bin's susceptibility to damage. For combinations with a Cramer's V of 0.3 or greater, conditional probabilities were found for each category. A value of 0.3 was selected as this threshold to be conservative. Table 4.4 shows the number of bins in the intersection of variables. Table 4.5 presents this data in the form of conditional probabilities:

$$P(\text{Diameter}|\text{Variable}) = \frac{P(\text{Diameter} \cap \text{Variable})}{P(\text{Variable})}$$

This showed that the fragility functions of bins with better prior condition, external vertical stiffeners, and wind ring stiffeners, which counterintuitively performed worse than their counterparts, tended to have a larger diameter than their counterparts.

Additionally, grouped bins tended to have a larger diameter than ungrouped bins. This suggests that size is a more significant factor than these other parameters.

Tab. 4.3 Cramer's V of select parameters

	Group	Condition	Diameter	Height	Aspect Ratio	Stiffened	Wind Rings	Terrain
Group	1	0.255	0.493	0.546	0.157	0.348	0.420	0.096
Condition		1	0.299	0.249	0.187	0.333	0.433	0.221
Diameter			1	0.545	0.274	0.454	0.596	0.185
Height				1	0.306	0.487	0.668	0.109
Aspect Ratio					1	0.216	0.247	0.223
Stiffened						1	0.723	0.111
Wind Rings							1	0.076
Terrain	sym.							1

Tab. 4.4 Number of bins of certain diameter given conditions

	Grouped/ Ungrouped		Condition			Stiffened/ Unstiffened		Rings/ No Rings	
	Grouped	Ungrouped	Poor	Good	New	Stiffened	Unstiffened	Rings	No Rings
D= [0,25] ft	29	212	58	159	3	17	210	1	226
D= (25,35] ft	71	157	15	197	8	27	190	4	213
D= (35,130] ft	122	50	5	124	32	81	76	73	83

Tab. 4.5 Conditional probabilities of certain diameter given conditions

	Grouped/ Ungrouped		Condition			Stiffened/ Unstiffened		Rings/ No Rings	
	Grouped	Ungrouped	Poor	Good	New	Stiffened	Unstiffened	Rings	No Rings
D= [0,25] ft	0.13	0.51	0.73	0.33	0.07	0.14	0.44	0.01	0.43
D= (25,35] ft	0.32	0.37	0.20	0.41	0.19	0.22	0.40	0.05	0.41
D= (35,130] ft	0.55	0.12	0.06	0.26	0.74	0.65	0.16	0.94	0.16

4.5. Fragility Functions of the Intersection of Parameters

Fragility function of the parameters of silo group, condition, presence of external vertical stiffeners, presence of ring stiffeners, and terrain were developed for a tighter range of diameters to eliminate this variability.

Impact of Grouping: For silo group, only bins with a diameter of 7.62 to 10.7 meters (25 to 35 feet) were considered. Figure 4.3 depicts fragility functions of grouped and ungrouped bins of all damage states. This showed better performance of ungrouped bins at the minor and major damage states. However, the grouped bins performed slightly better at the severe damage state. This is an area that needs further research, as past literature reveals mixed results when it comes to the effects of grouping, even within a single study.

Impact of Vertical Stiffeners: For the presence of external vertical stiffeners, diameters were restricted to 10.7 to 15.2 meters (35 to 50 feet). These fragility functions showed little difference in performance of bins with external vertical stiffeners versus those without (Fig. 4.4). This helps resolve the counterintuitive results of the fragility functions of stiffened and unstiffened bins of all diameters. However, these are still not the expected results of the much better performance of stiffened bins. It is possible that within the range of diameters chosen, the stiffened bins are more likely to be at the top end of that range. Additionally, there could be other confounding issues that cannot be easily observed in the field.

Impact of Wind Rings: For the presence of wind rings, diameters were restricted to 10.7 to 15.2 meters (35 to 50 feet). Figure 4.5 shows that bins with wind rings follow the same trend as bins with stiffeners. Although in this case, while the means are very

close, there is some crossing due to differences in variability. It is important to note that all fragility functions were built with windspeed data ranging from about 31.3 to 53.6 m/s (70 to 120 mi/h), as this is the portion of the graph where bins with wind rings clearly have lower probability of failure.

Impact of Roof Vents: When looking at the effects of the presence of roof vents, diameter was restricted to 7.62 to 10.7 meters (25 to 35 feet). The fragility function showed a slightly higher susceptibility of bins with roof vents (Fig. 4.6). However, the effect is far less significant than suggested in literature (Maleki and Mehretehran 2019). Reasons for this discrepancy could include differences between wind tunnel tests and field behavior, differences between grain bins built in accordance with Eurocode and grain bins built in the United States, or other confounding variables unable to be eliminated from the empirical analysis.

Impact of Condition: Since some combinations of condition and diameter had very small numbers of data points, not all combinations were able to produce fragility functions. In Figure 4.7 diameter is categorized as small ([0,7.6]m ([0,25]ft)), medium ((7.6,10.7]m ((25,35]ft)), or large ((10.7,39.6]m ((35,130]ft)). The results of the condition versus diameter show that better condition has little to no positive effect on performance. This indicates that over time the structural integrity of grain bins likely remains substantially intact.

Impact of Terrain: In Figure 4.8 diameter is categorized as small ([0,7.6]m ([0,25]ft)), medium ((7.6,10.7]m ((25,35]ft)), or large ((10.7,39.6]m ((35,130]ft)). There were several combinations of diameter and terrain with too few datapoints to produce fragility functions. However, from the results that were able to be obtained, the fragility

functions in Figure 4.8 show that the more exposed and the larger the grain bins are the more susceptible to damage. This is due to the terrain providing shelter to and changing the wind pressure distribution on the effected grain bins. At the extremes, large diameter bins, 10.7 to 39.6 meters (35 to 130 feet), located on open terrain are the most susceptible of all diameter and terrain combinations while small diameter bins, less than 7.62 meters (25 feet), located in-town were mostly undamaged regardless of windspeed.

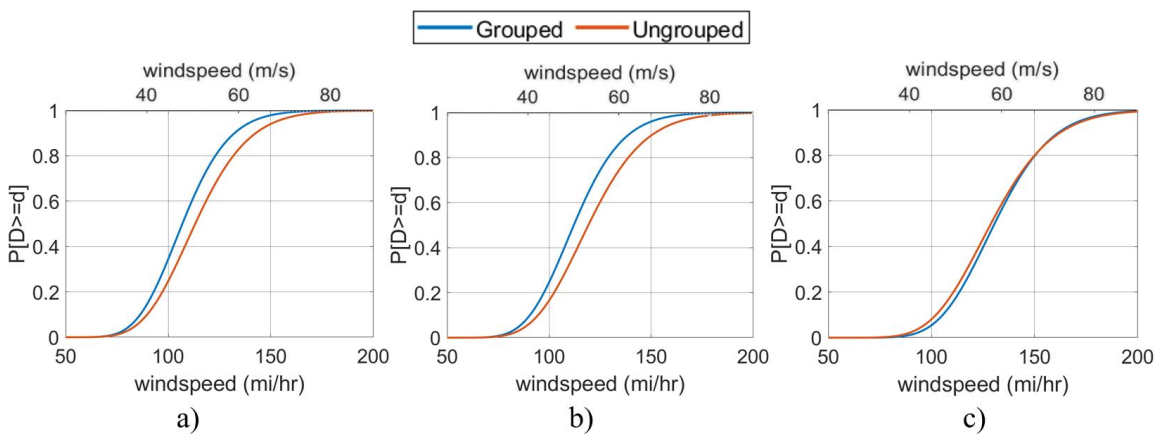


Fig. 4.3 Fragility functions of a) $D = (7.62, 10.7]m$ ((25,35]ft), grouped, minor damage, b) $D = (7.62, 10.7]m$ ((25,35]ft), grouped, major damage, and c) $D = (7.62, 10.7]m$ ((25,35]ft), grouped, severe damage

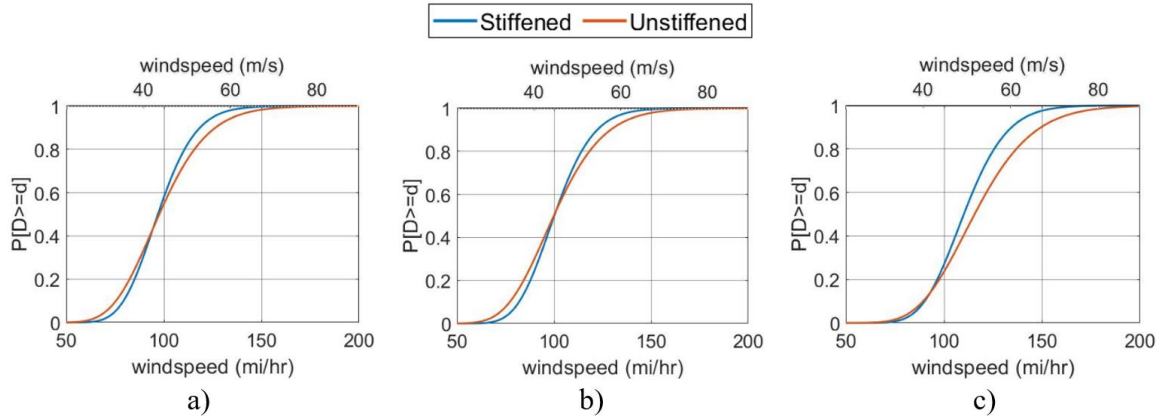


Fig. 4.4 Fragility functions of a) $D = (10.7, 15.2]m$ ((35,50]ft), stiffened, minor damage, b) $D = (10.7, 15.2]m$ ((35,50]ft), stiffened, major damage, and c) $D = (10.7, 15.2]m$ ((35,50]ft), stiffened, severe damage

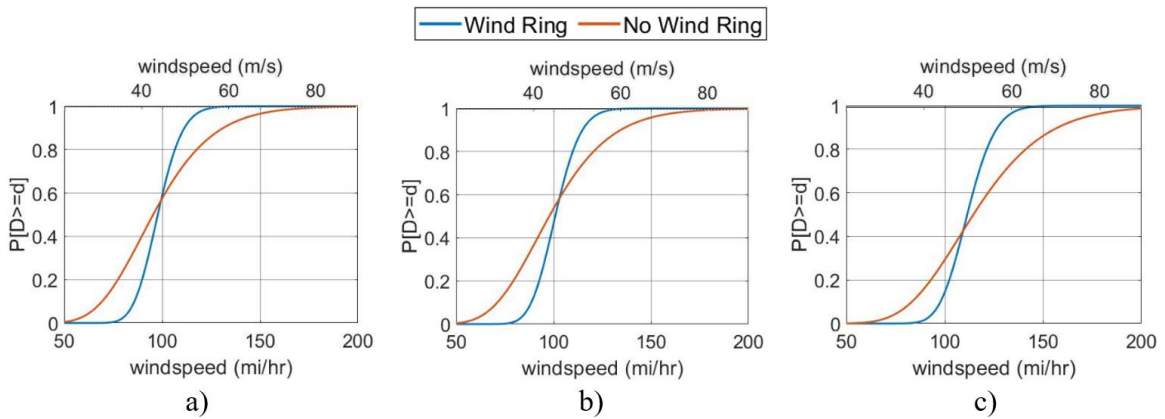


Fig. 4.5 Fragility functions of a) $D = (10.7, 15.2]m$ ((35,50]ft), wind rings, minor damage, b) $D = (10.7, 15.2]m$ ((35,50]ft), wind rings, major damage, and c) $D = (10.7, 15.2]m$ ((35,50]ft), wind rings, severe damage

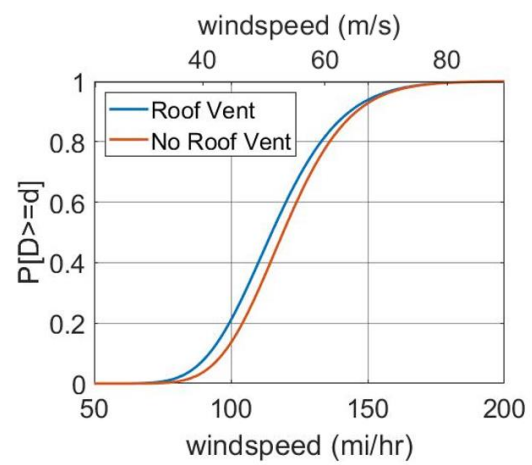


Fig. 4.6 Fragility Functions of $D = (7.62, 10.7]m$ ((25, 35]ft), Vented/Unvented Bins, major damage

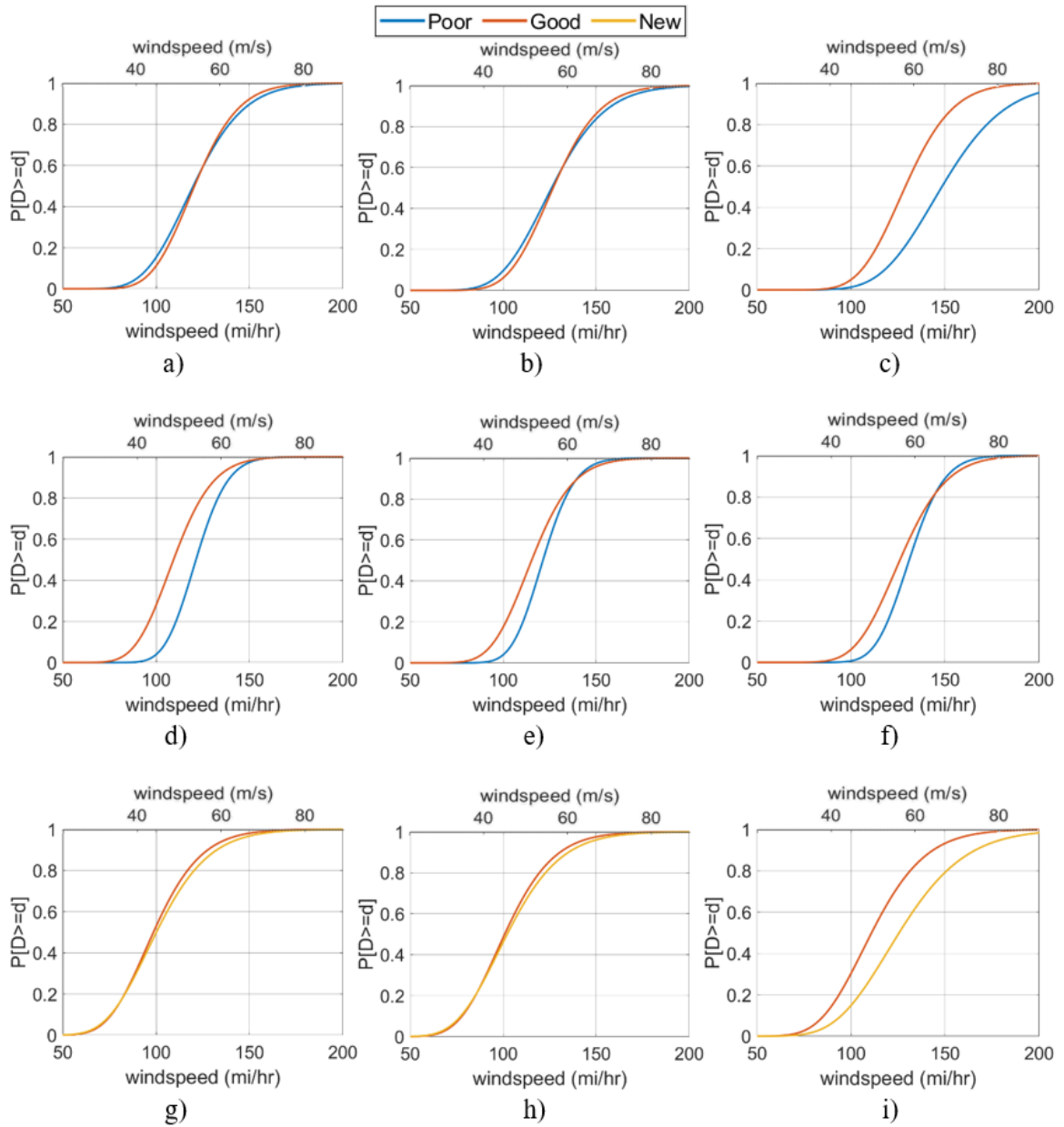


Fig. 4.7 Fragility functions of Diameter and Condition, a) minor damage, small diameter
 b) major damage, small diameter c) severe damage, small diameter d) minor damage,
 medium diameter e) major damage, medium diameter f) severe damage, medium
 diameter g) minor damage, large diameter h) major damage, large diameter i) severe
 damage, large diameter

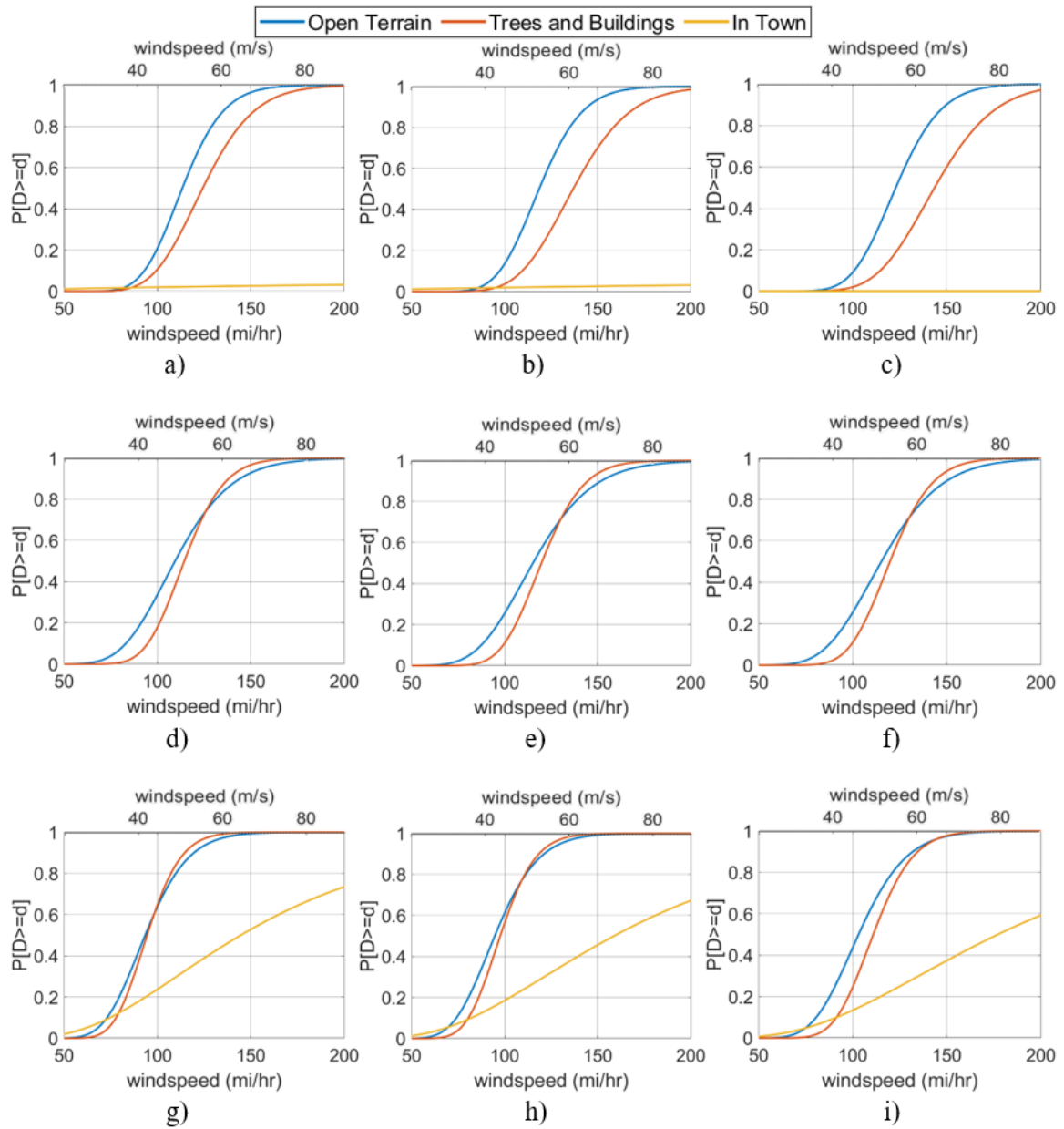


Fig. 4.8 Fragility functions of Diameter and Terrain, a) minor damage, small diameter b) major damage, small diameter c) severe damage, small diameter d) minor damage, medium diameter e) major damage, medium diameter f) severe damage, medium diameter g) minor damage, large diameter h) major damage, large diameter i) severe damage, large diameter

4.6. Conclusions

The complexity of correlations between numerous parameters made it difficult to isolate the effects of individual variables. This led to several apparently counterintuitive relationships between parameters and exceedance of damage state. However, performing a study of conditional probabilities between parameters revealed several strong correlations between variables that have opposite effects on performance. Building fragility functions based on these conditional probabilities revealed that diameter, with large bins being the most susceptible and small bins being the least, and terrain, with bins exposed on open terrain being the most susceptible and in town bins being the least, had the greatest effect on the performance of grain bins in high winds. However, these parameters act in different ways. While diameter affects the strength of the grain bin directly, terrain has no effect on actual strength. Rather, it affects the local windspeed. Additionally, even though the set contained over 600 grain bins, some parameters had too small sample sizes to build relevant fragility functions.

Chapter 5: Finite Element Modelling

5.1. Abstract

Due to the complexity of stresses in and wind load profile on cylindrical grain bins, the traditional and most accurate analysis approach has been finite element modelling. In this study LS-DYNA was used to calculate the critical buckling wind load on a wide range of grain bin configurations. In the numerical models, bins were considered empty, as this is the simplest and most critical case for wind load analysis. The consideration of filled or partially filled bins could significantly impact the buckling behavior. Bin geometry and material properties were based on current manufacturing practices and past literature. Eurocode was used to develop wind load profiles. The arc-length method was used to determine critical buckling load. This was chosen despite its high computational expense because of its ability to capture non-linear behavior and ease of implementation in LS-DYNA. A validation model was made based on a physical bin and past literature to confirm the accuracy of the approach. Then the parametric analysis was carried out. The parametric analysis revealed the failure modes and effectiveness of a wide range of configurations. Since such a large set of parameters was considered in one study, the effectiveness of individual variables could be compared more easily than in the past due to previous studies only being able to look at smaller data sets.

5.2. Model Development

5.2.1. *Geometry*

In order to set up a parametric analysis, a baseline was set down. Any variation from this was specifically denoted in the study. Figure 5.1 depicts the baseline model in

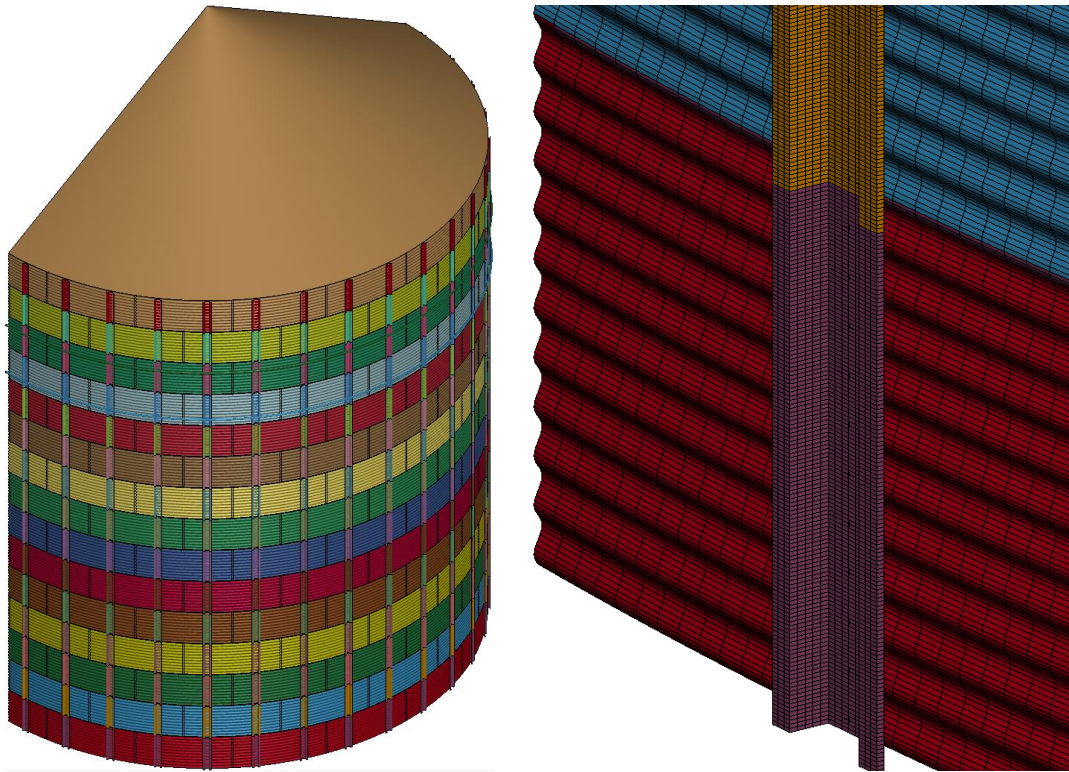
comparison to an annotated photo of a grain bin in the field. Bin height was defined as the top of cylindrical wall. To represent physical bins as accurately as possible, walls were modelled as being constructed of rings of overlapping panels, where element thickness at the overlap is the sum of adjacent panels. These panels were 1.143 m (45 in) tall and approximately 2.92 m (9.59 ft) long. Panels were arranged in a running bond pattern, with a 25.4 mm (1 in) horizontal overlap between rings, and a 50.8 mm (2 in) vertical overlap between panels in the same ring. Since wall thickness usually varies with height and height is not constant for all bins modelled, wall panels were modelled as uniform thickness from base to roof to eliminate inconsistencies in variation due to different heights. Diameter was measured from the average depth of the corrugation profile. The corrugation profile was sinusoidal, with a wavelength of 101.6 mm (4 in) and a depth (crest to trough) of 19.05 mm (0.75 in). The wall panels were meshed with 12 elements per corrugation wavelength and a seed size of 50 mm along the circumferential direction. The roof of the bin was conical with a slope of 30 degrees.

The stiffener geometry shown in Figure 5.2 was based on the shape of stiffeners used by most major manufacturers in the United States. Stiffener thickness was kept constant with height for the same reason as wall panel thickness. Wind rings were modelled as a tube of shell elements with a diameter of 63.5 mm (2.5 in) and thickness of 2.54 mm (0.1 in).

The wall of the cylinder and the vertical stiffeners were pinned in all three principal directions at the base. One simplification that was made was to only model half of the bin and to impose a plane of symmetry on the cut edge. In this way, half as many elements need to be analyzed.



a)



b)

c)

Fig. 5.1 Grain bin a) in the field b) finite element model c) close-up of wall and stiffener elements

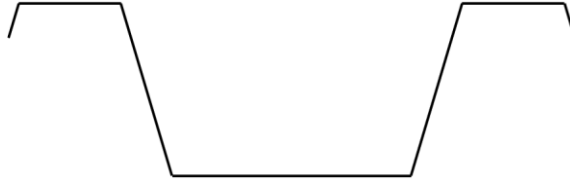


Fig. 5.2 Stiffener cross-section

5.2.2. Elements and Material Model

For the entire model, the same element type and material model was used. Material properties were selected to be consistent with standards referenced by most grain bin manufacturers in the United States. All parts were modelled as steel that was elastic-perfectly plastic with a Young's Modulus of 200 GPa, Poisson's ratio of 0.29, and a yield stress of 340 MPa. All elements were modelled as fully integrated 4-node shells.

5.2.3. Wind Loading

Wind loading is based on the provisions of Eurocode EN 1991-1-4 as this has a more detailed load development than ASCE 7 of wind on cylindrical structures, is based on the wind tunnel tests of MacDonald et al. (1988) and is used by several other past studies. These tests were performed to replicate the effects of straight-line winds and are not applicable to tornadic winds. Eurocode distributes pressure over vertical and circumferential directions. In this distribution, wind pressure varies vertically according to EN 1991-1-4:

$$q_p(z) = C_e(z)q_b$$

where:

$$q_b = \frac{1}{2} \rho v_b^2$$

In this distribution, peak velocity pressure $q_p(z)$ as function of height z , air density ρ (taken as 1.25 kg/m^3), basic wind speed velocity v_b at a height of 10 m above the ground.

The value of the exposure factor $C_e(z)$ comes from the equations:

$$C_e(z) = [1 + 7I_v(z)]c_r^2(z)c_o^2(z)$$

$$\begin{cases} c_r(z) = k_r \ln\left(\frac{z}{z_0}\right) & \text{for } z_{min} \leq z \leq z_{max} \\ c_r(z) = c_r(z_{min}) & \text{for } z \leq z_{min} \end{cases}$$

$$k_r = 0.19 \left(\frac{z_0}{z_{0,II}}\right)^{0.07}$$

$$\begin{cases} I_v(z) = \frac{k_I}{c_o(z) \ln(z/z_0)} & \text{for } z_{min} \leq z \leq z_{max} \\ I_v(z) = I_v(z_{min}) & \text{for } z \leq z_{min} \end{cases}$$

where, $c_o(z)$ is taken as 1.0, z_0 and $z_{0,II}$ are taken as 0.05 m, z_{min} and z_{max} are taken as 2 m and 200 m respectively, and k_I is taken as 1. The vertical distribution of wind pressure is shown in Figure 5.3.

Similarly, the circumferential distribution was taken from Eurocode (EN1993-4-1 Annex C). In this code, wind pressure is a function of bin aspect ratio and polar angle as shown:

$$C_p(\theta) = -0.54 + 0.16(d_c/H) + \{0.28 + 0.04(d_c/H)\}\cos\theta + \{1.04 -$$

$$0.20(d_c/H)\}\cos2\theta + \{0.36 - 0.05(d_c/H)\}\cos3\theta - \{0.14 - 0.05(d_c/H)\}\cos4\theta$$

where, θ is the polar angle measured from the stagnation zone, d_c is the diameter of the cylinder, and H is the maximum wall height. The circumferential wind pressure distribution is shown in Figure 5.4. Therefore, the final wind pressure distribution as a function of both elevation and circumferential coordinate is given as:

$$P(z, \theta) = q_p(z)C_p(\theta)c_s c_d = C_e(z)C_p(\theta)q_b$$

where, $c_s c_d$ can be taken as 1. Wind loads were applied as point loads to the nodes of the grain bin wall rather than as a pressure applied to the face of the shell elements for simplicity. Each node was loaded with a force equivalent to the pressure at the point of the node multiplied by the area of the wall elements.

Some physical bins have vents in their roof to help with moisture control in the bin. Eurocode prescribes a uniform inward pressure coefficient $\Delta C_p = +0.4$ (EN 1993-4-1 Annex C). The corresponding circumferential pressure coefficient is shown in Figure 5.5. Wind loads on the roof were taken from EN 1991-1-4 provisions for loads on a dome roof due to lack of provisions for a conical roof and to stay consistent with past literature. For bins considering both vented roofs and wind load on the roof, the uniform inward pressure coefficient $\Delta C_p = +0.4$ was applied to roof wind loads as well.

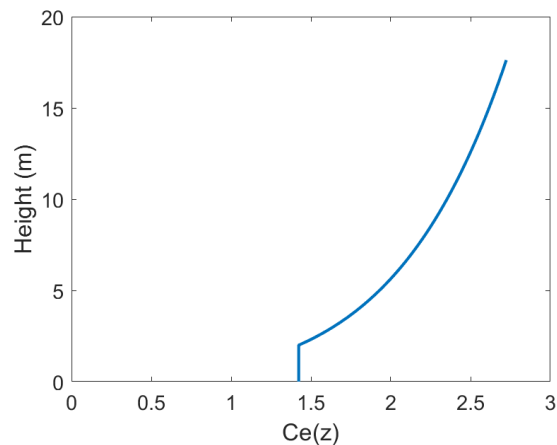


Fig. 5.3 Meridional wind pressure distribution

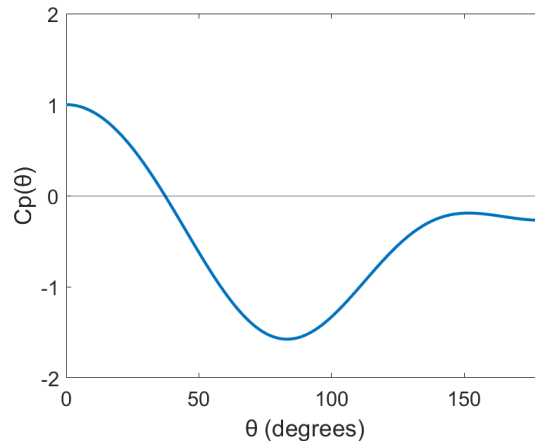


Fig. 5.4 Circumferential wind pressure distribution for unvented bin

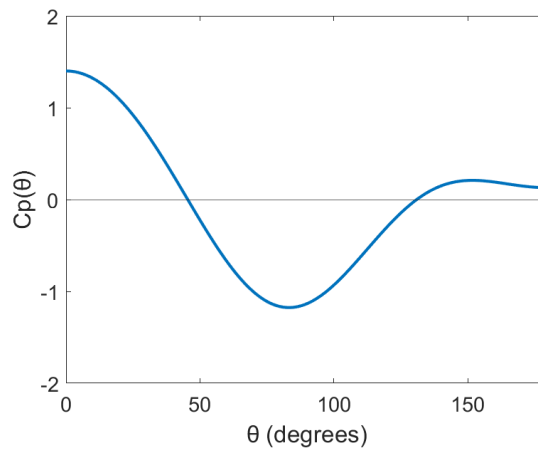


Fig. 5.5 Circumferential wind pressure distribution for vented bin

5.2.4. Arc-Length Method

The goal of the parametric numerical study was to determine the critical buckling load of each grain bin included in the study. There were two methods considered for determining these critical buckling loads. First, elastic buckling load can be determined by eigen analysis. This provides a computationally cheap solution at the expense of the ability to capture geometric and material nonlinearity. However, for this study it was determined that the benefits of a non-linear buckling analysis outweighed the additional

computational expense. Therefore, the arc-length method was implemented in LS-DYNA's implicit solver.

Traditionally, finite element software solves the finite element equation using the Newton's Method. However, since Newton's method requires load to increase monotonically with every timestep, it is only able to capture behavior up to a critical point (Vasios 2015). Due to the complex behavior of grain bins under wind loads, it was necessary to be able to fully capture buckling behavior. The arc-length method overcomes this by stepping through force-displacement space by varying both parameters simultaneously along the equilibrium path (Vasios 2015). A feature of the arc-length method is that it requires applied loads to be linear with respect to time. Due to the nature of this analysis, it was required that gravity forces be constant. However, the implicit solver was unable to converge under the instantaneous loading of gravity. This was solved by implementing dynamic relaxation, in which stresses and displacements due to gravity were initialized before starting the arc-length analysis. The first step was to calculate the Eigen-frequencies and record the frequency of the mode shape corresponding to vertical oscillation. This frequency was then used to calculate critical damping by the equation,

$$c_c = \frac{4\pi}{T}$$

where c_c is the critical damping coefficient and T is period in $kN\ ms/mm$ and ms respectively for the system of units used in this model. Next, an explicit transient analysis was run with only gravity forces and critical damping applied until the structure reached equilibrium. The output of this analysis was the stresses and displacement of all nodes

and elements. These were then used to initialize the final implicit arc-length analysis. Therefore, gravity loads could be kept constant during the analysis.

5.2.5. Model Validation

In the absence of physical test data, model validation was conducted by comparison with limited literature. Specifically, the studies of Maleki and Mehrehtehran (2018) and Iwicki et al. (2015) were utilized in which experimental modal analysis of a constructed steel grain bin yielded the first several natural frequencies, which were subsequently modeled in ABAQUS.

The model built for validation incorporated the geometry and materials of the tested bin, which is not the same as the baseline bin analyzed in this chapter. However, the modeling and analysis approaches are the same. The validation bin had a height of 17.62 meters and diameter of 8.02 meters. A sinusoidal corrugation profile, with a wavelength and amplitude of 76 mm and 18 mm respectively, was used for the corrugation profile of the bin walls. The bin was modelled with a uniform wall thickness of 0.75 mm, with no increased thickness for overlaps. A total of 18 vertical stiffeners were distributed evenly around the circumference of the bin. These stiffeners were open-section shapes of two different profiles, shown in Figure 5.6, that switch around one-third height and vary in thickness with height at outlined in Table 5.1. The roof of the bin was modelled as a 7.5 mm thick flat steel plate to prevent out-of-round stiffness to the top of the bin. The material model of the validation bin is characterized by a Young's Modulus of 210 GPa, a Poisson's ratio of 0.3, and a yield stress of 355 MPa.

From the analysis of the first Eigen-frequency, a value of 7.51 Hz, with a mode shape shown in Figure 5.7, compared to 6.9 Hz as measured experimentally. Figure 5.8

shows the resultant node displacements at the critical windspeed. Maximum displacement occurs in the stagnation zone at a height of about 70% of the total bin height. Since wind load, geometry, material model, and boundary conditions are symmetric with respect to the vertical plane parallel to windward, the left half of the deflected shape would be the mirror image of Figure 5.8. In reality, neither loading, geometry, nor material are perfect, causing behavior that is not perfectly symmetrical. However, imperfections like these were not considered in the present study. Investigation of the effects of geometric imperfection have been carried out by several authors, including Godoy and Flores (2002), Portela and Godoy (2005a), and Maleki and Mehretehran (2018 and 2019). They showed that geometric imperfections significantly reduced the critical wind load for grain bins. While modelling grain bins as accurately as possible was a major consideration, the main focus of the present research was the effects of individual parameters, not calculating the exact windspeed at failure. From the arc-length analysis a critical windspeed of 53.72 m/s was calculated. The Von Mises stress distribution in Figure 5.9 shows shear ripples in the lower portion of the bin wall and the failure of the stiffener nearest the stagnation zone at the critical windspeed.

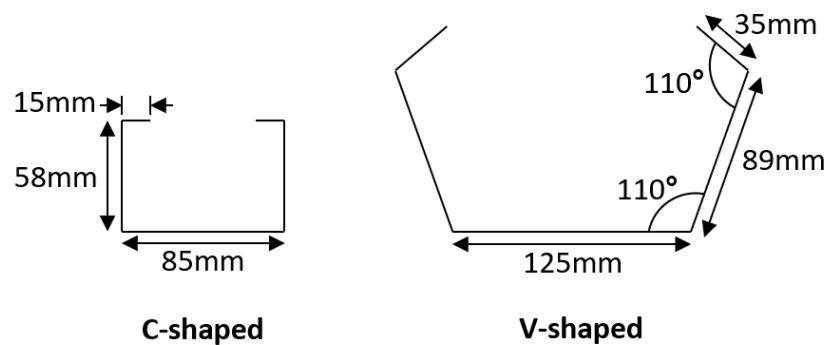


Fig. 5.6 Stiffener cross-sections

Tab. 5.1 Stiffener Variation

Stiffener number	Cross-section	Thickness (mm)
7 (top)	C-shaped	1.5
6	C-shaped	2.0
5	C-shaped	3.0
4	V-shaped	4.0
3	V-shaped	4.0
2	V-shaped	4.0
1 (bottom)	V-shaped	5.0

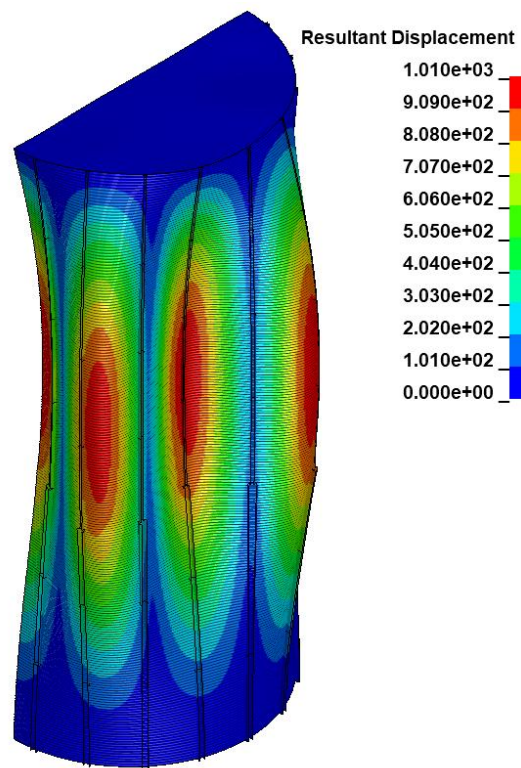


Fig. 5.7 First eigen-frequency mode shape

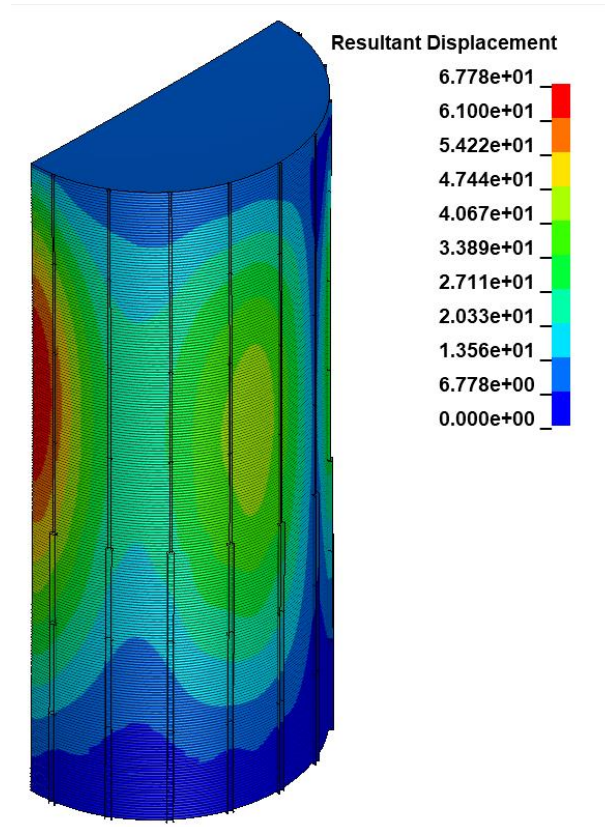


Fig. 5.8 Non-linear buckled form with resultant displacement

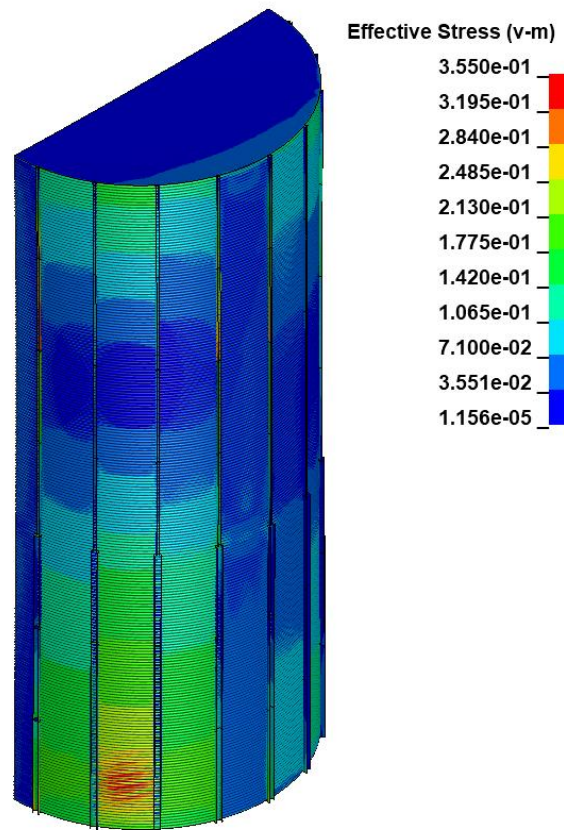


Fig. 5.9 Non-linear buckled form with Von Mises stress distribution

5.3. Parametric Analysis of Finite Element Model Configurations

5.3.1. Methodology

The set of variables considered in the parametric analysis were diameter, height, stiffeners, wind rings, wind on roof, vented, corrugation length, corrugation depth, wall thickness, stiffener thickness. The variables of wind on roof and vented wind pressure distribution are binary. The rest of the variables were analyzed over the ranges shown in Table 5.2. These ranges were selected to cover the majority of variation found in physical bins. In order to analyze a single variable at a time, a standard bin was created. Therefore, all bins compared to each other have these parameters unless explicitly labelled otherwise. These standard values are shown in red in Table 5.2. Additionally, the

standard bin was modelled without wind loads on the roof and with an unvented pressure distribution. To keep variables as consistent as possible wall and stiffener thickness was kept constant with height. Even though this is not consistent with physical bins, it helped eliminate additional variables between bins. For example, taller bins would not be able to have the same sequence of thicknesses, as they have a greater number of panels. The force-displacement plot and resultant displacement plot at critical wind pressure for every bin considered in the parametric study are included in **Appendix B** of this thesis.

Tab. 5.2 Variation of parametric analysis

Variable	Values Considered
Diameter, m (ft)	5.49, 9.14, 12.8, 16.5 , 20.1, 23.8, 27.4 (18, 30, 42, 54 , 66, 78, 90)
Height, panels	5, 10, 15 , 20, 25, 30
Stiffeners per Panel	0, 1, 2 , 3
Number of Wind Rings	0, 1, 2 , 3, 4, 5
Wind on Roof	True, False
Vented Wind Pressure	True, False
Corrugation Length, mm (in)	20.8, 76.2, 101.6 , 152.4 (2, 3, 4 , 6)
Corrugation Depth, mm (in)	6.35, 12.7, 19.1 , 25.4, 38.1 (0.25, 0.5, 0.75 , 1.0, 1.5)
Wall Thickness, mm	1, 1.5, 2 , 3, 4
Stiffener Thickness, mm	3, 4, 5 , 7, 9

5.3.2. Impact of Bin Geometry and Load Application

In order to more accurately gauge the effects of diameter on critical wind load, datasets were built for all combinations of unstiffened bins, bins with stiffeners, bins with stiffeners and wind rings, bins with and without wind loads applied to the roof, and bins with vented and unvented pressure distributions. When looking at all levels of

reinforcement for bins without wind loads on their roof and modelled as unvented, there is a clear inverse relationship between diameter and critical buckling load. This is consistent with all past literature. Figures 5.10 and 5.11 present the critical buckling strength as a function of bin diameter for unvented and vented bins, respectively, assuming all other variables are held constant. Three scenarios are included on each plot for comparison: unstiffened, stiffened, and the case of stiffeners combined with wind rings. In both plots, it can be seen that stiffened bins have a higher critical buckling load than unstiffened bins. The effect is striking with unstiffened bins having buckling strength consistently less than 1000 compared to stiffened bins which exceed 3000 Pa at low diameters. Additionally, stiffened bins with rings had the highest critical load of all. Although, they are only slightly higher than stiffened bins without wind rings. However, there is a somewhat anomalous dip and increase in buckling strength for bins with diameters of 9.14 meters (30 feet) and 12.8 meters (42 feet) (Fig. 5.10). This dip and increase are not present for other combinations of roof loading and venting (Fig 5.11). Looking at load-displacement curves gives some insight into this anomaly. Figure 5.12 shows that the load-displacement curves for bins with larger diameters experience a shallower slope as they near their peak, indicating a more gradual loss in stiffness before snap-through. However, bins with a smaller diameter have an abrupt reversal in path, indicating a more sudden snap-through behavior. The smallest diameter bins do not follow this trend. Figure 5.13 shows the Von Mises stress distribution for the 5.49 m (18 ft) diameter unstiffened bin that is unvented and has no wind load applied to its roof. This figure shows that, at the critical load, a significant area of the bin wall has yielded. This accounts for the softening seen in Figure 5.12. Conversely, the Von Mises stress

distribution for the corresponding bin with a diameter of 16.5 m (54 ft), in Figure 5.14, shows much less yielding of the bin wall. This is consistent with the abrupt snap through behavior exhibited in Figure 5.12. Furthermore, Figure 5.15 and Figure 5.16 show the resultant displacement for the same two bins. This shows a more cantilever like behavior at failure of the smaller diameter bin compared to the more plate-bending like behavior of the larger diameter bin. The dip in critical wind pressure occurs at the transition between these two stress distributions and displacement patterns. Looking at the same data in a different way, with wind on roof and venting variable for bins with the same reinforcement, shows the same inverse relationship between diameter and critical load. Figure 5.17 shows this for unstiffened bins. Furthermore, it shows that for bins with and without roof wind loads, vented bins have a lower critical load than unvented bins due to the increased negative internal pressure. Also, for both vented and unvented bins, wind loads applied to the roof increased critical load. This is due to roof wind pressures being negative for the roof slope in this study, therefore relieving some compressive stress in bin walls and stiffeners. Figure 5.18 shows that, for stiffened bins, there is a crossing between unvented bins with no roof wind loads and vented bins with wind loads. Since there are two variables between these lines, they cannot be compared directly. However, when comparing them to the lines sharing one constant, the graph implies that at smaller diameters, roof wind loads have a much more significant effect than venting, with the opposite being true at larger diameters. The parameter of height was looked at regarding unstiffened bins, bins with stiffeners, and bins with stiffeners and rings. Figure 5.19, shows buckling load and height had a clear inverse relationship, as expected. Similar to

bins with variable diameter, bins with variable height had higher buckling loads the more reinforced they were.

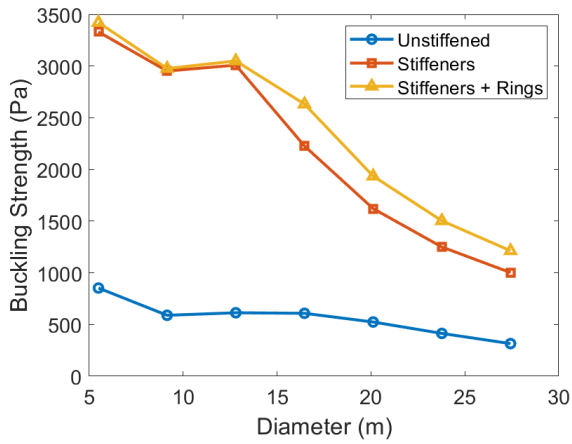


Fig. 5.10 Critical Buckling Load versus Diameter for unvented bins without wind loads applied to the roof

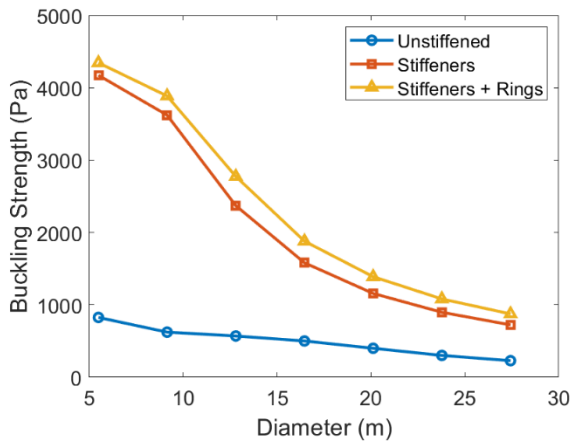


Fig. 5.11 Critical Buckling Load versus Diameter for vented bins with wind loads applied to the roof

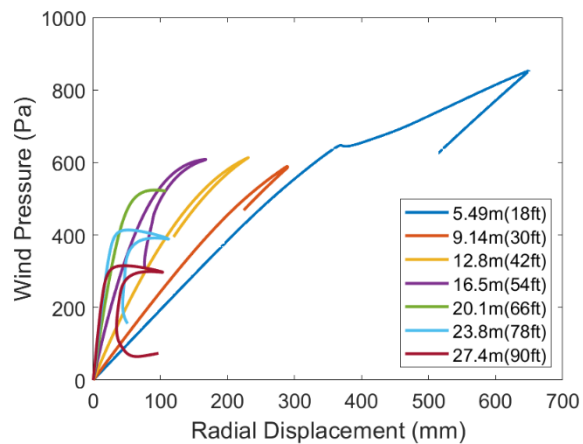


Fig. 5.12 Load-Displacement Curves for unstiffened bins of varying diameter

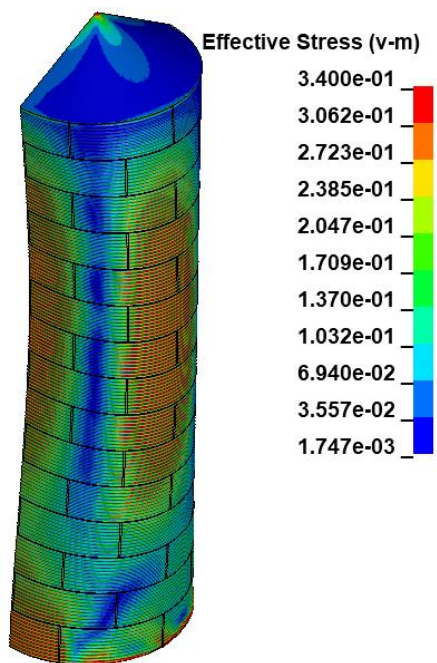


Fig. 5.13 Von Mises Stress Distribution of 5.49 m (18 ft) Diameter Bin

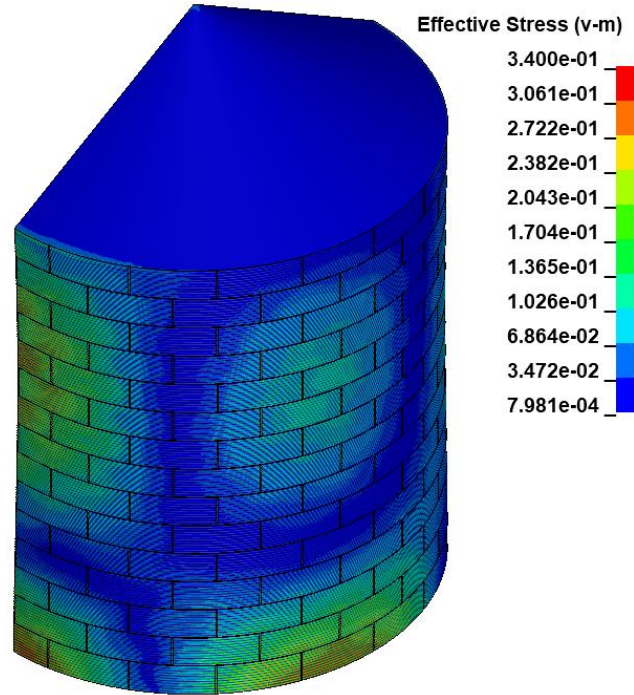


Fig. 5.14 Von Mises Stress Distribution of 16.5 m (54 ft) Diameter Bin

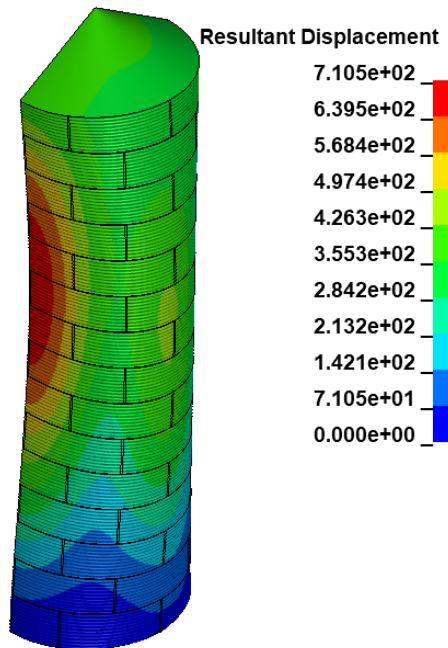


Fig. 5.15 Resultant Displacement of 5.49 m (18 ft) Diameter Bin

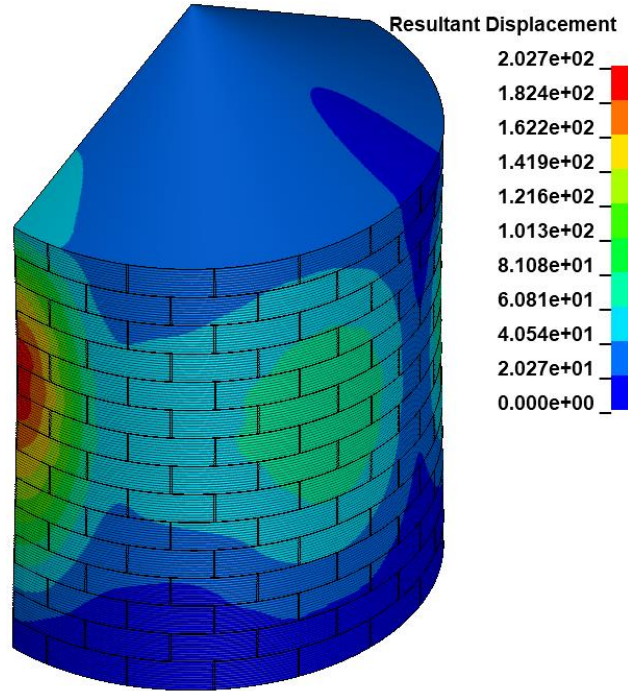


Fig. 5.16 Resultant Displacement of 16.5 m (54 ft) Diameter Bin

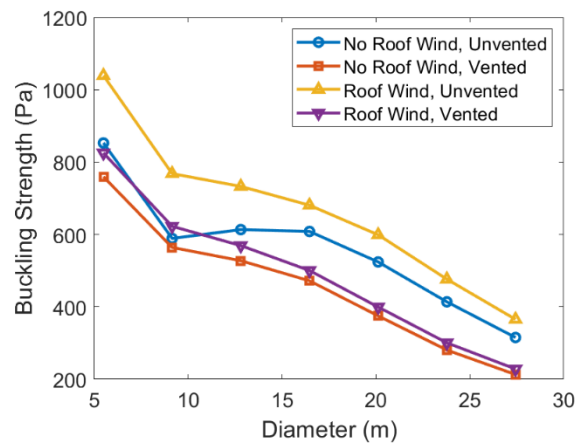


Fig. 5.17 Critical Buckling Load versus Diameter for unstiffened bins

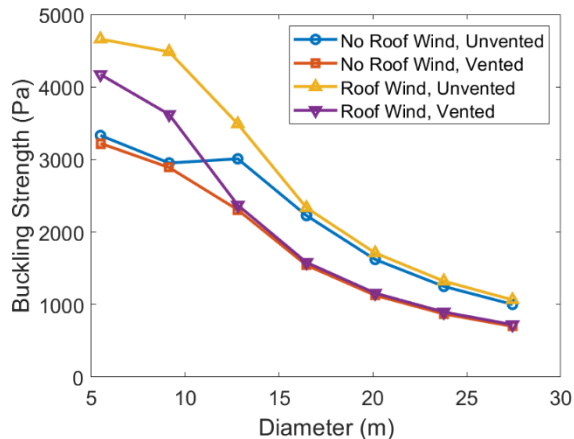


Fig. 5.18 Critical Buckling Load versus Diameter for stiffened bins

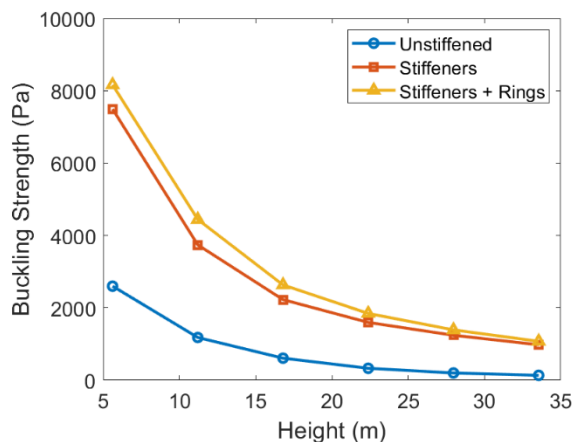


Fig. 5.19 Critical Buckling Load versus Height

5.3.3. Impact of Stiffener and Wind Ring Configuration

Stiffener and wind ring configuration were looked at in tandem, as the two forms of reinforcement are commonly used together. From Figures 5.20 and 5.21, it can be seen that critical wind load increases significantly as number of stiffeners per panel goes from zero to three, but with diminishing returns for heavily stiffened bins. Additionally, the number of wind rings has a smaller effect on critical load. However, wind rings had a more substantial effectiveness for bins with two stiffeners per panel. Figures 5.22, 5.23,

and 5.24 show the resultant displacement at critical wind load of bins with zero, two, and four wind rings respectively. From these figures, it can be seen that the addition of two wind rings stiffens the bin wall at the height where they are located and shifts the maximum displacement lower when compared to the bin with no rings. However, with the addition of four rings, the displaced shape changes, with maximum displacement occurring in the roof. This indicates a change in failure mode. Since the bin with five rings has the same roof geometry as the bin with four, they have nearly identical critical wind speeds. Additionally, the effectiveness of wind rings is variable with robustness of wind rings. Standard ring diameter was 63.5 mm (2.5 in), and ring thickness was 2.54 mm (0.1 in). To investigate the lower and upper limit of wind ring effectiveness, bins were also modelled with a diameter of 38.1 mm (1.5 in) and thickness of 1.27 mm (0.05 in) or a diameter of 88.9 mm (3.5 in) and thickness of 3.81 mm (0.15 in). Error bars on the data for bins with two stiffeners per panel show increasing or decreasing wind ring diameter and thickness can have a significant effect on critical wind load (Fig 5.21). Lightly modelled wind rings have little effect on critical load. Standard model wind rings stop significantly increasing critical load with four rings, at which point resultant displacement profile changes. Heavily modelled wind rings stop significantly increasing critical load at two rings, where displacement likewise changed to a maximum at the roof. The same change in displacement profile accounts for the small difference in critical windspeed between bins with two stiffeners per panel and bins with three stiffeners per panel.

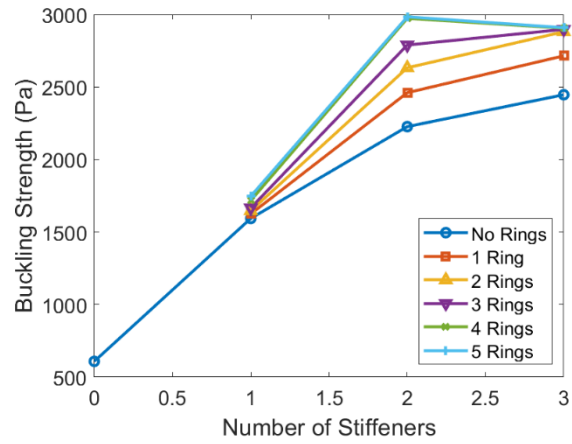


Fig. 5.20 Critical Buckling Load versus Number of Stiffeners

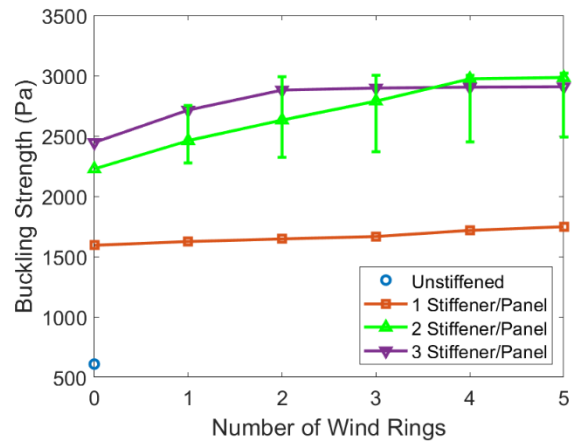


Fig. 5.21 Critical Buckling Load versus Number of Wind Rings

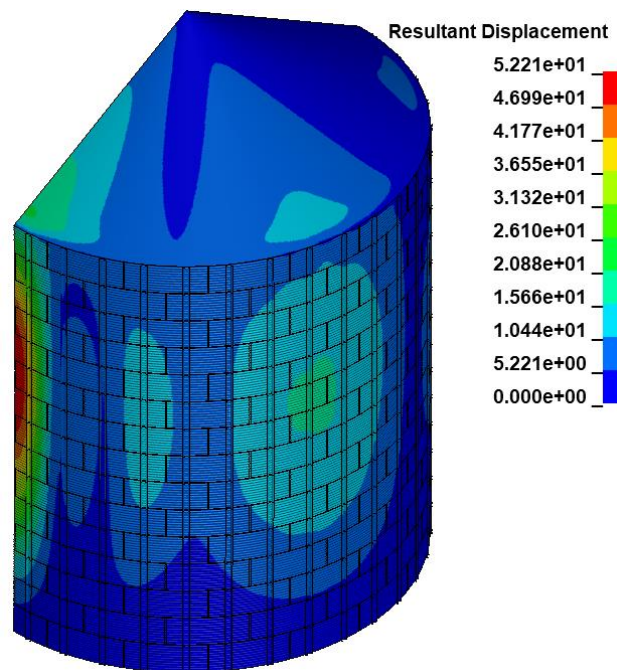


Fig. 5.22 Resultant Displacement of Stiffened Bin without Wind Rings

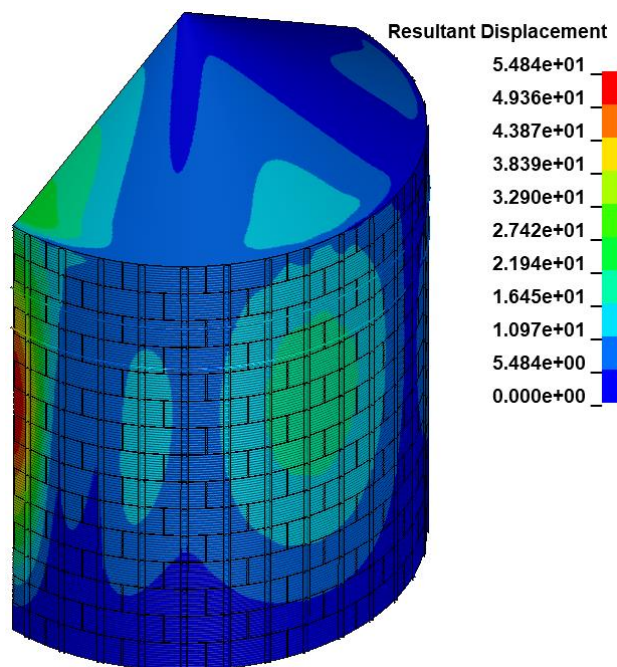


Fig. 5.23 Resultant Displacement of Stiffened Bin with Two Wind Rings

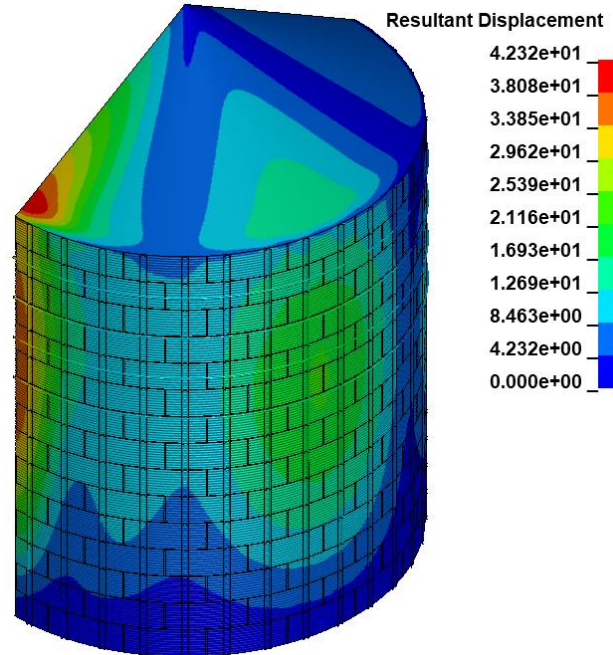


Fig. 5.24 Resultant Displacement of Stiffened Bin with Four Wind Rings

5.3.4. Impact of Corrugation Profile

Like stiffeners and wind rings, corrugation profile wavelength and depth were looked at together. Figure 5.25 shows that corrugation length has little effect on critical wind load for most corrugation depths for unstiffened bins. At the same time corrugation depth does have an effect of critical wind load. Figure 5.26 more clearly shows the benefits of corrugation depth have a maximum at about 19 mm. This is due to increased depth adding flexural strength in the circumferential direction, while at the same time having a detrimental effect on flexural resistance in the meridional direction. Therefore, bins with a very shallow corrugation depth failed due to lack resistance in the circumferential direction. The effects of this can be seen by comparing the high number of waves in the circumferential direction of the bin walls as seen in Figure 5.27 to the displacement profile of Figure 5.16. Alternately, bins with very deep corrugation

depths experienced severe snap-through behavior. Figure 5.28 shows that bins with a deep corrugation profile have a similar displacement pattern to the standard (Fig. 5.16) but with a higher magnitude. Since these bins were unstiffened and corrugation depth lost effectiveness due to increased orthotropic behavior, it was worthwhile to investigate the effects of corrugation depth for bins with stiffeners which provide stability in the softer direction and brace against snap-through. Figure 5.29 shows the effect of corrugation depth on critical wind load for bins with stiffeners. As expected, for bins with stiffeners, critical buckling load continued to increase with corrugation depth. However, returns significantly diminish beyond a depth of 19 mm. Similar to the dimensioning returns of stiffeners per panel and number of wind rings, the apparent maximum benefit occurs when the location of maximum displacement changes from the bin wall to the roof.

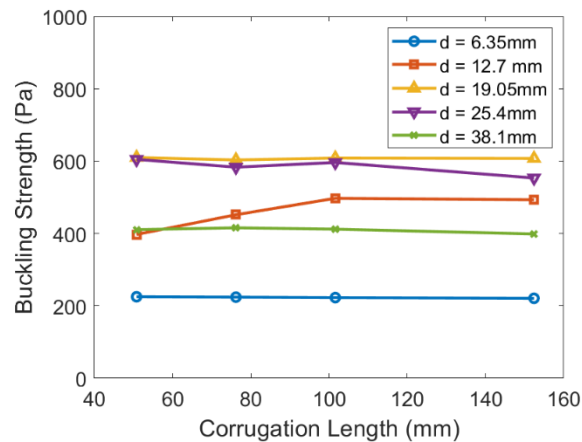


Fig. 5.25 Critical Buckling Load versus Corrugation Length (unstiffened)

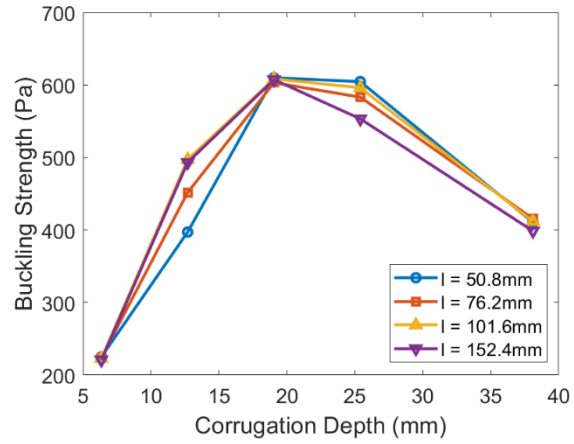


Fig. 5.26 Critical Buckling Load versus Corrugation Depth (unstiffened)

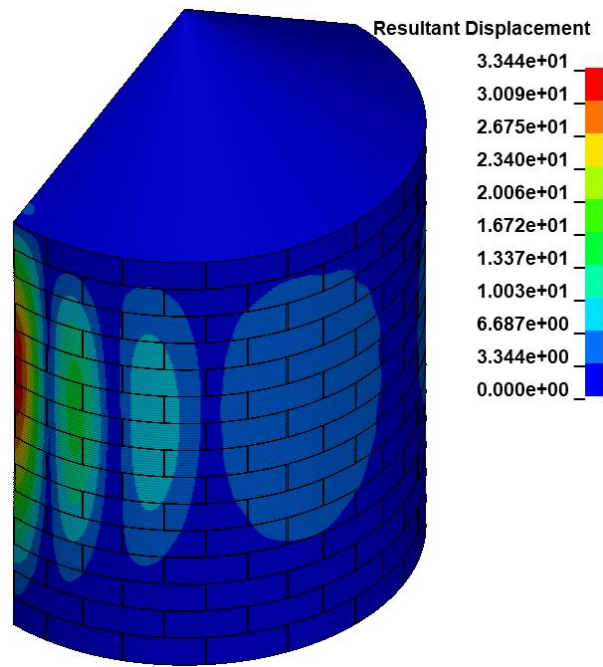


Fig. 5.27 Resultant Displacement of Bin with Corrugation Depth of 6.35 mm (0.25 in)

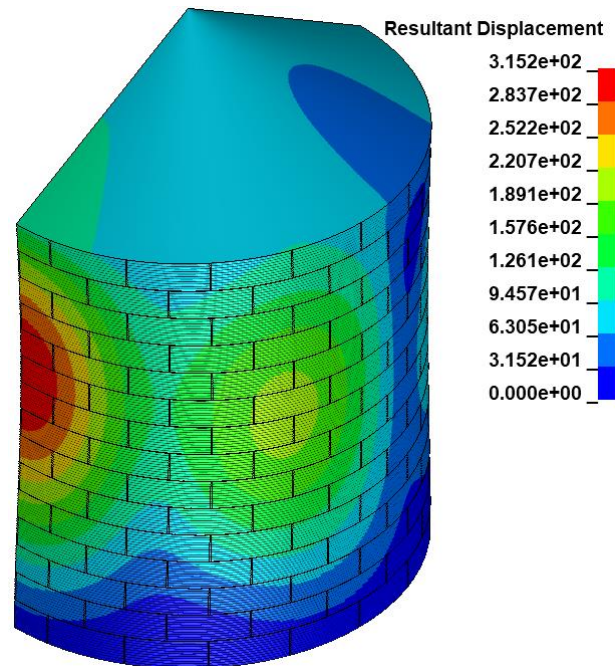


Fig. 5.28 Resultant Displacement of Bin with Corrugation Depth of 38.1 mm (1.5 in)

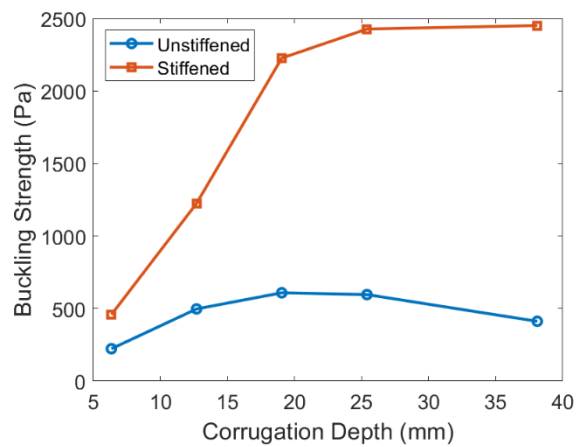


Fig. 5.29 Critical Buckling Load versus Corrugation Depth

5.3.5. Impact of Wall and Stiffener Thickness

Looking at Figures 5.30 and 5.31 together reveal that the presence of stiffeners has a major contribution to the buckling load, but stiffener thickness has limited effect for the values considered in this study. This is due to a buckle wave forming between the

stiffeners adjacent to the stagnation zone (Fig. 5.22). Therefore, the stiffener is deformed in torsion, which has a relatively low stiffness. On the other hand, wall thickness has a direct and fairly linear relationship with critical load.

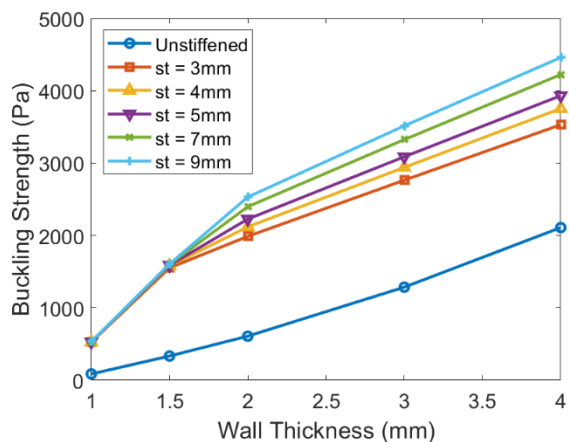


Fig. 5.30 Critical Buckling Load versus Wall Thickness

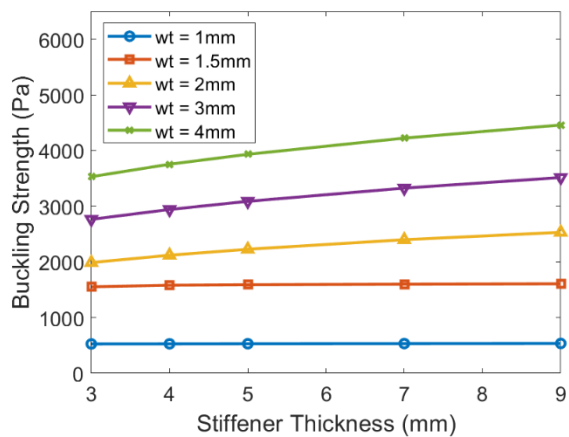


Fig. 5.31 Critical Buckling Load versus Stiffener Thickness

5.4. Conclusions

Through the parametric analysis of grain bin configurations using finite element modelling, the individual effects of numerous variables were qualitatively determined. Diameter and height are both inversely related to critical wind load. Critical pressures

went from 853 Pa to 608 Pa to 314 Pa as diameter increased from 5.49 m (18 ft) to 16.5 m (54 ft) to 27.4 m (90 ft). These pressures correspond to windspeeds of 36.9 m/s (82.5 mi/h), 31.2 m/s (69.8 mi/h), and 22.5 m/s (50.3 mi/h) respectively. Increasing the number of stiffeners per panel and number of wind rings both had a direct relationship with critical wind load until a level of diminishing returns was met. For the standard bin, the maximum benefit that could be reached by varying these parameters approached 3000 Pa corresponding to a windspeed of approximately 70 m/s (157 mi/h). The modelling of grain bins with wind loads applied to the roof was beneficial to critical wind load as the negative pressure reduced the vertical compression on bin walls caused by gravity. The application of a vented pressure distribution had a negative effect on critical wind load due to the increased pressure in the stagnation zone. This became more significant at greater diameters. Corrugation length had little effect on critical wind load. Conversely, corrugation depth had a significant effect on critical wind load, with effectiveness tied to both circumferential and meridional stiffness. Stiffener thickness had only a small effect on critical wind load, while wall thickness is approximately linear with crucial wind load over the range tested in this study.

Based on the results of this study, in the practice of grain bin design it might be beneficial to devise a system to seal the vents of empty grain bins. As airflow is not needed when the bin is empty and most susceptible to wind damage, the resulting change in pressure distribution would be beneficial to critical wind load. Future research is needed to take a more in-depth look at the geometry of the roof and roof-wall connections in addition to anchorage. Further refinement would be needed to develop an optimization of height, diameter, and wall thickness given a target volume. These would

include varying wall and stiffener thickness with height, refining connection details, and varying stiffener geometry.

Chapter 6: Comparison of Empirical and Numerical Results

6.1. Abstract

Given the large number of parameters that can have an effect on critical windspeed, it became relevant to assess the effectiveness of individual parameters compared to others. This was done by comparing the strengths of bins with a range of values for a specific variable. From the empirical fragility functions, median windspeeds associated with specific damage states were compared. From the finite element models, critical windspeeds resulting in buckling were compared. The results showed that for real bins in the field, decreasing diameter and height had the greatest increase on median windspeed at failure. For the numerically modelled bins, the addition of stiffeners had the greatest benefit to critical windspeed. However, the numerical models did not account for imperfections in construction and the increases are expected to be exaggerated.

6.2. Comparison

In order to compare the effectiveness of individual parameters of grain bin construction, strengths of bins with a range of values for a specific variable were compared. This was done with both physical bins and numerical models. For certain parameters that were considered in both studies, the effectiveness of that parameter could then be compared across them both. From the empirical fragility functions, the windspeed used was that at which there is a 50% probability of exceeding the damage state. Critical windspeed of finite element models occurred at the first failure mechanism, which was typically wall buckling. Since wall buckling was considered “Minor Damage” in the empirical fragility analysis, exceedance of this damage state was deemed as failure for

the purpose of this comparison. Figure 6.1 depicts the changes in this windspeed for several variables considered in the empirical fragility analysis. Furthermore, since diameter was determined to be the most influential variable on probability of failure and highly correlated with other parameters, windspeed values were taken from the conditional fragility functions of bins with diameters restricted to 25 feet to 35 feet. The exception to this was when the effects of diameter itself and height were analyzed. From the finite element models, critical buckling windspeed was compared to determine effectiveness of individual parameters. Figure 6.2 depicts the changes in the critical windspeeds for several parameters considered in the numerical analysis. For these comparisons, the standard bin was used, with only the explicitly called out parameters varying over the range specified.

The results of the empirical fragility analysis showed that changing the surrounding terrain from open to trees and buildings had the smallest effect on median windspeed at failure. They showed that isolated bins had a moderate increase over grouped bins. Likewise, unvented bins had a moderate increase in median windspeed over vented bins. However, the addition of stiffeners and wind rings and decreasing diameter and height both had significant increases in median windspeed at failure. For the comparison of numerically modelled bins, corrugation length and stiffener thickness were shown to have little effect on critical buckling windspeed. The addition of two wind rings had a moderate increase on critical windspeed, with all other parameters held constant. Increasing wall thickness, unvented roofs, decreasing diameter, and decreasing height all have significant improvement on critical windspeed. However, the addition of stiffeners has more than double the impact as the second most relevant variable, height.

Comparing the results of the two different studies to each other gives insight into the actual effectiveness of each variable. First, not all variables were considered in both studies due to limitations of field reconnaissance and numerical modeling. The effects of grouping and surrounding terrain were not considered in the numerical analysis as they impact the wind pressures applied to the bin, rather than the bin itself. The effects of corrugation depth, wall thickness, and stiffener thickness were not considered in the empirical analysis as they could not be easily observed or recorded for a large number of bins. Figure 6.3 depicts a side-by-side comparison of the effects of parameters considered by both studies. The percent increases shown are those that correspond to the appropriate windspeed metric of the respective analysis as described above. Of the variables that both studies had in common, the effect of roof venting, decreasing diameter, and decreasing height had comparable effects. However, the effects were less pronounced in the empirical analysis in all three cases. This is likely due to the fact that, in the numerical analysis, wall thickness was uniform and did not increase with diameter or height as would be the case in physical specimens. For numerical models, wind rings were found to have a moderate increase on critical windspeed, while the effects of the fragility analysis showed a slightly higher percent increase. The largest discrepancy between the empirical and numerical analyses came from the comparison between the effects of stiffeners. In the numerical analysis, all parameters were kept constant except those explicitly called out. Therefore, when adding stiffeners to the unstiffened bin, the same wall thickness was used. However, in reality, this would not be the case. The unstiffened bin would have significantly thicker wall panels than a stiffened bin of the same dimensions. Additionally, the empirical data might be skewed by other confounding factors.

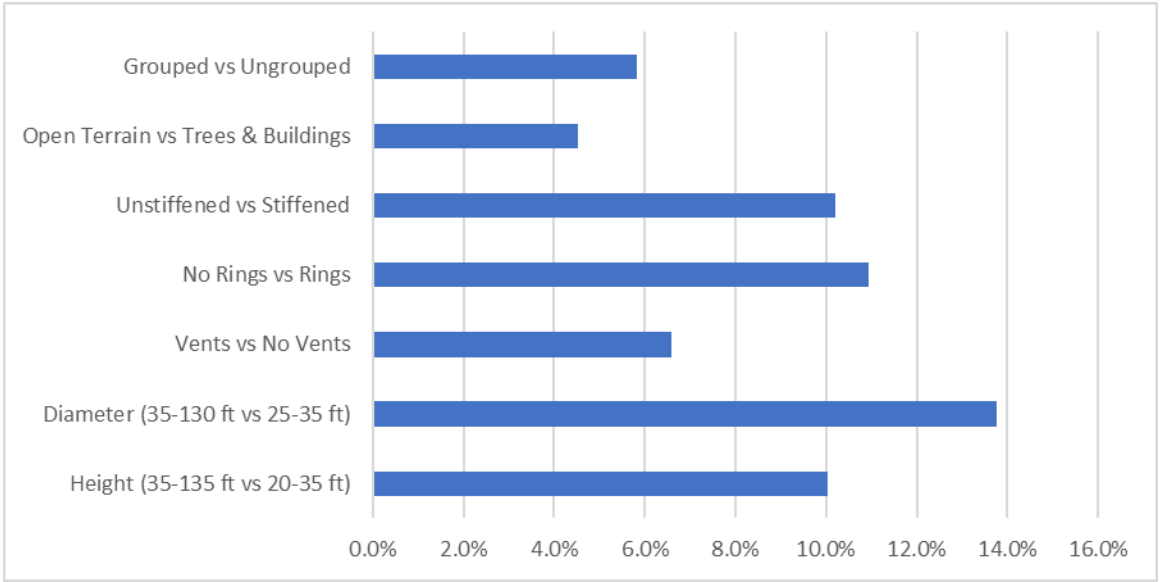


Fig. 6.1 Percent increase in windspeed at 50% rate of exceeding minor damage for condition B compared to condition A (A vs B)

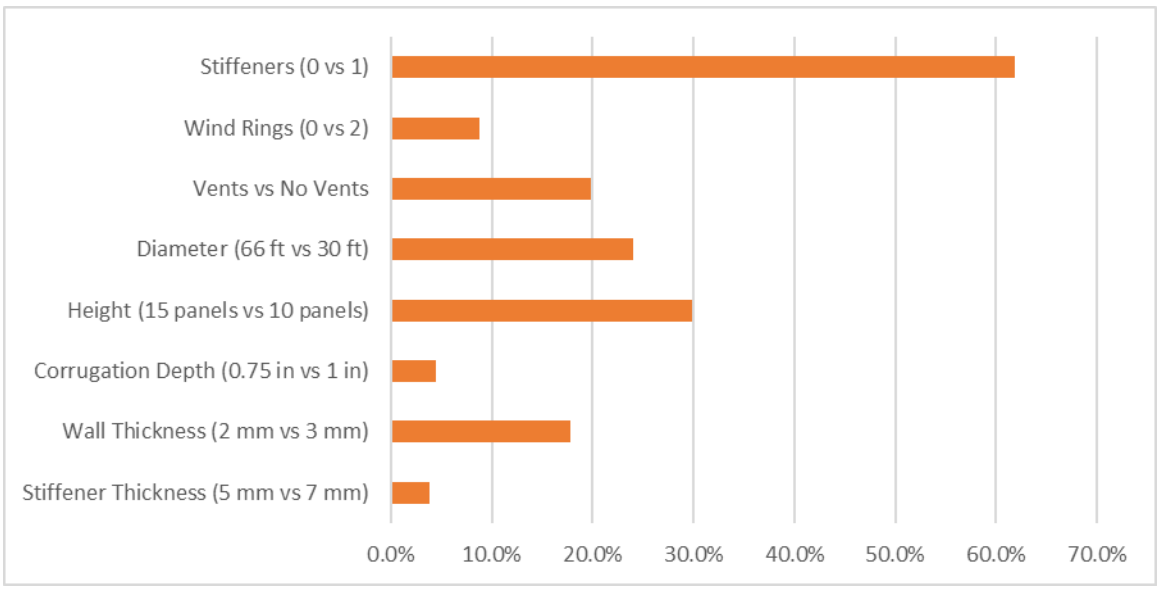


Fig. 6.2 Percent increase in windspeed at buckling for condition B compared to condition A (A vs B)

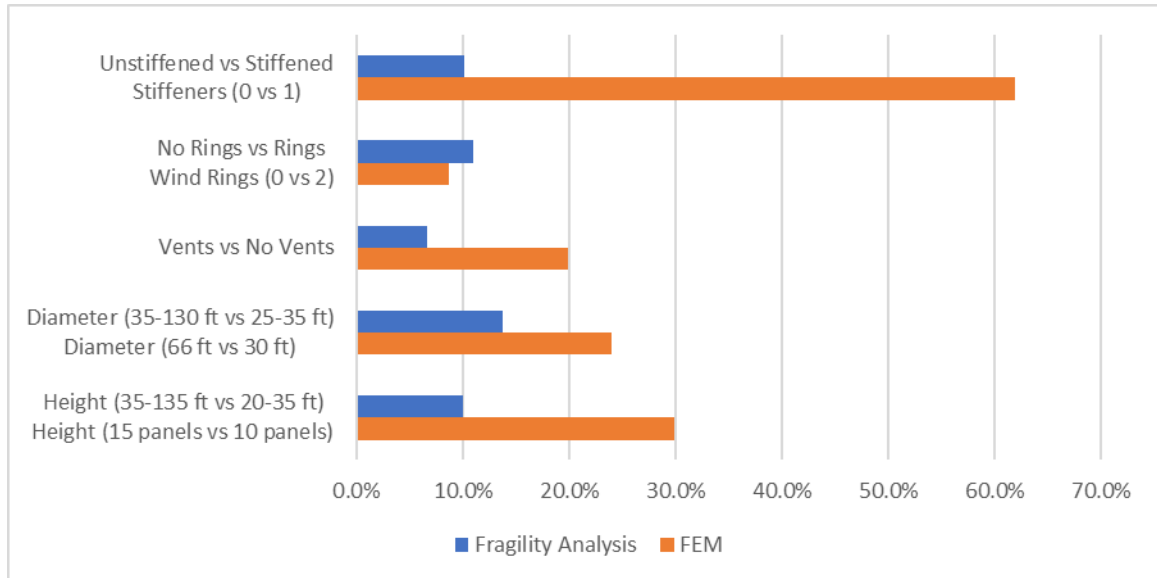


Fig. 6.3. Comparison of percent increase in windspeed at 50% rate of exceeding minor damage (Fragility Analysis) or buckling (FEM) for condition B compared to condition A (A vs B)

6.3. Conclusions

Comparing the results of both studies, they appear to generally agree on which parameters have the greatest effect on performance. However, since parameters in the empirical study are so highly correlated and interconnected, they are not as effective at determining the benefit of individual parameters. At the same time, the numerical analysis is better at determining these individual effects, but potentially unrealistic in the variations it makes. Despite this, the results of the two studies together show that decreasing diameter, decreasing height, having a roof that is unvented, and increasing wall thickness have the most significant increase on critical windspeed.

Chapter 7: Conclusions

7.1. Summary

While rural infrastructure is critical to the agricultural industry, it has been historically more susceptible to damage and slower to recover following natural disasters than its urban and suburban counterparts. Steel grain bins, a key component of rural infrastructure, which are used by farmers and co-ops to dry and store certain commodities, are among some of the most frequently damaged structures. They are particularly susceptible to damage in high wind events due to a number of factors, including: a lack of consistent design standards for wind loads, lightweight construction, high surface area, and complex structural responses.

The goal of this thesis is to enhance current understanding of the performance of steel grain bins in high wind events by development of empirical fragility functions and conducting a numerical parametric study. To accomplish this, a detailed literature review was conducted on wind pressure distribution, stresses, numerical modelling, and performance of grain bins. Field reconnaissance in the immediate aftermath of the August 10, 2020, derecho was used to develop a detailed map of maximum windspeeds over a study area. This data was then used to develop empirical fragility functions for a set of over 600 effected grain bins. In this way a probabilistic approach was taken to diminish structure-to-structure variation and help present a more realistic expectation of structural performance. Next, the finite element software LS-DYNA was used to perform a parametric numerical analysis of grain bin buckling strength to confirm and give quantitative support to the trends observed in the fragility analysis. Finally, the results of the fragility analysis were compared to the results of parametric numerical analysis.

7.2. Conclusions

From the events of the August 10, 2020, derecho, windspeed data was used to develop a windspeed map to interpolate the maximum windspeed at the locations of over 600 steel grain bins. These maximum windspeeds, along with field reconnaissance, were then used to perform a fragility analysis of the grain bins in high winds. This fragility analysis revealed several trends in susceptibility in high winds, some of which were counterintuitive. Through an investigation of correlation between characteristics and creating fragility functions of conditional parameters, it was determined that all counterintuitive results could be explained by having a higher correlation with large diameter bins, which had the most influence on median windspeed at failure. Additionally, surrounding terrain was found to have a large influence as well but was determined to have little to no correlation with other characteristics. From the parametric finite element analysis, the effects of several variables were determined. Diameter and height had a strong inverse relationship with critical wind pressure. The number of stiffeners per panel and number of wind rings were shown to have a direct relationship with critical wind pressure that had diminishing returns within the ranges considered. Effects of correlation length were negligible. However, corrugation depth was found to have significant effect, but with an optimum for unstiffened bins. Stiffened bins continued to increase critical wind pressure with corrugation depth, but with significant diminishing returns. Additionally, stiffener thickness had little effect, while wall thickness had direct and fairly linear relationship with critical wind pressure over the ranges considered. In the comparison of effectiveness of various parameters between the two analyses, the fragility analysis showed that decreasing height and diameter had the

greatest increase on median windspeed of failure. The results of the finite element analysis agreed with this. However, it also showed a significant increase in critical windspeed with the closing of roof vents and increase of wall thickness. The fragility analysis showed only moderate contributions from unvented roofs and was unable to consider wall thickness. Therefore, the parameters of diameter, height, wall thickness, presence of stiffeners, number of wind rings, and roof venting have the greatest potential for increasing resistance to wind loads.

7.3. Recommendations

Based on the results of this thesis, some recommendations can be made to the owners, designers, and constructors of steel grain bins. First, the simplest way to decrease susceptibility to damage in high winds is to construct grain bins in locations that are sheltered by structures or trees of similar height. From a structural perspective, increasing number of stiffeners, increasing wall thickness, decreasing bin height, and decreasing bin diameter all improve performance under wind loads but with significant financial costs. More economical solutions are increasing the number and robustness of wind rings and increasing corrugation depth of stiffened bins. Closing roof vents showed significant increase in performance of numerical models, but much more limited benefits in the field.

7.4. Future Work

Although this thesis considered a broader set of parameters than previous studies and combined the results of empirical fragility functions with numerical modelling, there are several topics that require further investigation to better evaluate and increase the

performance of steel grain bins in high wind conditions. To this end, a few recommendations are suggested as a basis for future studies:

- Conduct further research on the effects of stiffeners, wind rings, and roof eaves on wind pressure distribution and use this information to update numerical models.
- Evaluate the performance of grain bins considering tornadic wind loads.
- Develop finer modelling of roof construction, roof to wall connections, and anchorage.
- Systematically vary wall panel and stiffener thickness in numerical modelling.
- Model grain bin behavior beyond first buckling, potentially with more complex material models.
- Conduct full scale testing to compare pressure coefficients from wind tunnel testing and to investigate failure in a controlled setting.

References

- Abdel-Sayed, G. et al. (1985). Cold-formed steel farm structures. Part I: Grain Bins. *Journal of Structural Engineering* (New York, N.Y.), 111(10), 2065–2089.
- Briassoulis, D., & Pecknold, D. A. (1986a). Anchorage requirements for wind-loaded empty silos. *Journal of Structural Engineering*, 112(2), 308-325.
- Briassoulis, D., & Pecknold, D. A. (1986b). Behaviour of empty steel grain silos under wind loading: part 1: the stiffened cylindrical shell. *Engineering Structures*, 8(4), 260-275.
- Briassoulis, D., & Pecknold, D. A. (1988). Behaviour of empty steel grain silos under wind loading: part 2: the stiffened conical roof shell. *Engineering Structures*, 10(1), 57-64.
- Briassoulis, D. (1992). Integrated physical model for cylindrical shells. *Journal of Structural Engineering*, 118(8), 2168-2185.
- Brito, L., and Wittich, C. (2019). Performance of Steel Grain Silos and Rural Communities to Windstorms. *Structures Congress 2019. Damage Assessment Toolkit*. ArcGIS web application. (n.d.). Retrieved February 17, 2022, from <https://apps.dat.noaa.gov/stormdamage/damageviewer/>
- EN 1991-1-4, Eurocode 1: Actions on Structures—Part 1–4: General Actions—Wind Actions, (2005).
- EN 1993-1-6, Eurocode 3: Design of Steel Structures -Part 1–6: Strength and Stability of Shell Structures, CEN, Brussels, 2007.
- Environment Canada (2014). Enhanced Fujita Scale. Retrieved November 4, 2022, from <https://www.canada.ca/en/environment-climate-change/services/seasonal->

weather-hazards/publications/enhanced-fujita-scale-damage-indicators/chapter-30.html#shr-pg0

- Godoy, L. A., & Flores, F. G. (2002). Imperfection sensitivity to elastic buckling of wind loaded open cylindrical tanks. *Structural Engineering and Mechanics*, 13(5), 533-542.
- Iwicki, P. et al. (2015). Stability of cylindrical steel silos composed of corrugated sheets and columns based on FE analyses versus Eurocode 3 approach. *Engineering Failure Analysis*, 57, 444-469.
- Kebeli, H. V. et al. (2001a). Wind pressure coefficients of conical roofs on grain bins. AAWE Americas Conference on Wind Engineering – 2001.
- Kebeli, H. V. et al. (2001b). Wind tunnel tests to establish pressure coefficients for grain bins. Paper No. 01-4017. ASAE, St. Joseph, MI.
- Kebeli, H. V. (2002). Determining pressure coefficients due to wind loading on grain bins. University of Florida.
- Kikitsu, H., & Sarkar, P. P. (2015). Building damage, wind speed estimation, and post disaster recovery in an EF5 Tornado. *Natural Hazards Review*, 16(2), 04014019.
- Loken, A. et al. (2020). Digital reconnaissance and performance assessment of rural infrastructure for 2018 natural hazards. *Journal of performance of constructed facilities*, 34(4), 04020054.
- Macdonald, P. A. et al. (1988). Wind loads on circular storage bins, silos and tanks: I. Point pressure measurements on isolated structures. *Journal of Wind Engineering and Industrial Aerodynamics*, 31(2-3), 165-187.

- Macdonald, P. A. et al. (1990a). Wind loads on circular storage bins, silos and tanks. II. Effect of grouping. *Journal of Wind Engineering and Industrial Aerodynamics*, 34(1), 77-95.
- Macdonald, P. A. et al. (1990b). Wind loads on circular storage bins, silos and tanks III. Fluctuating and peak pressure distributions. *Journal of Wind Engineering and Industrial Aerodynamics*, 34(3), 319-337.
- Maleki, S., & Mehrehtehran, A. M. (2018). 3D wind buckling analysis of long steel corrugated silos with vertical stiffeners. *Engineering Failure Analysis*, 90, 156-167.
- Maleki, S., & Mehrehtehran, A. M. (2019). 3D wind buckling analysis of steel silos with stepped walls. *Thin-Walled Structures*, 142, 236-261.
- McDonald, J. R. et al. (2006). "A recommendation for an enhanced Fujita scale (EF-Scale)." In *Report to the National Weather Service, Revision 2, wind science and engineering center*.
- National Oceanic and Atmospheric Administration (NOAA) (2022). Damage Assessment Toolkit. <https://apps.dat.noaa.gov/stormdamage/damageviewer/>
- NOAA National Centers for Environmental Information (NCEI) (2022). U.S. Billion-Dollar Weather and Climate Disasters. <https://www.ncdc.noaa.gov/billions/>
- NOAA National Weather Service (NWS) (2021). August 10, 2020, Midwest derecho. *ArcGIS StoryMaps*. Retrieved January 31, 2022, from <https://storymaps.arcgis.com/stories/f98352e2153b4865b99ba53b86021b65>
- Pecknold, D. A. (1989). Load transfer mechanisms in wind-loaded cylinders. *Journal of engineering mechanics*, 115(11), 2353-2367.

- Pecknold, D. A., & Rahman, S. (1990). Ovaling of ring-stiffened cylindrical shells. *Journal of engineering mechanics*, 116(12), 2681-2701.
- Portela, G., & Godoy, L. A. (2005a). Wind pressures and buckling of cylindrical steel tanks with a conical roof. *Journal of Constructional Steel Research*, 61(6), 786-807.
- Portela, G., & Godoy, L. A. (2005b). Wind pressures and buckling of cylindrical steel tanks with a dome roof. *Journal of Constructional Steel Research*, 61(6), 808-824.
- Raeesi, A. et al. (2017). Failure analysis of steel silos subject to wind load. *Engineering Failure Analysis*, 79, 749-761.
- Shouse, S. et al. (2021). Derecho Emphasizes Engineers' Role in Agricultural Structure Design. *Resource Magazine*, 28(4), 4-7.
- Troulis, E. and Wittich, C.E. (2022). Functionality recovery of steel grain bins in rural communities following the August 2020 Iowa Derecho. *Proceedings of the 3rd International Conference on Natural Hazards & Infrastructure*. Athens, Greece, July 5-7.
- U.S. Census Bureau (2016). New Census Data Show Difference Between Urban and Rural Populations, *Census Newsroom*. Retrieved from <https://census.gov>
- Vasios, N. (2015). Nonlinear Analysis of Structures; The Arc Length Method: Formulation, Implementation and Applications.
- Zeybek, Ö. et al. (2019). Stress resultants for wind girders in open-top cylindrical steel tanks. *Engineering Structures*, 196, 109347.

Appendix A: Empirical Fragility Functions

Appendix A contains all the relevant fragility functions calculated in this thesis. All fragility functions appear twice, once depicted in the traditional way, with all successive damage states for a specific set on a single plot. They appear a second time in a comparison of consistent damage states between different sets. Even though the full set of grain bins contained over 600 specimens, some subsets contained too few specimens to build meaningful fragility functions. These curves have been removed from the plots.

List of Figures

Fig. A.1 Full Set.....	104
Fig. A.2 Grouped	104
Fig. A.3 Ungrouped	105
Fig. A.4 Grouped-Ungrouped, Minor.....	105
Fig. A.5 Grouped-Ungrouped, Major	106
Fig. A.6 Grouped-Ungrouped, Severe	106
Fig. A.7 Behind Other Bins	107
Fig. A.8 Exposed Bins	107
Fig. A.9 Behind Other Bins, Minor	108
Fig. A.10 Behind Other Bins, Major.....	108
Fig. A.11 Behind Other Bins, Severe	109
Fig. A.12 Manufacturer 1.....	109
Fig. A.13 Manufacturer 2.....	110
Fig. A.14 Manufacturer 3.....	110

Fig. A.15 Manufacturer 4.....	111
Fig. A.16 Manufacturer, Minor.....	111
Fig. A.17 Manufacturer, Major.....	112
Fig. A.18 Manufacturer, Severe.....	112
Fig. A.19 Condition-Poor	113
Fig. A.20 Condition-Good	113
Fig. A.21 Condition-New	114
Fig. A.22 Condition, Minor	114
Fig. A.23 Condition, Major.....	115
Fig. A.24 Condition, Severe	115
Fig. A.25 Diameter [0,25] ft	116
Fig. A.26 Diameter (25,35] ft	116
Fig. A.27 Diameter (35,130] ft	117
Fig. A.28 Diameter, Minor	117
Fig. A.29 Diameter, Major.....	118
Fig. A.30 Diameter, Severe.....	118
Fig. A.31 Height [0,20] ft	119
Fig. A.32 Height (20,35] ft	119
Fig. A.33 Height (35,135] ft	120
Fig. A.34 Height, Minor	120
Fig. A.35 Height, Major.....	121
Fig. A.36 Height, Severe.....	121
Fig. A.37 Aspect Ratio [0,0.75].....	122

Fig. A.38 Aspect Ratio (0.75,1.0].....	122
Fig. A.39 Aspect Ratio, Minor.....	123
Fig. A.40 Aspect Ratio, Major.....	123
Fig. A.41 Aspect Ratio, Severe.....	124
Fig. A.42 Stiffened.....	124
Fig. A.43 Unstiffened	125
Fig. A.44 Stiffened-Unstiffened, Minor	125
Fig. A.45 Stiffened-Unstiffened, Major.....	126
Fig. A.46 Stiffened-Unstiffened, Severe.....	126
Fig. A.47 Wind Rings	127
Fig. A.48 No Wind Rings	127
Fig. A.49 Wind Rings, Minor	128
Fig. A.50 Wind Rings, Major	128
Fig. A.51 Wind Rings, Severe	129
Fig. A.52 Terrain-Open.....	129
Fig. A.53 Terrain-Trees & Buildings.....	130
Fig. A.54 Terrain-In Town.....	130
Fig. A.55 Terrain-Grain Bins.....	131
Fig. A.56 Terrain, Minor.....	131
Fig. A.57 Terrain, Major.....	132
Fig. A.58 Terrain, Severe.....	132
Fig. A.59 Distance to Obstruction [0,50] ft	133
Fig. A.60 Distance to Obstruction (50,150] ft	133

Fig. A.61 Distance to Obstruction (150,1000] ft	134
Fig. A.62 Distance to Obstruction, Minor	134
Fig. A.63 Distance to Obstruction, Major.....	135
Fig. A.64 Distance to Obstruction, Severe	135
Fig. A.65 Prominence [-20,-4] ft	136
Fig. A.66 Prominence (-4,4] ft.....	136
Fig. A.67 Prominence (4,30] ft.....	137
Fig. A.68 Prominence, Minor	137
Fig. A.69 Prominence, Major	138
Fig. A.70 Prominence, Severe	138
Fig. A.71 Slope [-0.07,-0.004].....	139
Fig. A.72 Slope (-0.004,0.004]	139
Fig. A.73 Slope (0.004,0.04].....	140
Fig. A.74 Slope, Minor	140
Fig. A.75 Slope, Major	141
Fig. A.76 Slope, Severe	141
Fig. A.77 Diameter (25,35] ft and Grouped.....	142
Fig. A.78 Diameter (25,35] ft and Ungrouped.....	142
Fig. A.79 Diameter (25,35] ft and Grouped-Ungrouped, Minor	143
Fig. A.80 Diameter (25,35] ft and Grouped-Ungrouped, Major	143
Fig. A.81 Diameter (25,35] ft and Grouped-Ungrouped, Severe	144
Fig. A.82 Diameter [0,25] ft and Condition-Poor.....	144
Fig. A.83 Diameter [0,25] ft and Condition-Good	145

Fig. A.84 Diameter (25,35] ft and Condition-Poor.....	145
Fig. A.85 Diameter (25,35] ft and Condition-Good	146
Fig. A.86 Diameter (35,135] ft and Condition-Good	146
Fig. A.87 Diameter (35,135] ft and Condition-New.....	147
Fig. A.88 Diameter and Condition, Minor.....	147
Fig. A.89 Diameter and Condition, Major	148
Fig. A.90 Diameter and Condition, Severe.....	148
Fig. A.91 Diameter (30,45] ft and Stiffened.....	149
Fig. A.92 Diameter (30,45] ft and Unstiffened.....	149
Fig. A.93 Diameter (30,45] ft and Stiffened-Unstiffened, Minor.....	150
Fig. A.94 Diameter (30,45] ft and Stiffened-Unstiffened, Major	150
Fig. A.95 Diameter (30,45] ft and Stiffened-Unstiffened, Severe.....	151
Fig. A.96 Diameter (30,45] ft and Wind Rings	151
Fig. A.97 Diameter (30,45] ft and No Wind Rings	152
Fig. A.98 Diameter (30,45] ft and Wind Rings, Minor	152
Fig. A.99 Diameter (30,45] ft and Wind Rings, Major.....	153
Fig. A.100 Diameter (30,45] ft and Wind Rings, Severe	153
Fig. A.101 Diameter [0,25] ft and Terrain-Open.....	154
Fig. A.102 Diameter [0,25] ft and Terrain-Trees & Buildings.....	154
Fig. A.103 Diameter [0,25] ft and Terrain-In Town.....	155
Fig. A.104 Diameter (25,35] ft and Terrain-Open.....	155
Fig. A.105 Diameter (25,35] ft and Terrain-Trees & Buildings.....	156
Fig. A.106 Diameter (35,130] ft and Terrain-Open.....	156

Fig. A.107 Diameter (35,130] ft and Terrain-Trees & Buildings.....	157
Fig. A.108 Diameter (35,130] ft and Terrain-In Town.....	157
Fig. A.109 Diameter and Terrain, Minor.....	158
Fig. A.110 Diameter and Terrain, Major.....	159
Fig. A.111 Diameter and Terrain, Severe.....	160

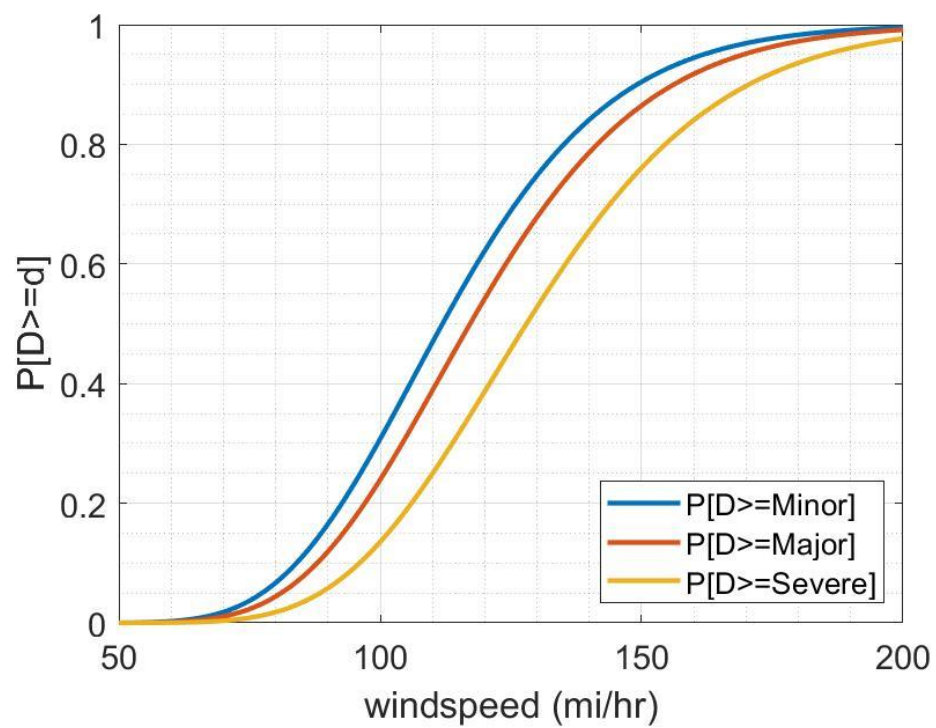


Fig. A.1 Full Set

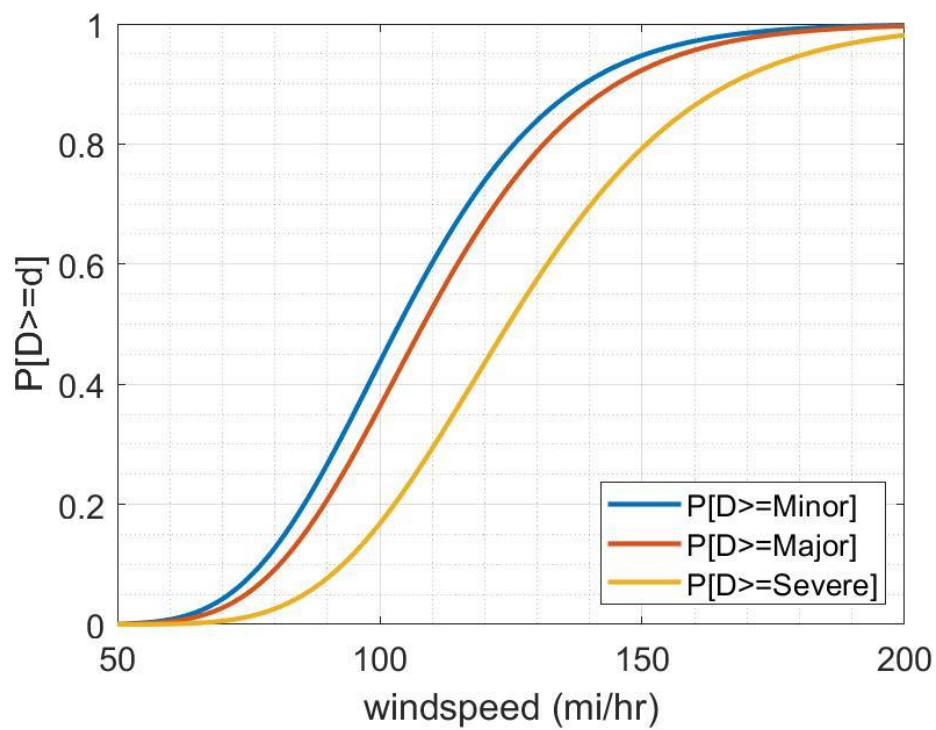


Fig. A.2 Grouped

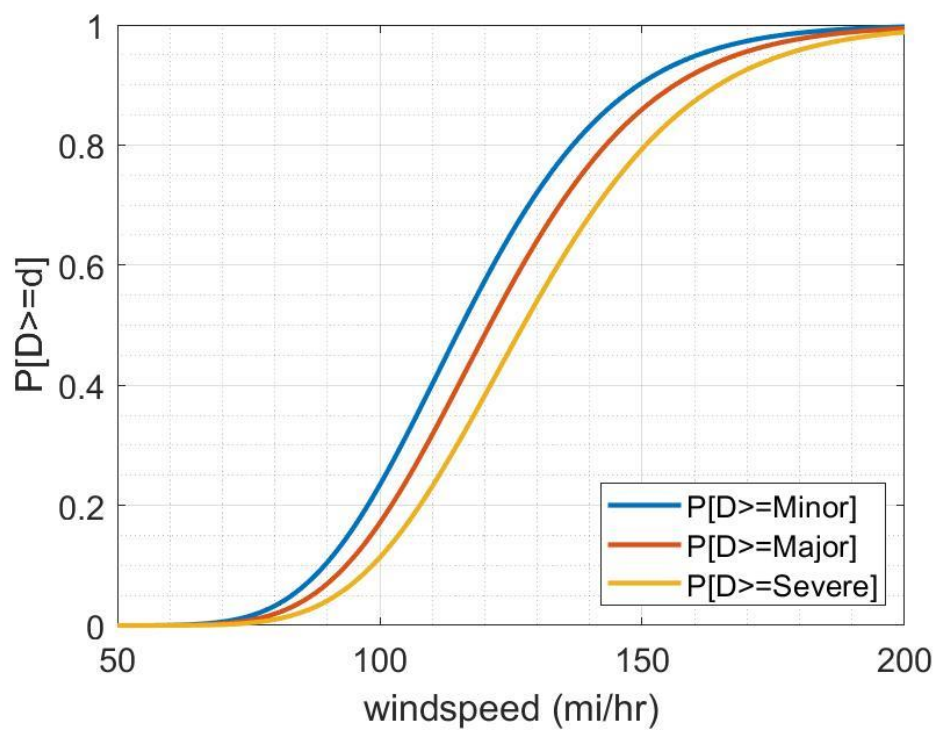


Fig. A.3 Ungrouped

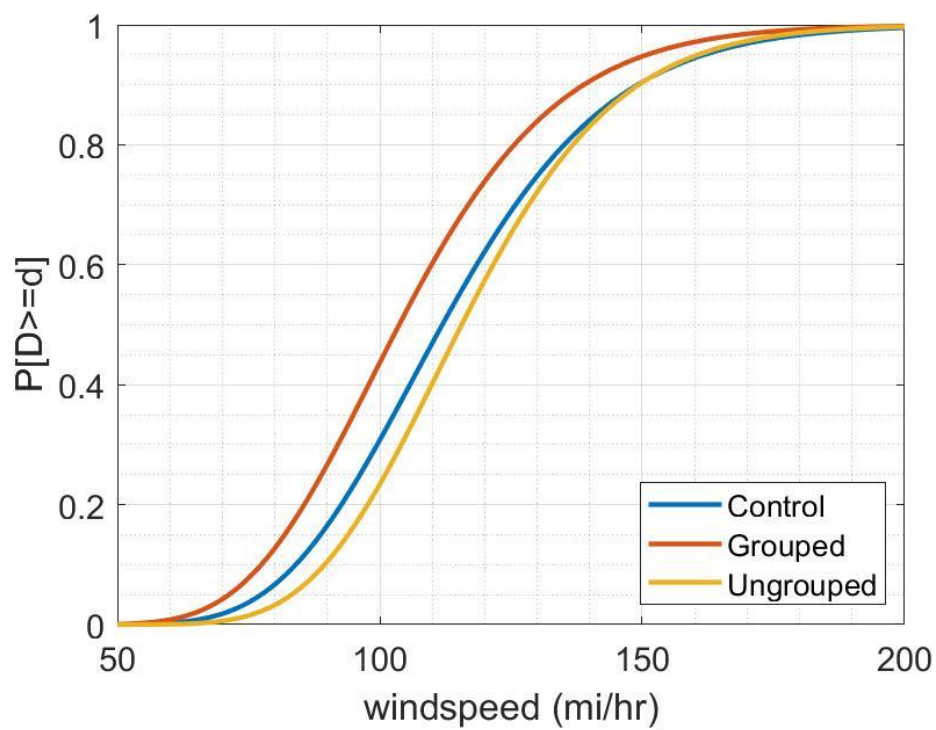


Fig. A.4 Grouped-Ungrouped, Minor

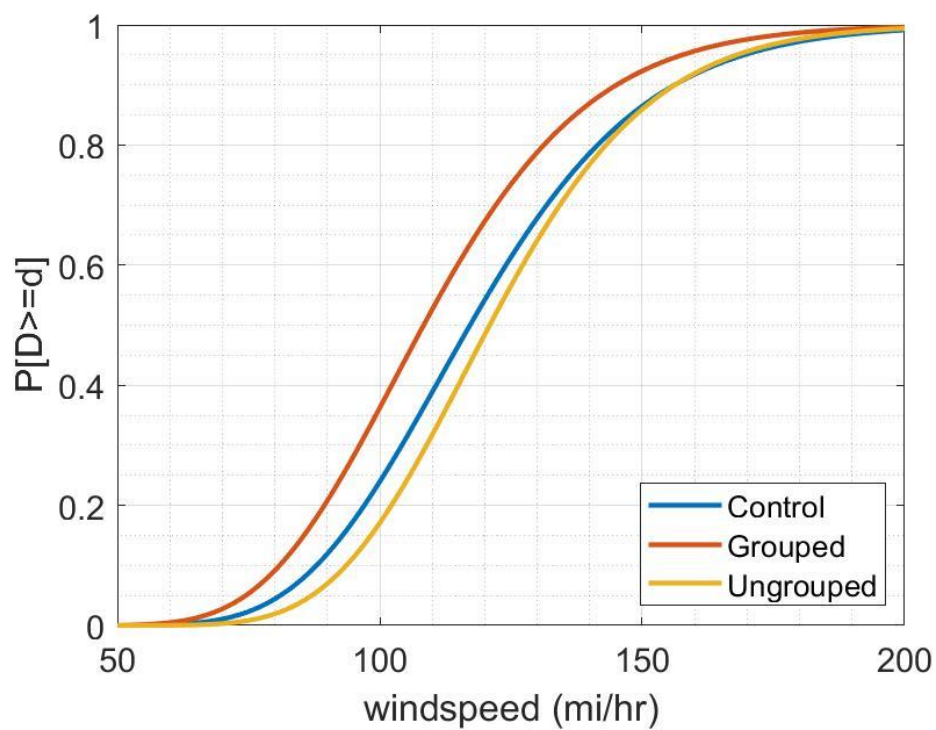


Fig. A.5 Grouped-Ungrouped, Major

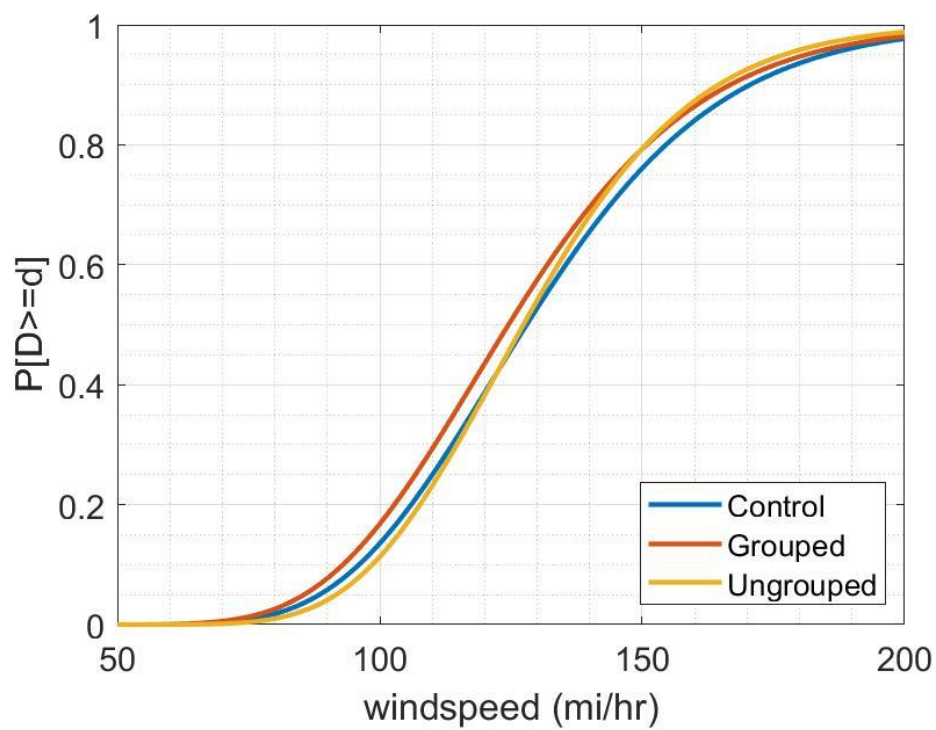


Fig. A.6 Grouped-Ungrouped, Severe

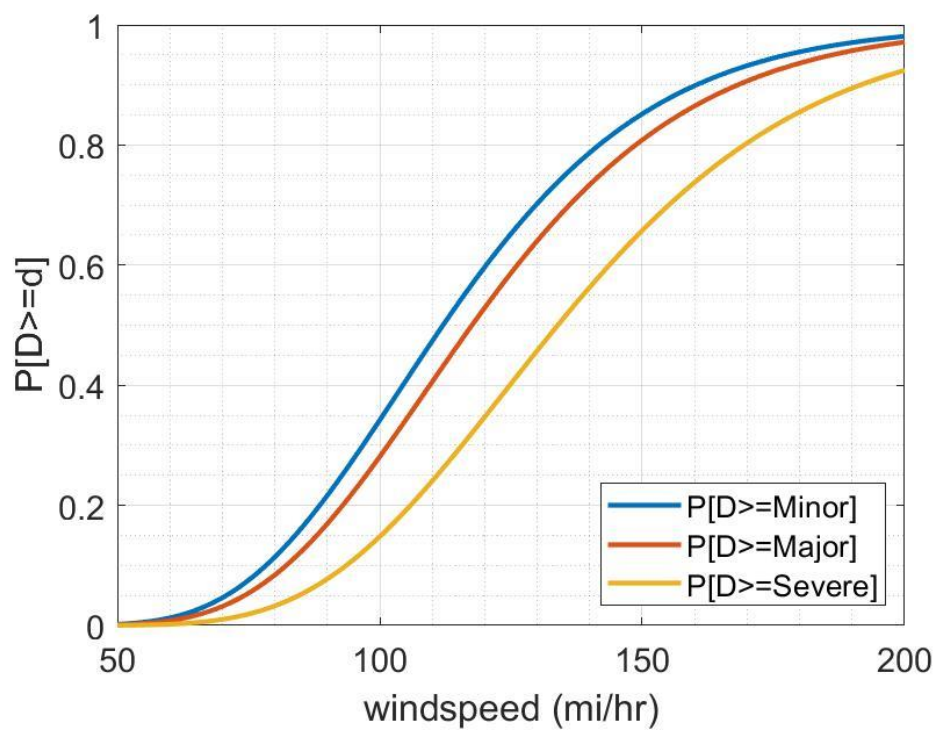


Fig. A.7 Behind Other Bins

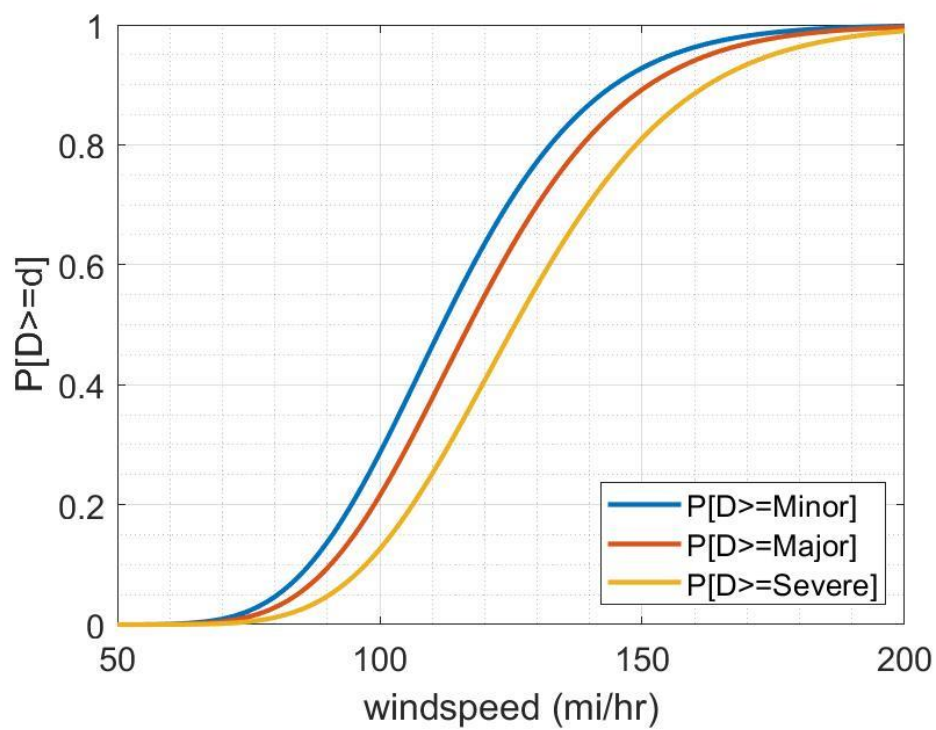


Fig. A.8 Exposed Bins

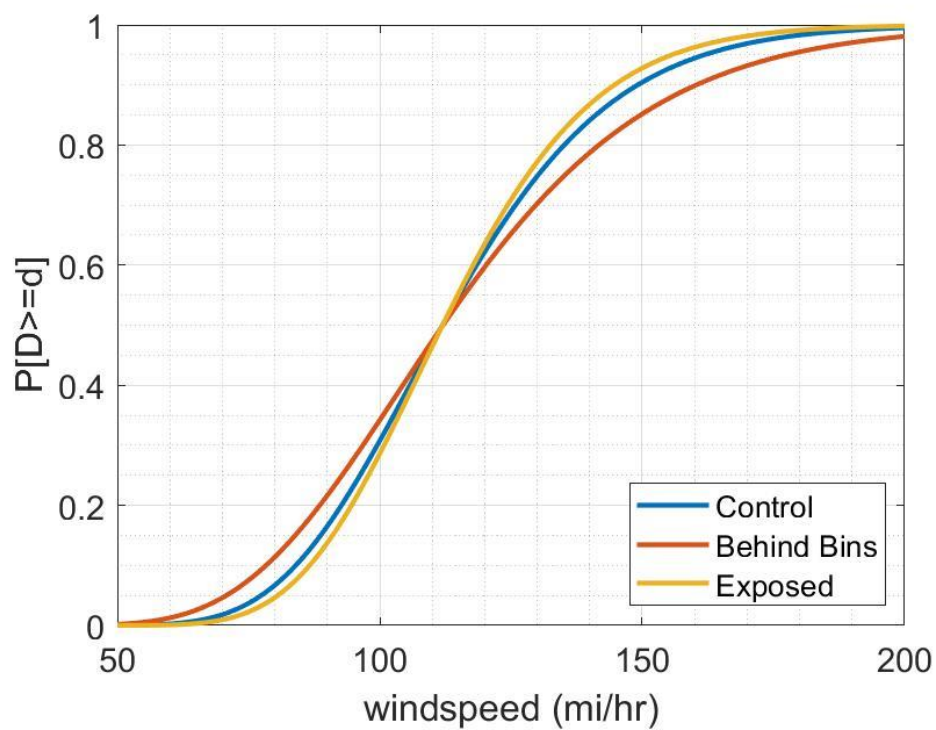


Fig. A.9 Behind Other Bins, Minor

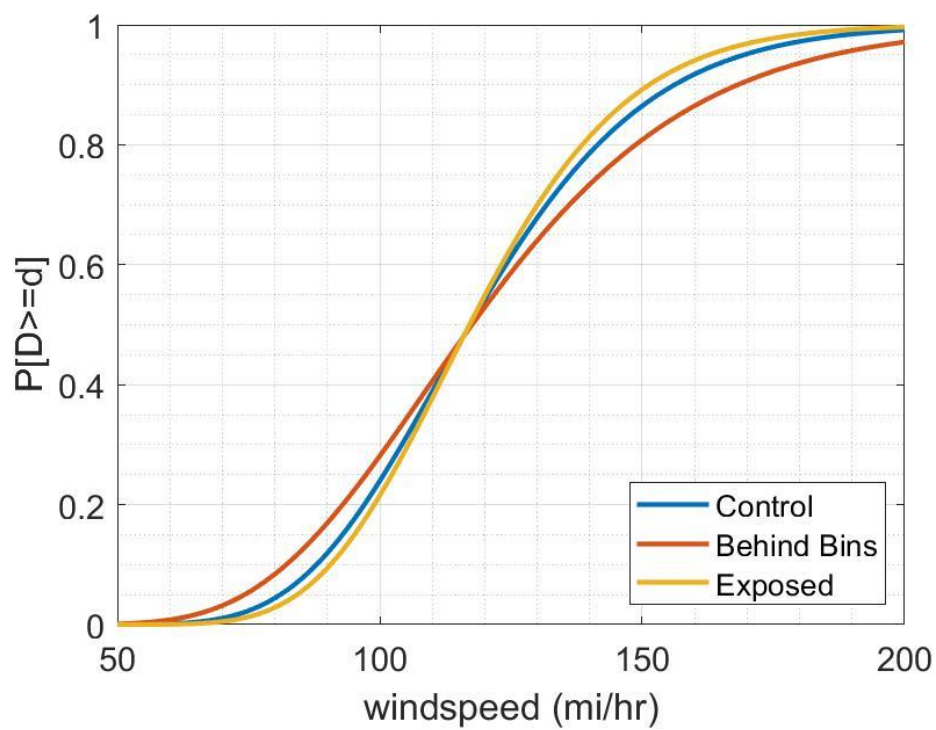


Fig. A.10 Behind Other Bins, Major

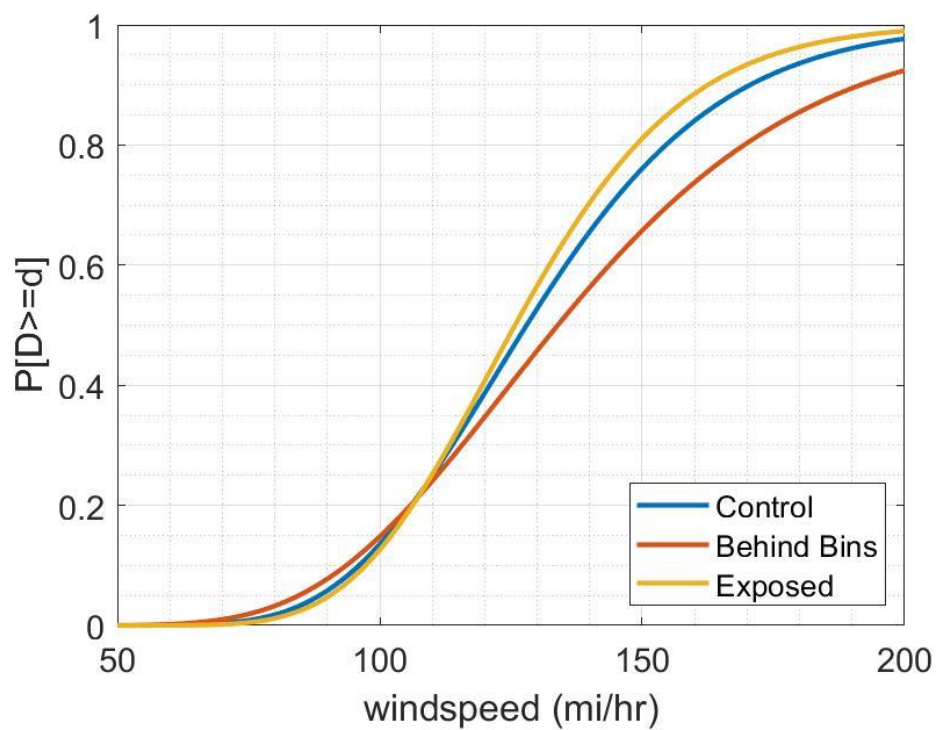


Fig. A.11 Behind Other Bins, Severe

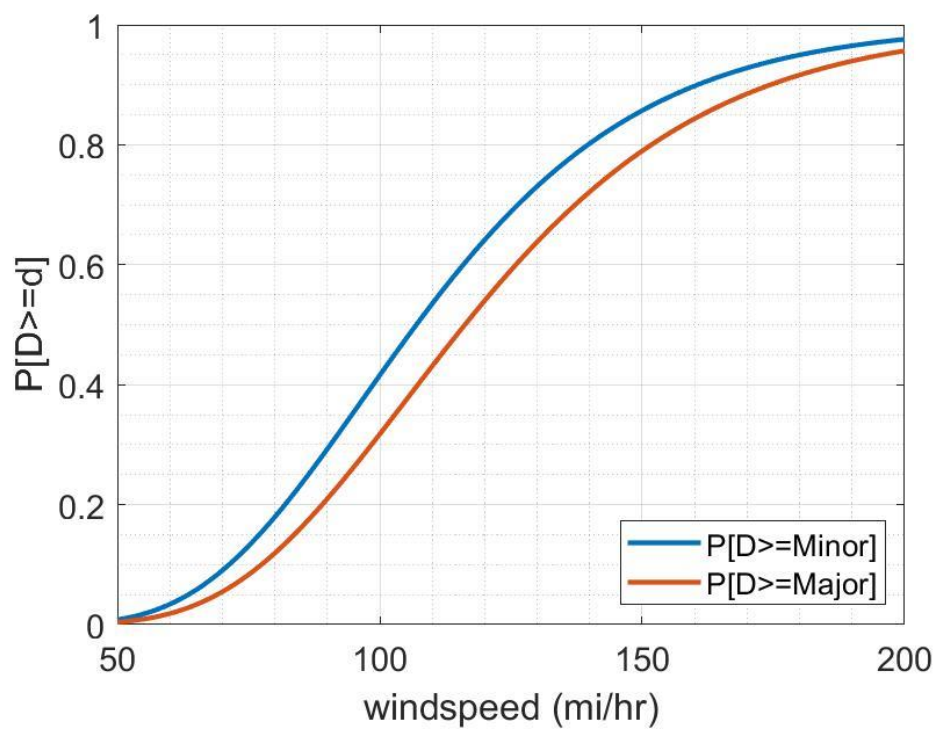


Fig. A.12 Manufacturer 1

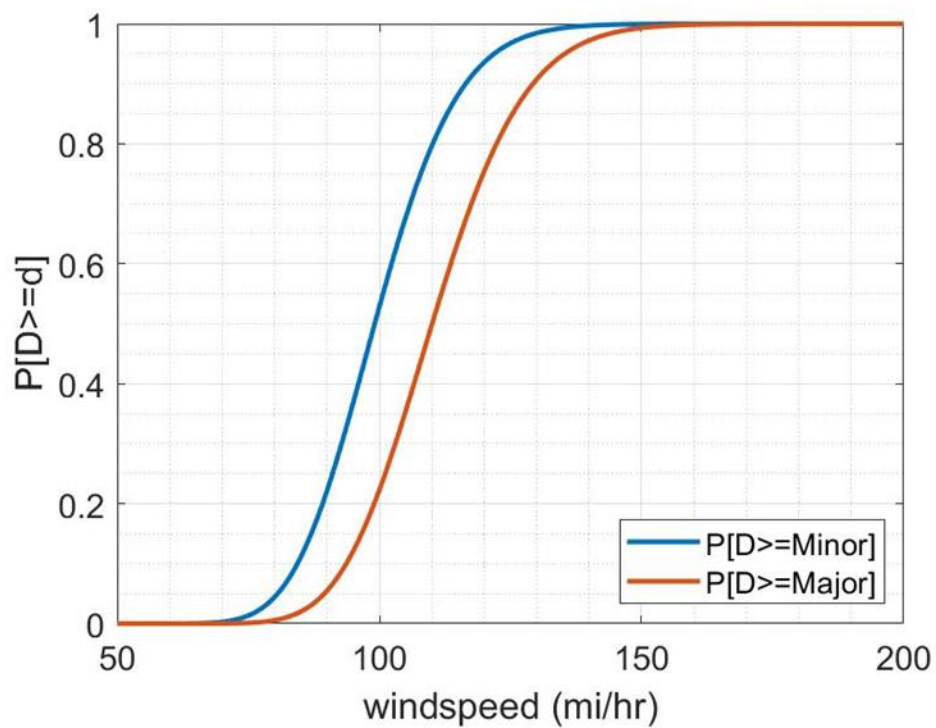


Fig. A.13 Manufacturer 2

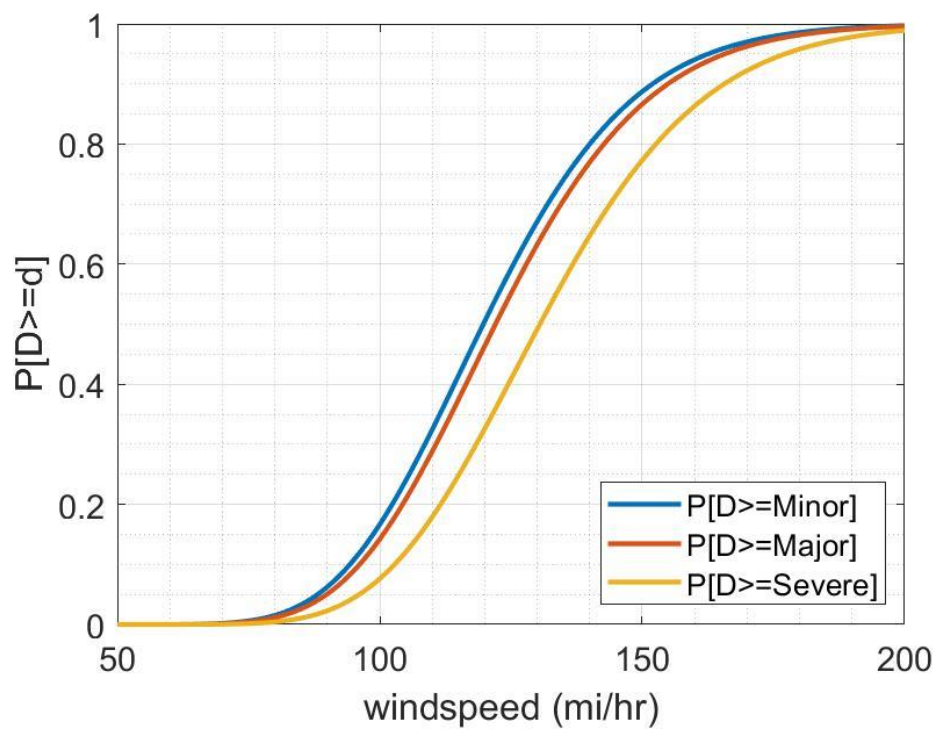


Fig. A.14 Manufacturer 3

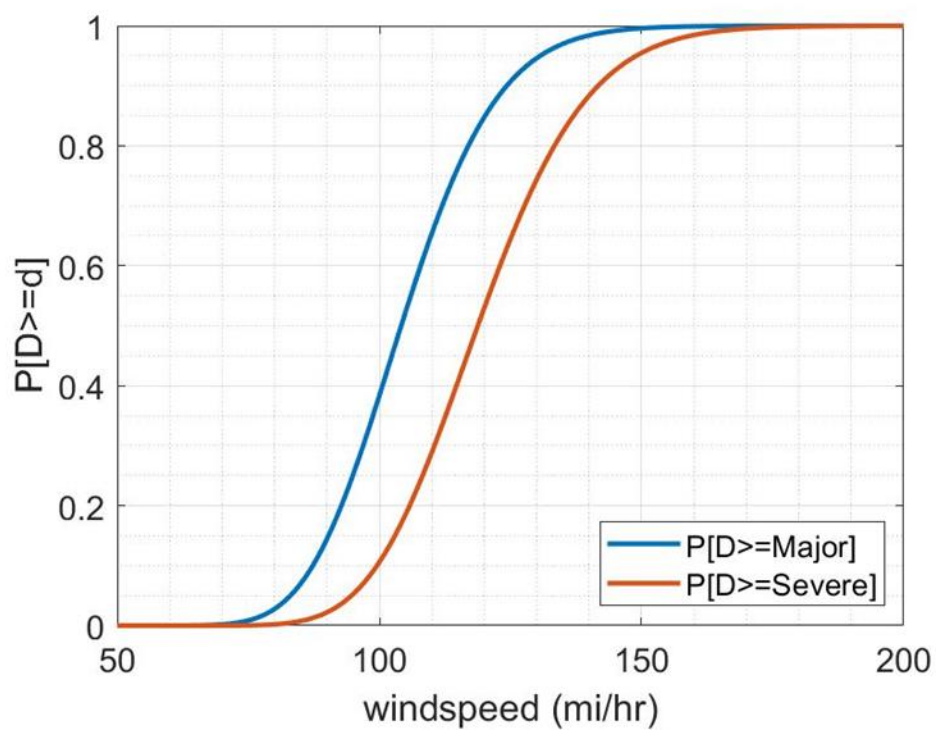


Fig. A.15 Manufacturer 4

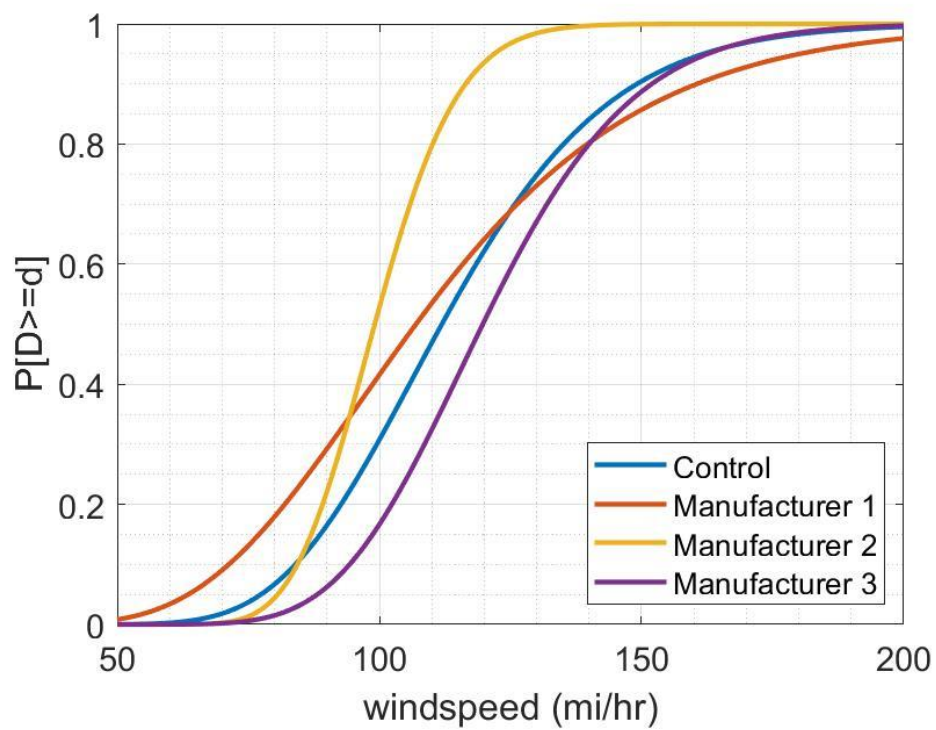


Fig. A.16 Manufacturer, Minor

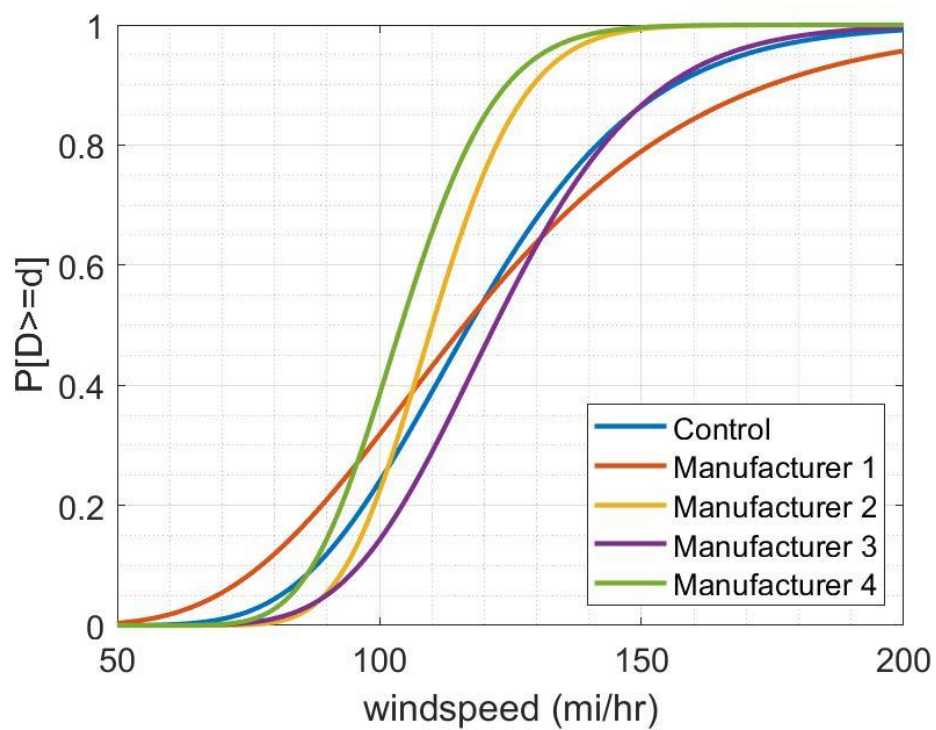


Fig. A.17 Manufacturer, Major

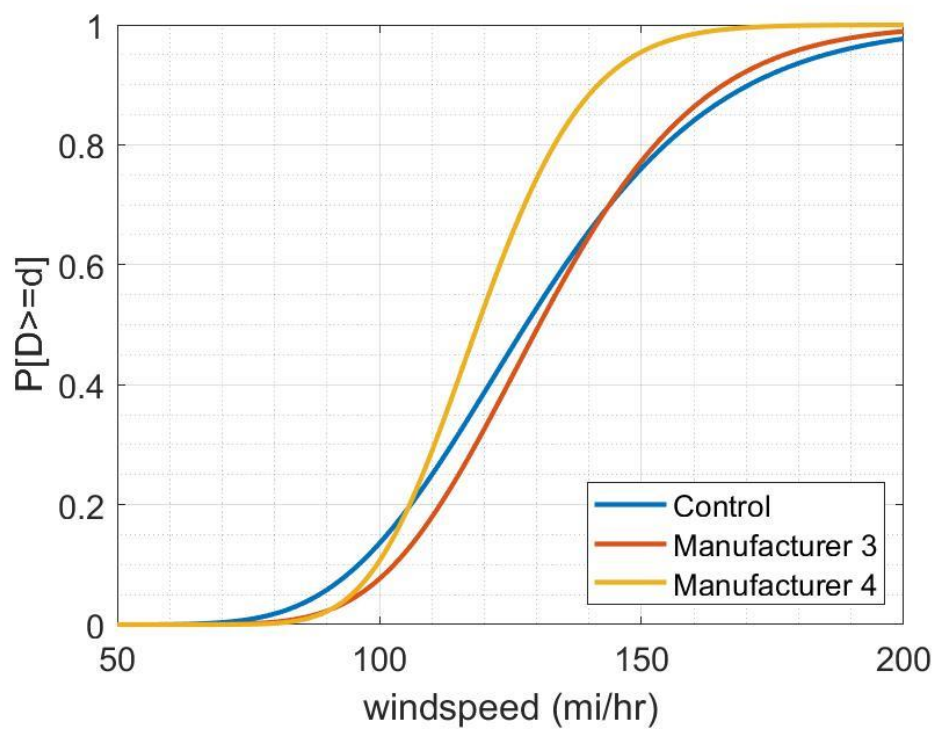


Fig. A.18 Manufacturer, Severe

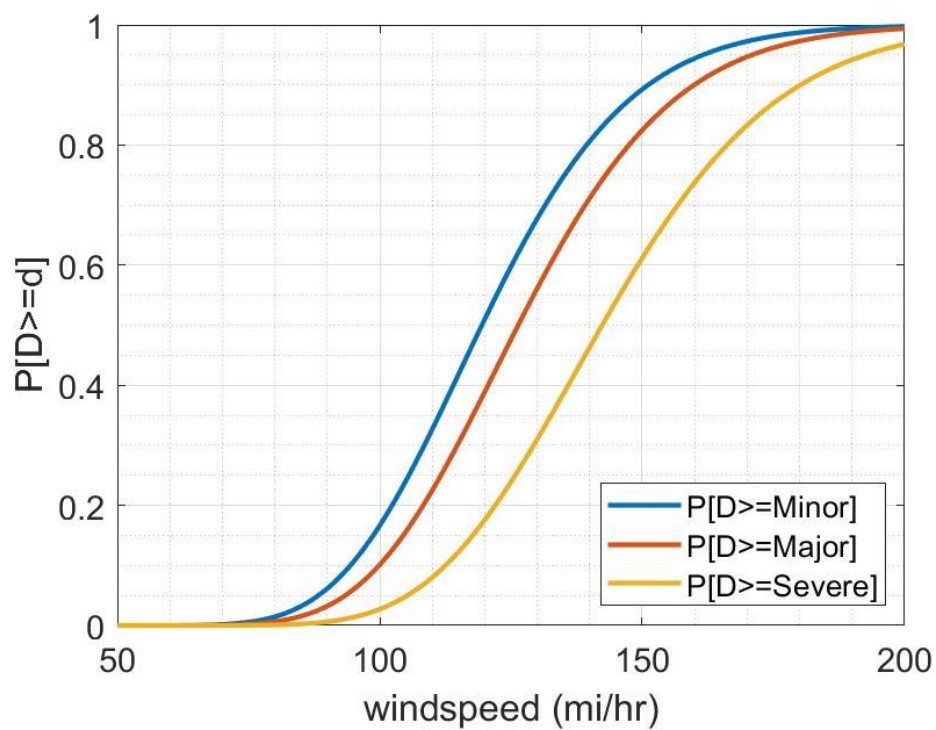


Fig. A.19 Condition-Poor

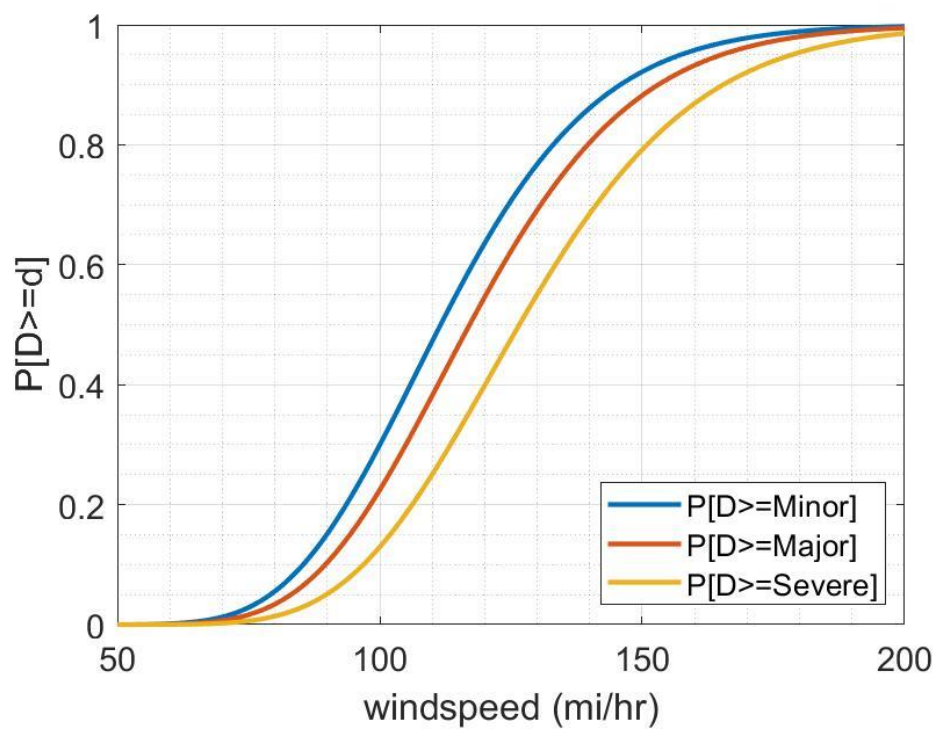


Fig. A.20 Condition-Good

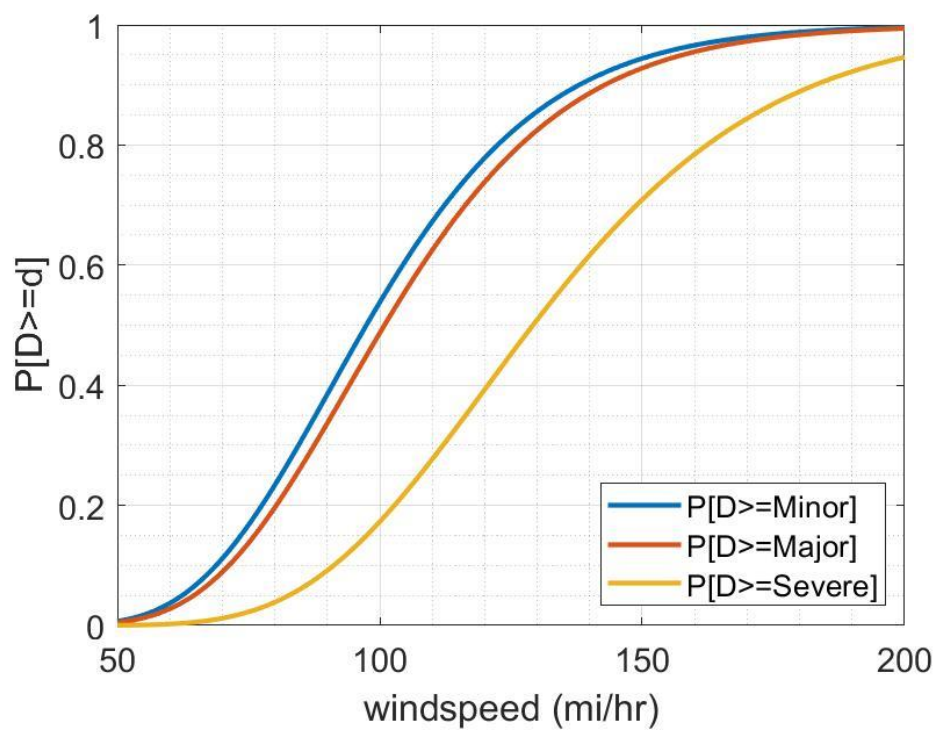


Fig. A.21 Condition-New

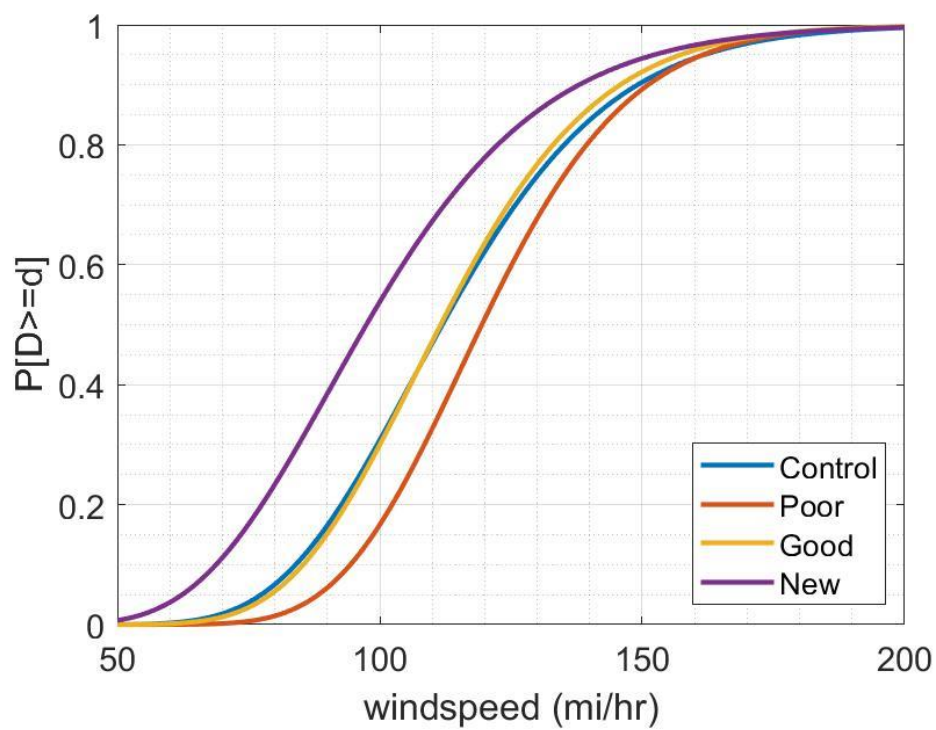


Fig. A.22 Condition, Minor

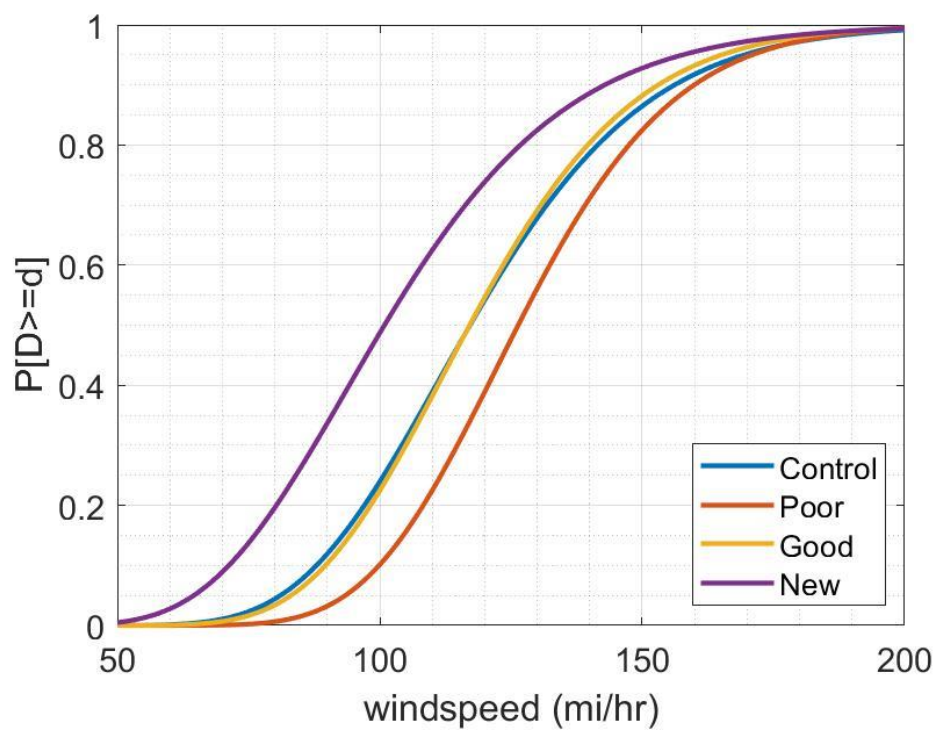


Fig. A.23 Condition, Major

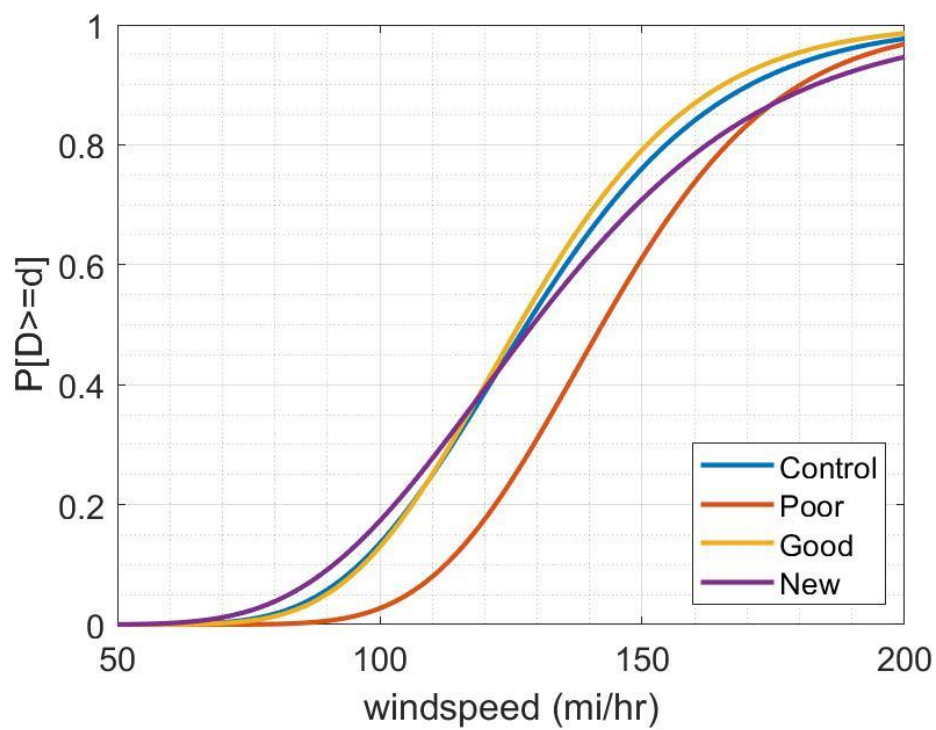


Fig. A.24 Condition, Severe

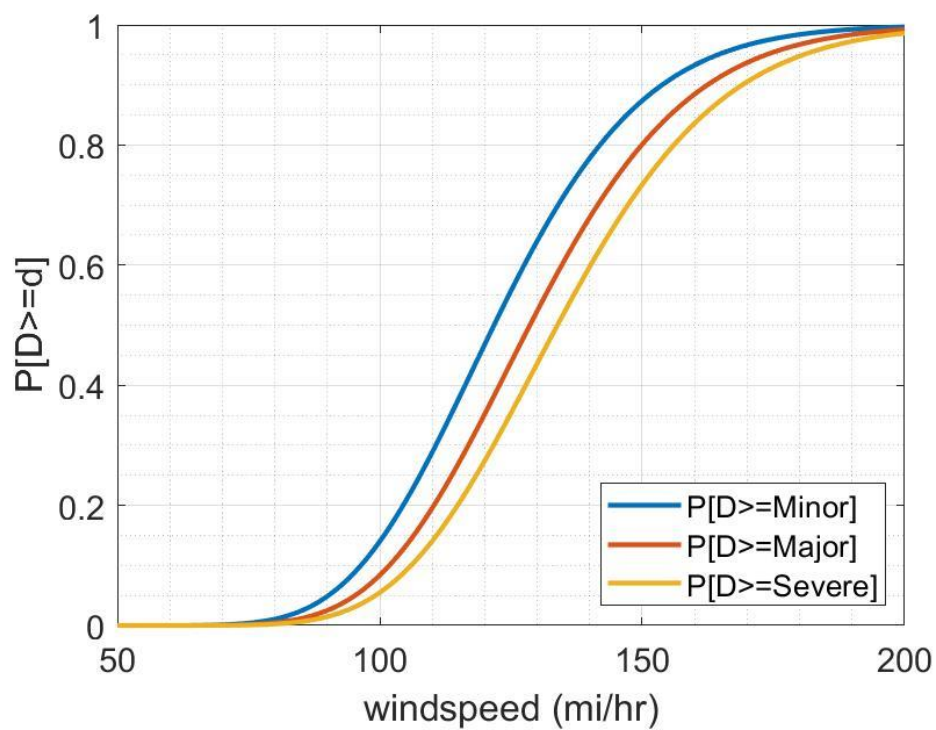


Fig. A.25 Diameter [0,25] ft

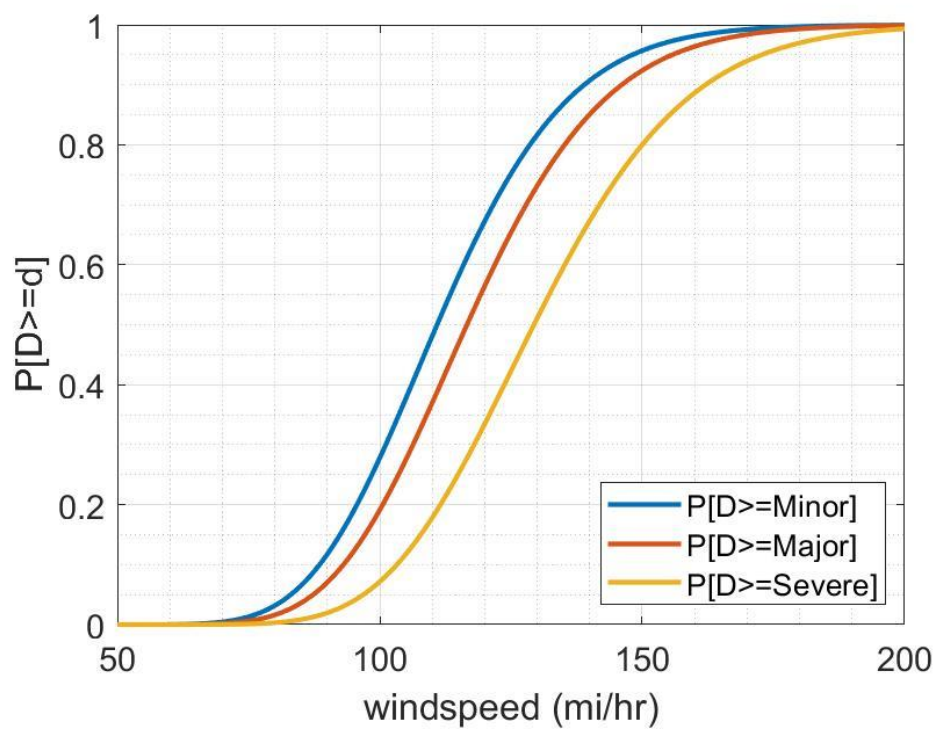


Fig. A.26 Diameter (25,35] ft

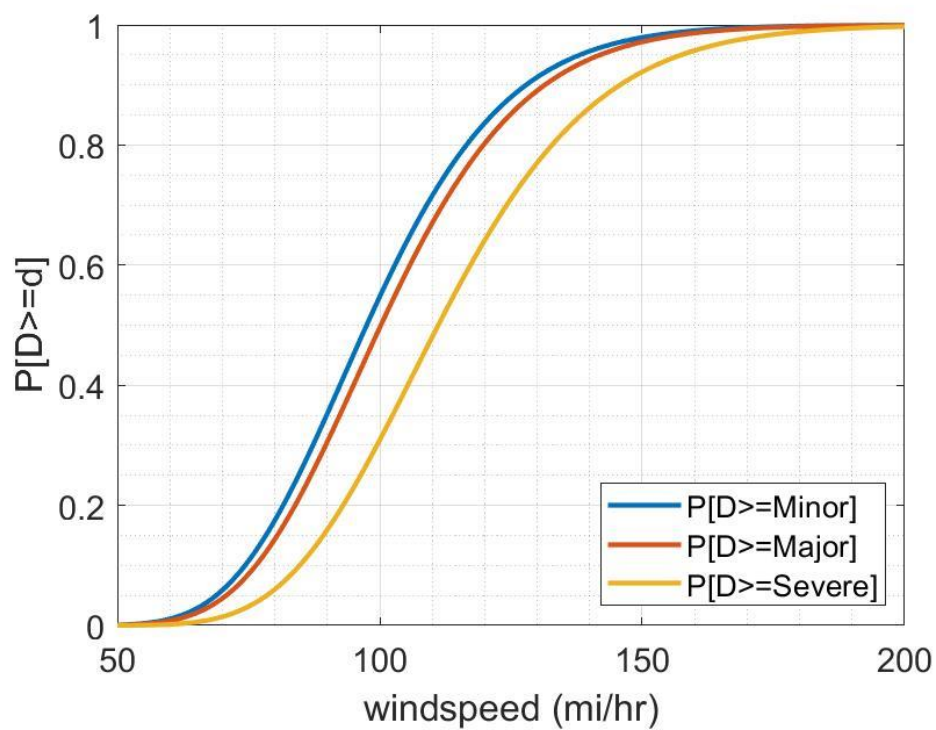


Fig. A.27 Diameter (35,130] ft

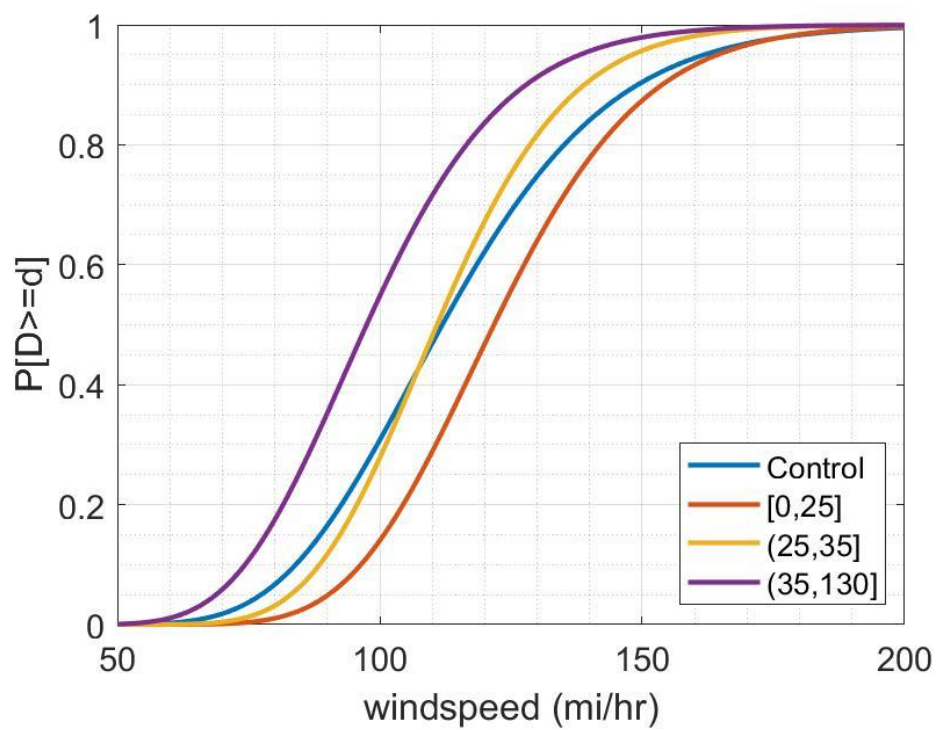


Fig. A.28 Diameter, Minor

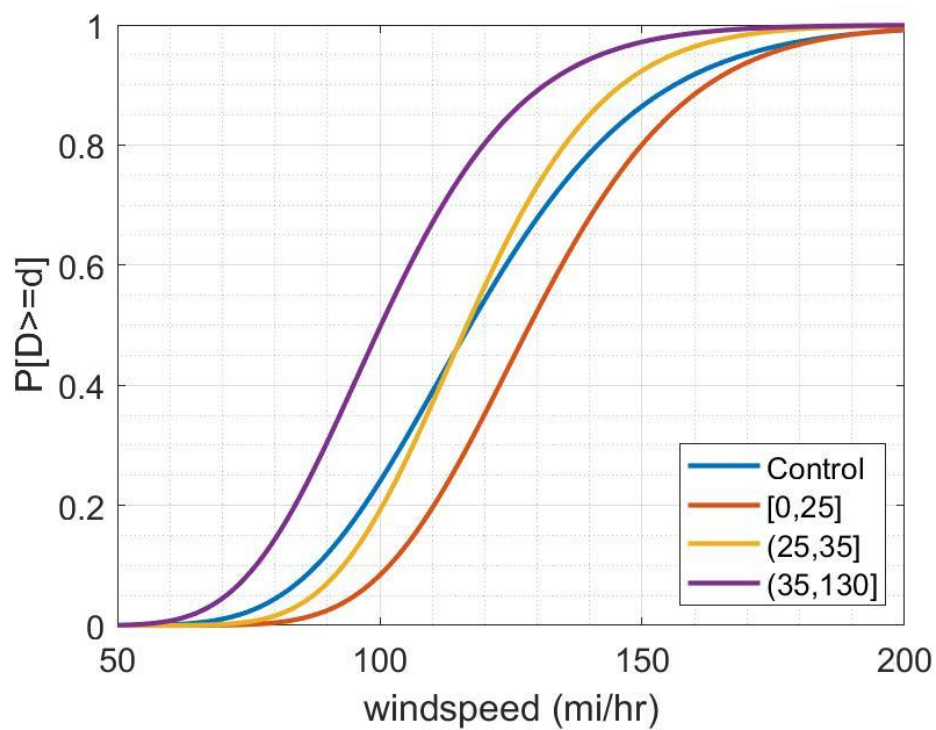


Fig. A.29 Diameter, Major

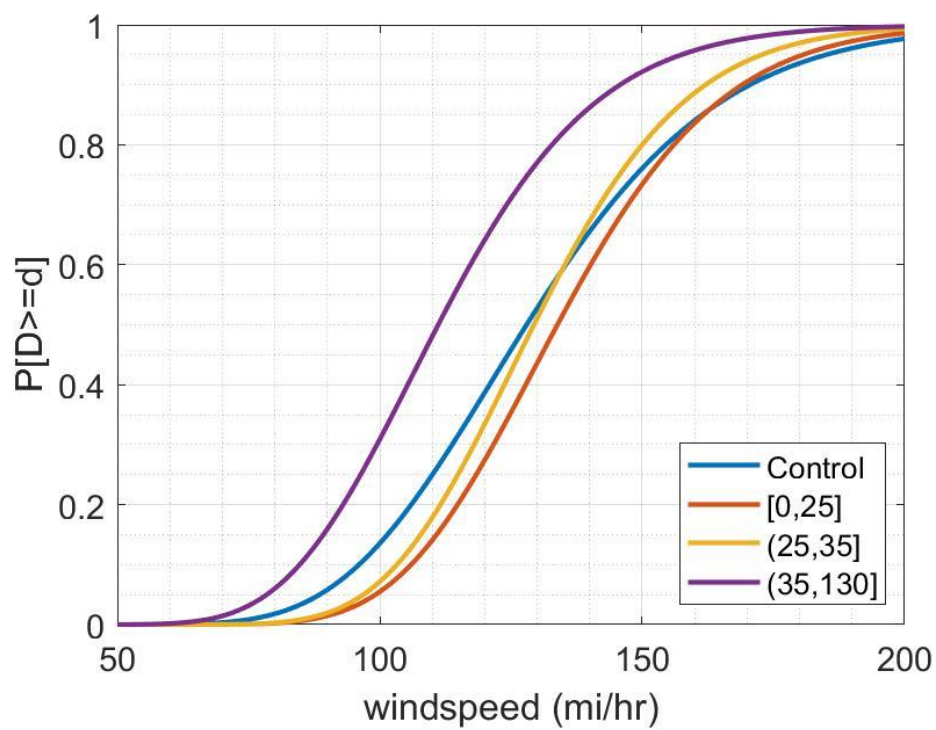


Fig. A.30 Diameter, Severe

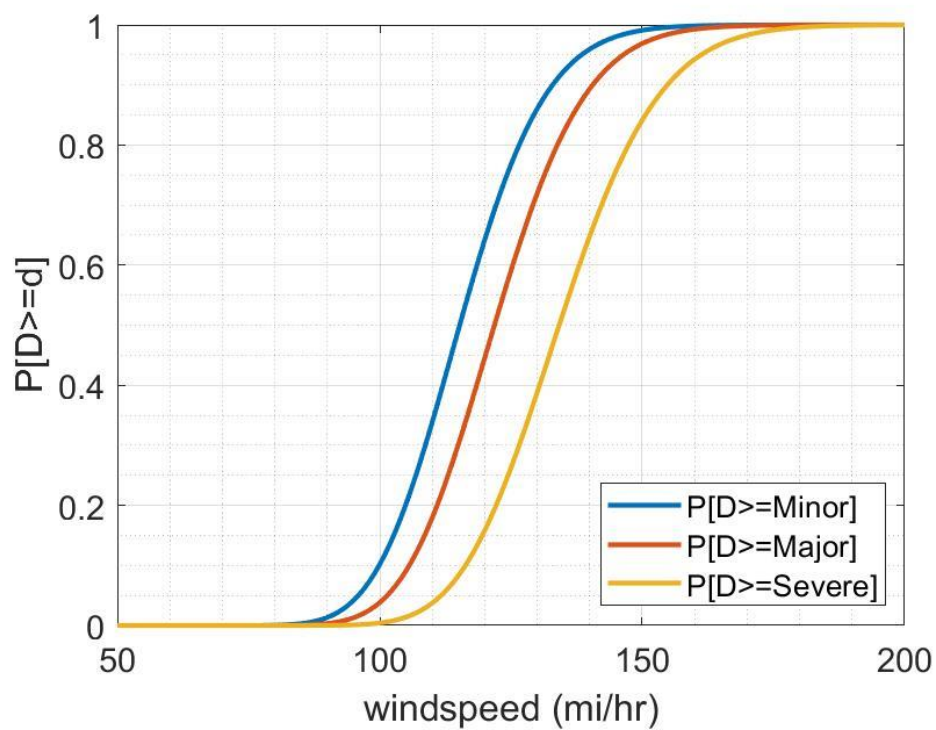


Fig. A.31 Height [0,20] ft

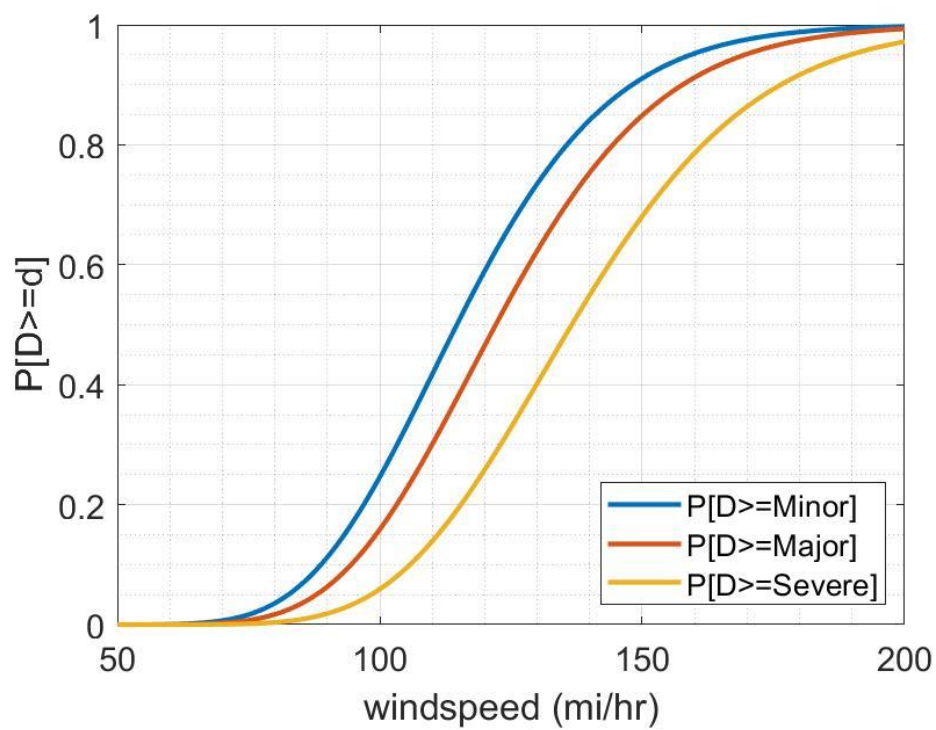


Fig. A.32 Height (20,35] ft

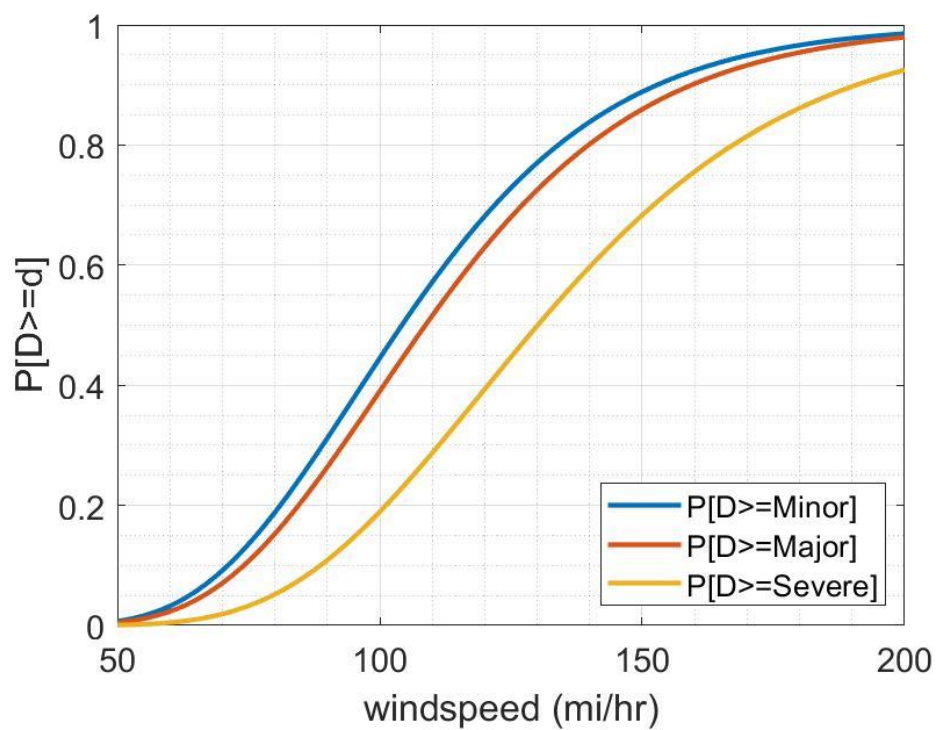


Fig. A.33 Height (35,135] ft

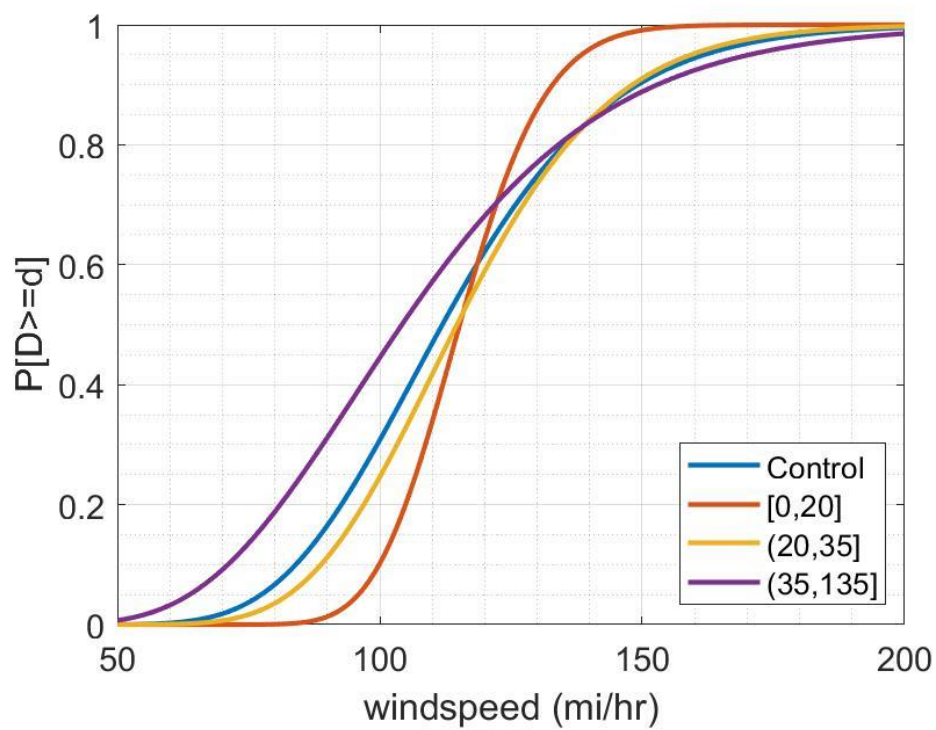


Fig. A.34 Height, Minor

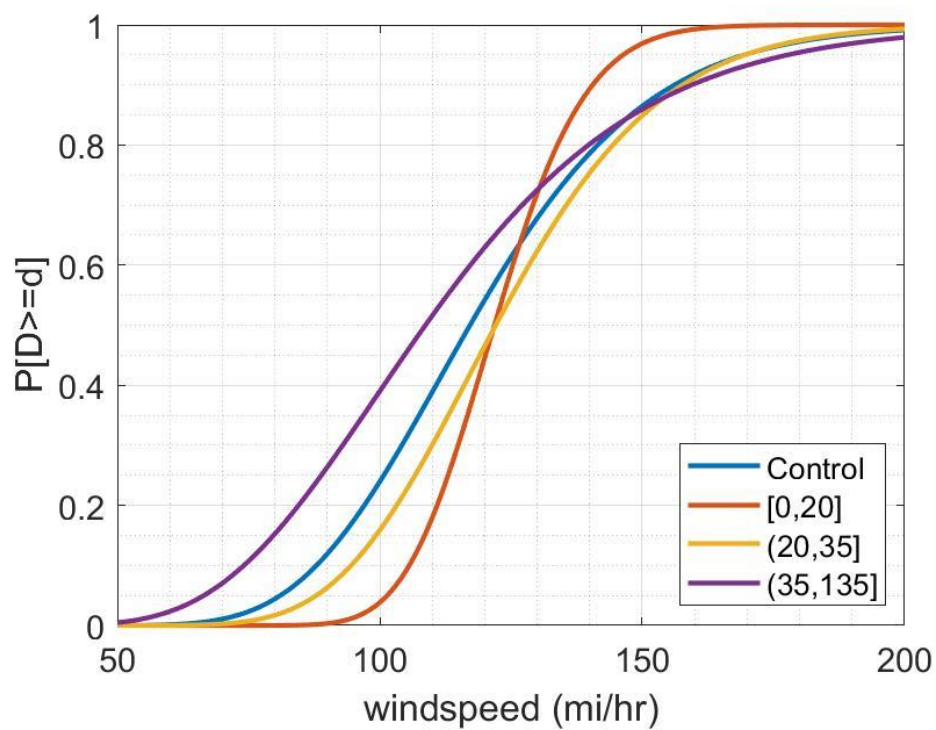


Fig. A.35 Height, Major

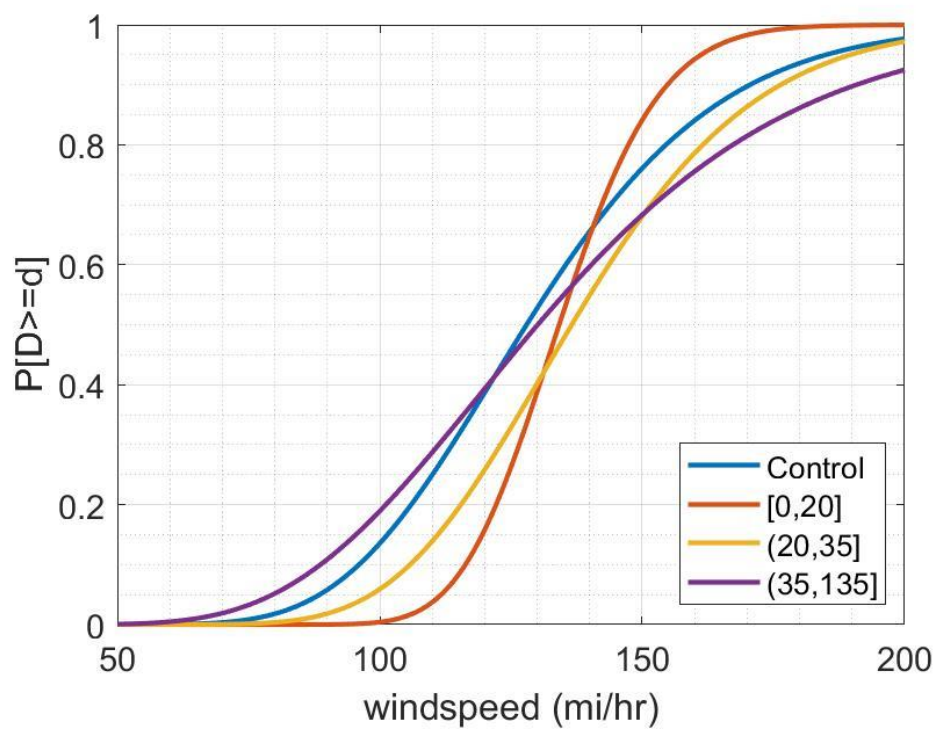
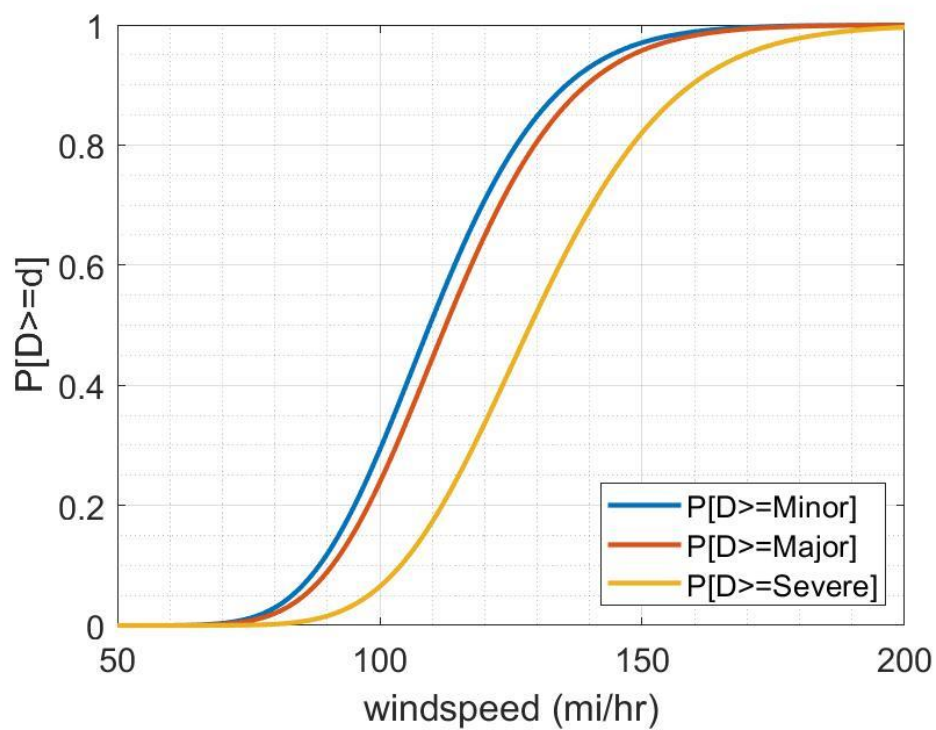
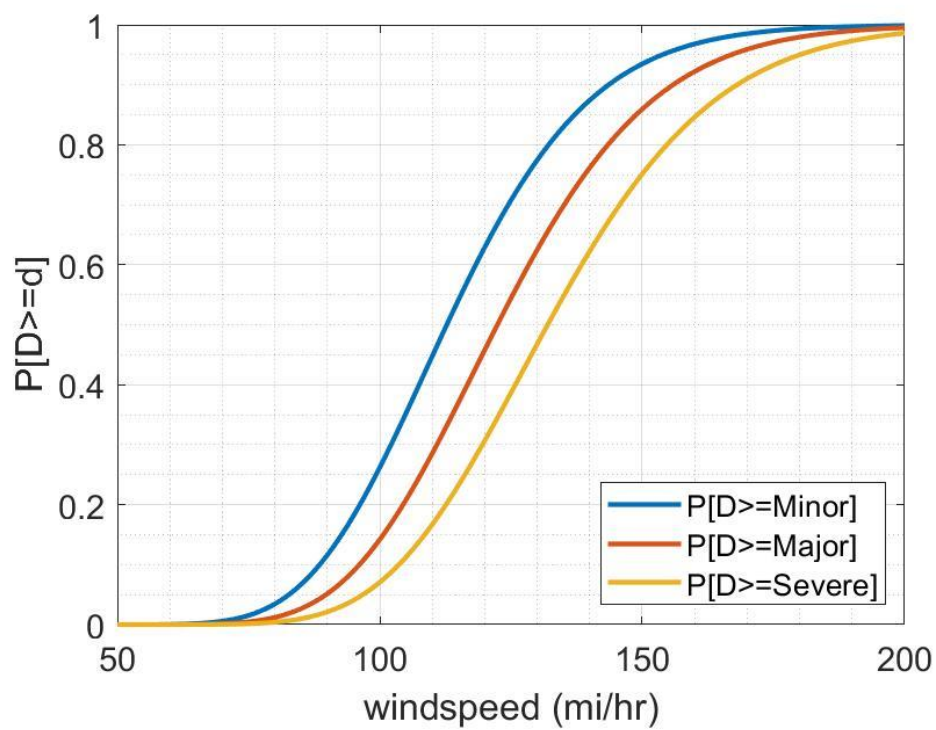


Fig. A.36 Height, Severe

Fig. A.37 Aspect Ratio $[0, 0.75]$ Fig. A.38 Aspect Ratio $(0.75, 1.0]$

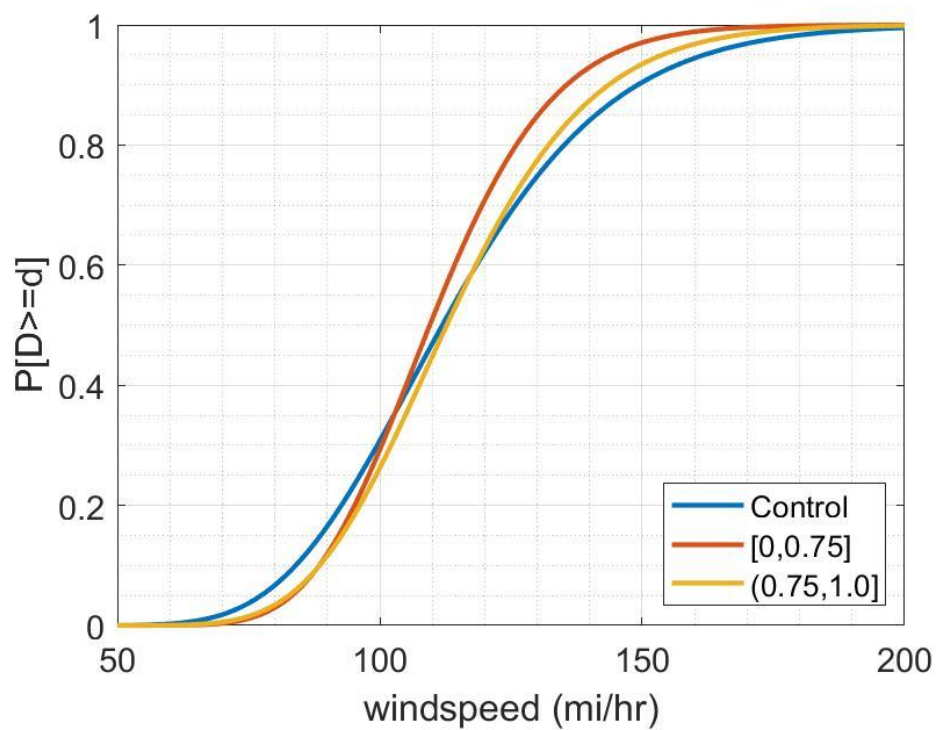


Fig. A.39 Aspect Ratio, Minor

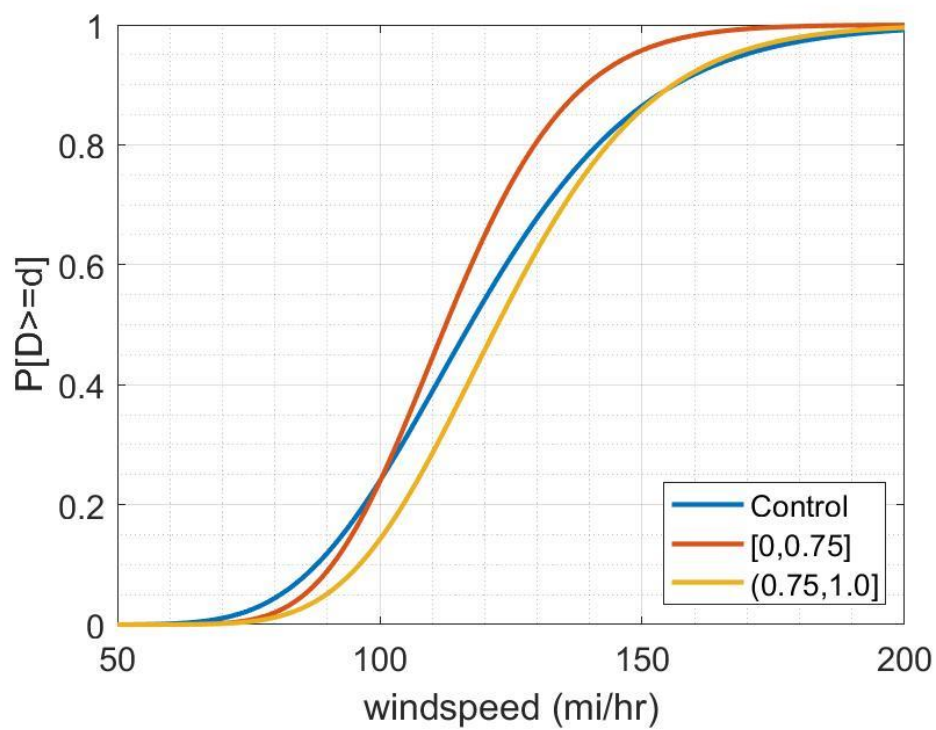


Fig. A.40 Aspect Ratio, Major

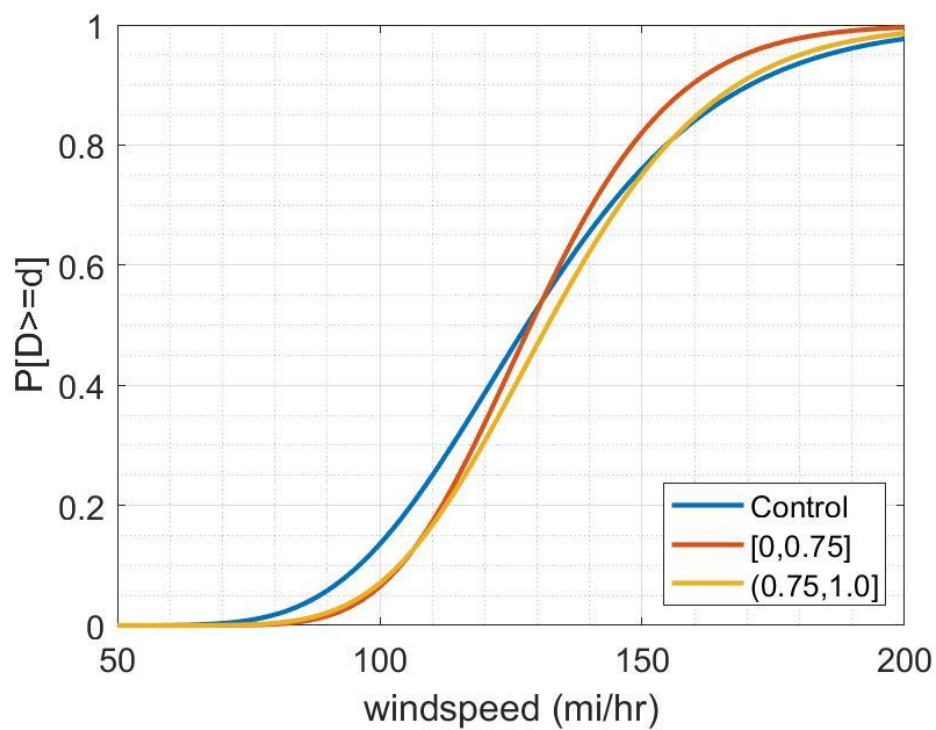


Fig. A.41 Aspect Ratio, Severe

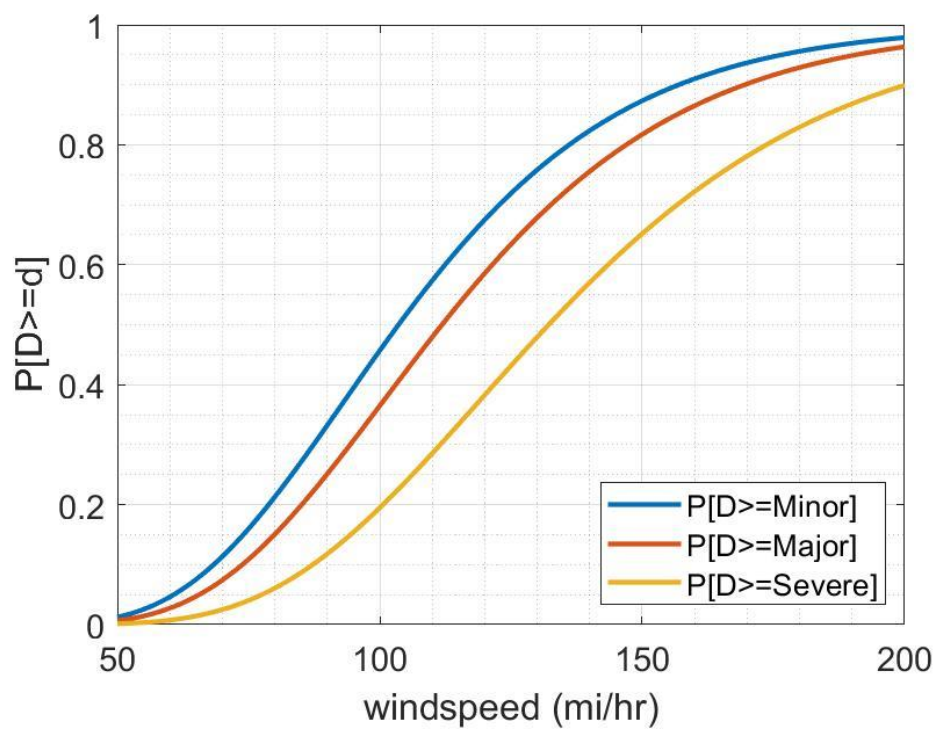


Fig. A.42 Stiffened

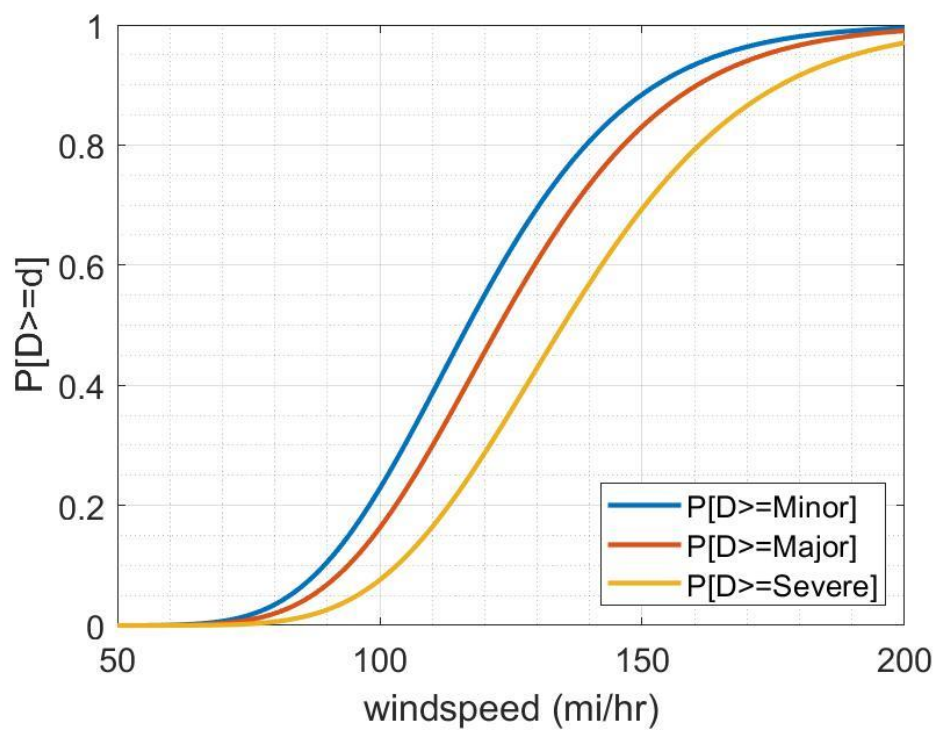


Fig. A.43 Unstiffened

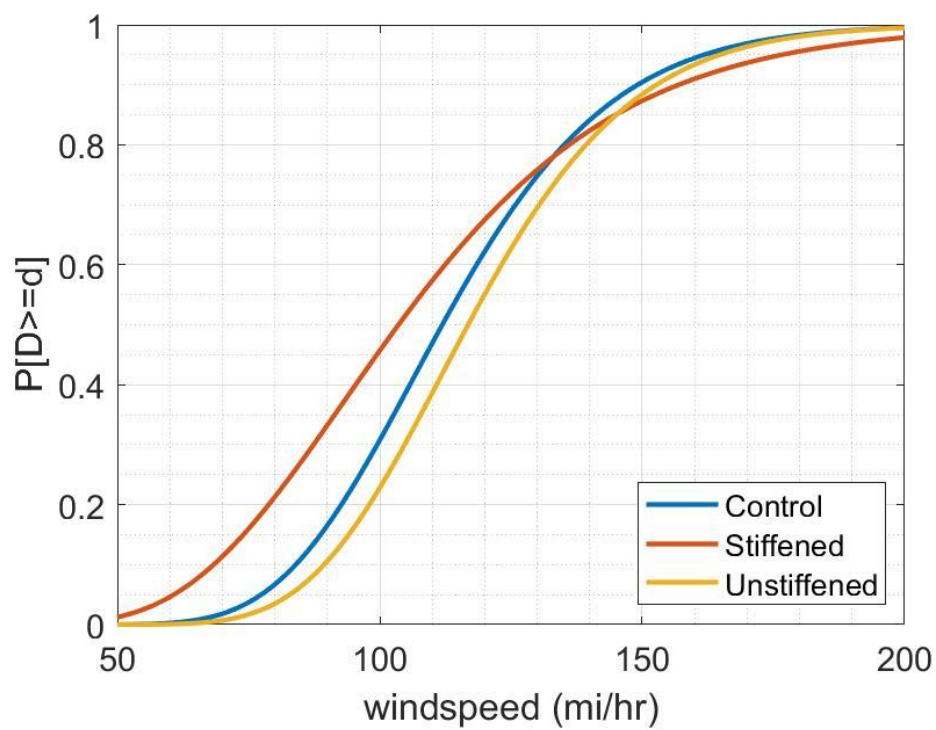


Fig. A.44 Stiffened-Unstiffened, Minor

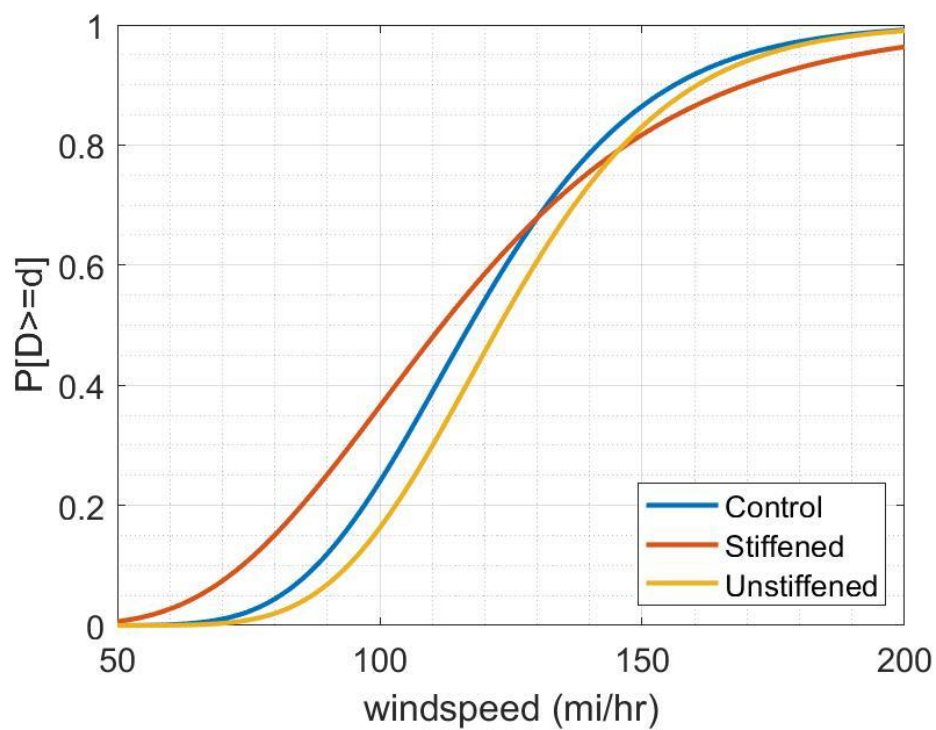


Fig. A.45 Stiffened-Unstiffened, Major

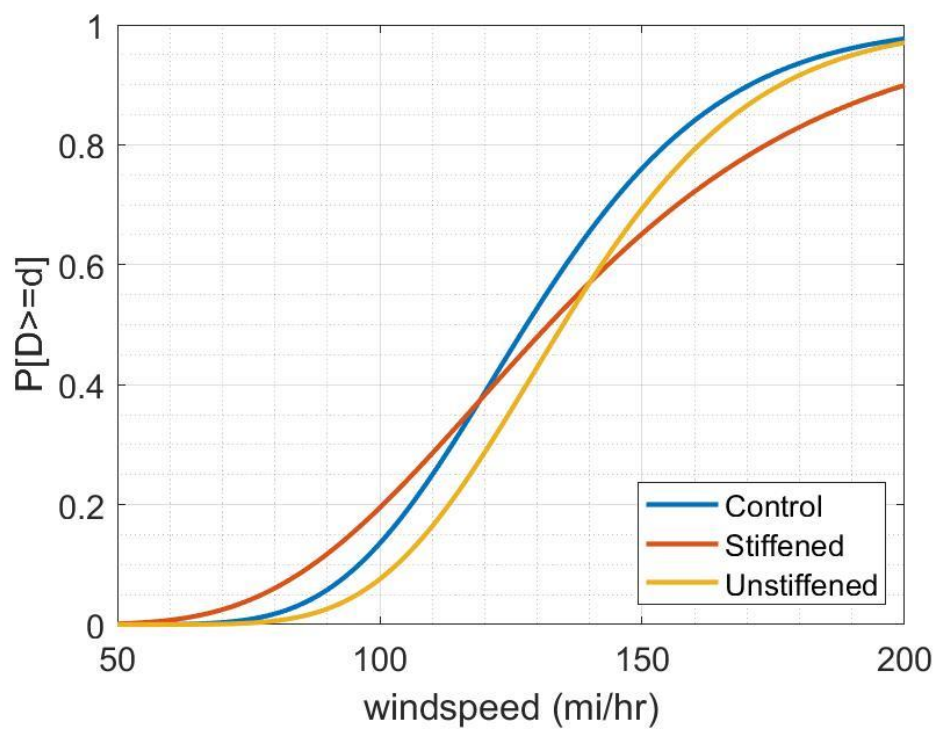


Fig. A.46 Stiffened-Unstiffened, Severe

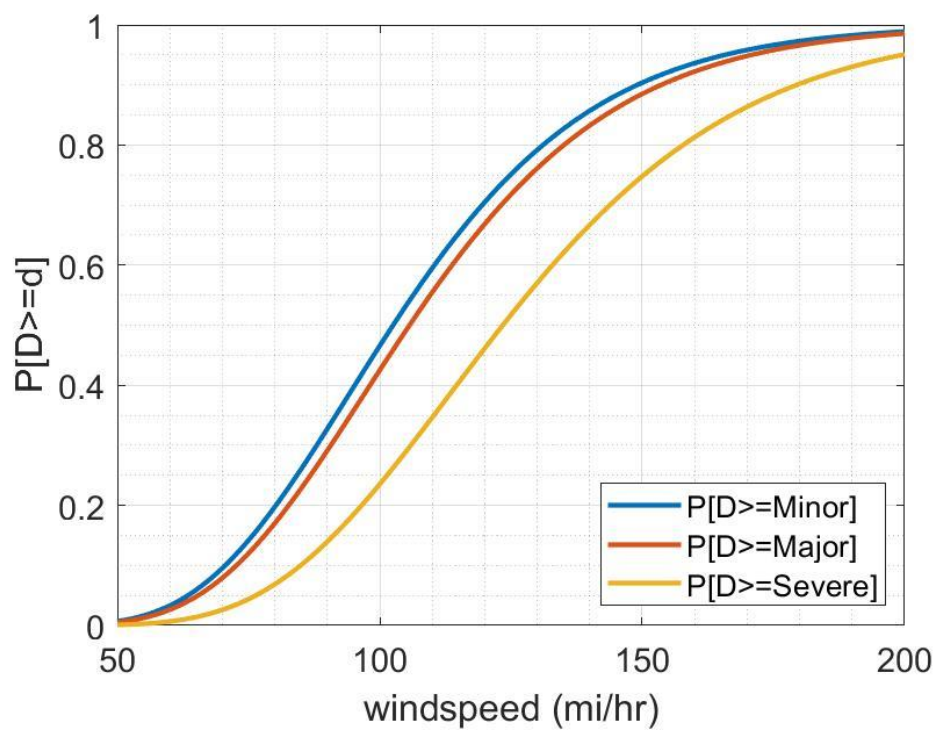


Fig. A.47 Wind Rings

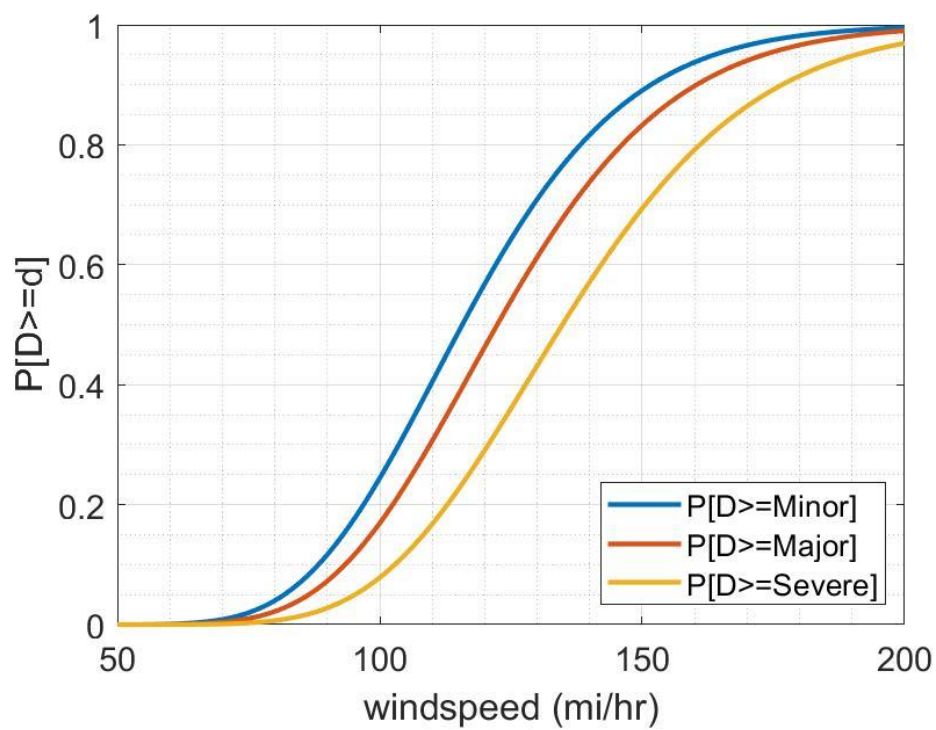


Fig. A.48 No Wind Rings

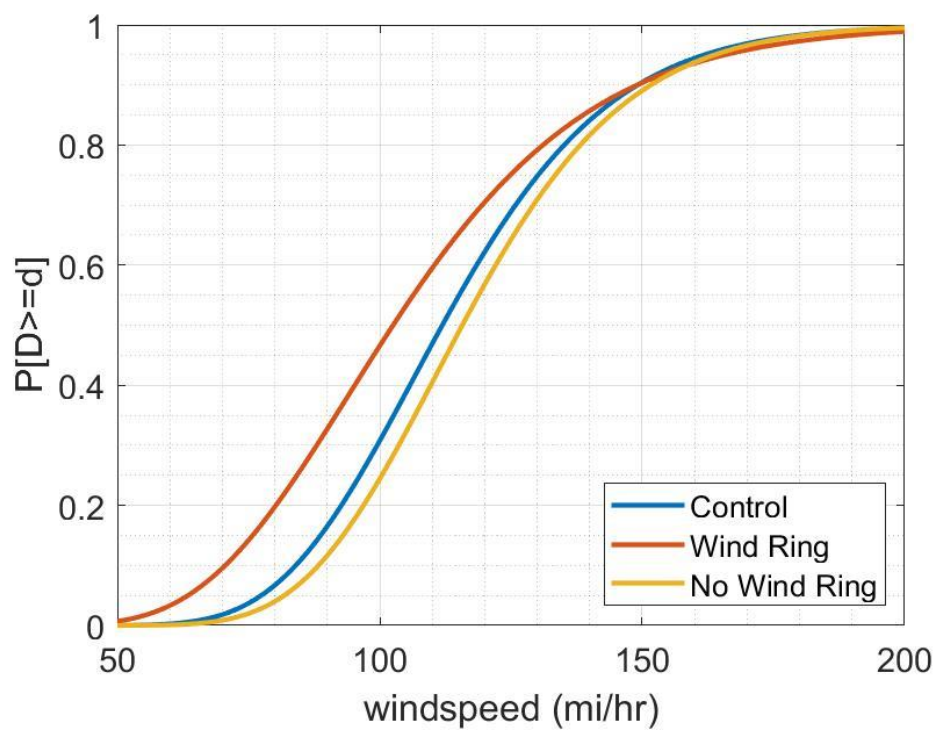


Fig. A.49 Wind Rings, Minor

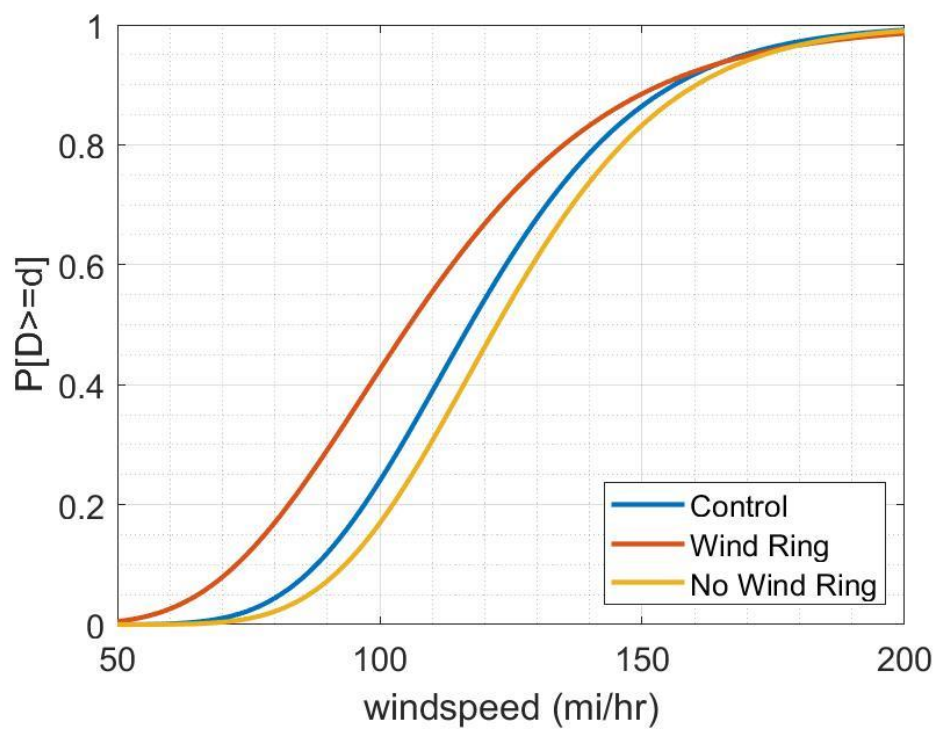


Fig. A.50 Wind Rings, Major

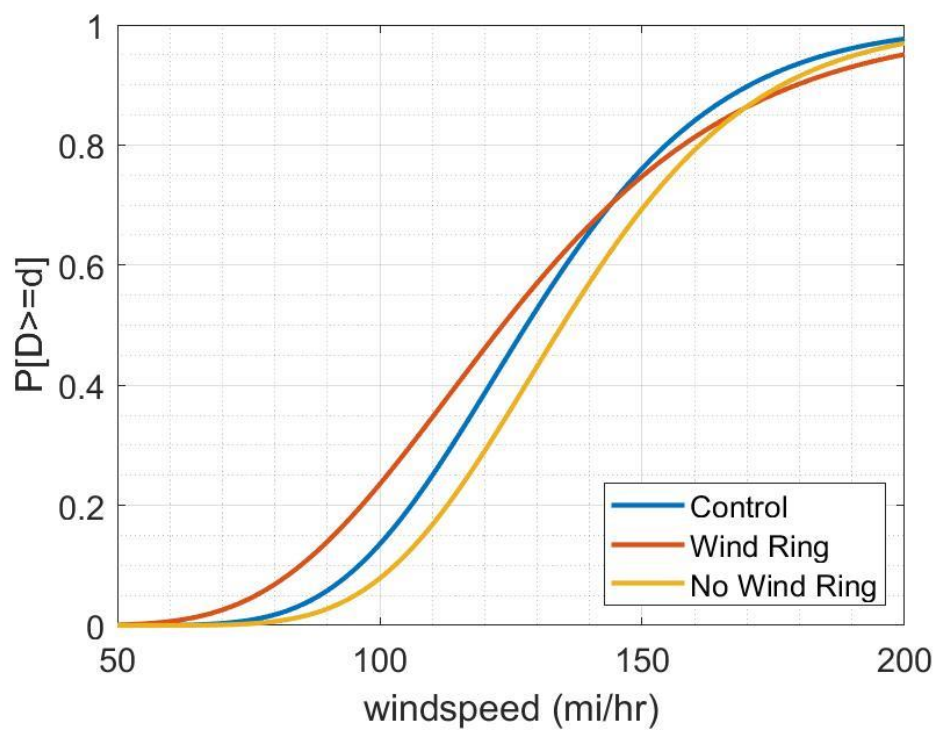


Fig. A.51 Wind Rings, Severe

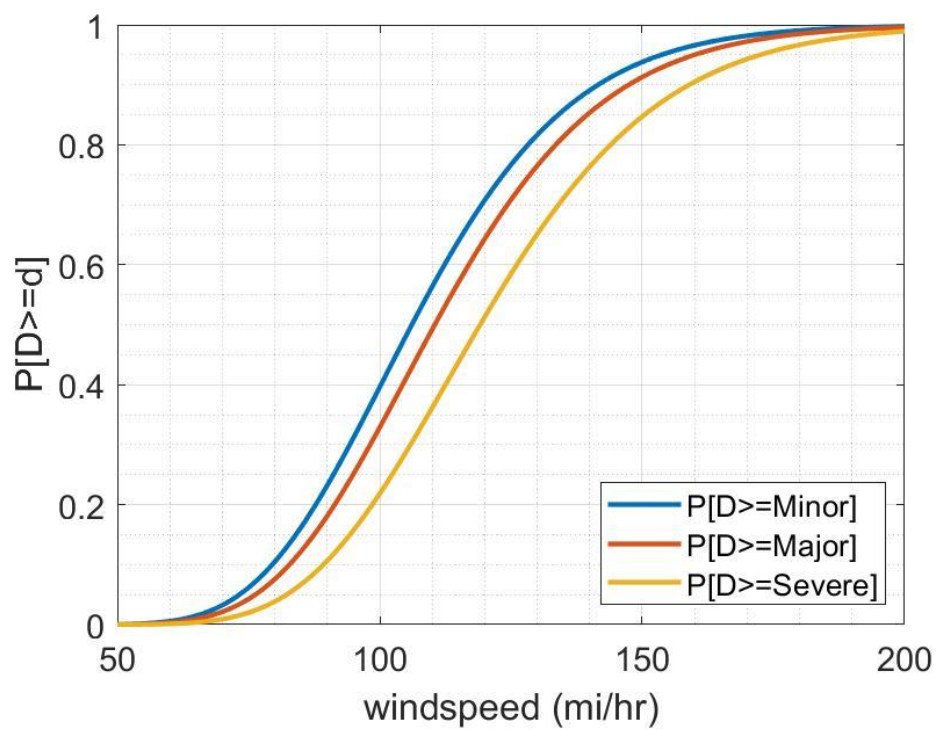


Fig. A.52 Terrain-Open

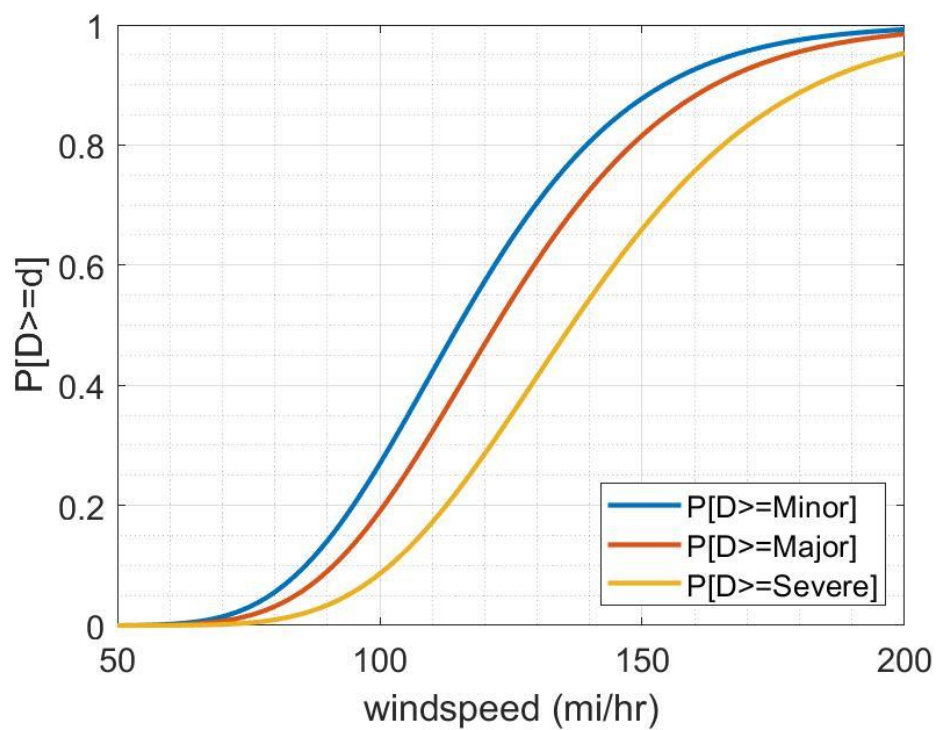


Fig. A.53 Terrain-Trees & Buildings

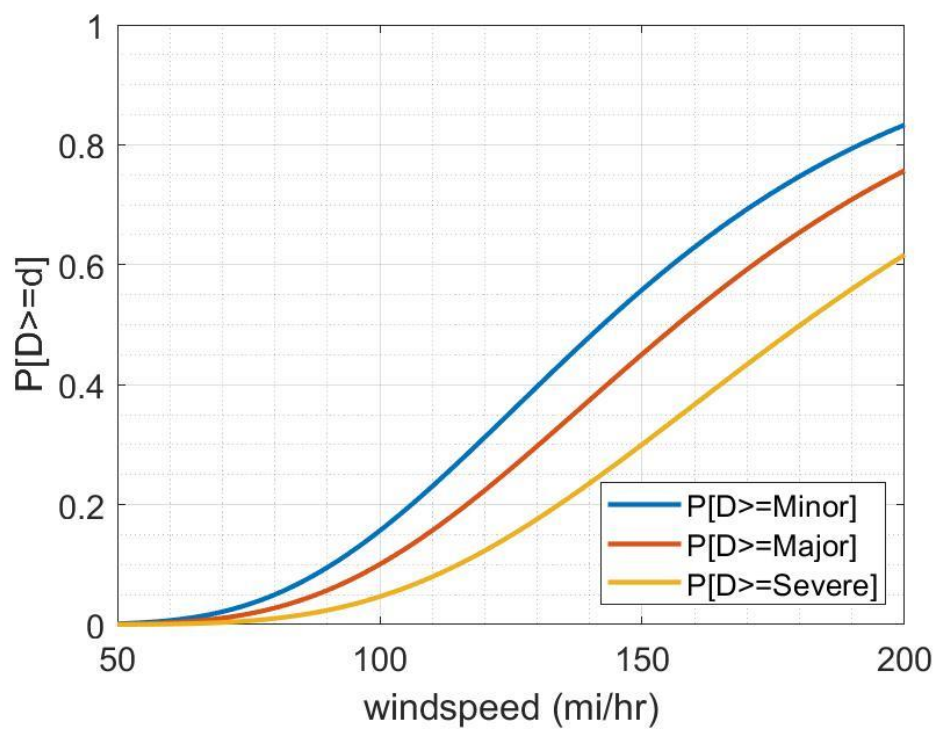


Fig. A.54 Terrain-In Town

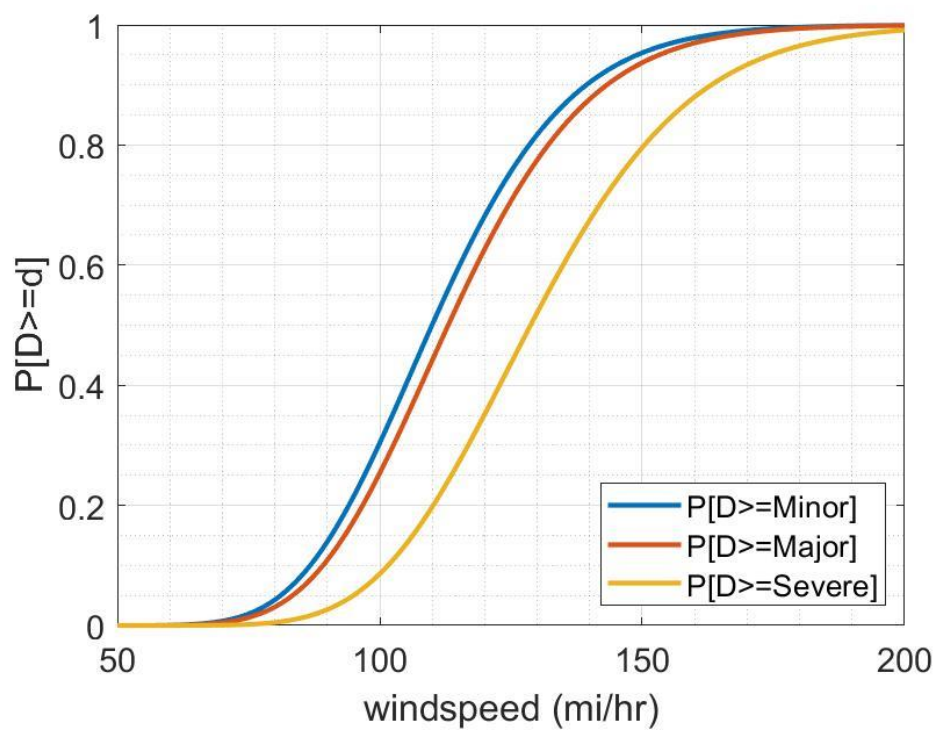


Fig. A.55 Terrain-Grain Bins

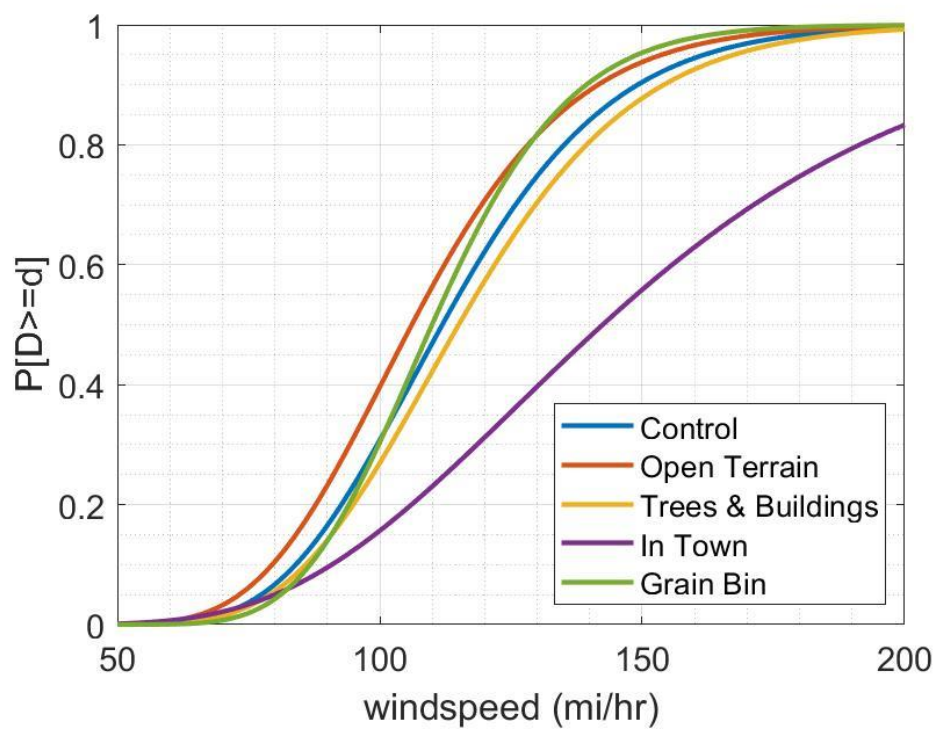


Fig. A.56 Terrain, Minor

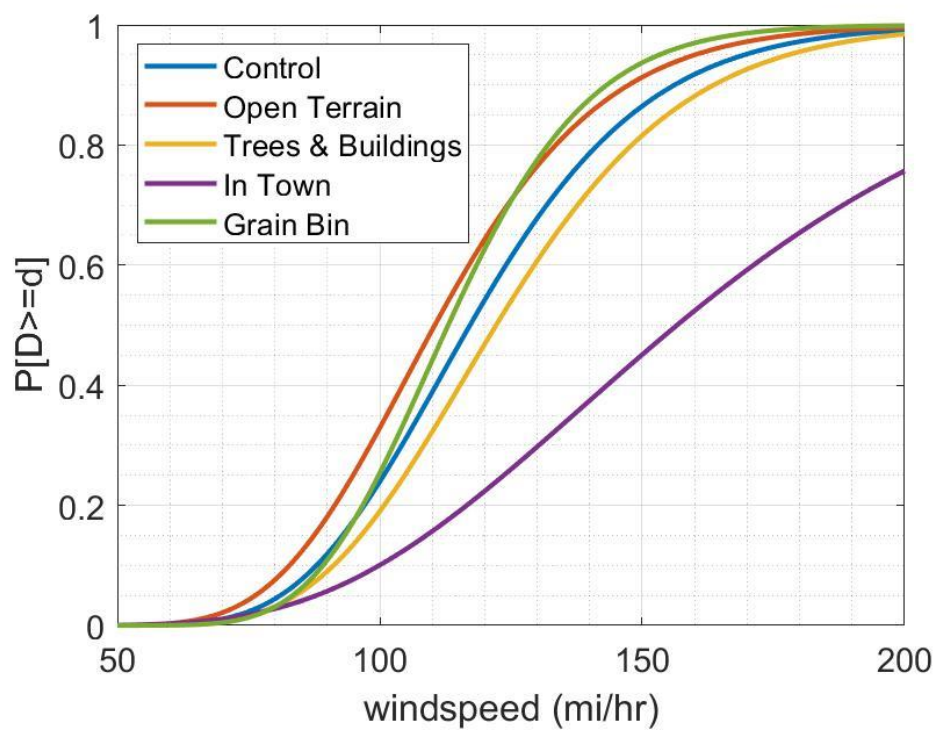


Fig. A.57 Terrain, Major

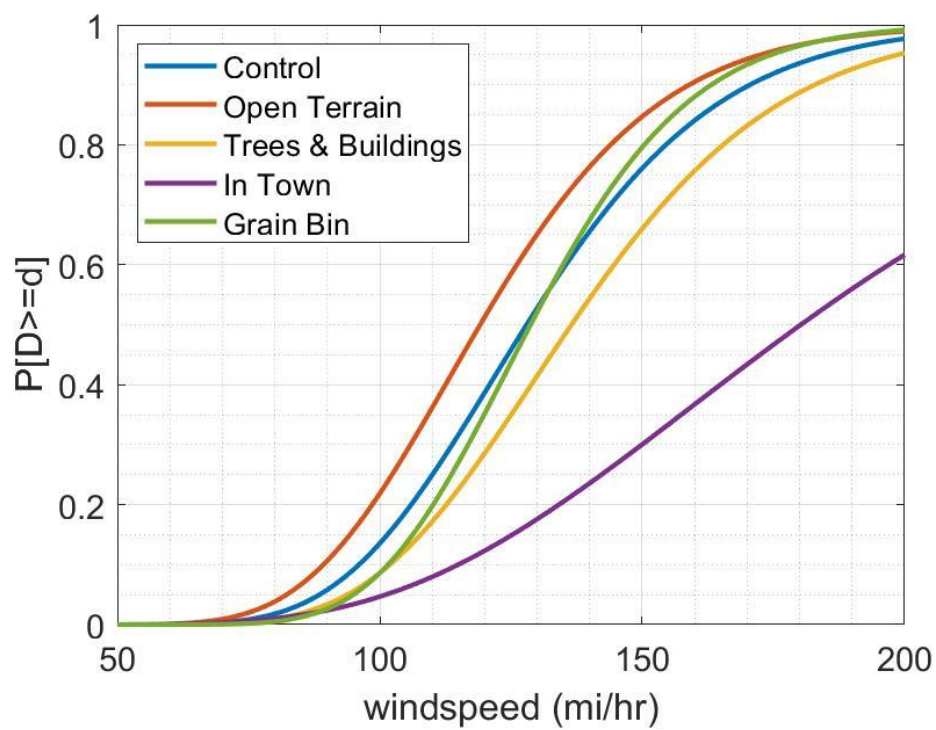


Fig. A.58 Terrain, Severe

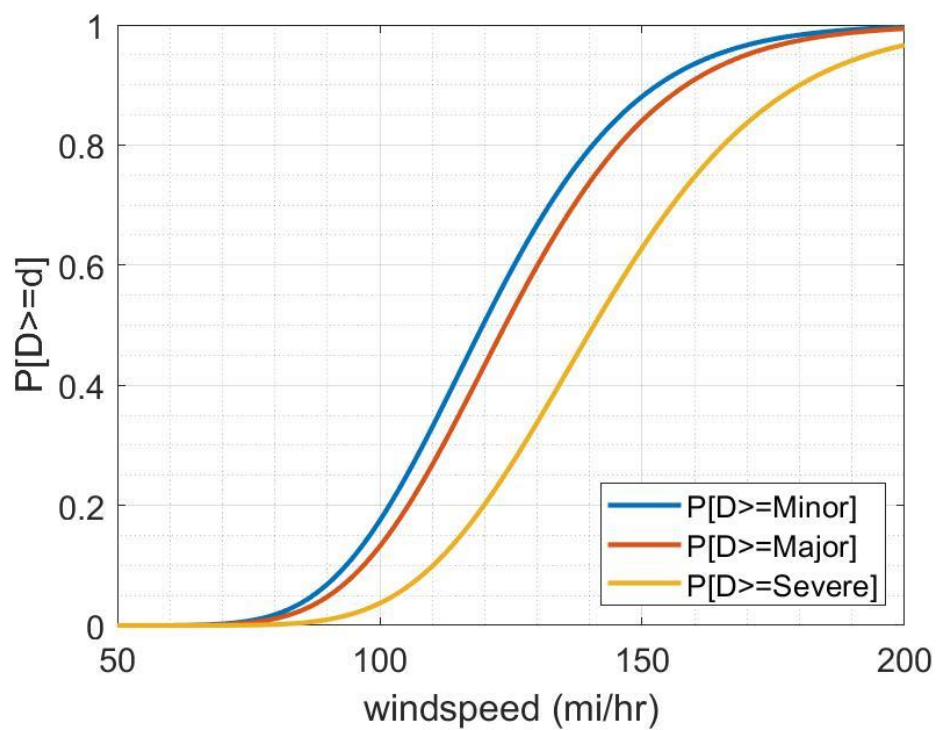


Fig. A.59 Distance to Obstruction [0,50] ft

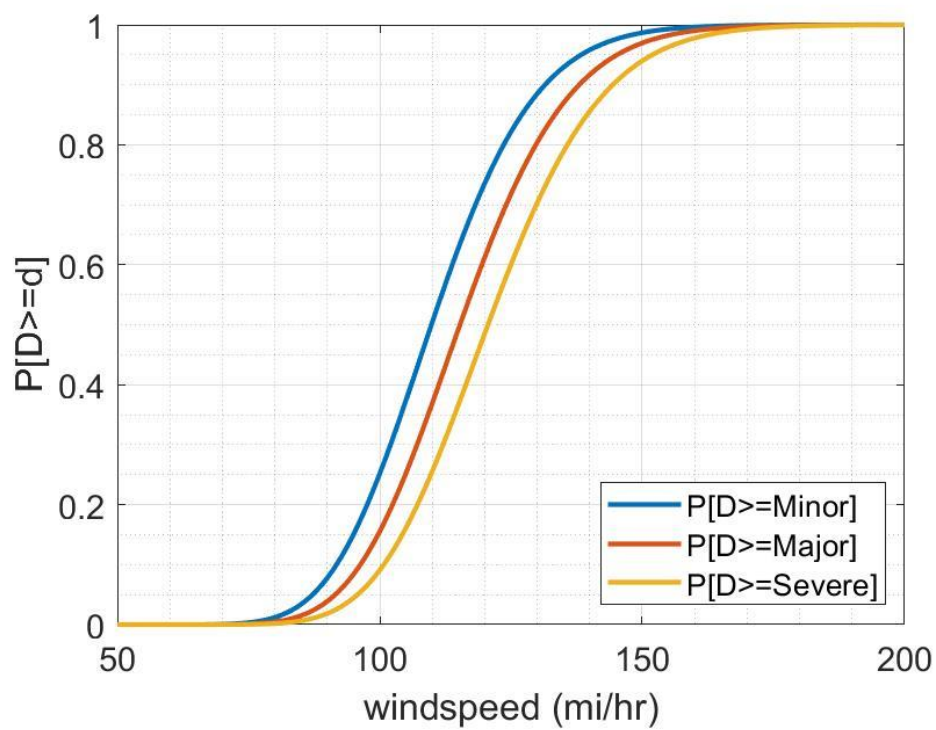


Fig. A.60 Distance to Obstruction (50,150] ft

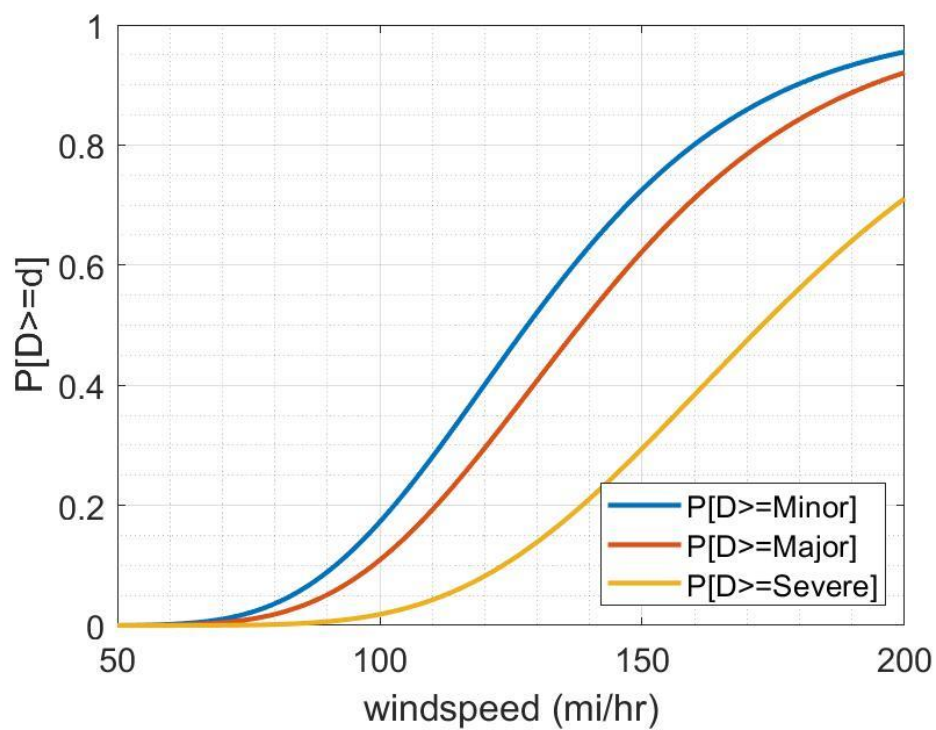


Fig. A.61 Distance to Obstruction (150,1000] ft

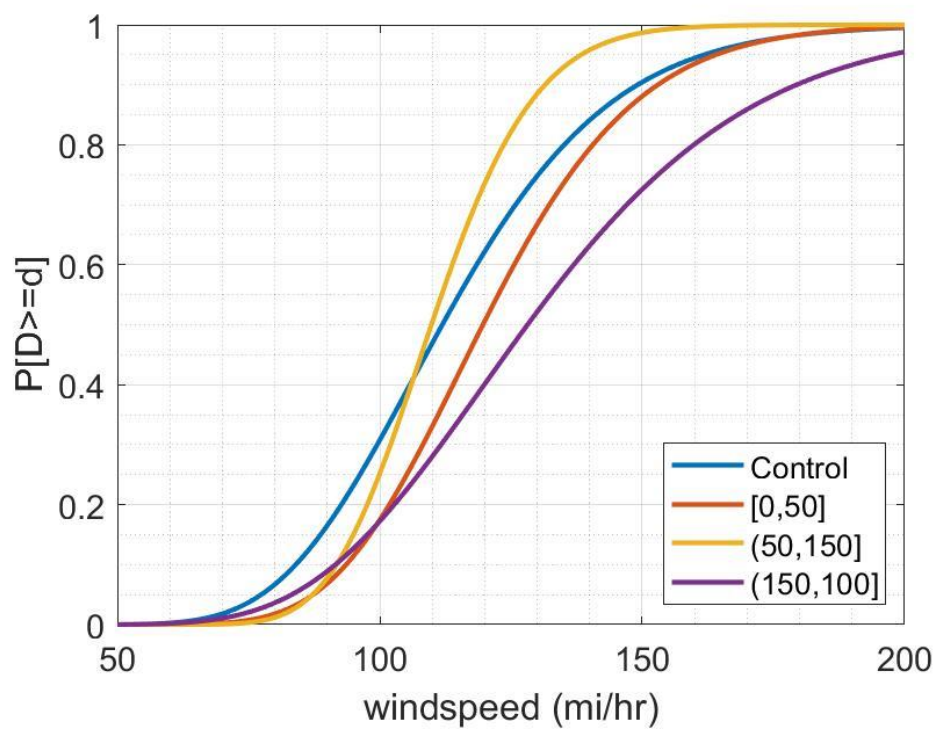


Fig. A.62 Distance to Obstruction, Minor

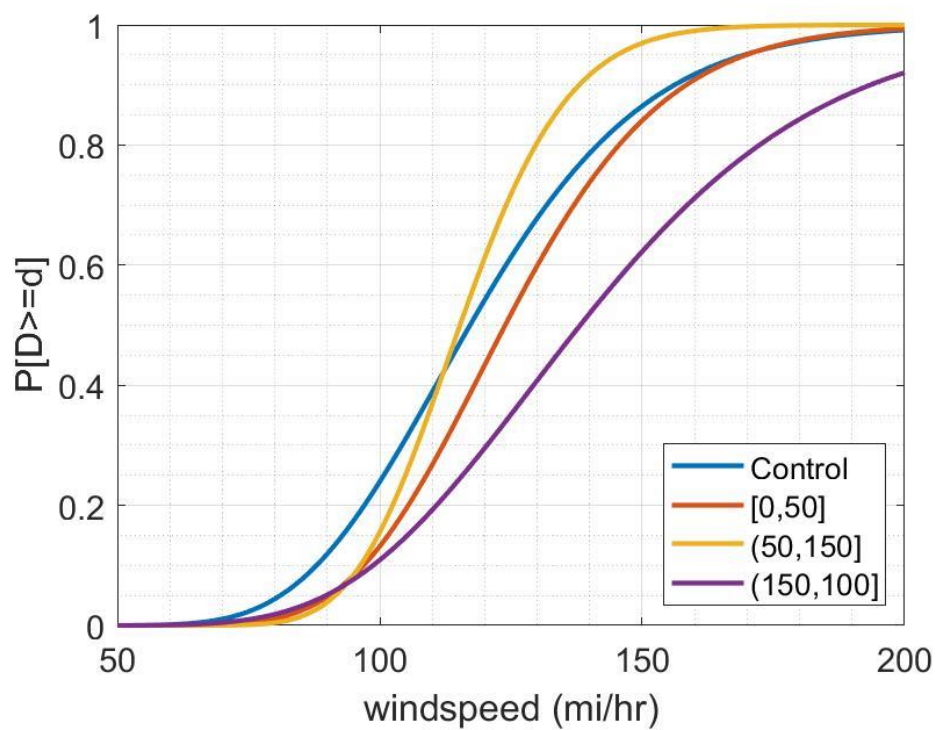


Fig. A.63 Distance to Obstruction, Major

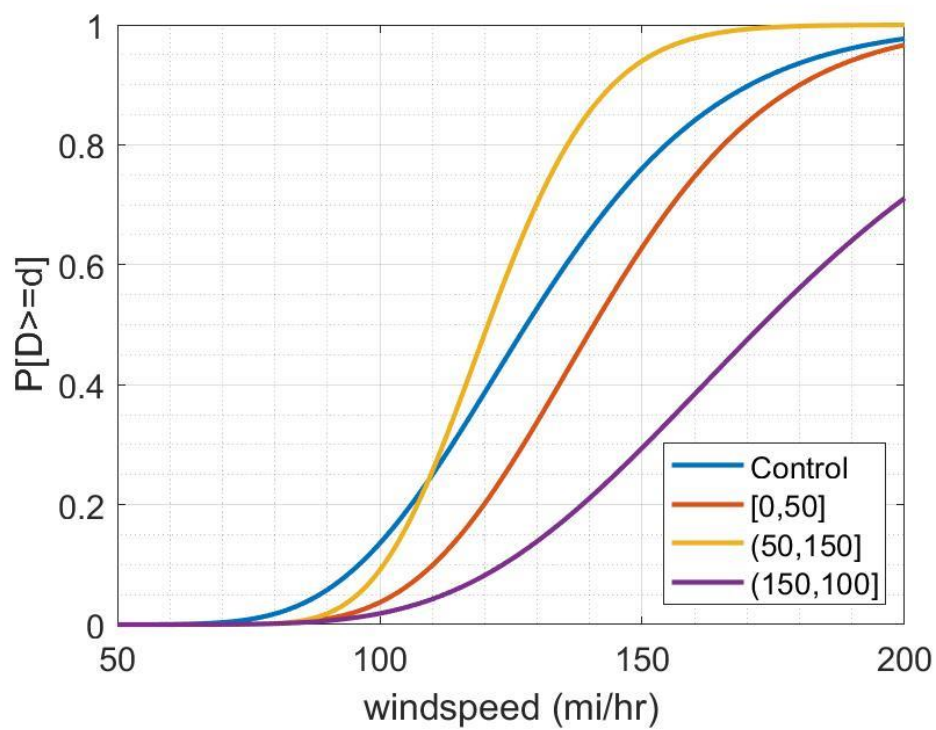


Fig. A.64 Distance to Obstruction, Severe

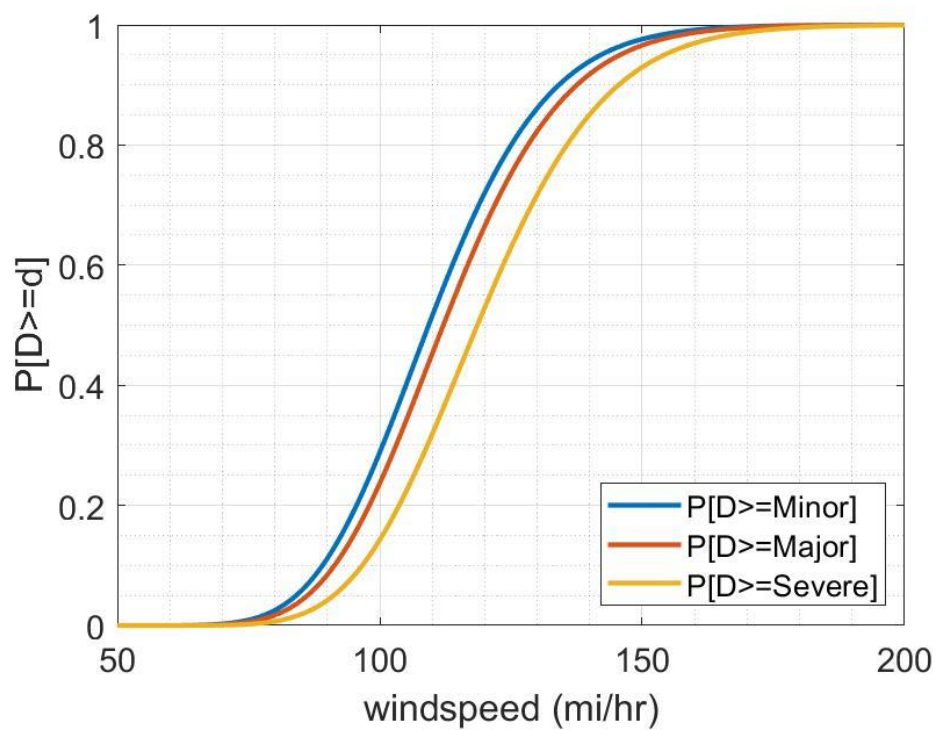


Fig. A.65 Prominence [-20,-4] ft

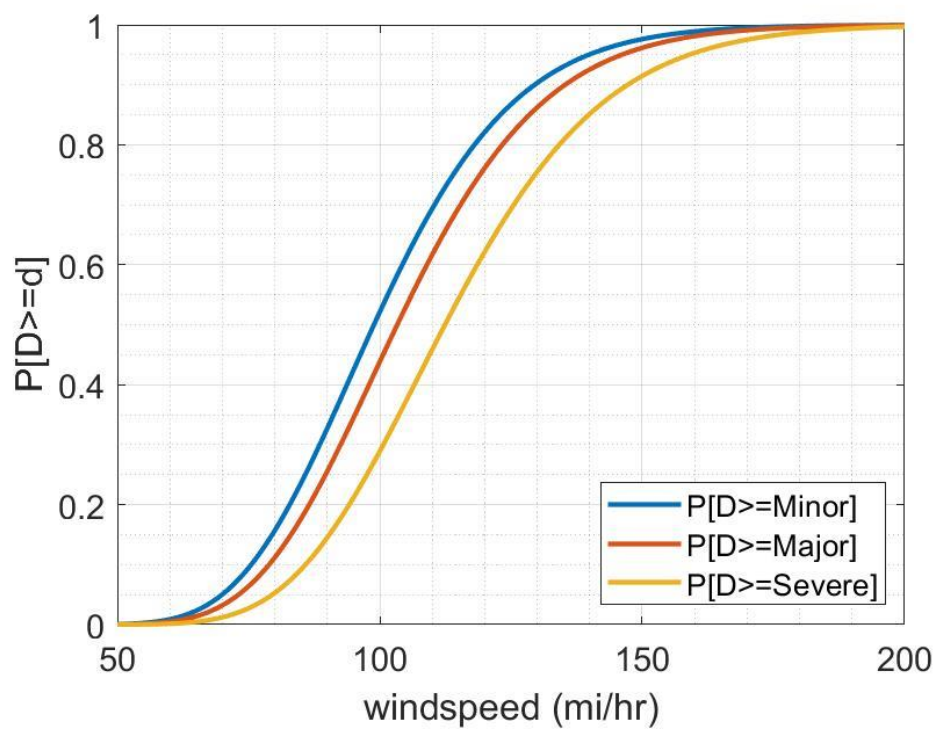


Fig. A.66 Prominence (-4,4] ft

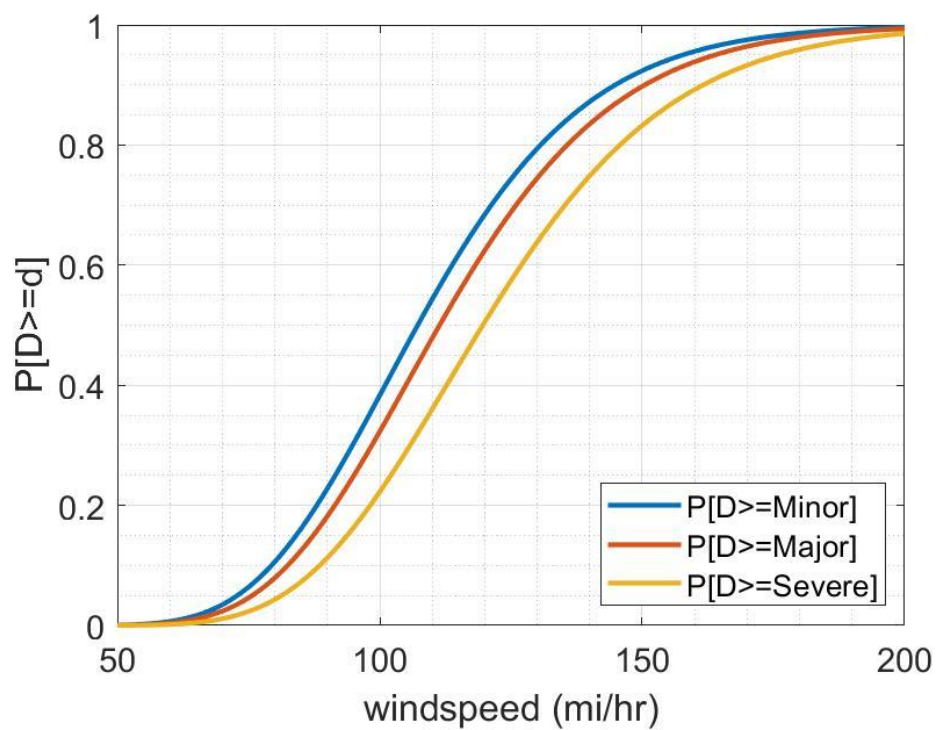


Fig. A.67 Prominence (4,30] ft

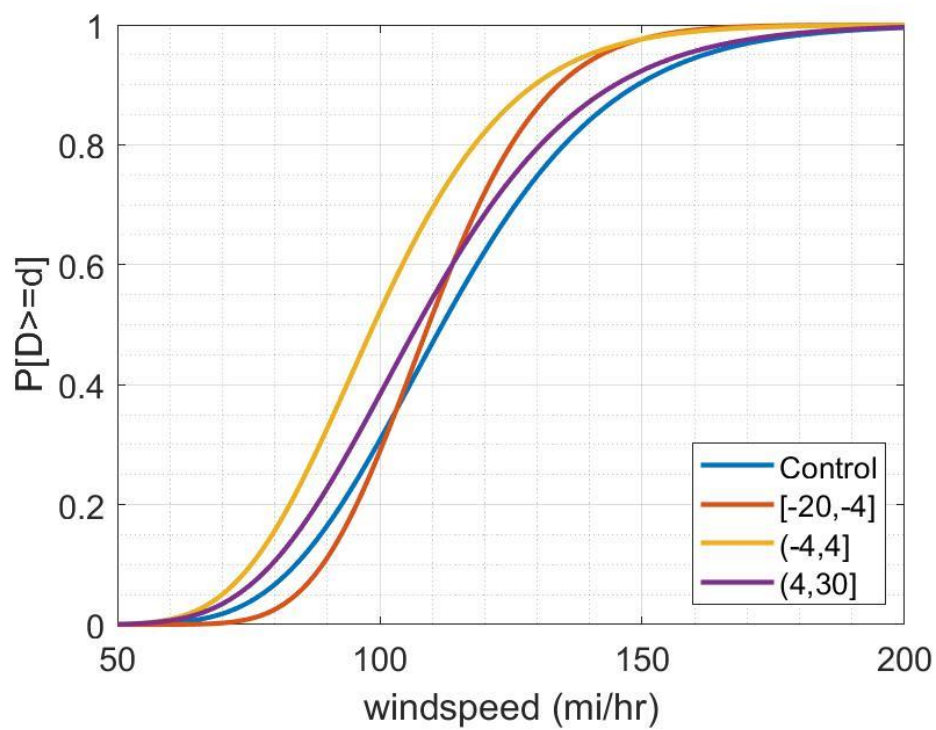


Fig. A.68 Prominence, Minor

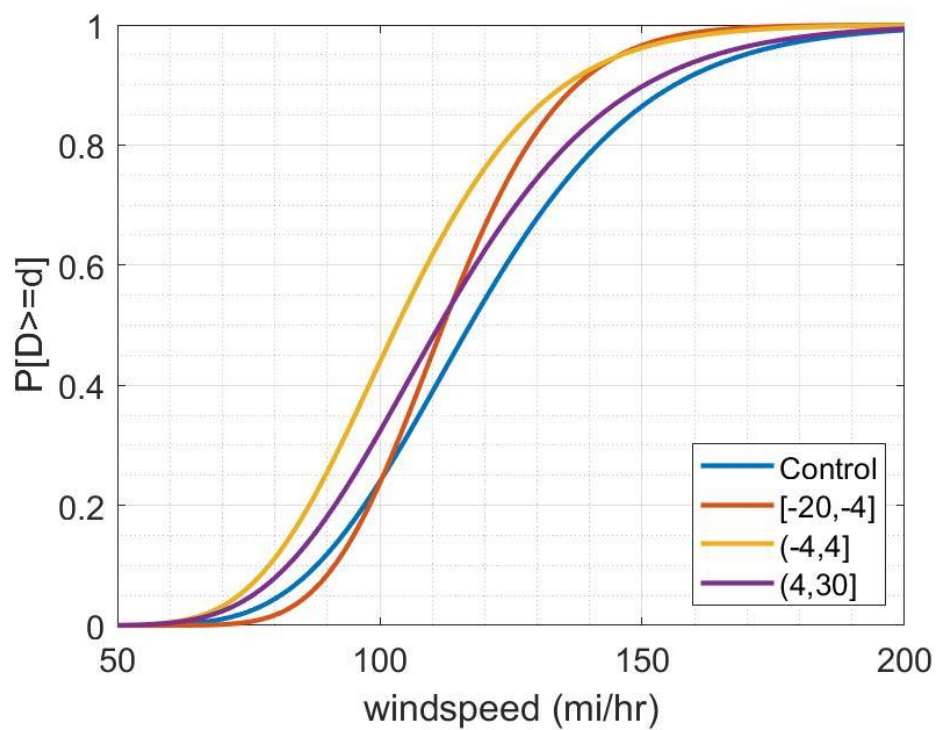


Fig. A.69 Prominence, Major

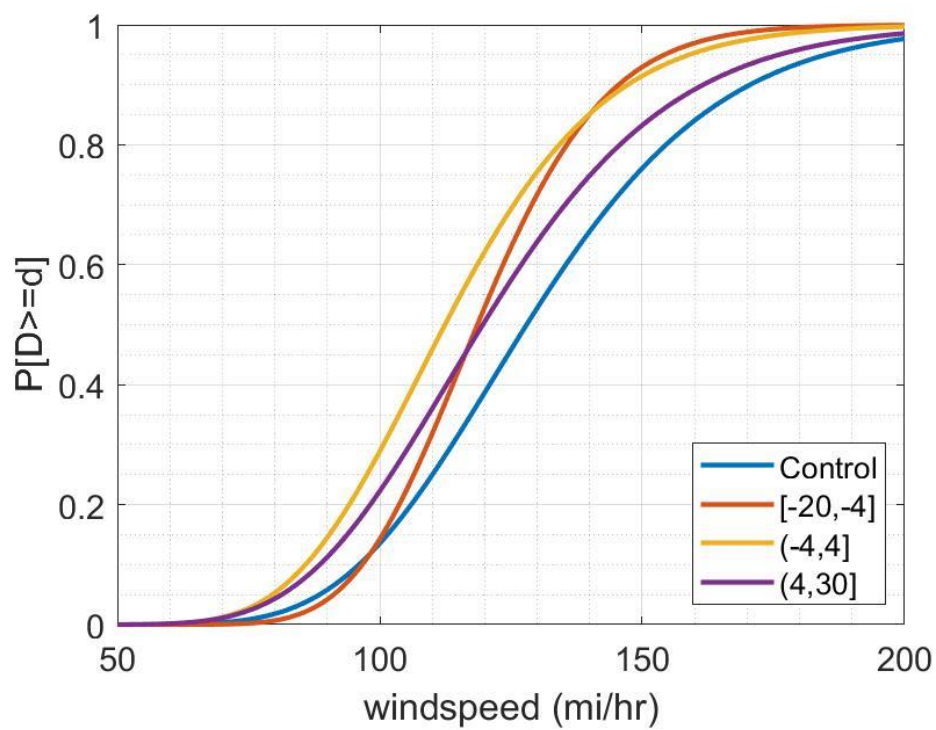


Fig. A.70 Prominence, Severe

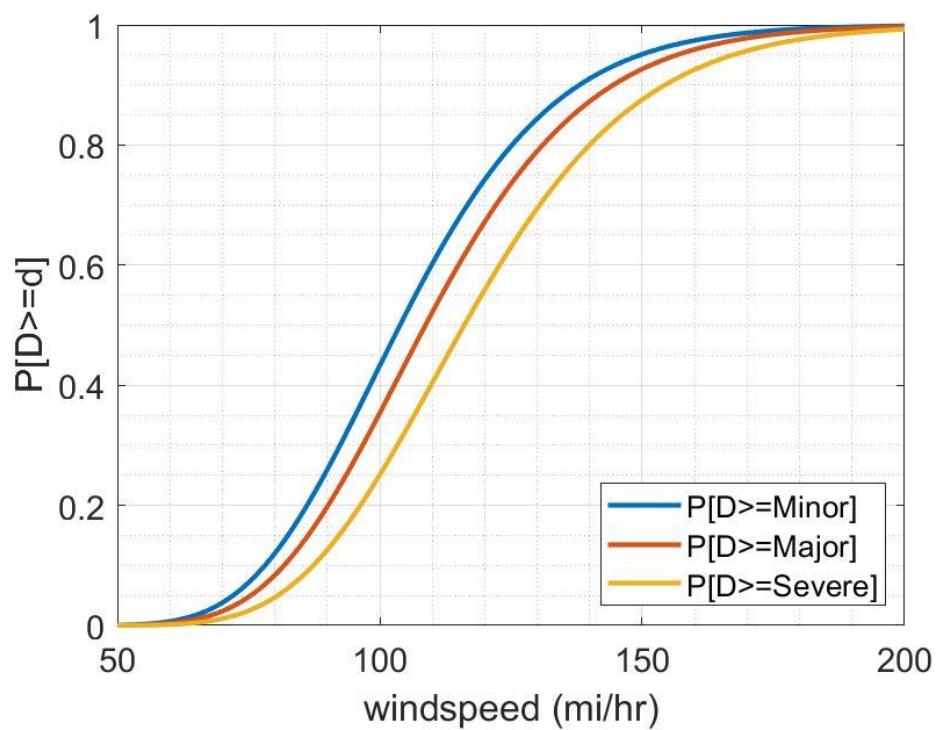


Fig. A.71 Slope [-0.07,-0.004]

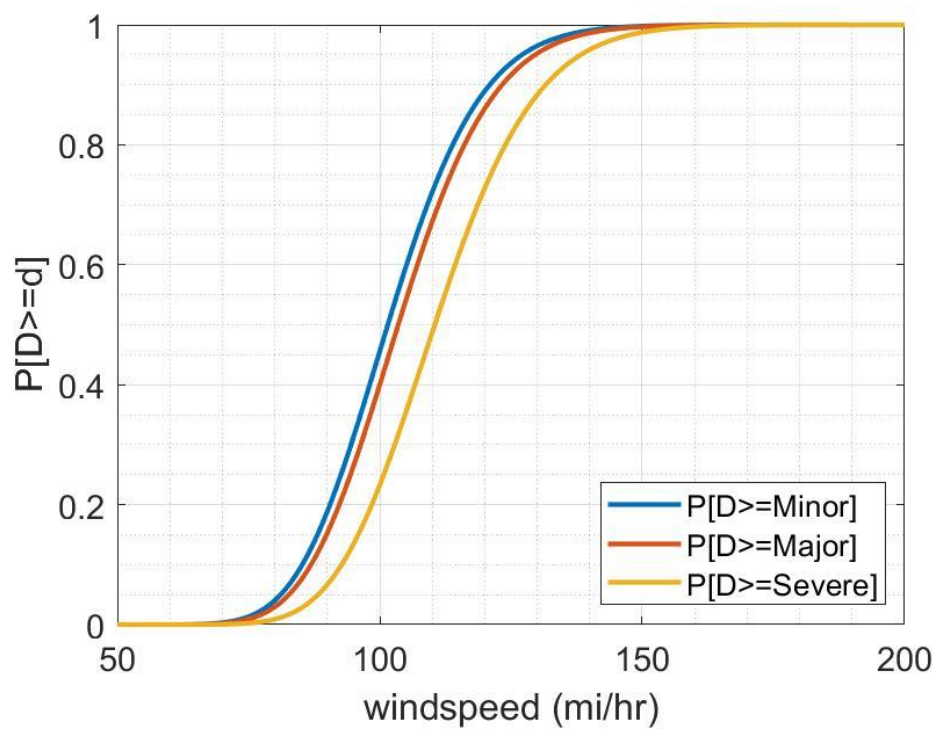


Fig. A.72 Slope (-0.004,0.004)

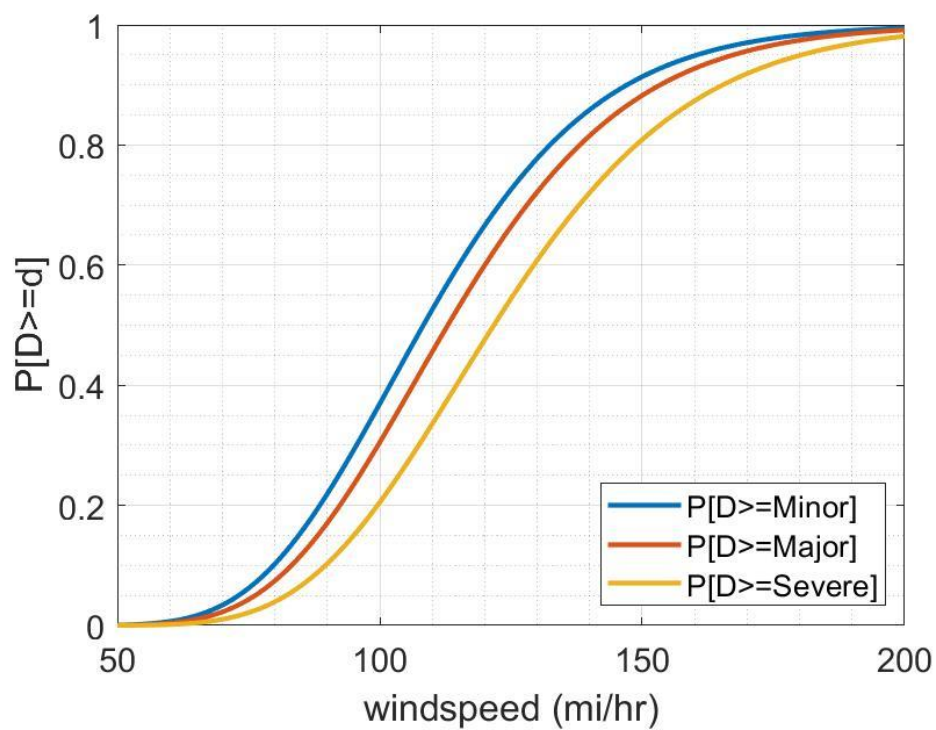


Fig. A.73 Slope (0.004,0.04]

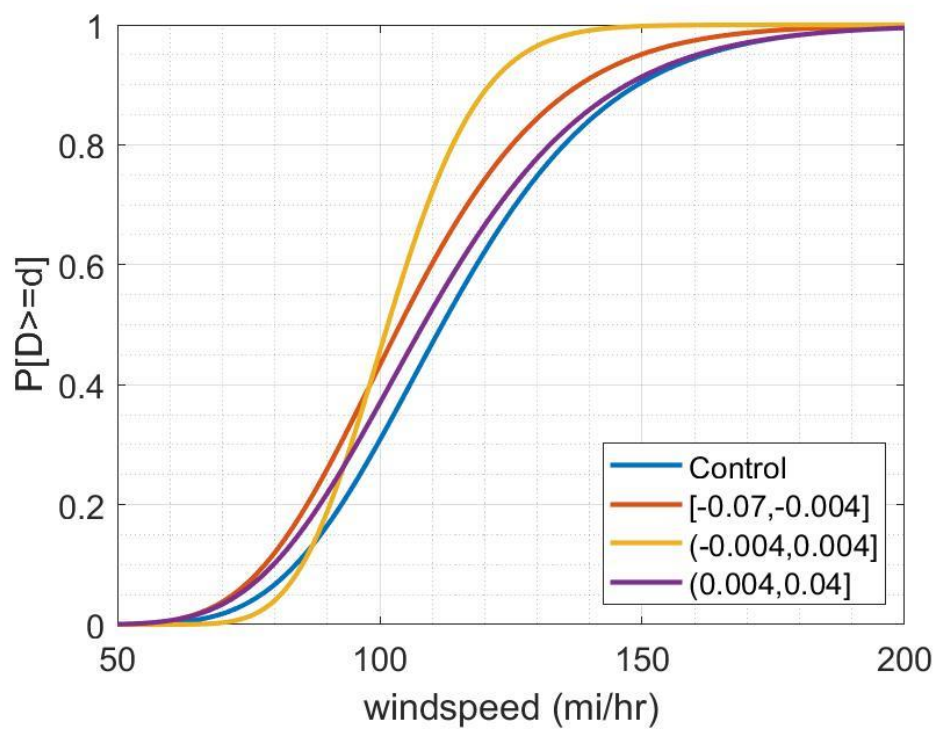


Fig. A.74 Slope, Minor

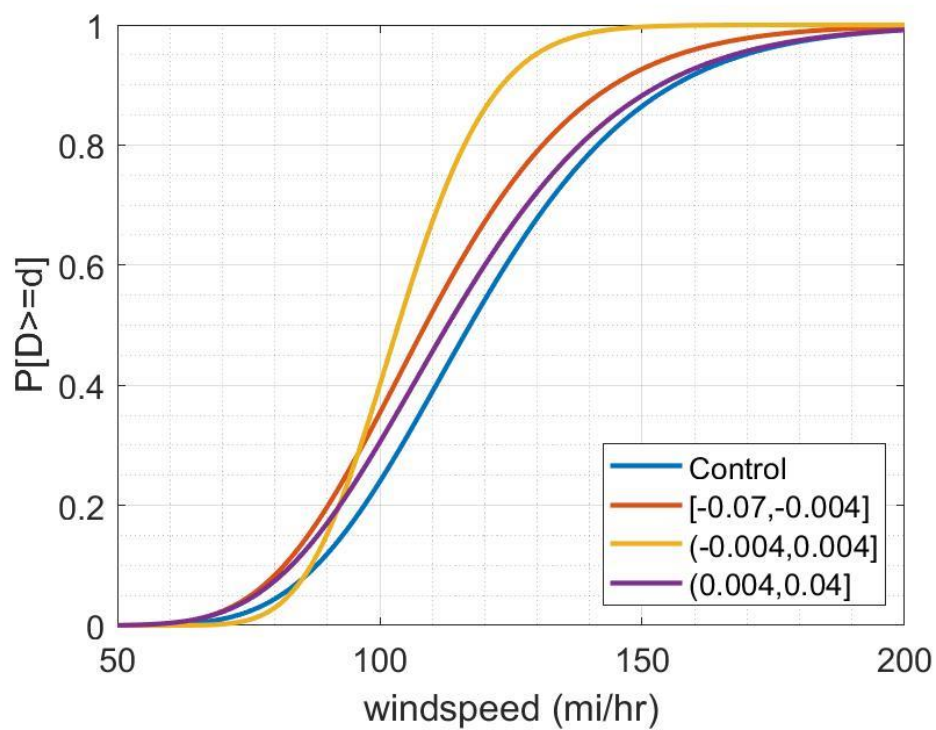


Fig. A.75 Slope, Major

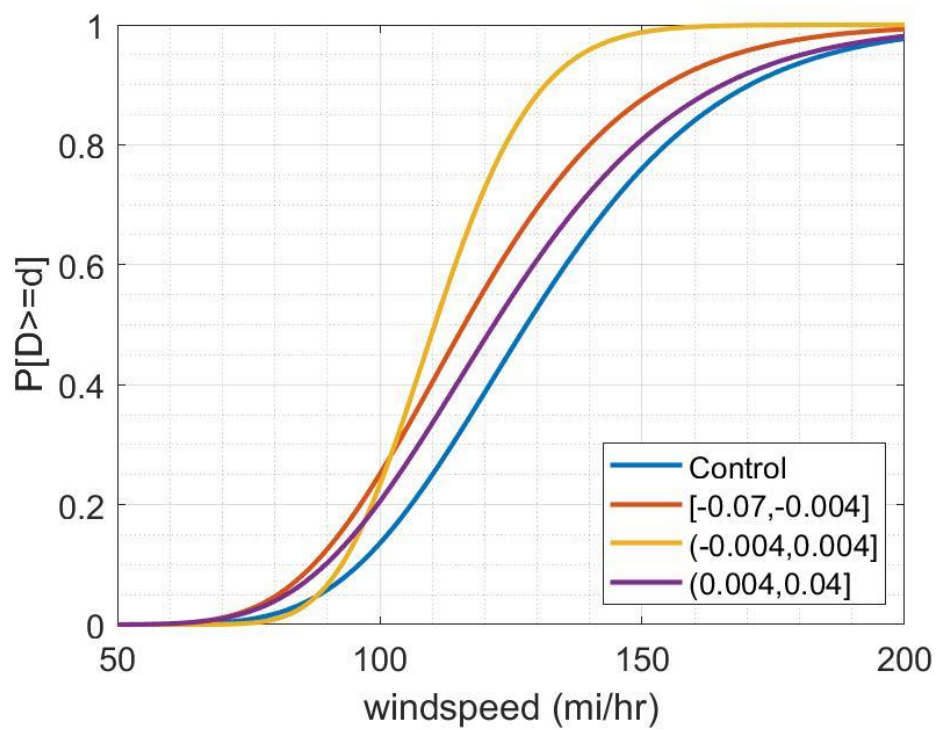


Fig. A.76 Slope, Severe

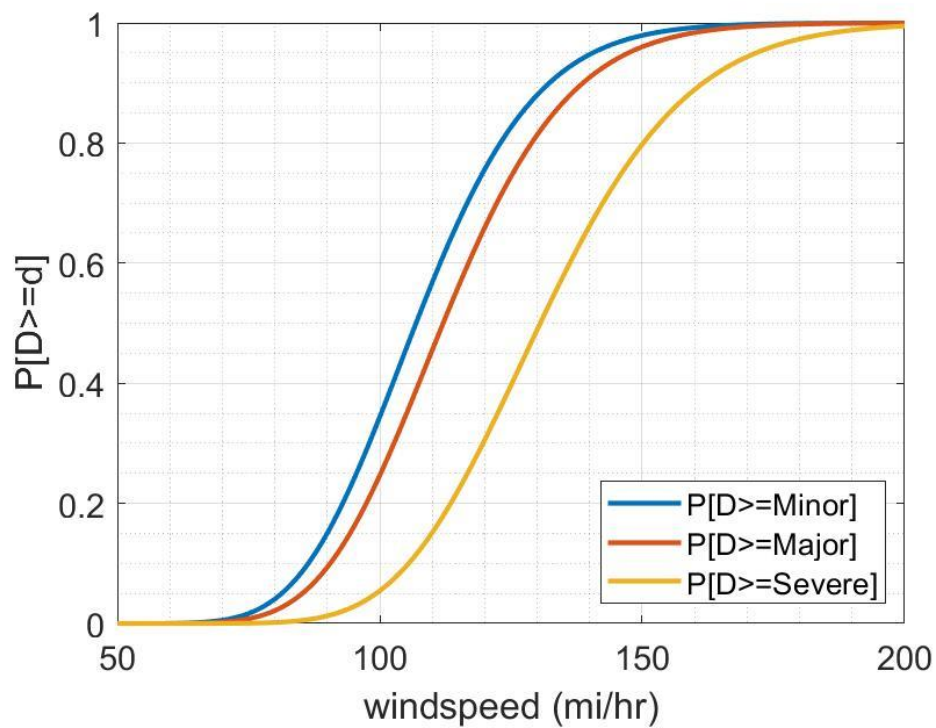


Fig. A.77 Diameter (25,35] ft and Grouped

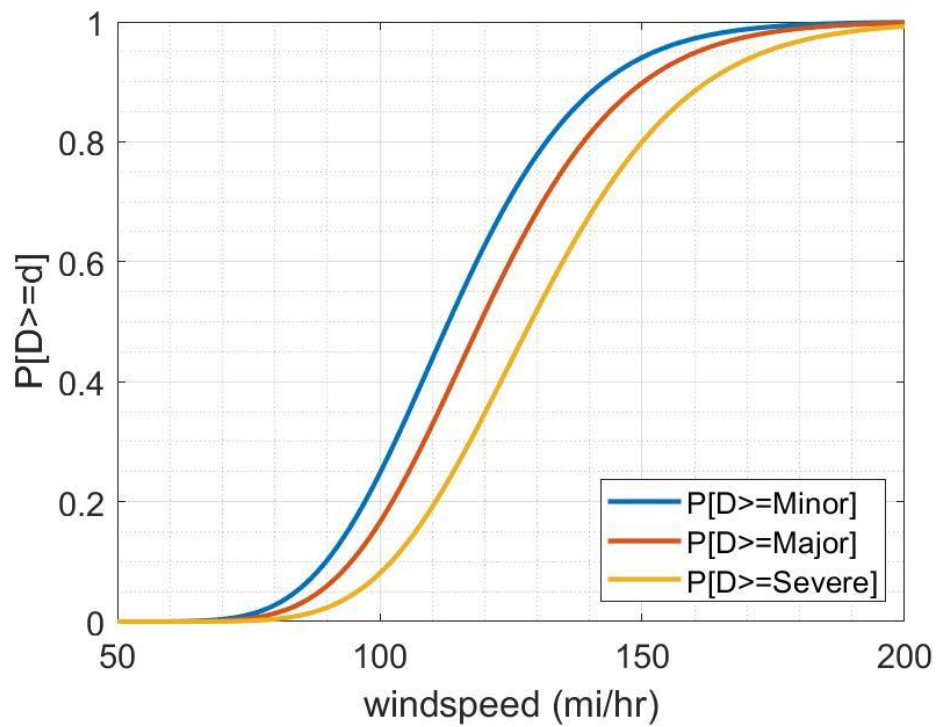


Fig. A.78 Diameter (25,35] ft and Ungrouped

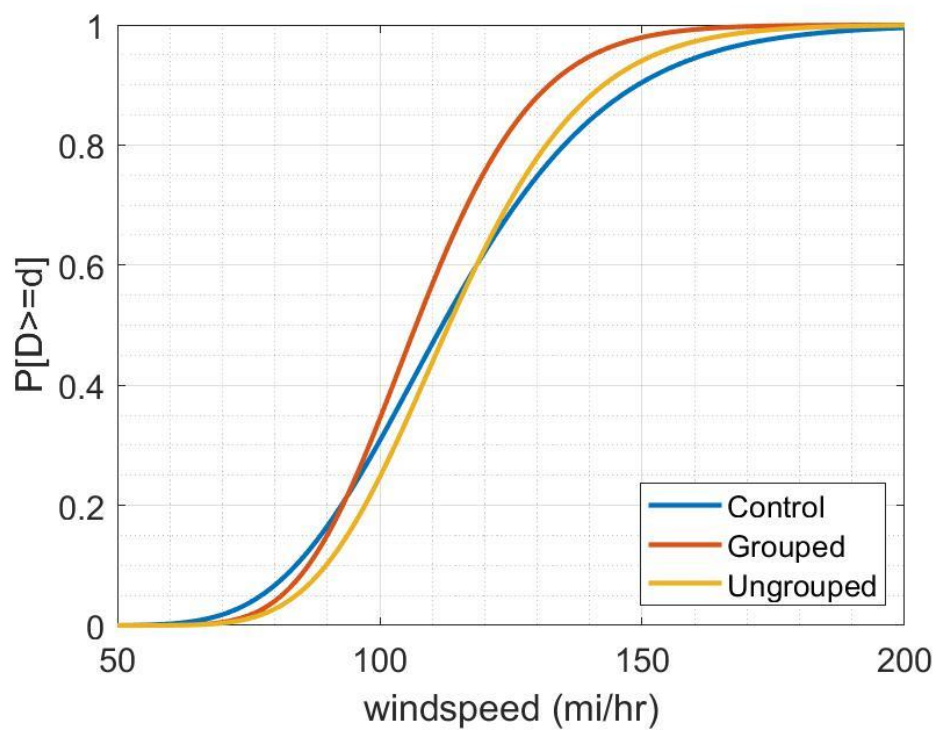


Fig. A.79 Diameter (25,35] ft and Grouped-Ungrouped, Minor

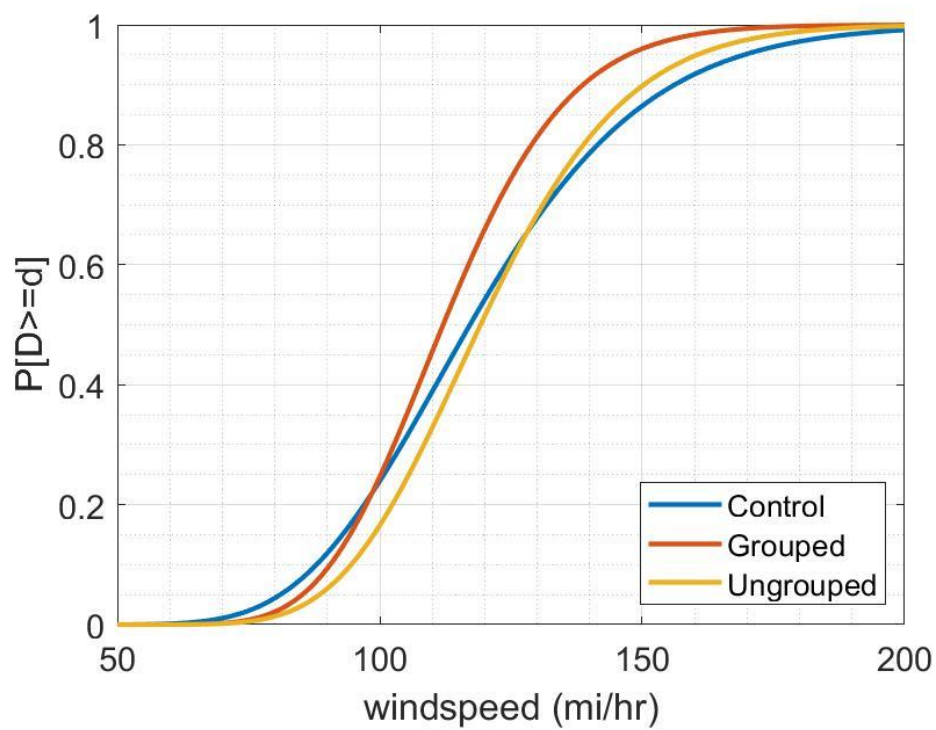


Fig. A.80 Diameter (25,35] ft and Grouped-Ungrouped, Major

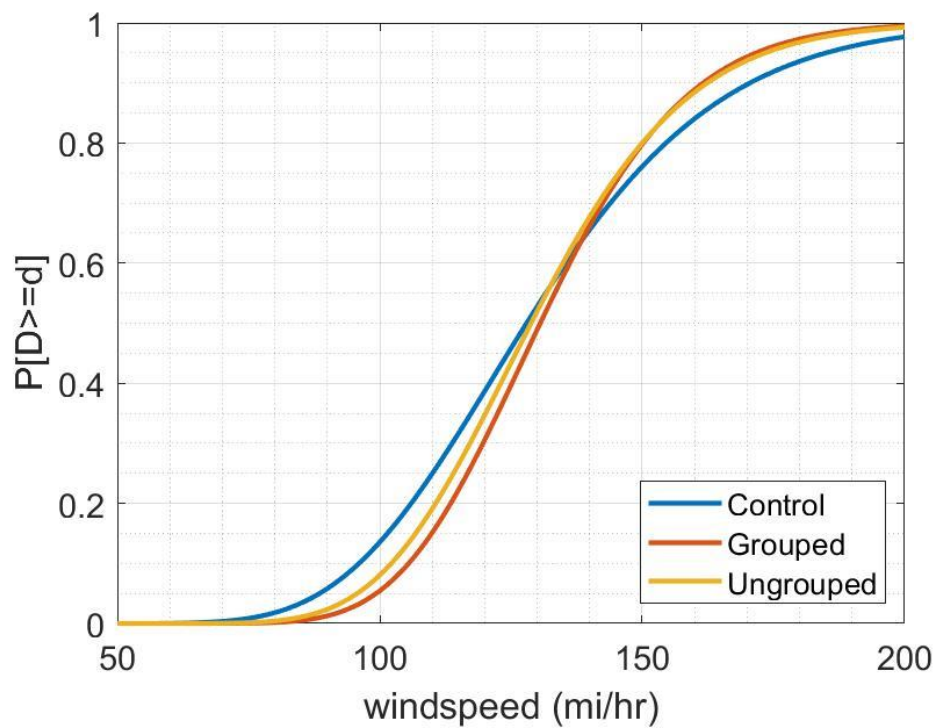


Fig. A.81 Diameter (25,35] ft and Grouped-Ungrouped, Severe

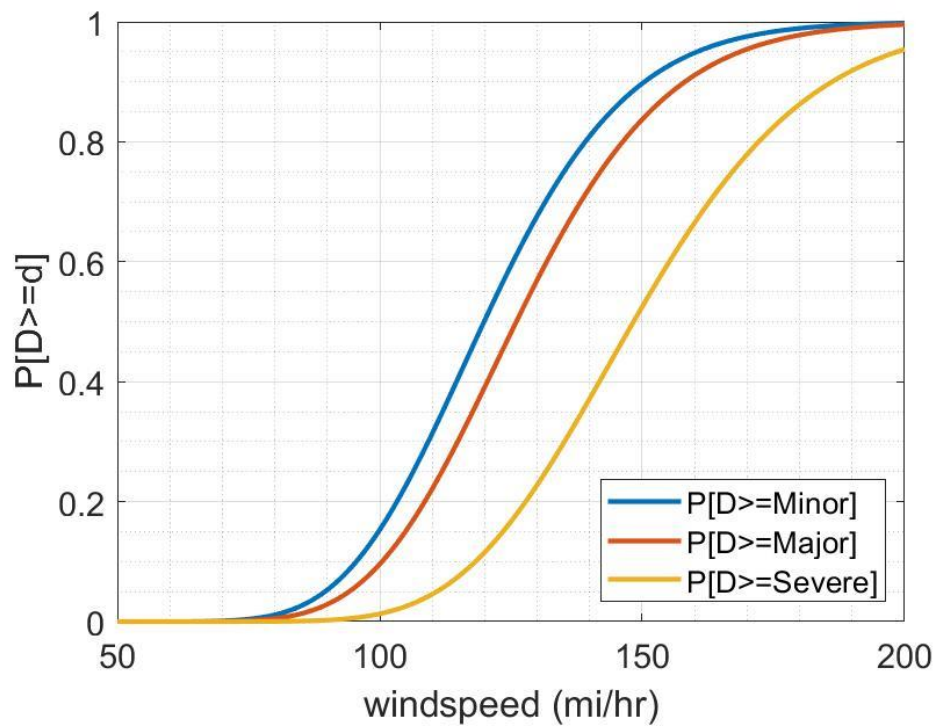


Fig. A.82 Diameter [0,25] ft and Condition-Poor

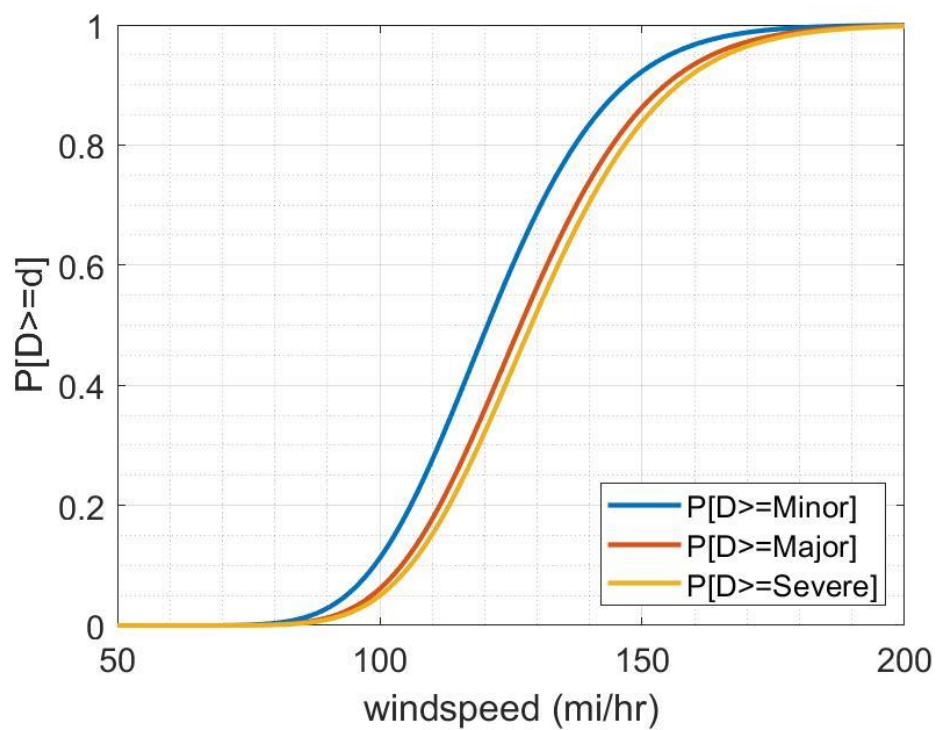


Fig. A.83 Diameter [0,25] ft and Condition-Good

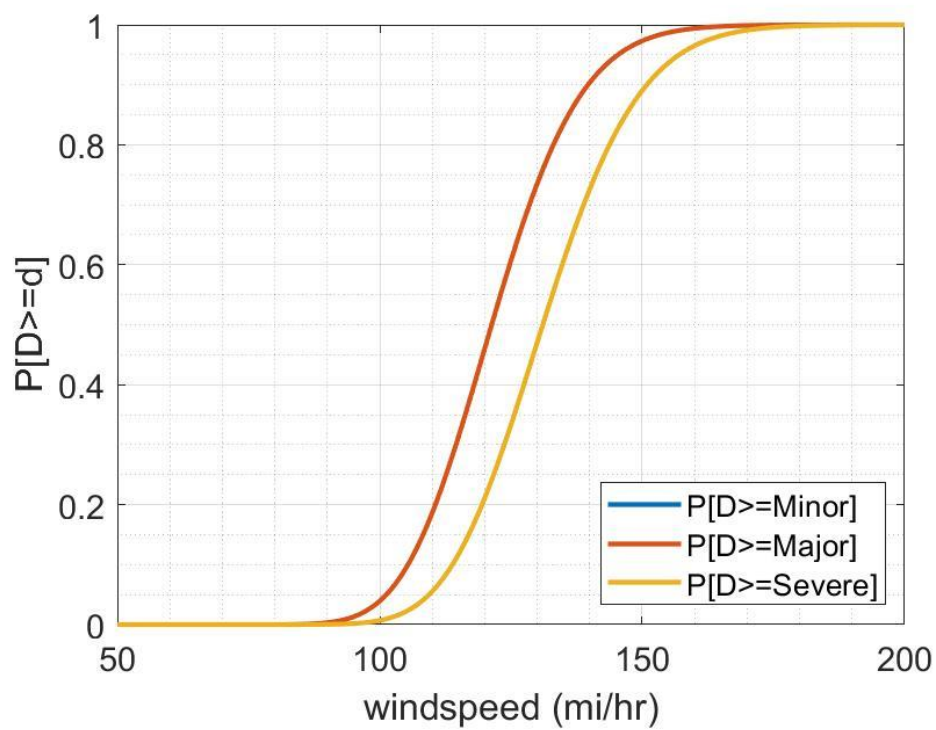


Fig. A.84 Diameter (25,35] ft and Condition-Poor

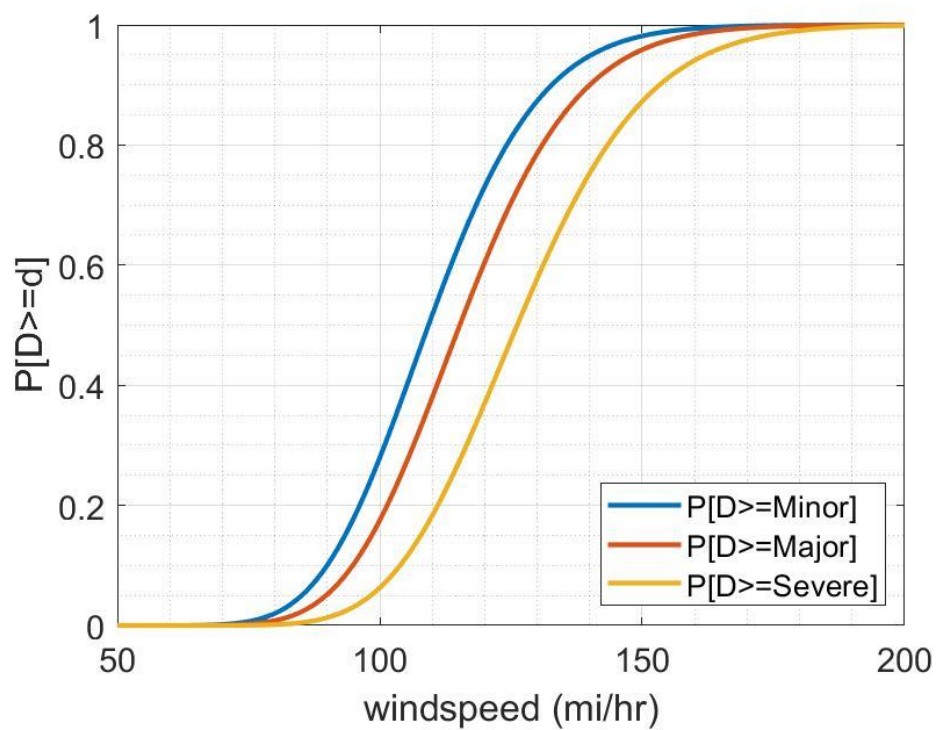


Fig. A.85 Diameter (25,35] ft and Condition-Good

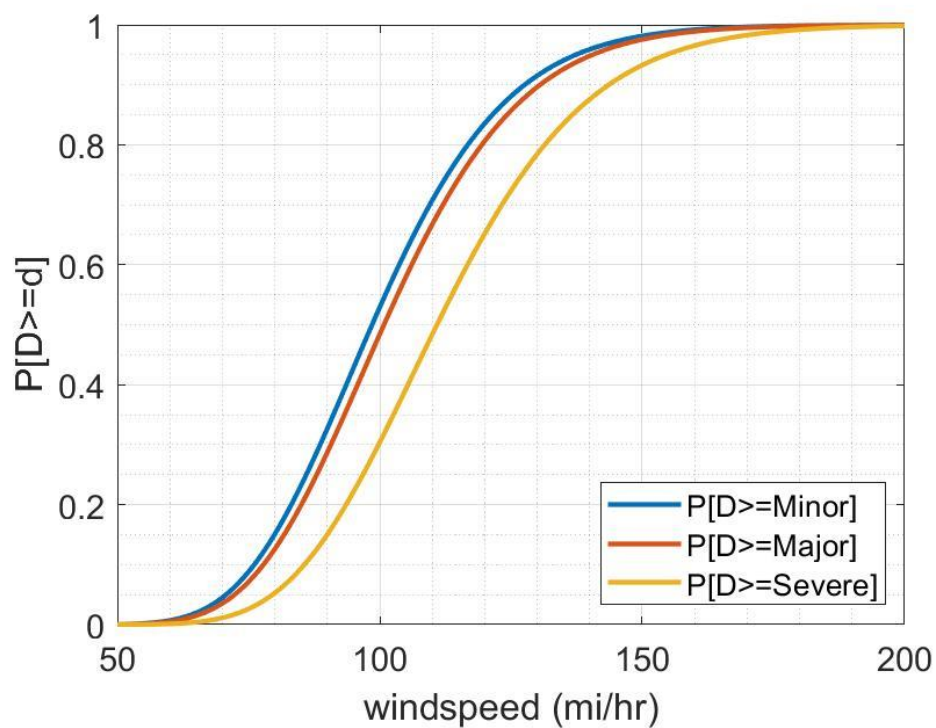


Fig. A.86 Diameter (35,135] ft and Condition-Good

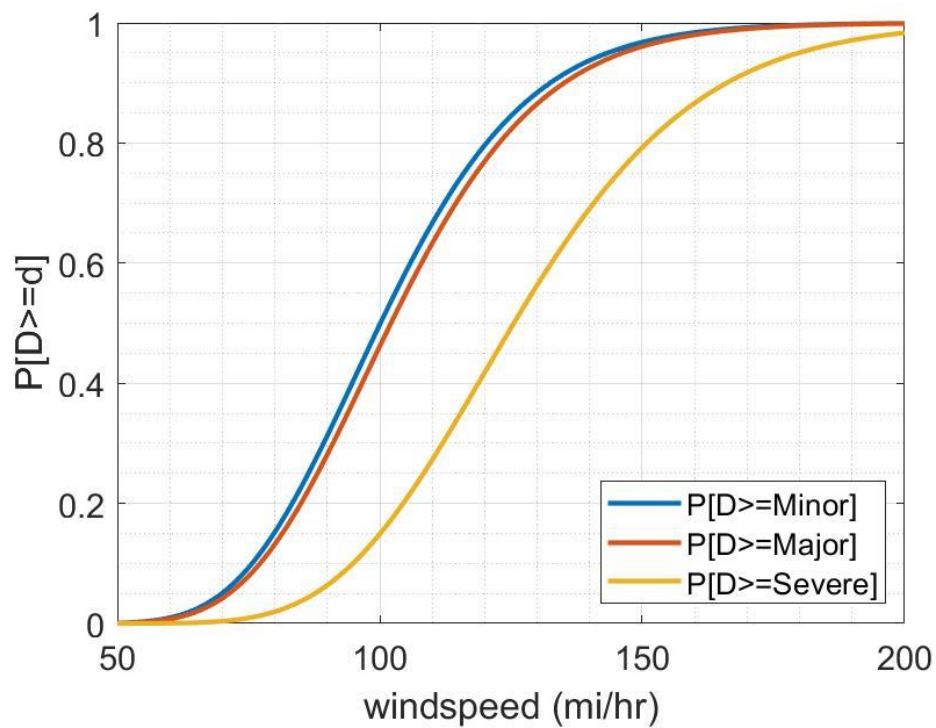


Fig. A.87 Diameter (35,135] ft and Condition-New

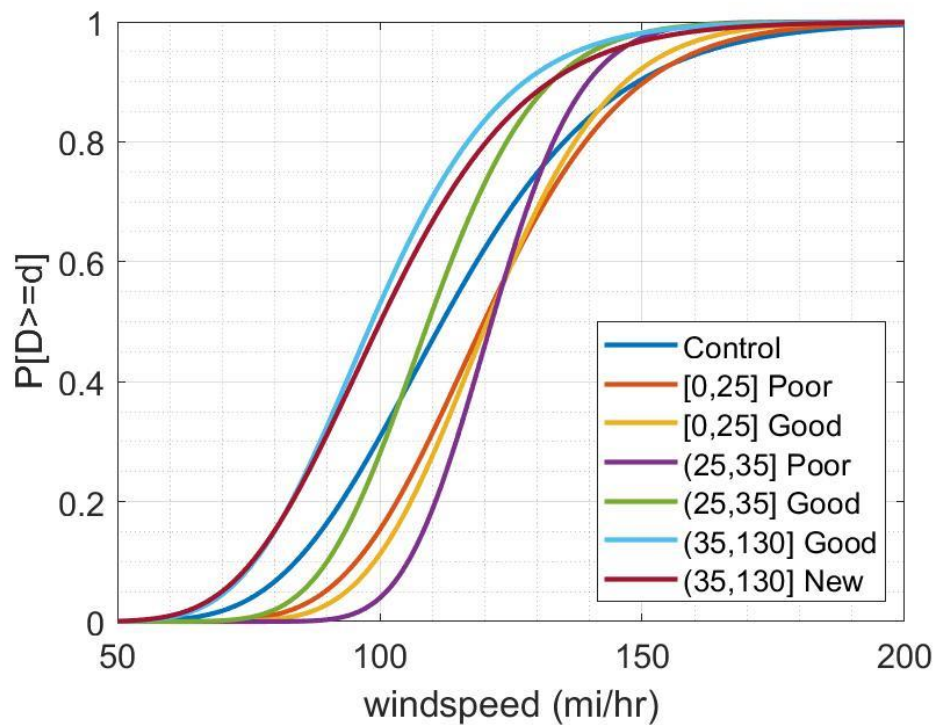


Fig. A.88 Diameter and Condition, Minor

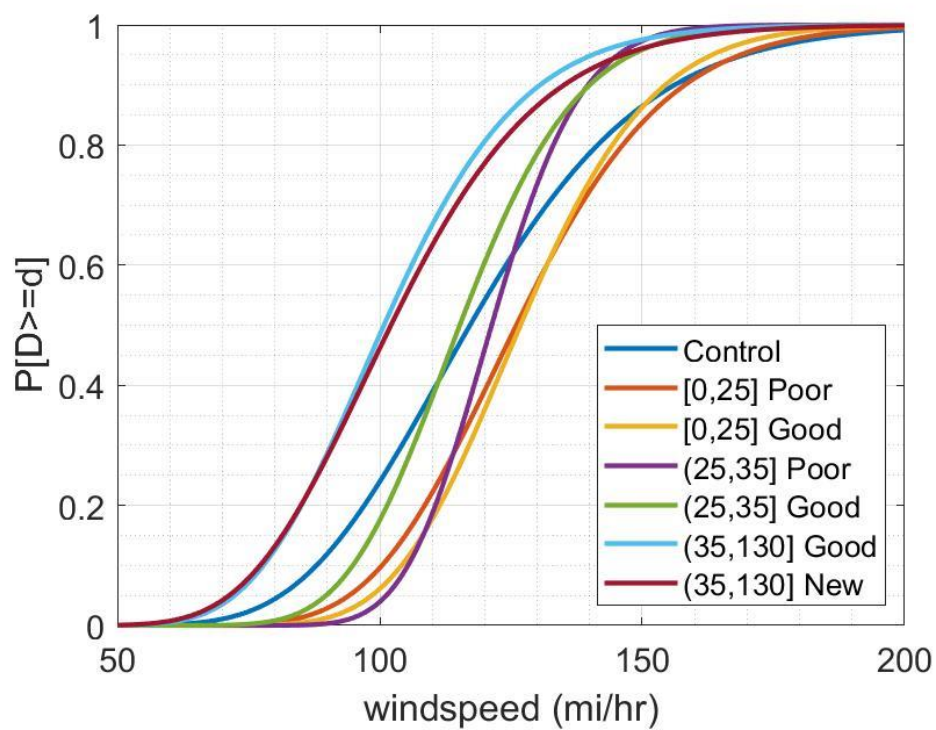


Fig. A.89 Diameter and Condition, Major

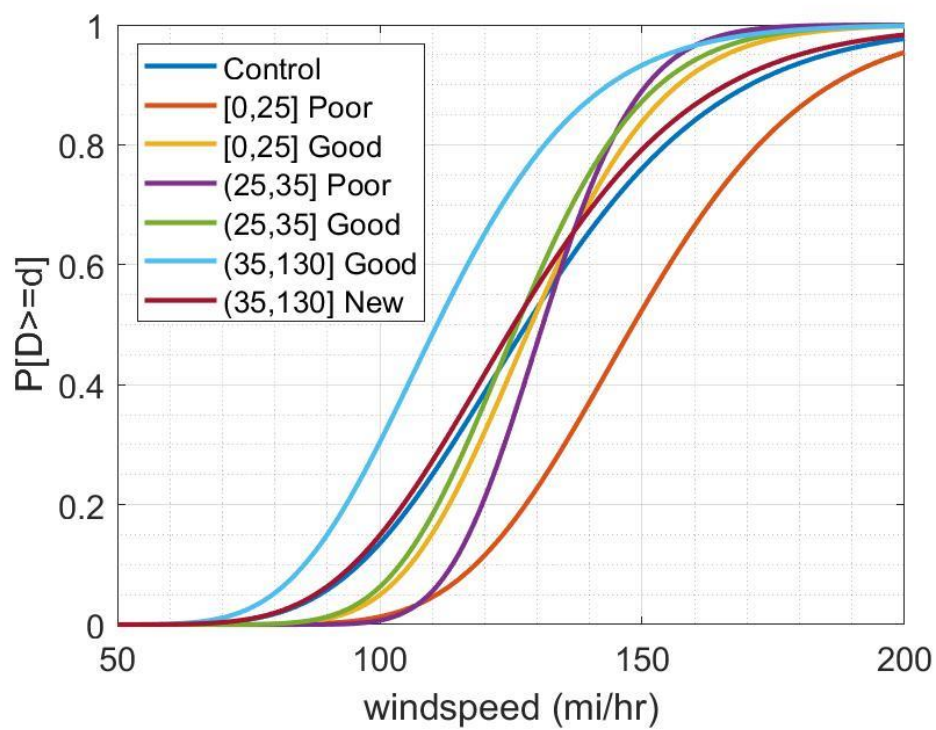


Fig. A.90 Diameter and Condition, Severe

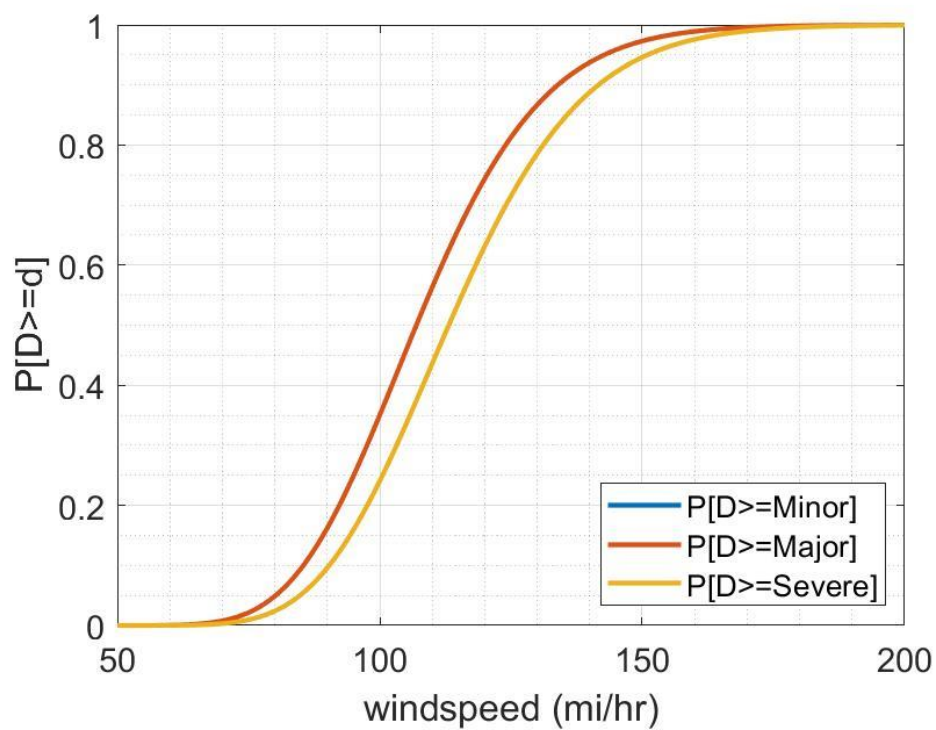


Fig. A.91 Diameter (30,45] ft and Stiffened

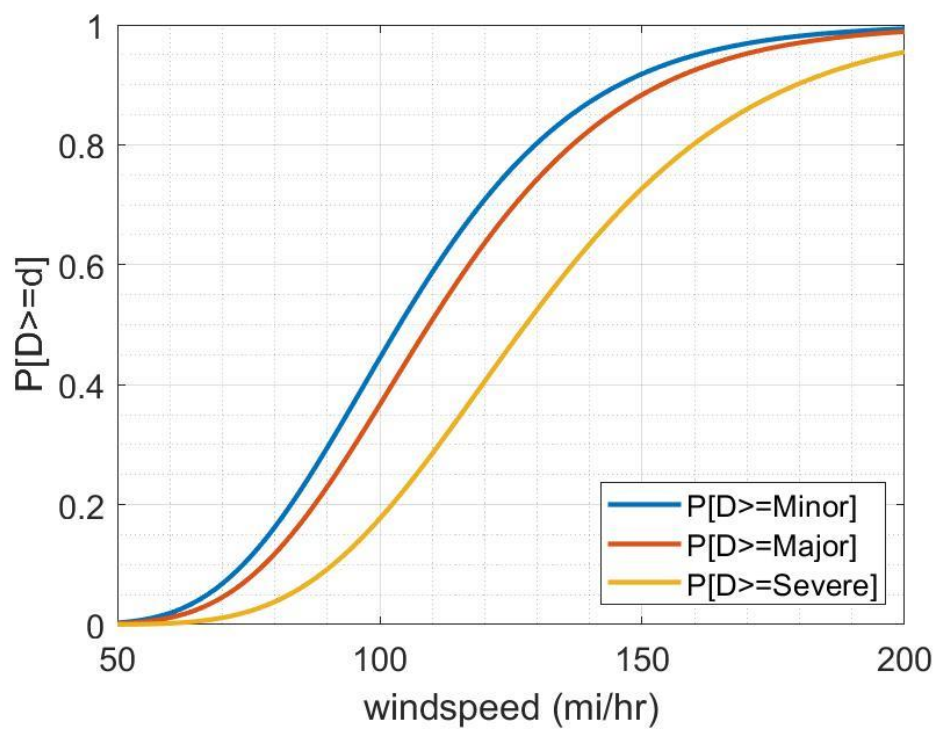


Fig. A.92 Diameter (30,45] ft and Unstiffened

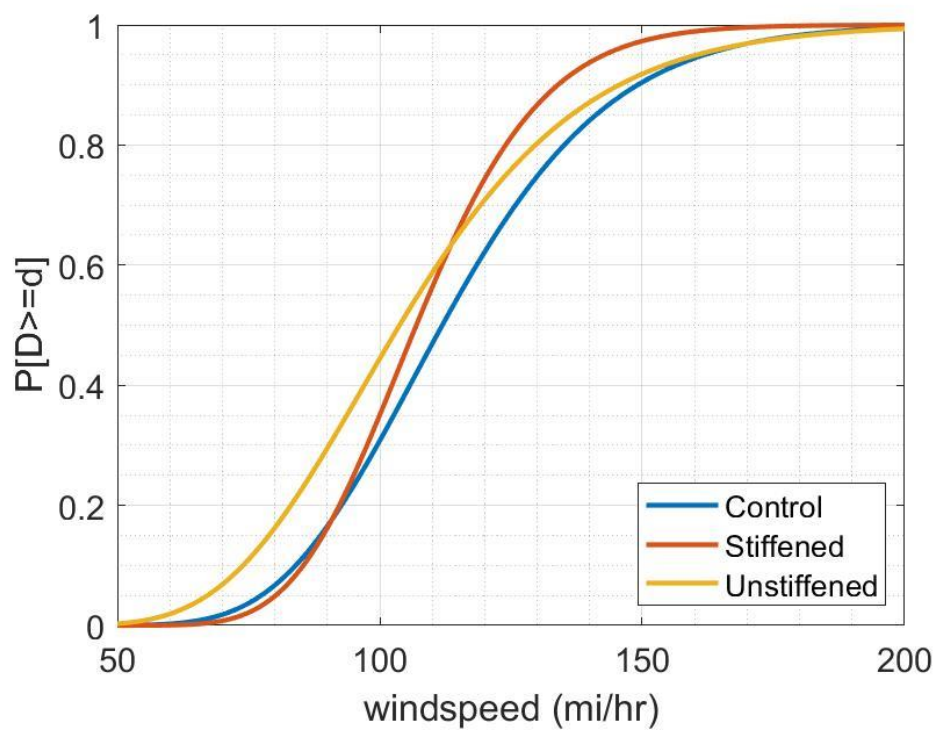


Fig. A.93 Diameter (30,45] ft and Stiffened-Unstiffened, Minor

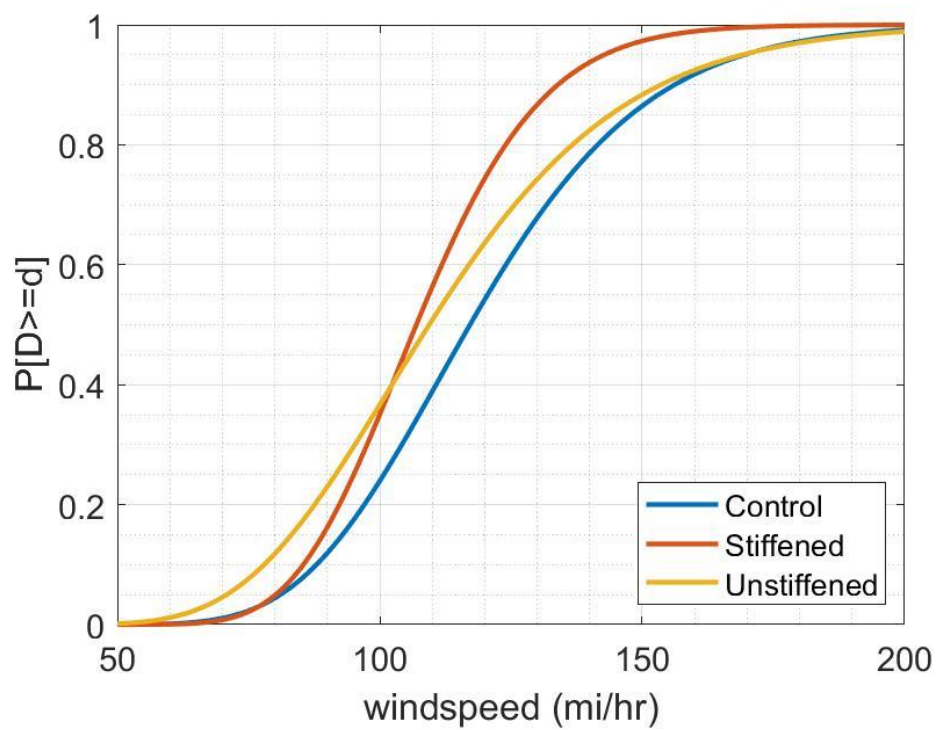


Fig. A.94 Diameter (30,45] ft and Stiffened-Unstiffened, Major

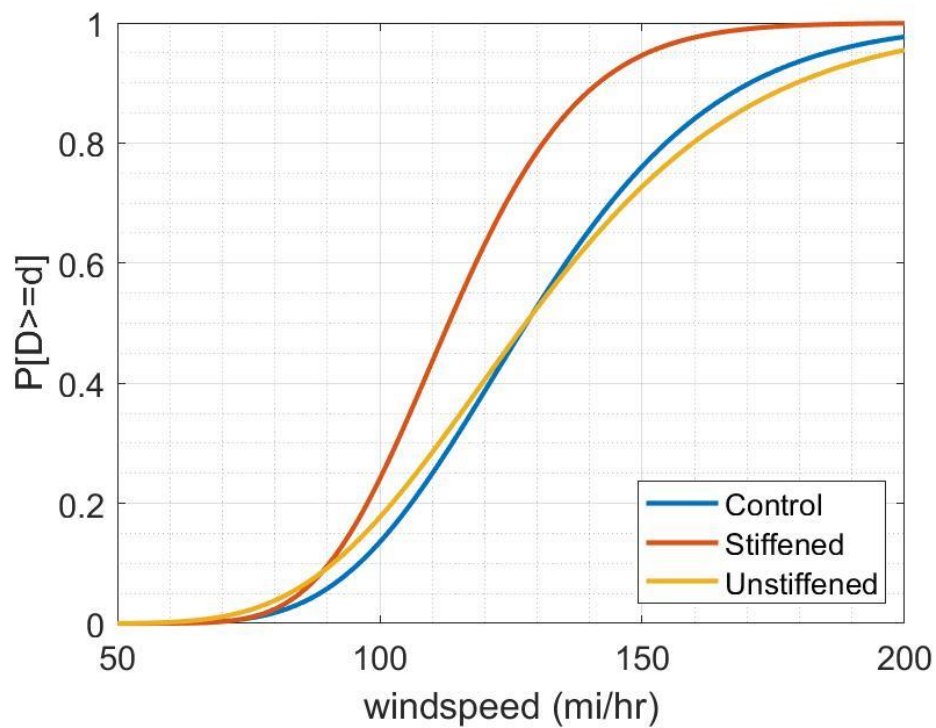


Fig. A.95 Diameter (30,45] ft and Stiffened-Unstiffened, Severe

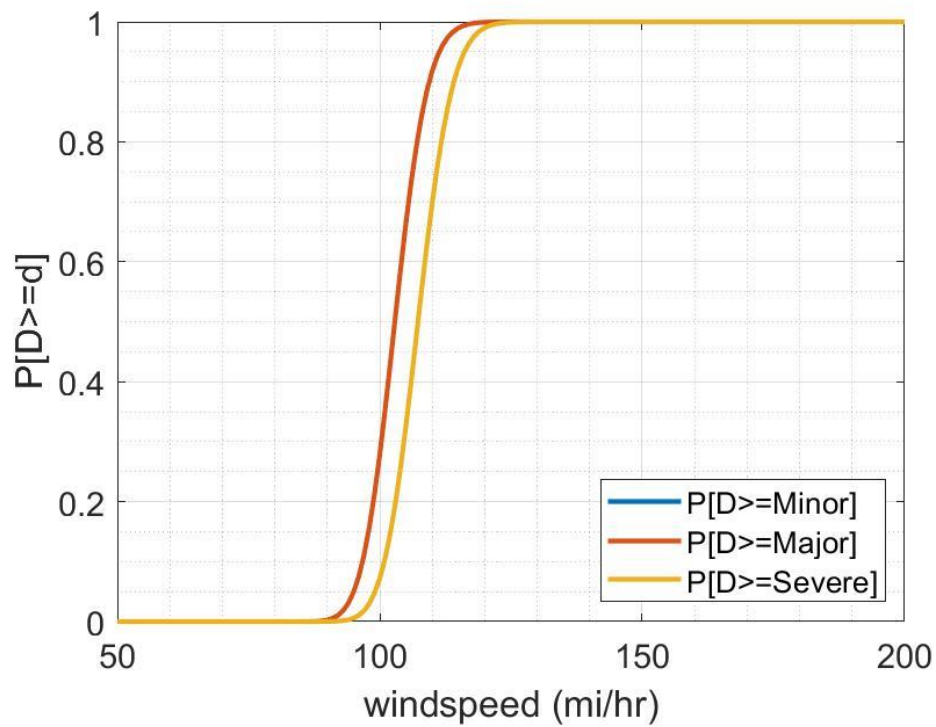


Fig. A.96 Diameter (30,45] ft and Wind Rings

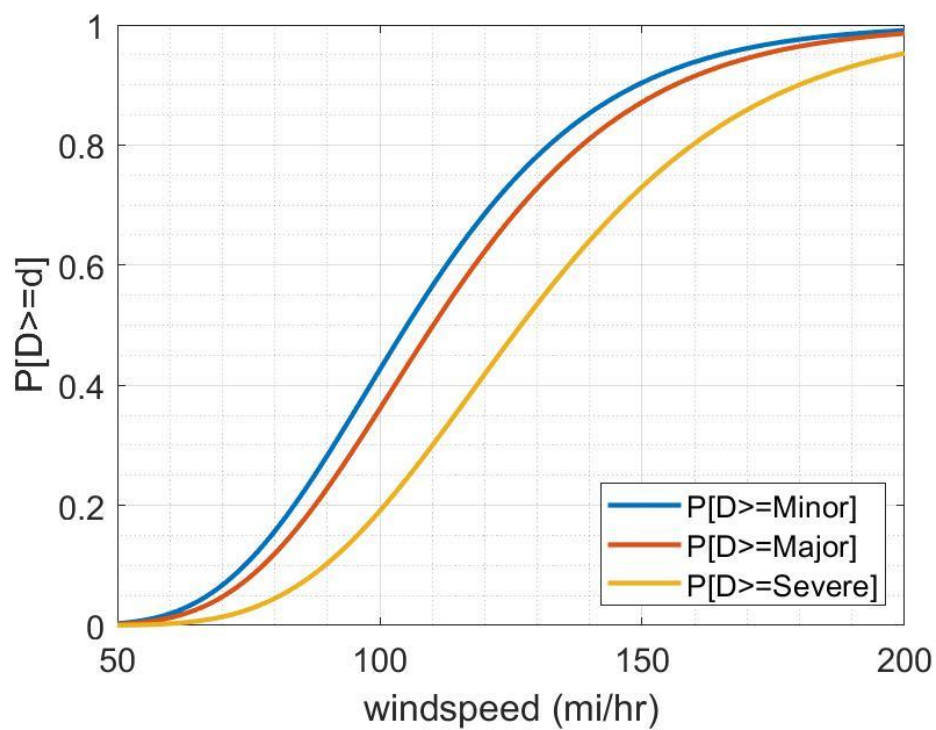


Fig. A.97 Diameter (30,45] ft and No Wind Rings

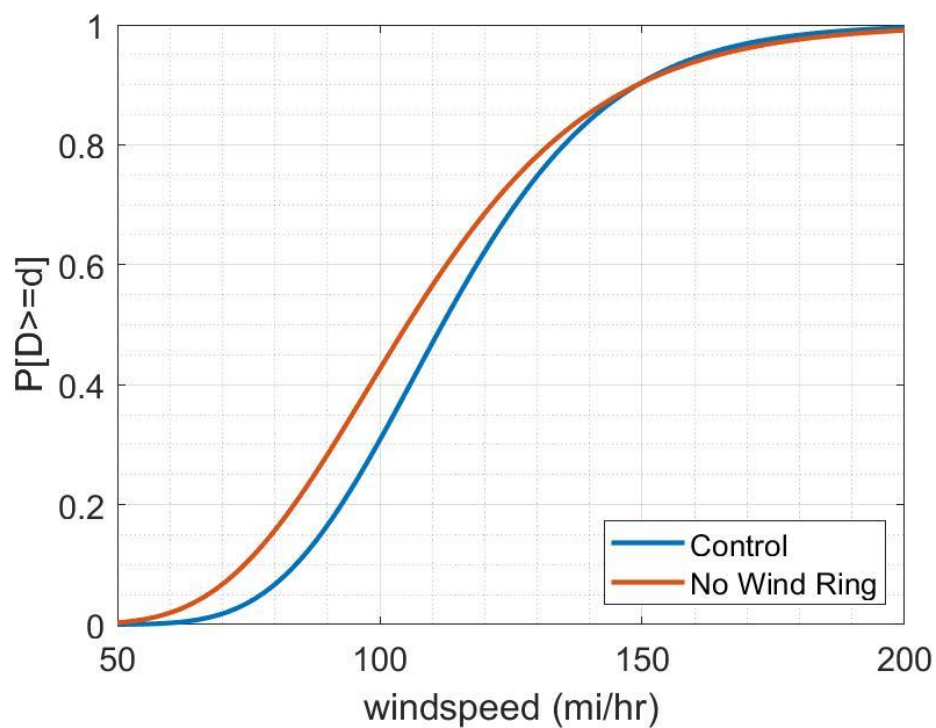


Fig. A.98 Diameter (30,45] ft and Wind Rings, Minor

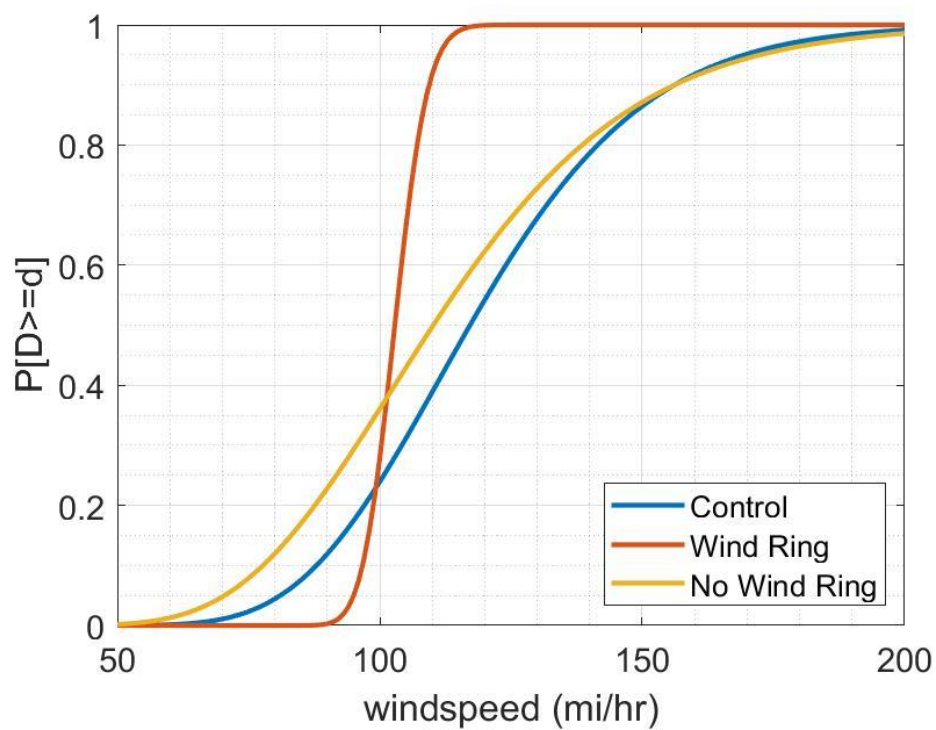


Fig. A.99 Diameter (30,45] ft and Wind Rings, Major

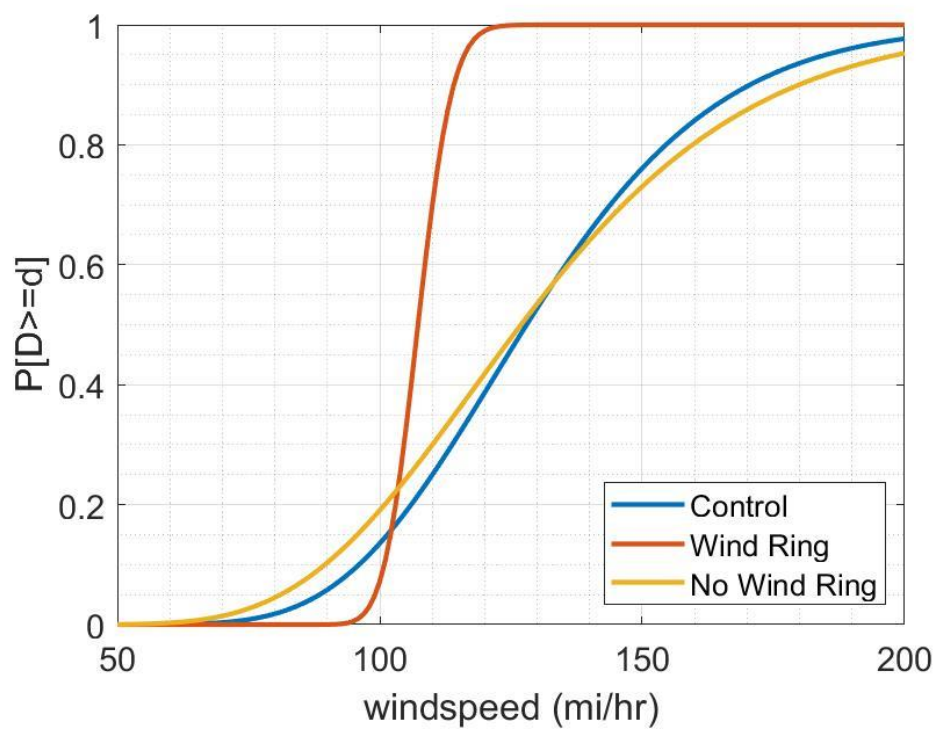


Fig. A.100 Diameter (30,45] ft and Wind Rings, Severe

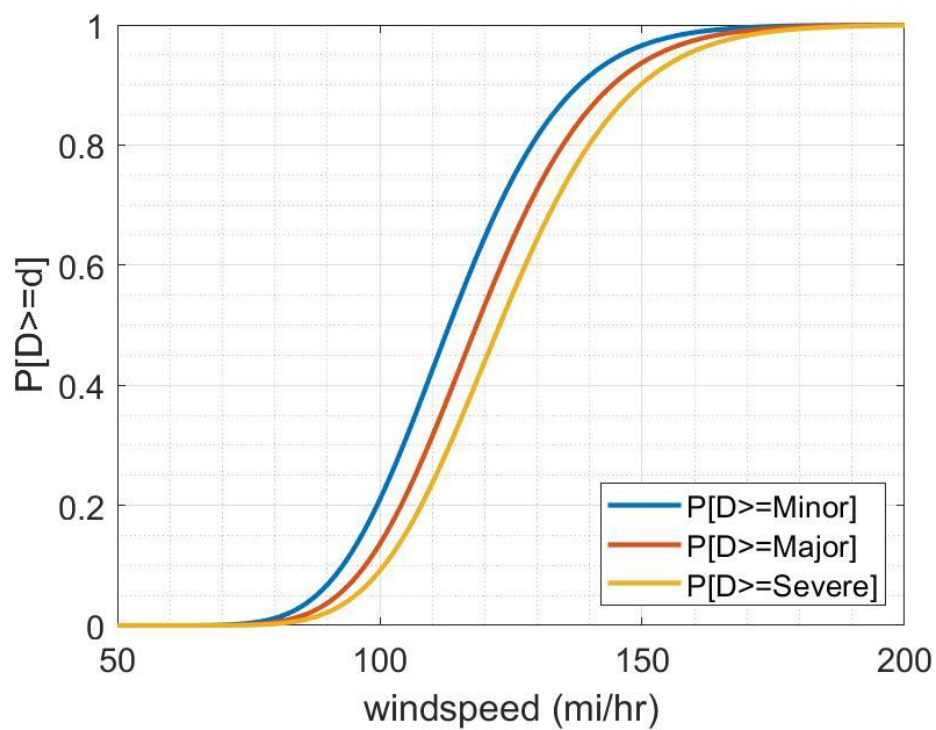


Fig. A.101 Diameter [0,25] ft and Terrain-Open

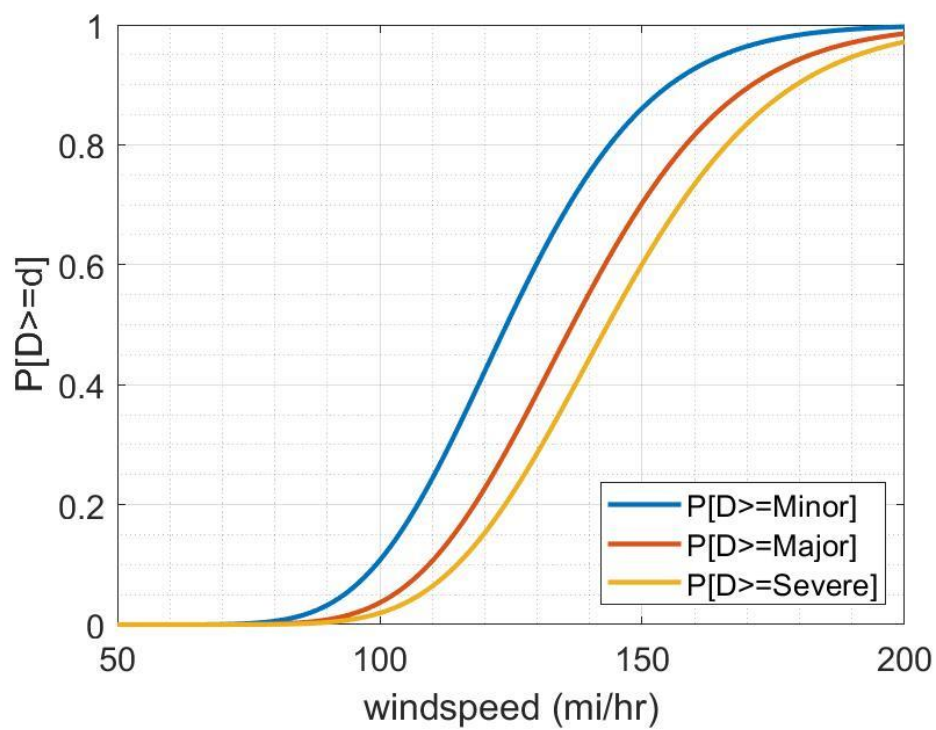


Fig. A.102 Diameter [0,25] ft and Terrain-Trees & Buildings

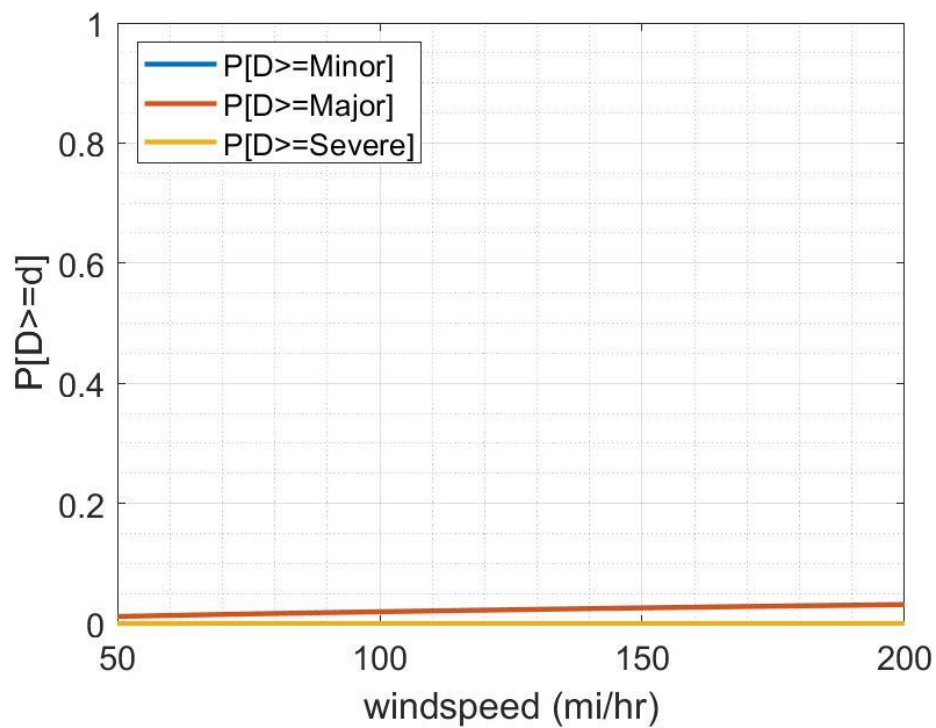


Fig. A.103 Diameter [0,25] ft and Terrain-In Town

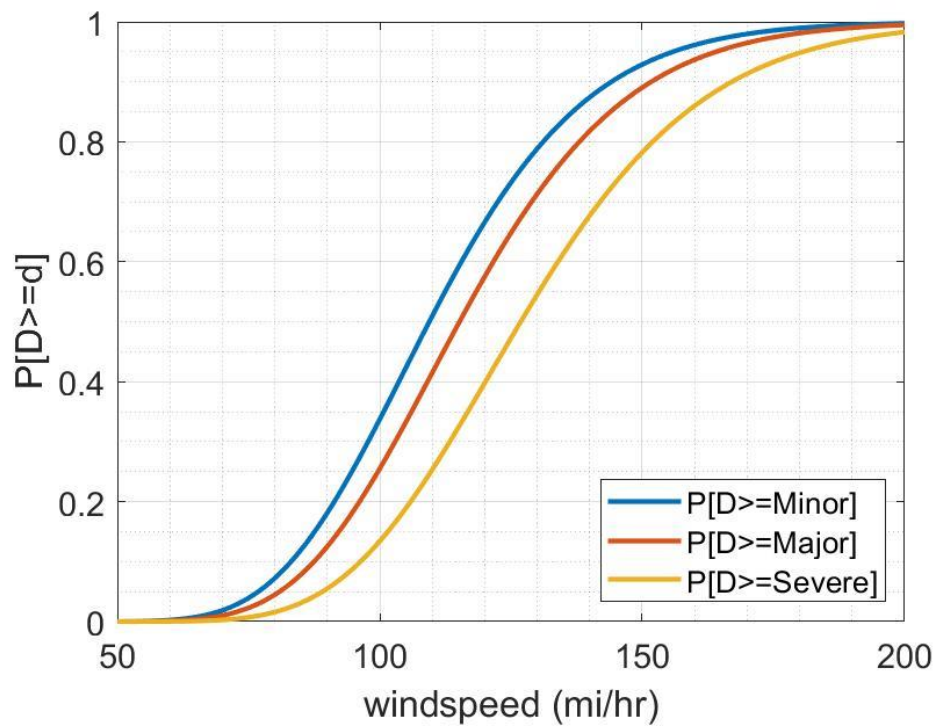


Fig. A.104 Diameter (25,35] ft and Terrain-Open

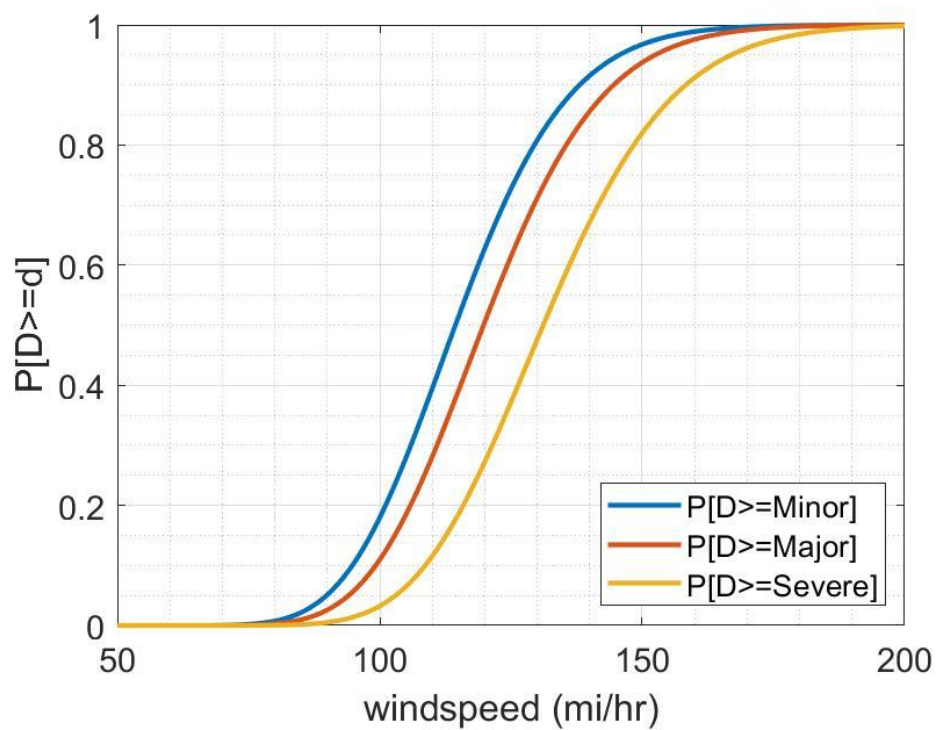


Fig. A.105 Diameter (25,35] ft and Terrain-Trees & Buildings

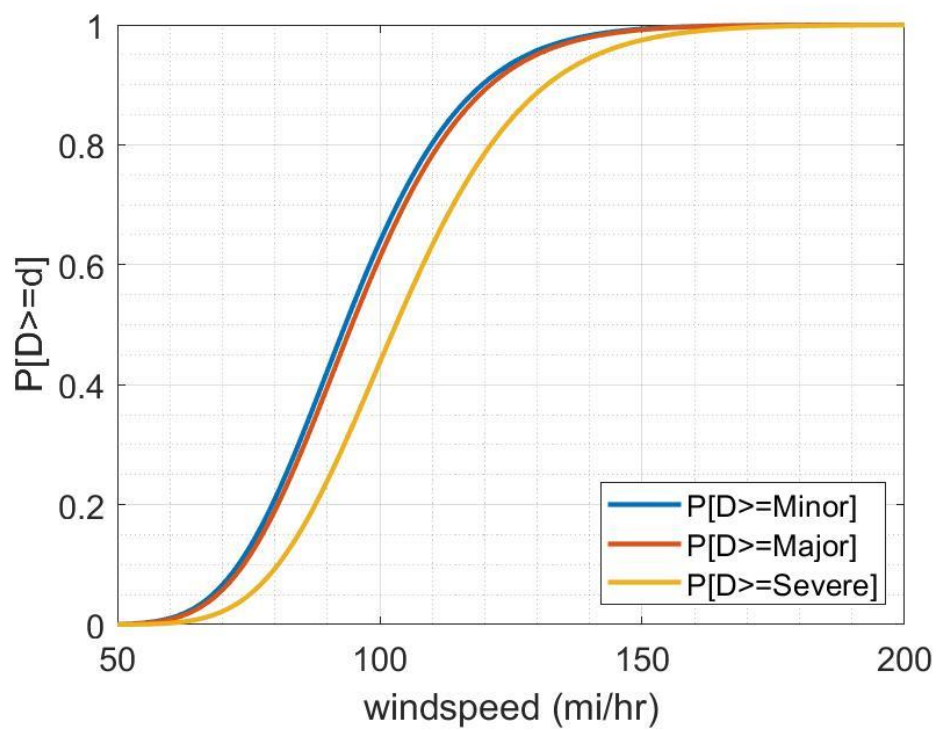


Fig. A.106 Diameter (35,130] ft and Terrain-Open

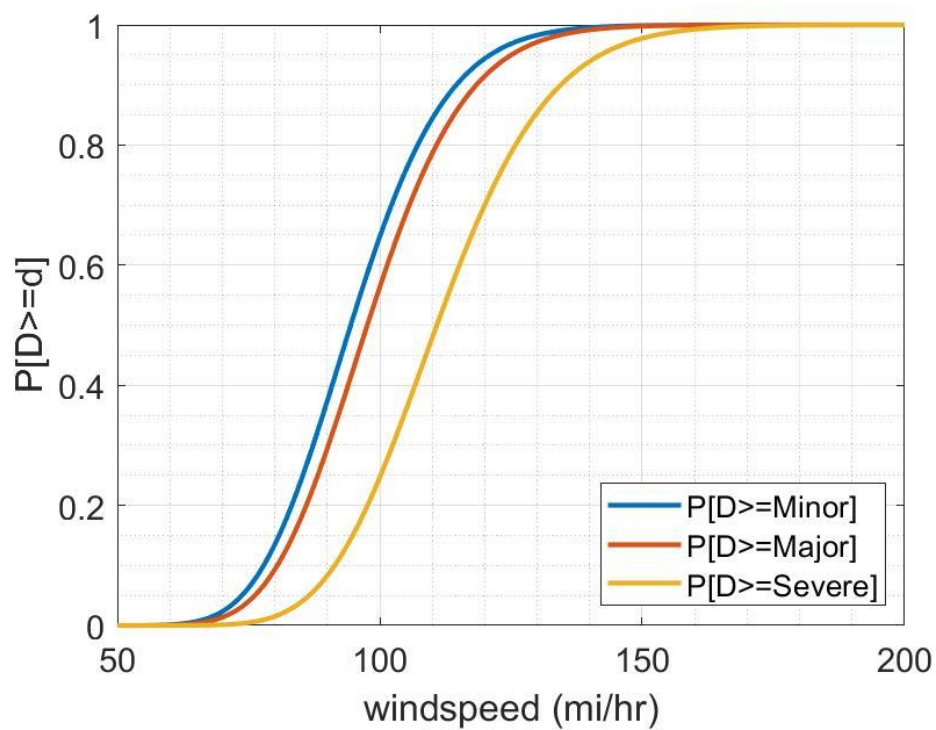


Fig. A.107 Diameter (35,130] ft and Terrain-Trees & Buildings

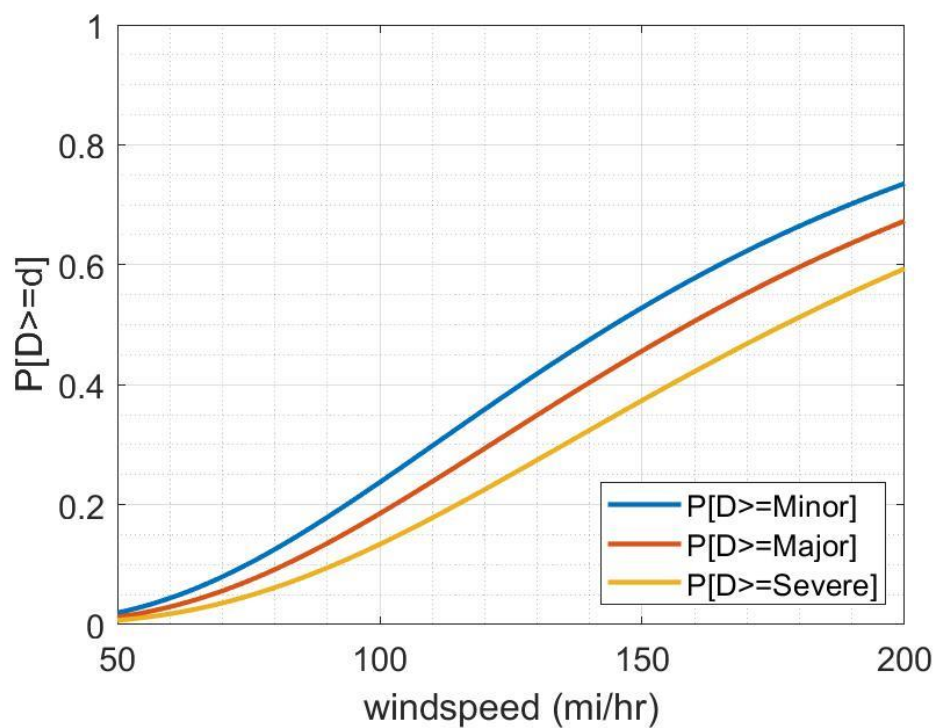


Fig. A.108 Diameter (35,130] ft and Terrain-In Town

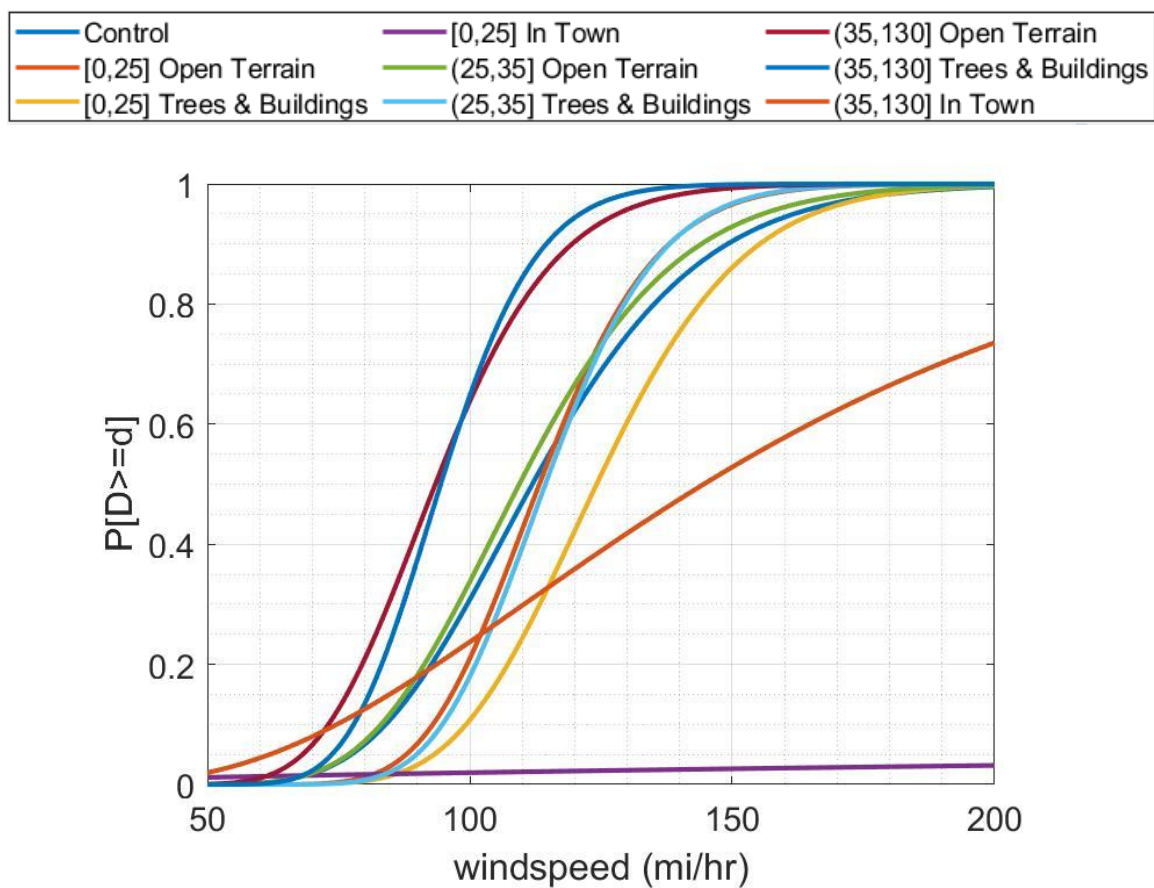


Fig. A.109 Diameter and Terrain, Minor

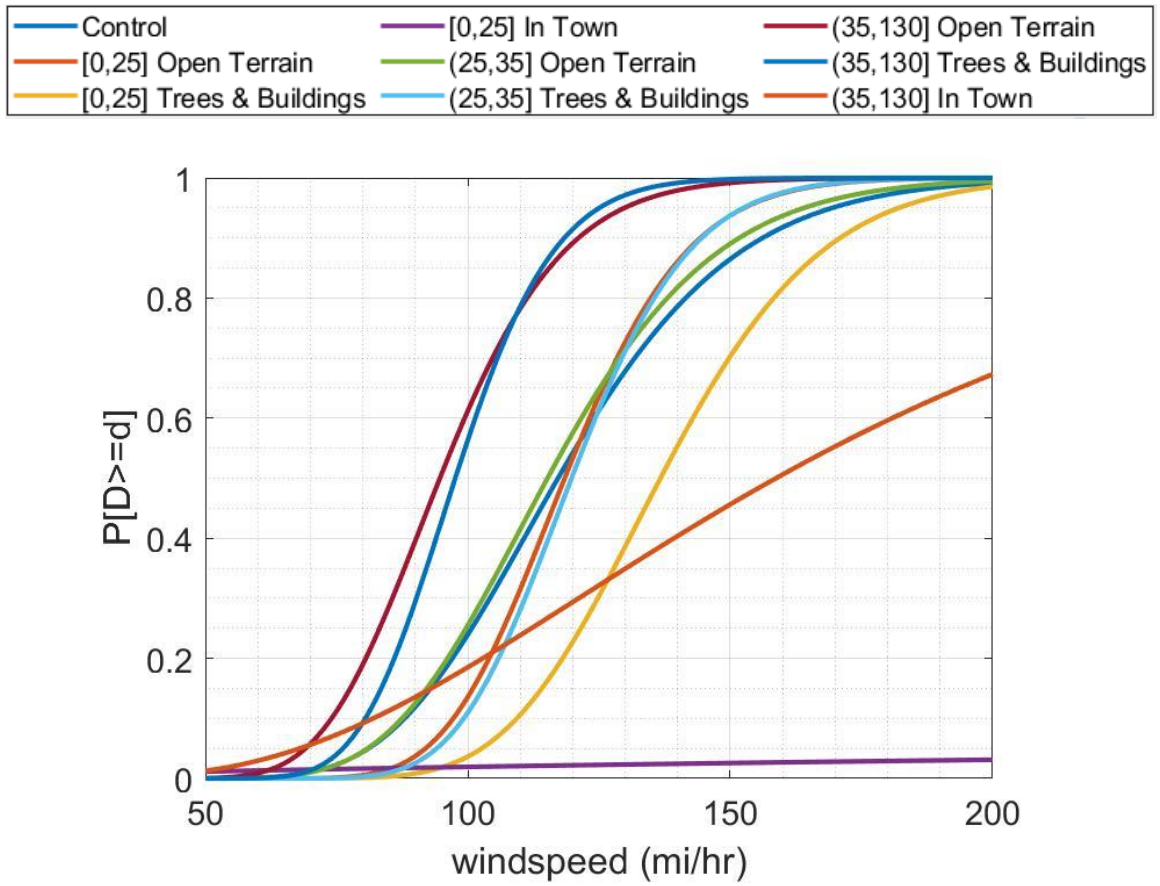


Fig. A.110 Diameter and Terrain, Major

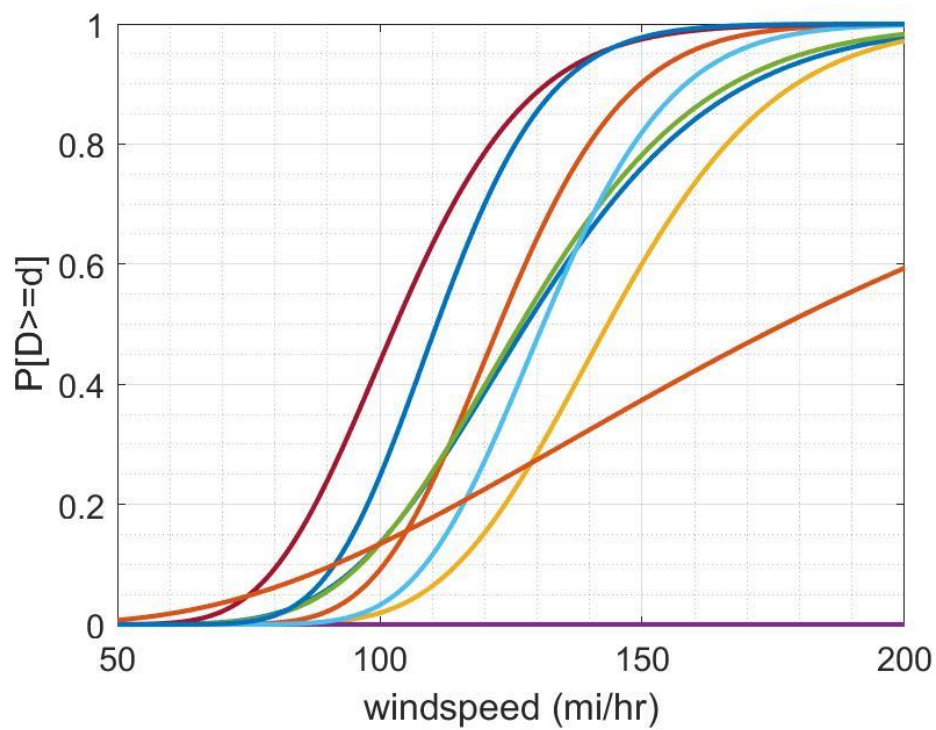
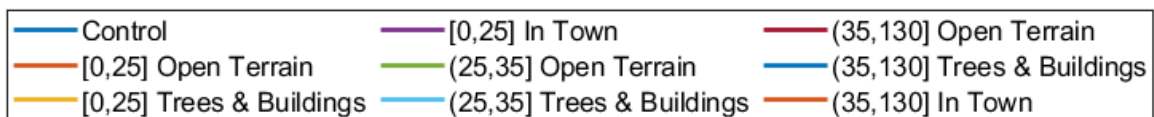


Fig. A.111 Diameter and Terrain, Severe

Appendix B: Buckling Results of FEA

Appendix B contains the force-displacement plots developed by the arc-length method and the resultant displacement plots for all grain bins modelled in the parametric numerical study. Additionally, Figures B1 and B2 illustrate the naming convention used to differentiate between bins in the parametric analysis. For example, the standard bin was D54_H15_S36_R02_W00_V00_CL03_CD03_WT03_ST03.

List of Figures

Fig. B.1 Naming Convention for Parametric Analysis	170
Fig. B.2 Naming convention identifier values	171
Fig. B.3 D18_H15_S00_R00_W00_V00_CL03_CD03_WT03_ST03.....	172
Fig. B.4 D18_H15_S00_R00_W00_V01_CL03_CD03_WT03_ST03.....	173
Fig. B.5 D18_H15_S00_R00_W01_V00_CL03_CD03_WT03_ST03.....	174
Fig. B.6 D18_H15_S00_R00_W01_V01_CL03_CD03_WT03_ST03.....	175
Fig. B.7 D18_H15_S12_R00_W00_V00_CL03_CD03_WT03_ST03.....	176
Fig. B.8 D18_H15_S12_R00_W00_V01_CL03_CD03_WT03_ST03.....	177
Fig. B.9 D18_H15_S12_R00_W01_V00_CL03_CD03_WT03_ST03.....	178
Fig. B.10 D18_H15_S12_R00_W01_V01_CL03_CD03_WT03_ST03.....	179
Fig. B.11 D18_H15_S12_R02_W00_V00_CL03_CD03_WT03_ST03.....	180
Fig. B.12 D18_H15_S12_R02_W00_V01_CL03_CD03_WT03_ST03.....	181
Fig. B.13 D18_H15_S12_R02_W01_V00_CL03_CD03_WT03_ST03.....	182
Fig. B.14 D18_H15_S12_R02_W01_V01_CL03_CD03_WT03_ST03.....	183
Fig. B.15 D30_H15_S00_R00_W00_V00_CL03_CD03_WT03_ST03.....	184

Fig. B.16 D30_H15_S00_R00_W00_V01_CL03_CD03_WT03_ST03.....	185
Fig. B.17 D30_H15_S00_R00_W01_V00_CL03_CD03_WT03_ST03.....	186
Fig. B.18 D30_H15_S00_R00_W01_V01_CL03_CD03_WT03_ST03.....	187
Fig. B.19 D30_H15_S20_R00_W00_V00_CL03_CD03_WT03_ST03.....	188
Fig. B.20 D30_H15_S20_R00_W00_V01_CL03_CD03_WT03_ST03.....	189
Fig. B.21 D30_H15_S20_R00_W01_V00_CL03_CD03_WT03_ST03.....	190
Fig. B.22 D30_H15_S20_R00_W01_V01_CL03_CD03_WT03_ST03.....	191
Fig. B.23 D30_H15_S20_R02_W00_V00_CL03_CD03_WT03_ST03.....	192
Fig. B.24 D30_H15_S20_R02_W00_V01_CL03_CD03_WT03_ST03.....	193
Fig. B.25 D30_H15_S20_R02_W01_V00_CL03_CD03_WT03_ST03.....	194
Fig. B.26 D30_H15_S20_R02_W01_V01_CL03_CD03_WT03_ST03.....	195
Fig. B.27 D42_H15_S00_R00_W00_V00_CL03_CD03_WT03_ST03.....	196
Fig. B.28 D42_H15_S00_R00_W00_V01_CL03_CD03_WT03_ST03.....	197
Fig. B.29 D42_H15_S00_R00_W01_V00_CL03_CD03_WT03_ST03.....	198
Fig. B.30 D42_H15_S00_R00_W01_V01_CL03_CD03_WT03_ST03.....	199
Fig. B.31 D42_H15_S28_R00_W00_V00_CL03_CD03_WT03_ST03.....	200
Fig. B.32 D42_H15_S28_R00_W00_V01_CL03_CD03_WT03_ST03.....	201
Fig. B.33 D42_H15_S28_R00_W01_V00_CL03_CD03_WT03_ST03.....	202
Fig. B.34 D42_H15_S28_R00_W01_V01_CL03_CD03_WT03_ST03.....	203
Fig. B.35 D42_H15_S28_R02_W00_V00_CL03_CD03_WT03_ST03.....	204
Fig. B.36 D42_H15_S28_R02_W00_V01_CL03_CD03_WT03_ST03.....	205
Fig. B.37 D42_H15_S28_R02_W01_V00_CL03_CD03_WT03_ST03.....	206
Fig. B.38 D42_H15_S28_R02_W01_V01_CL03_CD03_WT03_ST03.....	207

Fig. B.39 D54_H05_S00_R00_W00_V00_CL03_CD03_WT03_ST03.....	208
Fig. B.40 D54_H05_S36_R00_W00_V00_CL03_CD03_WT03_ST03.....	209
Fig. B.41 D54_H05_S36_R02_W00_V00_CL03_CD03_WT03_ST03.....	210
Fig. B.42 D54_H10_S00_R00_W00_V00_CL03_CD03_WT03_ST03.....	211
Fig. B.43 D54_H10_S36_R00_W00_V00_CL03_CD03_WT03_ST03.....	212
Fig. B.44 D54_H10_S36_R02_W00_V00_CL03_CD03_WT03_ST03.....	213
Fig. B.45 D54_H15_S00_R00_W00_V00_CL01_CD01_WT03_ST03.....	214
Fig. B.46 D54_H15_S00_R00_W00_V00_CL01_CD02_WT03_ST03.....	215
Fig. B.47 D54_H15_S00_R00_W00_V00_CL01_CD03_WT03_ST03.....	216
Fig. B.48 D54_H15_S00_R00_W00_V00_CL01_CD04_WT03_ST03.....	217
Fig. B.49 D54_H15_S00_R00_W00_V00_CL01_CD05_WT03_ST03.....	218
Fig. B.50 D54_H15_S00_R00_W00_V00_CL02_CD01_WT03_ST03.....	219
Fig. B.51 D54_H15_S00_R00_W00_V00_CL02_CD02_WT03_ST03.....	220
Fig. B.52 D54_H15_S00_R00_W00_V00_CL02_CD03_WT03_ST03.....	221
Fig. B.53 D54_H15_S00_R00_W00_V00_CL02_CD04_WT03_ST03.....	222
Fig. B.54 D54_H15_S00_R00_W00_V00_CL02_CD05_WT03_ST03.....	223
Fig. B.55 D54_H15_S00_R00_W00_V00_CL03_CD01_WT03_ST03.....	224
Fig. B.56 D54_H15_S00_R00_W00_V00_CL03_CD02_WT03_ST03.....	225
Fig. B.57 D54_H15_S00_R00_W00_V00_CL03_CD03_WT01_ST01.....	226
Fig. B.58 D54_H15_S00_R00_W00_V00_CL03_CD03_WT02_ST01.....	227
Fig. B.59 D54_H15_S00_R00_W00_V00_CL03_CD03_WT03_ST01.....	228
Fig. B.60 D54_H15_S00_R00_W00_V00_CL03_CD03_WT03_ST03.....	229
Fig. B.61 D54_H15_S00_R00_W00_V00_CL03_CD03_WT04_ST01.....	230

Fig. B.62 D54_H15_S00_R00_W00_V00_CL03_CD03_WT05_ST01.....	231
Fig. B.63 D54_H15_S00_R00_W00_V00_CL03_CD04_WT03_ST03.....	232
Fig. B.64 D54_H15_S00_R00_W00_V00_CL03_CD05_WT03_ST03.....	233
Fig. B.65 D54_H15_S00_R00_W00_V00_CL04_CD01_WT03_ST03.....	234
Fig. B.66 D54_H15_S00_R00_W00_V00_CL04_CD02_WT03_ST03.....	235
Fig. B.67 D54_H15_S00_R00_W00_V00_CL04_CD03_WT03_ST03.....	236
Fig. B.68 D54_H15_S00_R00_W00_V00_CL04_CD04_WT03_ST03.....	237
Fig. B.69 D54_H15_S00_R00_W00_V00_CL04_CD05_WT03_ST03.....	238
Fig. B.70 D54_H15_S00_R00_W00_V01_CL03_CD03_WT03_ST03.....	239
Fig. B.71 D54_H15_S00_R00_W01_V00_CL03_CD03_WT03_ST03.....	240
Fig. B.72 D54_H15_S00_R00_W01_V01_CL03_CD03_WT03_ST03.....	241
Fig. B.73 D54_H15_S18_R00_W00_V00_CL03_CD03_WT03_ST03.....	242
Fig. B.74 D54_H15_S18_R01_W00_V00_CL03_CD03_WT03_ST03.....	243
Fig. B.75 D54_H15_S18_R02_W00_V00_CL03_CD03_WT03_ST03.....	244
Fig. B.76 D54_H15_S18_R03_W00_V00_CL03_CD03_WT03_ST03.....	245
Fig. B.77 D54_H15_S18_R04_W00_V00_CL03_CD03_WT03_ST03.....	246
Fig. B.78 D54_H15_S18_R05_W00_V00_CL03_CD03_WT03_ST03.....	247
Fig. B.79 D54_H15_S36_R00_W00_V00_CL03_CD01_WT03_ST03.....	248
Fig. B.80 D54_H15_S36_R00_W00_V00_CL03_CD02_WT03_ST03.....	249
Fig. B.81 D54_H15_S36_R00_W00_V00_CL03_CD03_WT01_ST01.....	250
Fig. B.82 D54_H15_S36_R00_W00_V00_CL03_CD03_WT01_ST02.....	251
Fig. B.83 D54_H15_S36_R00_W00_V00_CL03_CD03_WT01_ST03.....	252
Fig. B.84 D54_H15_S36_R00_W00_V00_CL03_CD03_WT01_ST04.....	253

Fig. B.85 D54_H15_S36_R00_W00_V00_CL03_CD03_WT01_ST05.....	254
Fig. B.86 D54_H15_S36_R00_W00_V00_CL03_CD03_WT02_ST01.....	255
Fig. B.87 D54_H15_S36_R00_W00_V00_CL03_CD03_WT02_ST02.....	256
Fig. B.88 D54_H15_S36_R00_W00_V00_CL03_CD03_WT02_ST03.....	257
Fig. B.89 D54_H15_S36_R00_W00_V00_CL03_CD03_WT02_ST04.....	258
Fig. B.90 D54_H15_S36_R00_W00_V00_CL03_CD03_WT02_ST05.....	259
Fig. B.91 D54_H15_S36_R00_W00_V00_CL03_CD03_WT03_ST01.....	260
Fig. B.92 D54_H15_S36_R00_W00_V00_CL03_CD03_WT03_ST02.....	261
Fig. B.93 D54_H15_S36_R00_W00_V00_CL03_CD03_WT03_ST03.....	262
Fig. B.94 D54_H15_S36_R00_W00_V00_CL03_CD03_WT03_ST04.....	263
Fig. B.95 D54_H15_S36_R00_W00_V00_CL03_CD03_WT03_ST05.....	264
Fig. B.96 D54_H15_S36_R00_W00_V00_CL03_CD03_WT04_ST01.....	265
Fig. B.97 D54_H15_S36_R00_W00_V00_CL03_CD03_WT04_ST02.....	266
Fig. B.98 D54_H15_S36_R00_W00_V00_CL03_CD03_WT04_ST03.....	267
Fig. B.99 D54_H15_S36_R00_W00_V00_CL03_CD03_WT04_ST04.....	268
Fig. B.100 D54_H15_S36_R00_W00_V00_CL03_CD03_WT04_ST05.....	269
Fig. B.101 D54_H15_S36_R00_W00_V00_CL03_CD03_WT05_ST01.....	270
Fig. B.102 D54_H15_S36_R00_W00_V00_CL03_CD03_WT05_ST02.....	271
Fig. B.103 D54_H15_S36_R00_W00_V00_CL03_CD03_WT05_ST03.....	272
Fig. B.104 D54_H15_S36_R00_W00_V00_CL03_CD03_WT05_ST04.....	273
Fig. B.105 D54_H15_S36_R00_W00_V00_CL03_CD03_WT05_ST05.....	274
Fig. B.106 D54_H15_S36_R00_W00_V00_CL03_CD04_WT03_ST03.....	275
Fig. B.107 D54_H15_S36_R00_W00_V00_CL03_CD05_WT03_ST03.....	276

Fig. B.108 D54_H15_S36_R00_W00_V01_CL03_CD03_WT03_ST03.....	277
Fig. B.109 D54_H15_S36_R00_W01_V00_CL03_CD03_WT03_ST03.....	278
Fig. B.110 D54_H15_S36_R00_W01_V01_CL03_CD03_WT03_ST03.....	279
Fig. B.111 D54_H15_S36_R01_W00_V00_CL03_CD03_WT03_ST03.....	280
Fig. B.112 D54_H15_S36_R02_W00_V00_CL03_CD03_WT03_ST03.....	281
Fig. B.113 D54_H15_S36_R02_W00_V01_CL03_CD03_WT03_ST03.....	282
Fig. B.114 D54_H15_S36_R02_W01_V00_CL03_CD03_WT03_ST03.....	283
Fig. B.115 D54_H15_S36_R02_W01_V01_CL03_CD03_WT03_ST03.....	284
Fig. B.116 D54_H15_S36_R03_W00_V00_CL03_CD03_WT03_ST03.....	285
Fig. B.117 D54_H15_S36_R04_W00_V00_CL03_CD03_WT03_ST03.....	286
Fig. B.118 D54_H15_S36_R05_W00_V00_CL03_CD03_WT03_ST03.....	287
Fig. B.119 D54_H15_S54_R00_W00_V00_CL03_CD03_WT03_ST03.....	288
Fig. B.120 D54_H15_S54_R01_W00_V00_CL03_CD03_WT03_ST03.....	289
Fig. B.121 D54_H15_S54_R02_W00_V00_CL03_CD03_WT03_ST03.....	290
Fig. B.122 D54_H15_S54_R03_W00_V00_CL03_CD03_WT03_ST03.....	291
Fig. B.123 D54_H15_S54_R04_W00_V00_CL03_CD03_WT03_ST03.....	292
Fig. B.124 D54_H15_S54_R05_W00_V00_CL03_CD03_WT03_ST03.....	293
Fig. B.125 D54_H20_S00_R00_W00_V00_CL03_CD03_WT03_ST03.....	294
Fig. B.126 D54_H20_S36_R00_W00_V00_CL03_CD03_WT03_ST03.....	295
Fig. B.127 D54_H20_S36_R02_W00_V00_CL03_CD03_WT03_ST03.....	296
Fig. B.128 D54_H25_S00_R00_W00_V00_CL03_CD03_WT03_ST03.....	297
Fig. B.129 D54_H25_S36_R00_W00_V00_CL03_CD03_WT03_ST03.....	298
Fig. B.130 D54_H25_S36_R02_W00_V00_CL03_CD03_WT03_ST03.....	299

Fig. B.131 D54_H30_S00_R00_W00_V00_CL03_CD03_WT03_ST03.....	300
Fig. B.132 D54_H30_S36_R00_W00_V00_CL03_CD03_WT03_ST03.....	301
Fig. B.133 D54_H30_S36_R02_W00_V00_CL03_CD03_WT03_ST03.....	302
Fig. B.134 D66_H15_S00_R00_W00_V00_CL03_CD03_WT03_ST03.....	303
Fig. B.135 D66_H15_S00_R00_W00_V01_CL03_CD03_WT03_ST03.....	304
Fig. B.136 D66_H15_S00_R00_W01_V00_CL03_CD03_WT03_ST03.....	305
Fig. B.137 D66_H15_S00_R00_W01_V01_CL03_CD03_WT03_ST03.....	306
Fig. B.138 D66_H15_S44_R00_W00_V00_CL03_CD03_WT03_ST03.....	307
Fig. B.139 D66_H15_S44_R00_W00_V01_CL03_CD03_WT03_ST03.....	308
Fig. B.140 D66_H15_S44_R00_W01_V00_CL03_CD03_WT03_ST03.....	309
Fig. B.141 D66_H15_S44_R00_W01_V01_CL03_CD03_WT03_ST03.....	310
Fig. B.142 D66_H15_S44_R02_W00_V00_CL03_CD03_WT03_ST03.....	311
Fig. B.143 D66_H15_S44_R02_W00_V01_CL03_CD03_WT03_ST03.....	312
Fig. B.144 D66_H15_S44_R02_W01_V00_CL03_CD03_WT03_ST03.....	313
Fig. B.145 D66_H15_S44_R02_W01_V01_CL03_CD03_WT03_ST03.....	314
Fig. B.146 D78_H15_S00_R00_W00_V00_CL03_CD03_WT03_ST03.....	315
Fig. B.147 D78_H15_S00_R00_W00_V01_CL03_CD03_WT03_ST03.....	316
Fig. B.148 D78_H15_S00_R00_W01_V00_CL03_CD03_WT03_ST03.....	317
Fig. B.149 D78_H15_S00_R00_W01_V01_CL03_CD03_WT03_ST03.....	318
Fig. B.150 D78_H15_S52_R00_W00_V00_CL03_CD03_WT03_ST03.....	319
Fig. B.151 D78_H15_S52_R00_W00_V01_CL03_CD03_WT03_ST03.....	320
Fig. B.152 D78_H15_S52_R00_W01_V00_CL03_CD03_WT03_ST03.....	321
Fig. B.153 D78_H15_S52_R00_W01_V01_CL03_CD03_WT03_ST03.....	322

Fig. B.154 D78_H15_S52_R02_W00_V00_CL03_CD03_WT03_ST03.....	323
Fig. B.155 D78_H15_S52_R02_W00_V01_CL03_CD03_WT03_ST03.....	324
Fig. B.156 D78_H15_S52_R02_W01_V00_CL03_CD03_WT03_ST03.....	325
Fig. B.157 D78_H15_S52_R02_W01_V01_CL03_CD03_WT03_ST03.....	326
Fig. B.158 D90_H15_S00_R00_W00_V00_CL03_CD03_WT03_ST03.....	327
Fig. B.159 D90_H15_S00_R00_W00_V01_CL03_CD03_WT03_ST03.....	328
Fig. B.160 D90_H15_S00_R00_W01_V00_CL03_CD03_WT03_ST03.....	329
Fig. B.161 D90_H15_S00_R00_W01_V01_CL03_CD03_WT03_ST03.....	330
Fig. B.162 D90_H15_S60_R00_W00_V00_CL03_CD03_WT03_ST03.....	331
Fig. B.163 D90_H15_S60_R00_W00_V01_CL03_CD03_WT03_ST03.....	332
Fig. B.164 D90_H15_S60_R00_W01_V00_CL03_CD03_WT03_ST03.....	333
Fig. B.165 D90_H15_S60_R00_W01_V01_CL03_CD03_WT03_ST03.....	334
Fig. B.166 D90_H15_S60_R02_W00_V00_CL03_CD03_WT03_ST03.....	335
Fig. B.167 D90_H15_S60_R02_W00_V01_CL03_CD03_WT03_ST03.....	336
Fig. B.168 D90_H15_S60_R02_W01_V00_CL03_CD03_WT03_ST03.....	337
Fig. B.169 D90_H15_S60_R02_W01_V01_CL03_CD03_WT03_ST03.....	338
Fig. B.170 D54_H15_S36_R01_W00_V00_CL03_CD03_WT03_ST03, Light Rings.	339
Fig. B.171 D54_H15_S36_R02_W00_V00_CL03_CD03_WT03_ST03, Light Rings.	340
Fig. B.172 D54_H15_S36_R03_W00_V00_CL03_CD03_WT03_ST03, Light Rings.	341
Fig. B.173 D54_H15_S36_R04_W00_V00_CL03_CD03_WT03_ST03, Light Rings.	342
Fig. B.174 D54_H15_S36_R05_W00_V00_CL03_CD03_WT03_ST03, Light Rings.	343
Fig. B.175 D54_H15_S36_R01_W00_V00_CL03_CD03_WT03_ST03, Heavy Rings	344
Fig. B.176 D54_H15_S36_R02_W00_V00_CL03_CD03_WT03_ST03, Heavy Rings	345

Fig. B.177 D54_H15_S36_R03_W00_V00_CL03_CD03_WT03_ST03, Heavy Rings346

Fig. B.178 D54_H15_S36_R04_W00_V00_CL03_CD03_WT03_ST03, Heavy Rings347

Fig. B.179 D54_H15_S36_R05_W00_V00_CL03_CD03_WT03_ST03, Heavy Rings348

DXX_HXX_SXX_**R**XX_WXX_VXX_CLXX_CDXX_WTXX_STXX

Parameter Identifier

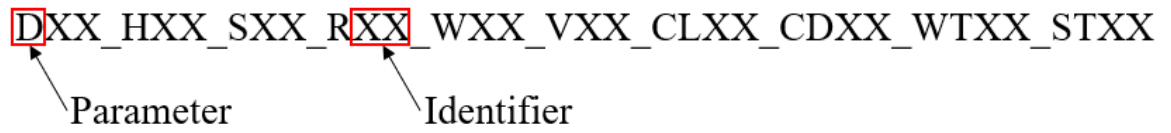


Fig. B.1 Naming Convention for Parametric Analysis

XX	D*	H**	S***	R	W	V	CL	CD	WT	ST
	Diameter, m (ft)	Height, panels	Stiffeners per panel	Wind Rings	Wind on Roof	Venting	Corrugation Length, mm (in)	Corrugation Depth, mm (in)	Wall Thickness, mm	Stiffener Thickness, mm
00			0	0	unloaded	unvented				
01	5.49 (18)	5	1	1	loaded	vented	20.8 (2)	6.35 (0.25)	1	3
02	9.14 (30)	10	2	2			76.2 (3)	12.7 (0.5)	1.5	4
03	12.8 (42)	15	3	3			101.6 (4)	19.1 (0.75)	2	5
04	16.5 (54)	20		4			152.4 (6)	25.4 (1.0)	3	7
05	20.1 (66)	25		5				38.1 (1.5)	4	9
06	23.8 (78)	30								
07	27.4 (90)									

*Diameter identifier is based on actual diameter (ft) rather than XX

**Height identifier is based on actual number of panels rather than XX

***Stiffener identifier is based on total number of stiffeners i.e. (stiffeners per panel * diameter (ft) / 3) rather than XX

Fig. B.2 Naming convention identifier values

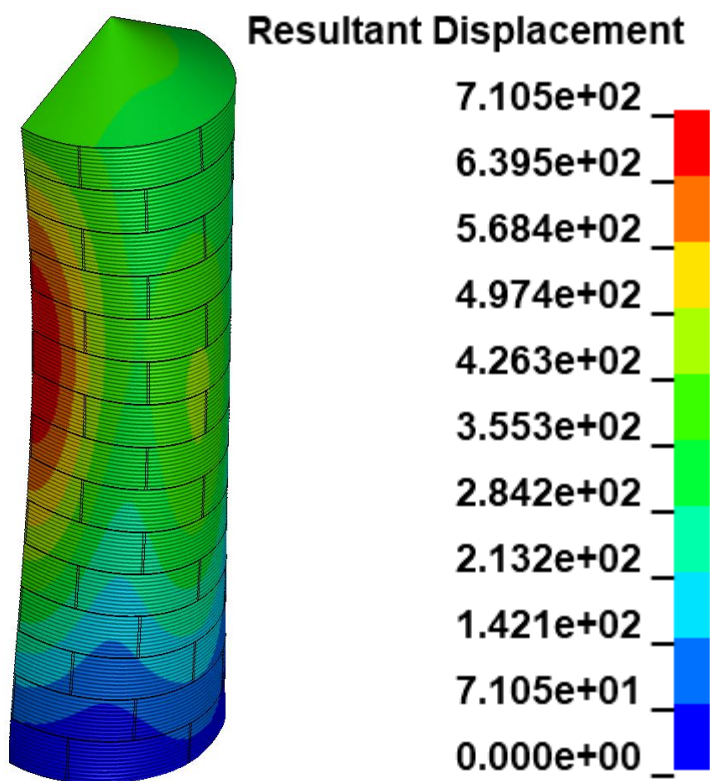
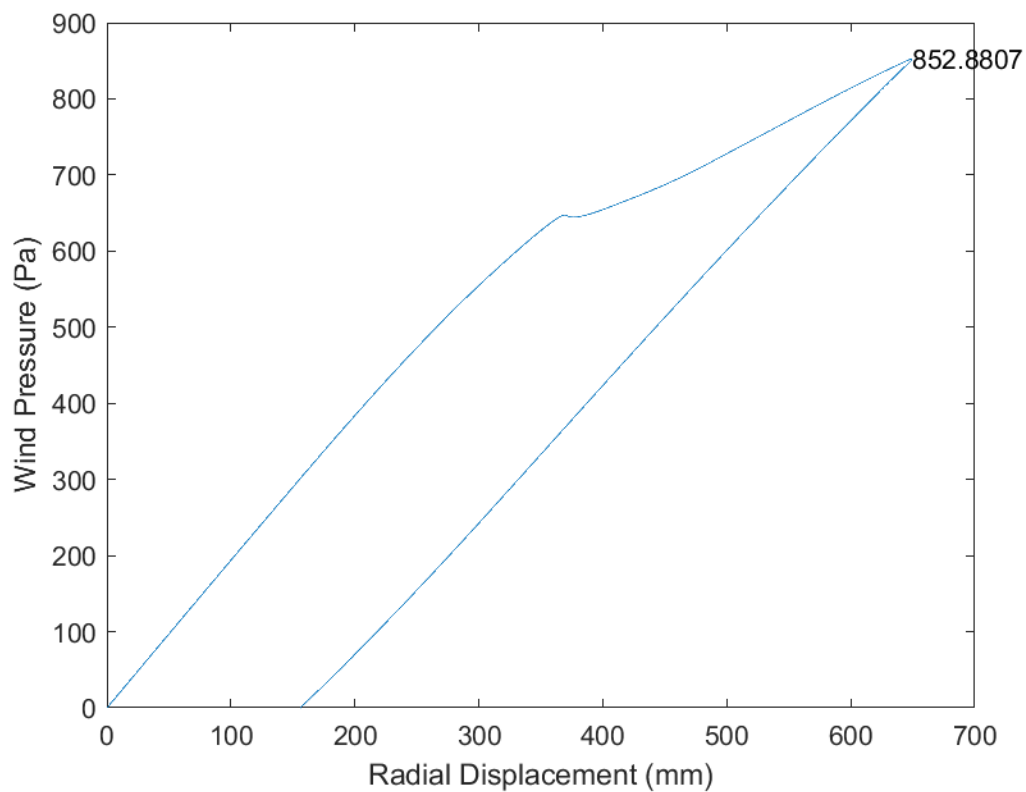


Fig. B.3 D18_H15_S00_R00_W00_V00_CL03_CD03_WT03_ST03

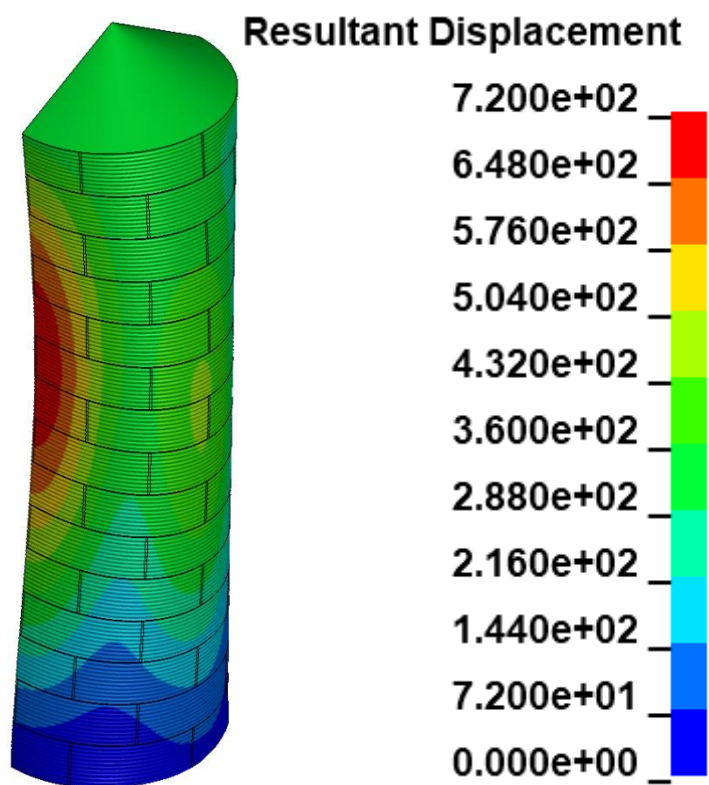
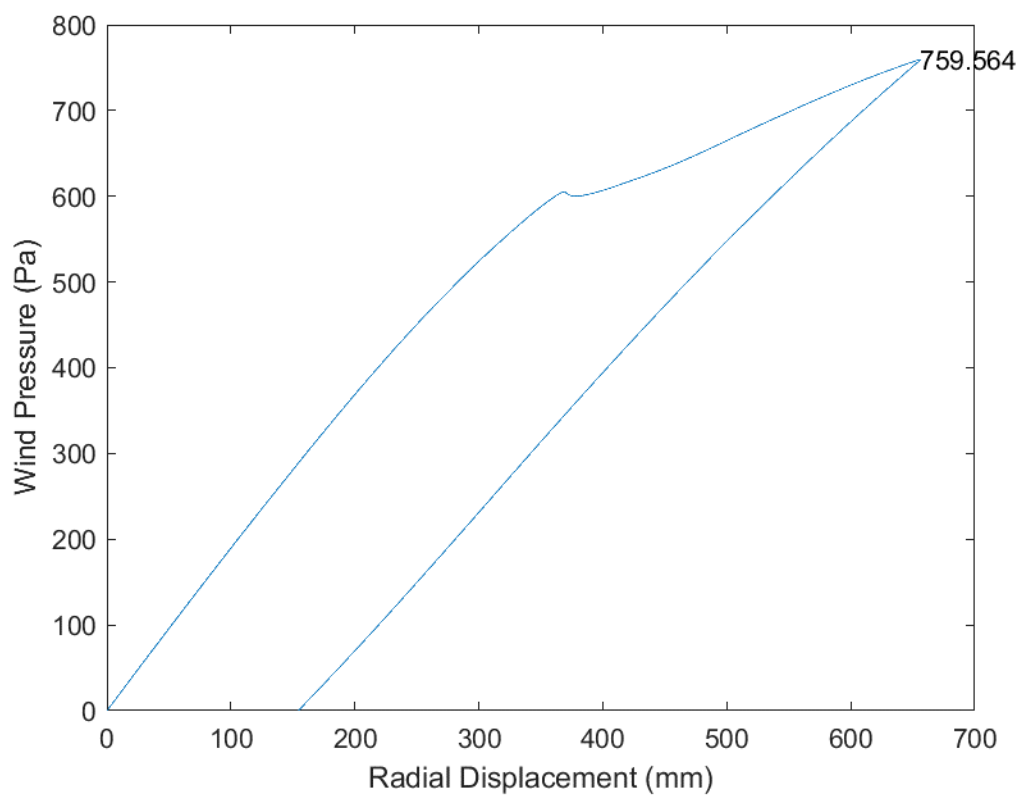


Fig. B.4 D18_H15_S00_R00_W00_V01_CL03_CD03_WT03_ST03

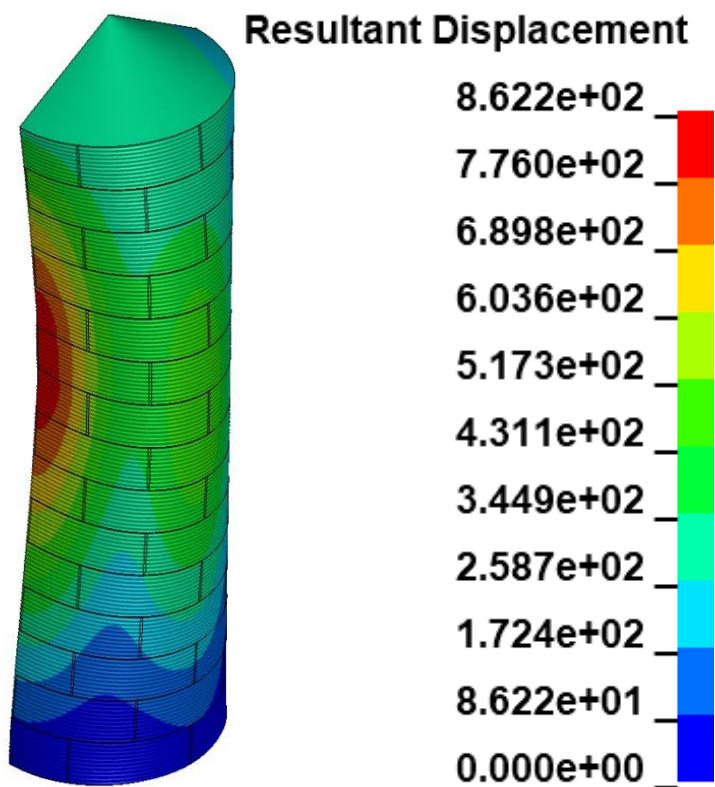
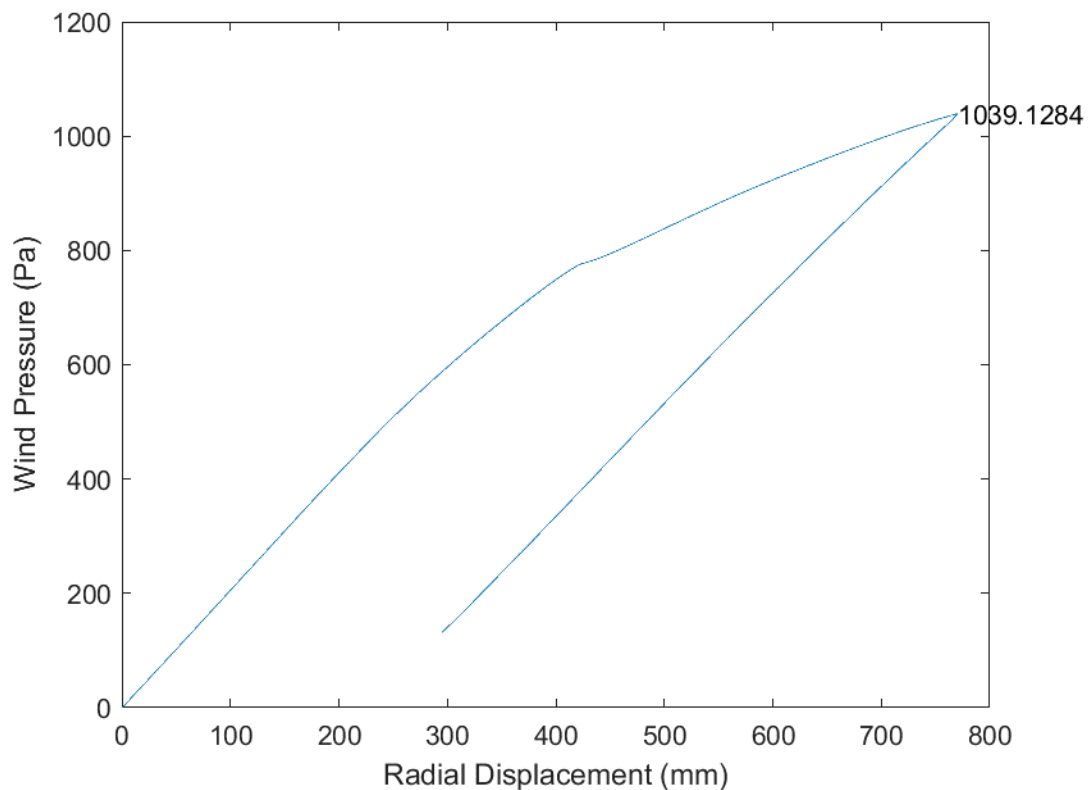


Fig. B.5 D18_H15_S00_R00_W01_V00_CL03_CD03_WT03_ST03

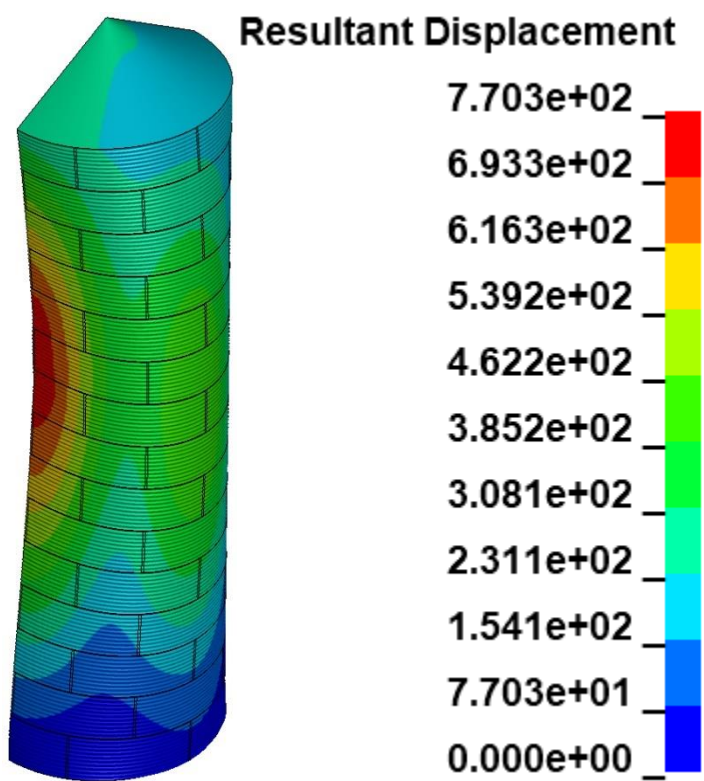
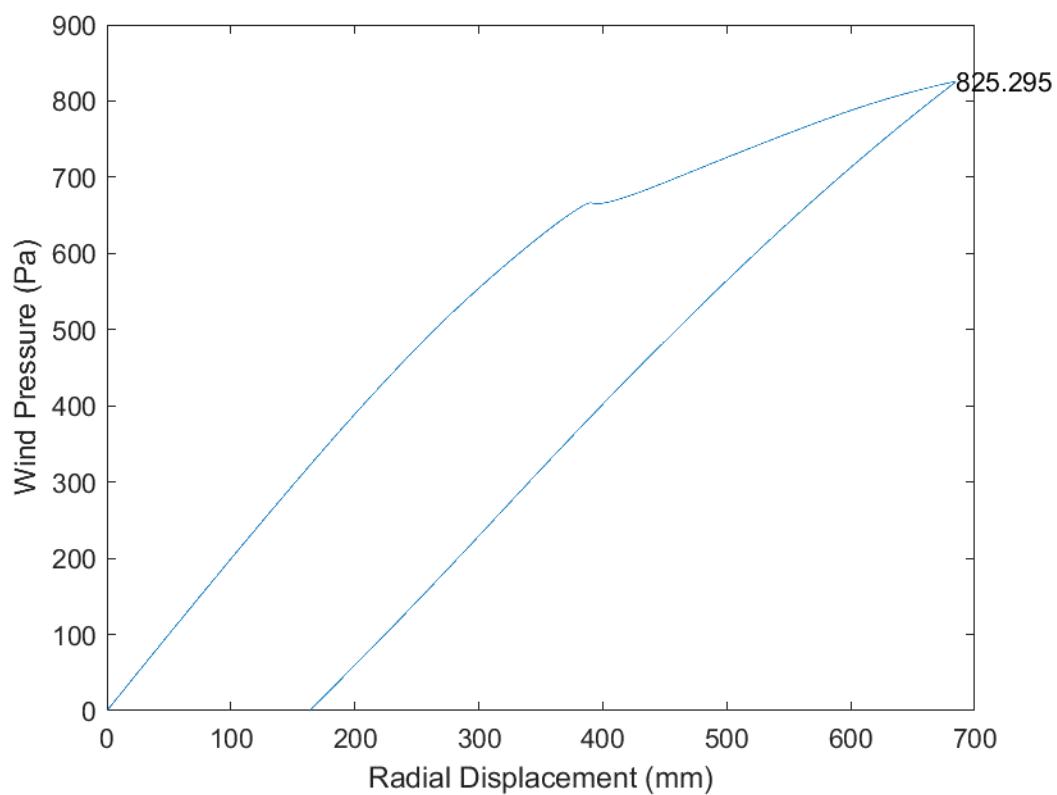


Fig. B.6 D18_H15_S00_R00_W01_V01_CL03_CD03_WT03_ST03

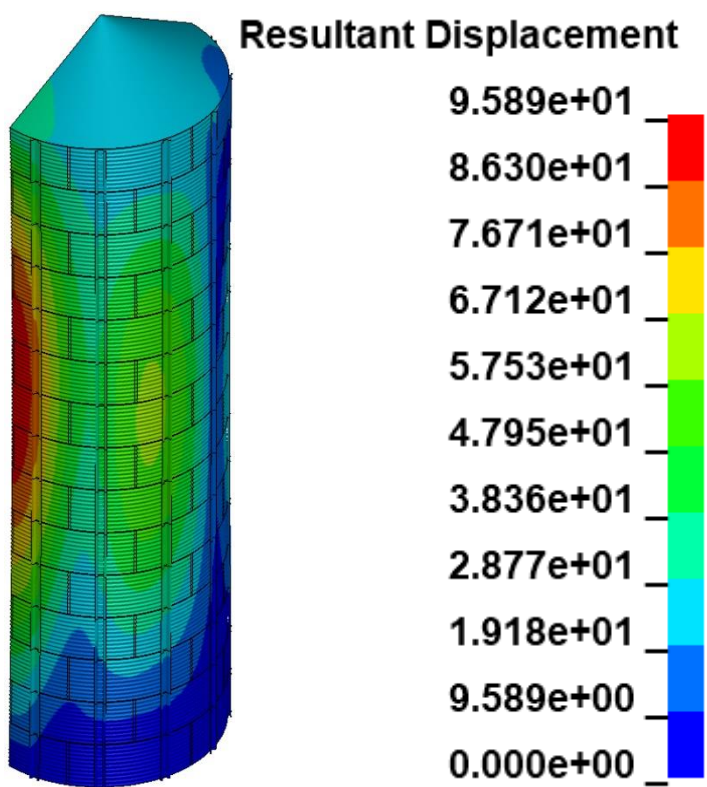
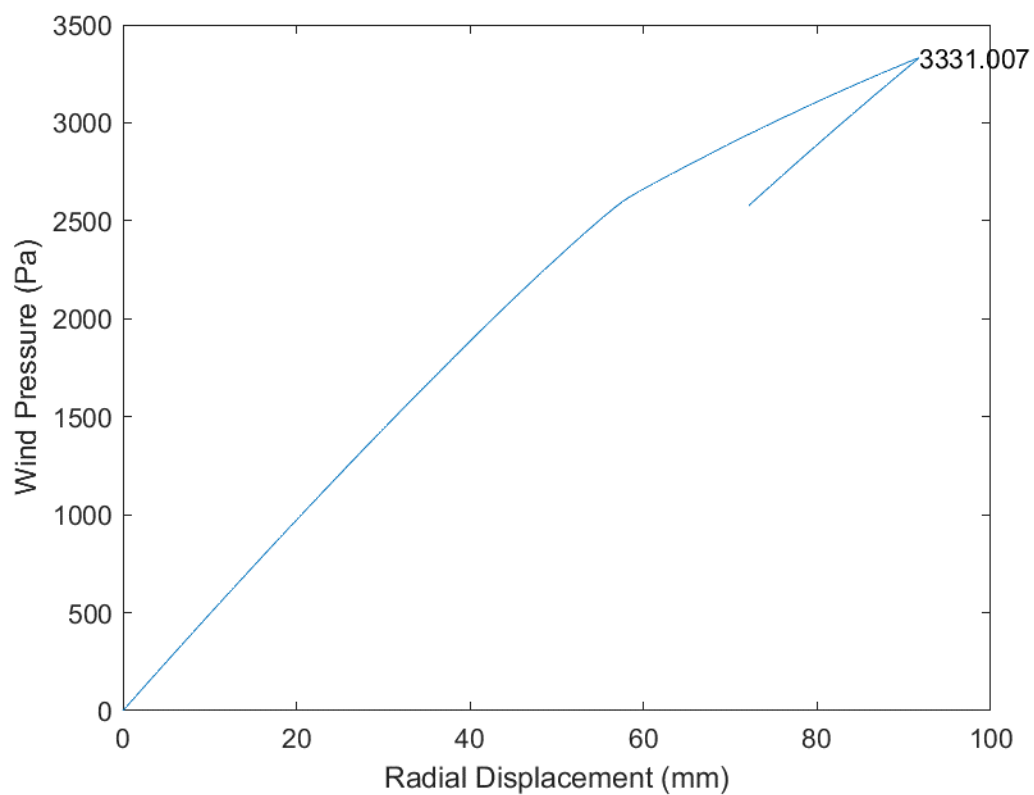


Fig. B.7 D18_H15_S12_R00_W00_V00_CL03_CD03_WT03_ST03

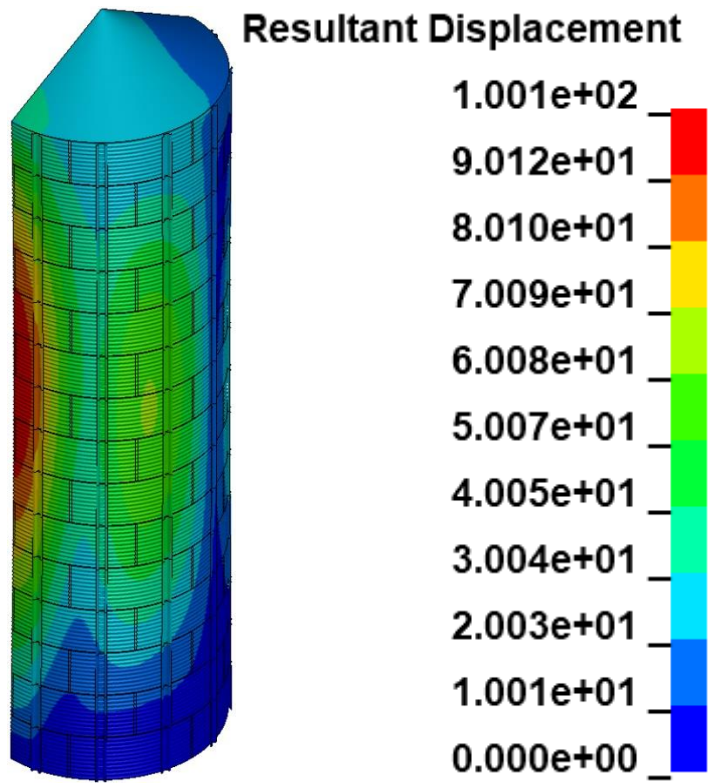
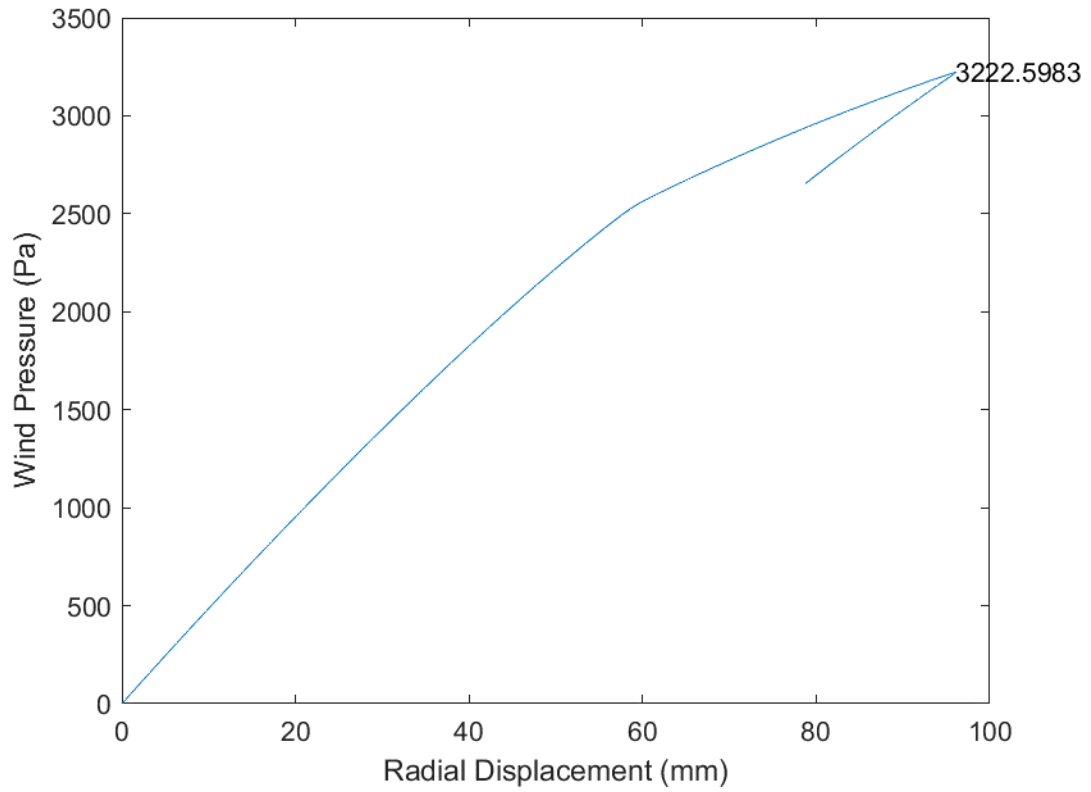


Fig. B.8 D18_H15_S12_R00_W00_V01_CL03_CD03_WT03_ST03

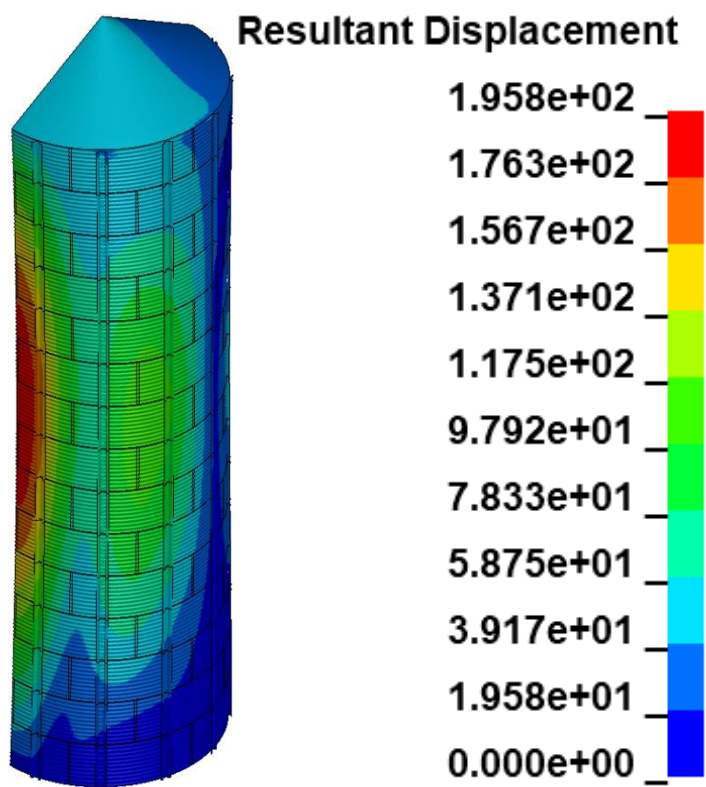
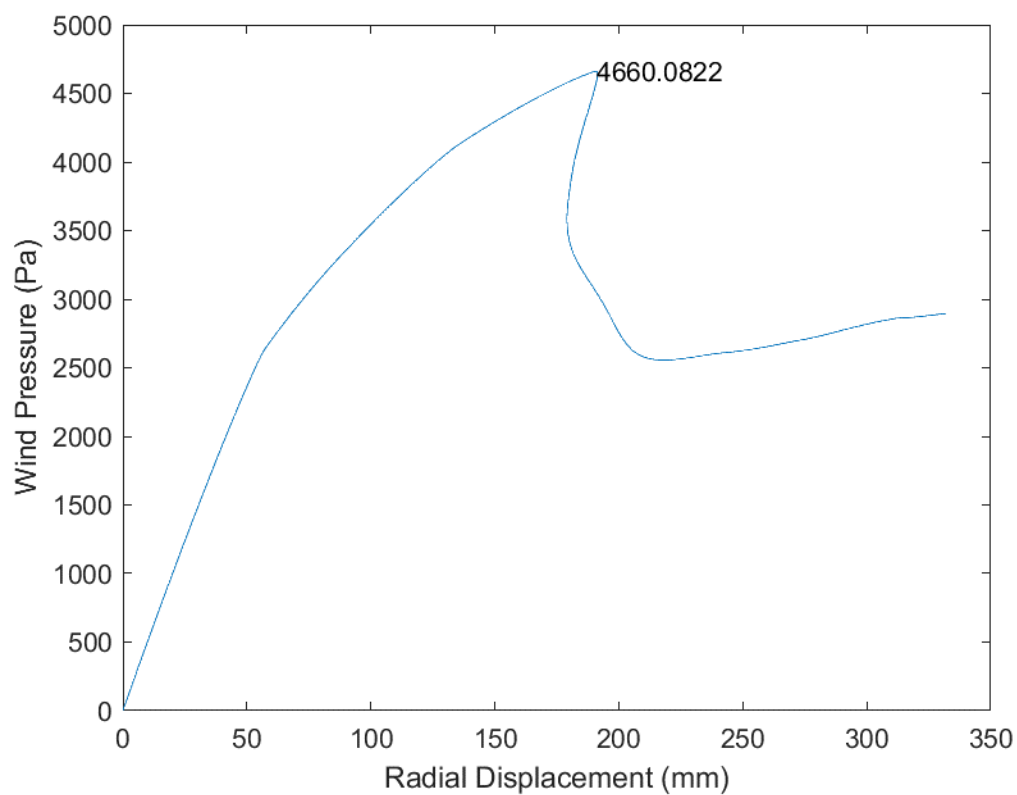


Fig. B.9 D18_H15_S12_R00_W01_V00_CL03_CD03_WT03_ST03

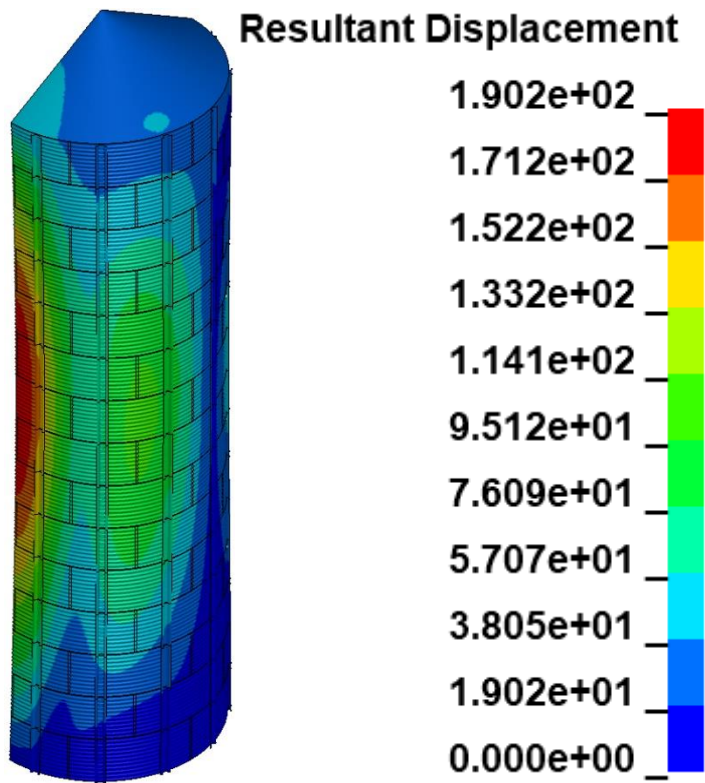
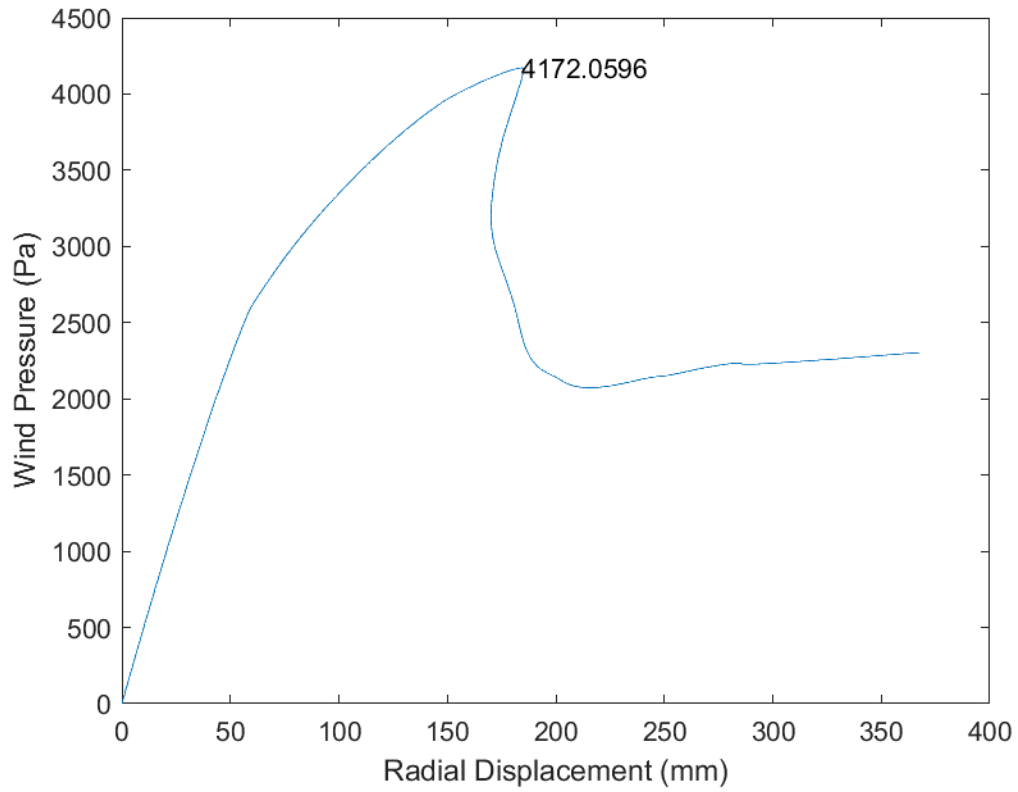


Fig. B.10 D18_H15_S12_R00_W01_V01_CL03_CD03_WT03_ST03

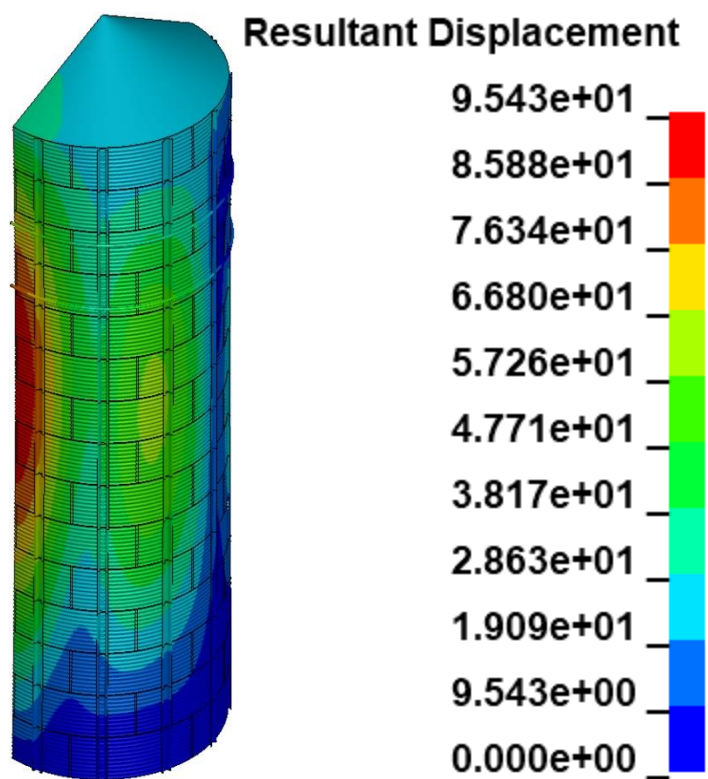
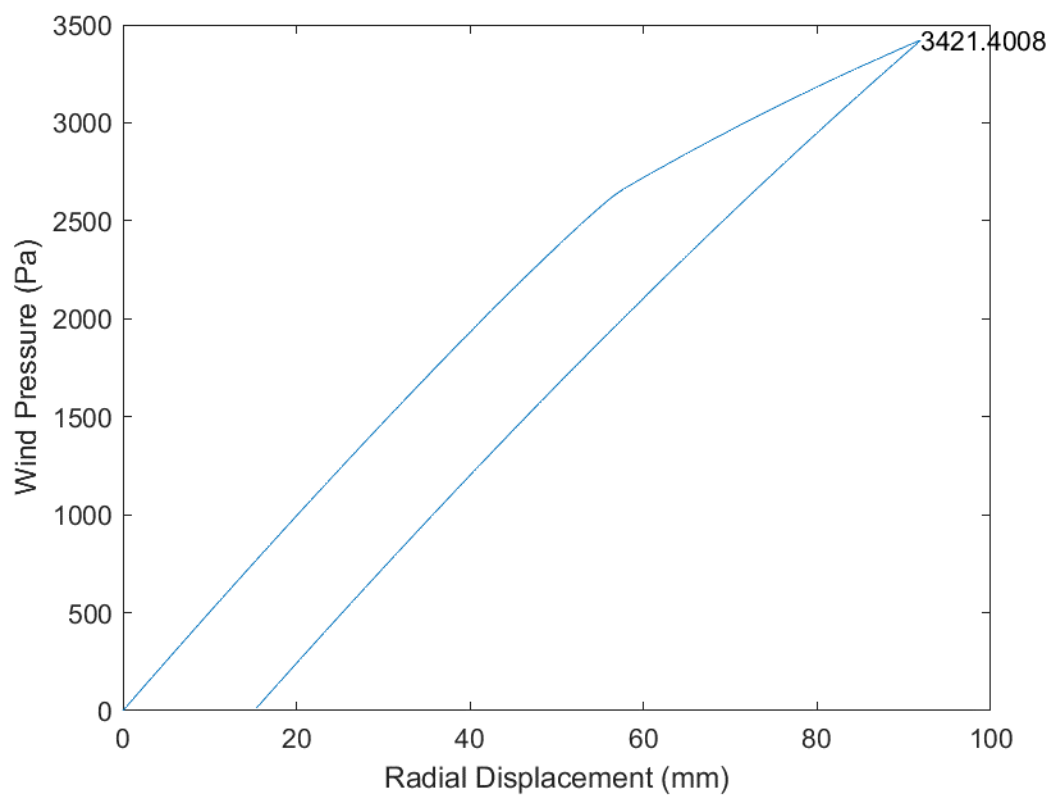


Fig. B.11 D18_H15_S12_R02_W00_V00_CL03_CD03_WT03_ST03

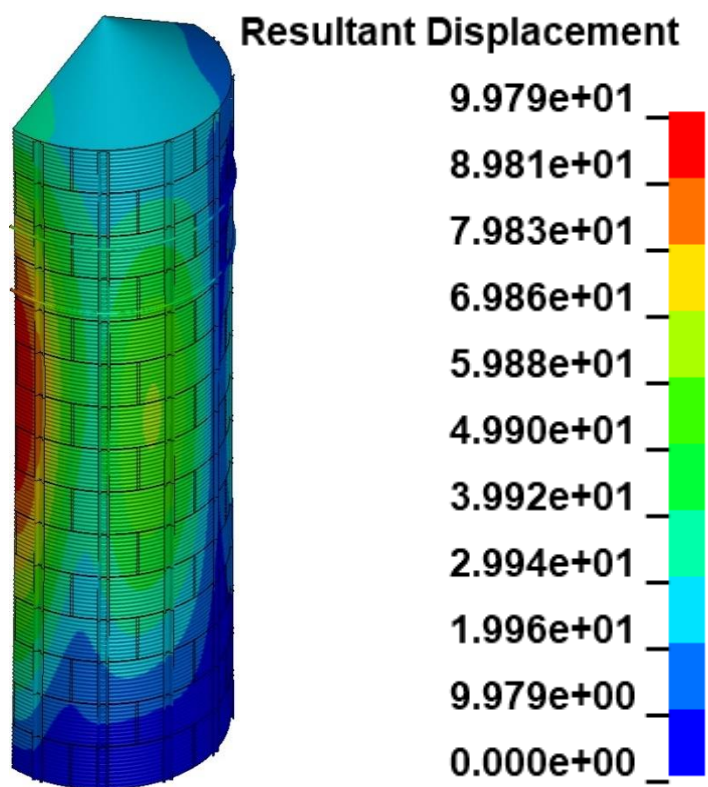
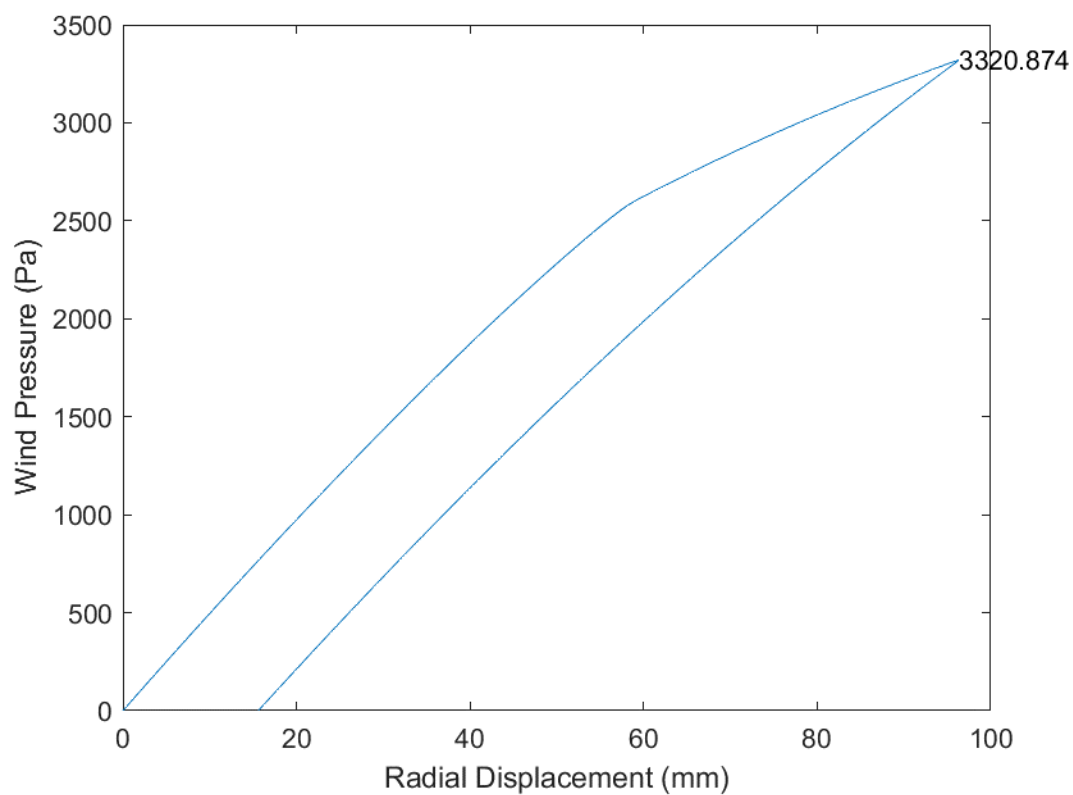


Fig. B.12 D18_H15_S12_R02_W00_V01_CL03_CD03_WT03_ST03

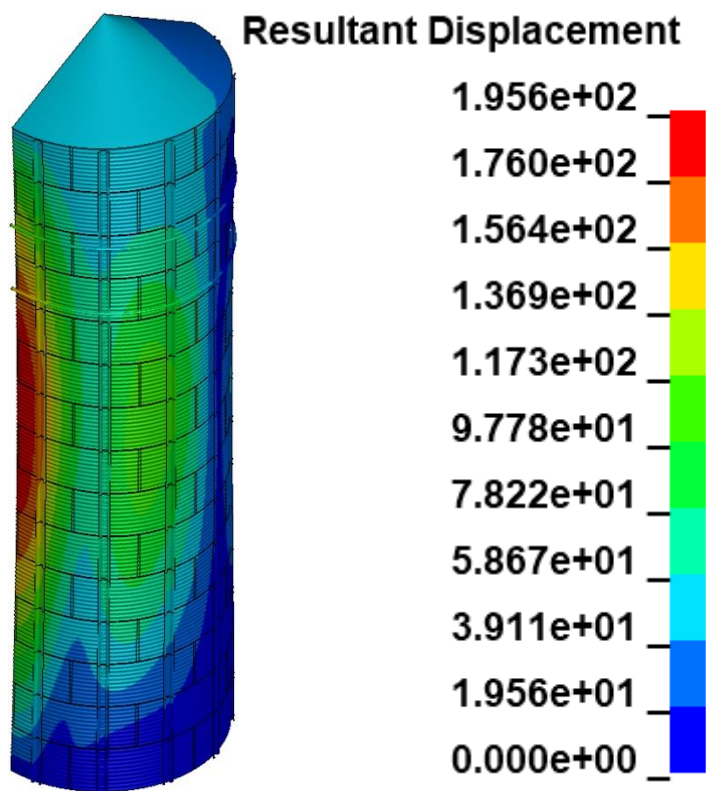
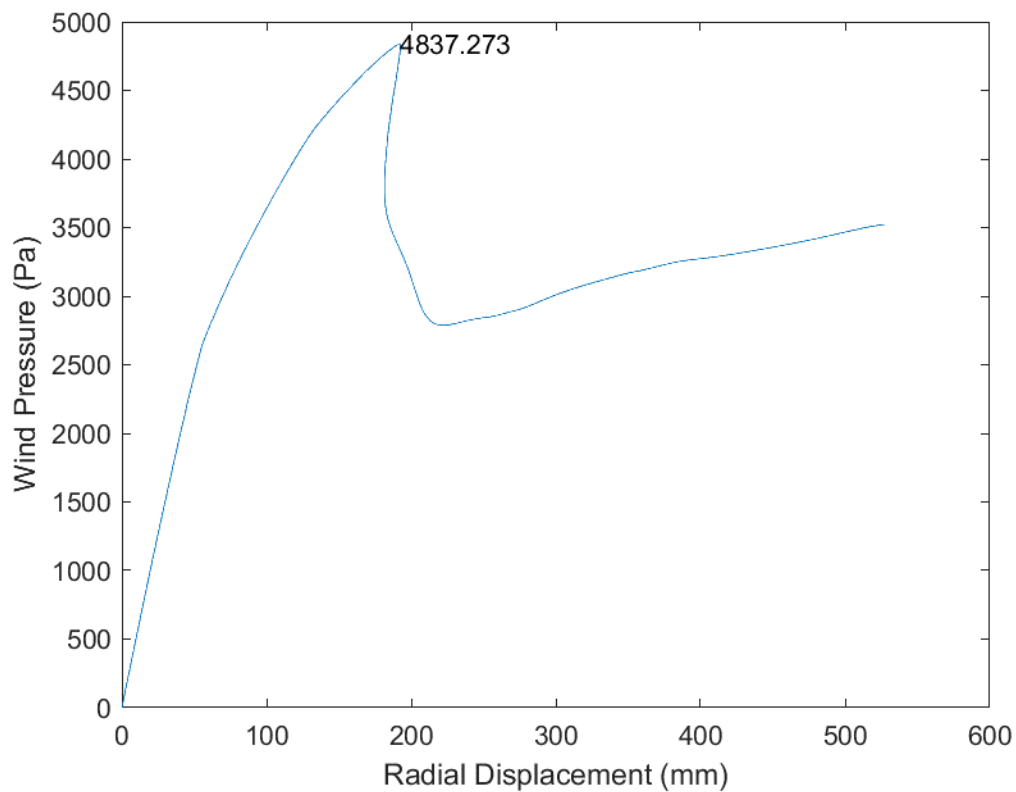


Fig. B.13 D18_H15_S12_R02_W01_V00_CL03_CD03_WT03_ST03

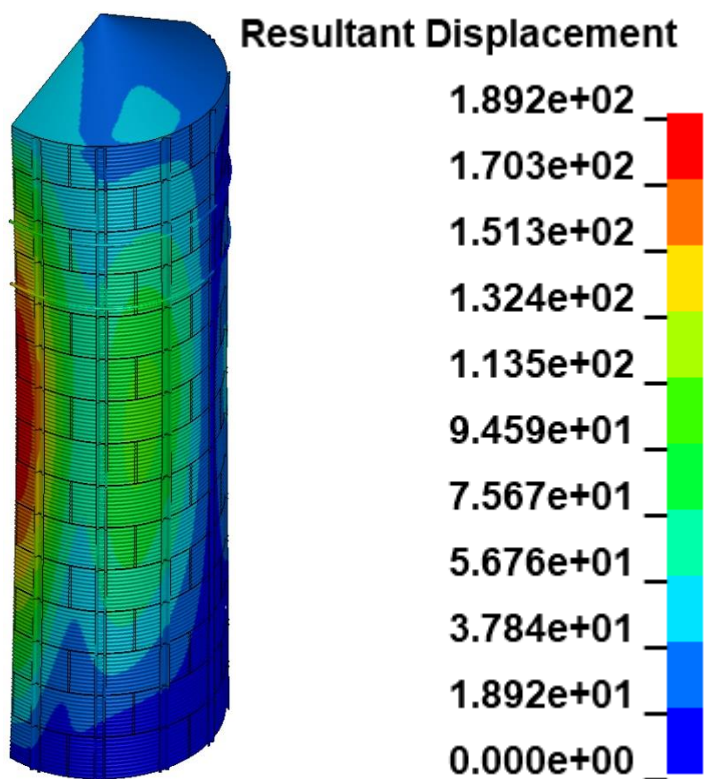
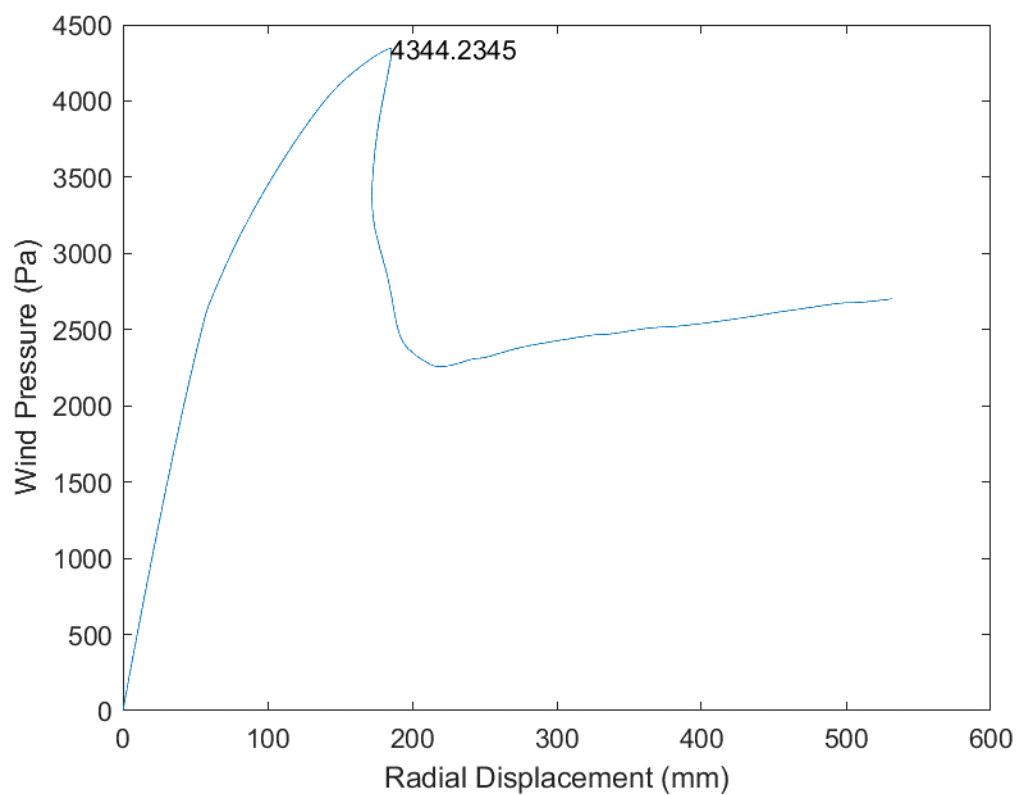


Fig. B.14 D18_H15_S12_R02_W01_V01_CL03_CD03_WT03_ST03

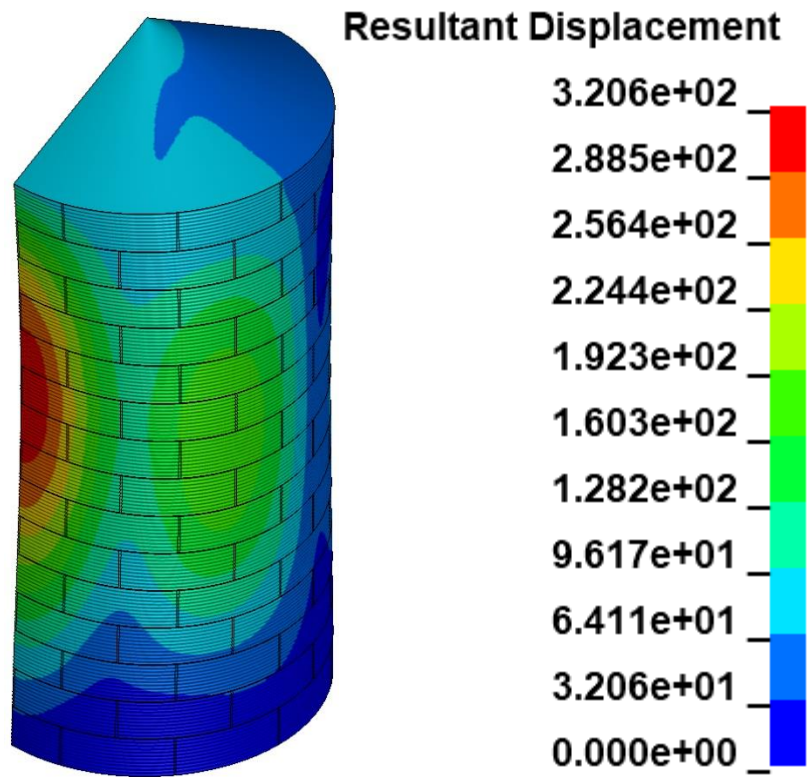
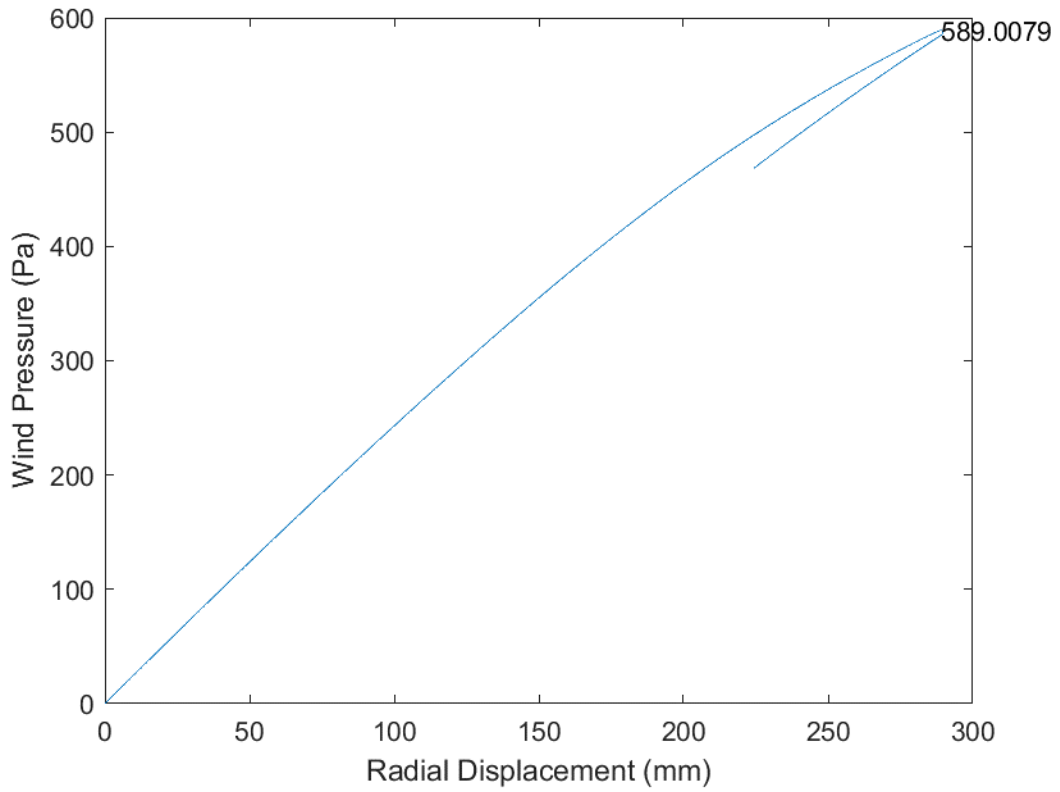


Fig. B.15 D30_H15_S00_R00_W00_V00_CL03_CD03_WT03_ST03

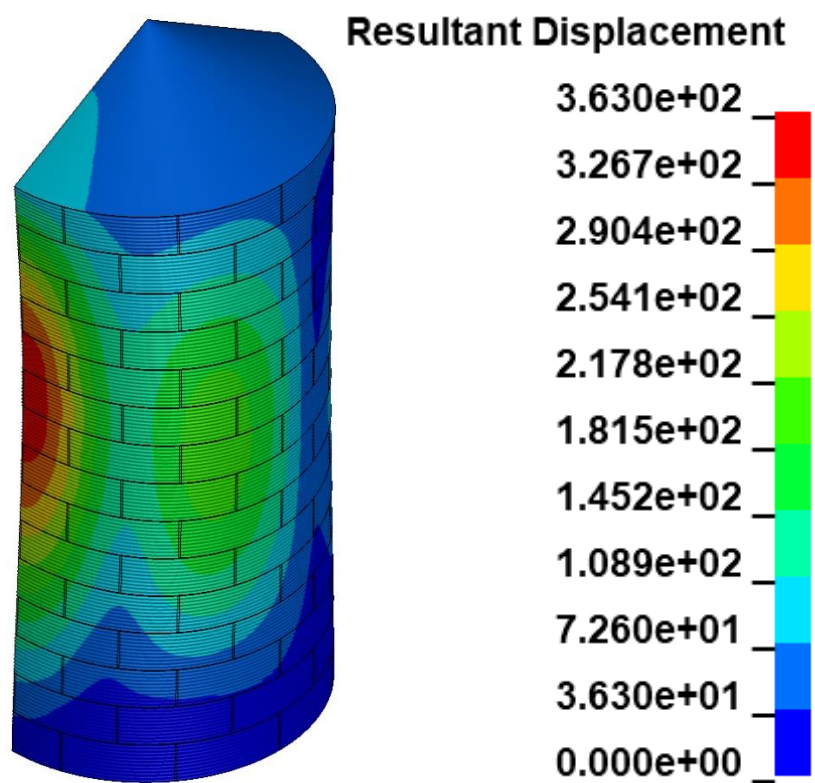
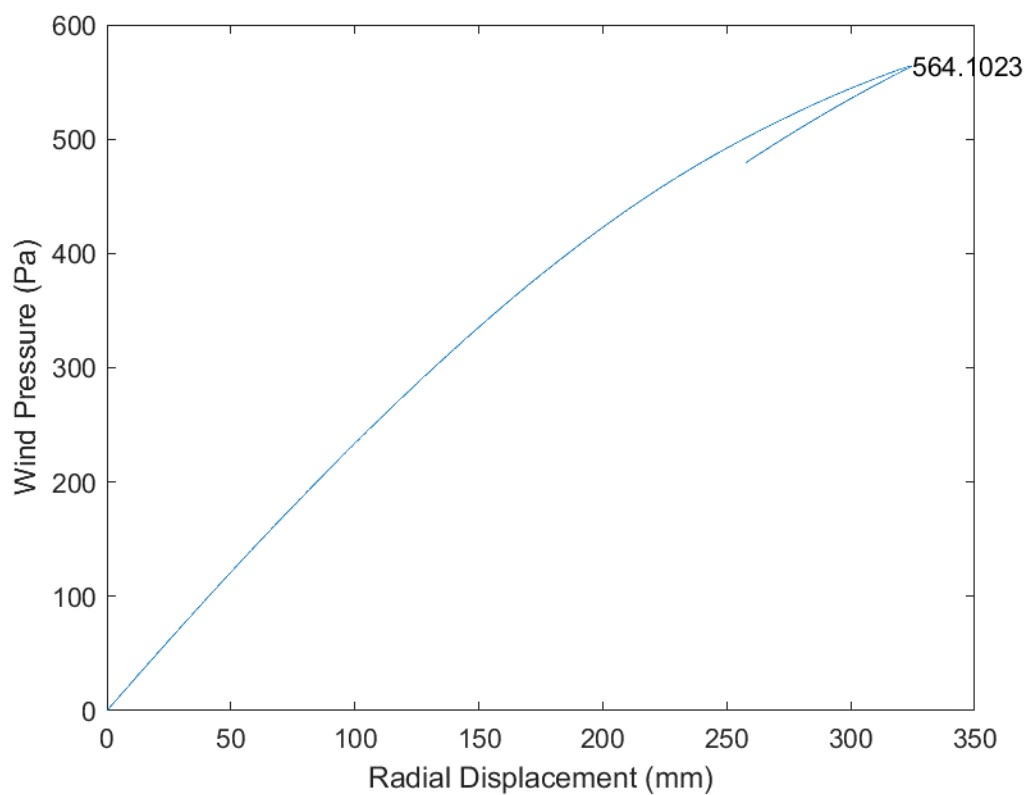


Fig. B.16 D30_H15_S00_R00_W00_V01_CL03_CD03_WT03_ST03

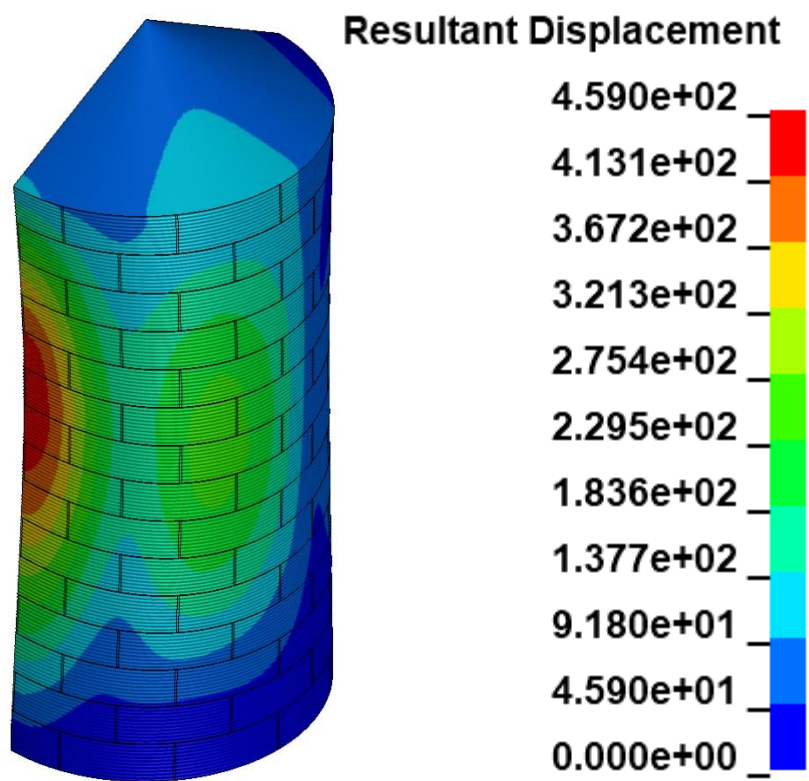
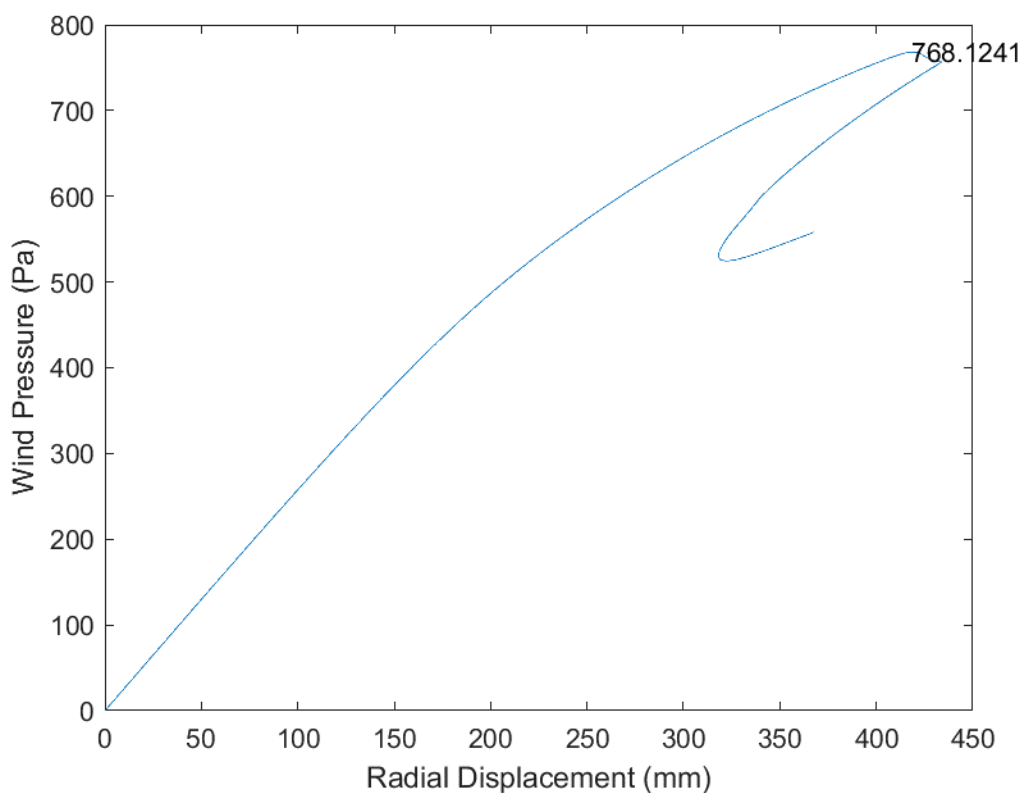


Fig. B.17 D30_H15_S00_R00_W01_V00_CL03_CD03_WT03_ST03

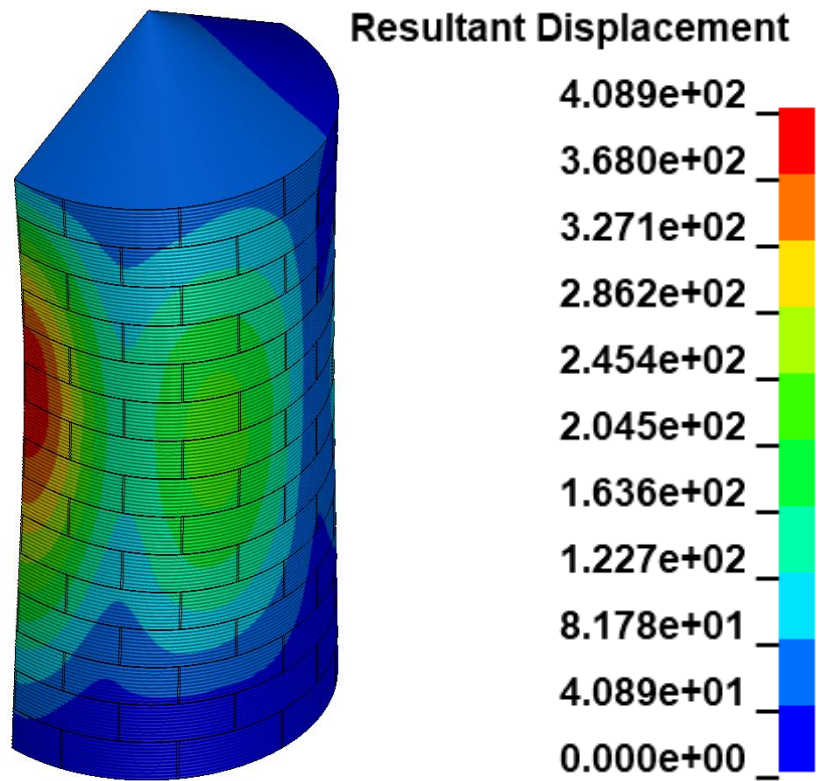
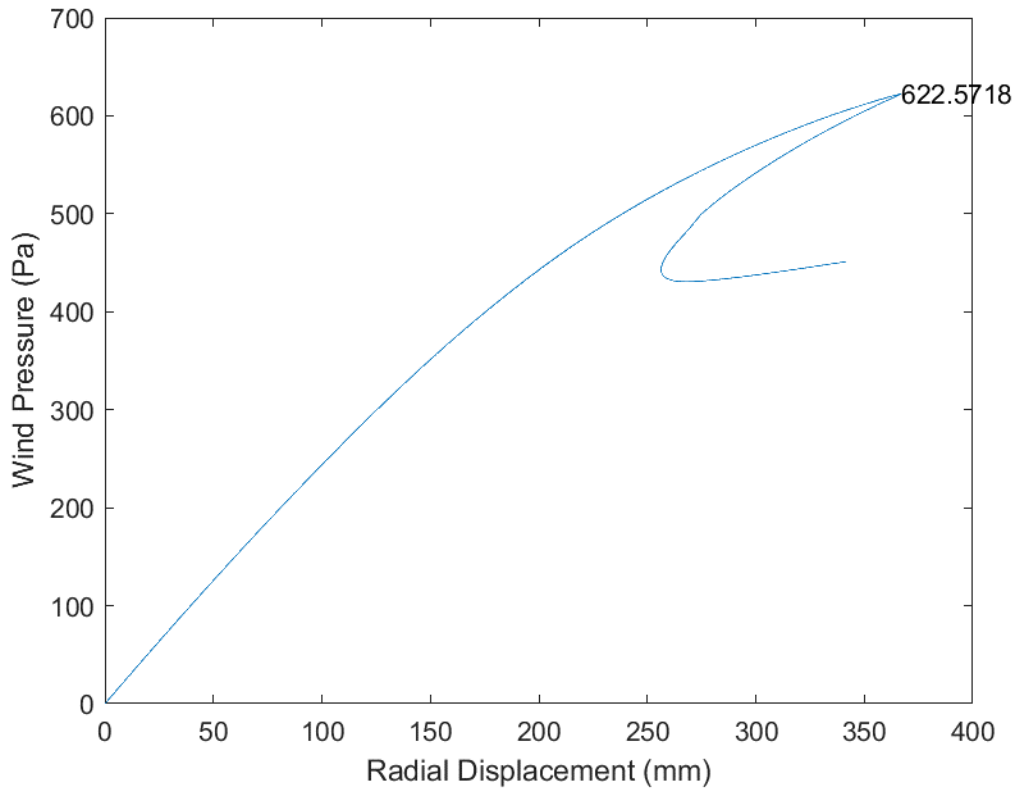


Fig. B.18 D30_H15_S00_R00_W01_V01_CL03_CD03_WT03_ST03

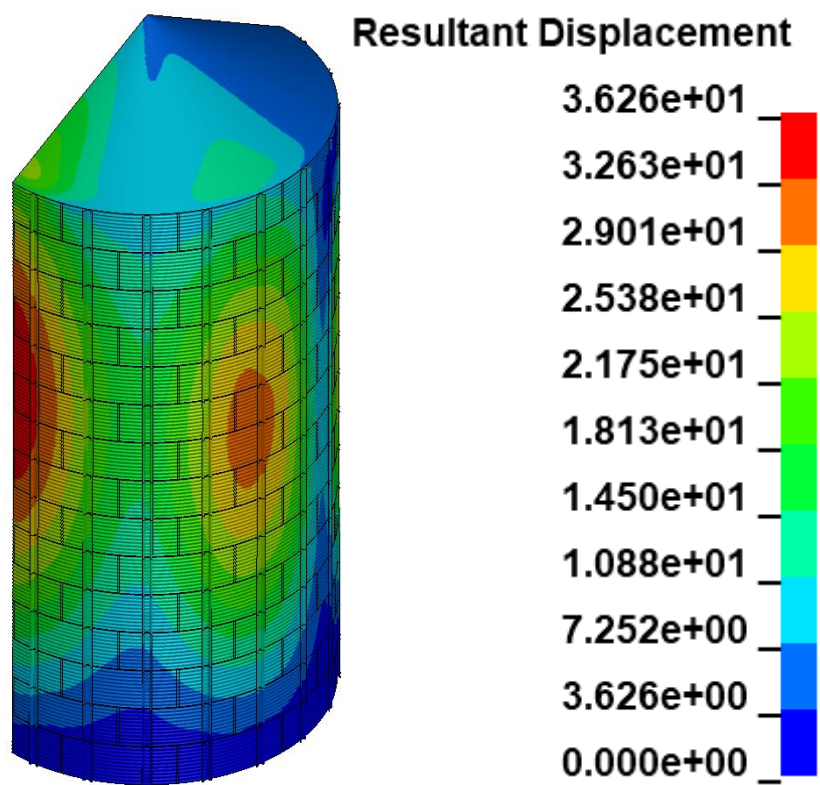
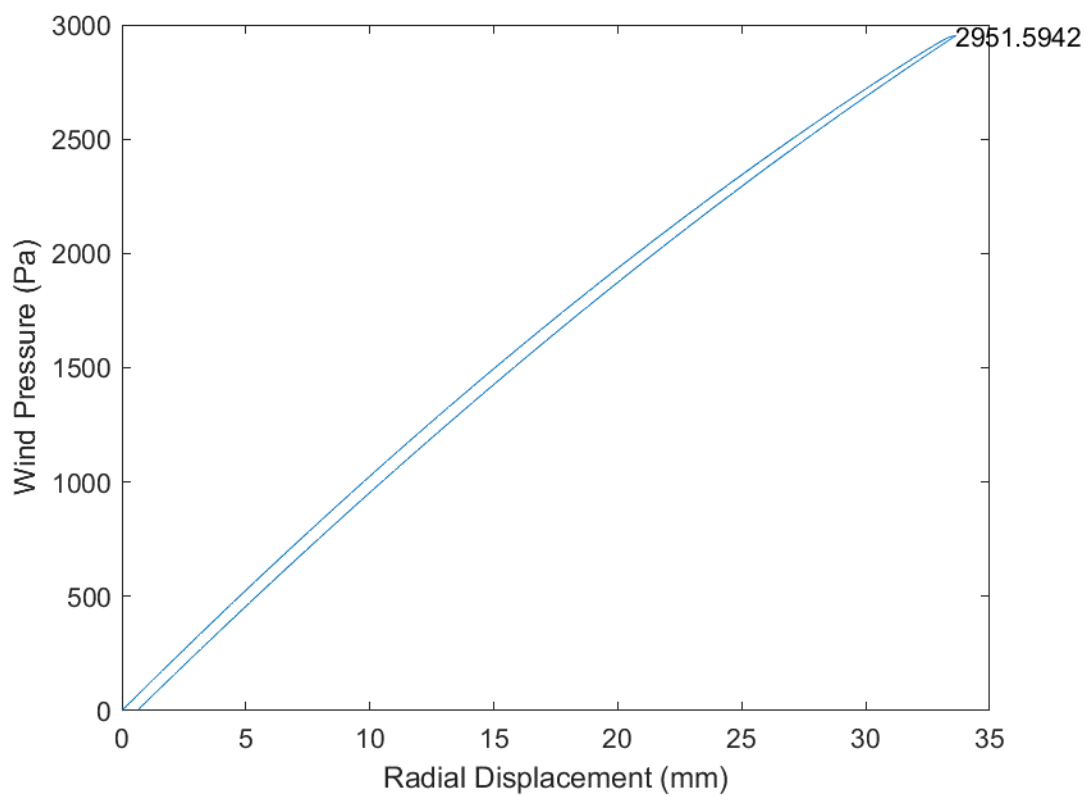


Fig. B.19 D30_H15_S20_R00_W00_V00_CL03_CD03_WT03_ST03

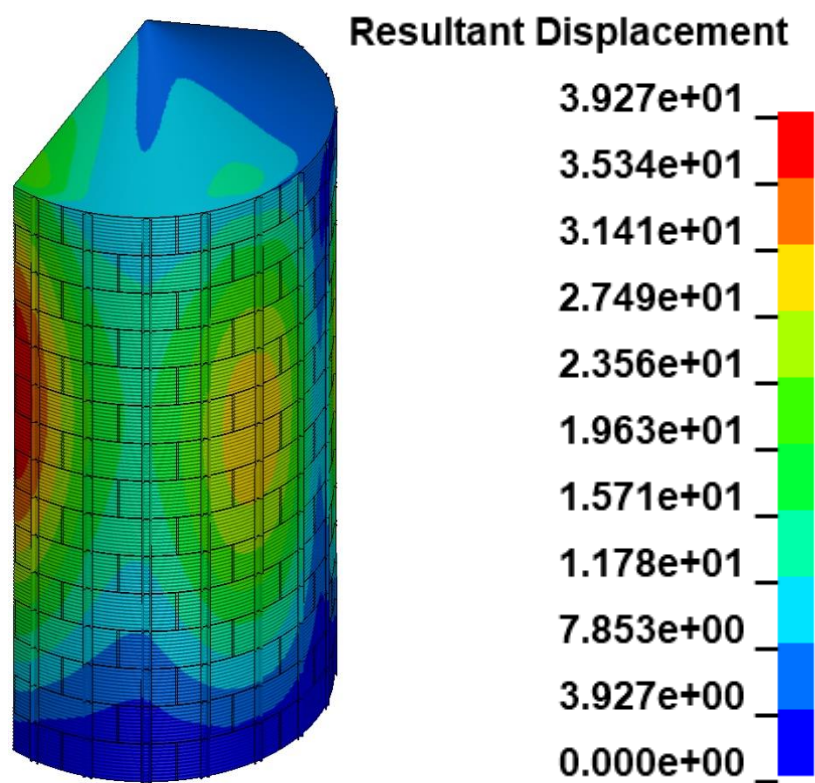
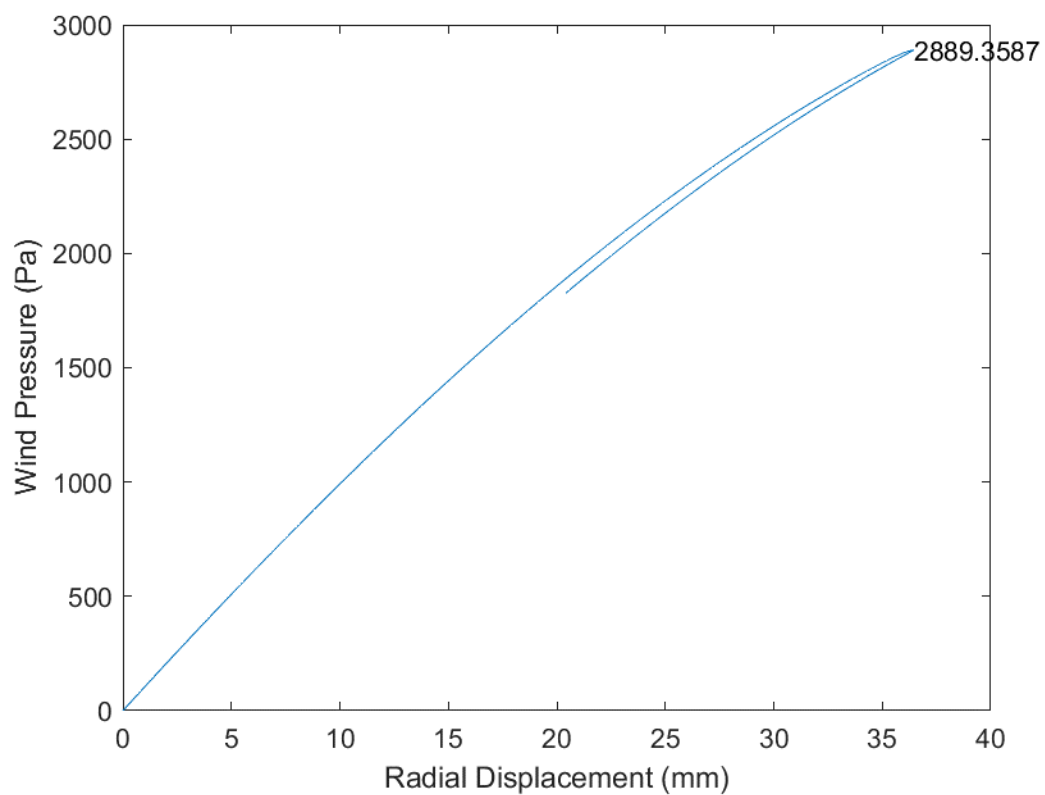


Fig. B.20 D30_H15_S20_R00_W00_V01_CL03_CD03_WT03_ST03

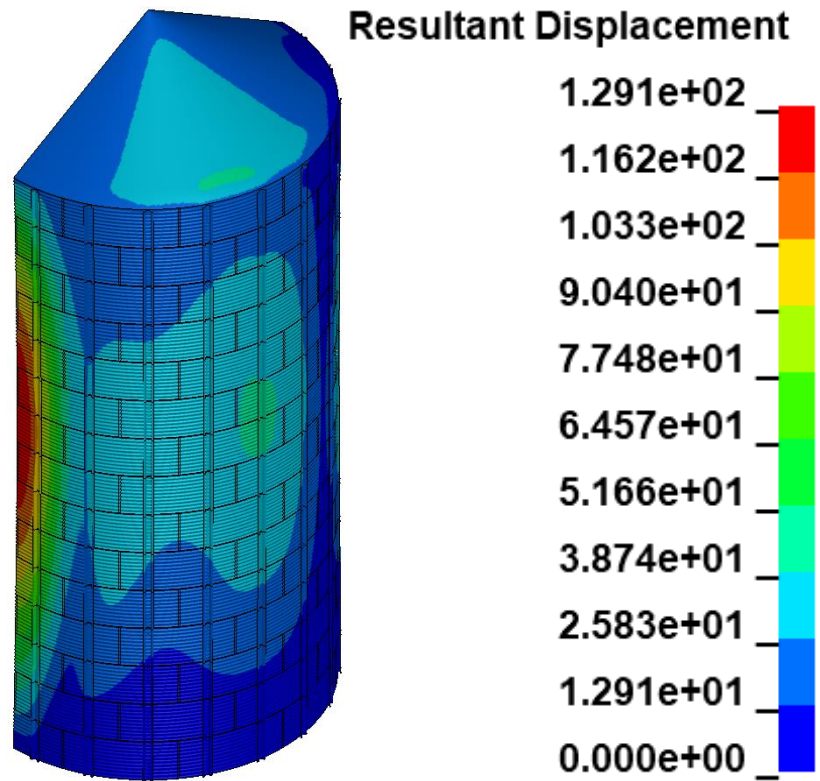
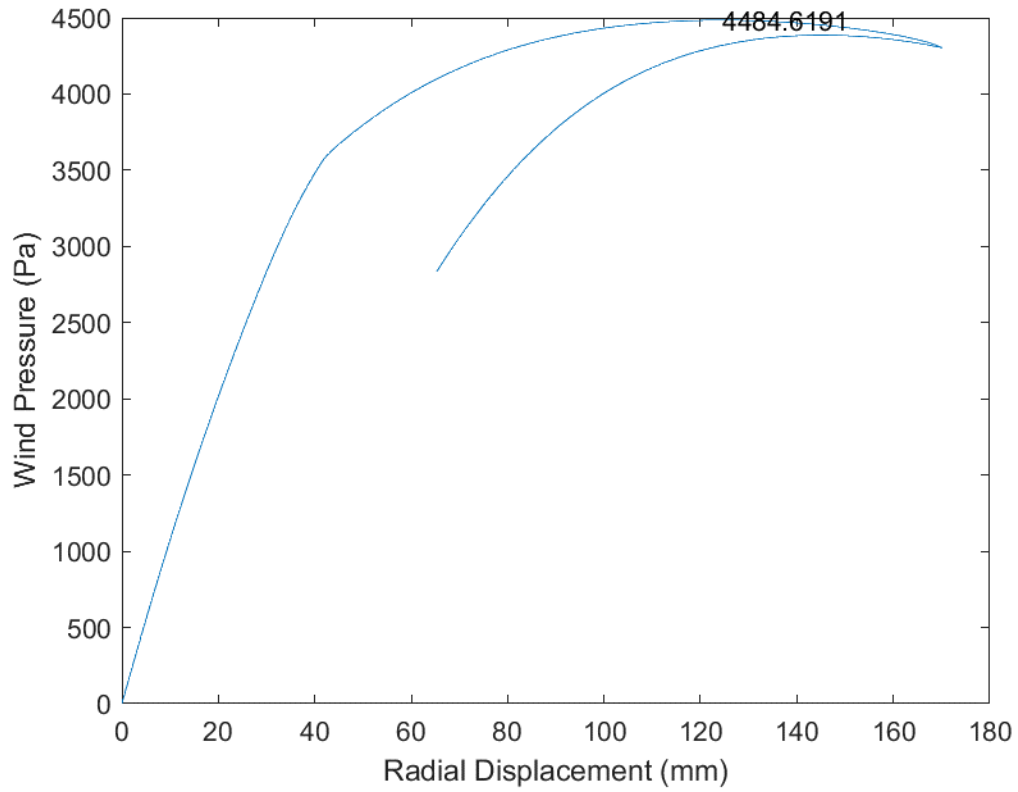


Fig. B.21 D30_H15_S20_R00_W01_V00_CL03_CD03_WT03_ST03

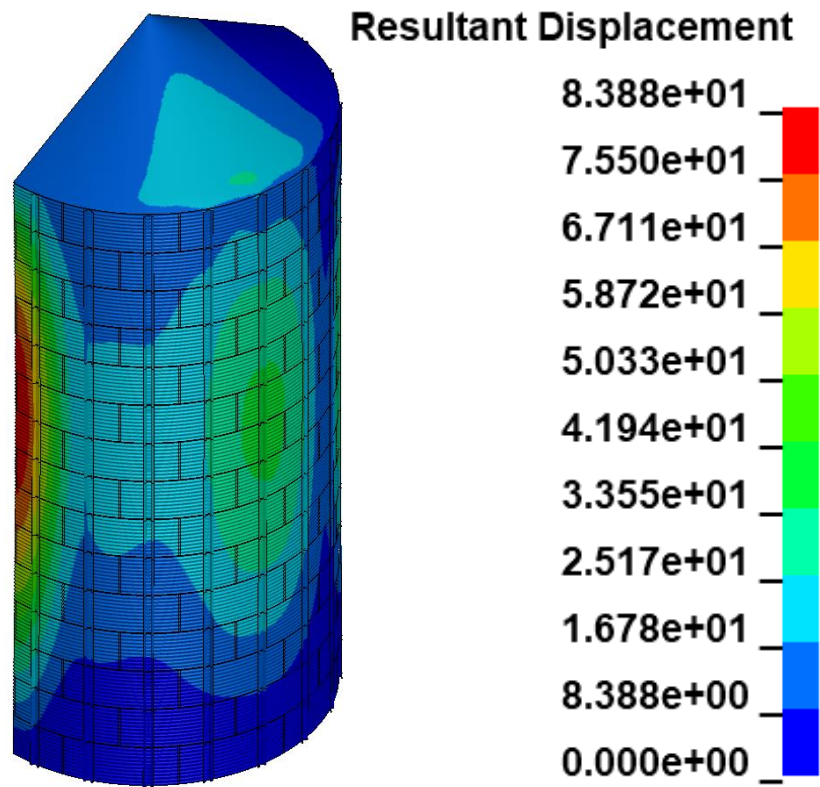
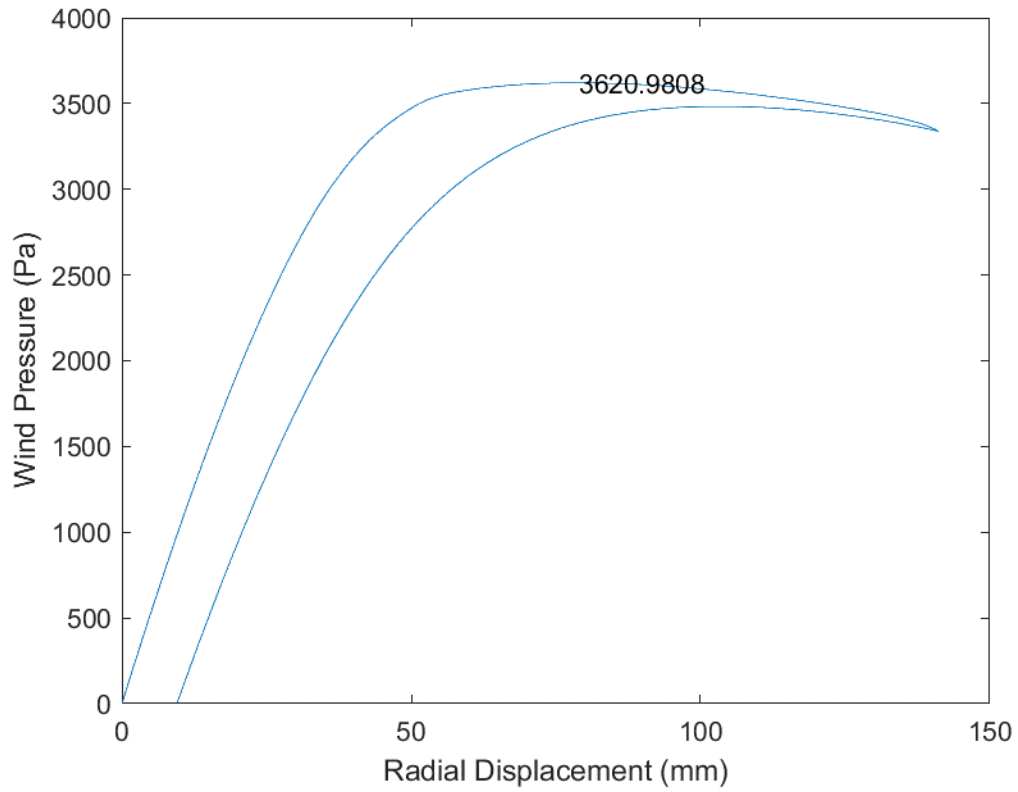


Fig. B.22 D30_H15_S20_R00_W01_V01_CL03_CD03_WT03_ST03

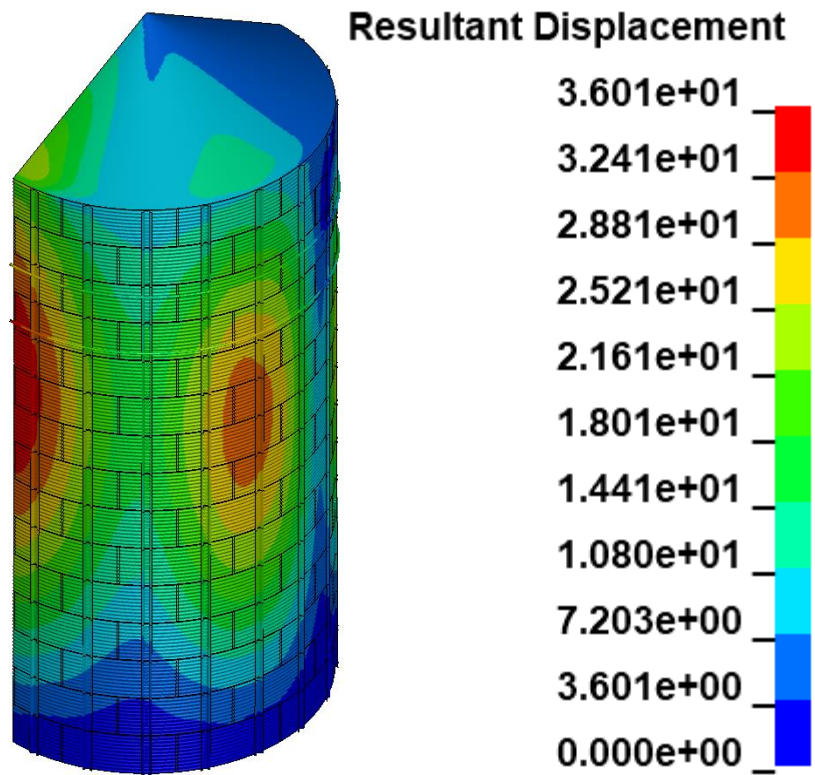
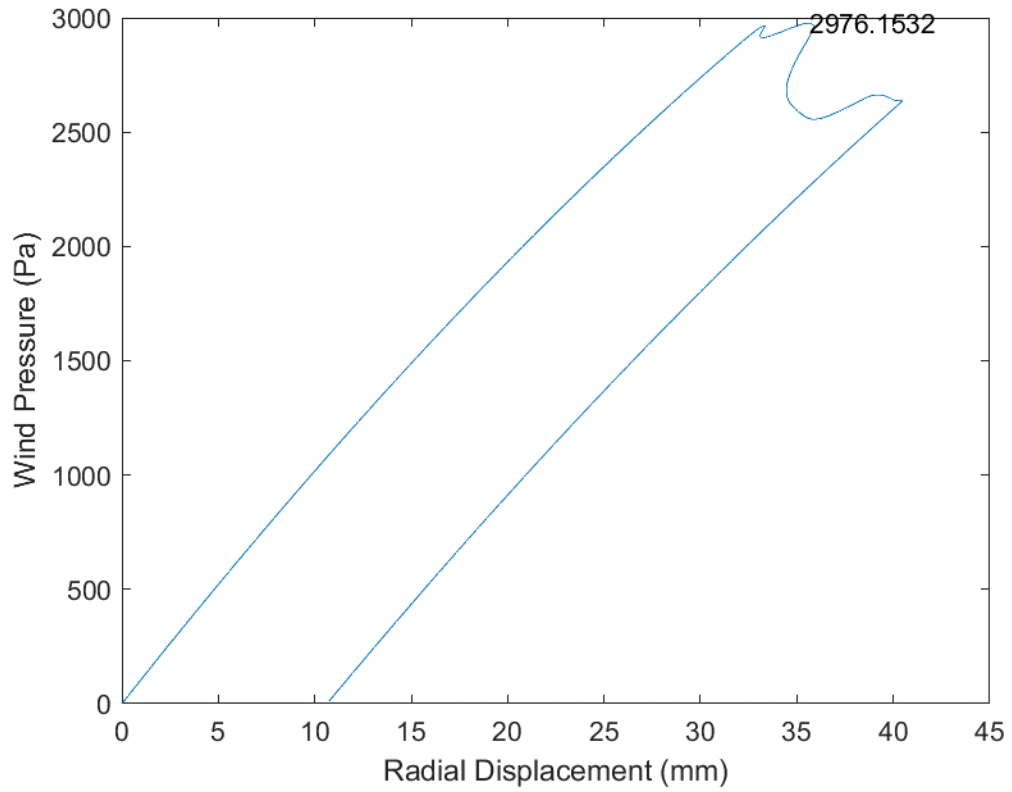


Fig. B.23 D30_H15_S20_R02_W00_V00_CL03_CD03_WT03_ST03

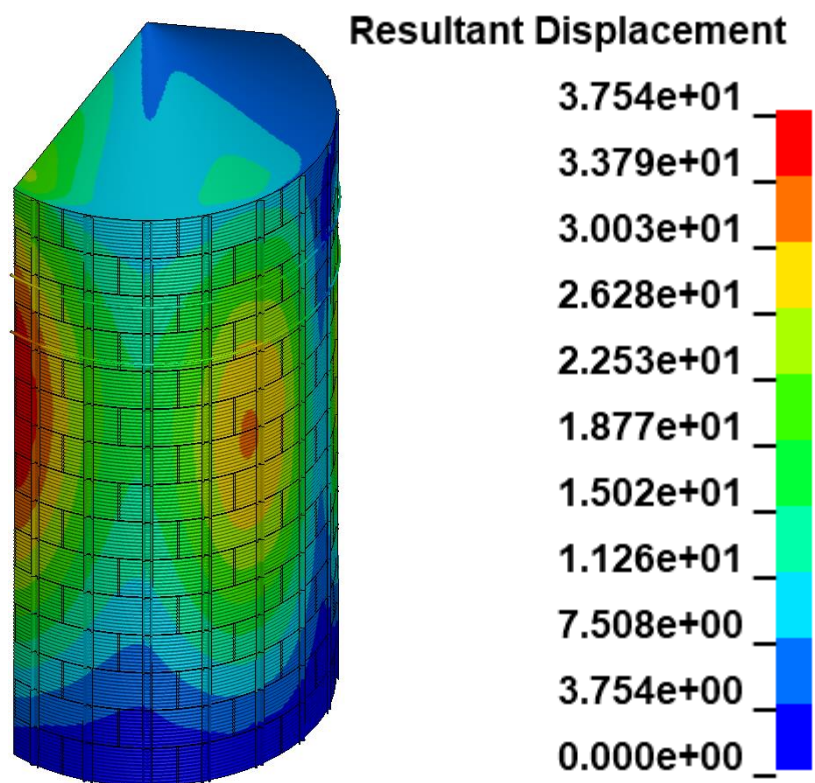
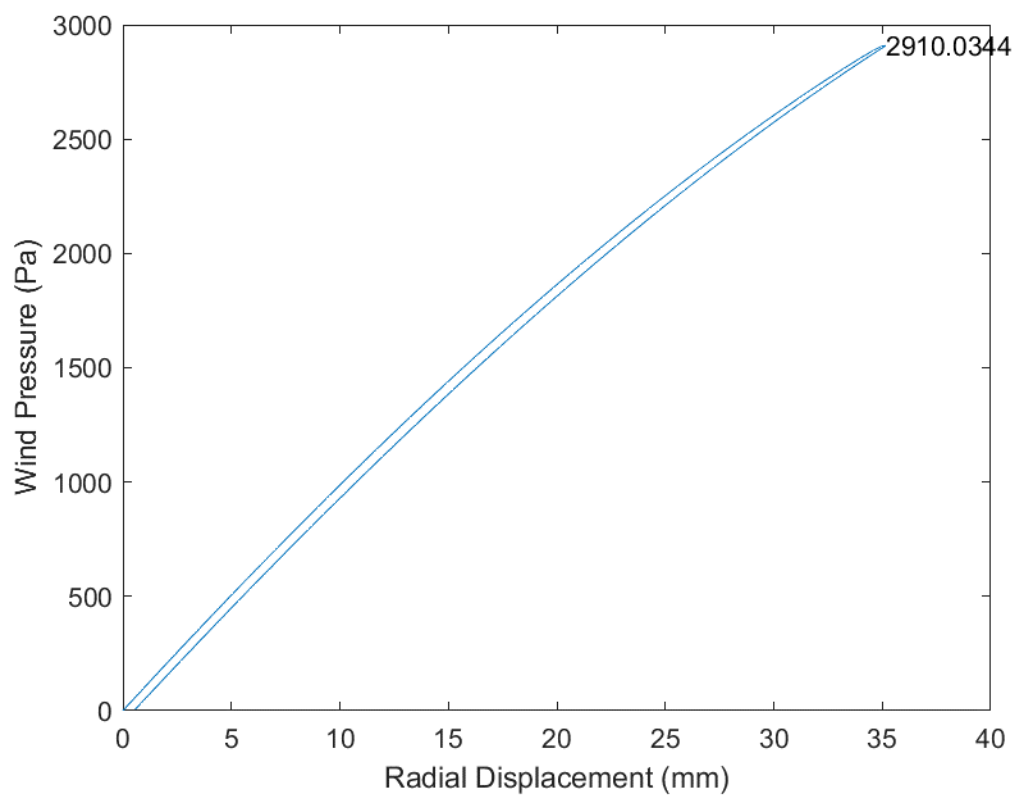


Fig. B.24 D30_H15_S20_R02_W00_V01_CL03_CD03_WT03_ST03

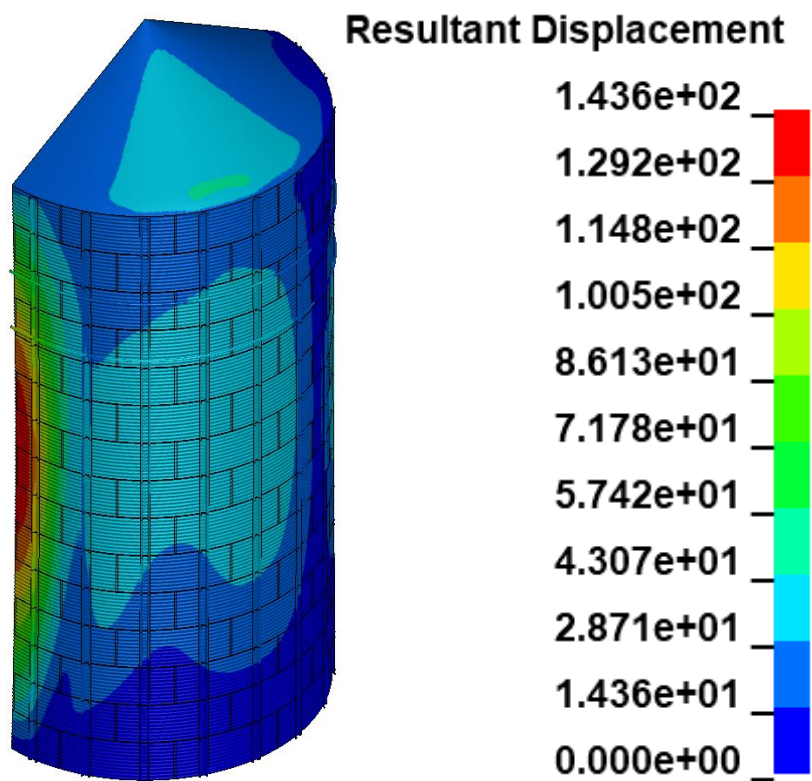
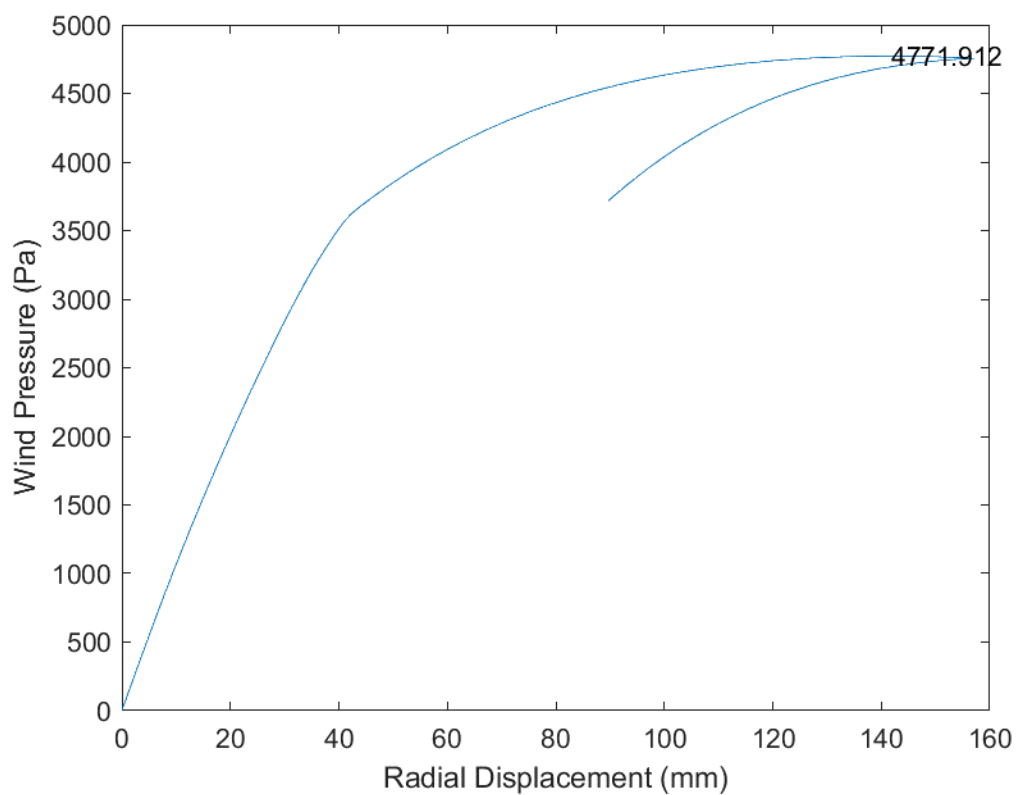


Fig. B.25 D30_H15_S20_R02_W01_V00_CL03_CD03_WT03_ST03

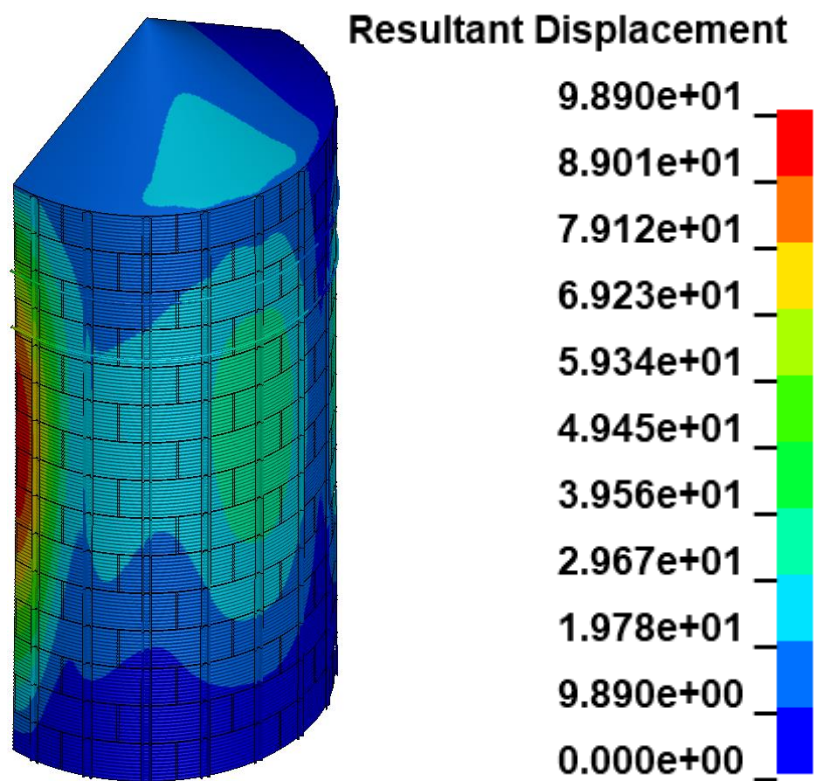
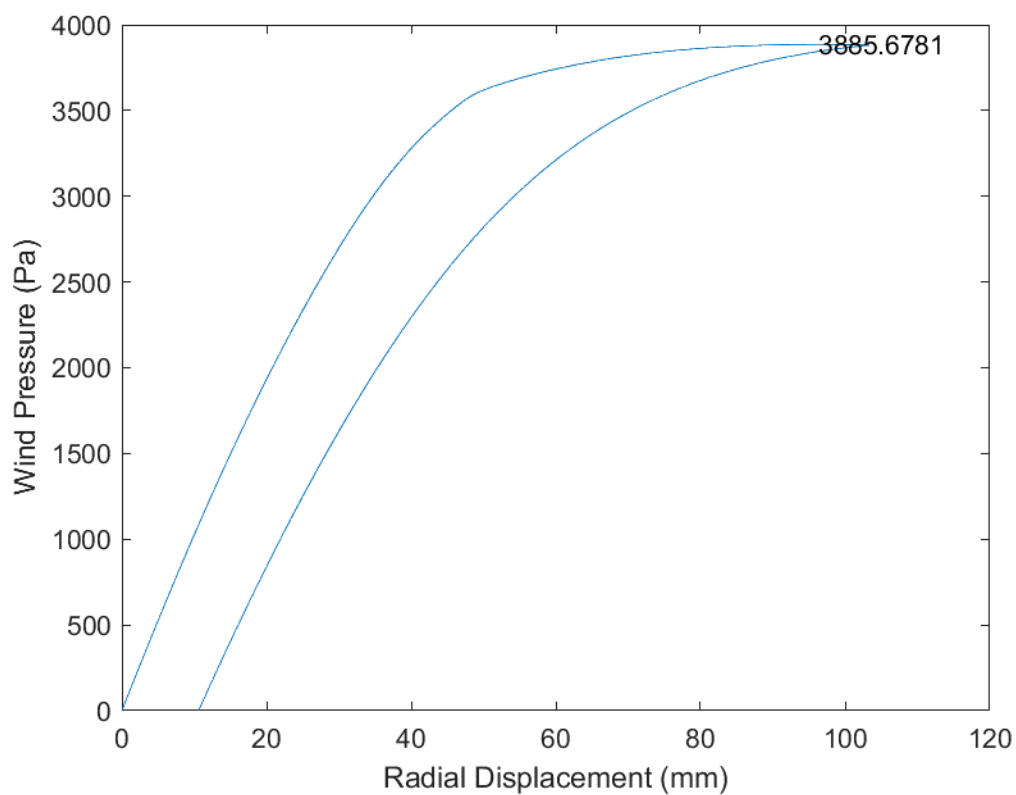


Fig. B.26 D30_H15_S20_R02_W01_V01_CL03_CD03_WT03_ST03

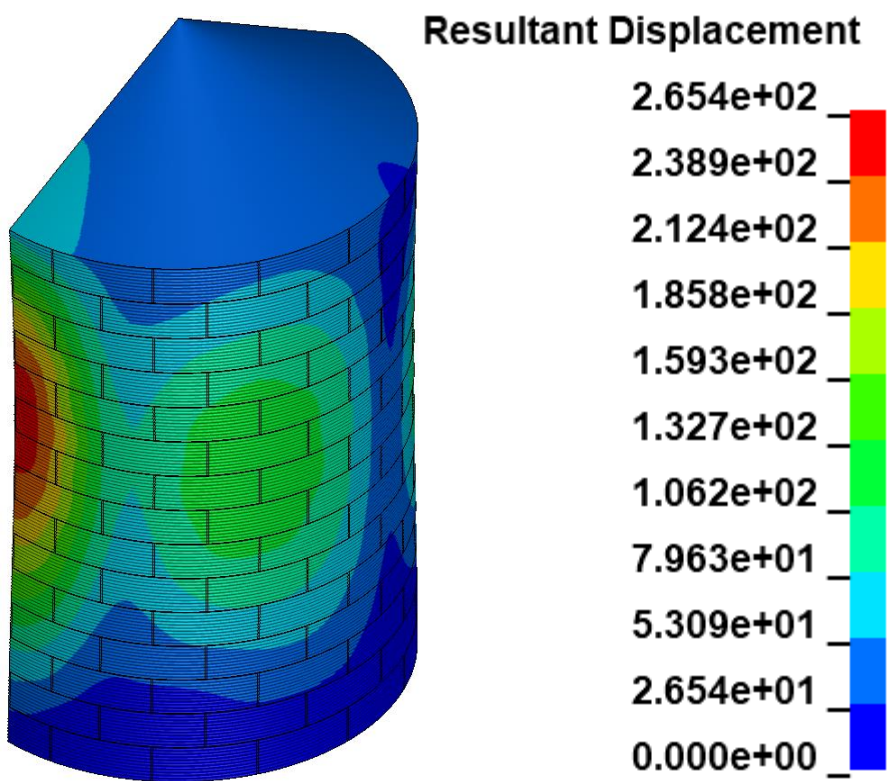
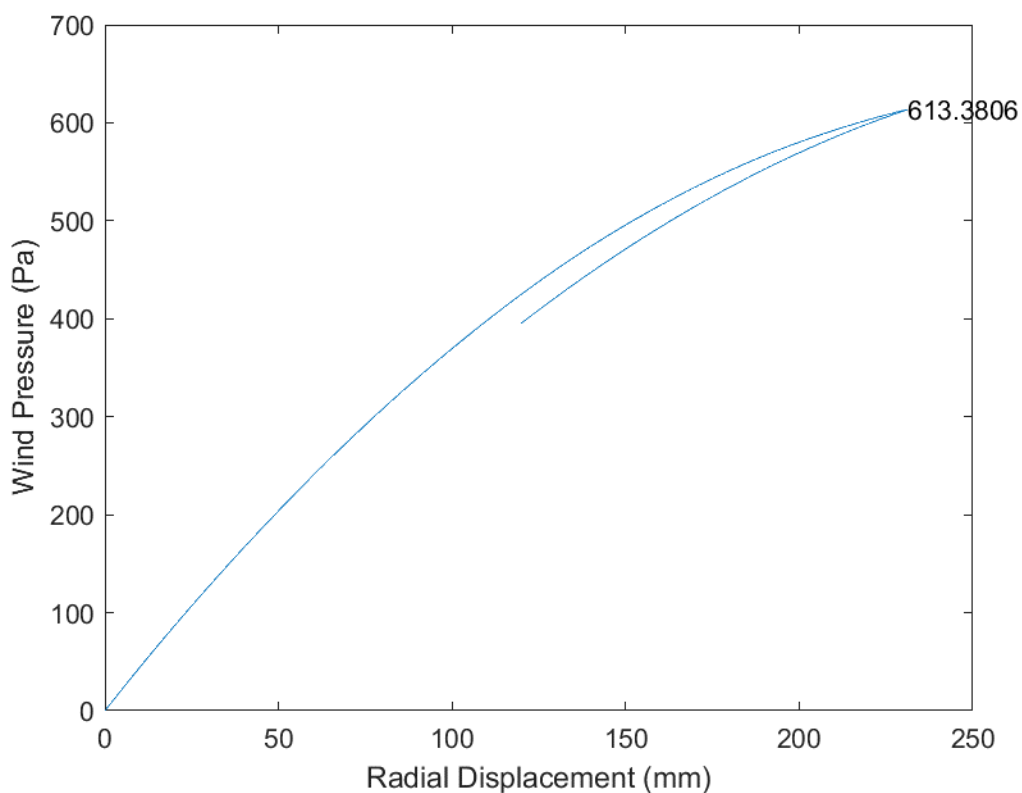


Fig. B.27 D42_H15_S00_R00_W00_V00_CL03_CD03_WT03_ST03

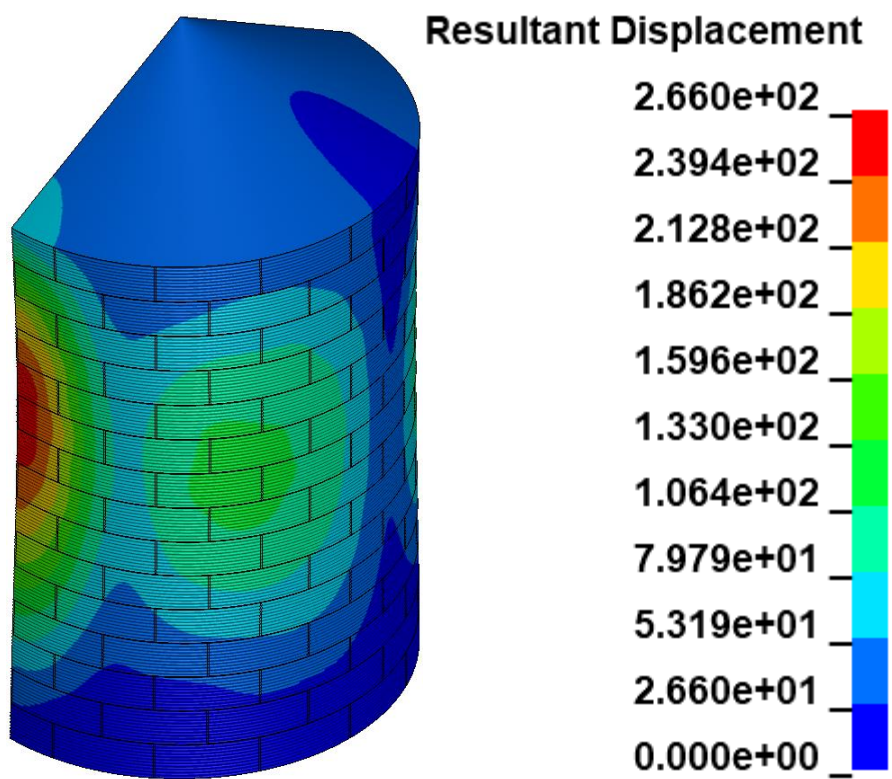
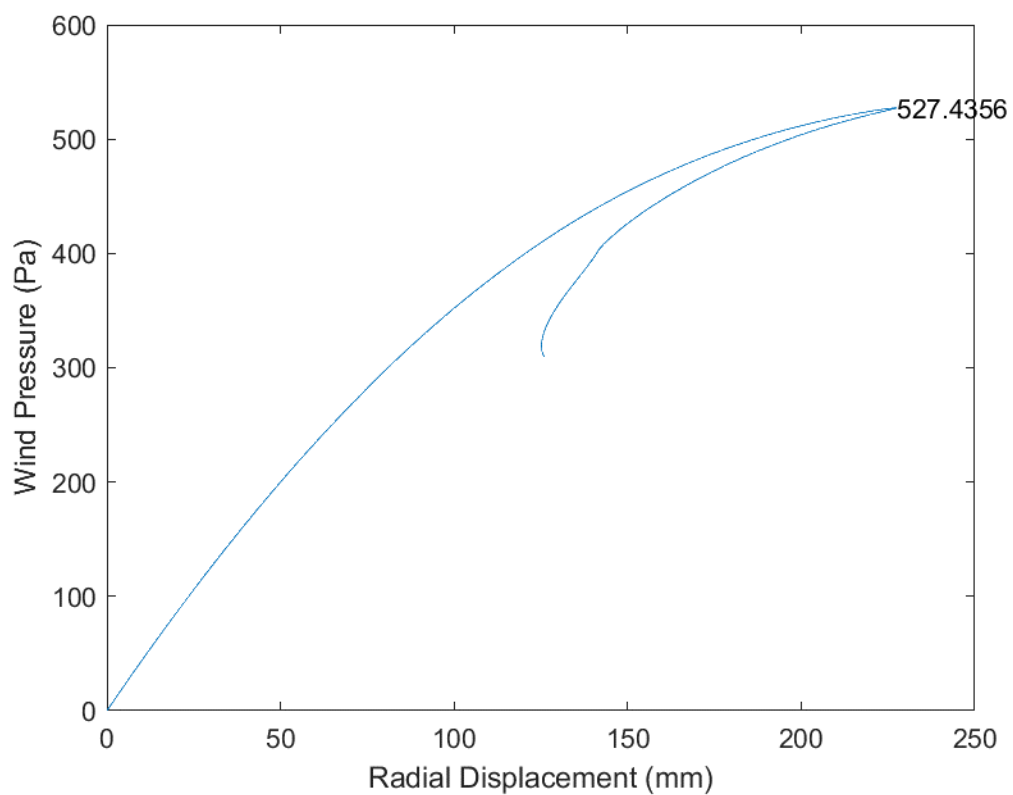


Fig. B.28 D42_H15_S00_R00_W00_V01_CL03_CD03_WT03_ST03

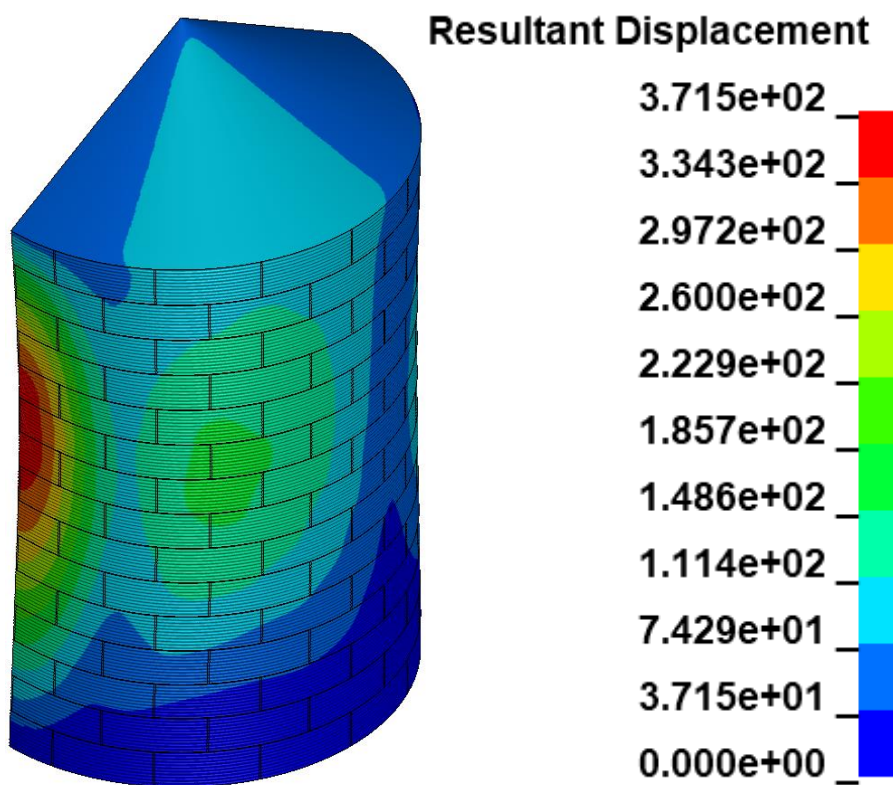
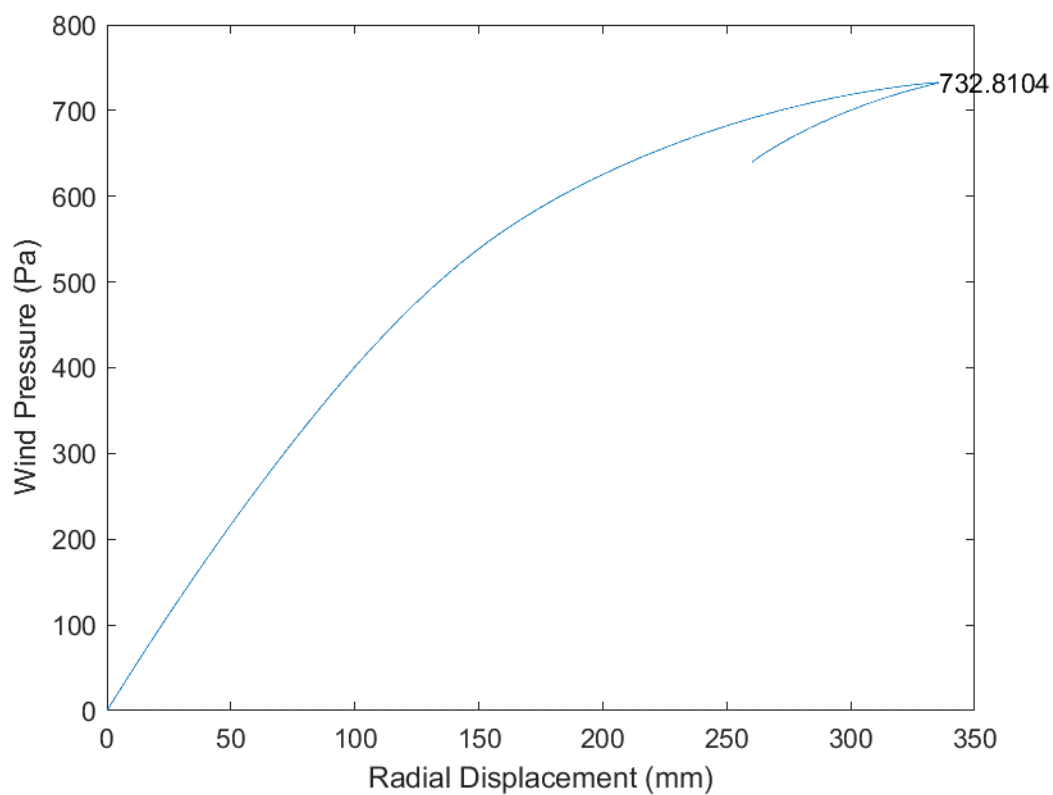


Fig. B.29 D42_H15_S00_R00_W01_V00_CL03_CD03_WT03_ST03

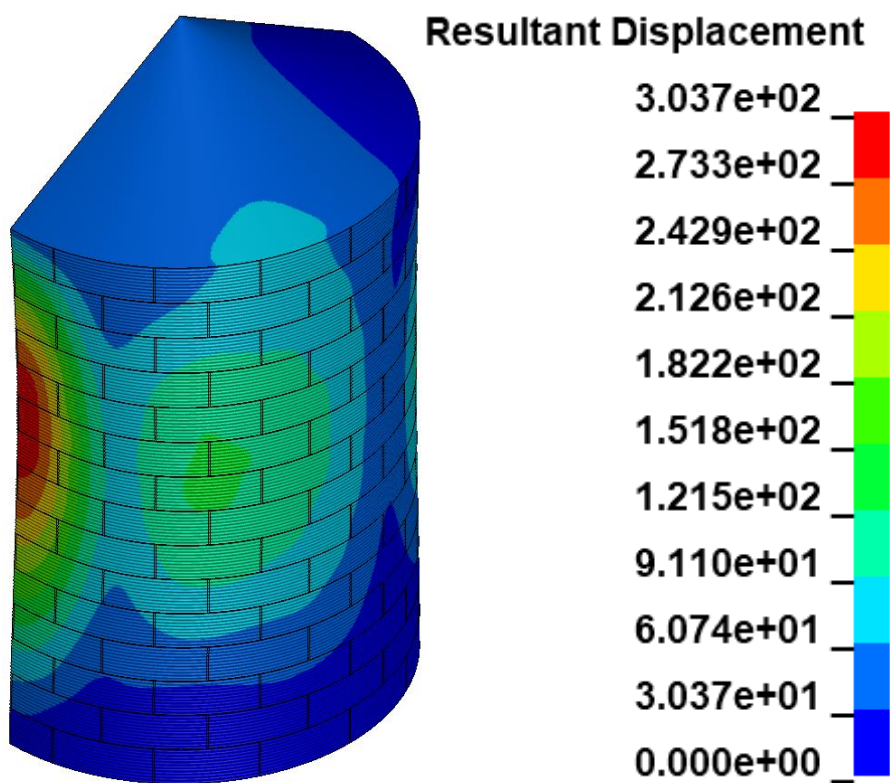
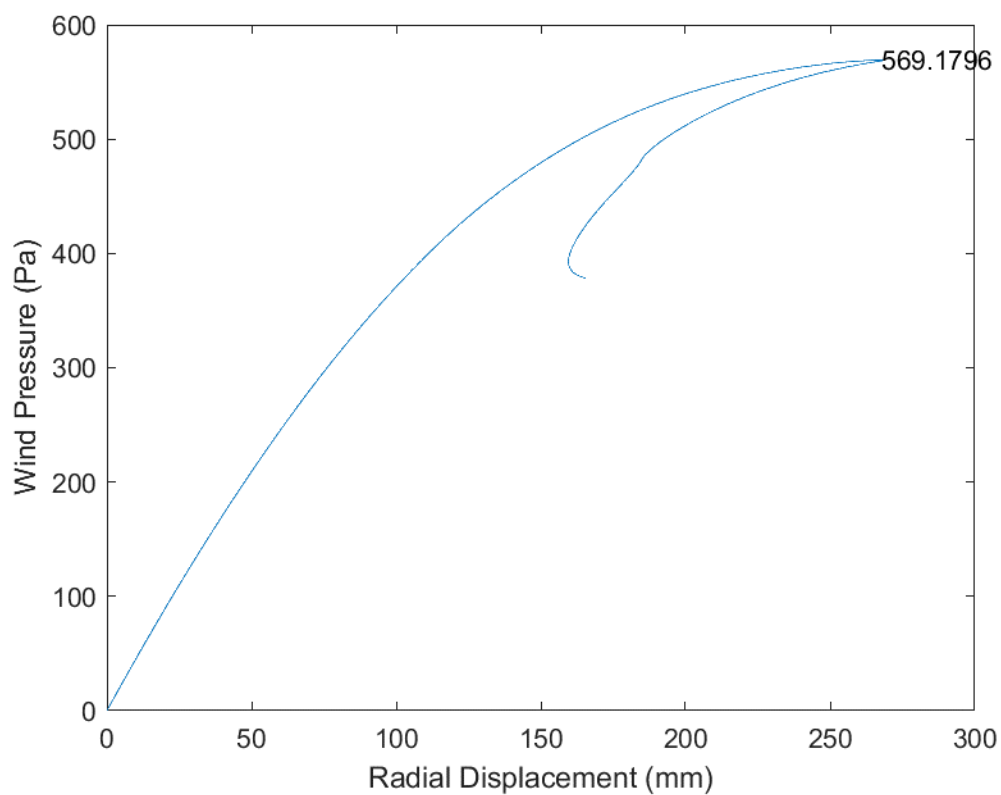


Fig. B.30 D42_H15_S00_R00_W01_V01_CL03_CD03_WT03_ST03

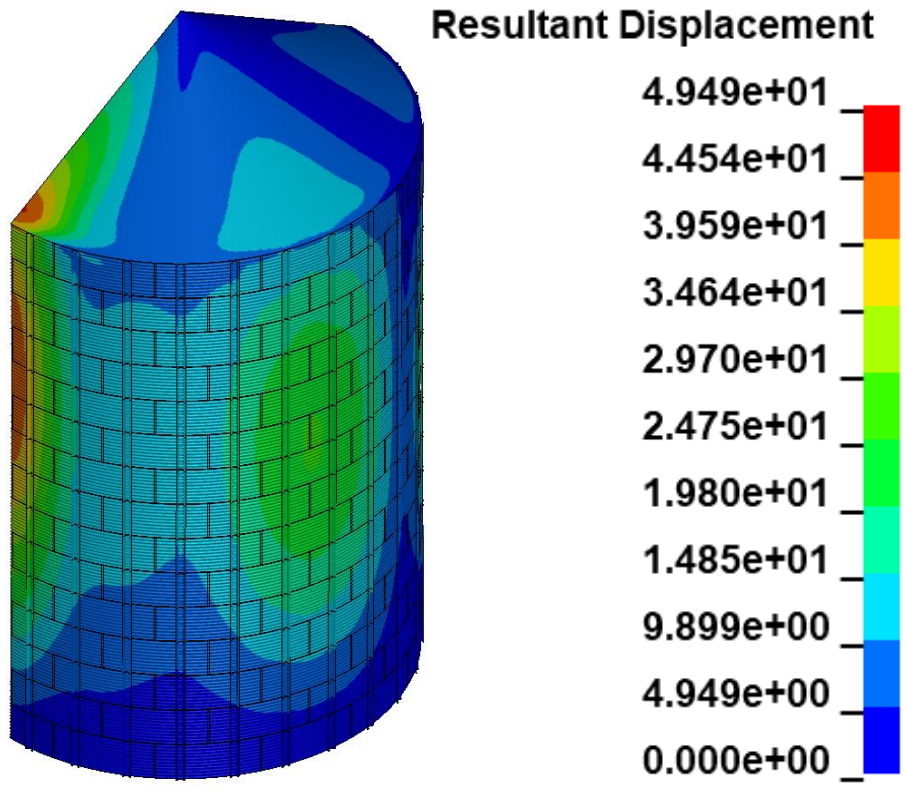
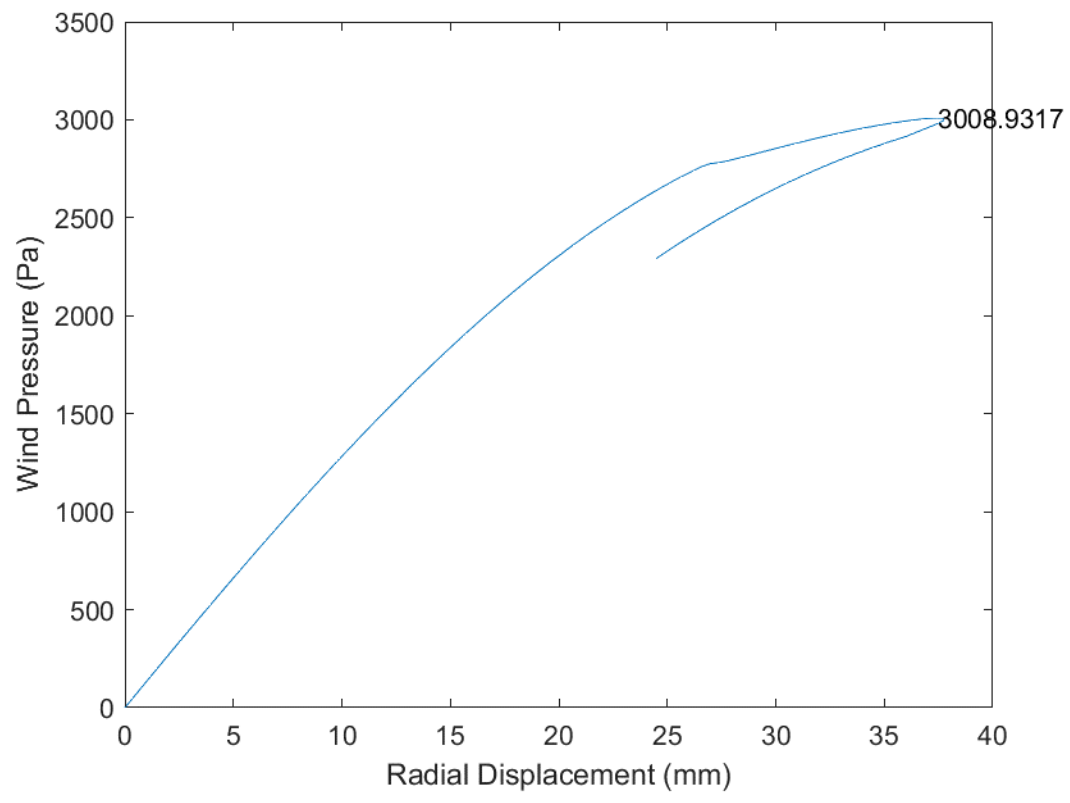


Fig. B.31 D42_H15_S28_R00_W00_V00_CL03_CD03_WT03_ST03

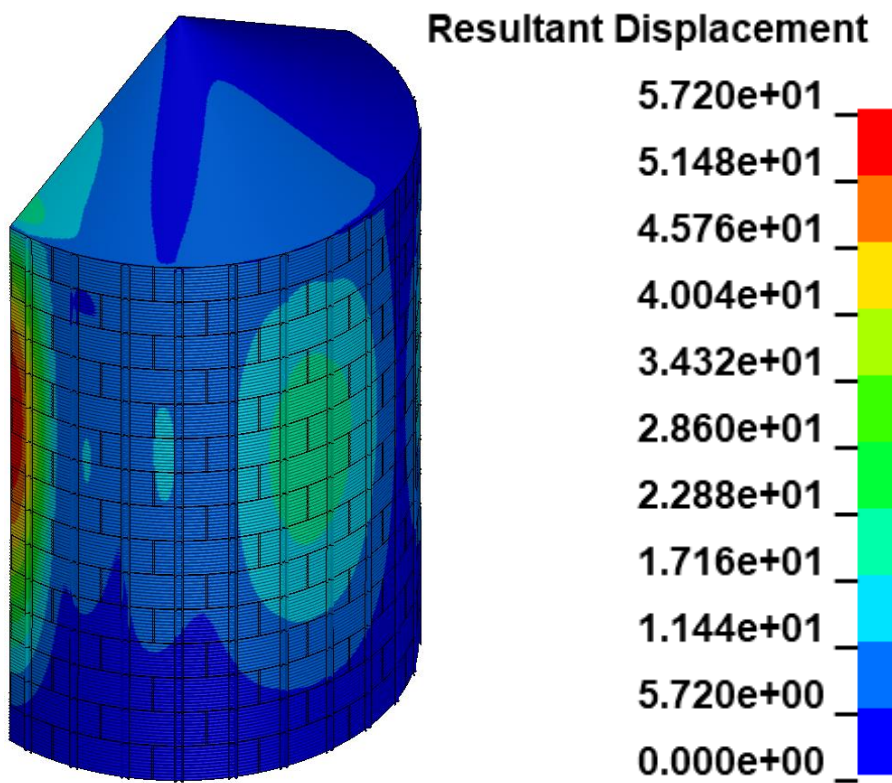
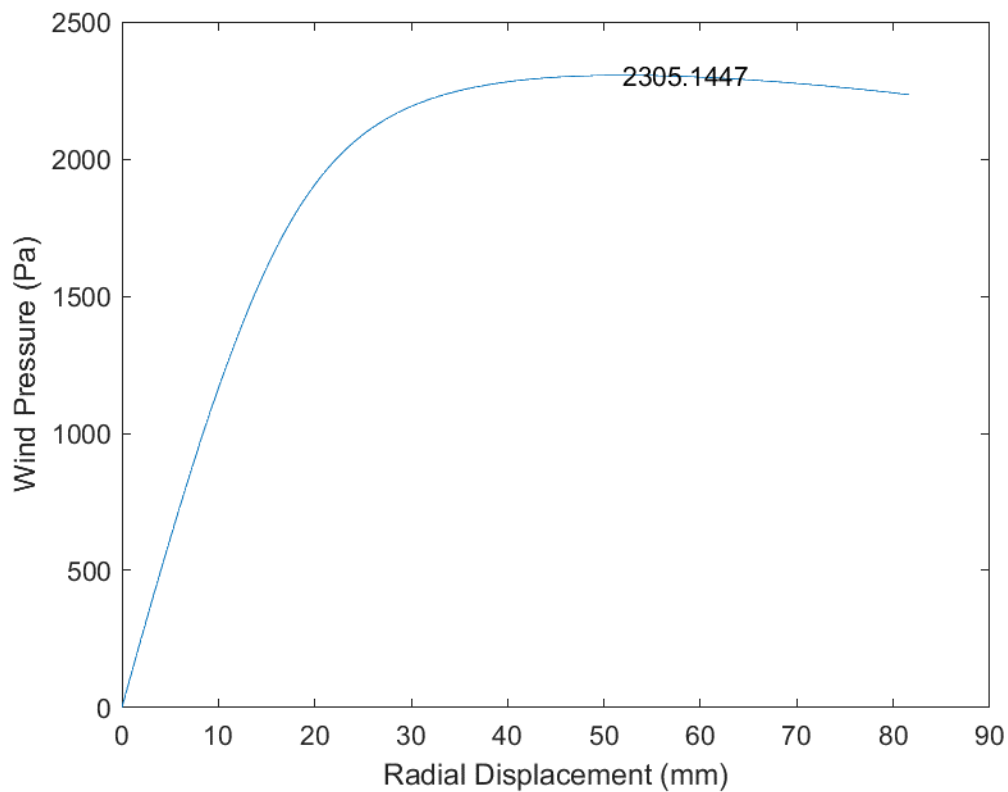


Fig. B.32 D42_H15_S28_R00_W00_V01_CL03_CD03_WT03_ST03

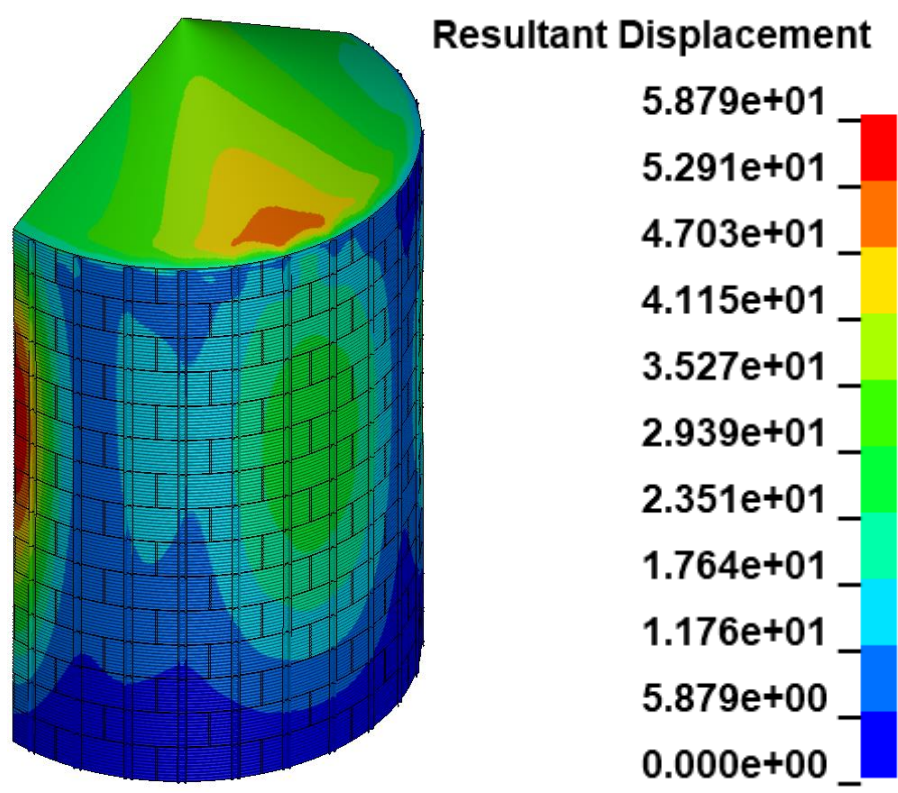
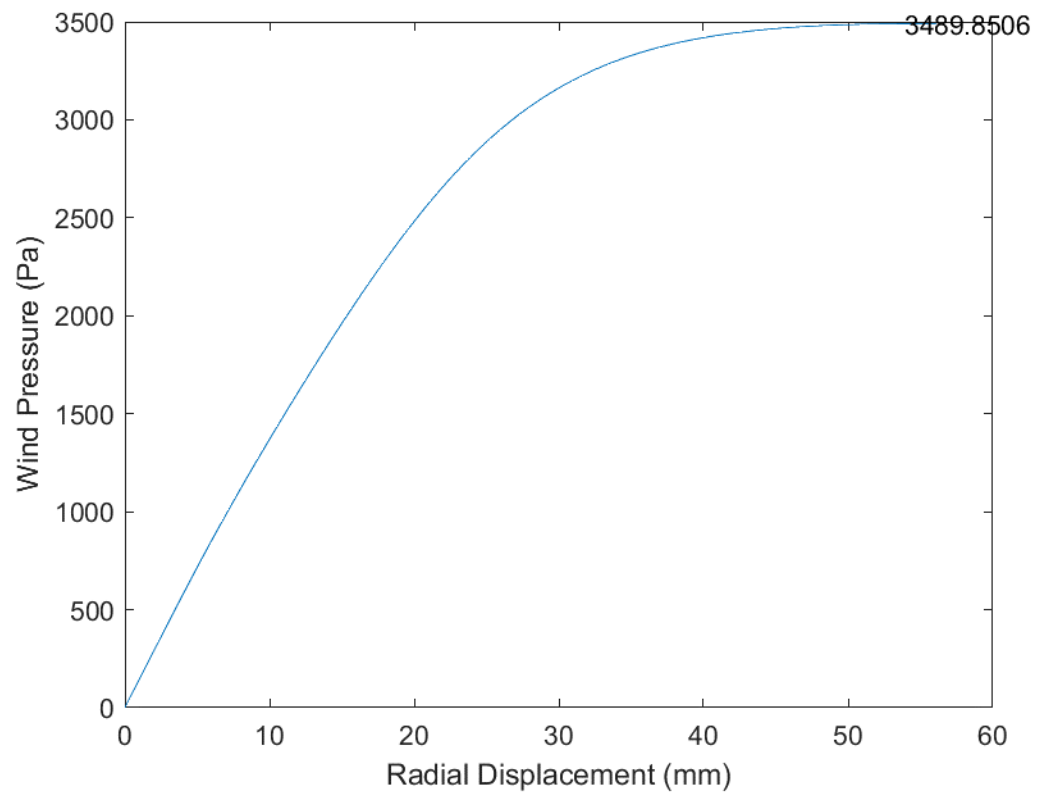


Fig. B.33 D42_H15_S28_R00_W01_V00_CL03_CD03_WT03_ST03

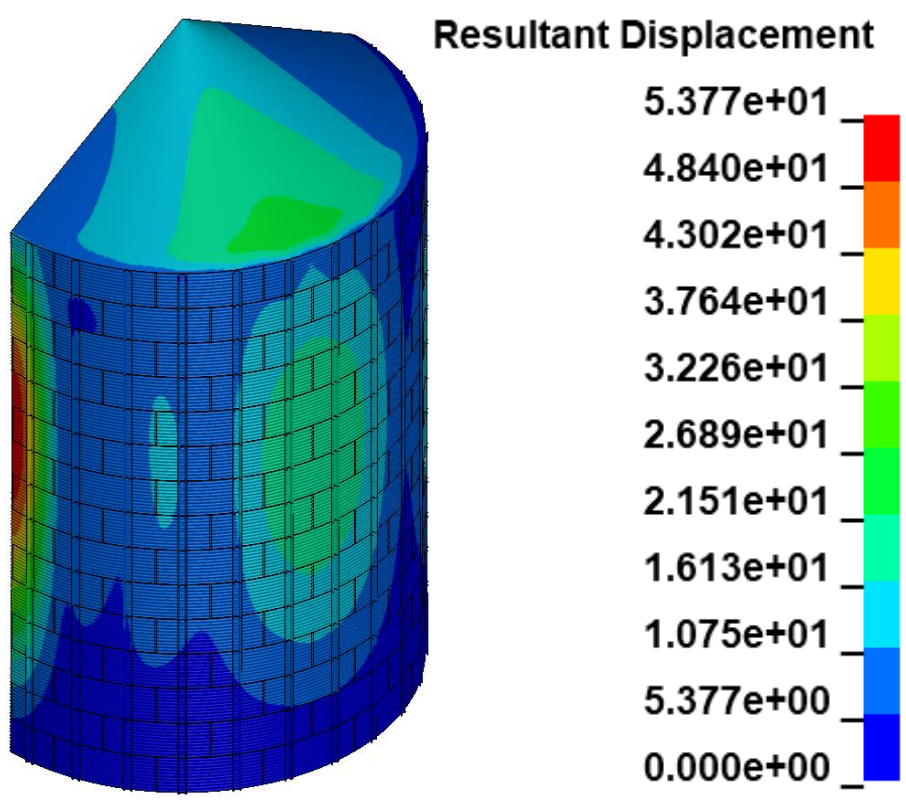
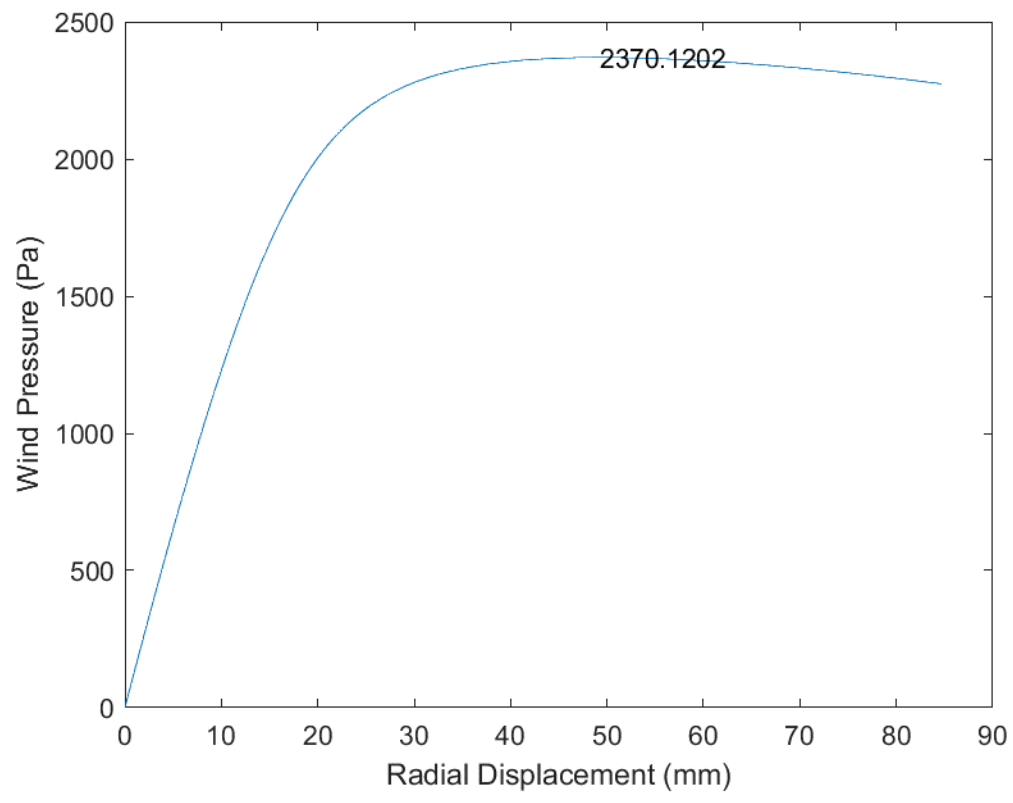


Fig. B.34 D42_H15_S28_R00_W01_V01_CL03_CD03_WT03_ST03

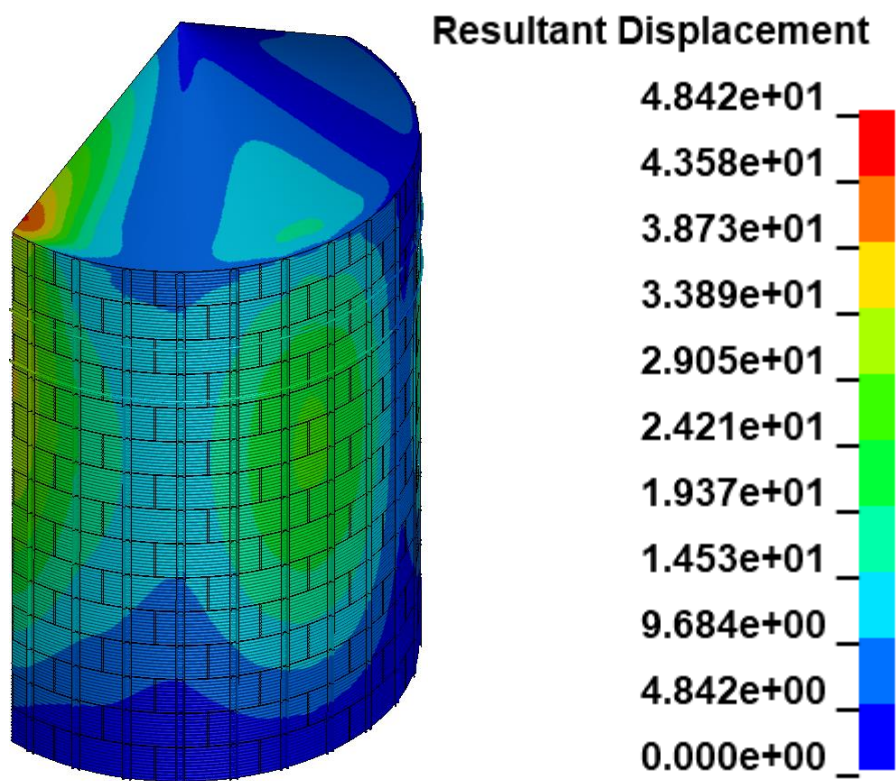
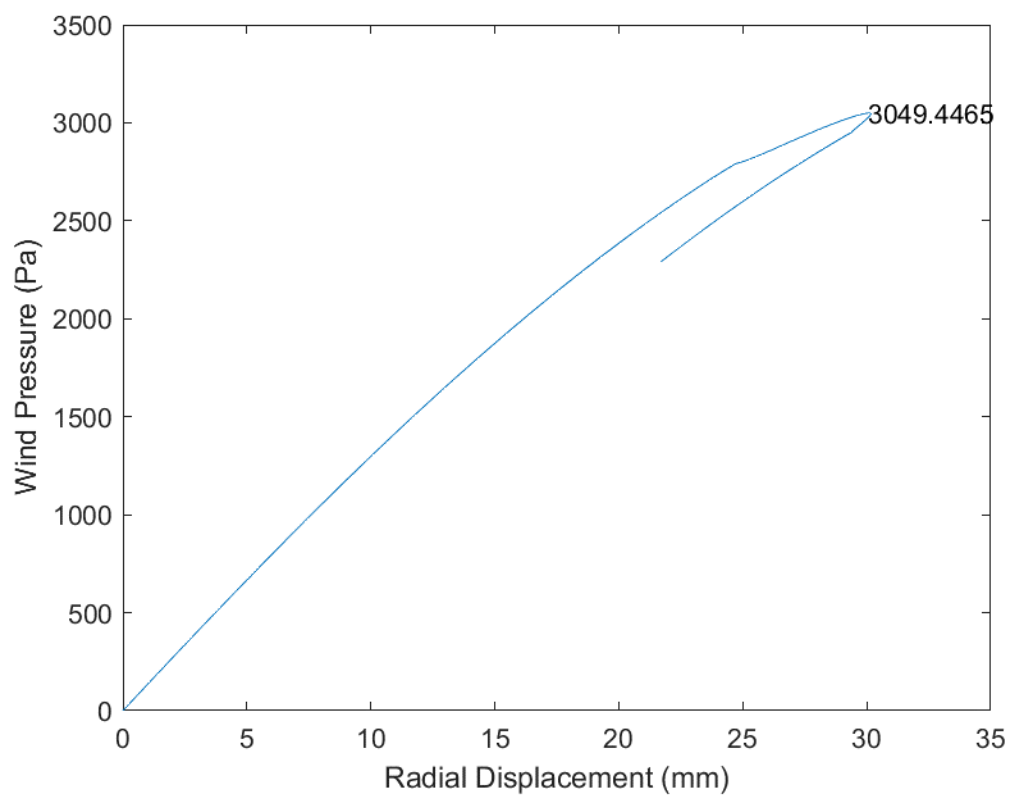


Fig. B.35 D42_H15_S28_R02_W00_V00_CL03_CD03_WT03_ST03

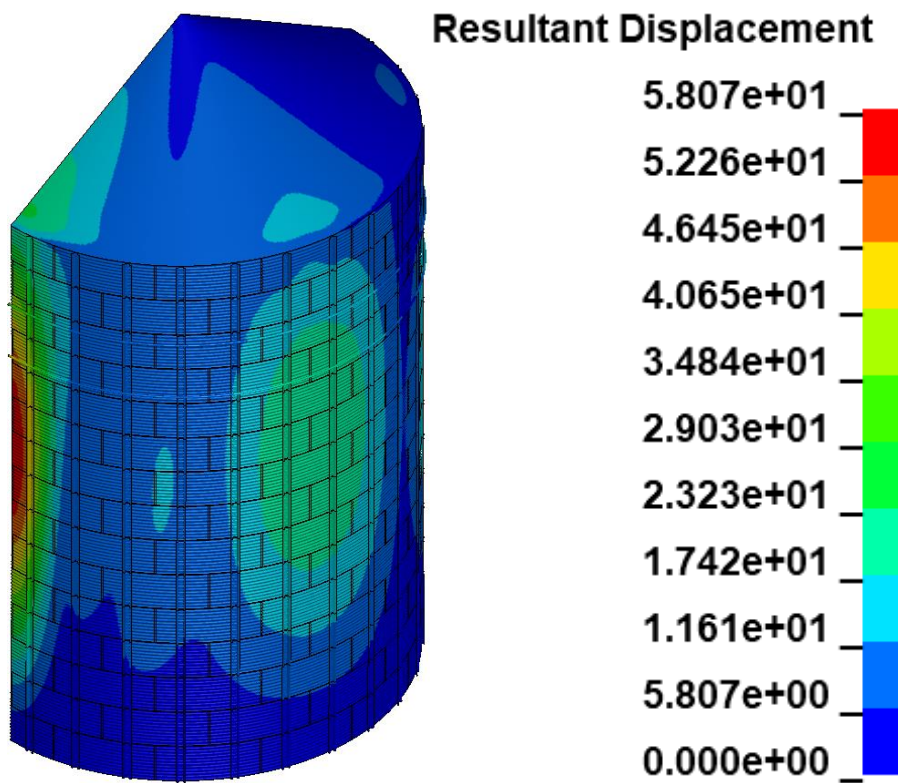
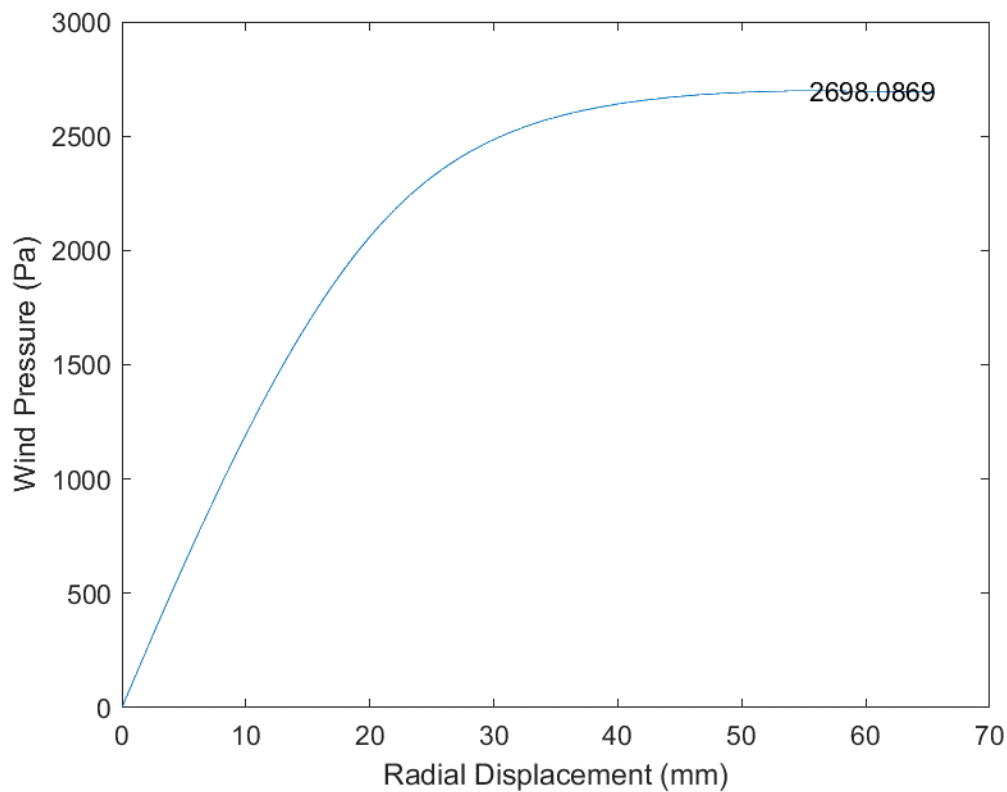


Fig. B.36 D42_H15_S28_R02_W00_V01_CL03_CD03_WT03_ST03

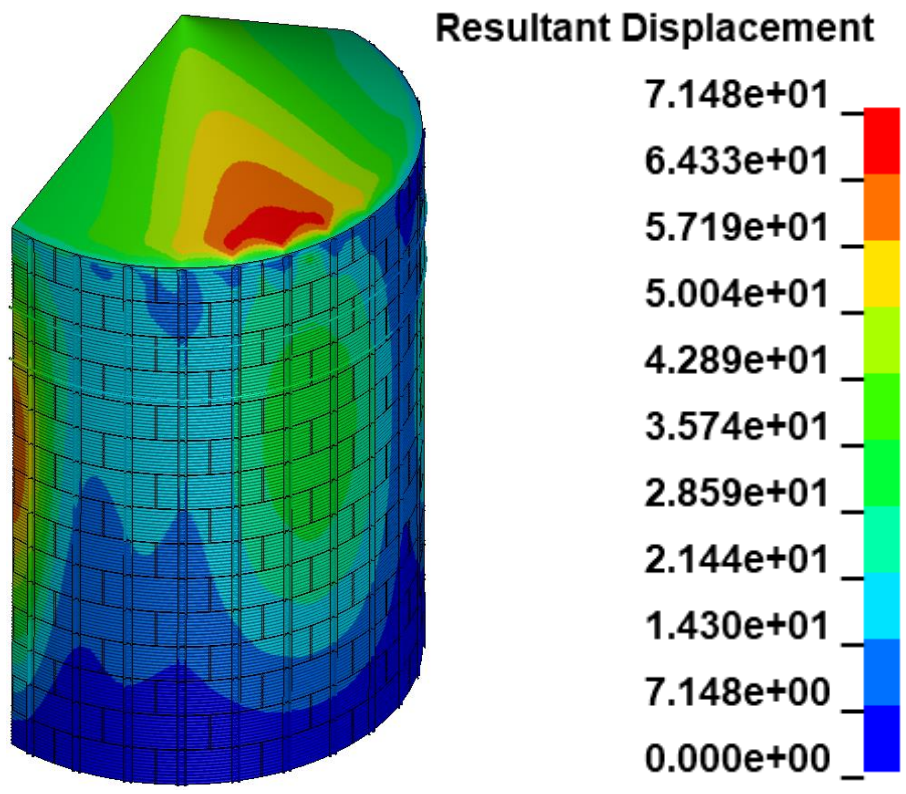
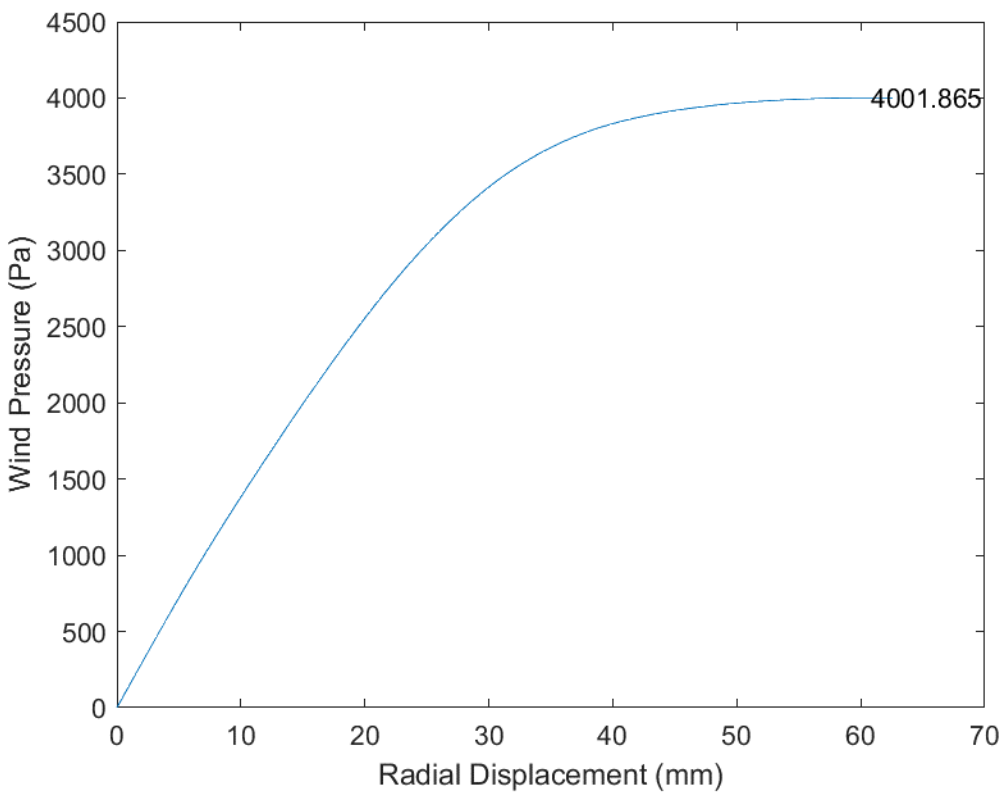


Fig. B.37 D42_H15_S28_R02_W01_V00_CL03_CD03_WT03_ST03

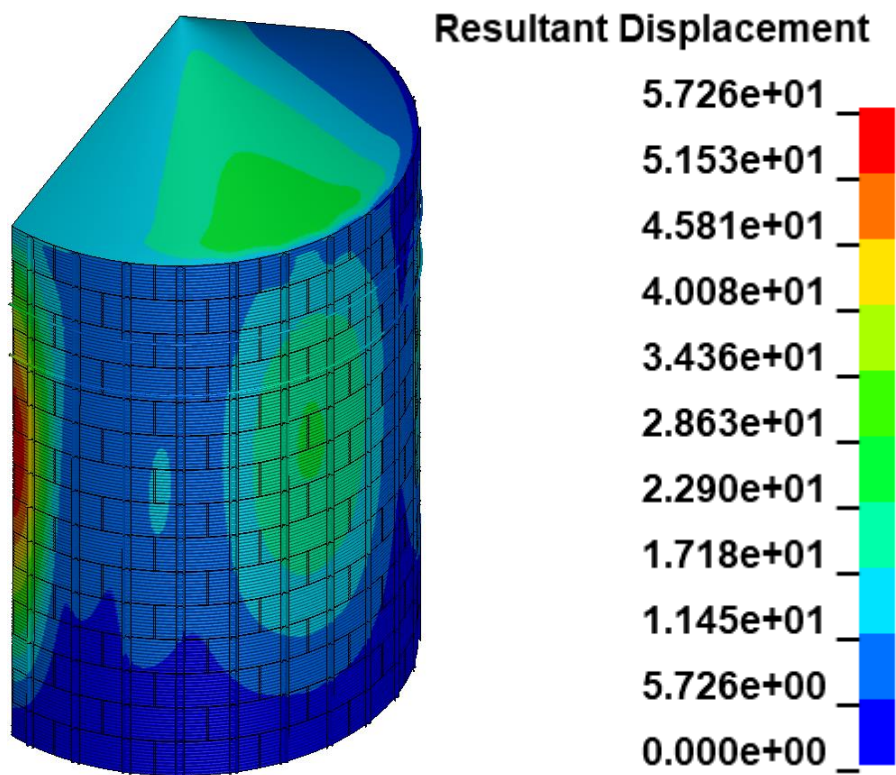
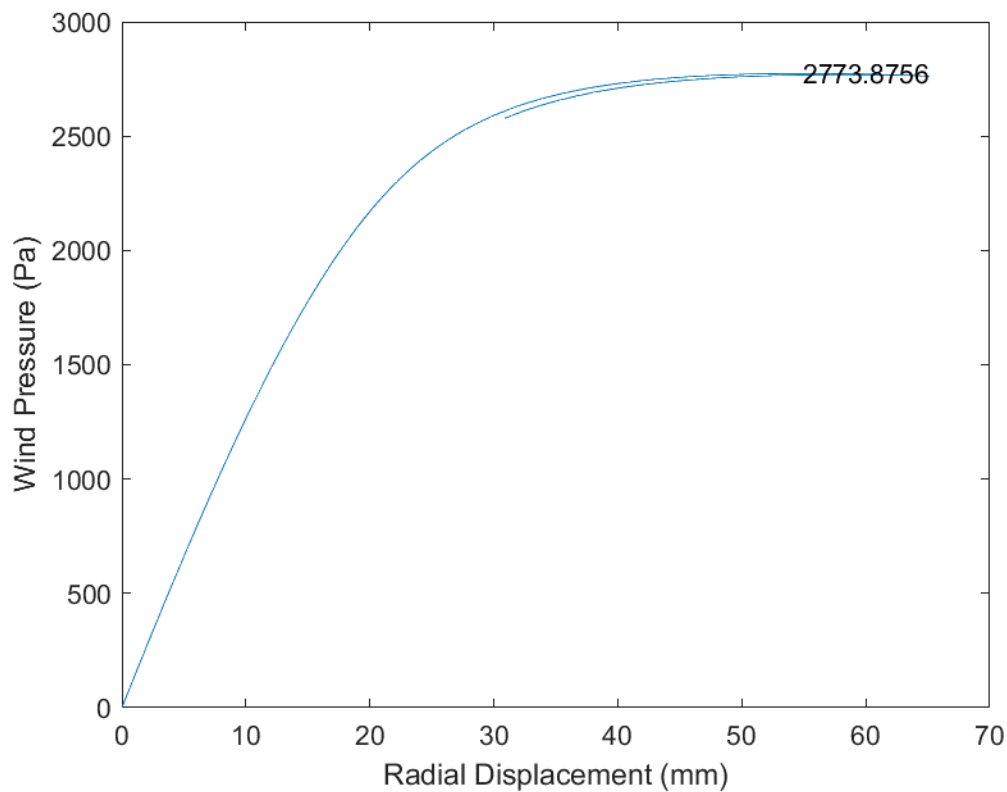


Fig. B.38 D42_H15_S28_R02_W01_V01_CL03_CD03_WT03_ST03

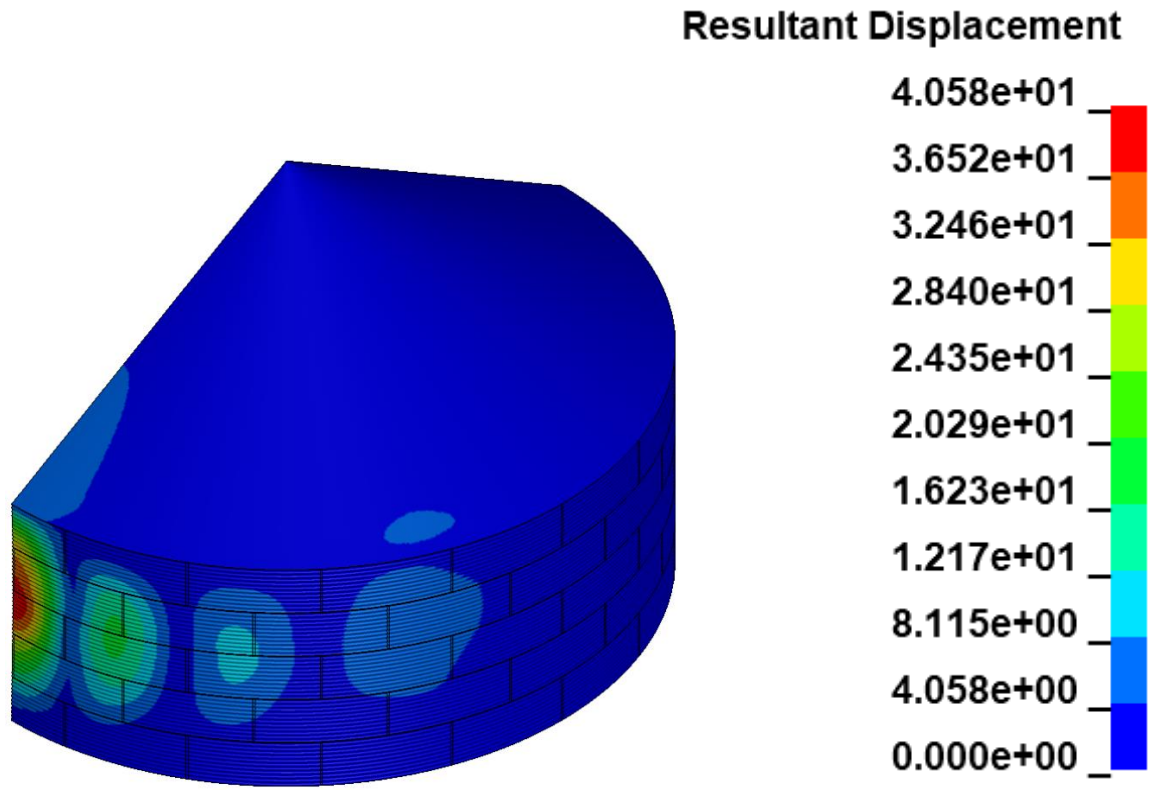
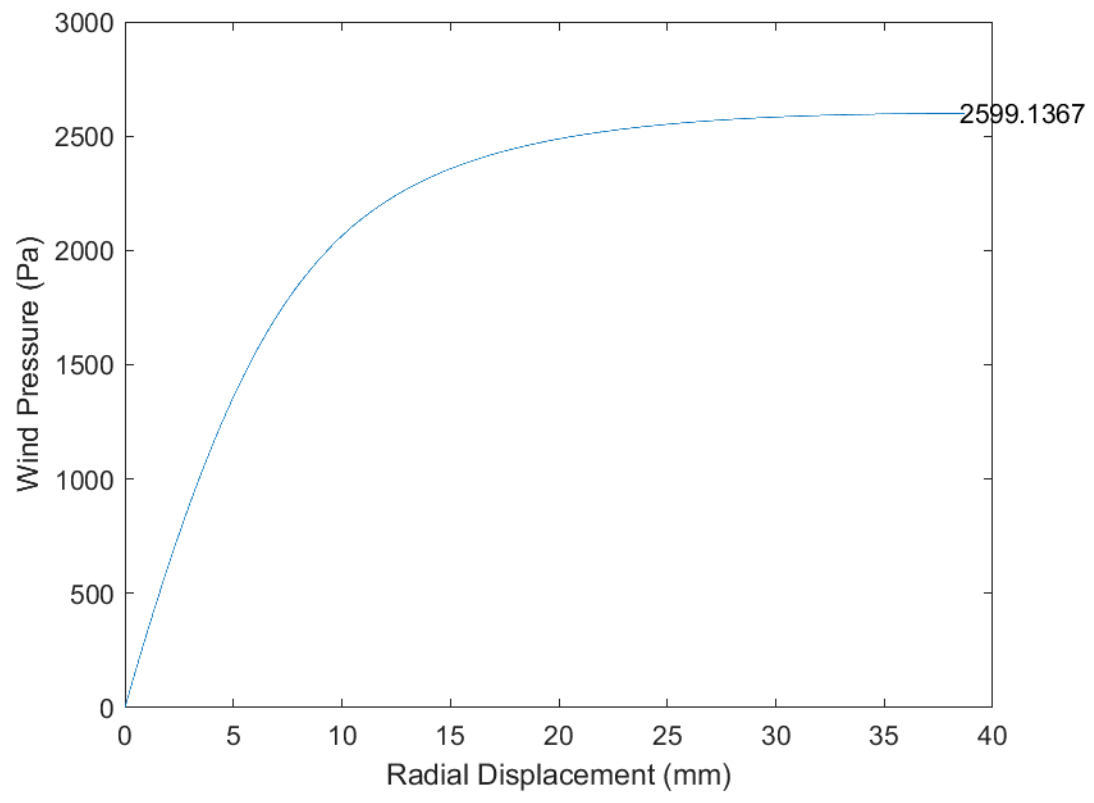


Fig. B.39 D54_H05_S00_R00_W00_V00_CL03_CD03_WT03_ST03

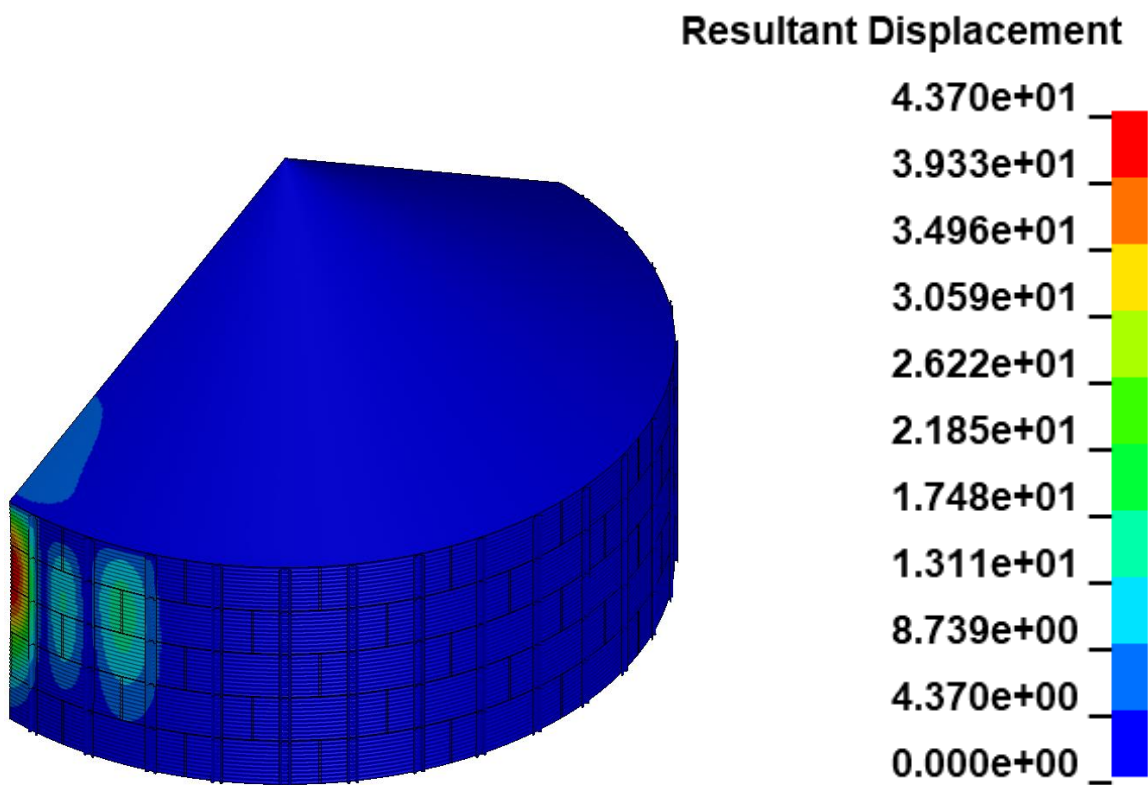
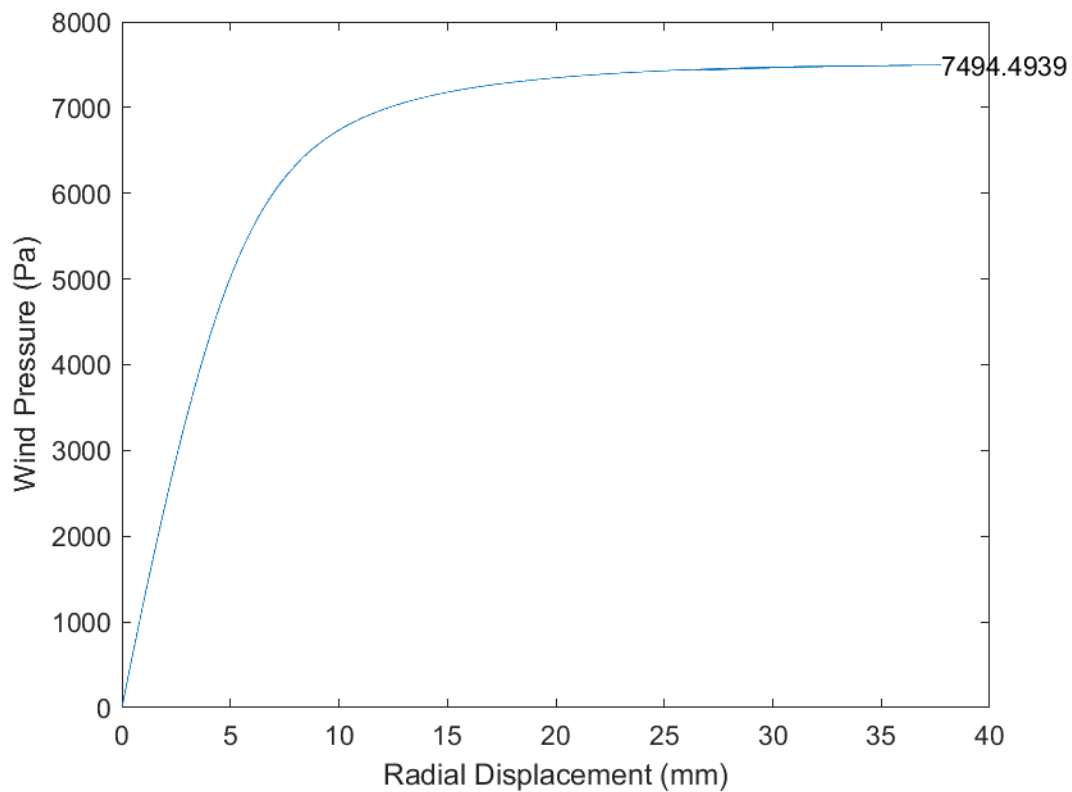


Fig. B.40 D54_H05_S36_R00_W00_V00_CL03_CD03_WT03_ST03

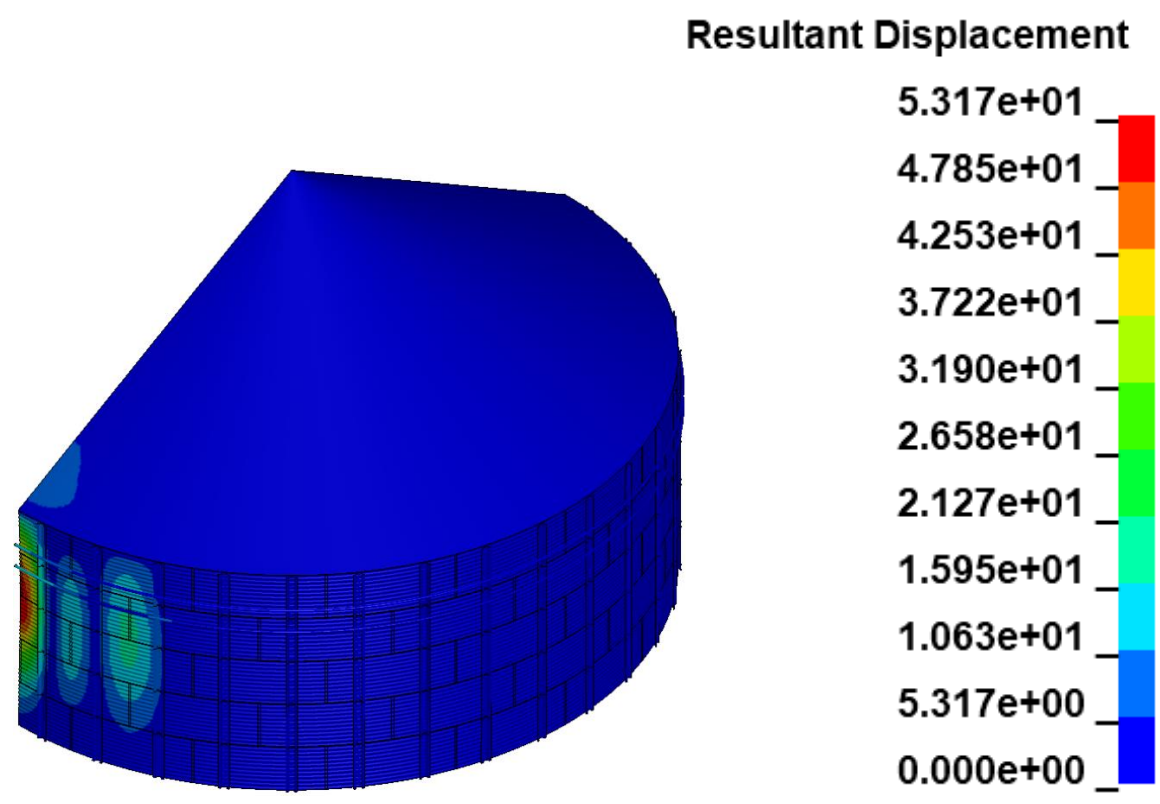
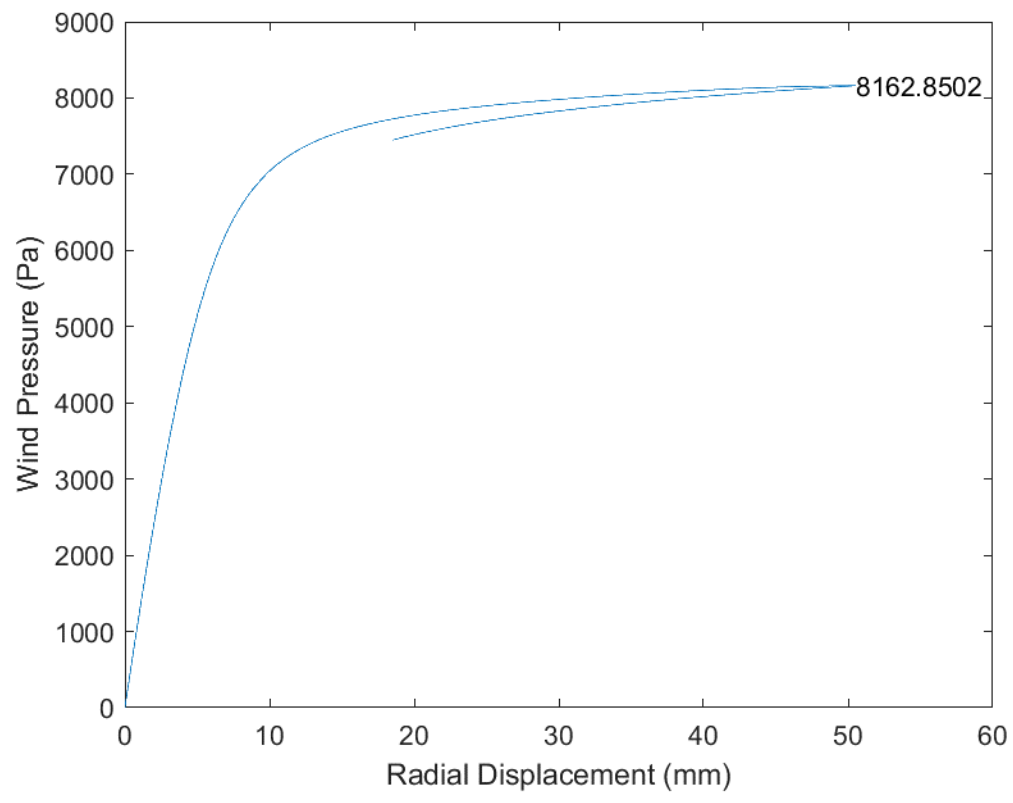


Fig. B.41 D54_H05_S36_R02_W00_V00_CL03_CD03_WT03_ST03

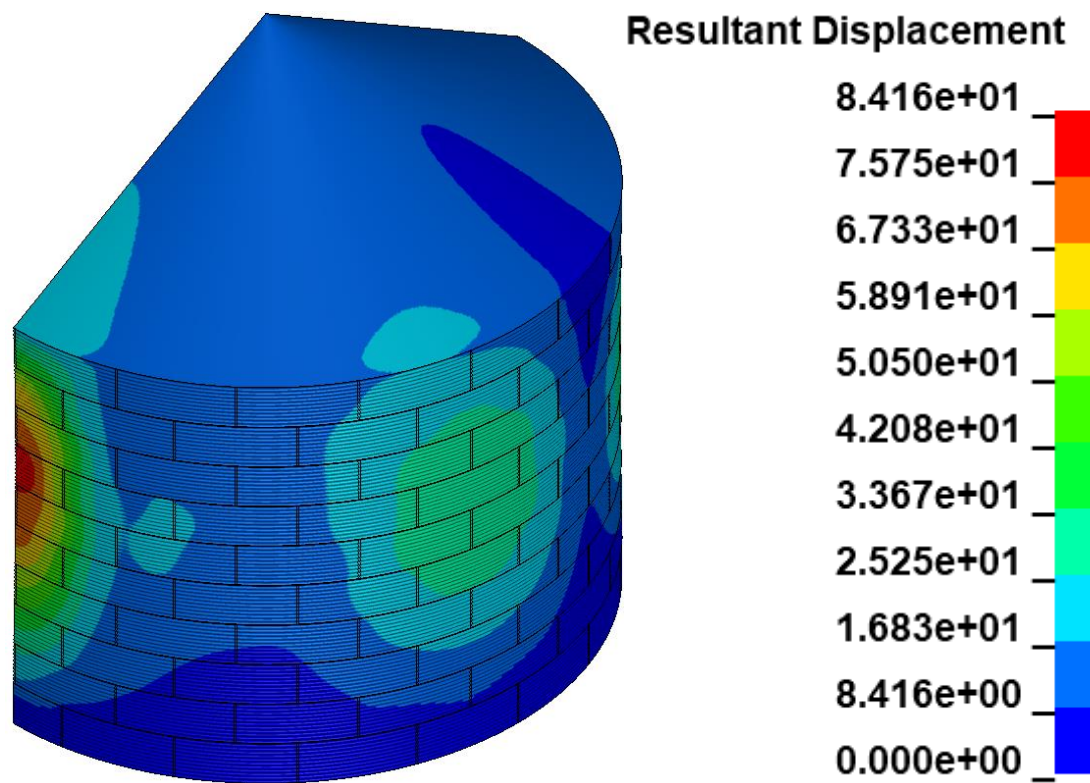
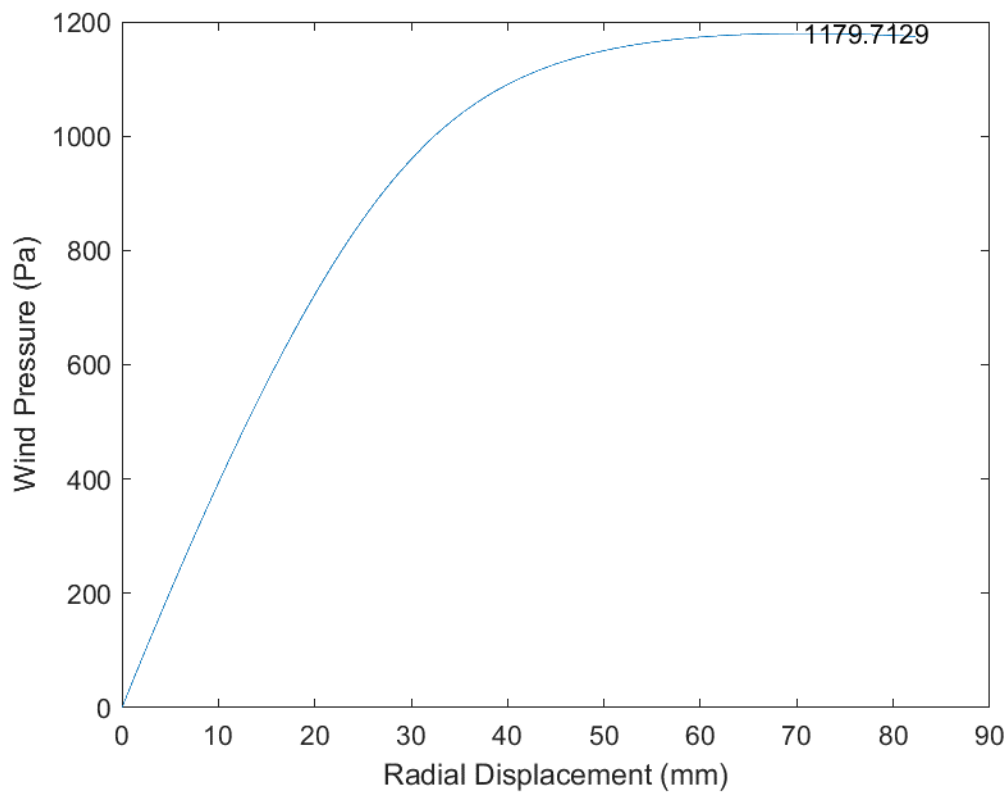


Fig. B.42 D54_H10_S00_R00_W00_V00_CL03_CD03_WT03_ST03

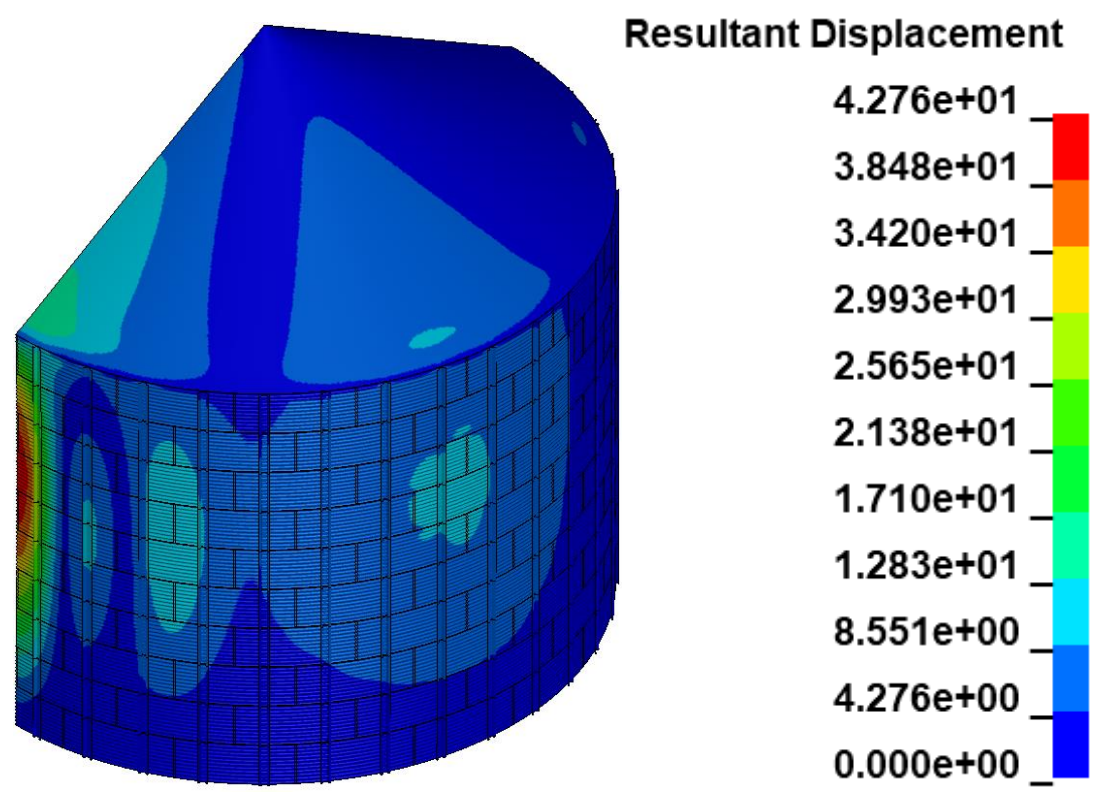
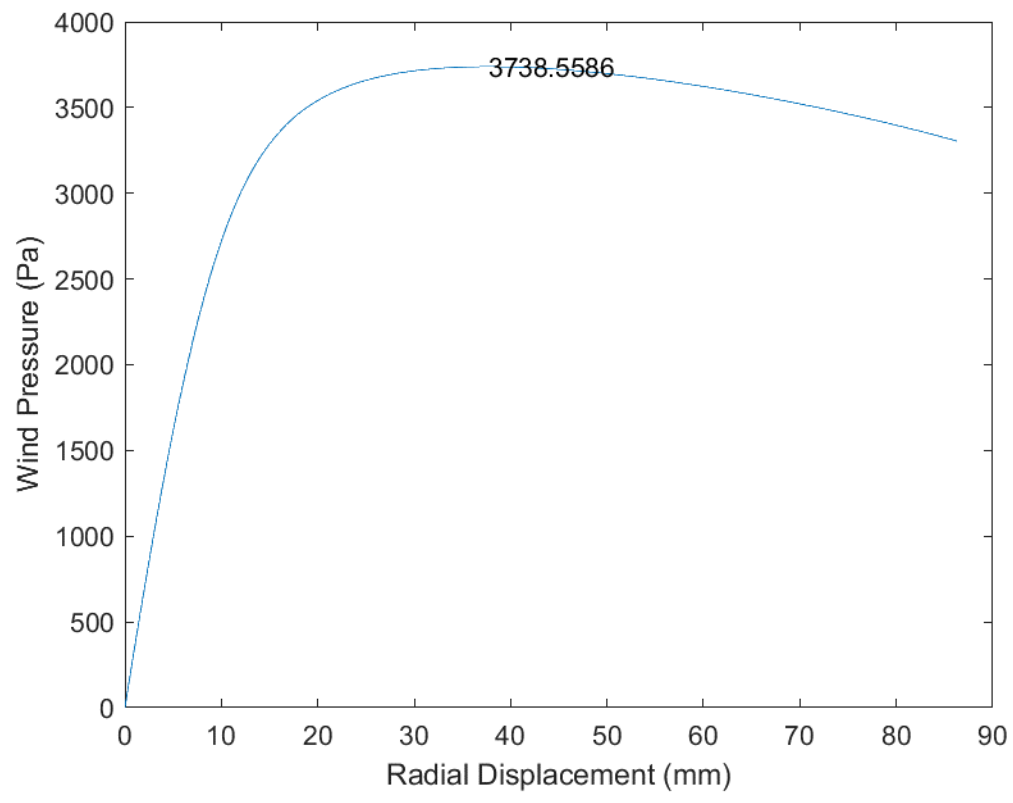


Fig. B.43 D54_H10_S36_R00_W00_V00_CL03_CD03_WT03_ST03

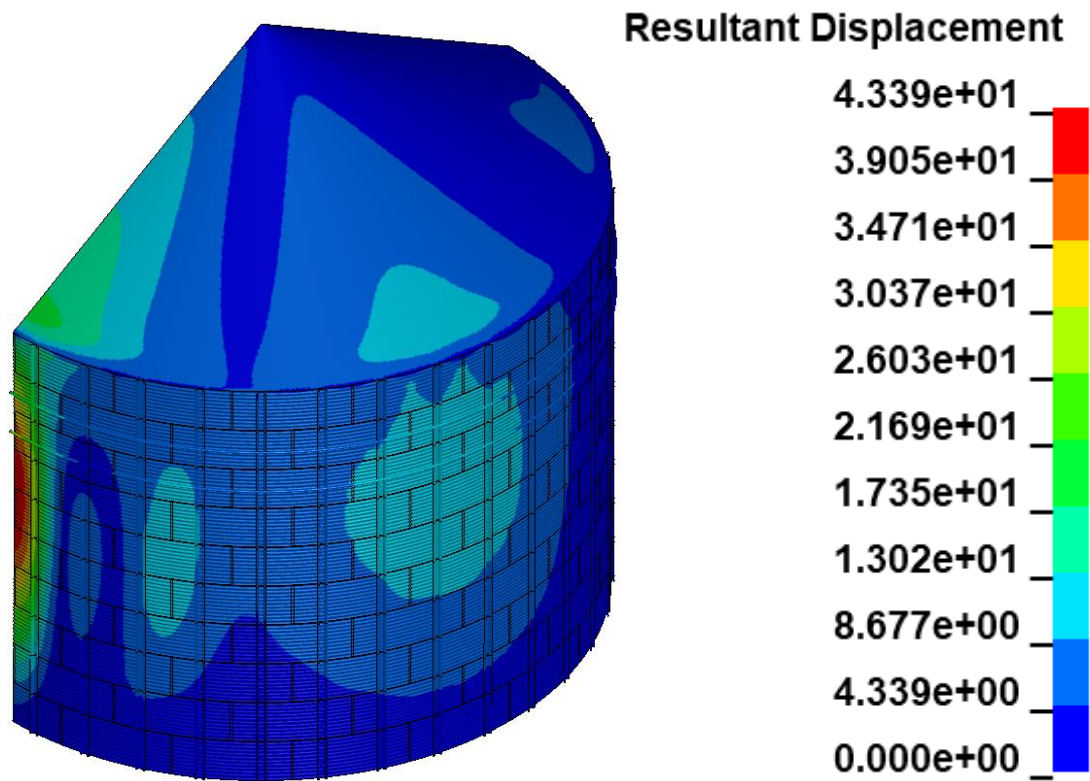
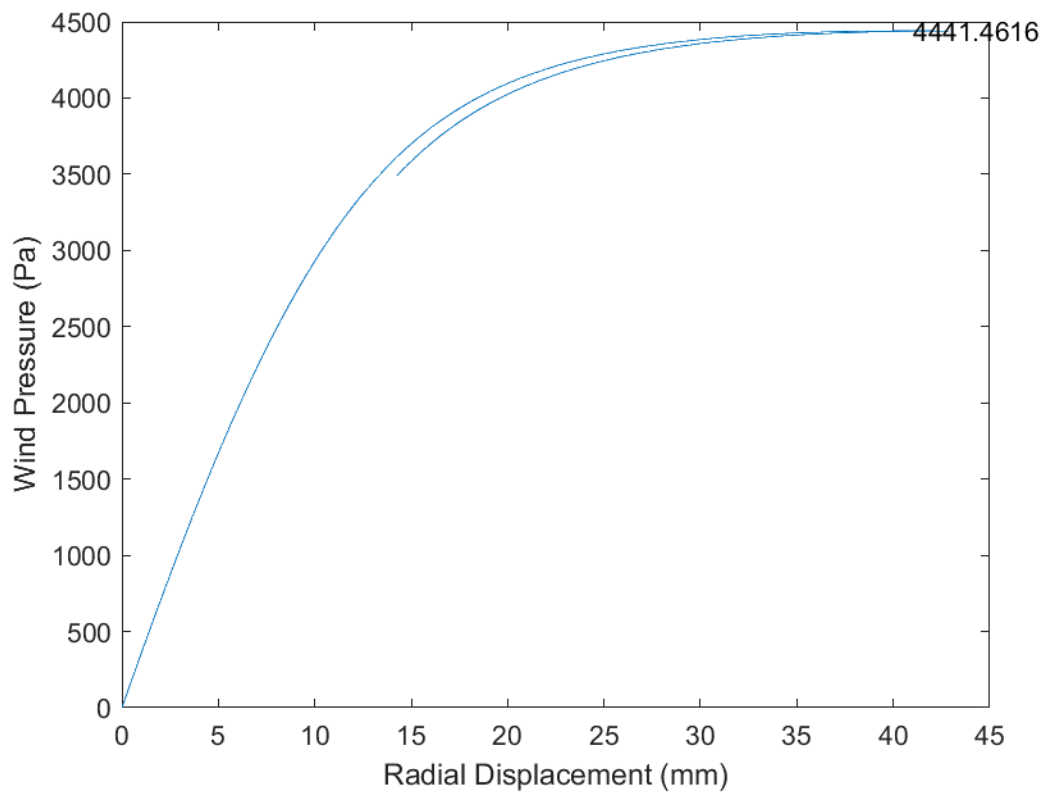


Fig. B.44 D54_H10_S36_R02_W00_V00_CL03_CD03_WT03_ST03

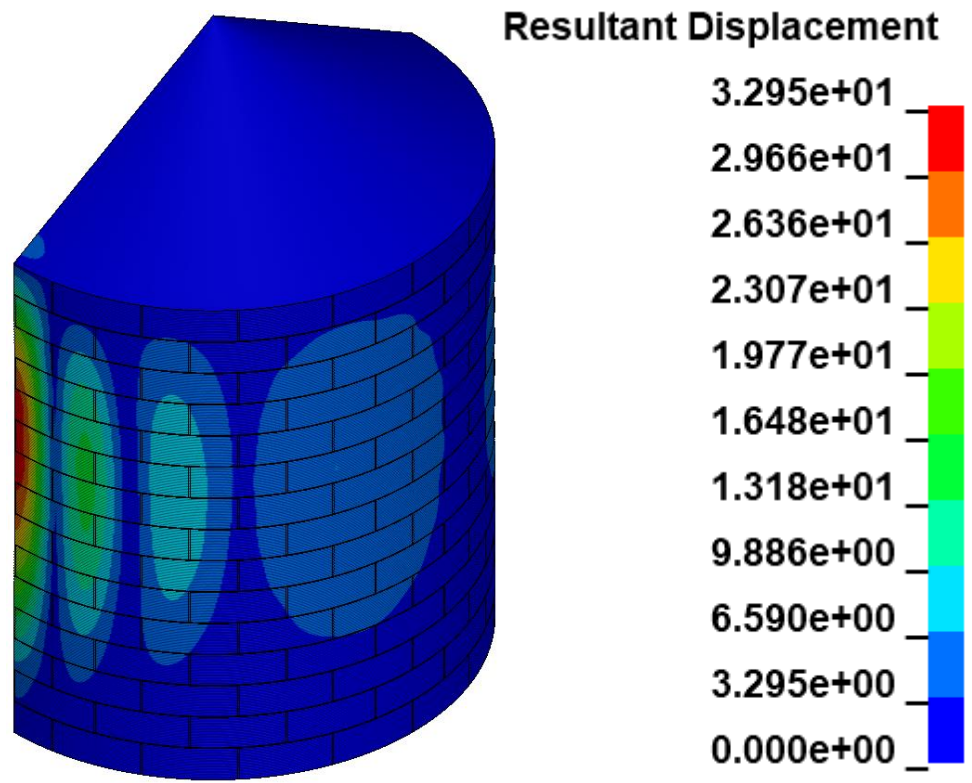
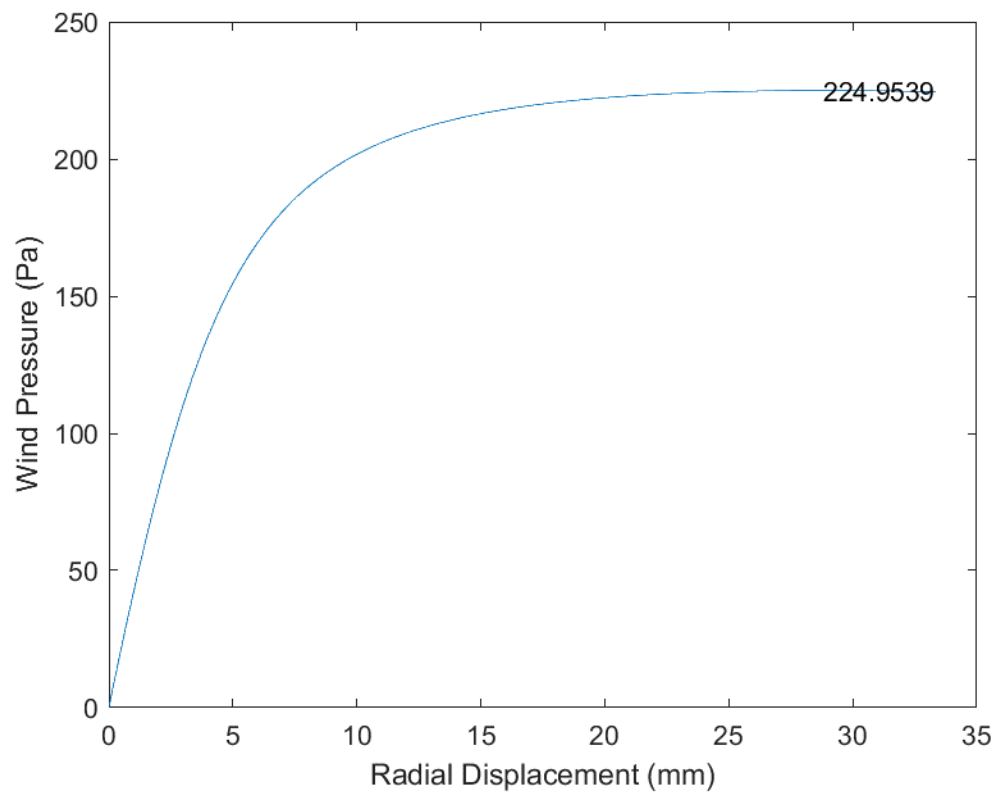


Fig. B.45 D54_H15_S00_R00_W00_V00_CL01_CD01_WT03_ST03

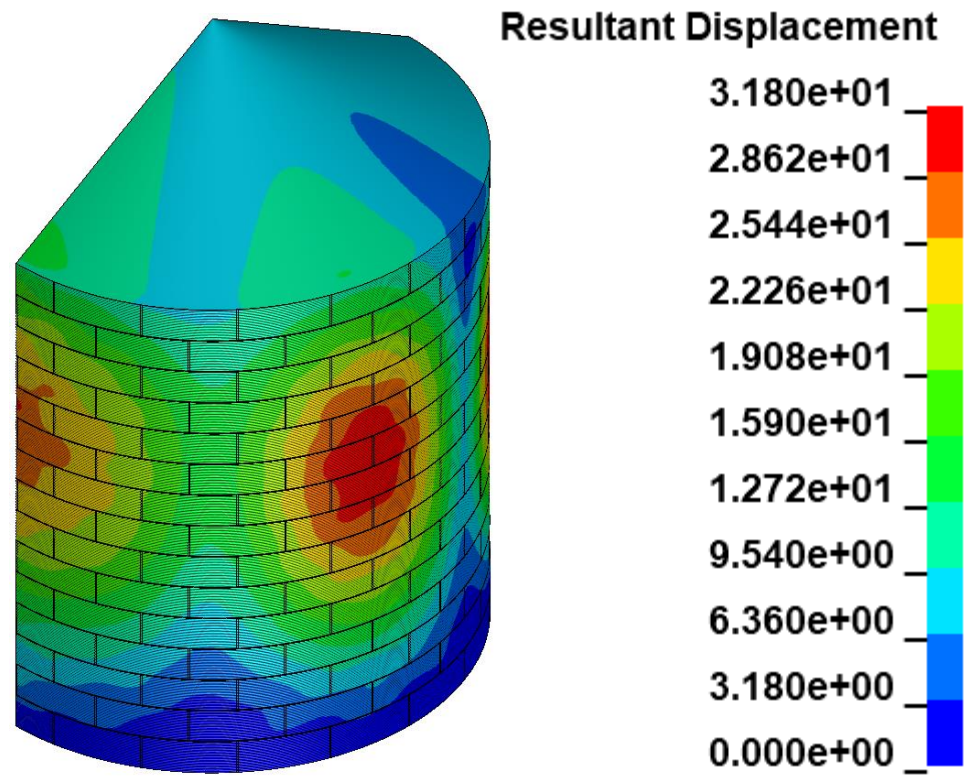
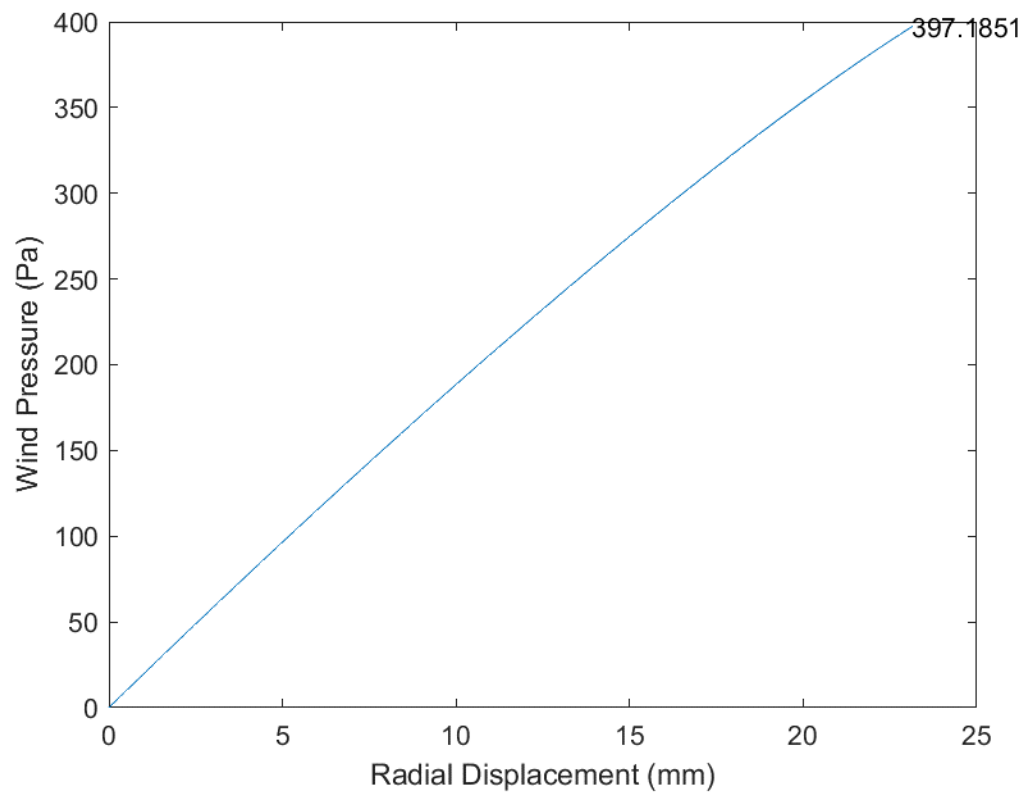


Fig. B.46 D54_H15_S00_R00_W00_V00_CL01_CD02_WT03_ST03

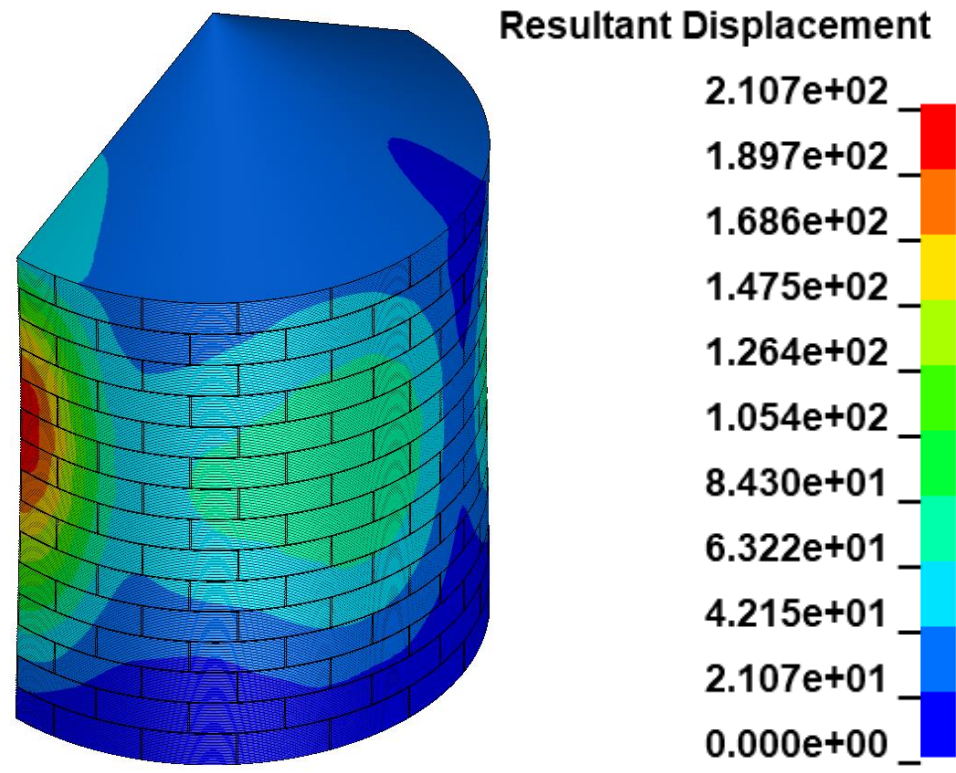
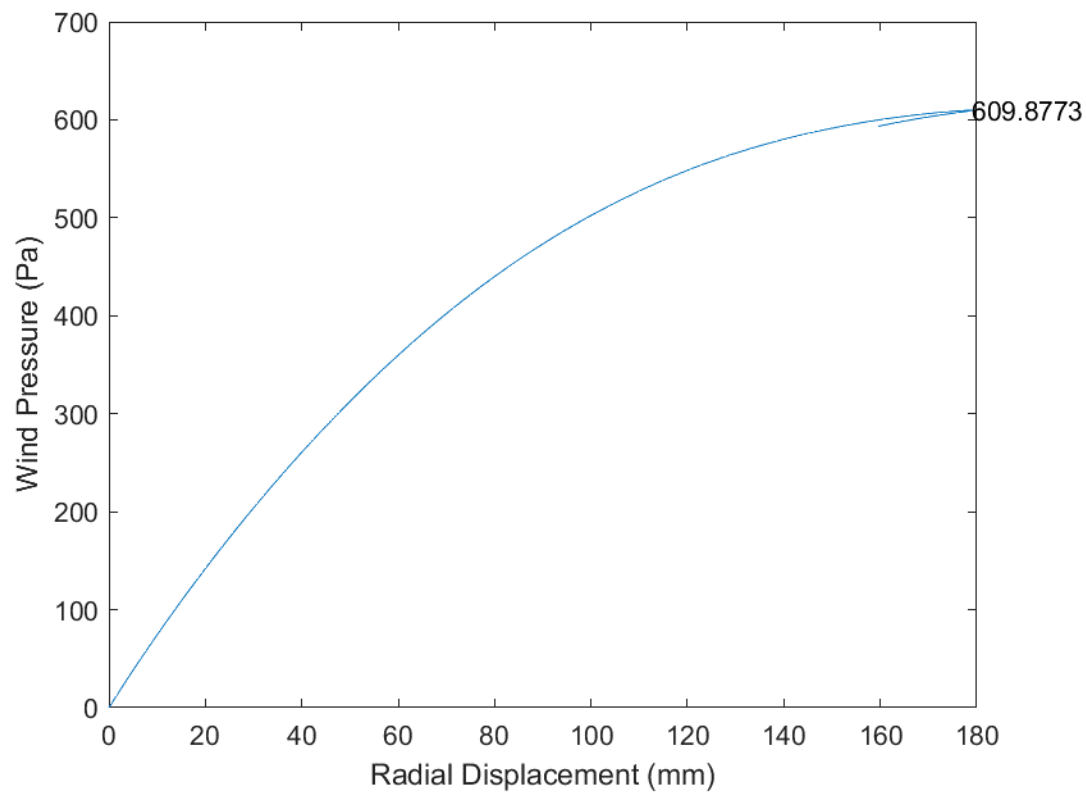


Fig. B.47 D54_H15_S00_R00_W00_V00_CL01_CD03_WT03_ST03

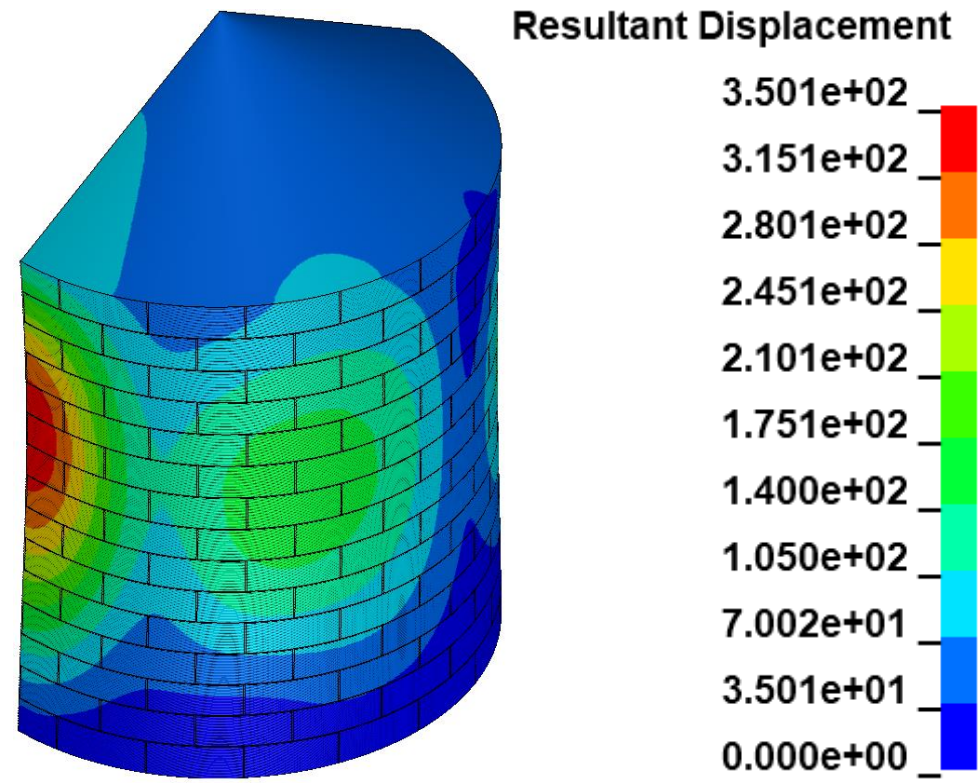
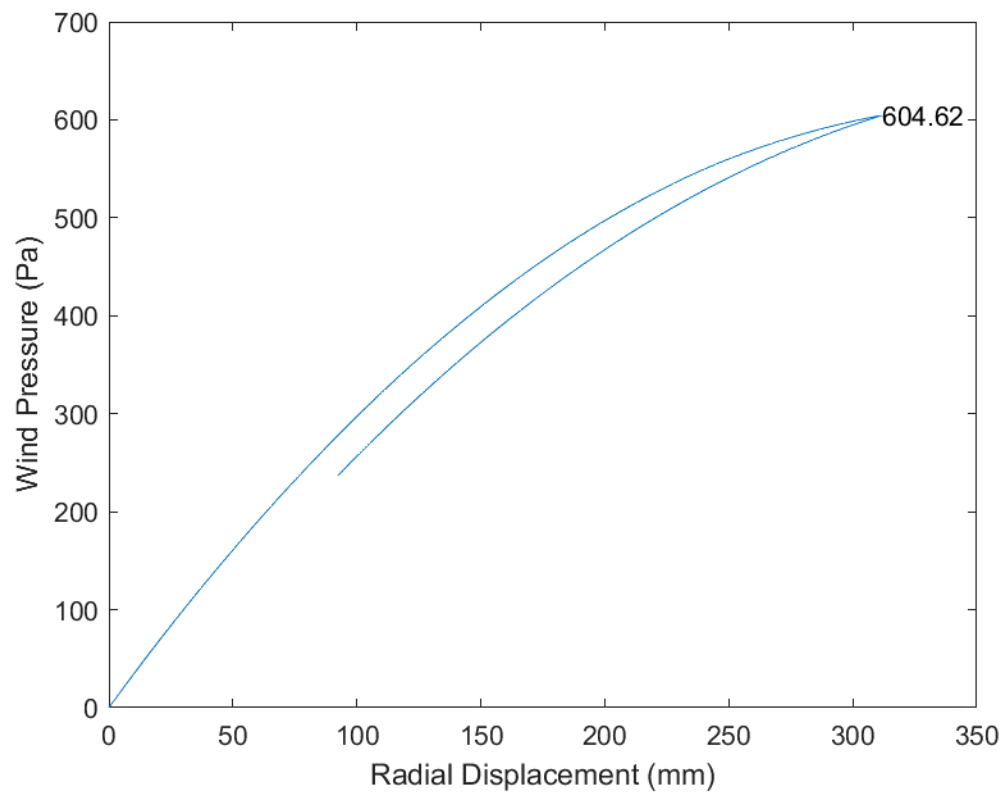


Fig. B.48 D54_H15_S00_R00_W00_V00_CL01_CD04_WT03_ST03

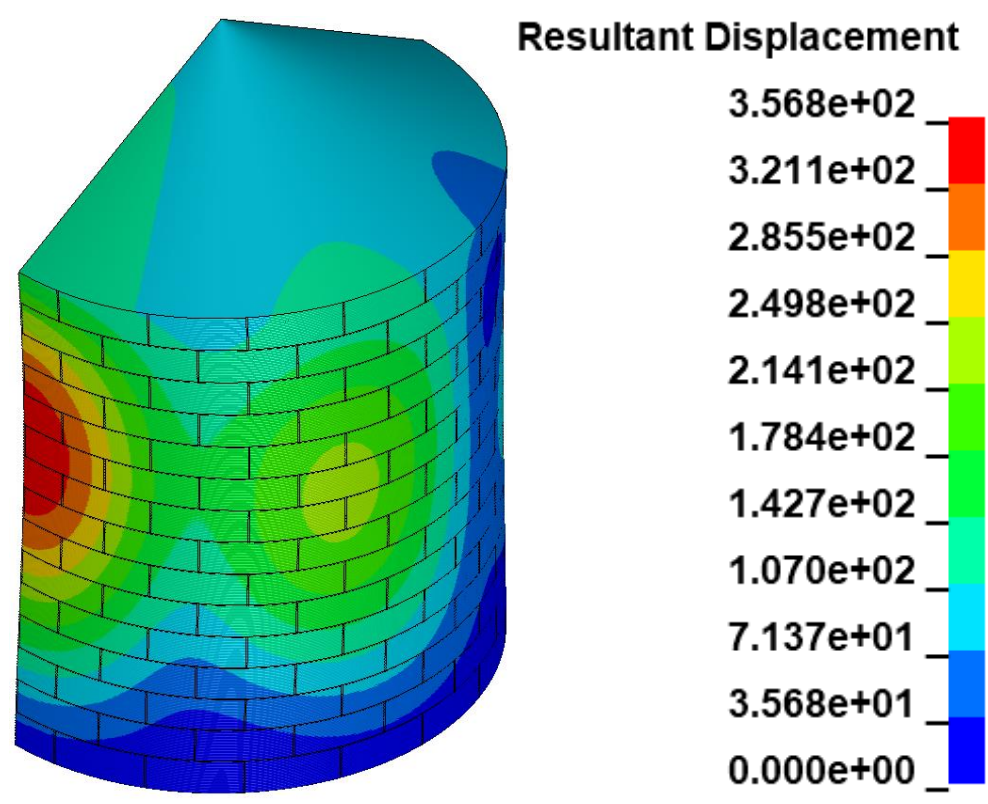
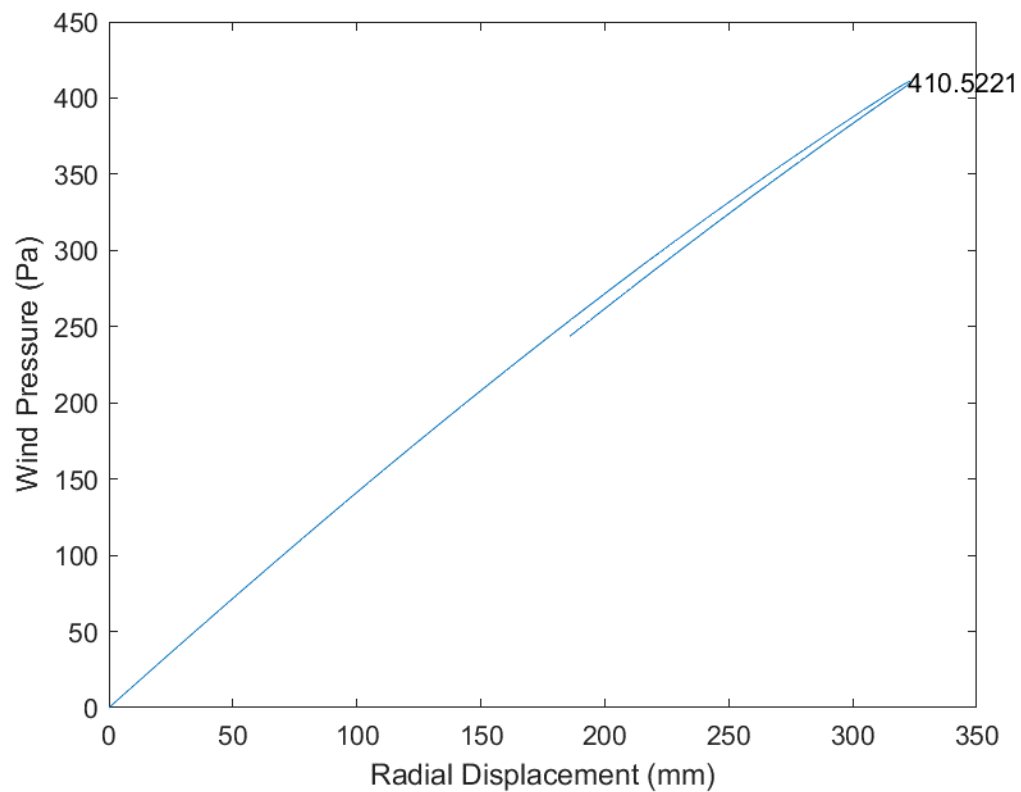


Fig. B.49 D54_H15_S00_R00_W00_V00_CL01_CD05_WT03_ST03

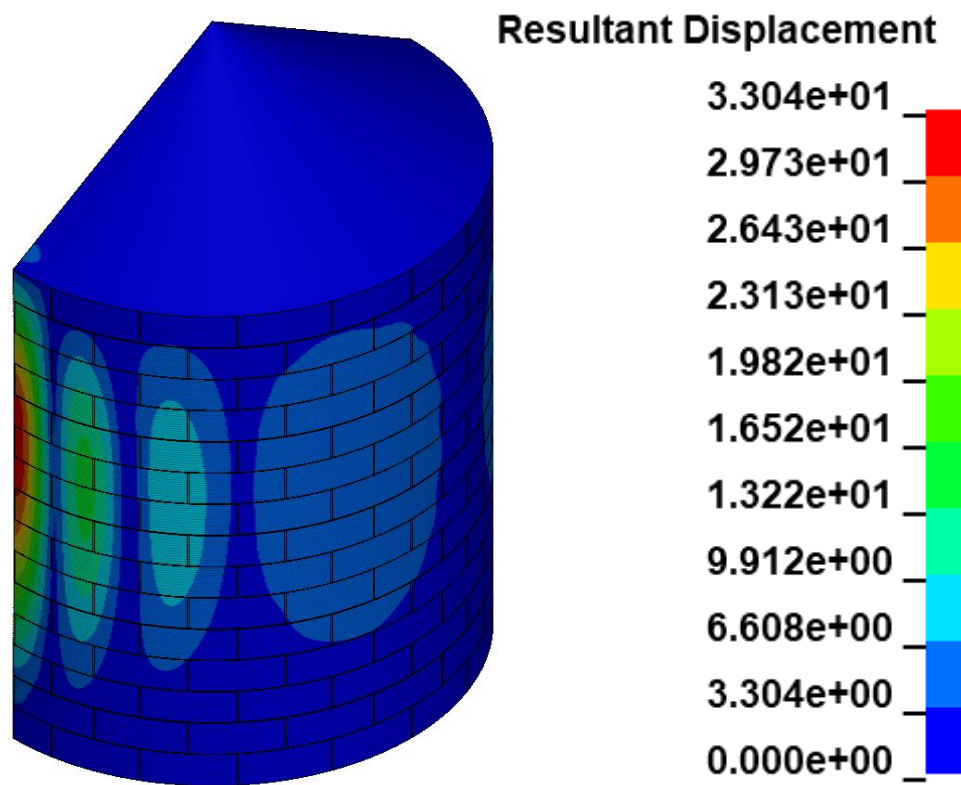
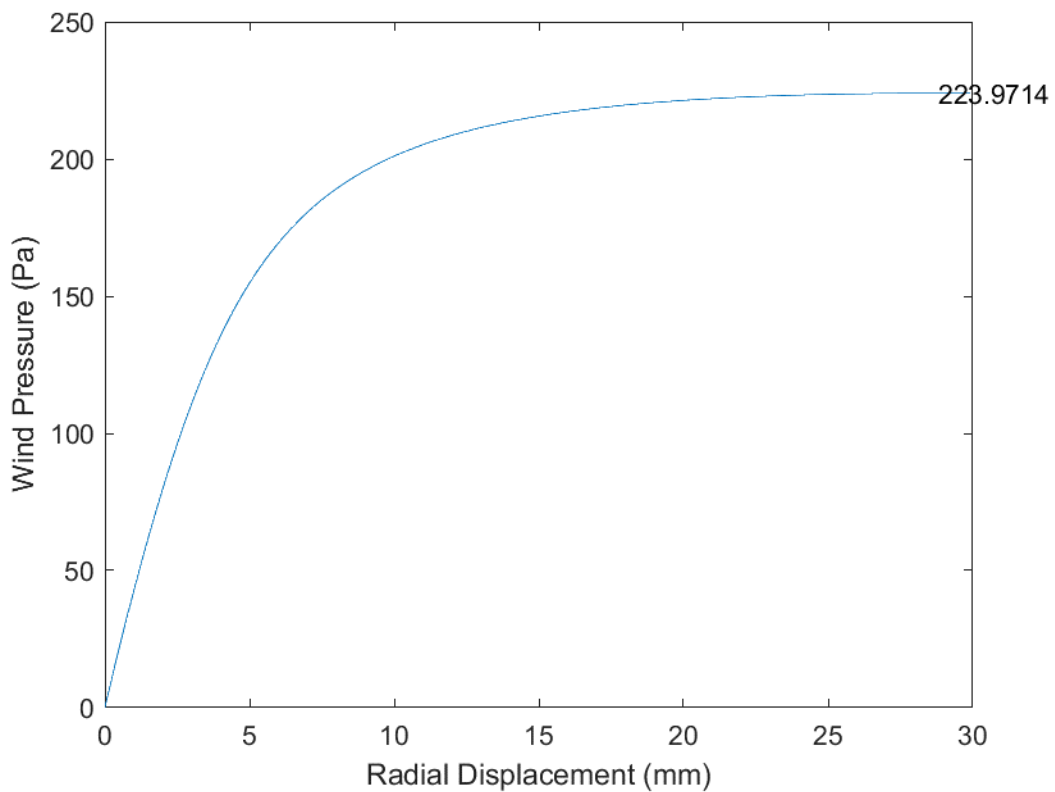


Fig. B.50 D54_H15_S00_R00_W00_V00_CL02_CD01_WT03_ST03

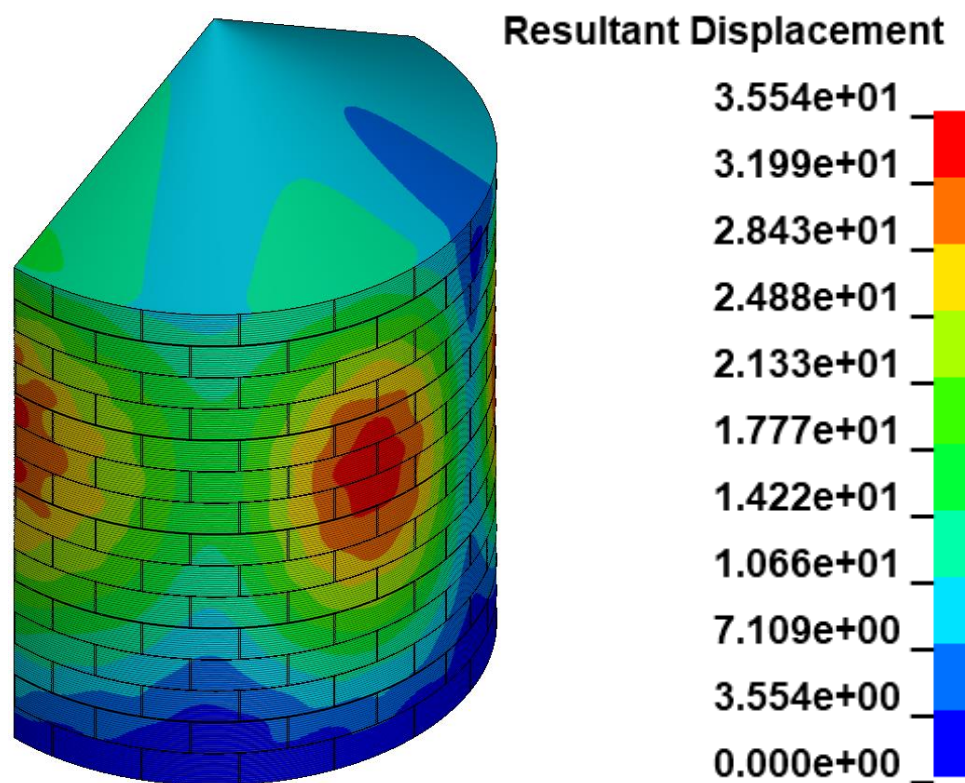
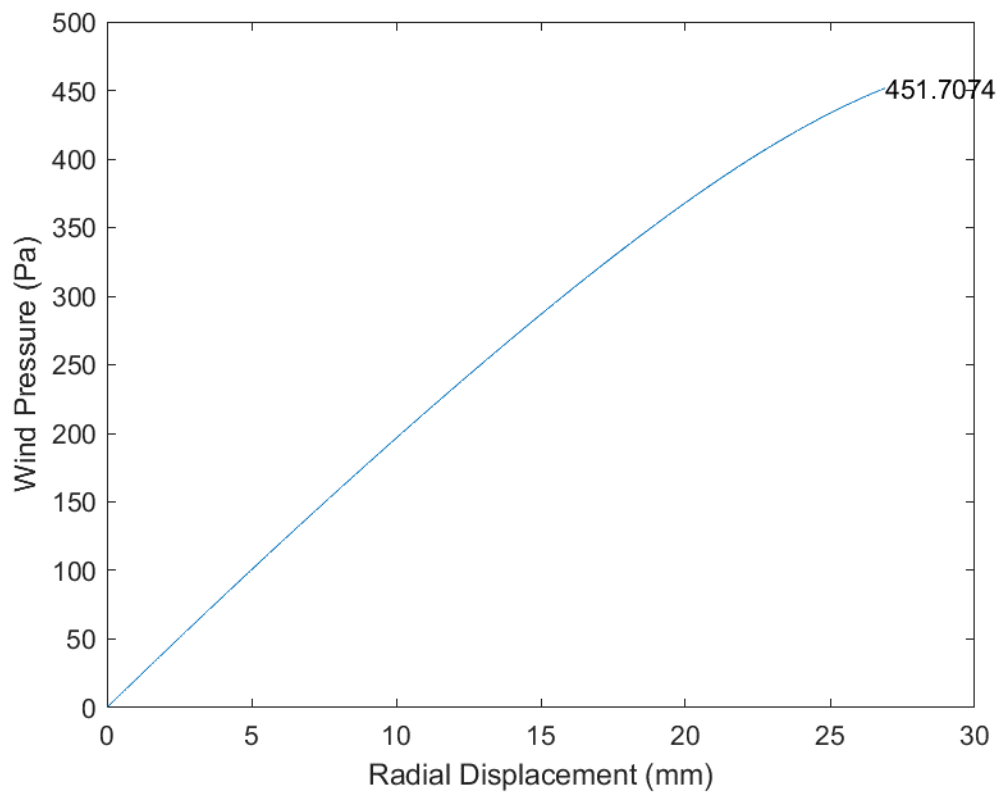


Fig. B.51 D54_H15_S00_R00_W00_V00_CL02_CD02_WT03_ST03

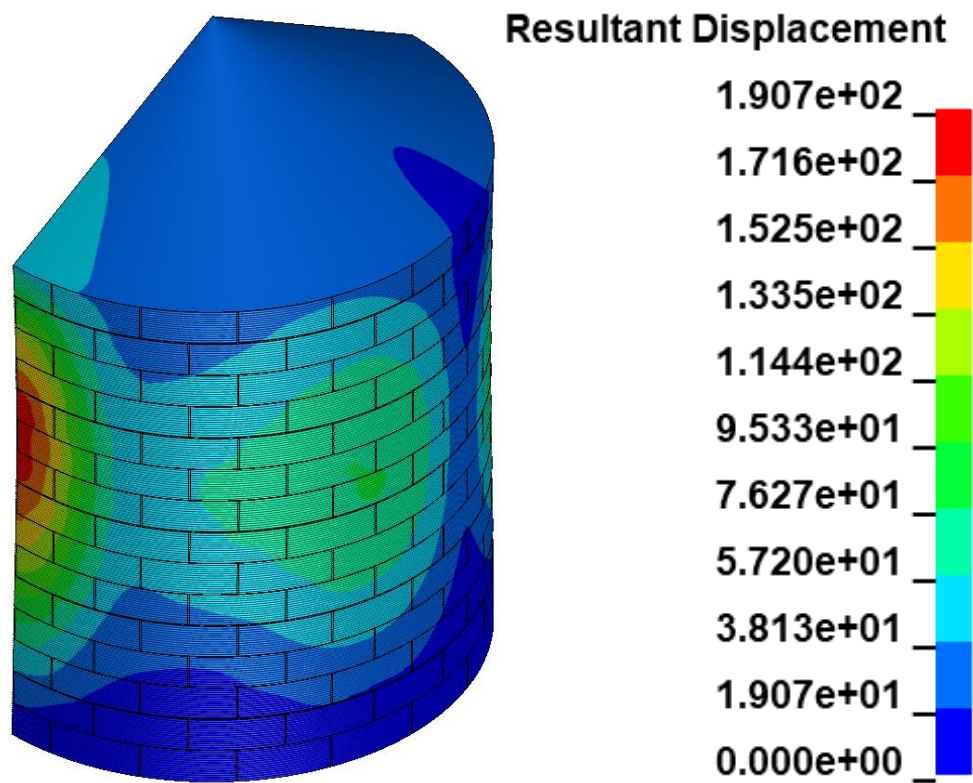
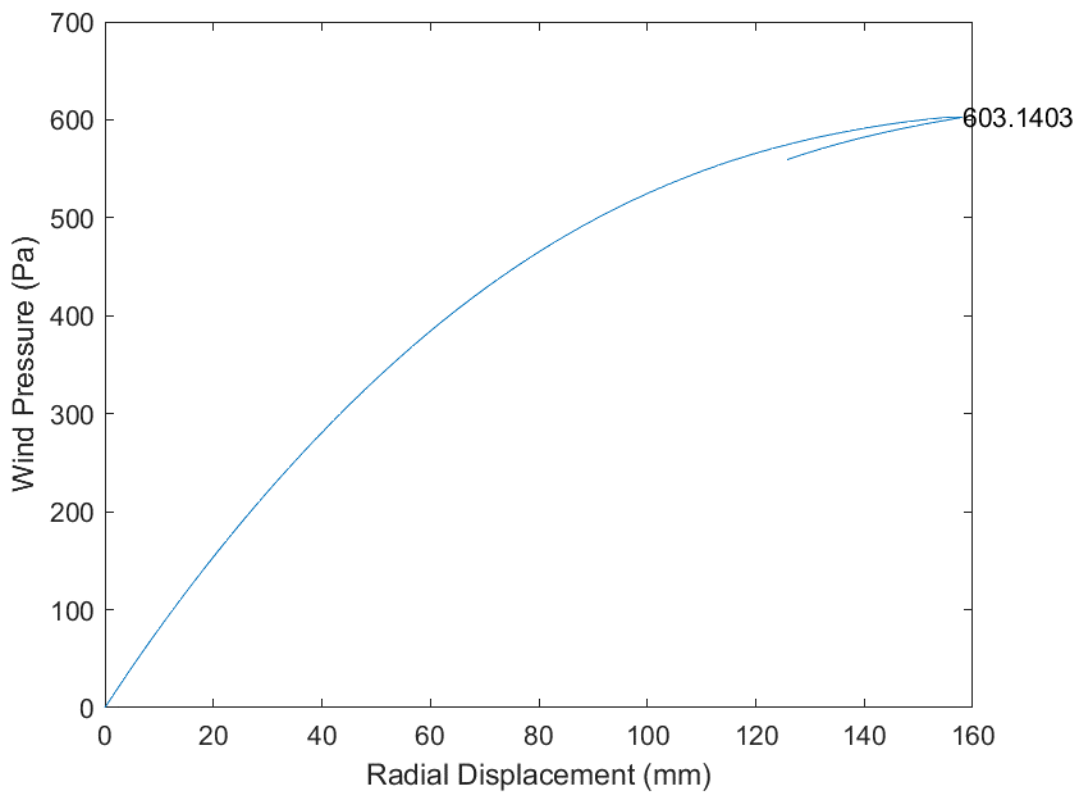


Fig. B.52 D54_H15_S00_R00_W00_V00_CL02_CD03_WT03_ST03

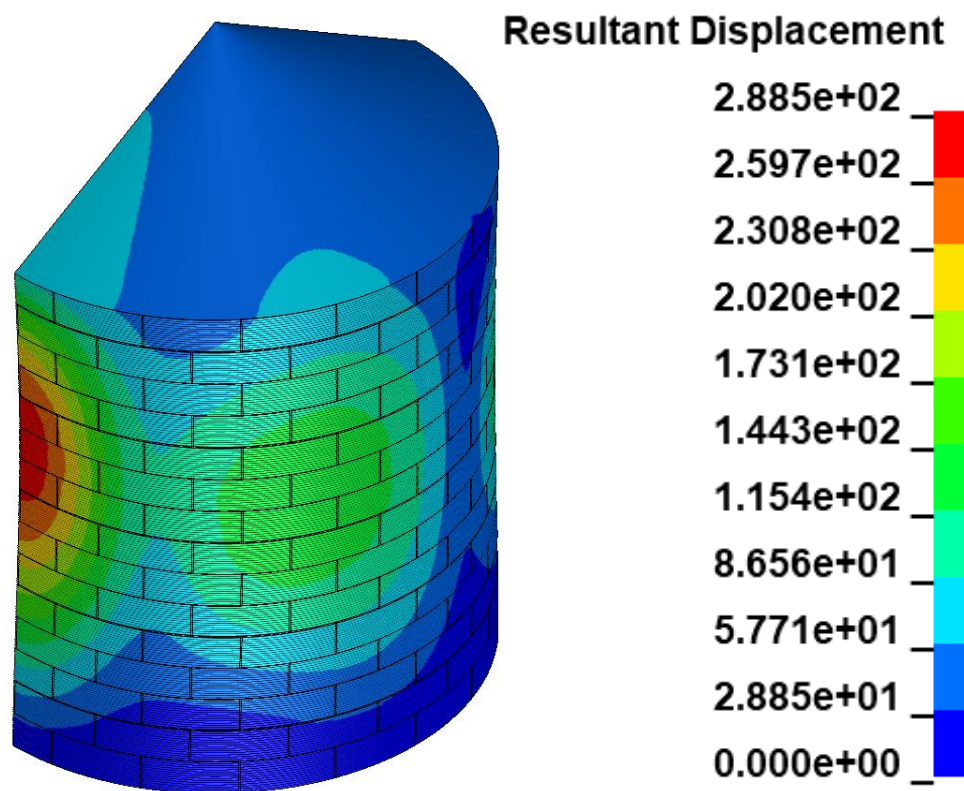
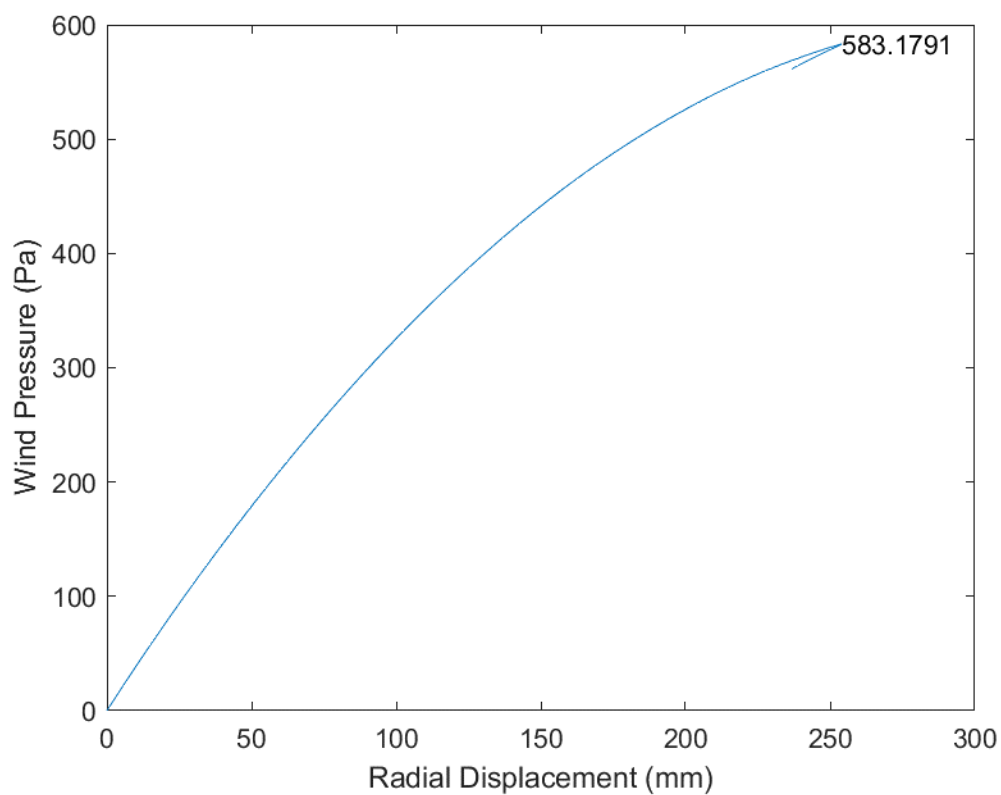


Fig. B.53 D54_H15_S00_R00_W00_V00_CL02_CD04_WT03_ST03

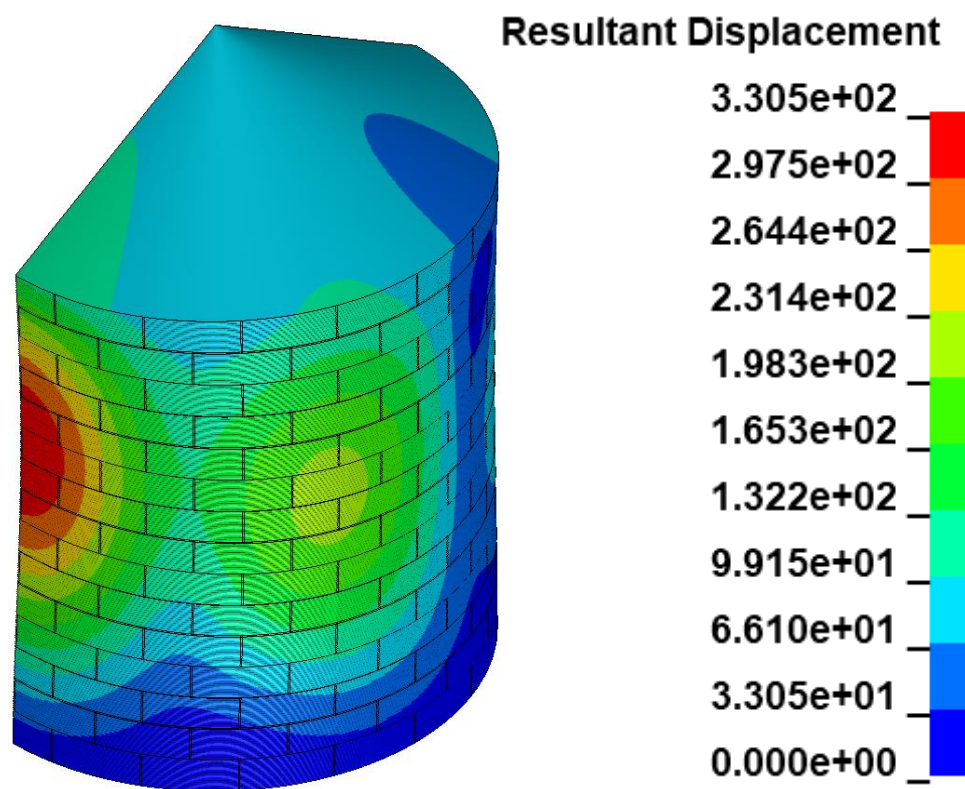
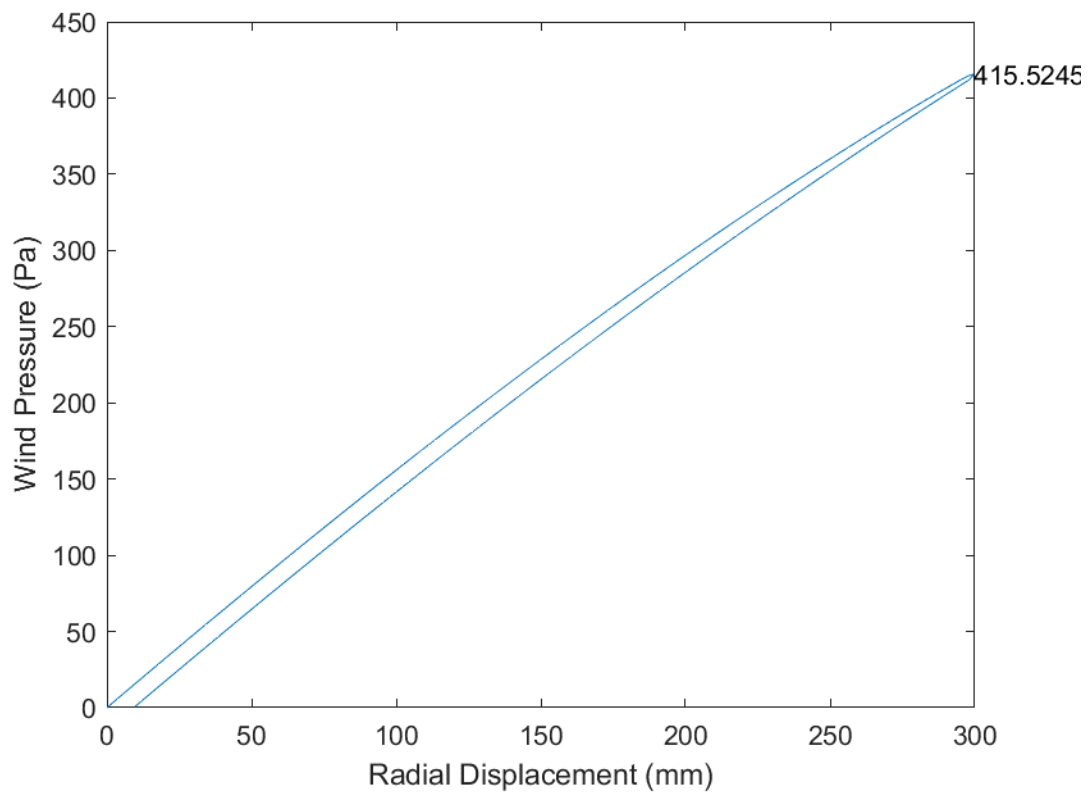


Fig. B.54 D54_H15_S00_R00_W00_V00_CL02_CD05_WT03_ST03

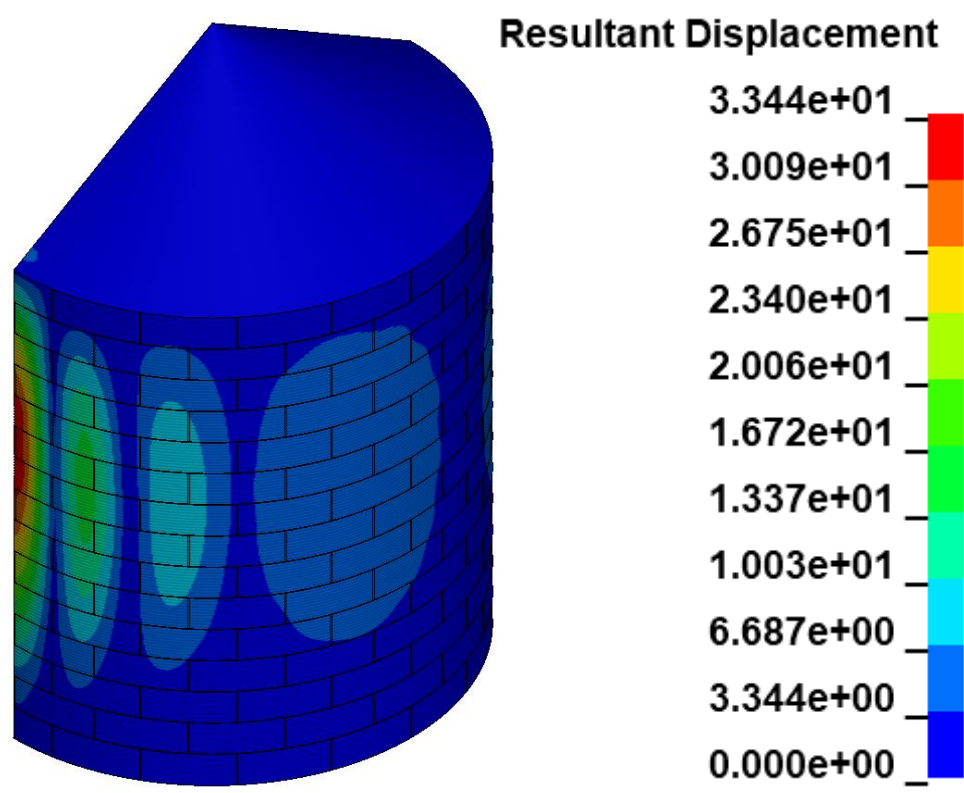
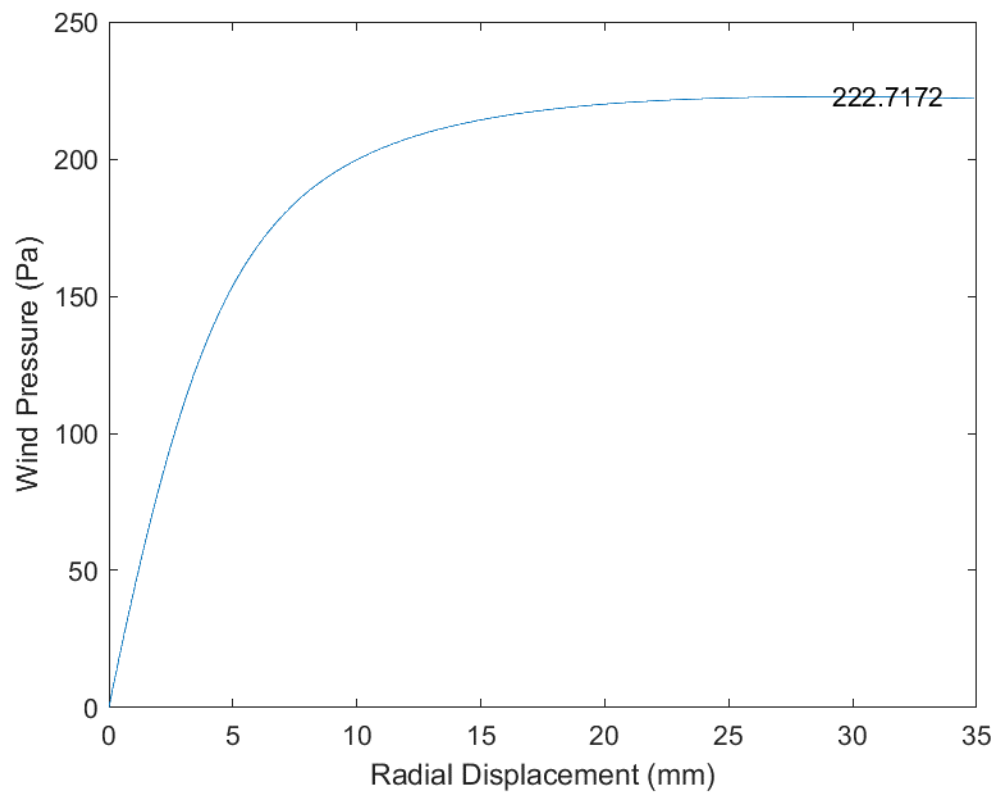


Fig. B.55 D54_H15_S00_R00_W00_V00_CL03_CD01_WT03_ST03

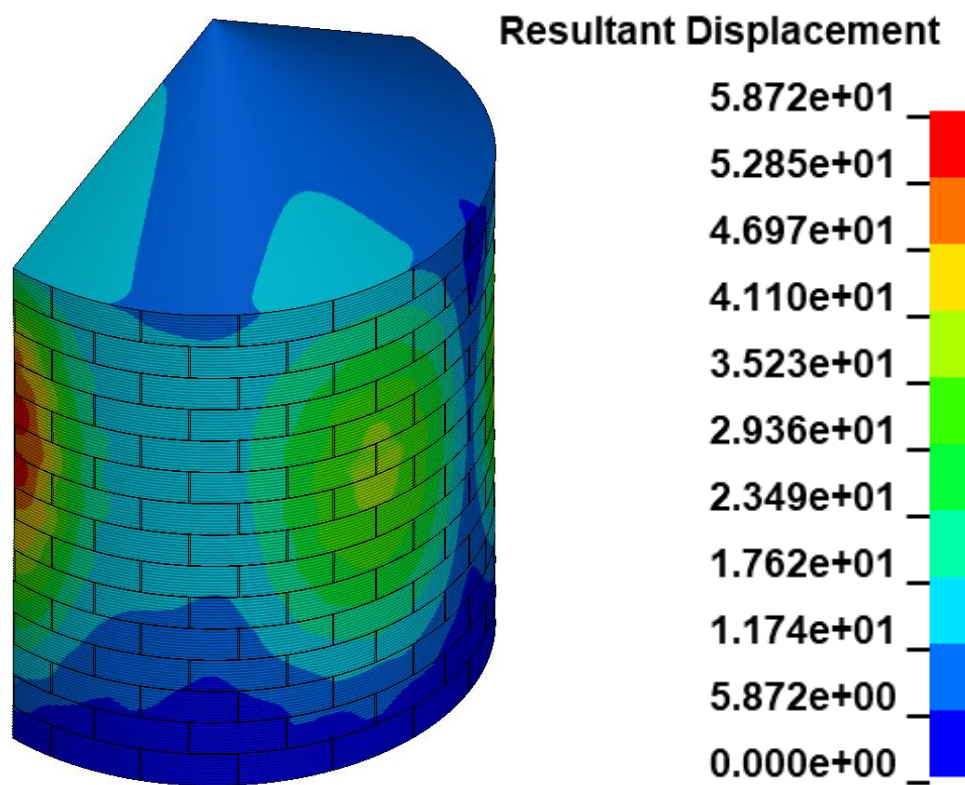
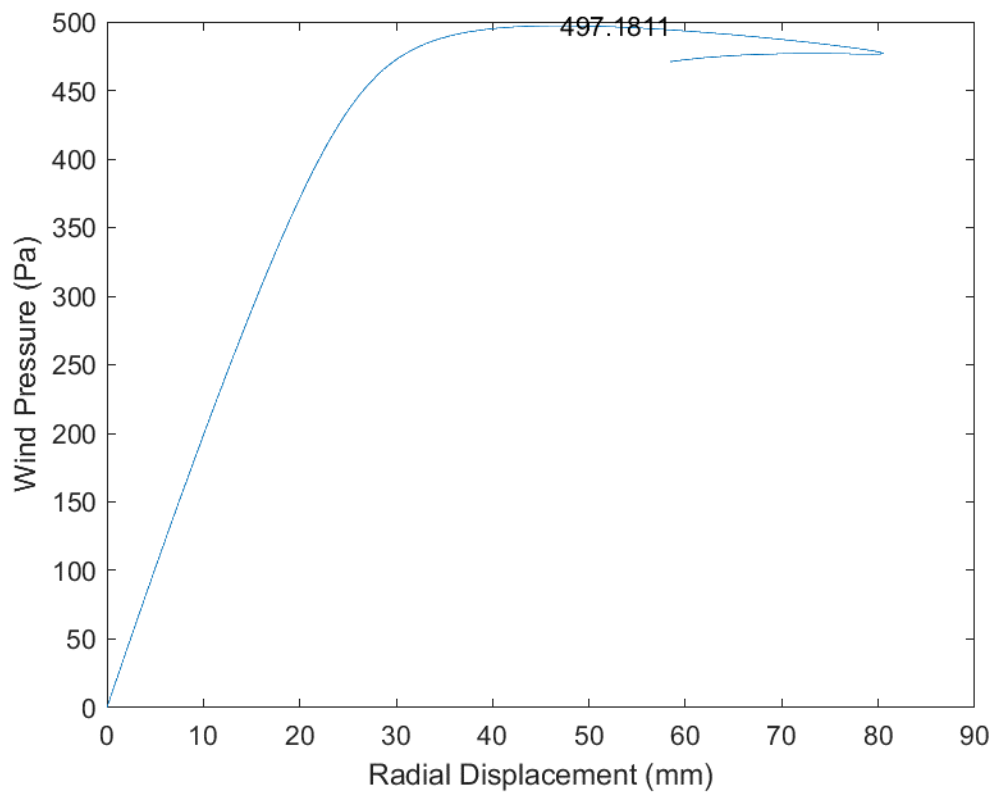


Fig. B.56 D54_H15_S00_R00_W00_V00_CL03_CD02_WT03_ST03

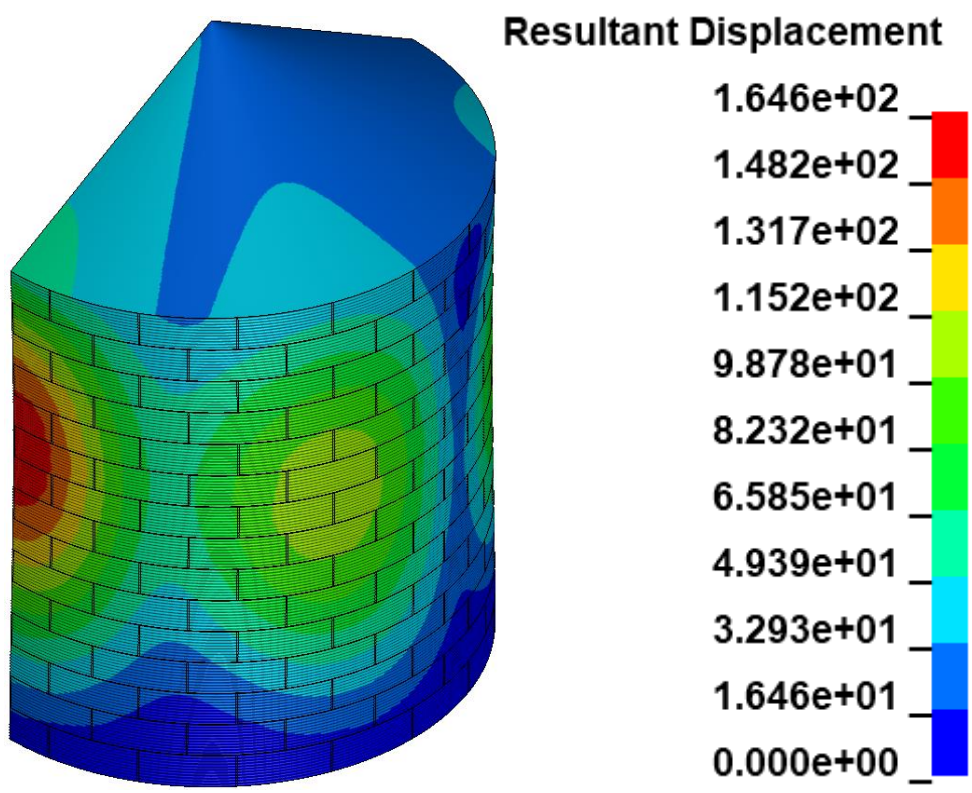
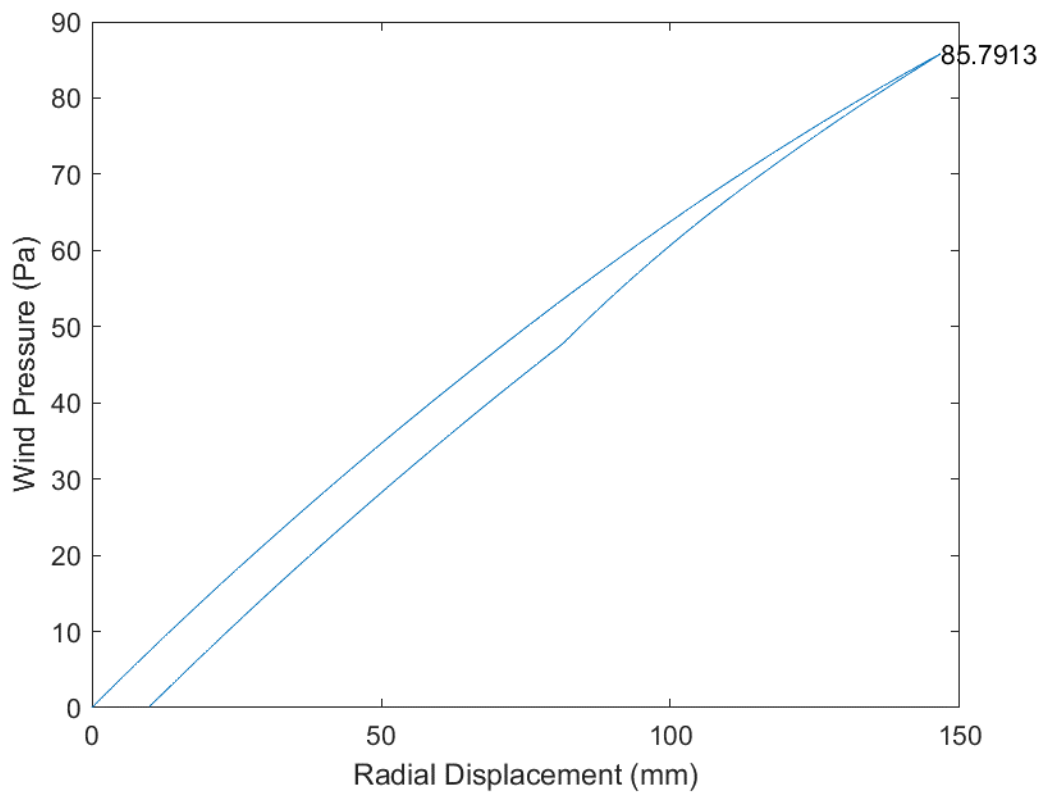


Fig. B.57 D54_H15_S00_R00_W00_V00_CL03_CD03_WT01_ST01

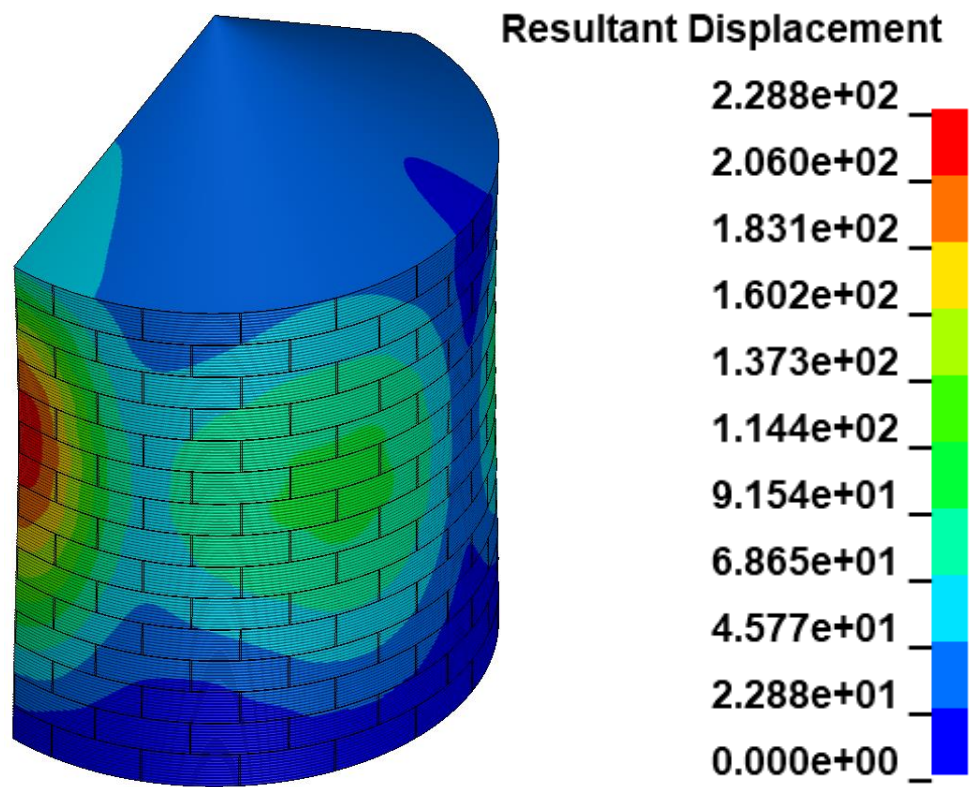
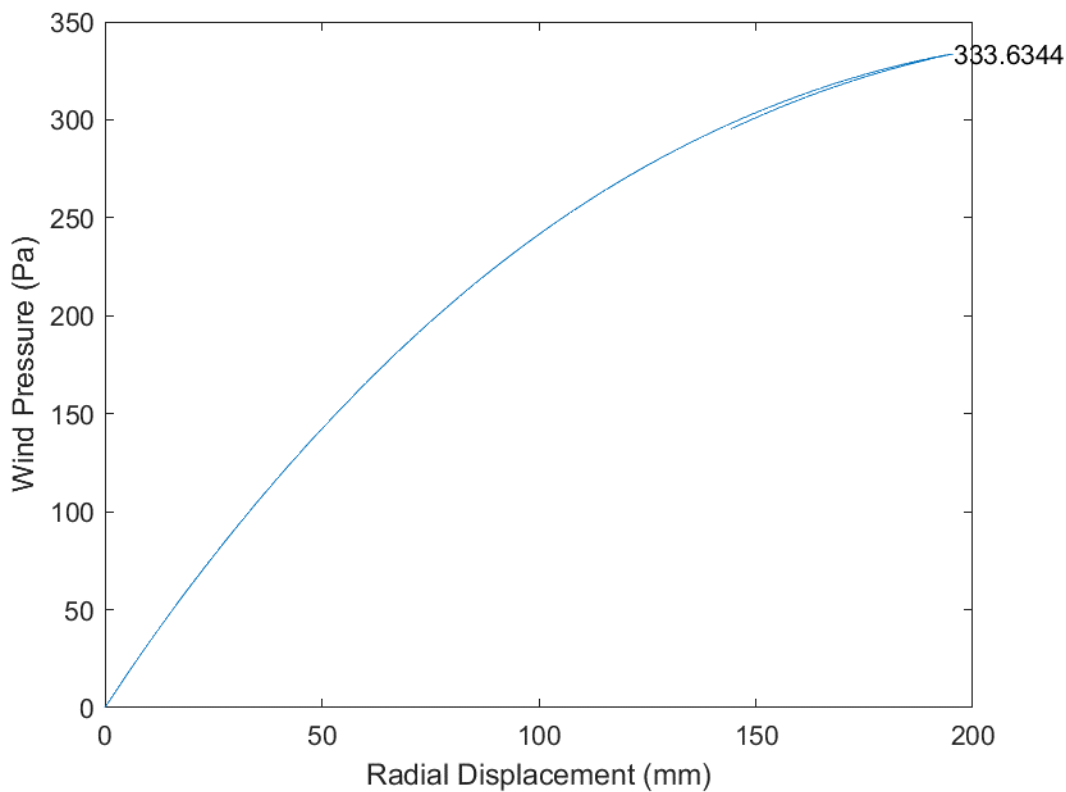


Fig. B.58 D54_H15_S00_R00_W00_V00_CL03_CD03_WT02_ST01

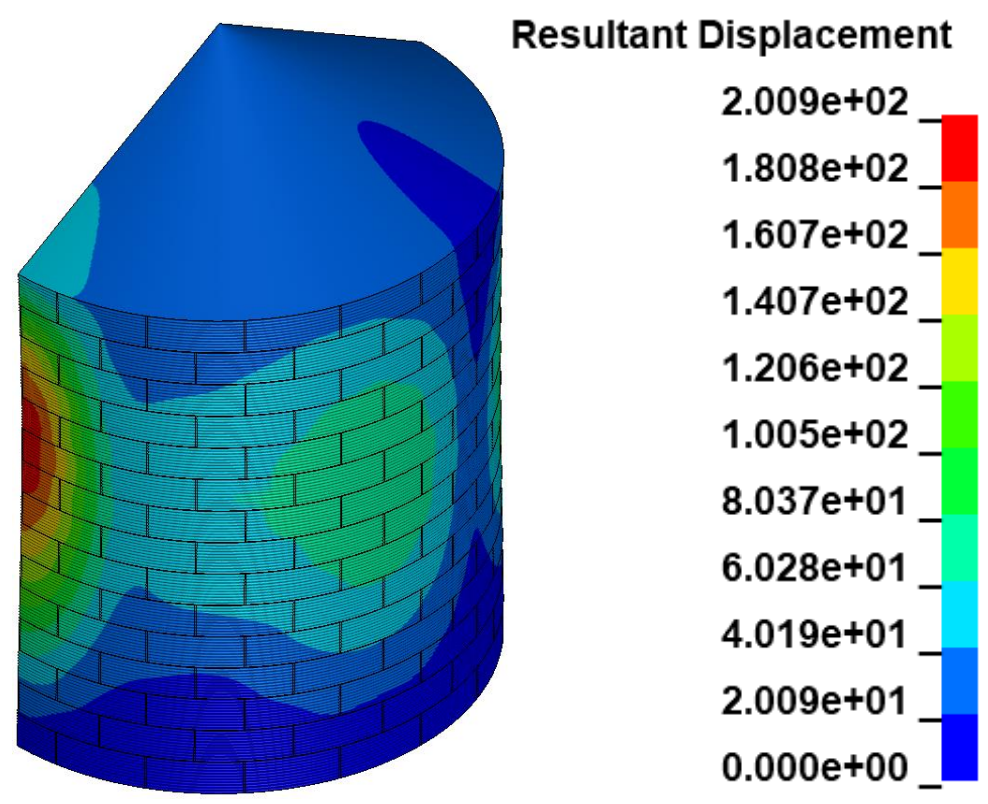
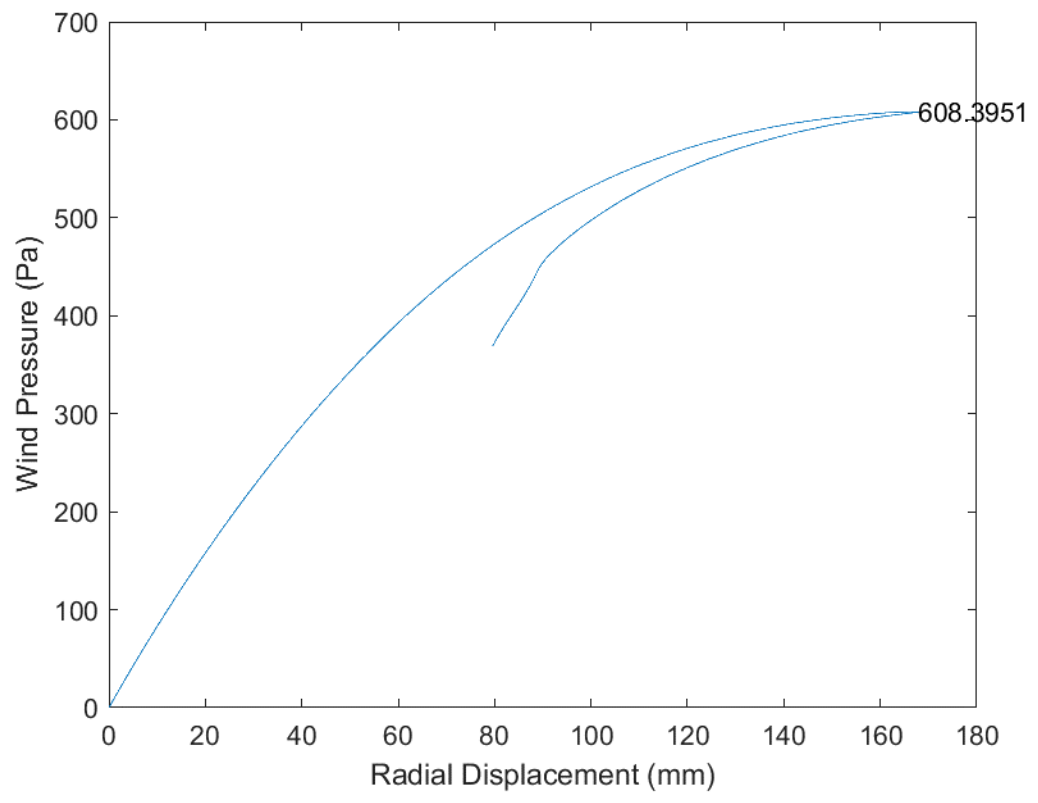


Fig. B.59 D54_H15_S00_R00_W00_V00_CL03_CD03_WT03_ST01

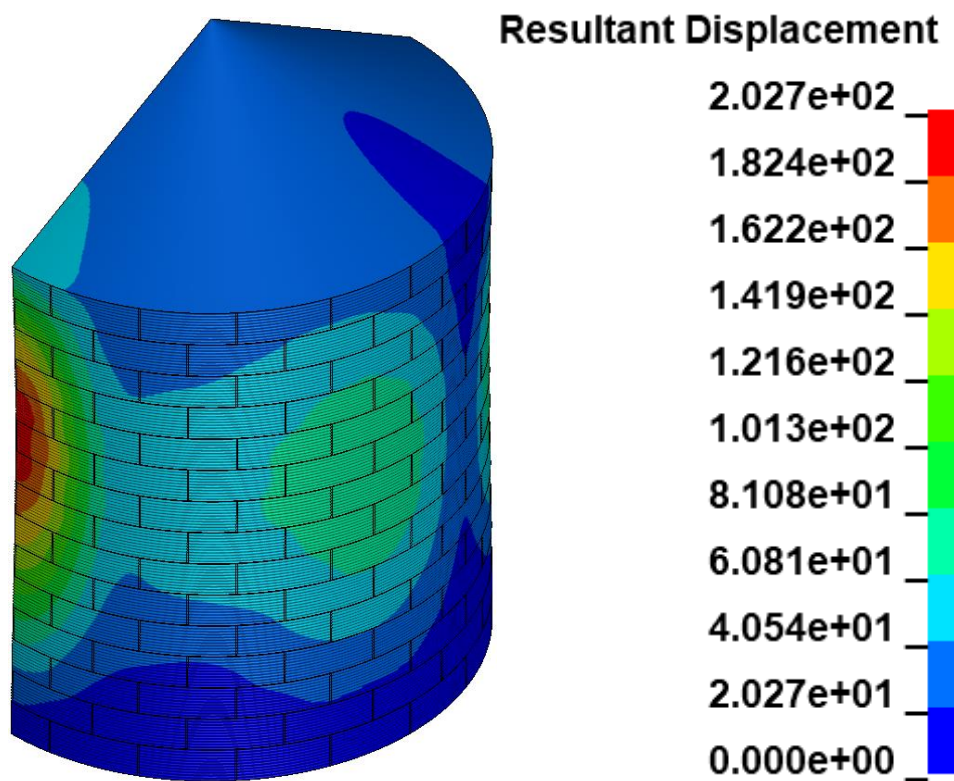
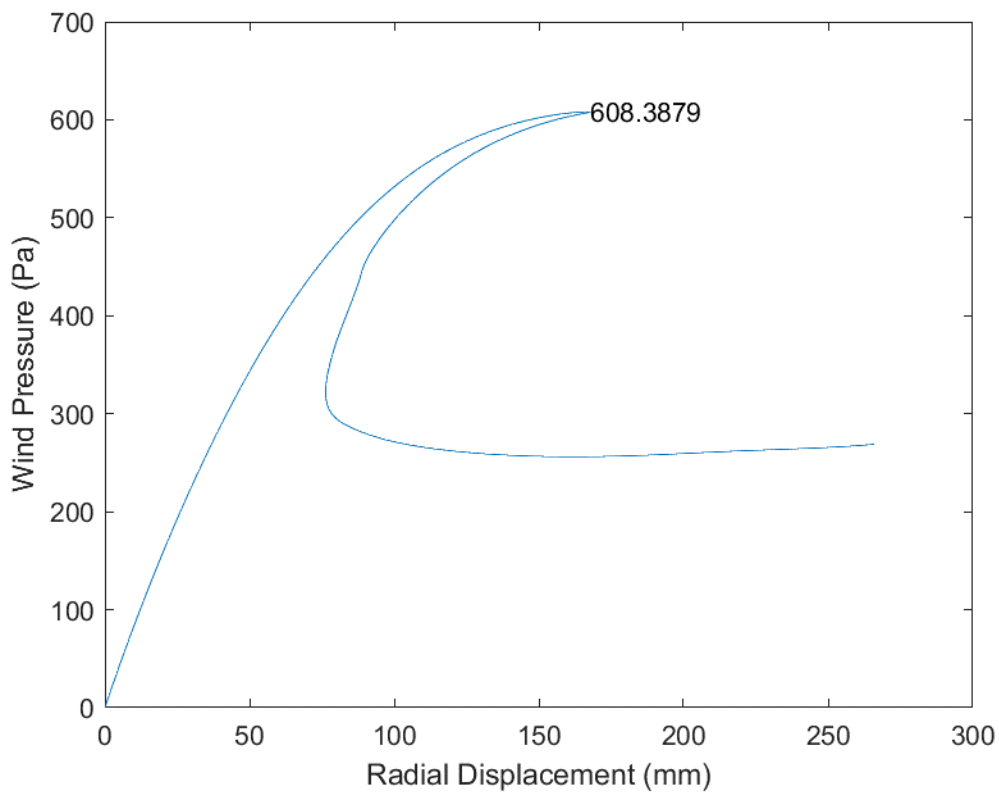


Fig. B.60 D54_H15_S00_R00_W00_V00_CL03_CD03_WT03_ST03

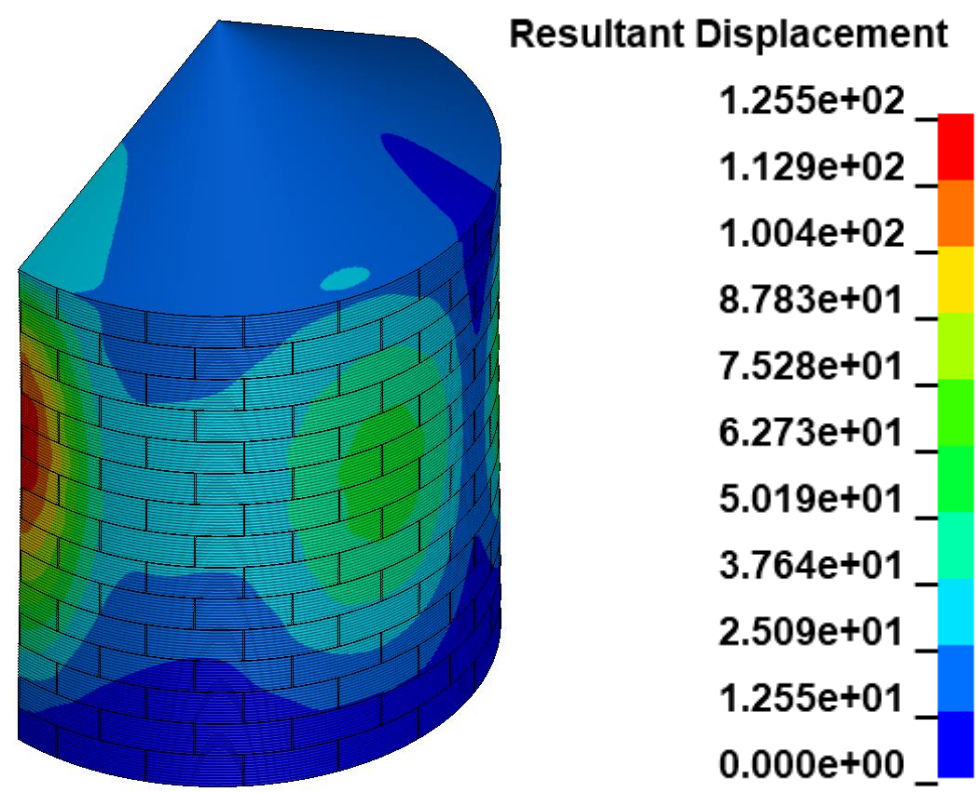
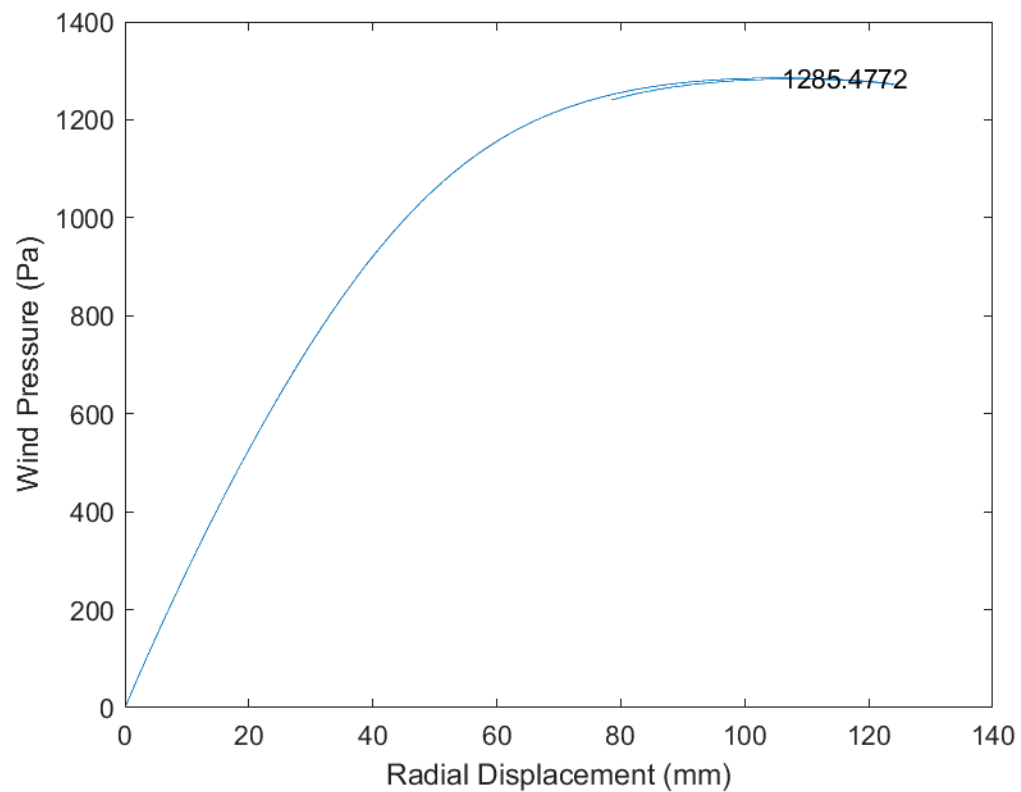


Fig. B.61 D54_H15_S00_R00_W00_V00_CL03_CD03_WT04_ST01

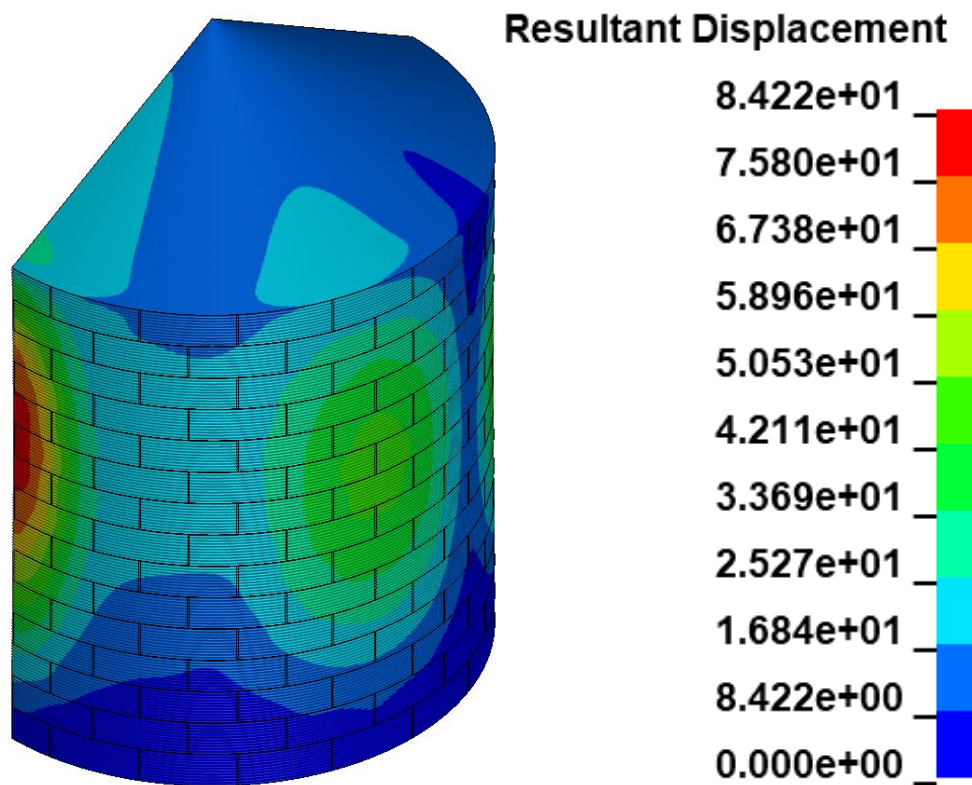
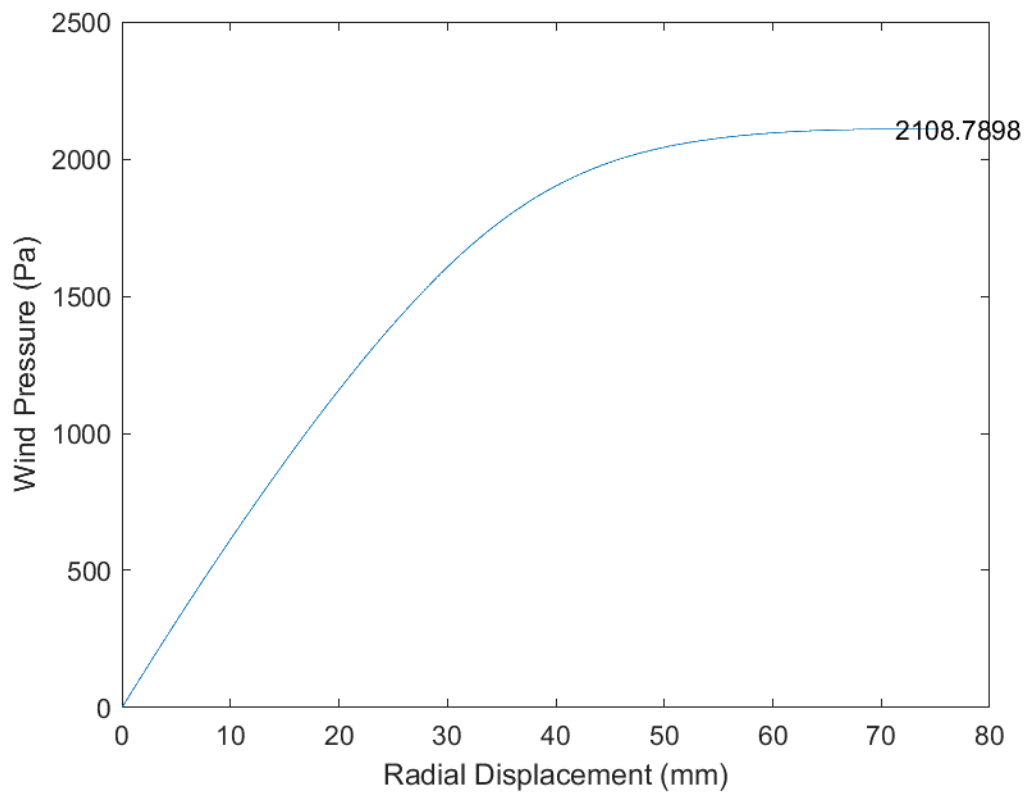


Fig. B.62 D54_H15_S00_R00_W00_V00_CL03_CD03_WT05_ST01

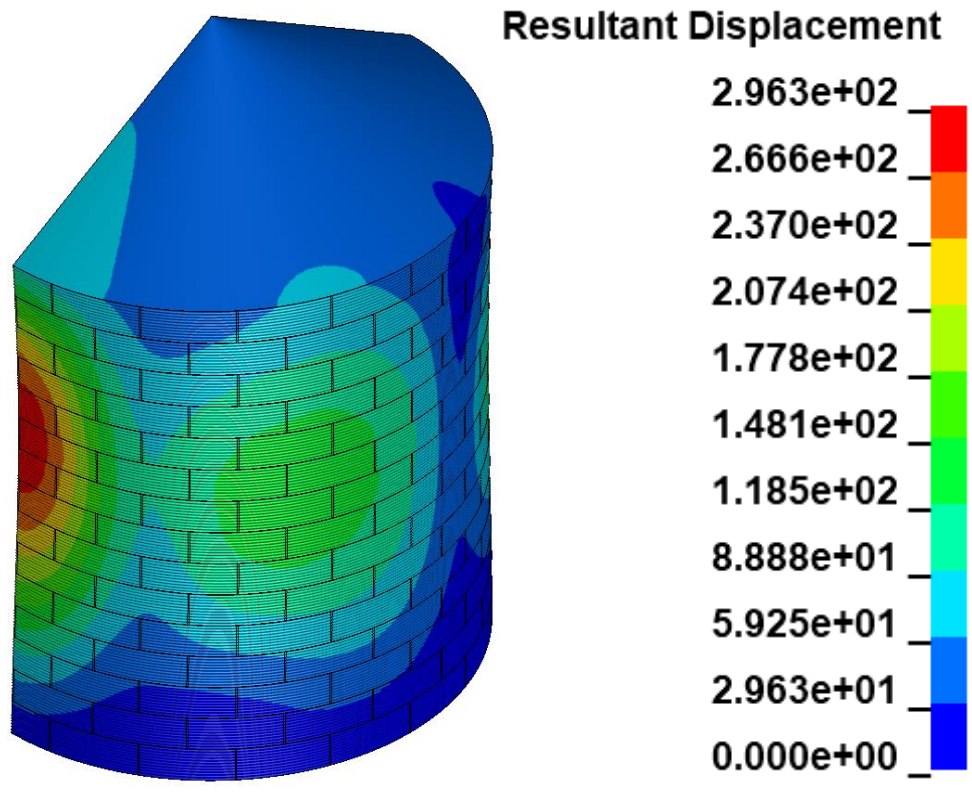
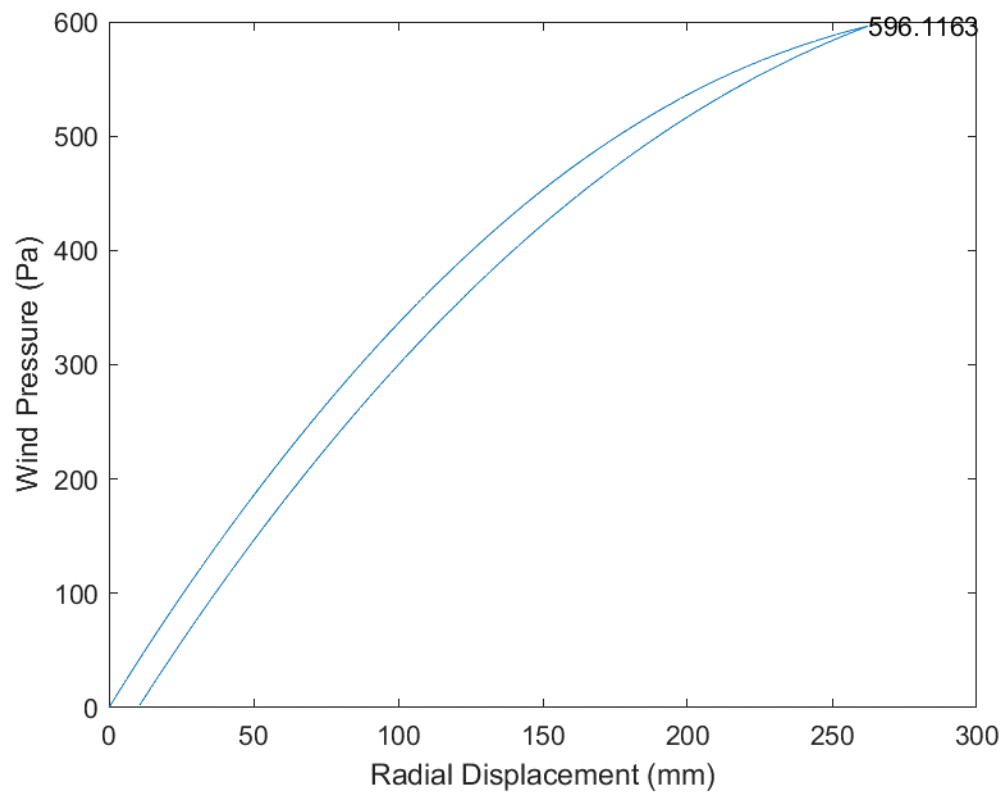


Fig. B.63 D54_H15_S00_R00_W00_V00_CL03_CD04_WT03_ST03

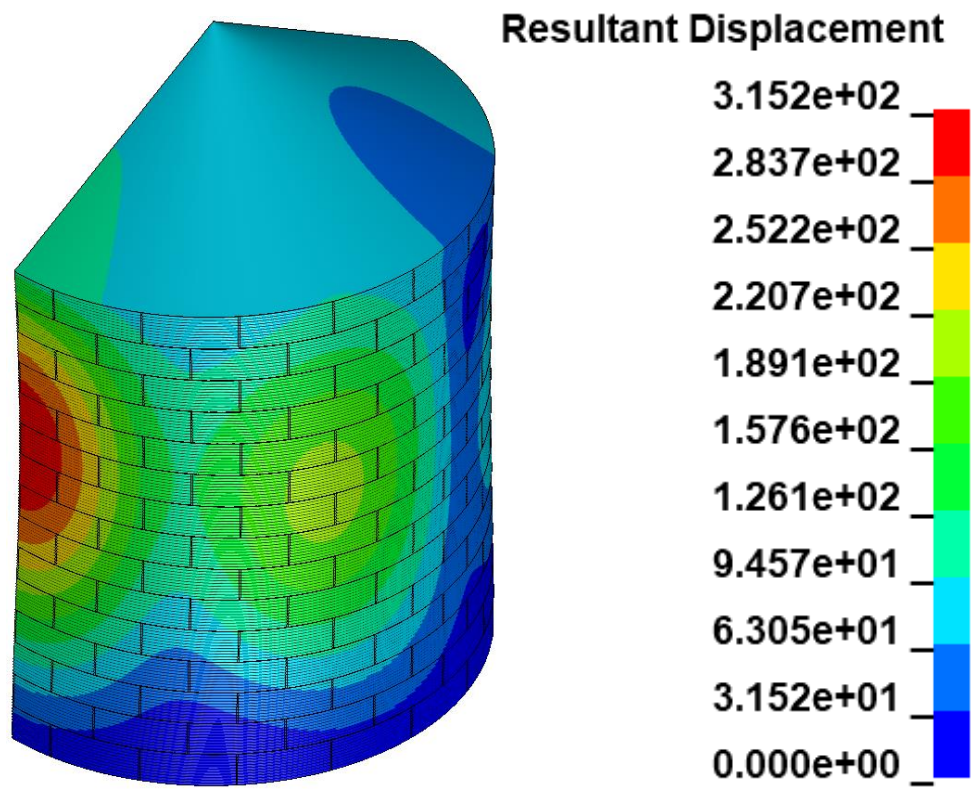
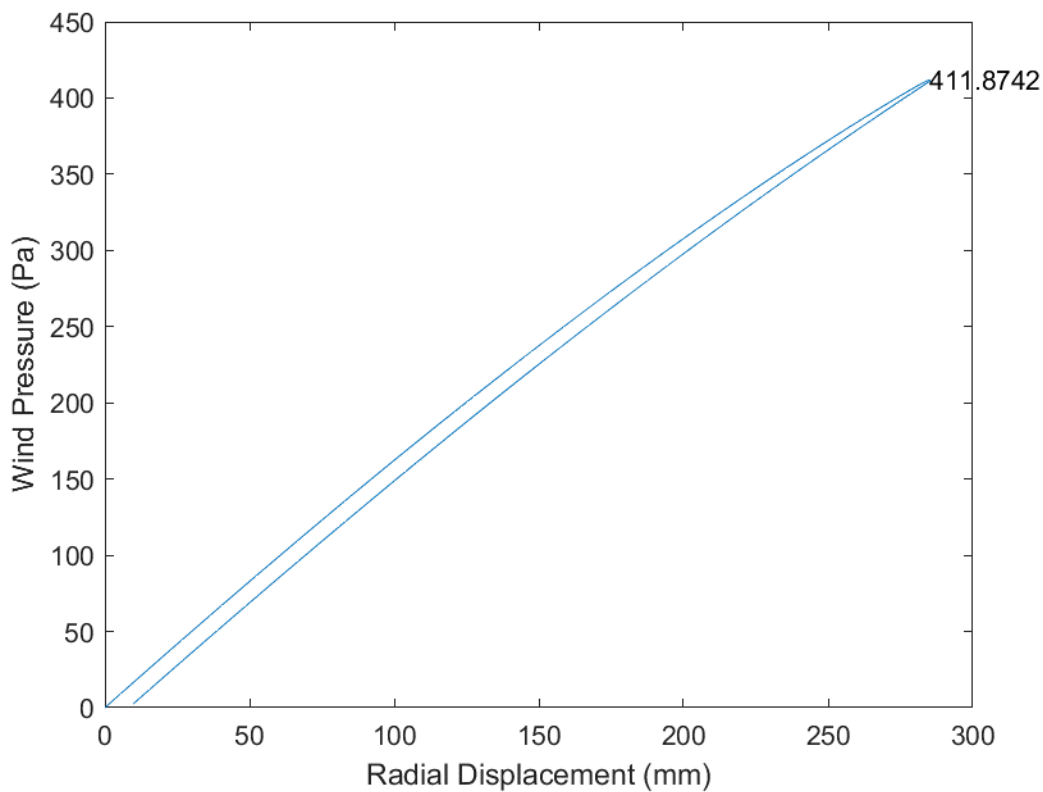


Fig. B.64 D54_H15_S00_R00_W00_V00_CL03_CD05_WT03_ST03

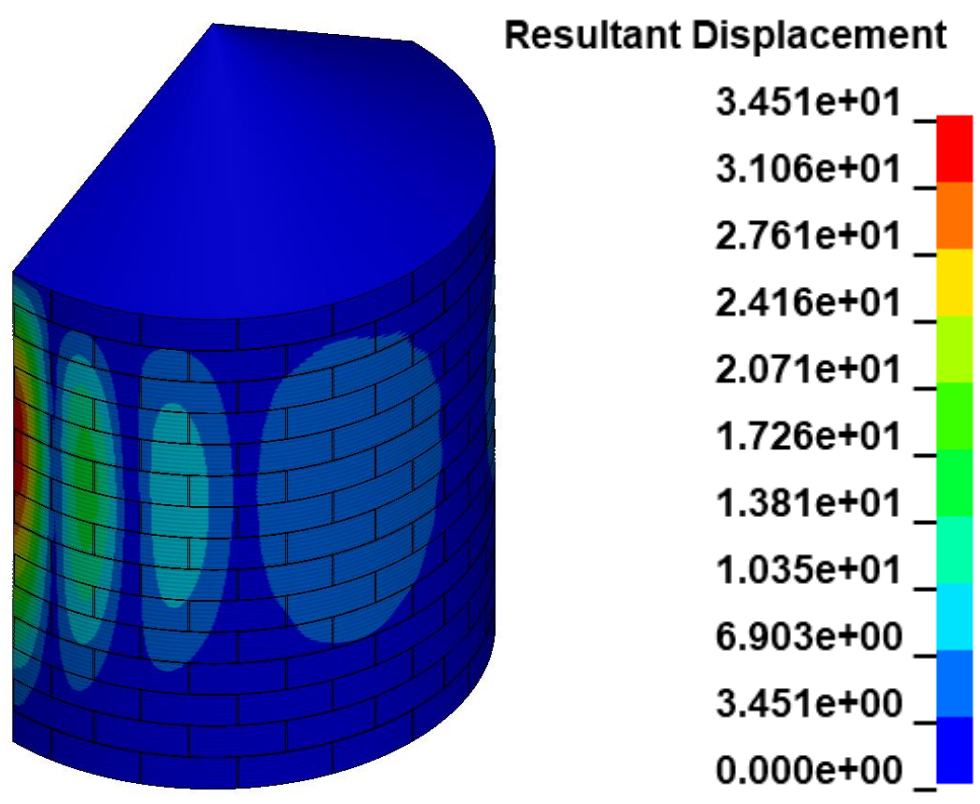
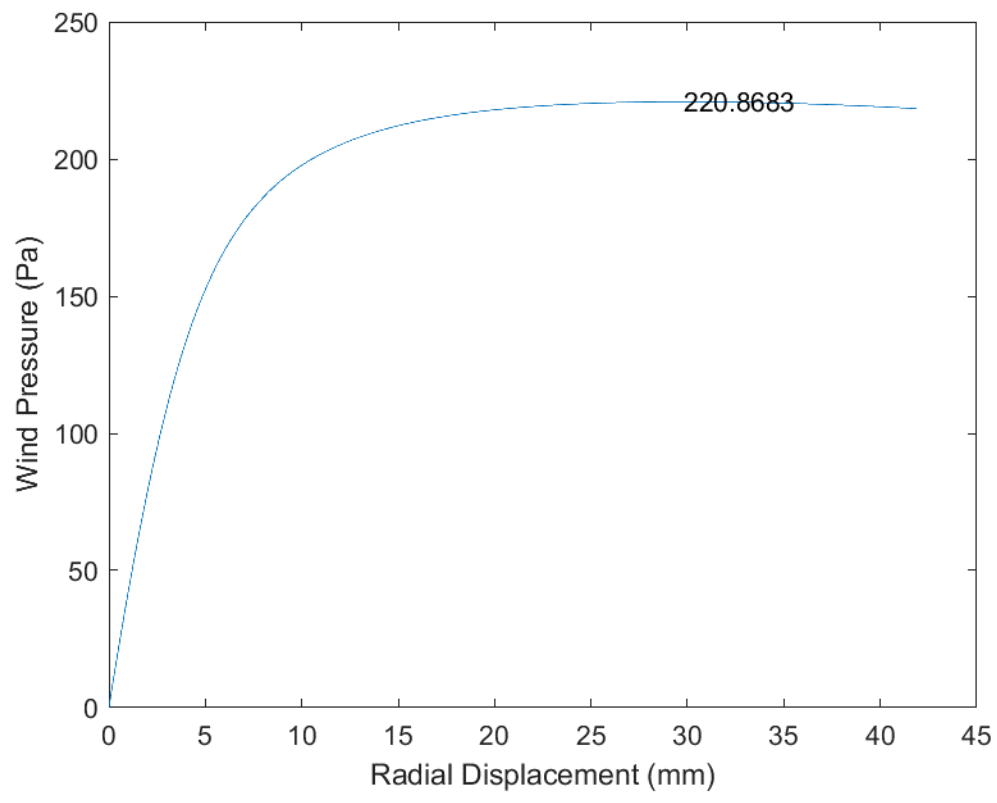


Fig. B.65 D54_H15_S00_R00_W00_V00_CL04_CD01_WT03_ST03

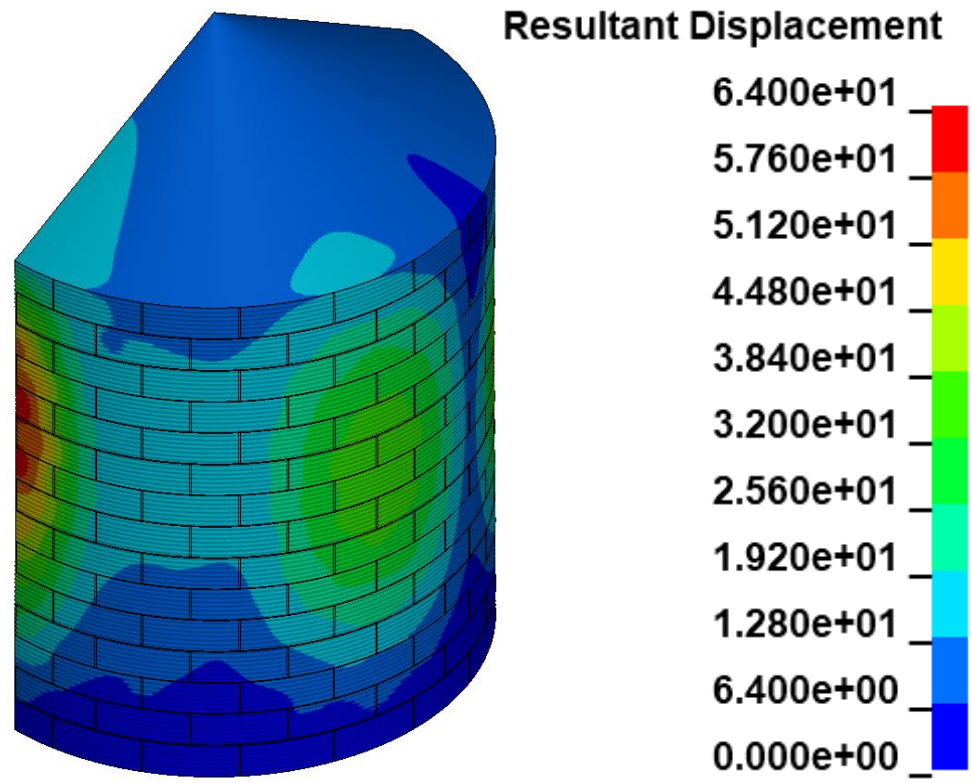
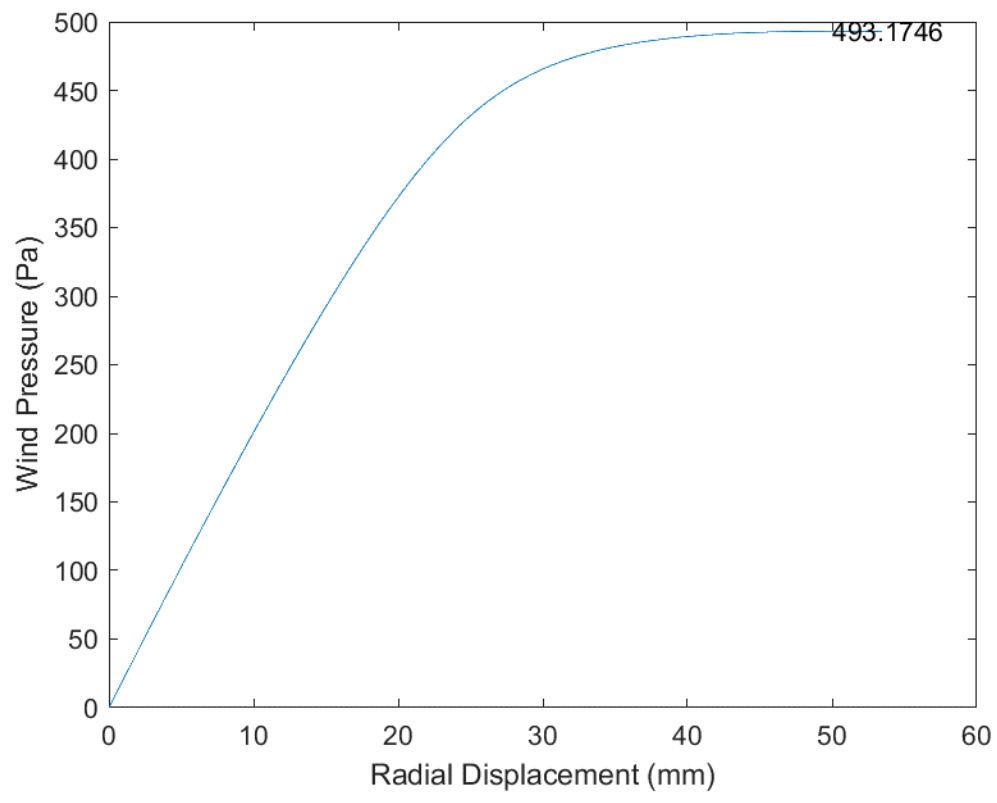


Fig. B.66 D54_H15_S00_R00_W00_V00_CL04_CD02_WT03_ST03

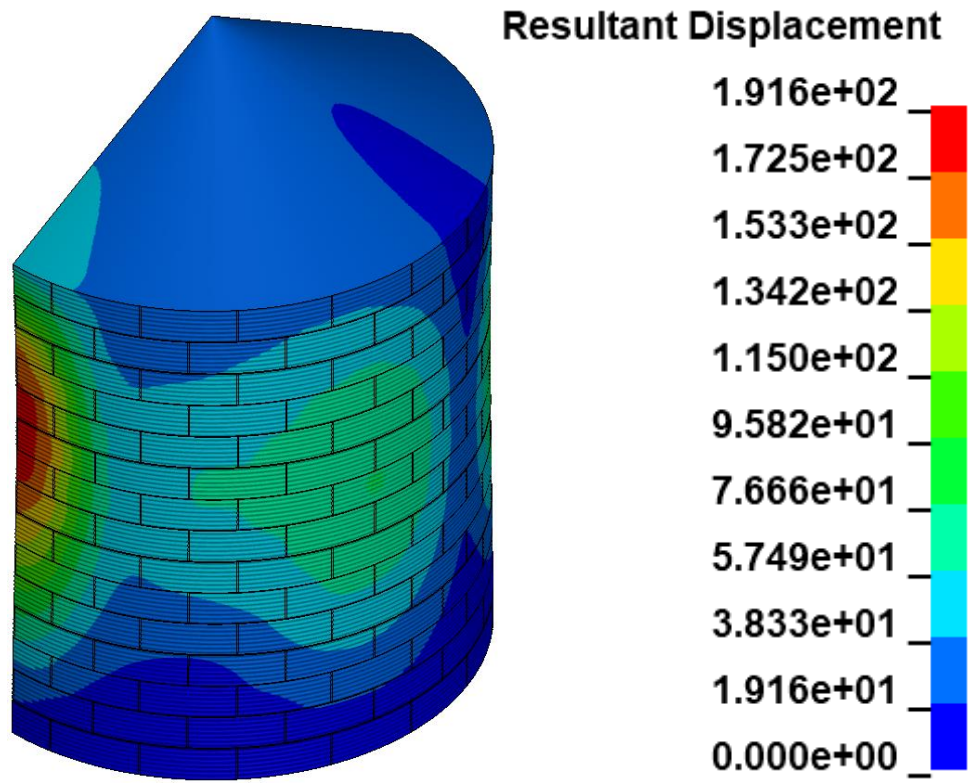
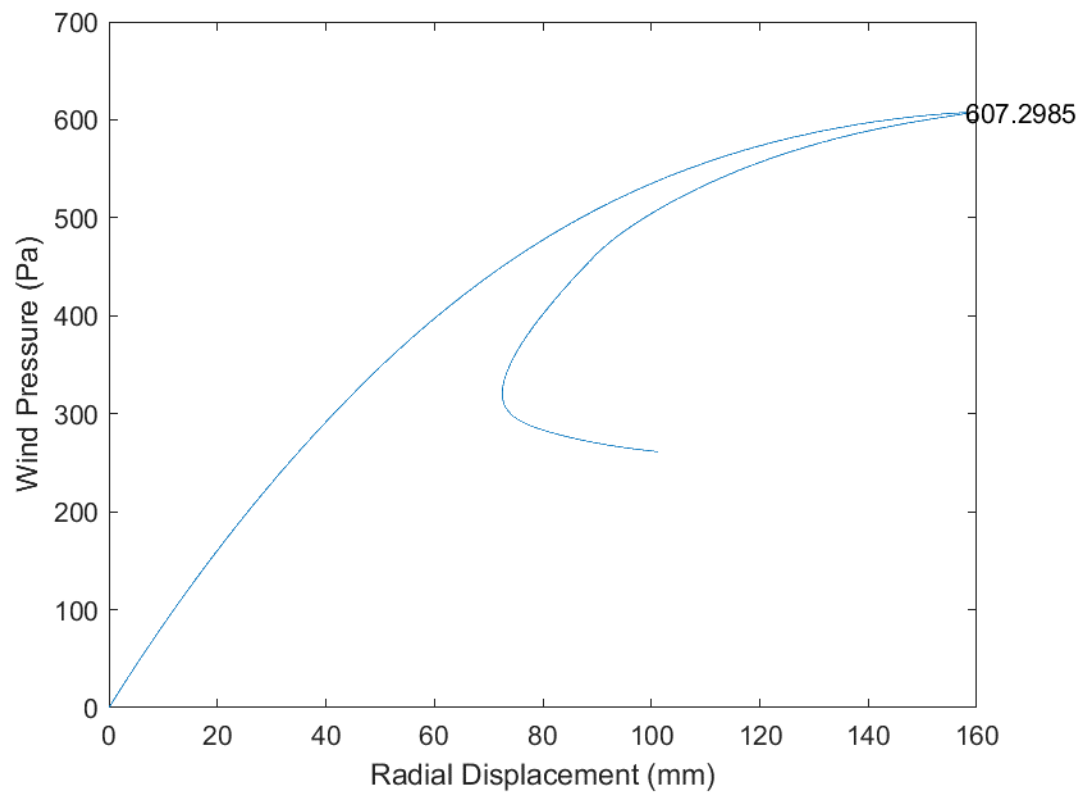


Fig. B.67 D54_H15_S00_R00_W00_V00_CL04_CD03_WT03_ST03

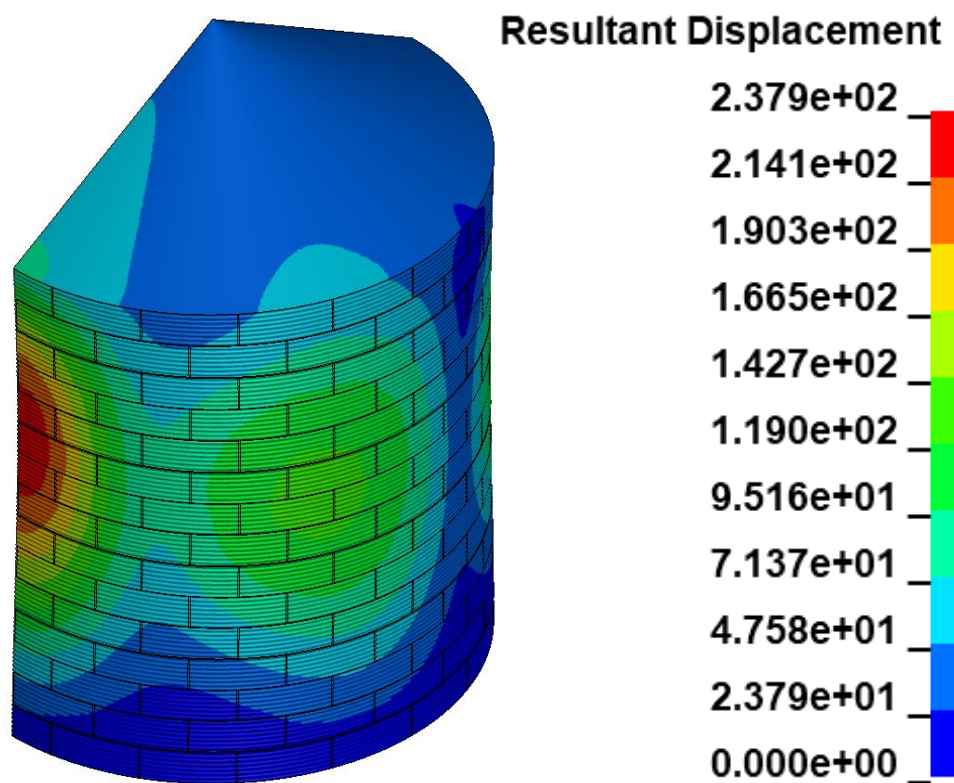
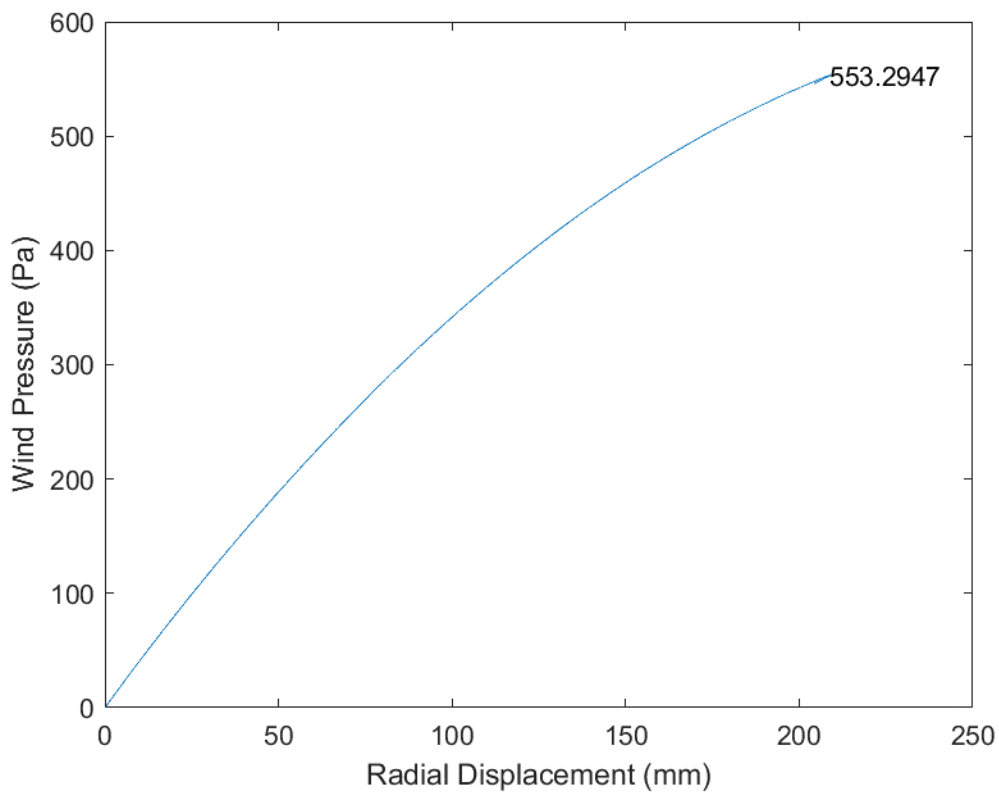


Fig. B.68 D54_H15_S00_R00_W00_V00_CL04_CD04_WT03_ST03

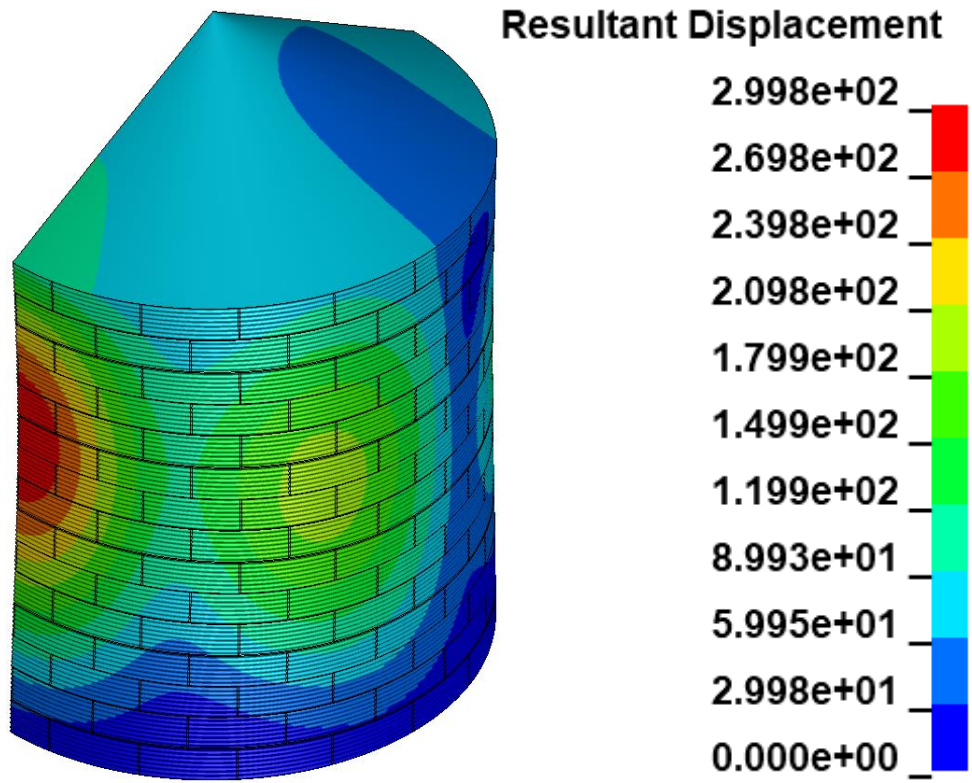
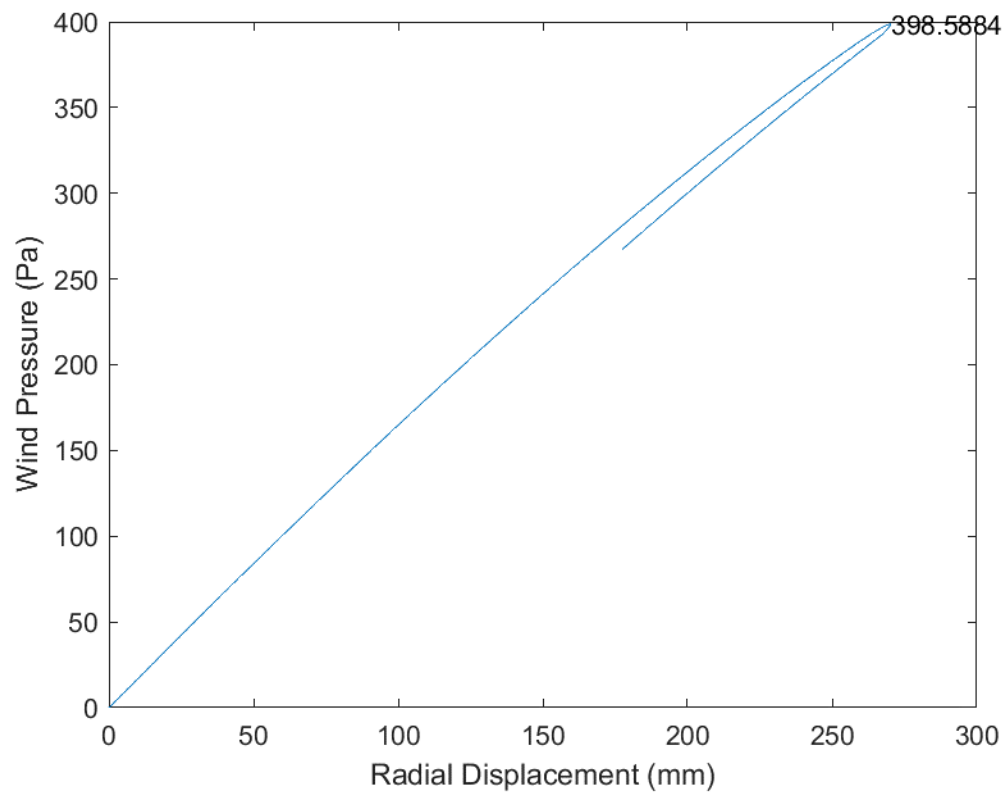


Fig. B.69 D54_H15_S00_R00_W00_V00_CL04_CD05_WT03_ST03

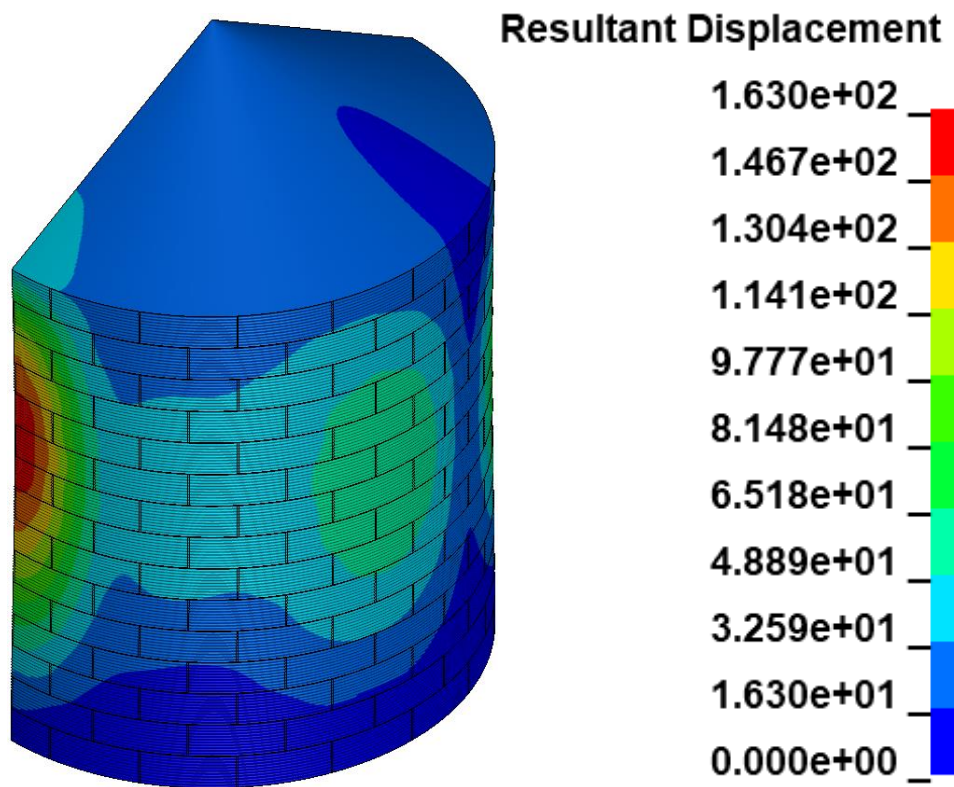
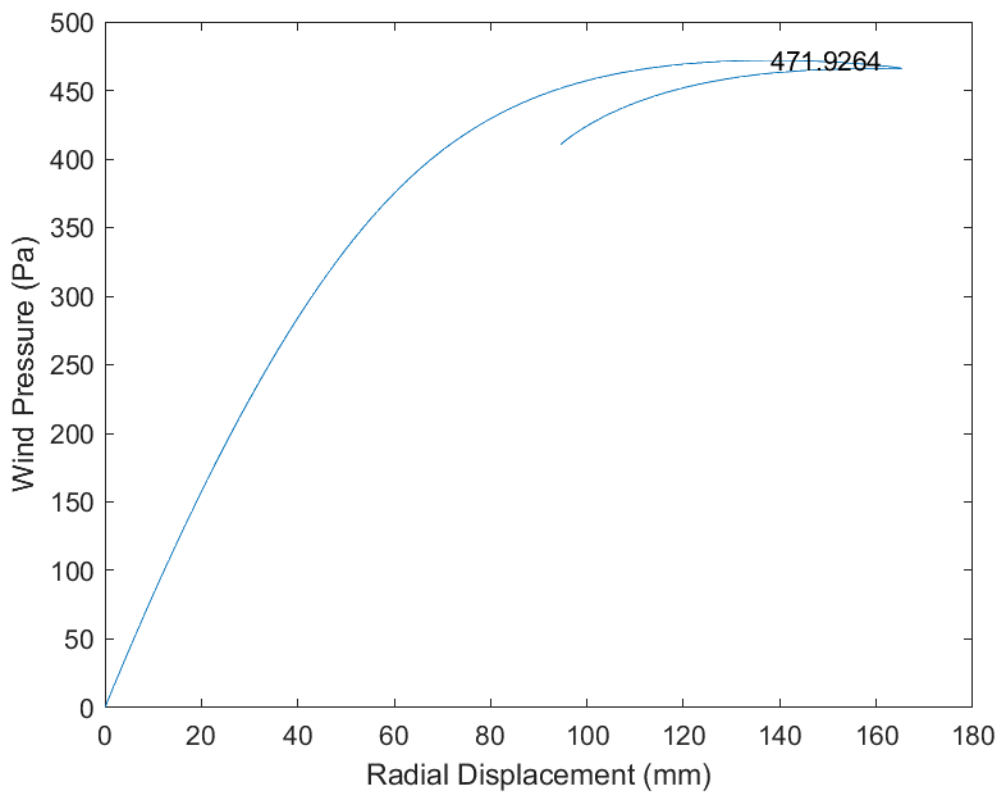


Fig. B.70 D54_H15_S00_R00_W00_V01_CL03_CD03_WT03_ST03

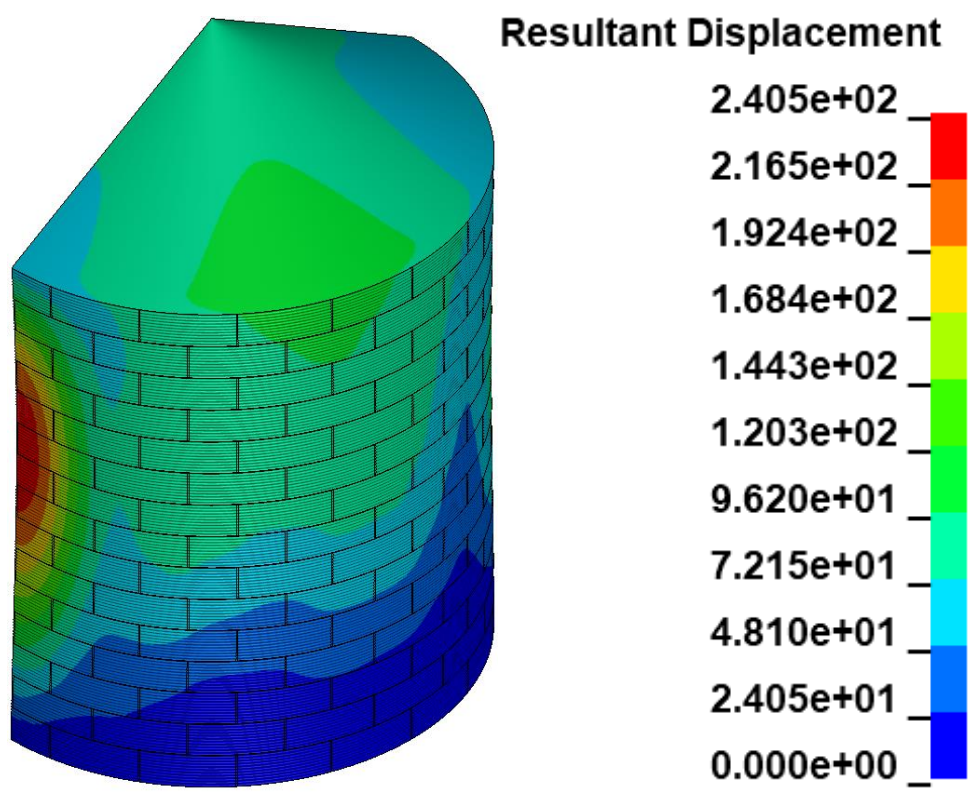
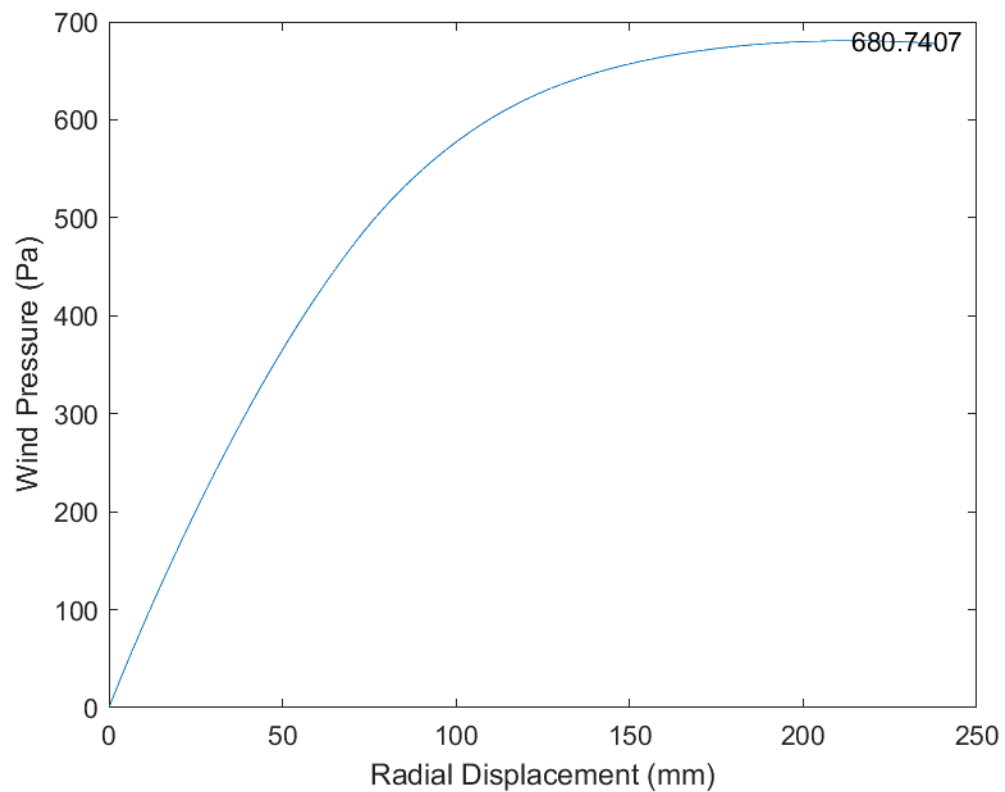


Fig. B.71 D54_H15_S00_R00_W01_V00_CL03_CD03_WT03_ST03

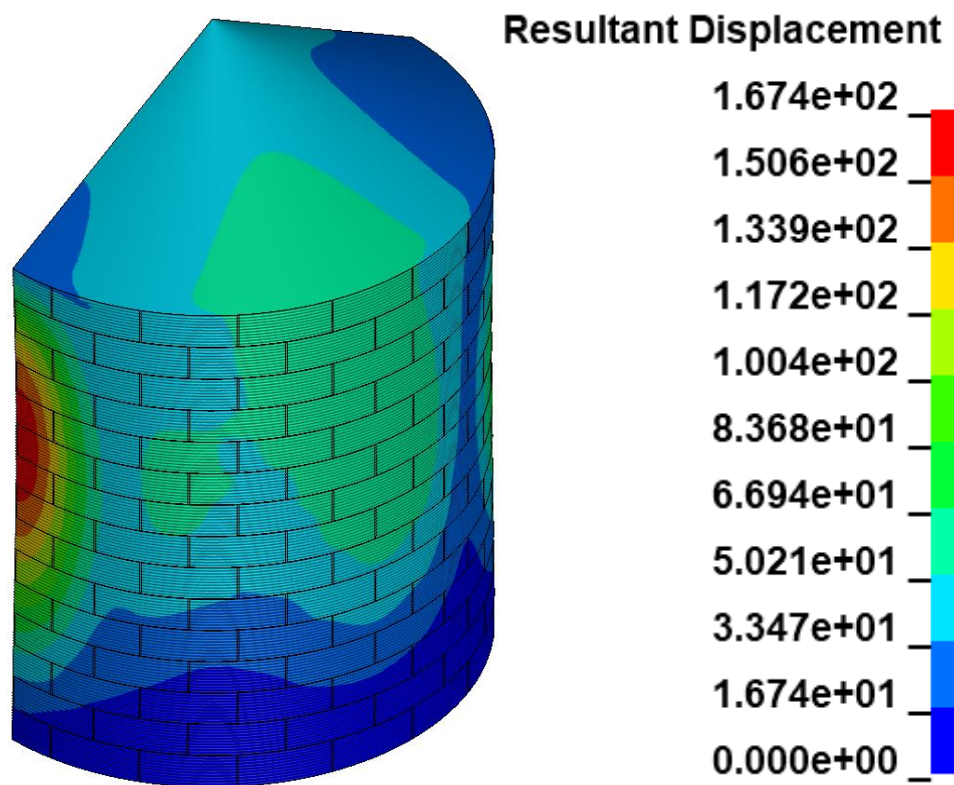
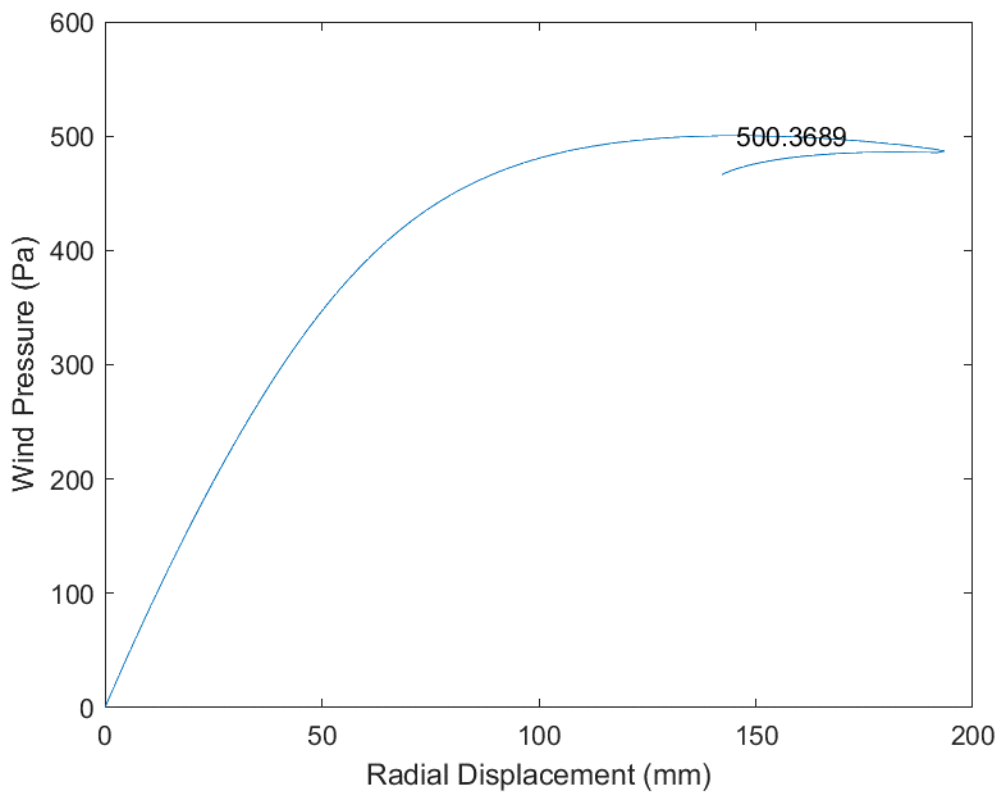


Fig. B.72 D54_H15_S00_R00_W01_V01_CL03_CD03_WT03_ST03

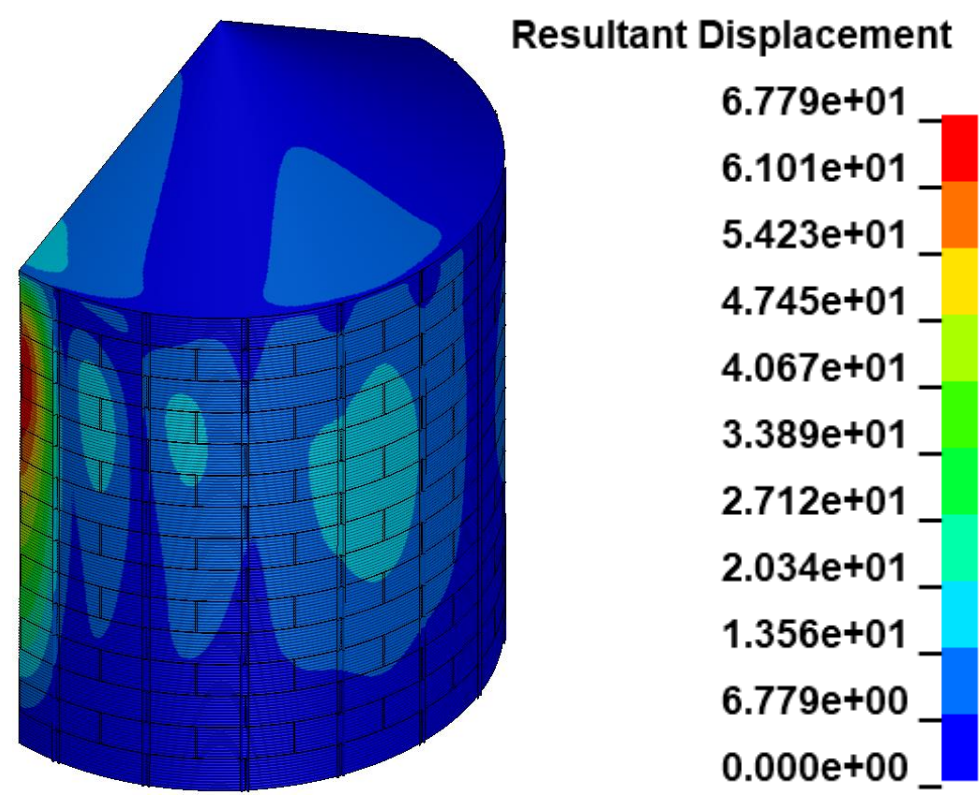
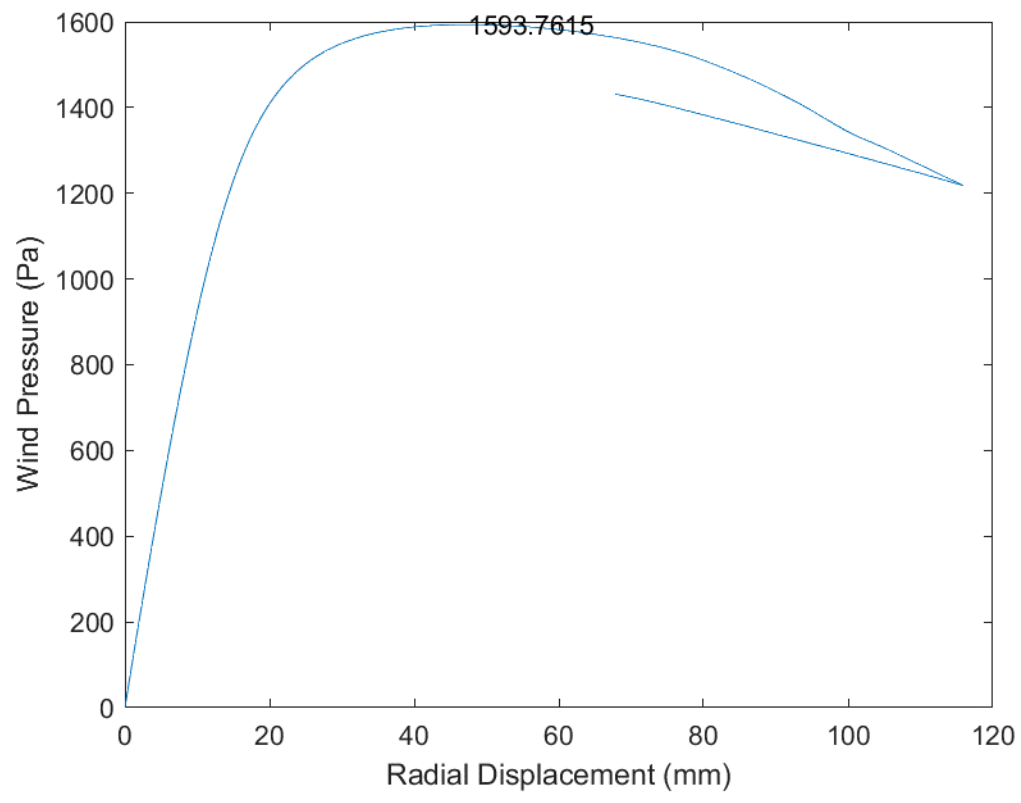


Fig. B.73 D54_H15_S18_R00_W00_V00_CL03_CD03_WT03_ST03

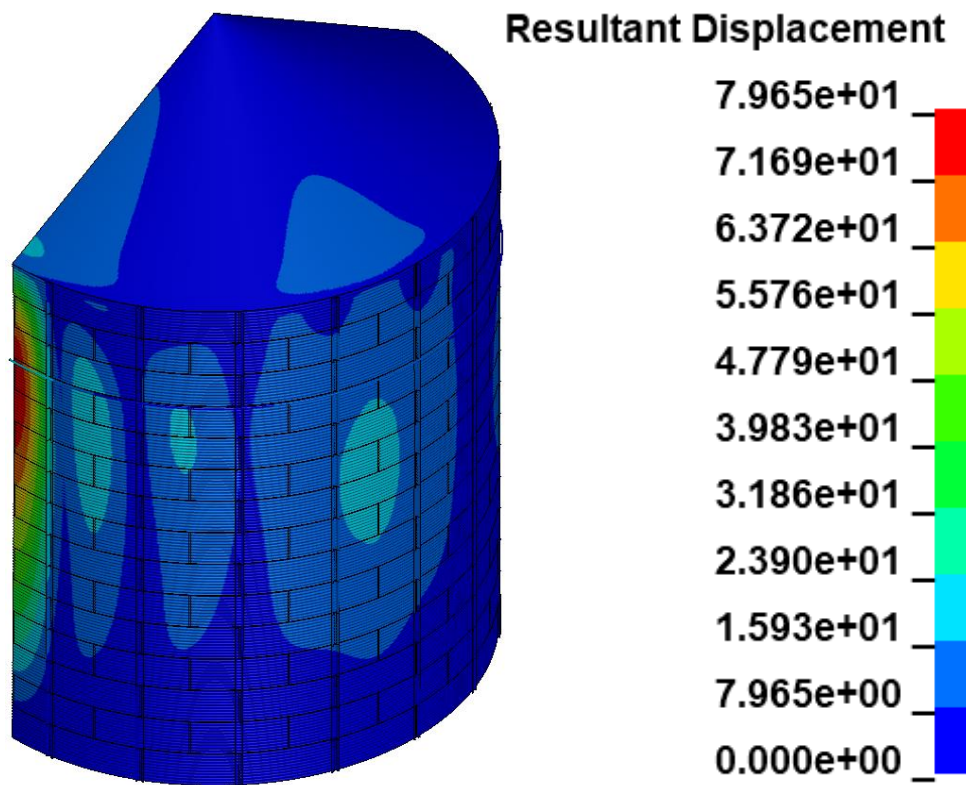
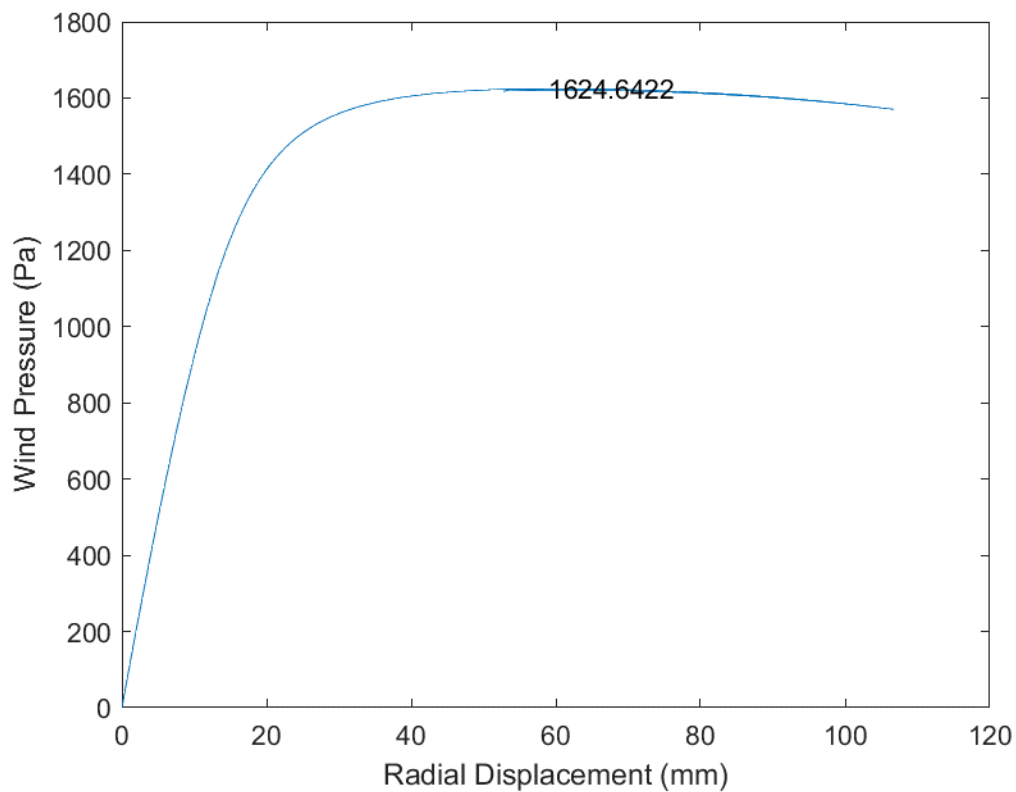


Fig. B.74 D54_H15_S18_R01_W00_V00_CL03_CD03_WT03_ST03

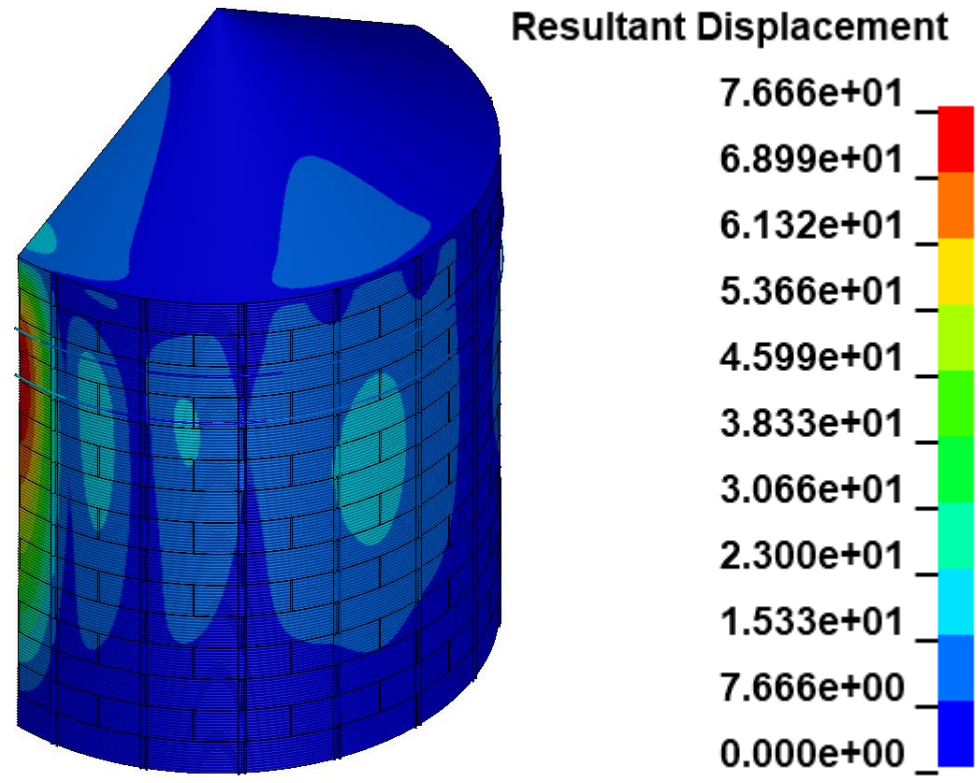
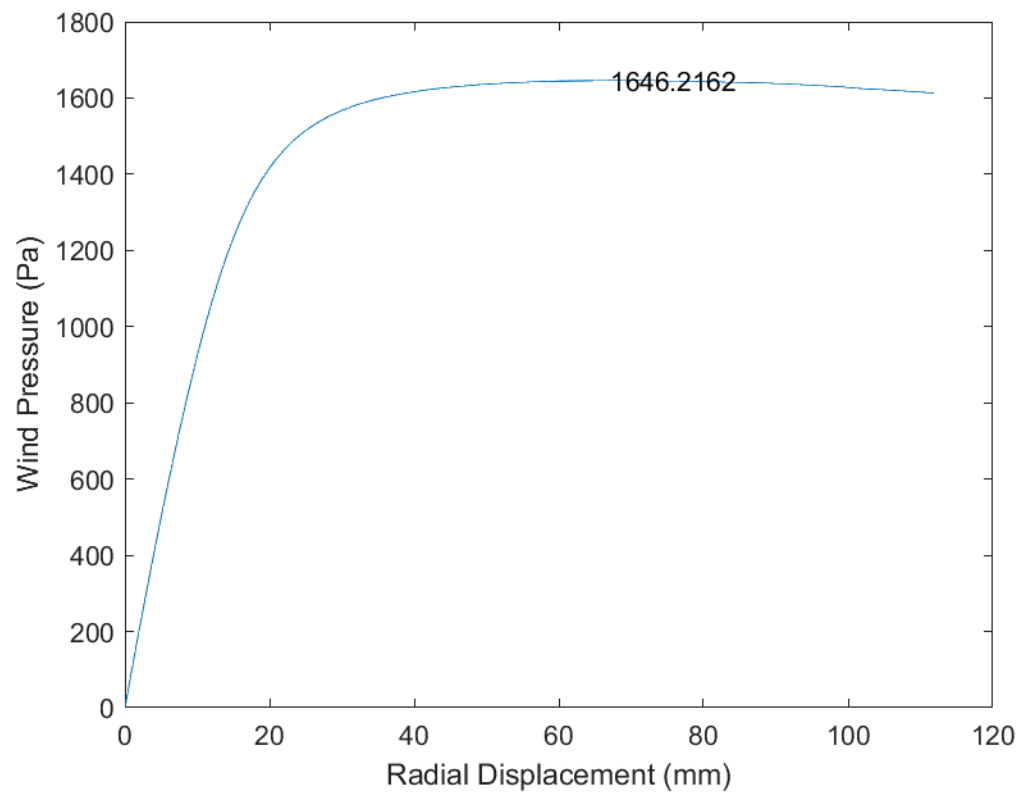


Fig. B.75 D54_H15_S18_R02_W00_V00_CL03_CD03_WT03_ST03

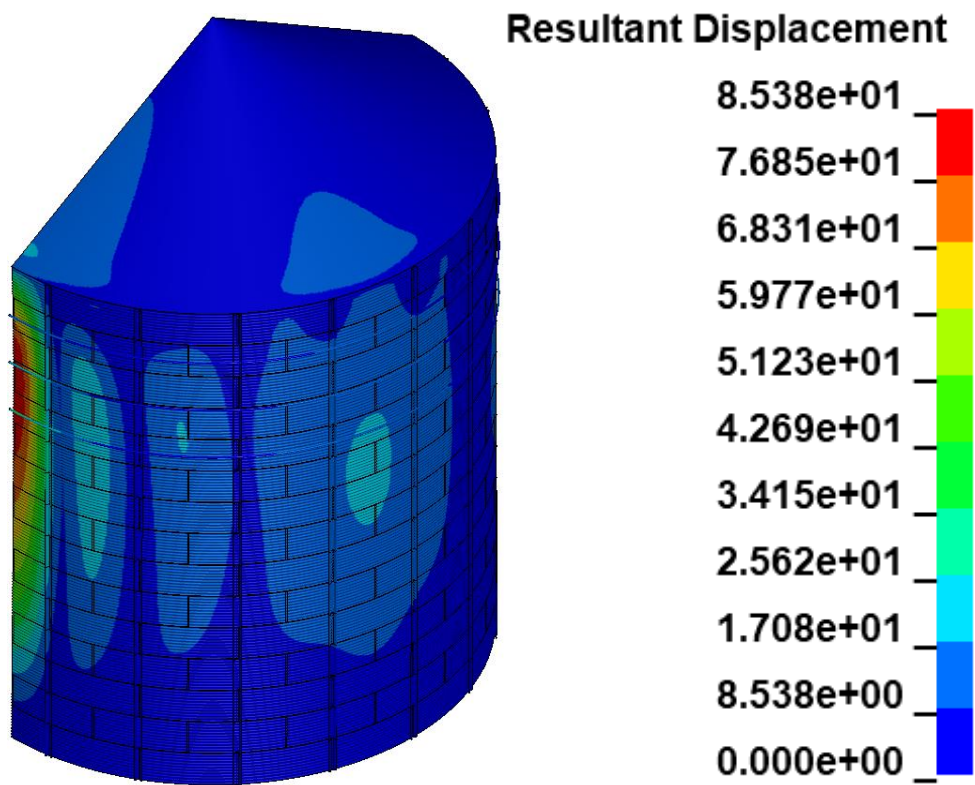
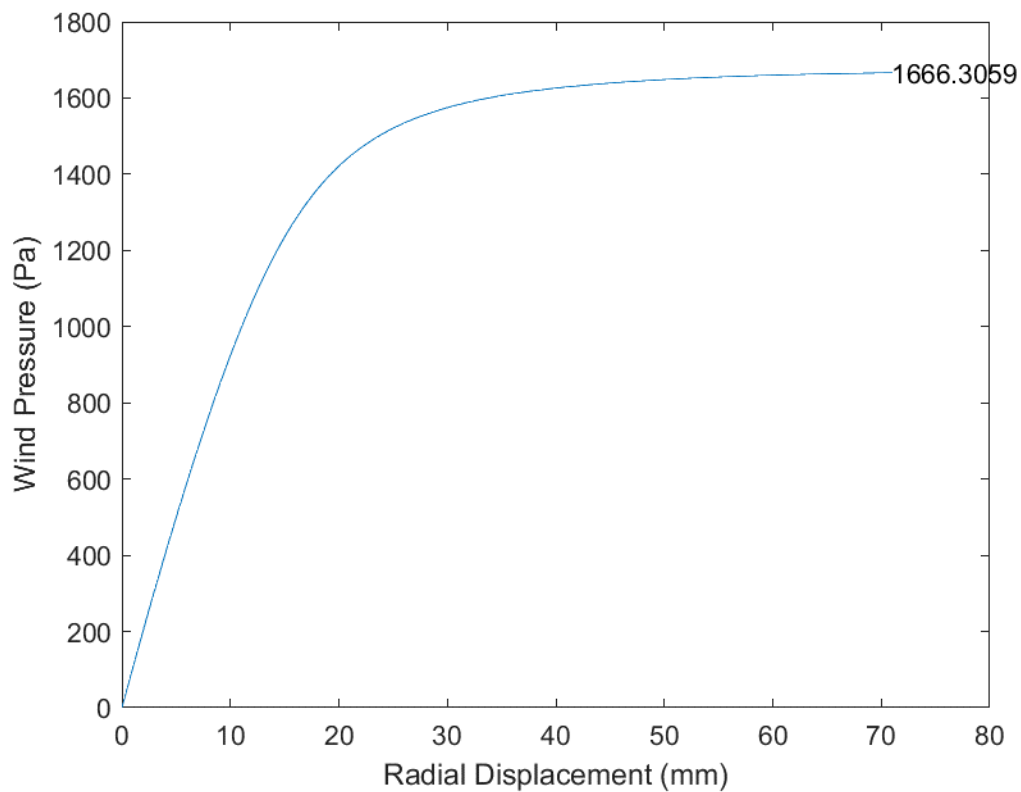


Fig. B.76 D54_H15_S18_R03_W00_V00_CL03_CD03_WT03_ST03

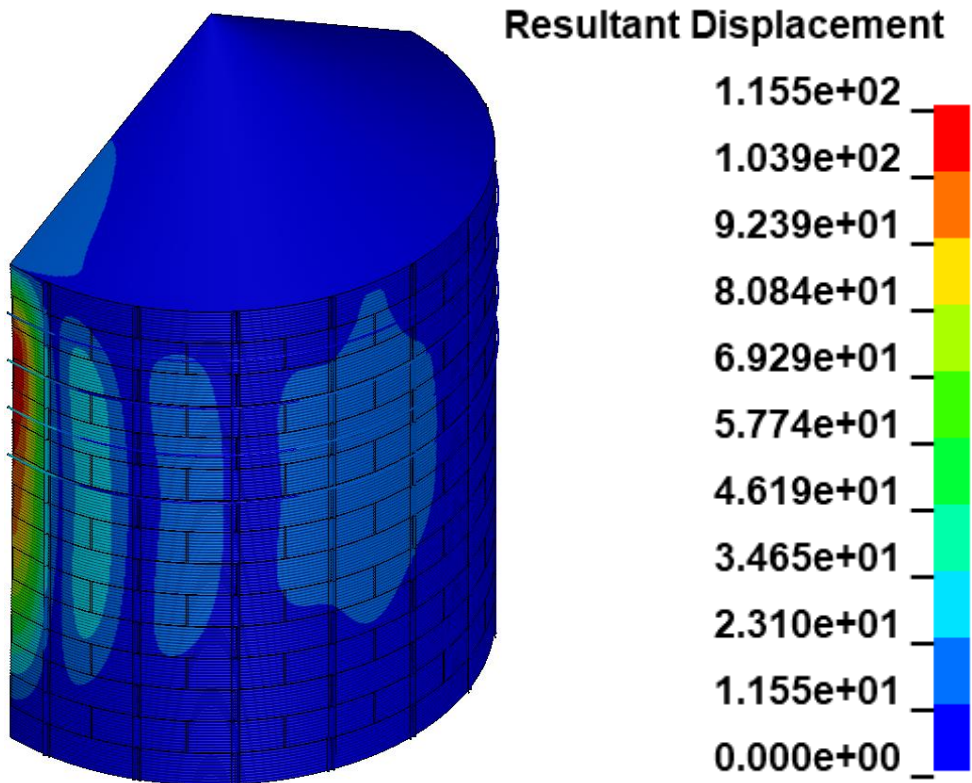
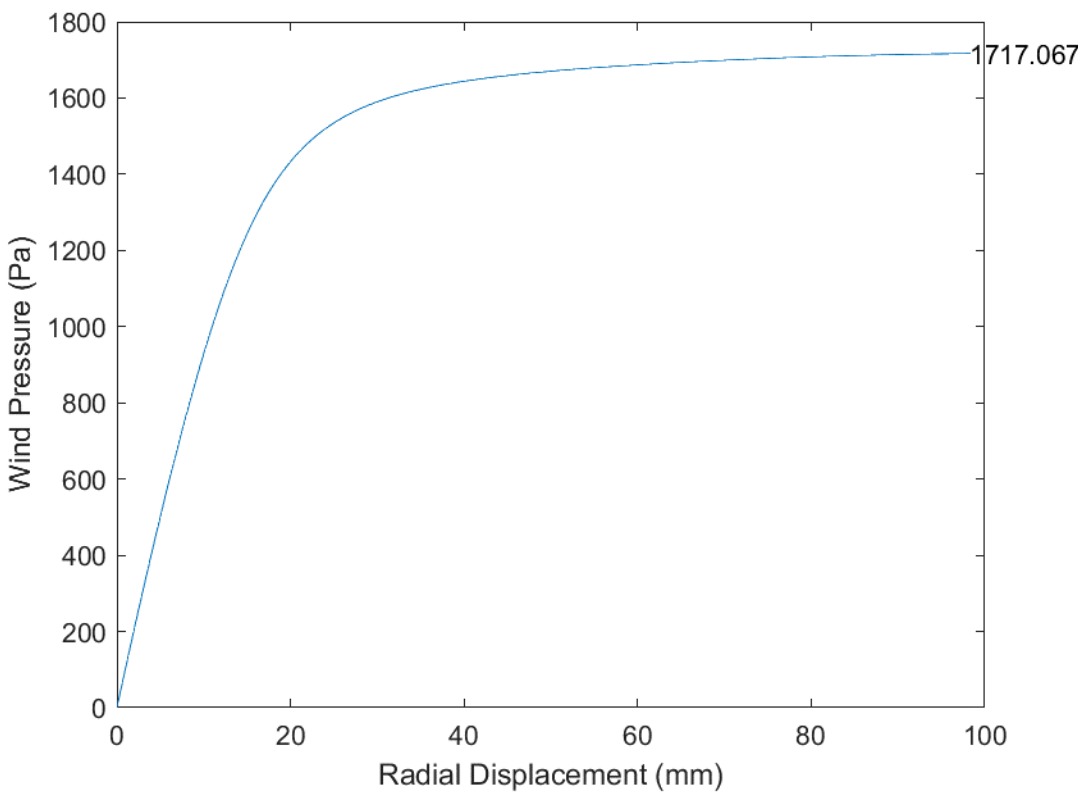


Fig. B.77 D54_H15_S18_R04_W00_V00_CL03_CD03_WT03_ST03

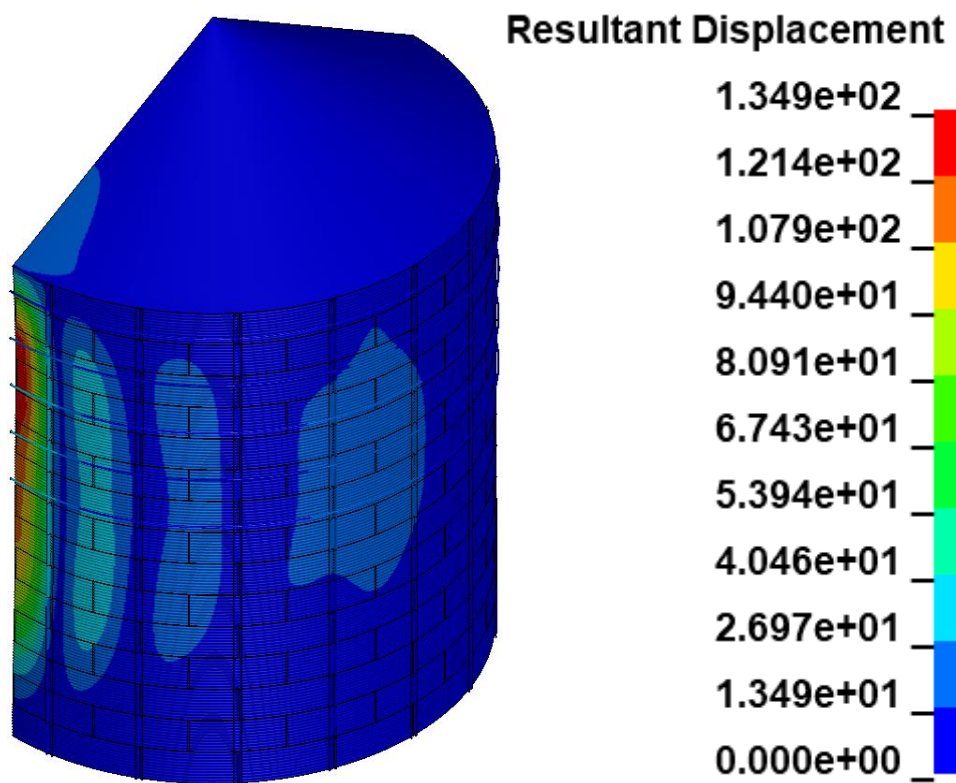
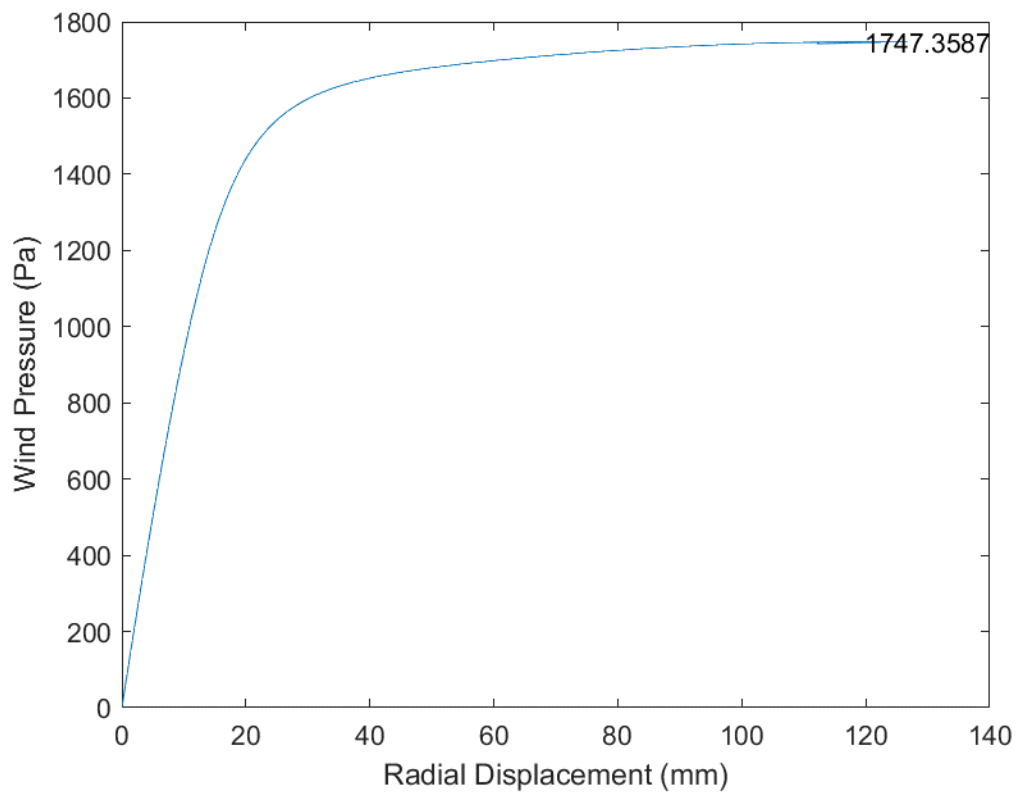


Fig. B.78 D54_H15_S18_R05_W00_V00_CL03_CD03_WT03_ST03

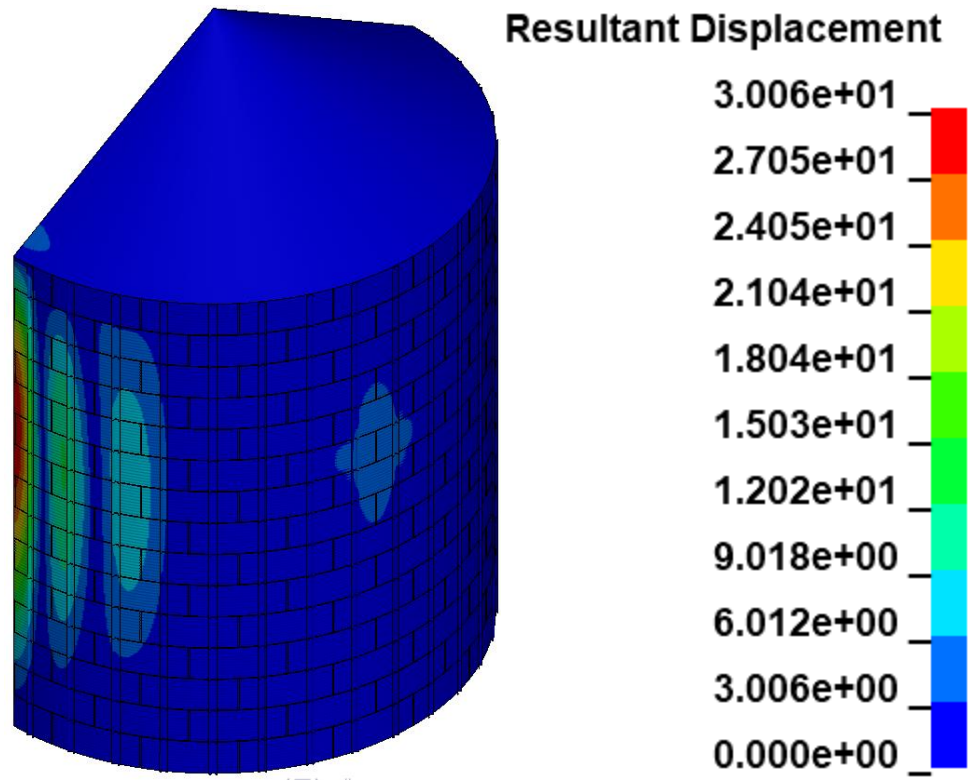
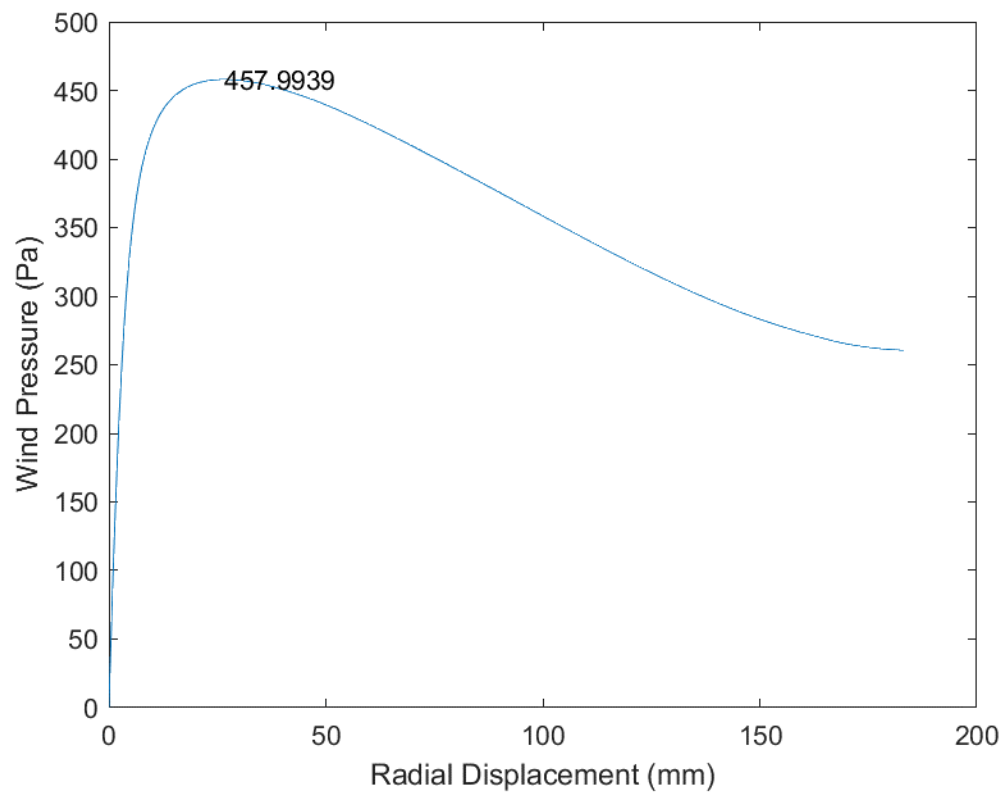


Fig. B.79 D54_H15_S36_R00_W00_V00_CL03_CD01_WT03_ST03

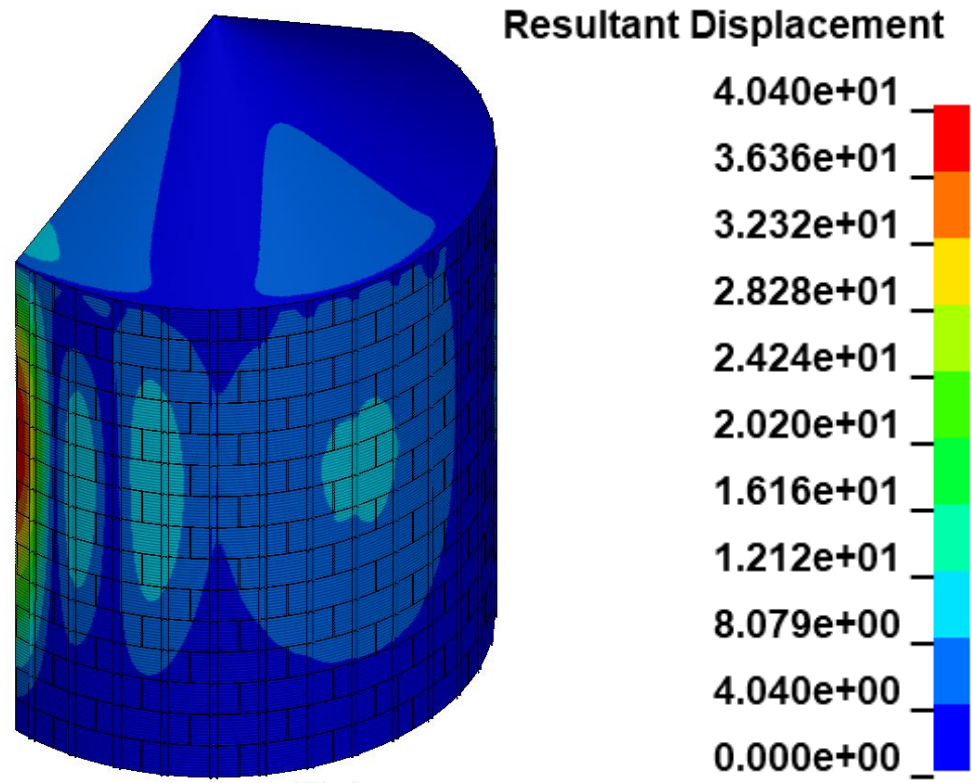
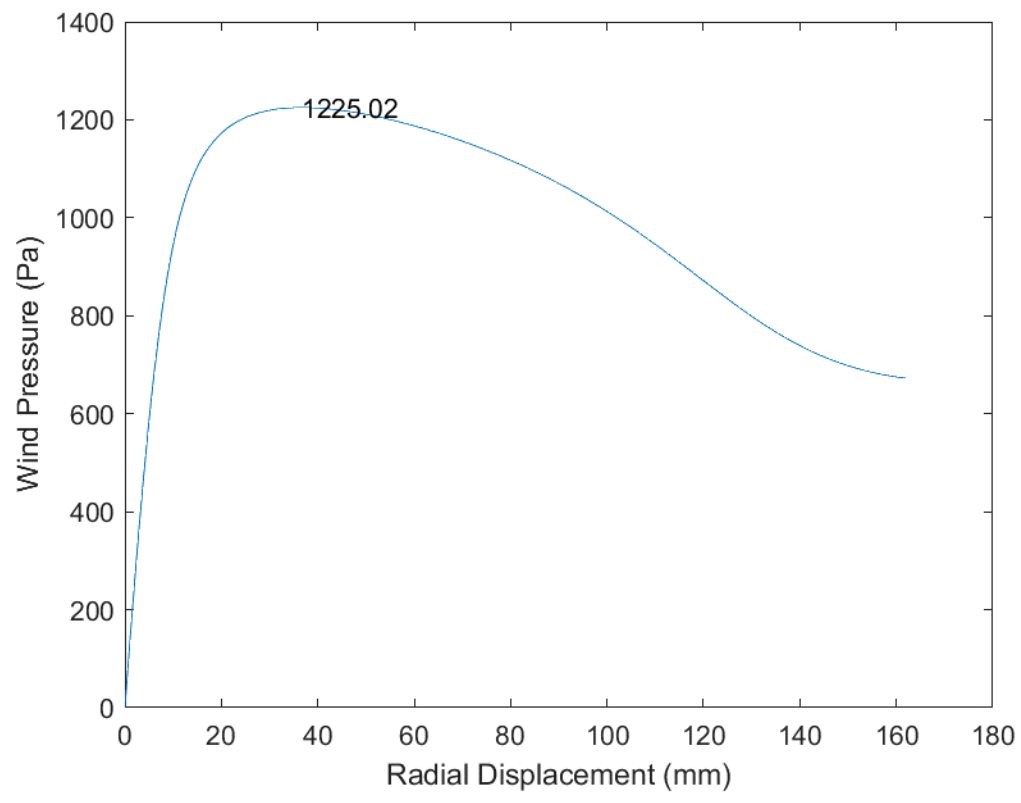


Fig. B.80 D54_H15_S36_R00_W00_V00_CL03_CD02_WT03_ST03

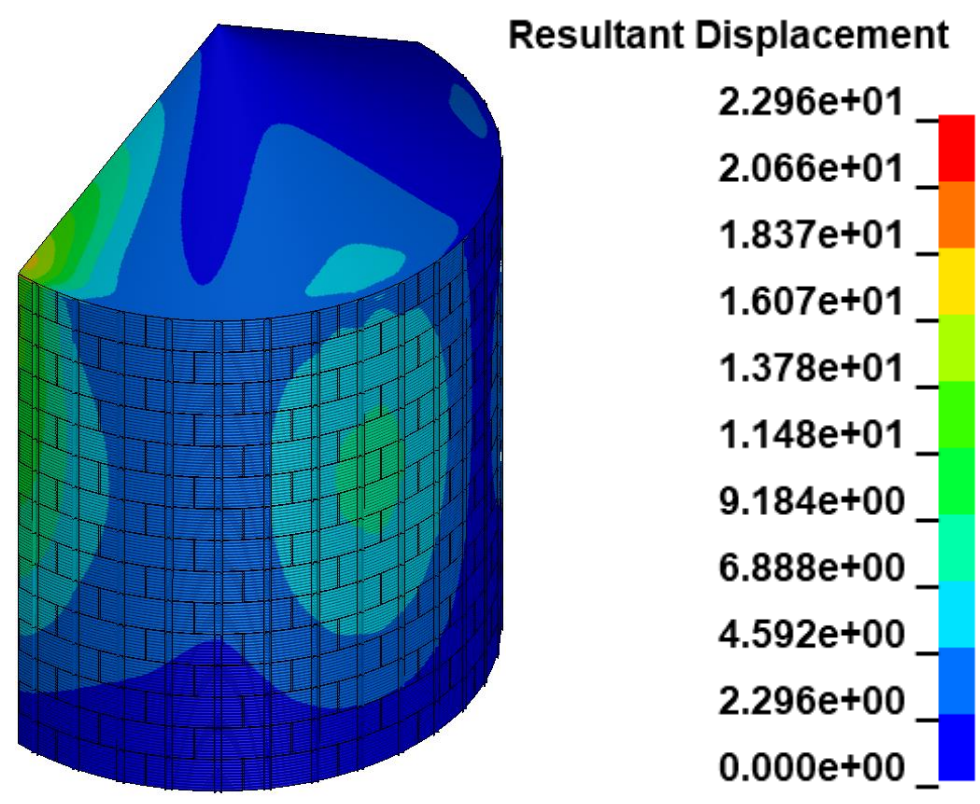
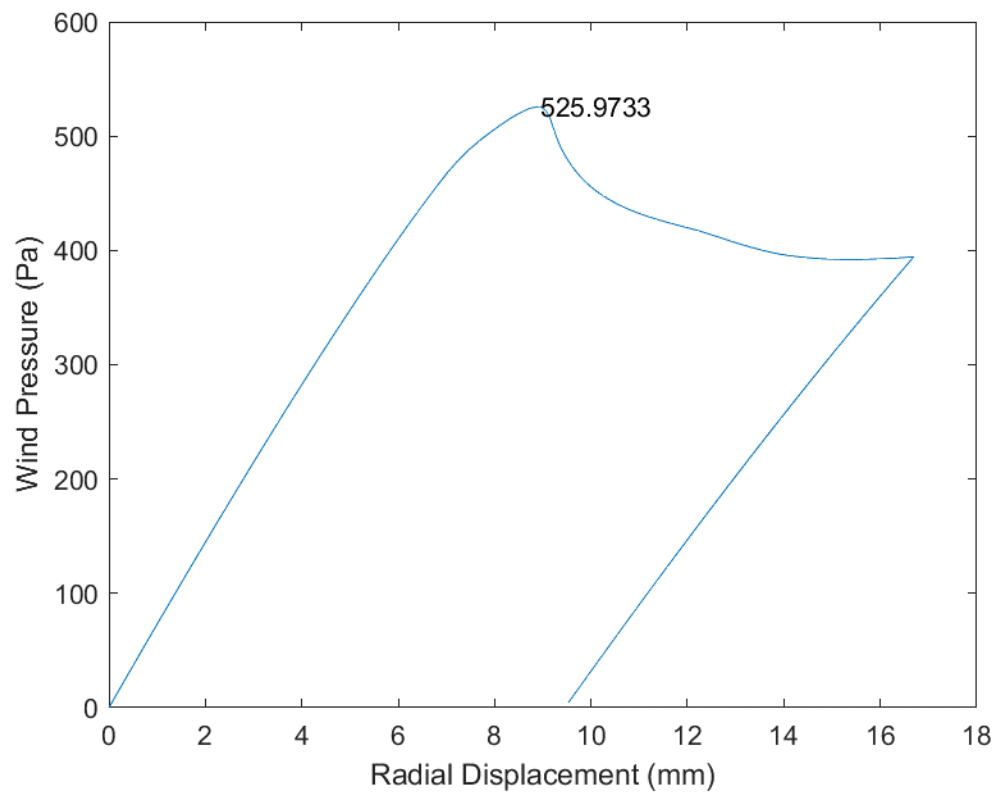


Fig. B.81 D54_H15_S36_R00_W00_V00_CL03_CD03_WT01_ST01

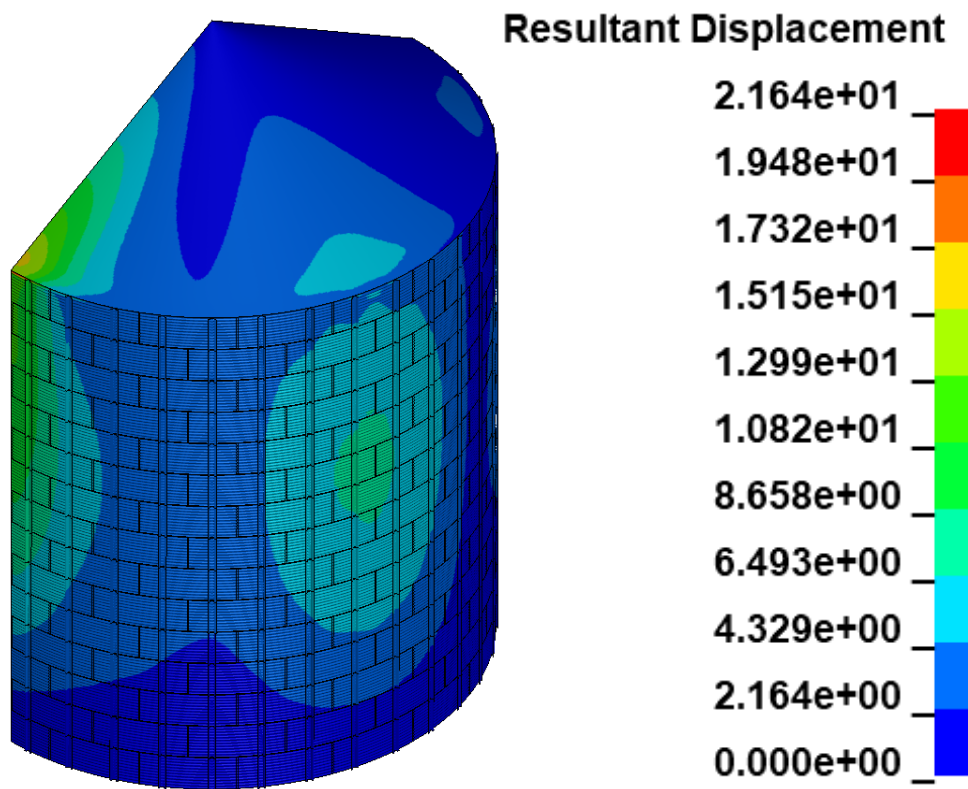
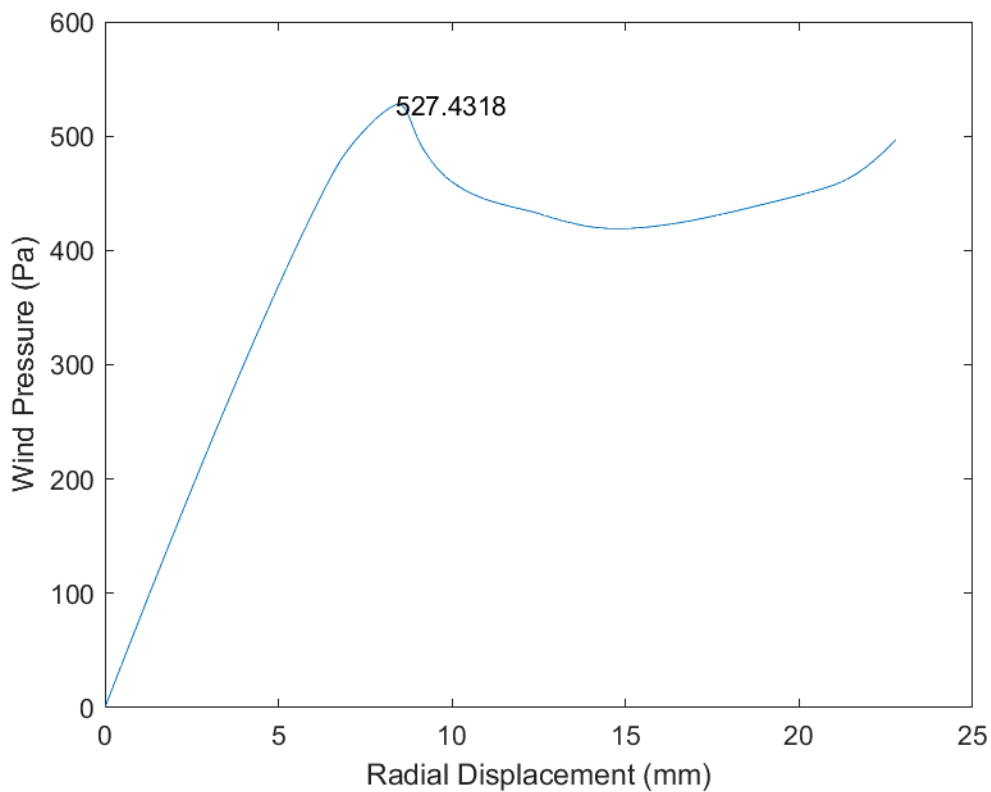


Fig. B.82 D54_H15_S36_R00_W00_V00_CL03_CD03_WT01_ST02

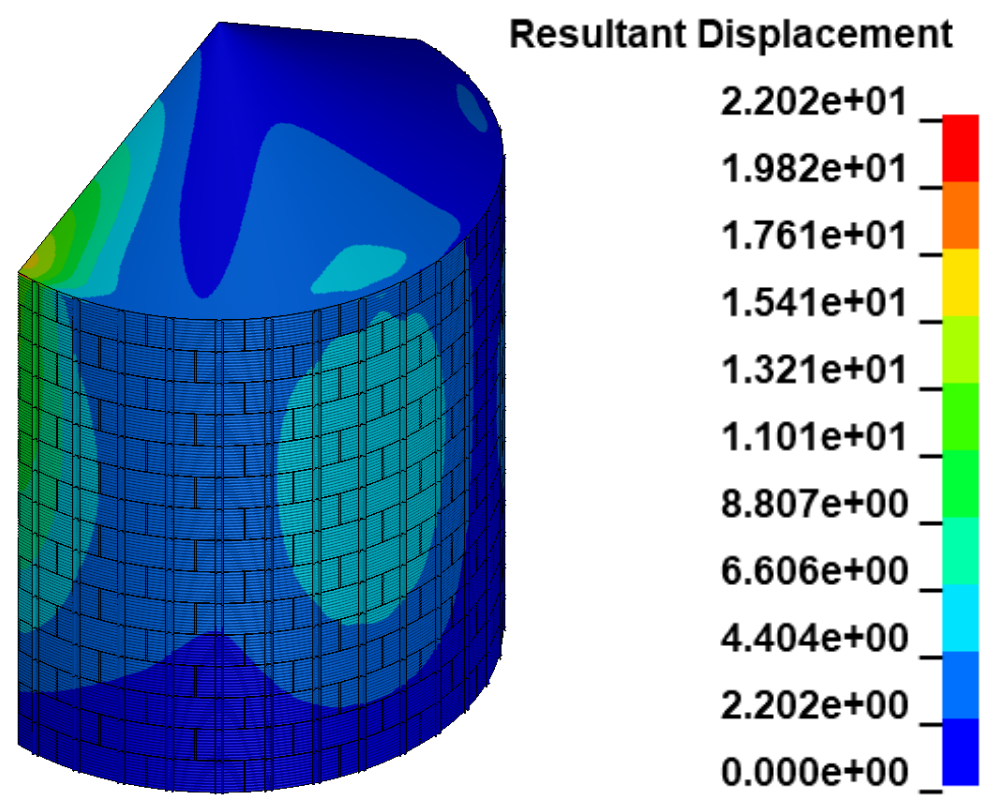
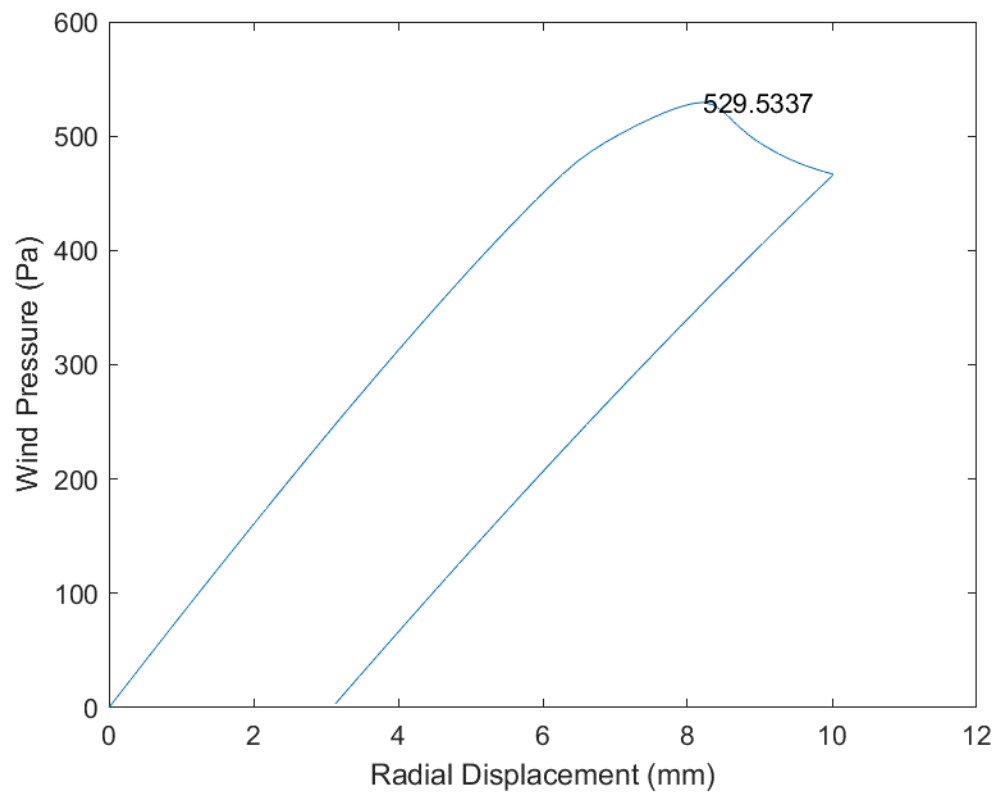


Fig. B.83 D54_H15_S36_R00_W00_V00_CL03_CD03_WT01_ST03

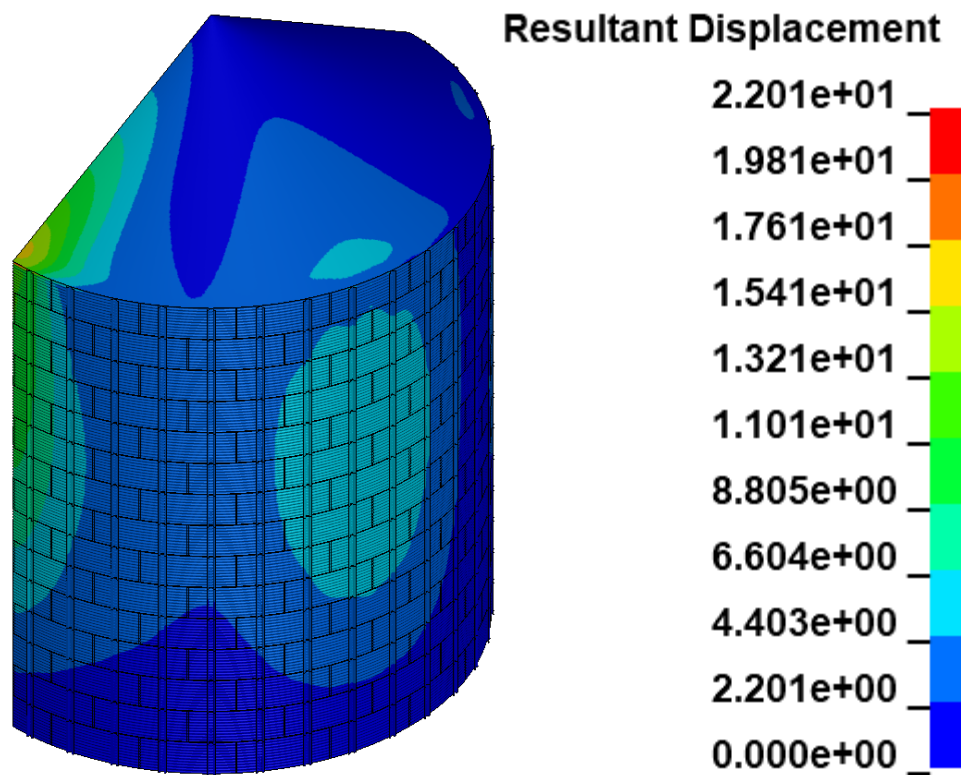
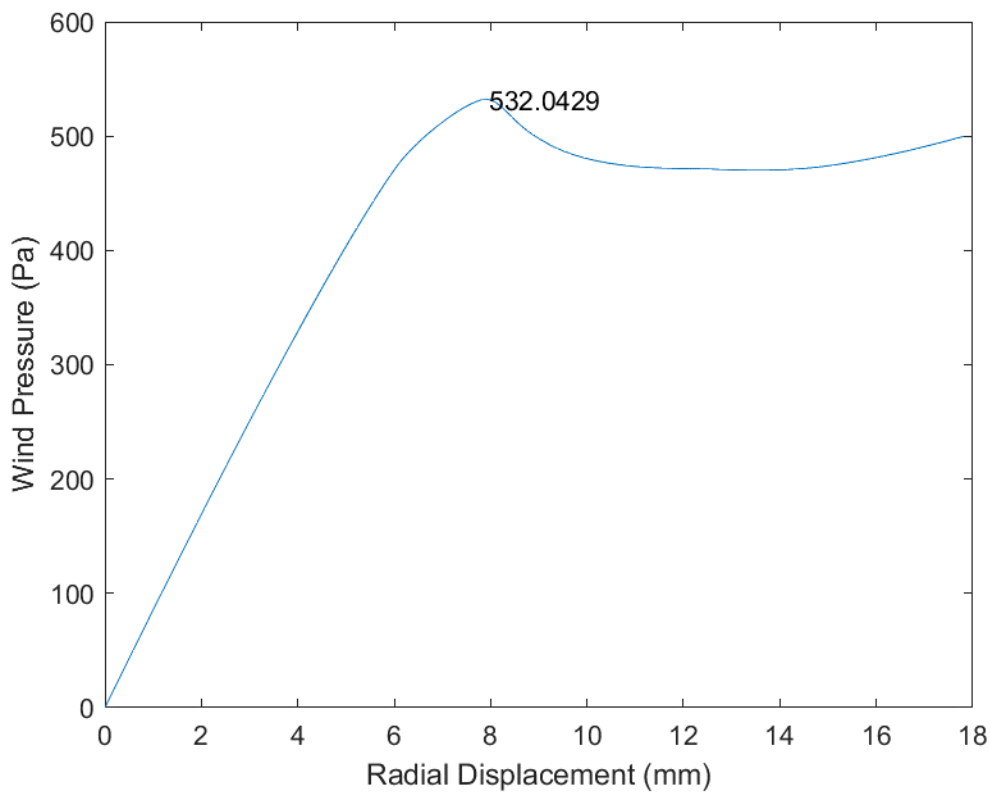


Fig. B.84 D54_H15_S36_R00_W00_V00_CL03_CD03_WT01_ST04

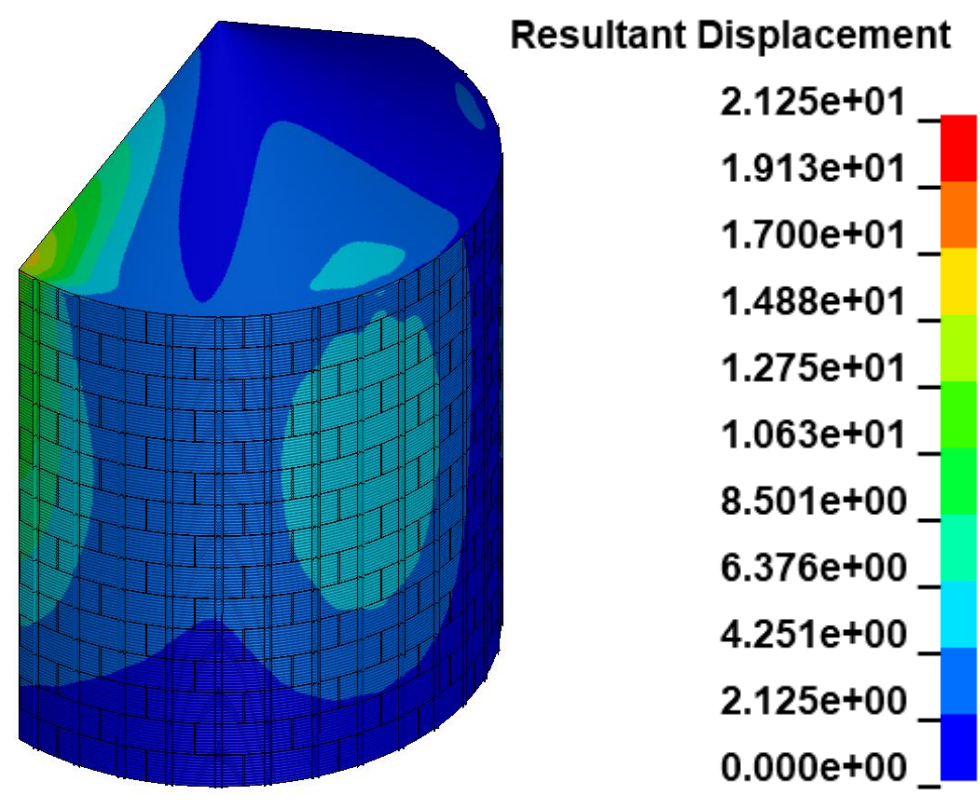
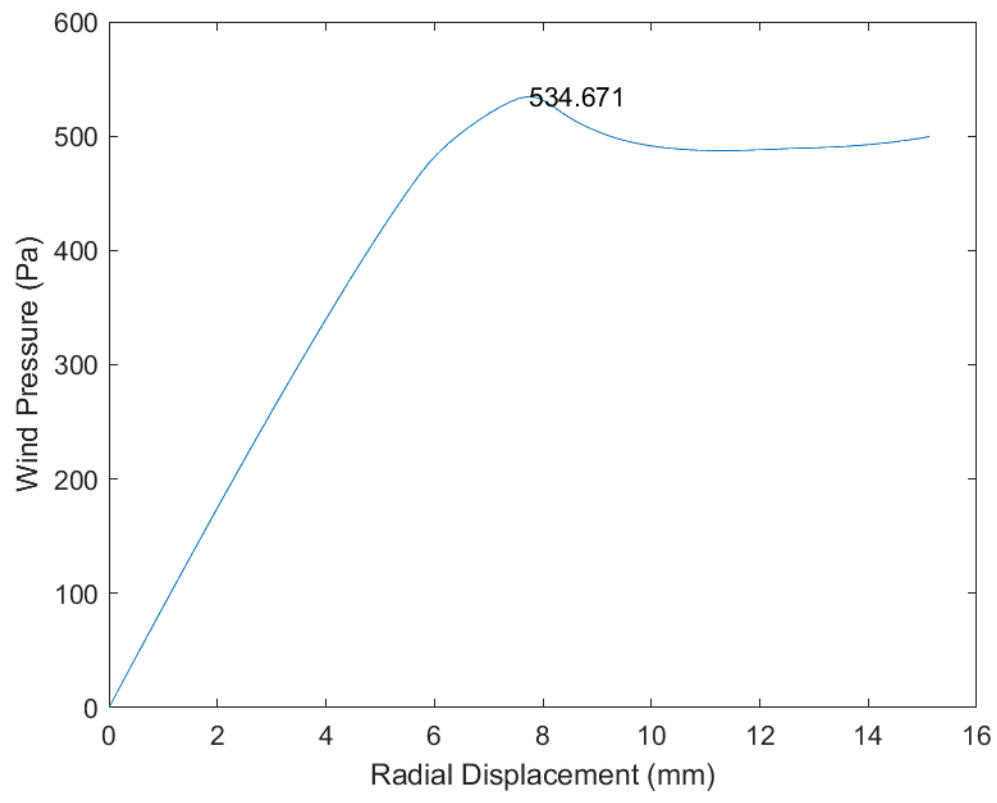


Fig. B.85 D54_H15_S36_R00_W00_V00_CL03_CD03_WT01_ST05

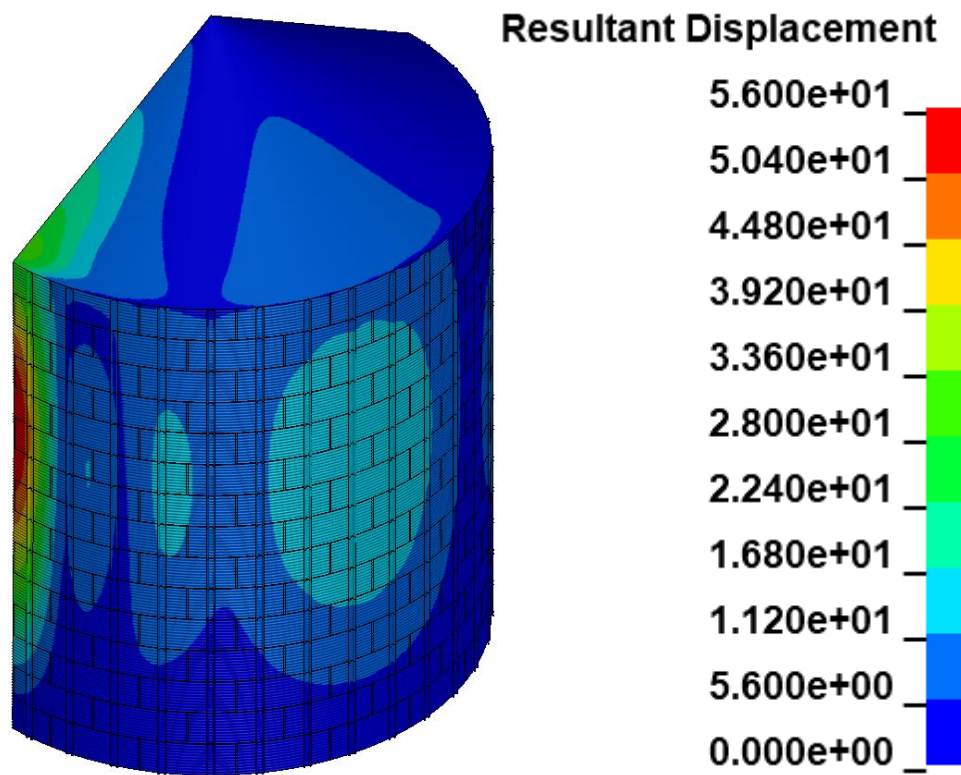
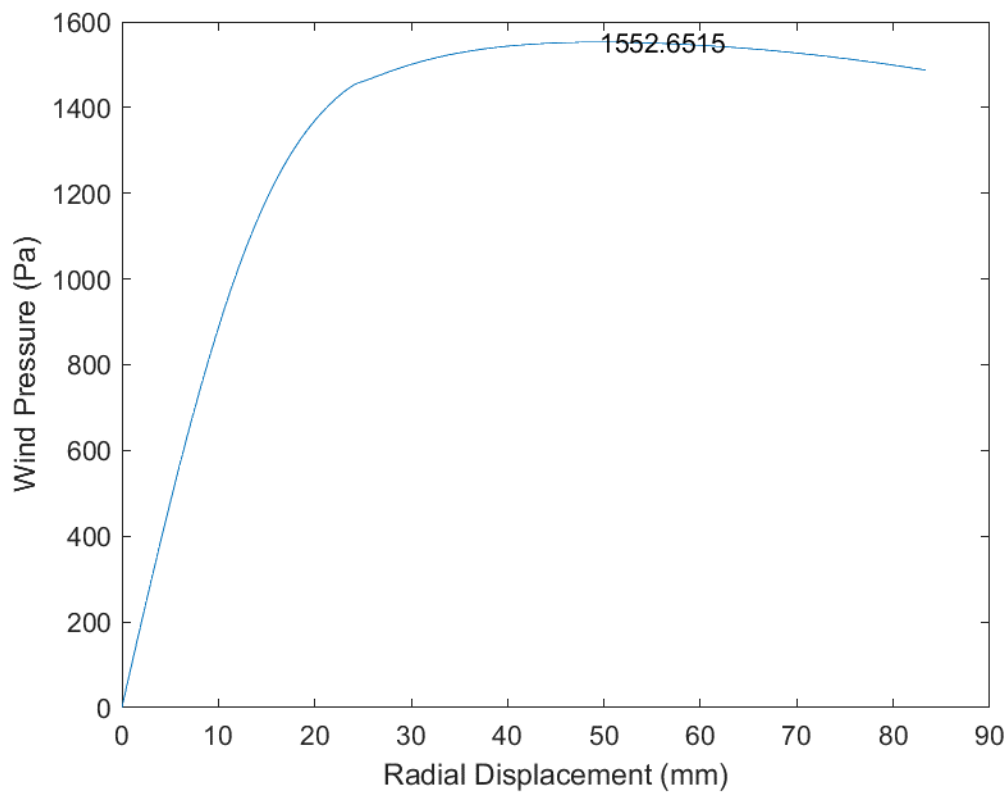


Fig. B.86 D54_H15_S36_R00_W00_V00_CL03_CD03_WT02_ST01

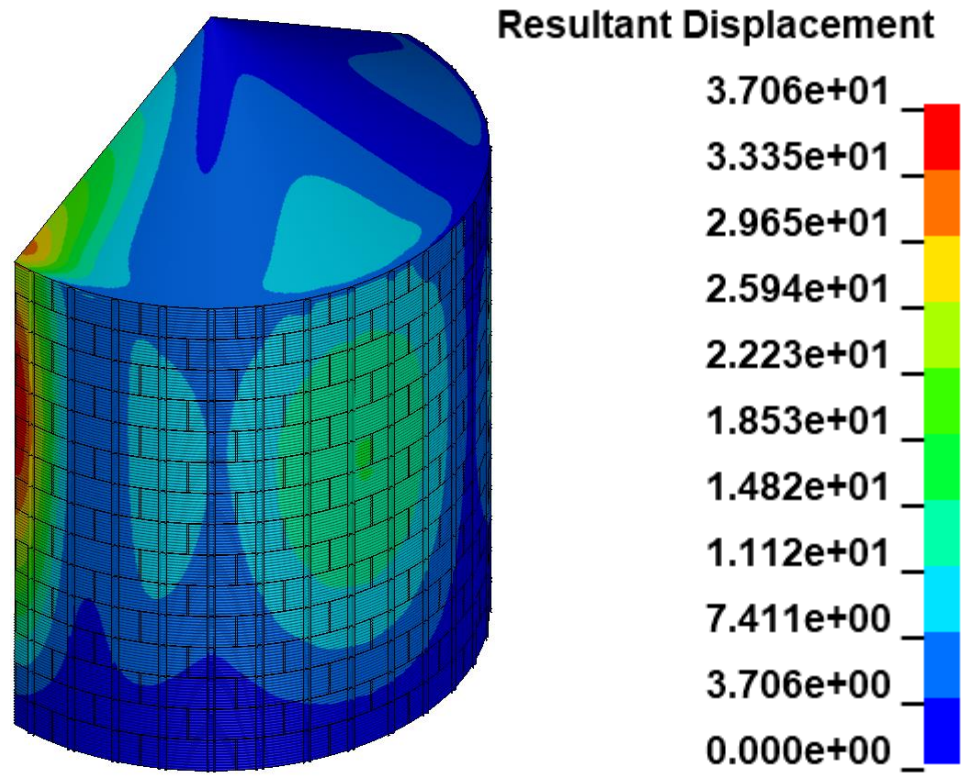
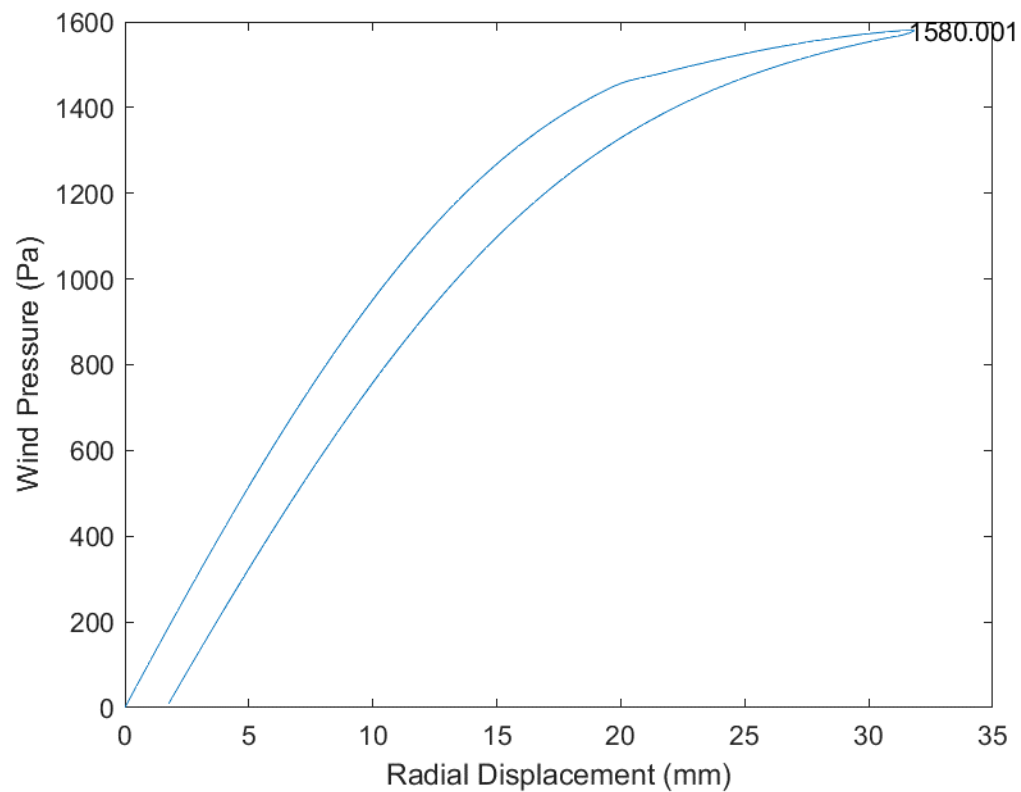


Fig. B.87 D54_H15_S36_R00_W00_V00_CL03_CD03_WT02_ST02

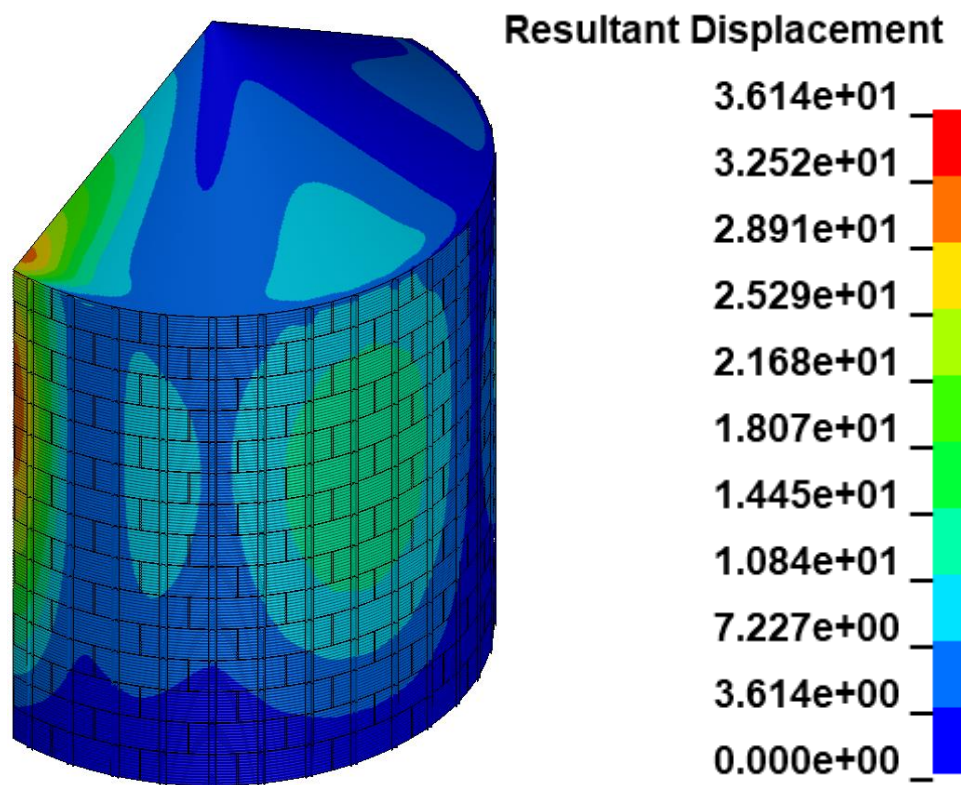
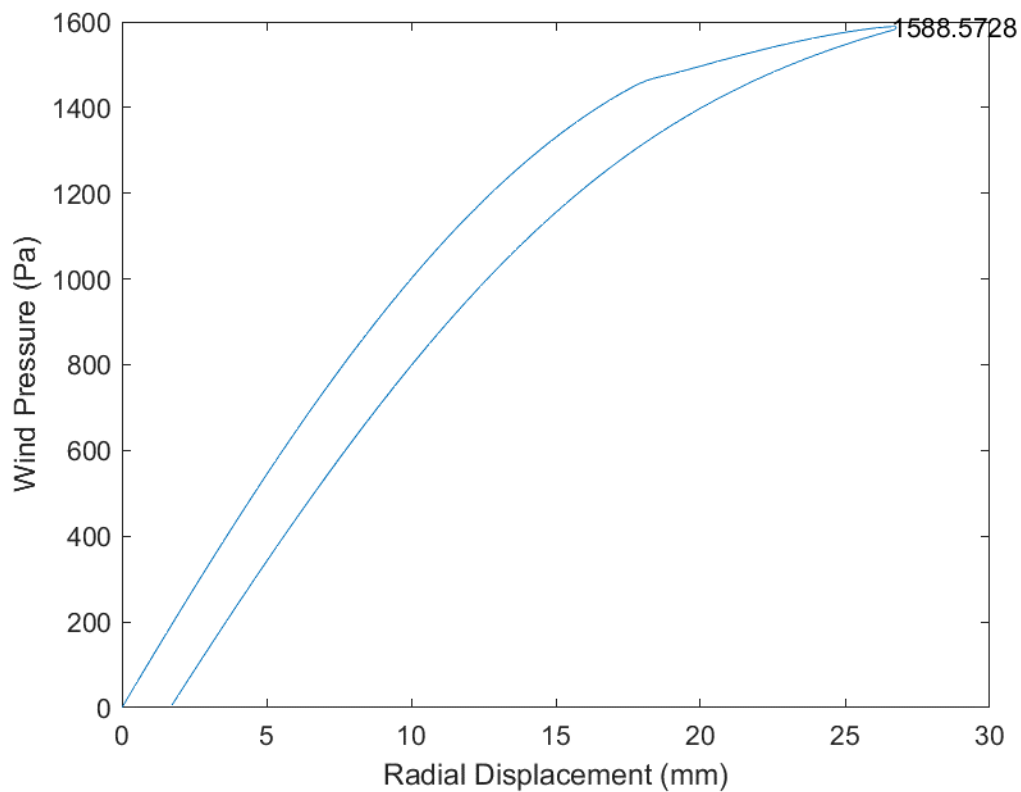


Fig. B.88 D54_H15_S36_R00_W00_V00_CL03_CD03_WT02_ST03

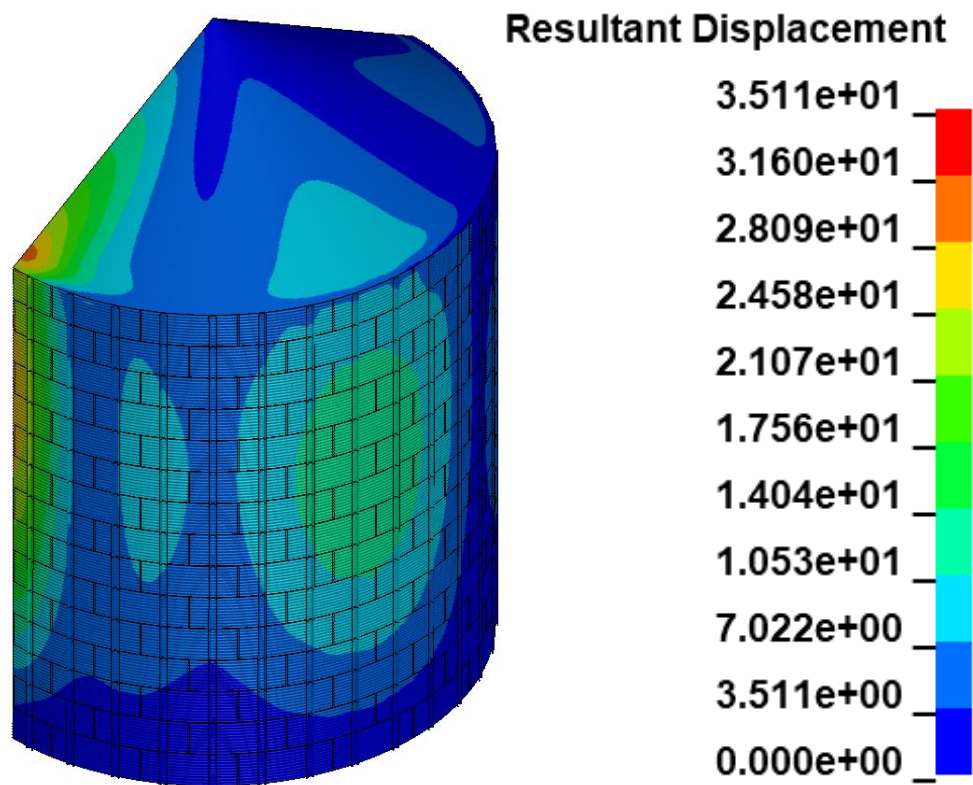
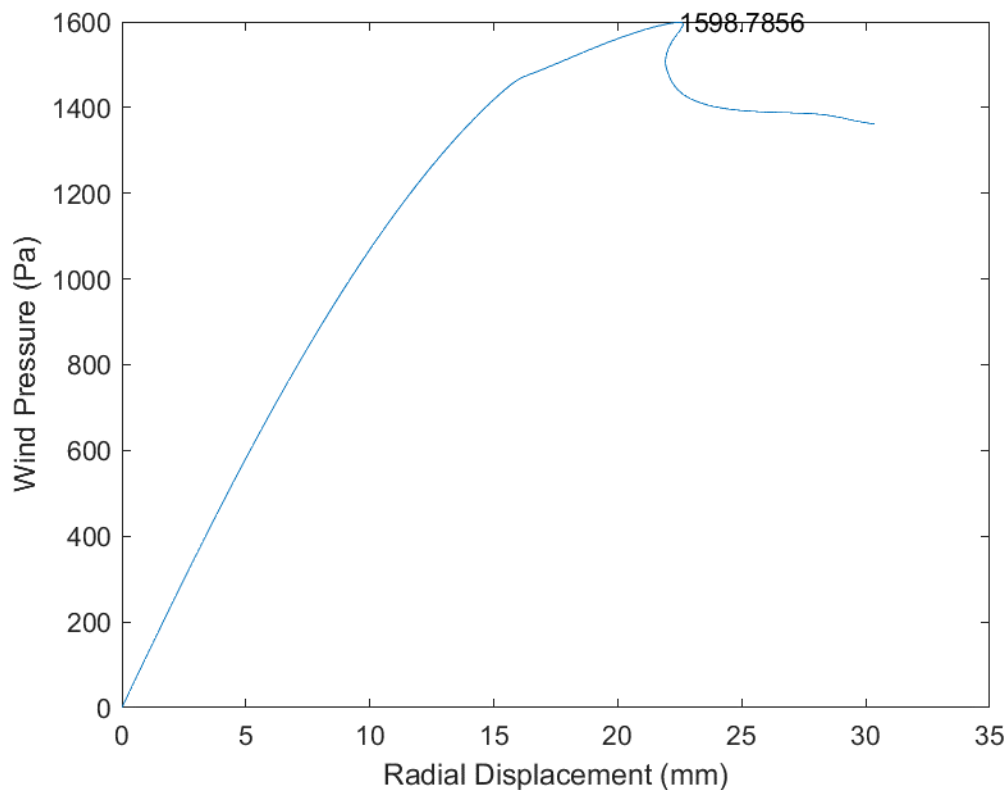


Fig. B.89 D54_H15_S36_R00_W00_V00_CL03_CD03_WT02_ST04

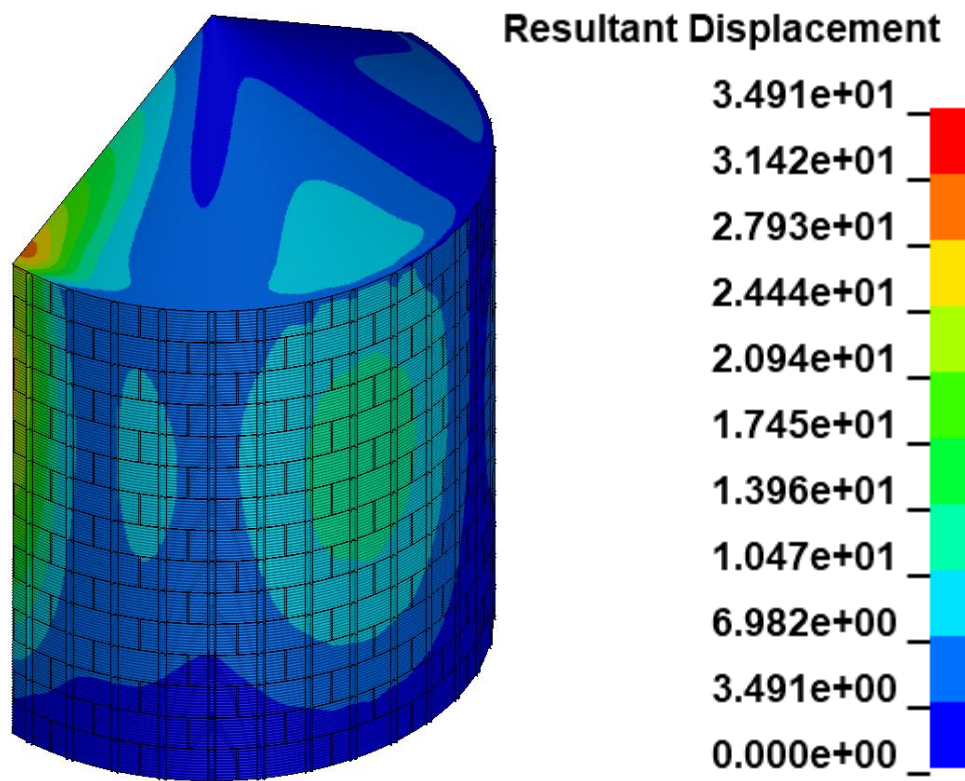
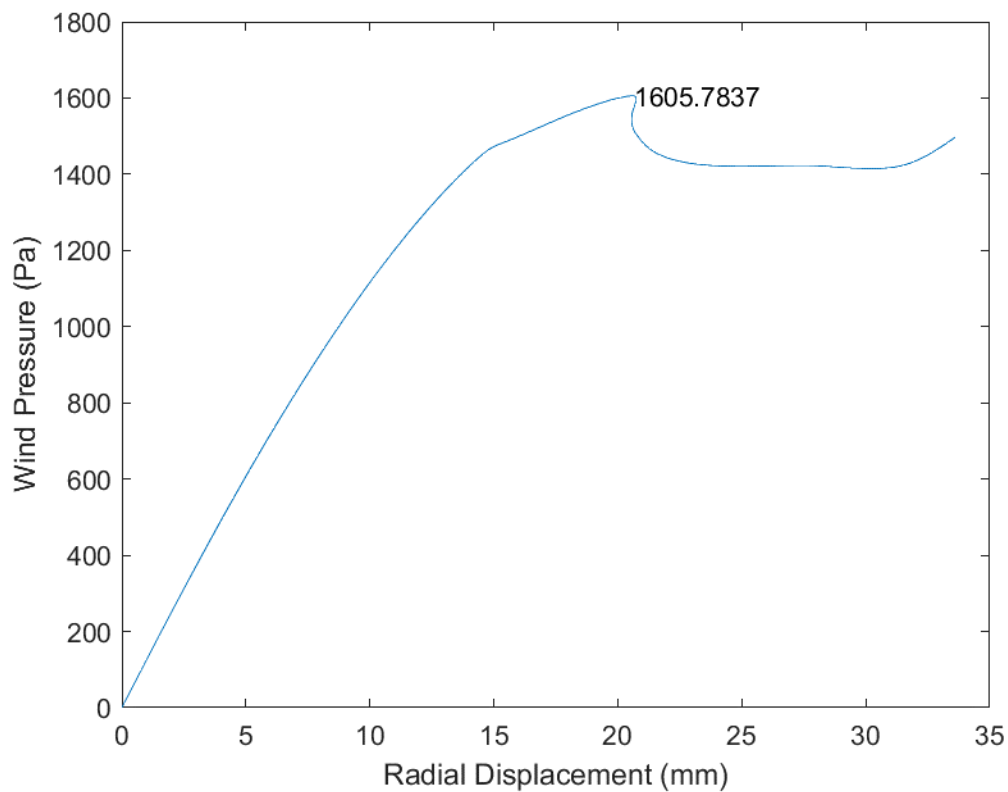


Fig. B.90 D54_H15_S36_R00_W00_V00_CL03_CD03_WT02_ST05

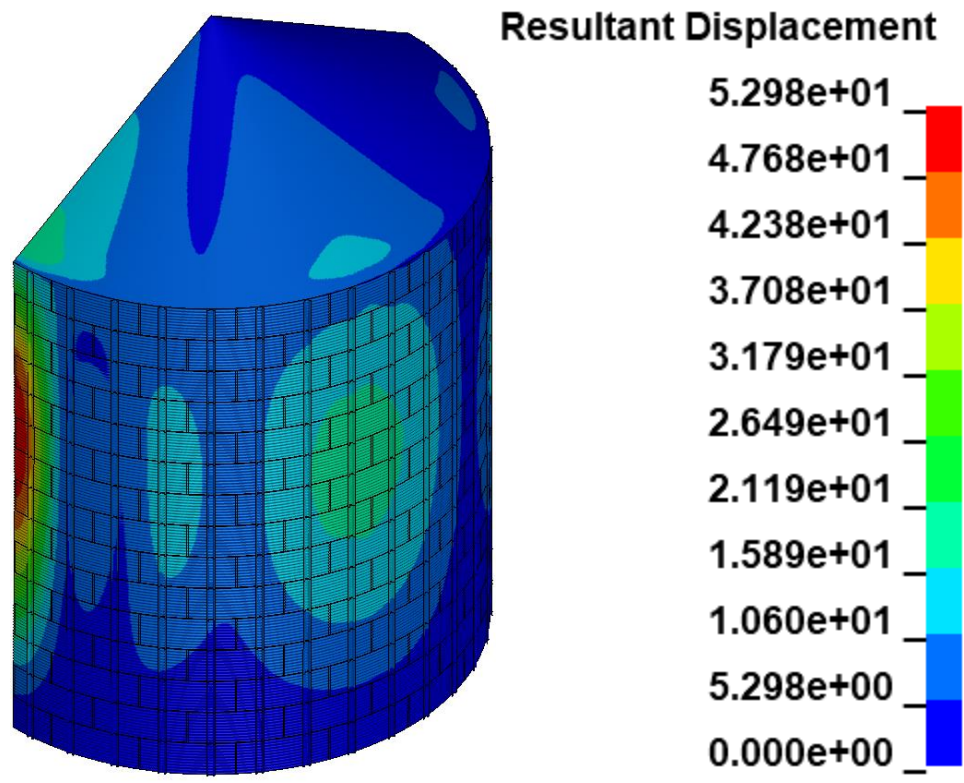
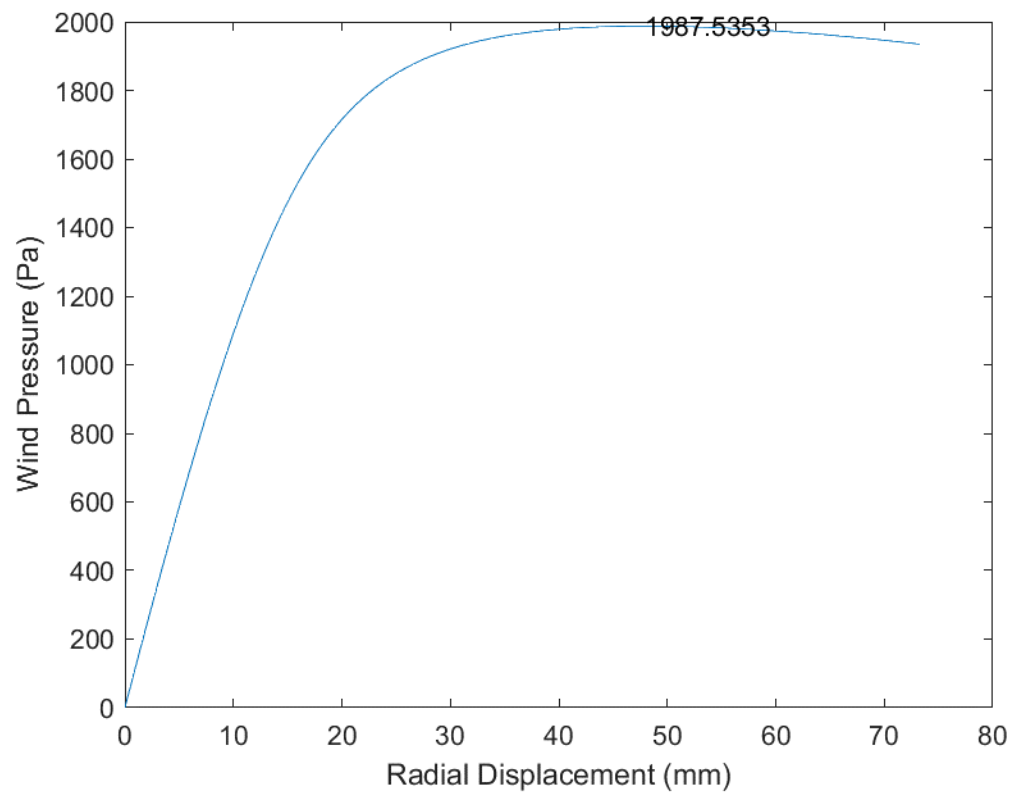


Fig. B.91 D54_H15_S36_R00_W00_V00_CL03_CD03_WT03_ST01

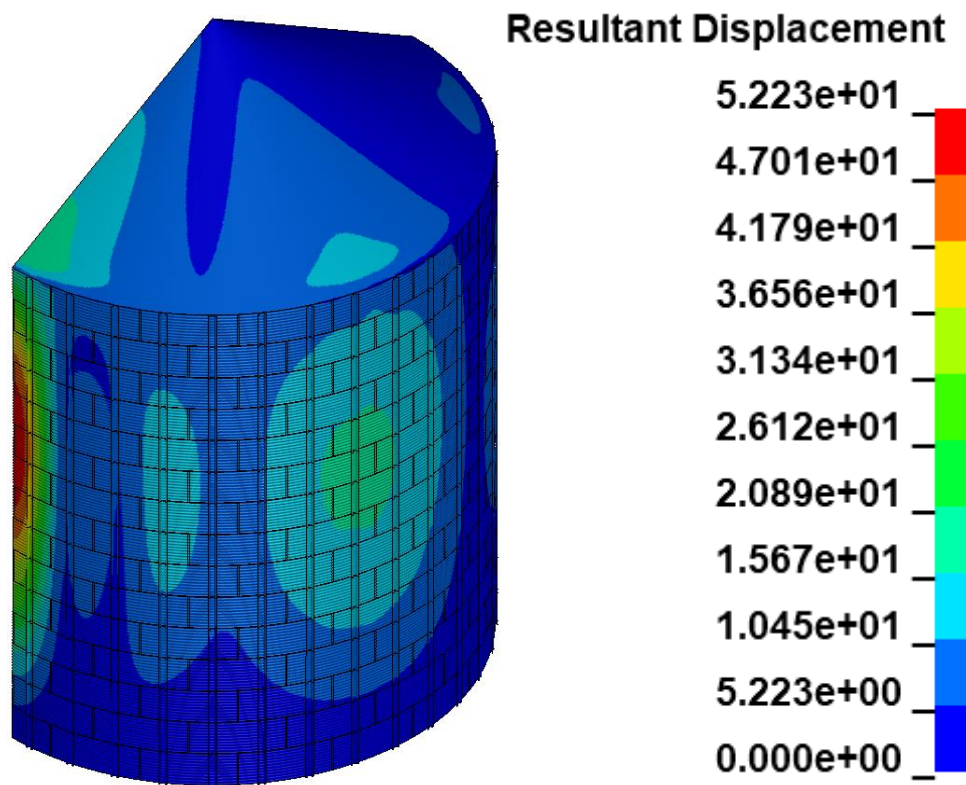
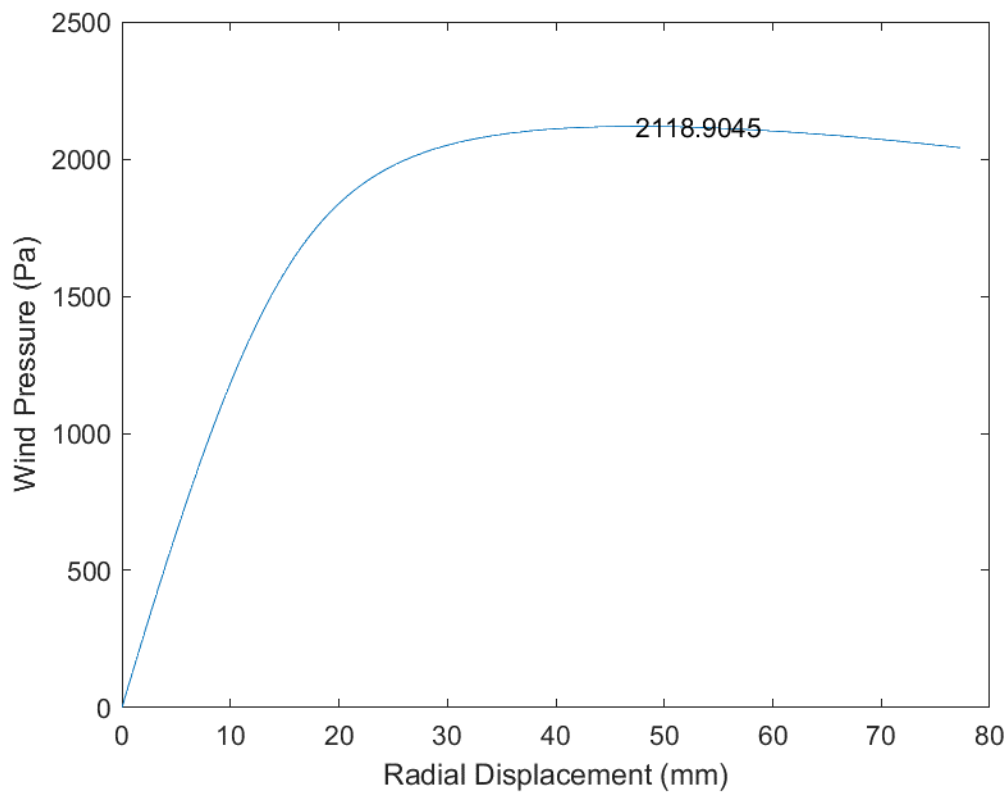


Fig. B.92 D54_H15_S36_R00_W00_V00_CL03_CD03_WT03_ST02

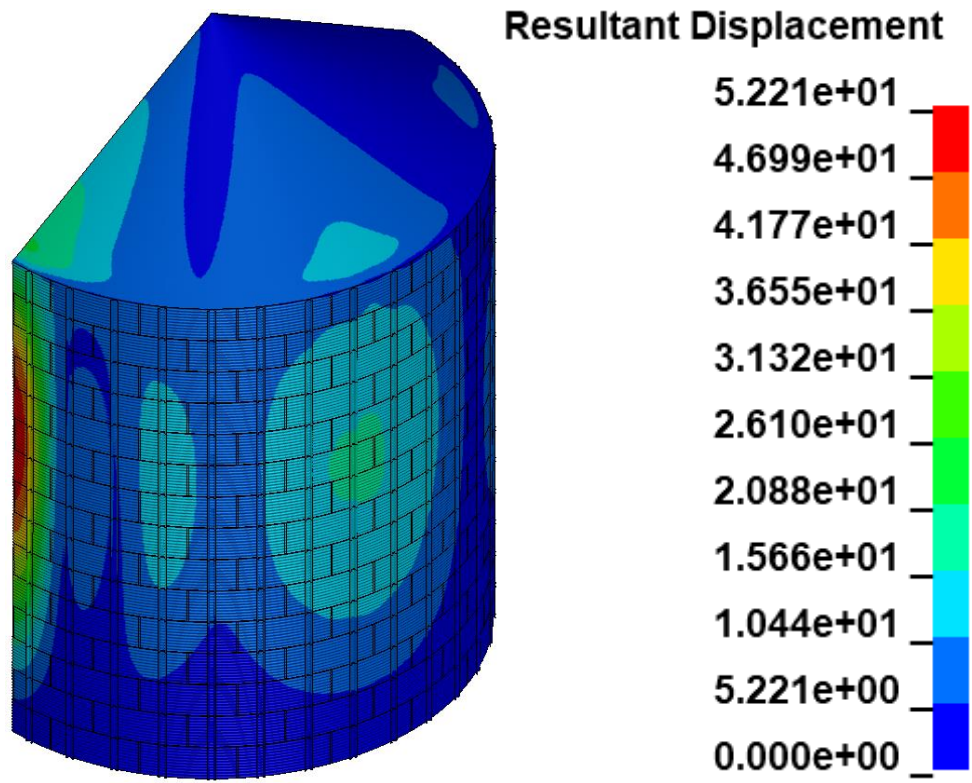
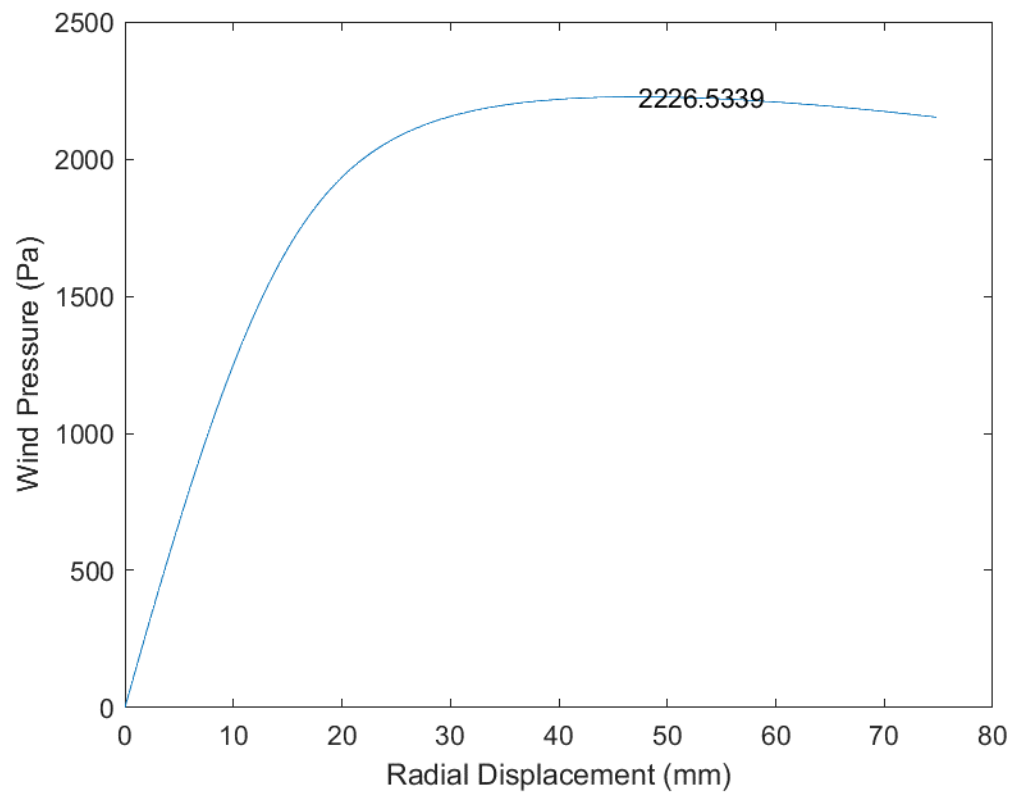


Fig. B.93 D54_H15_S36_R00_W00_V00_CL03_CD03_WT03_ST03

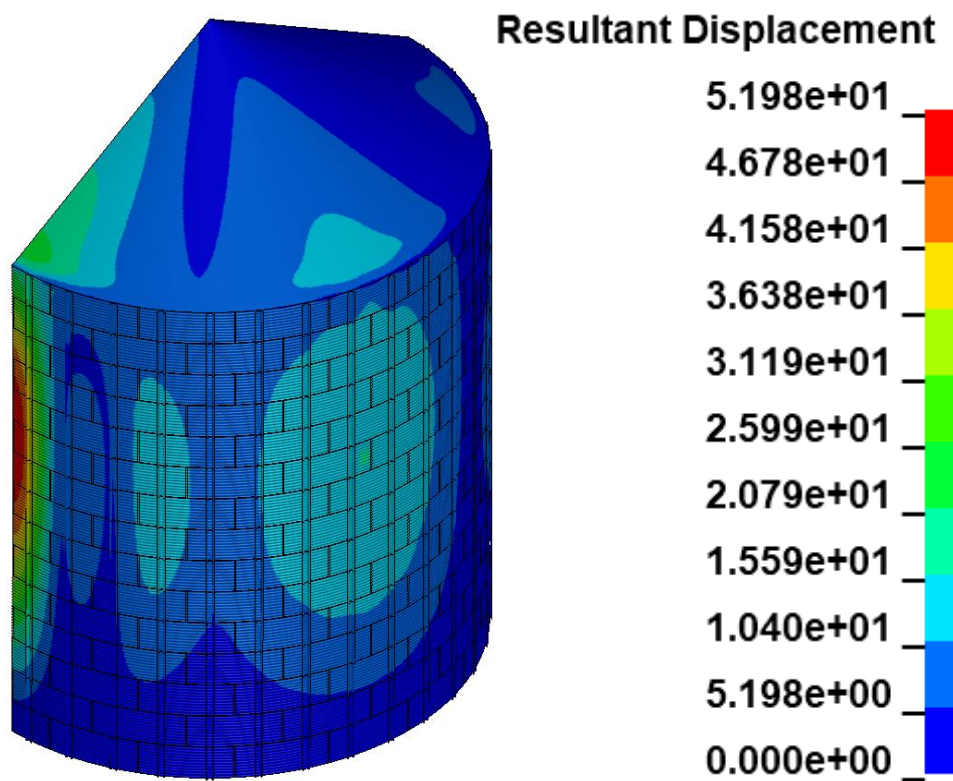
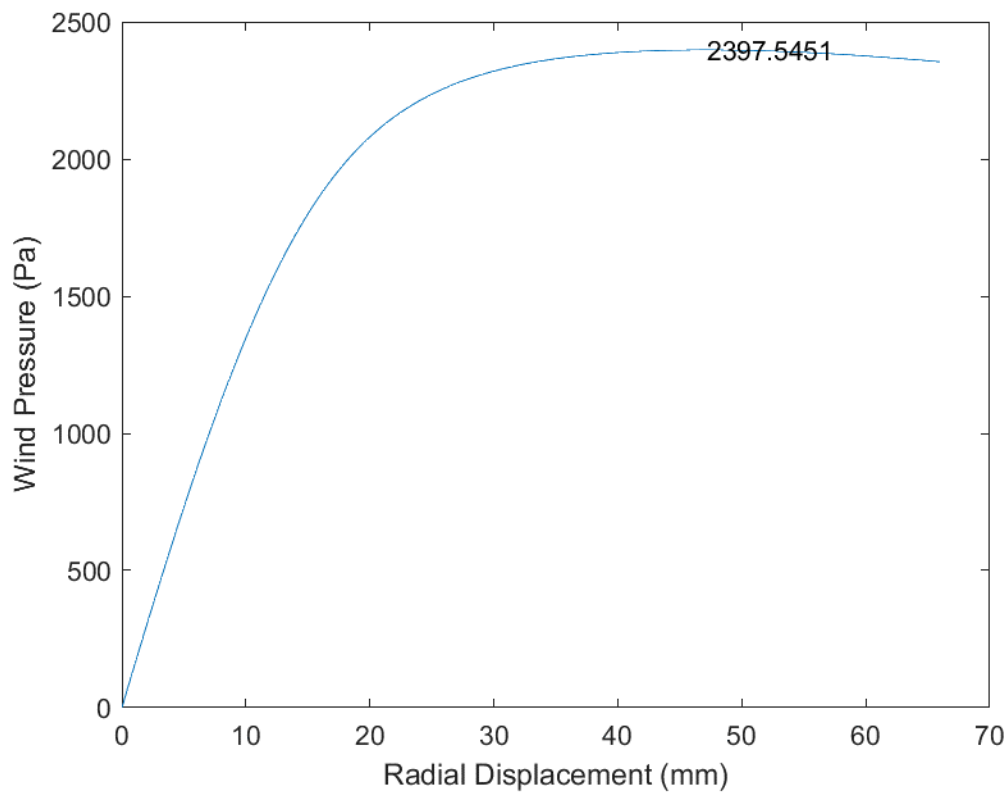


Fig. B.94 D54_H15_S36_R00_W00_V00_CL03_CD03_WT03_ST04

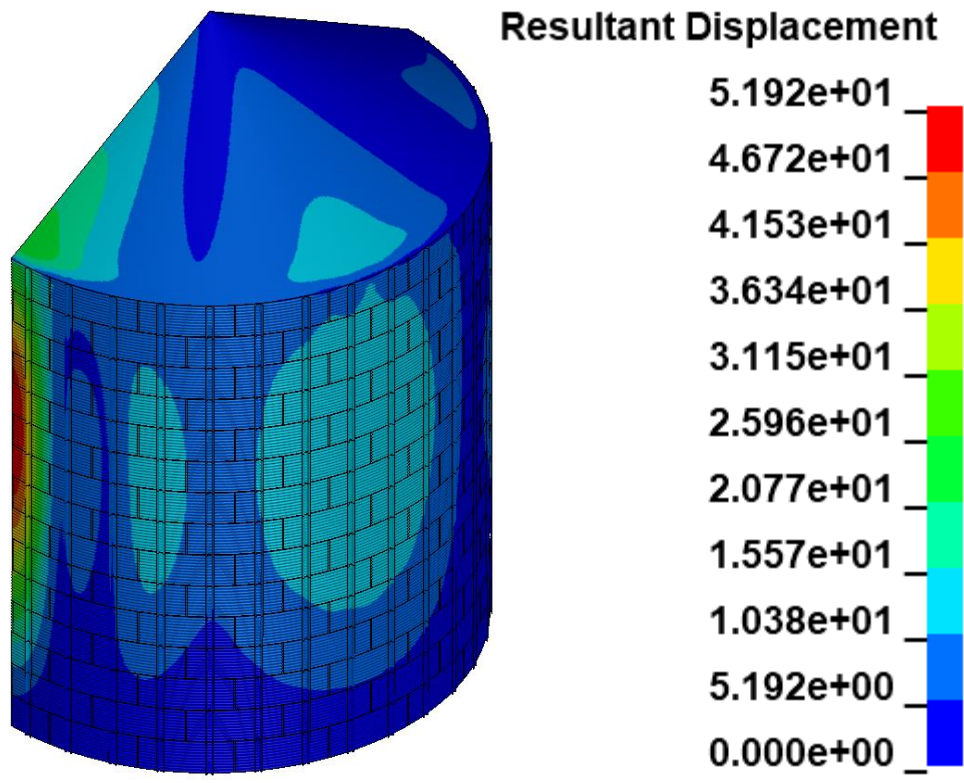
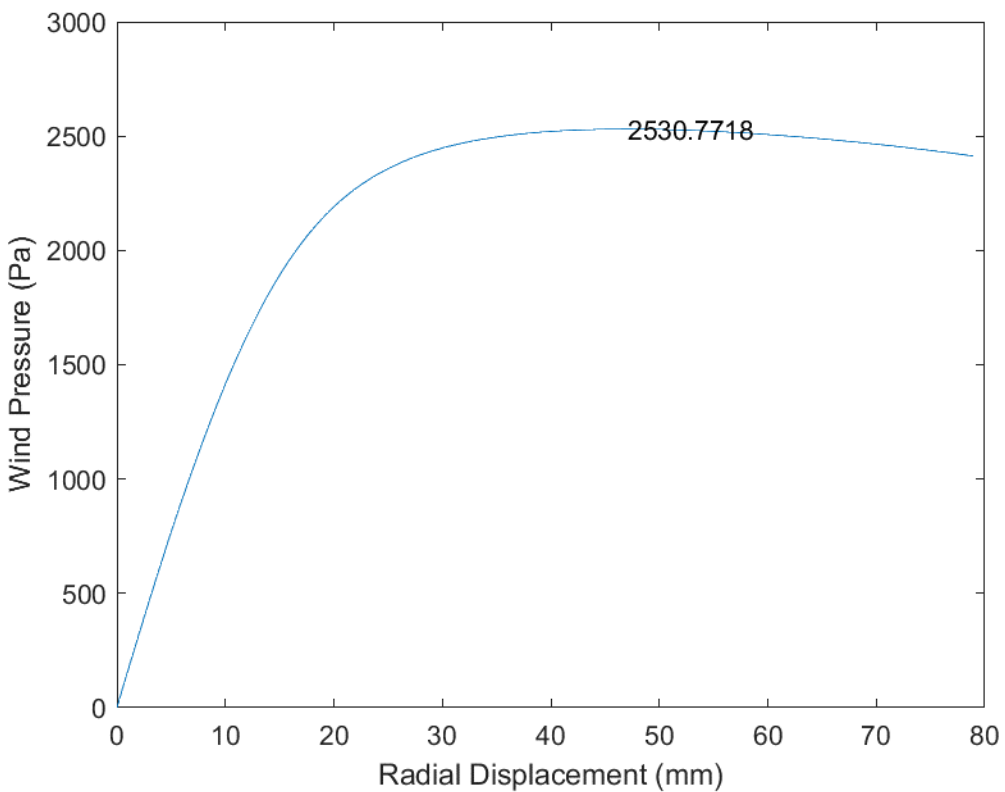


Fig. B.95 D54_H15_S36_R00_W00_V00_CL03_CD03_WT03_ST05

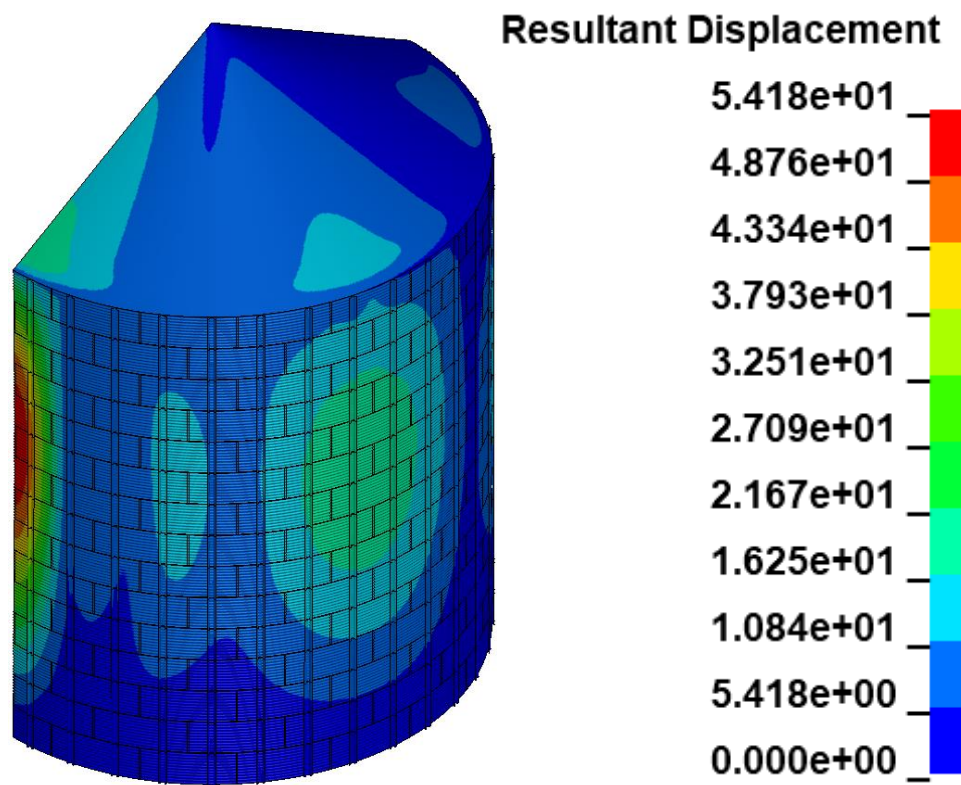
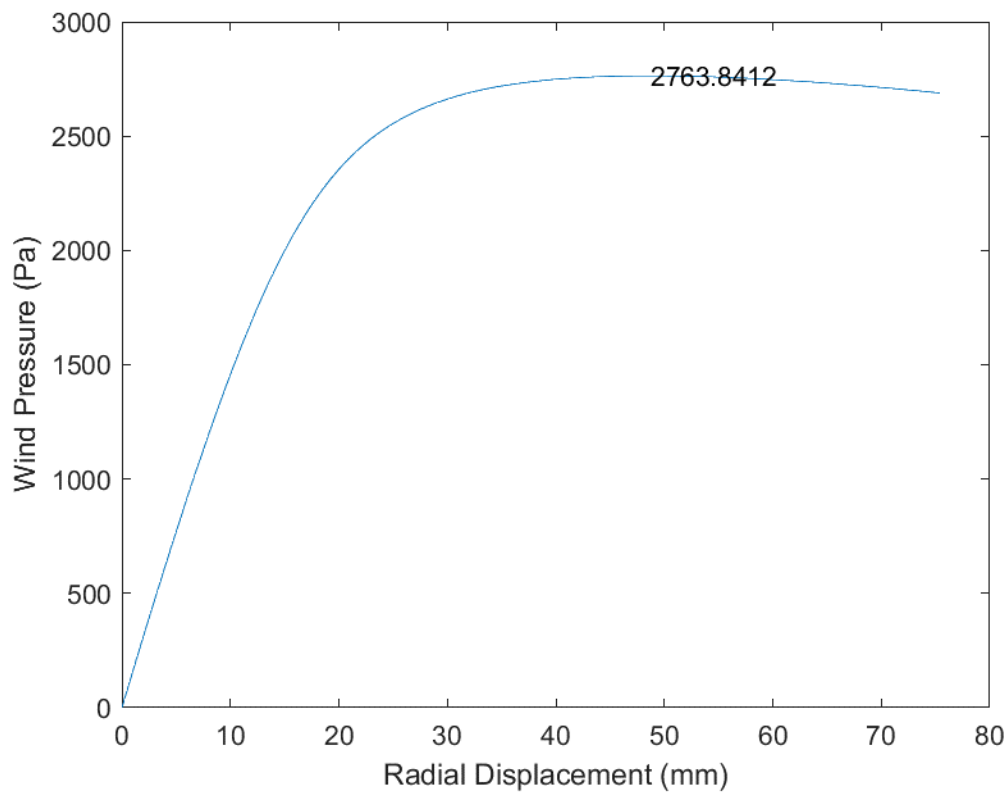


Fig. B.96 D54_H15_S36_R00_W00_V00_CL03_CD03_WT04_ST01

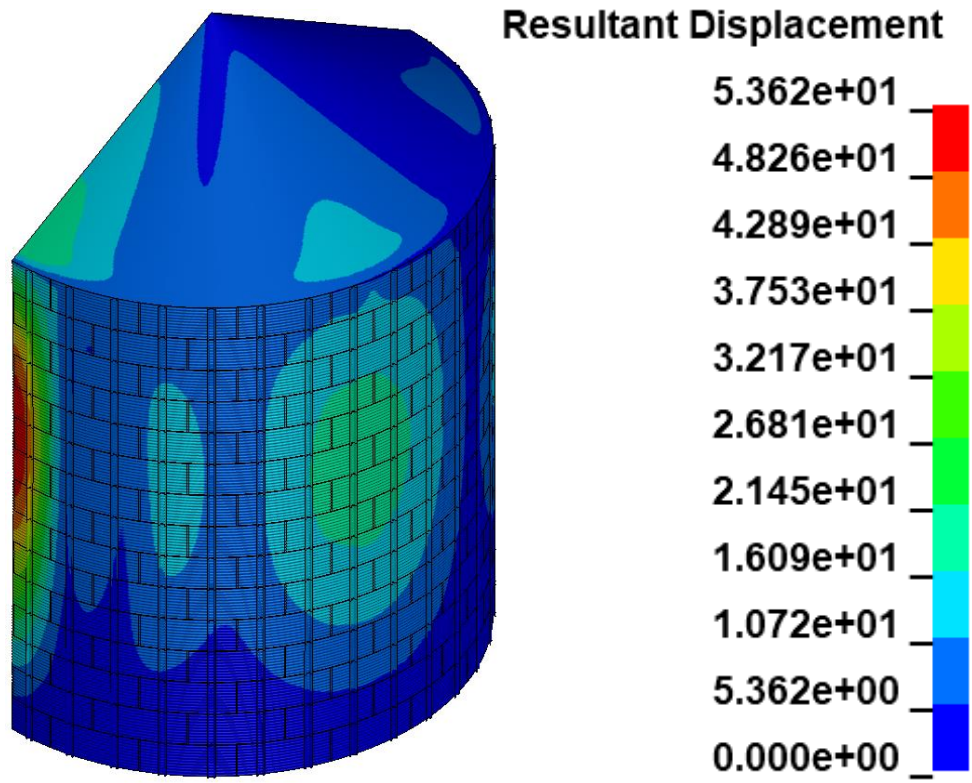
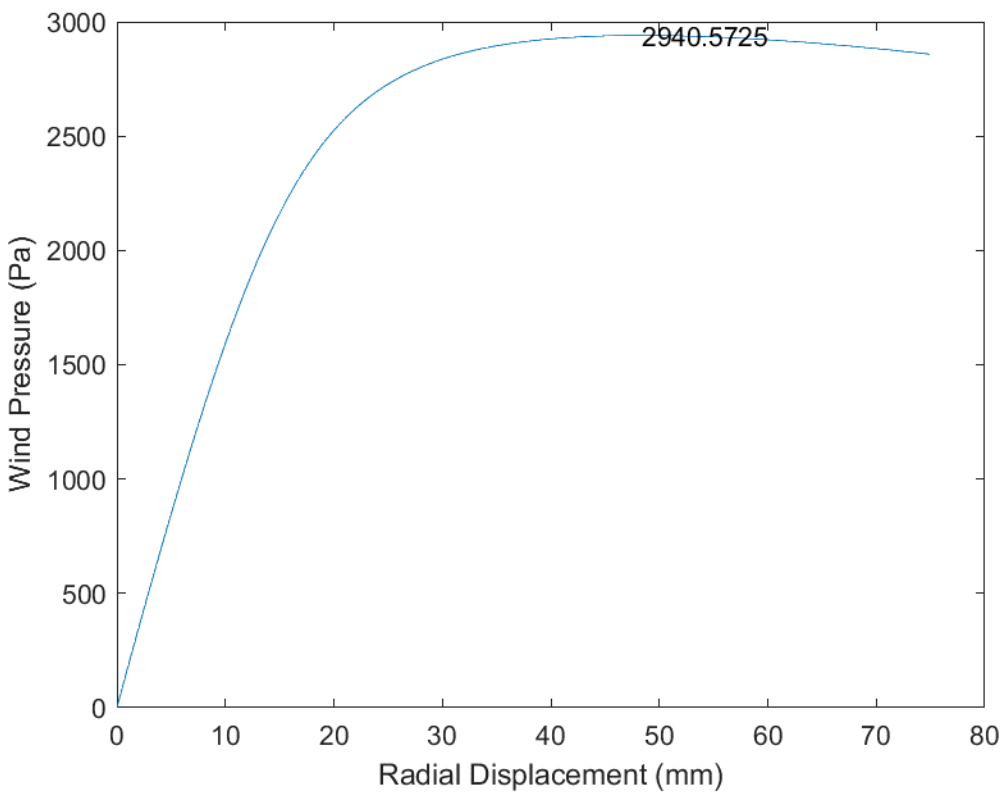


Fig. B.97 D54_H15_S36_R00_W00_V00_CL03_CD03_WT04_ST02

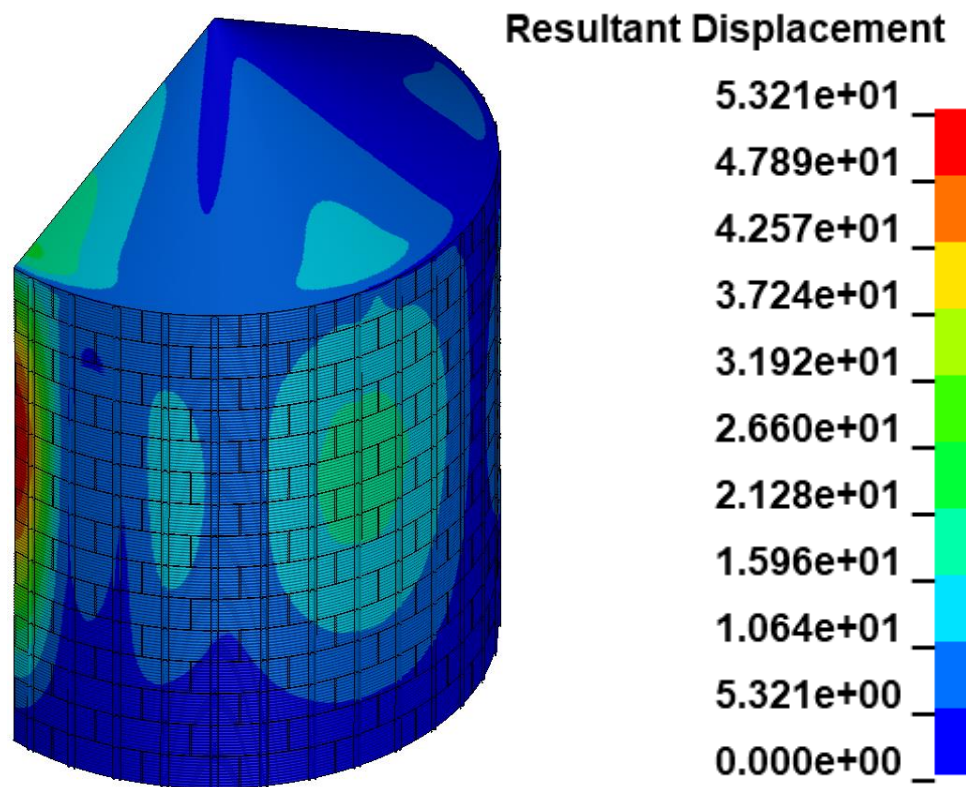
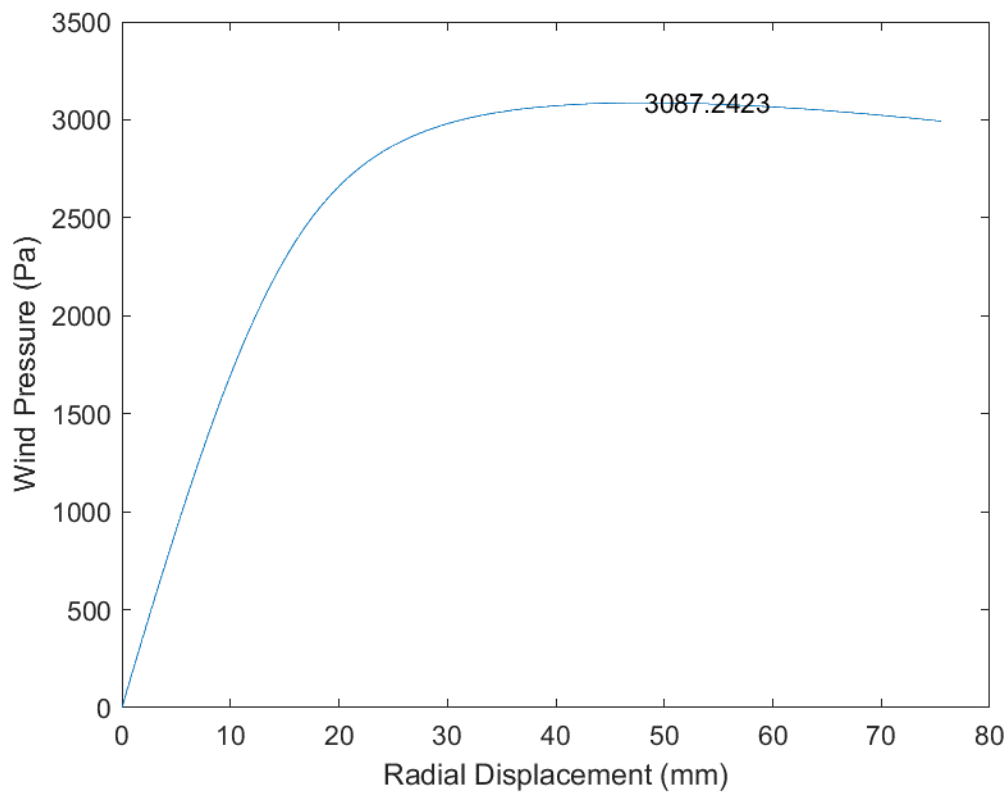


Fig. B.98 D54_H15_S36_R00_W00_V00_CL03_CD03_WT04_ST03

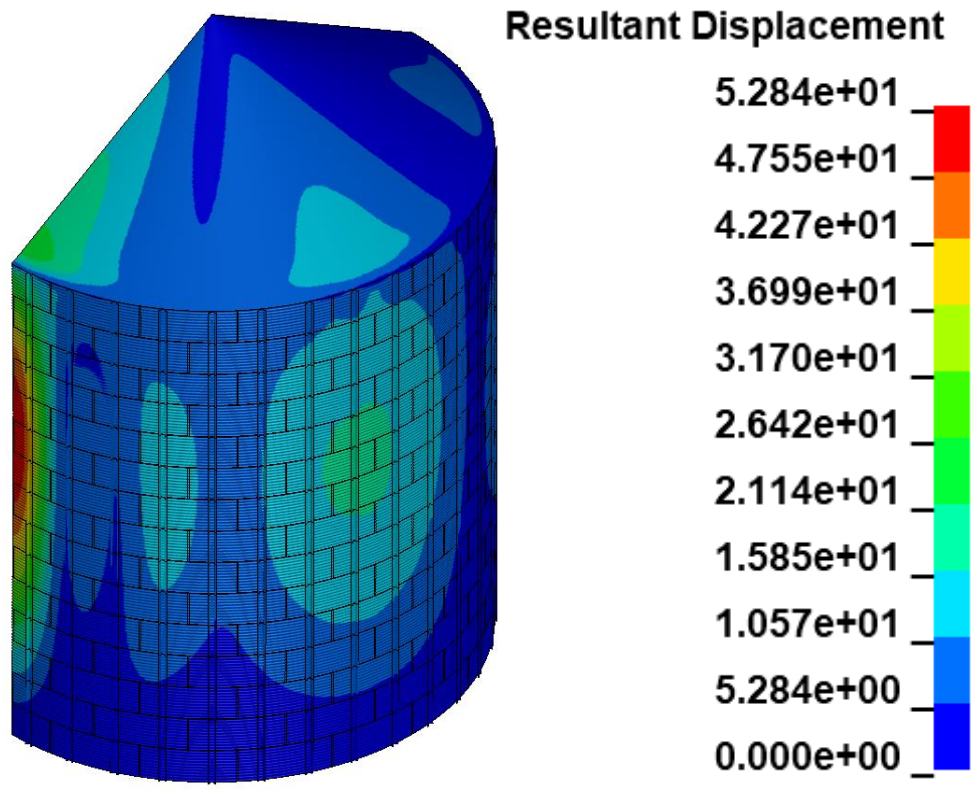
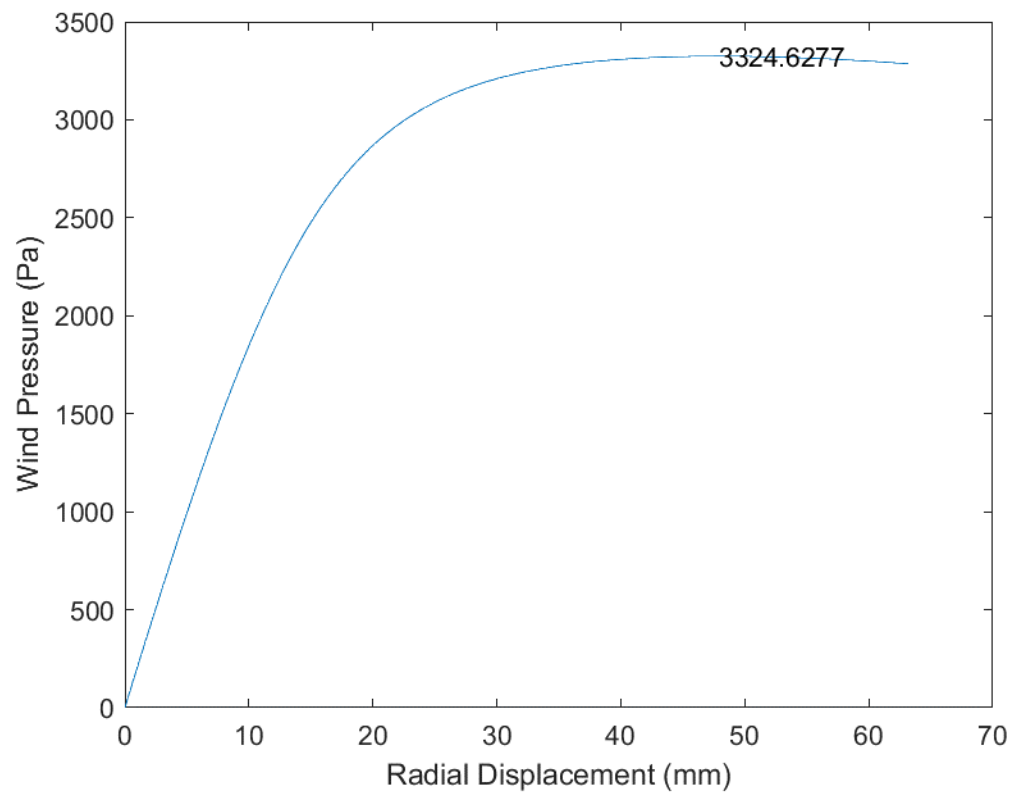


Fig. B.99 D54_H15_S36_R00_W00_V00_CL03_CD03_WT04_ST04

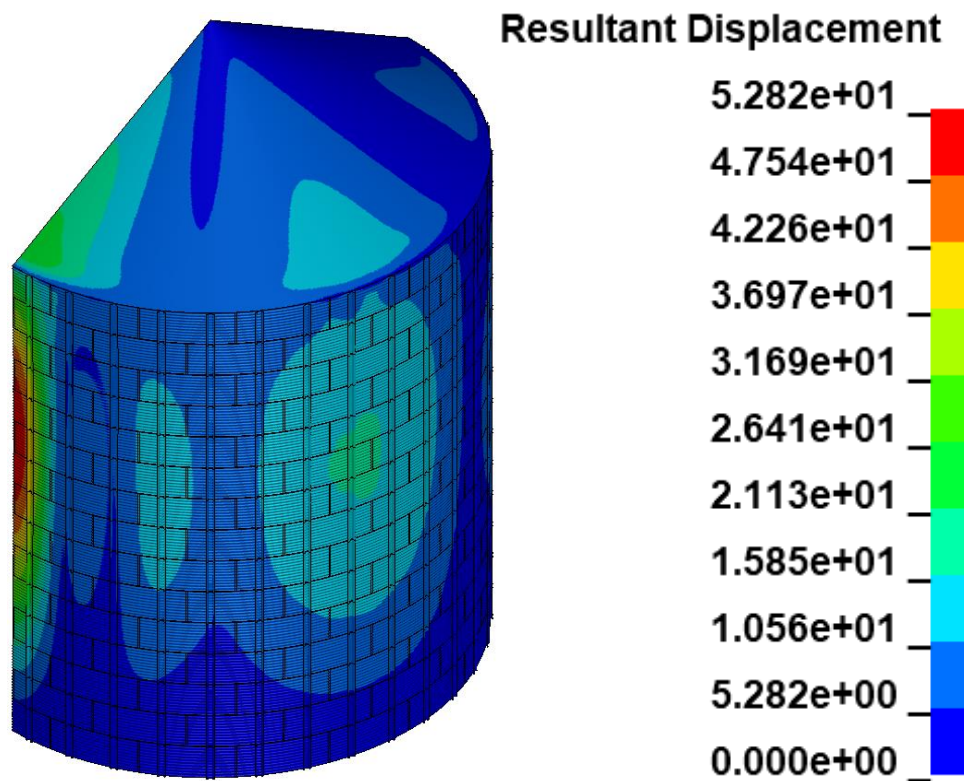
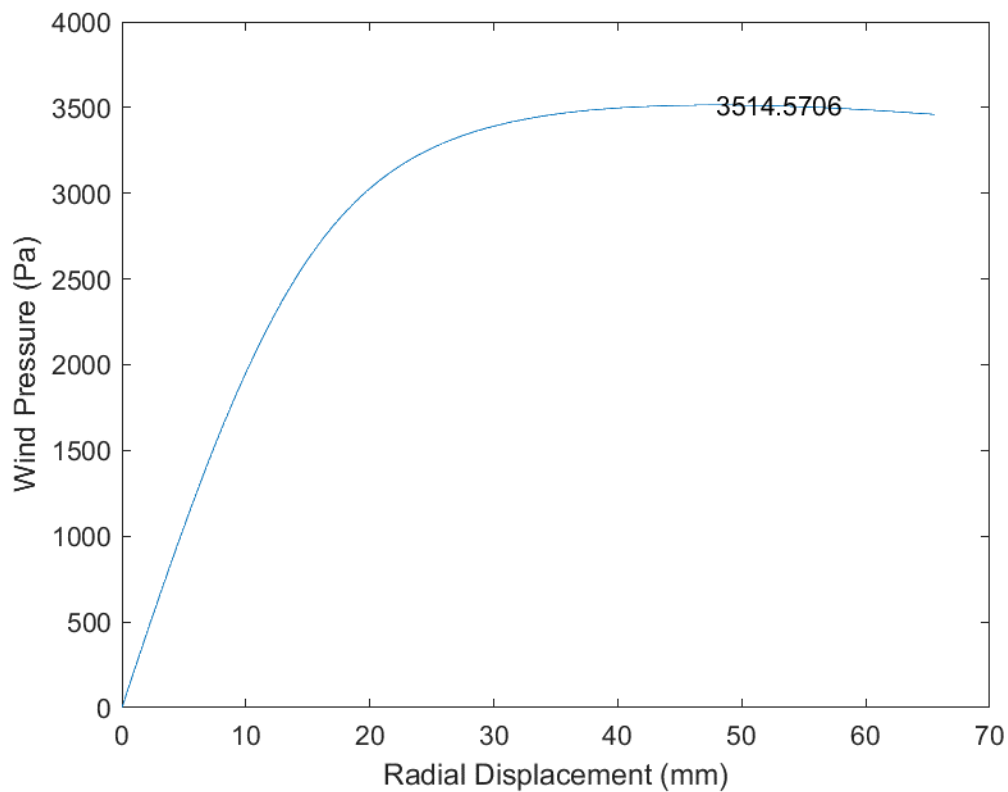


Fig. B.100 D54_H15_S36_R00_W00_V00_CL03_CD03_WT04_ST05

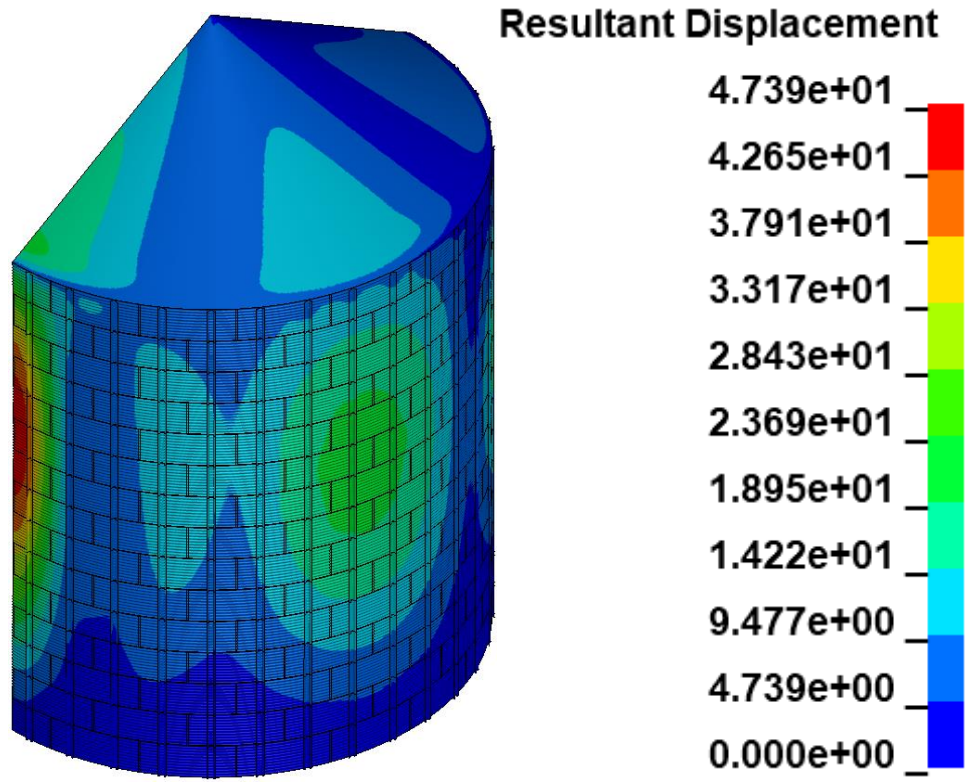
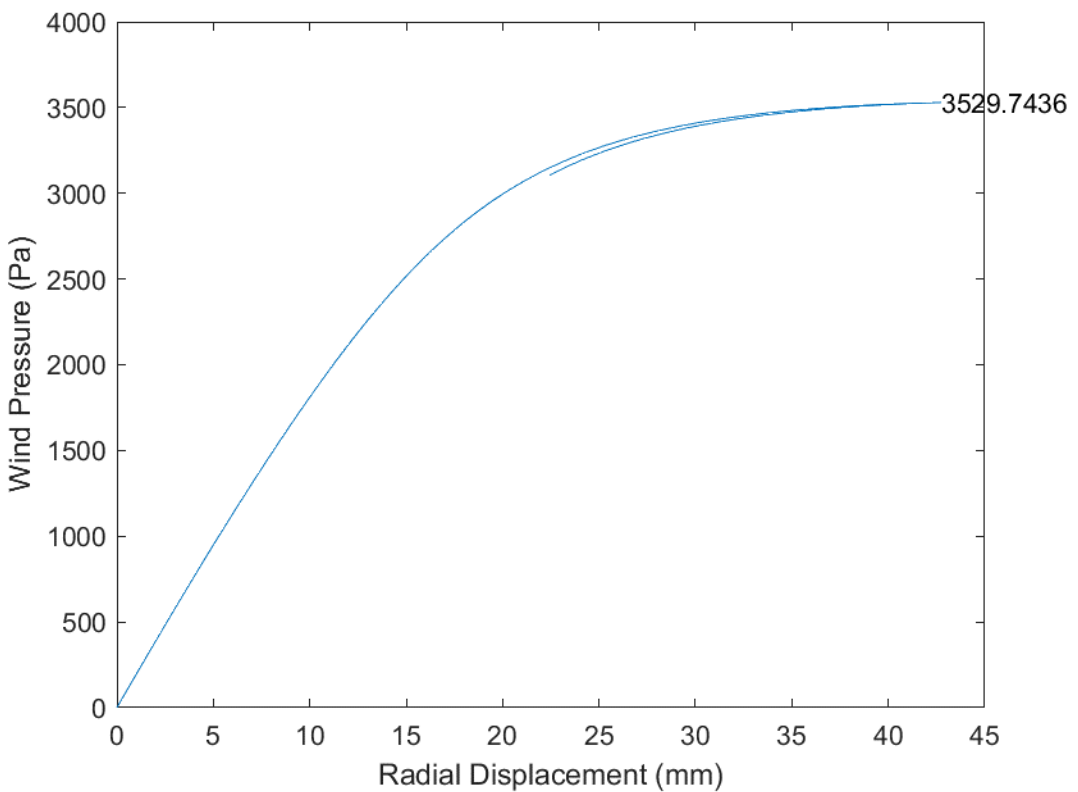


Fig. B.101 D54_H15_S36_R00_W00_V00_CL03_CD03_WT05_ST01

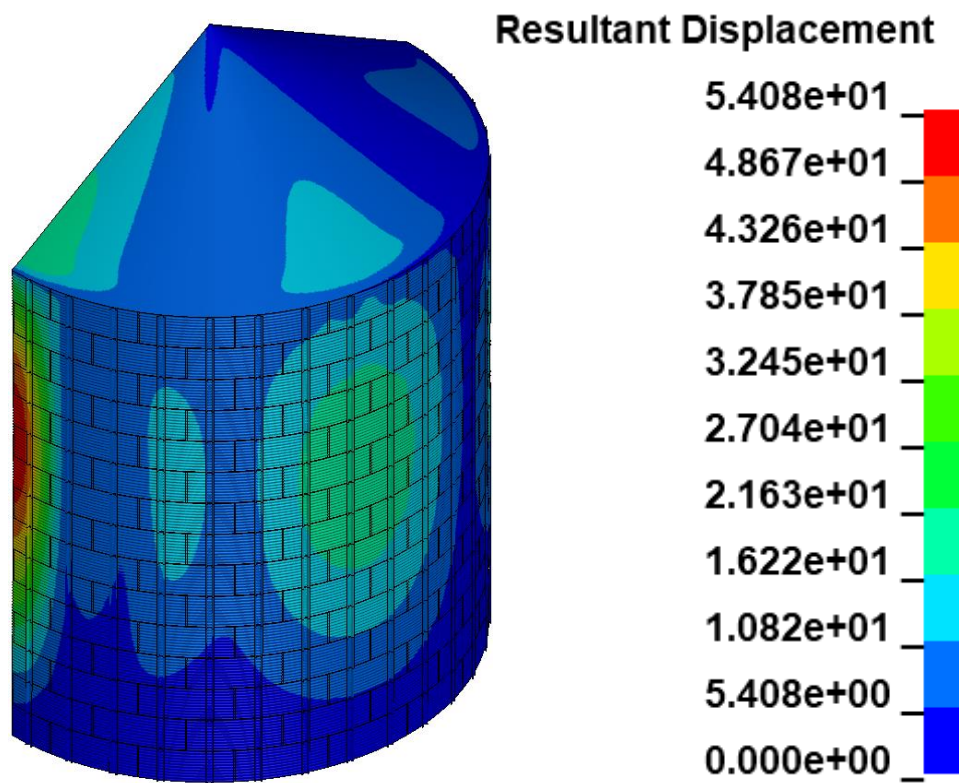
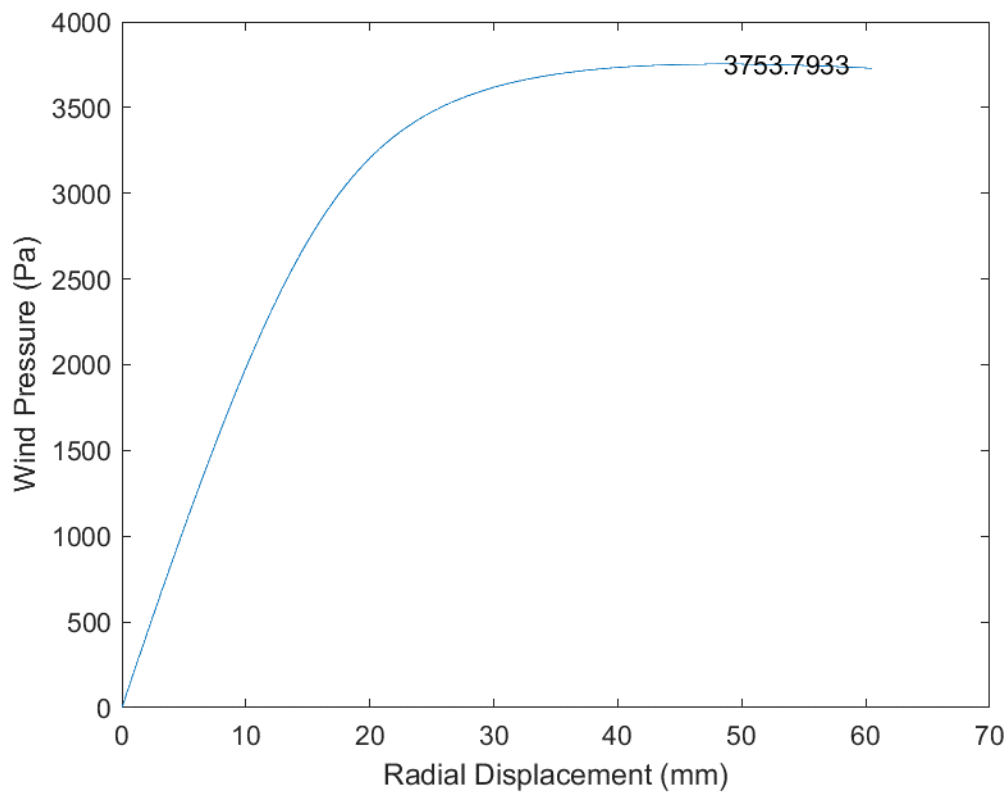


Fig. B.102 D54_H15_S36_R00_W00_V00_CL03_CD03_WT05_ST02

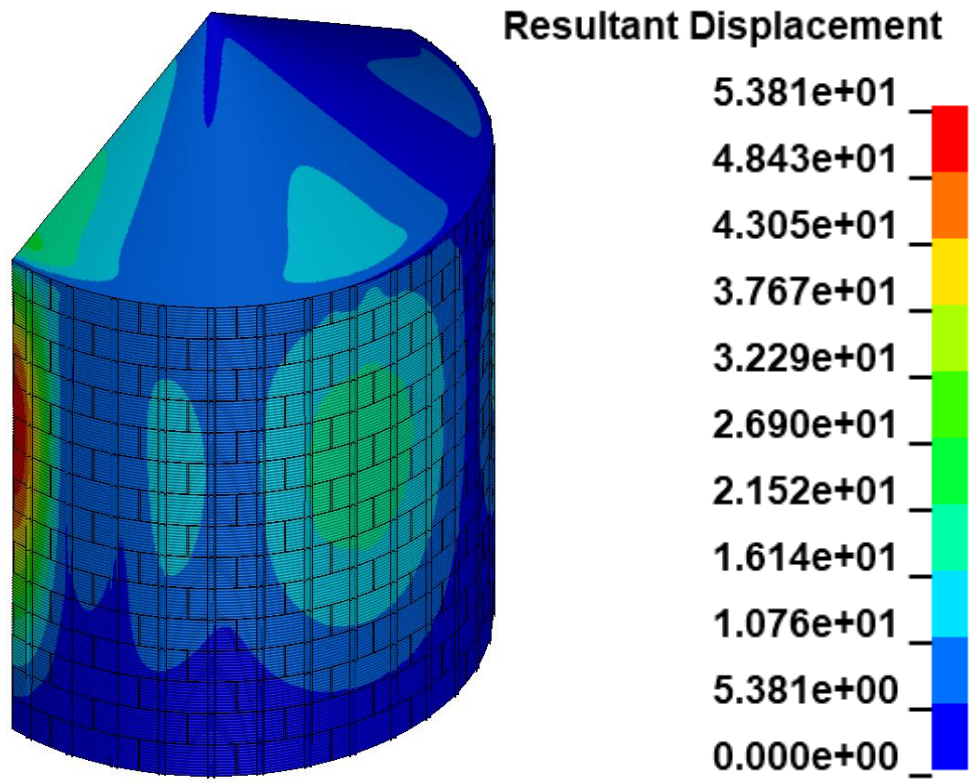
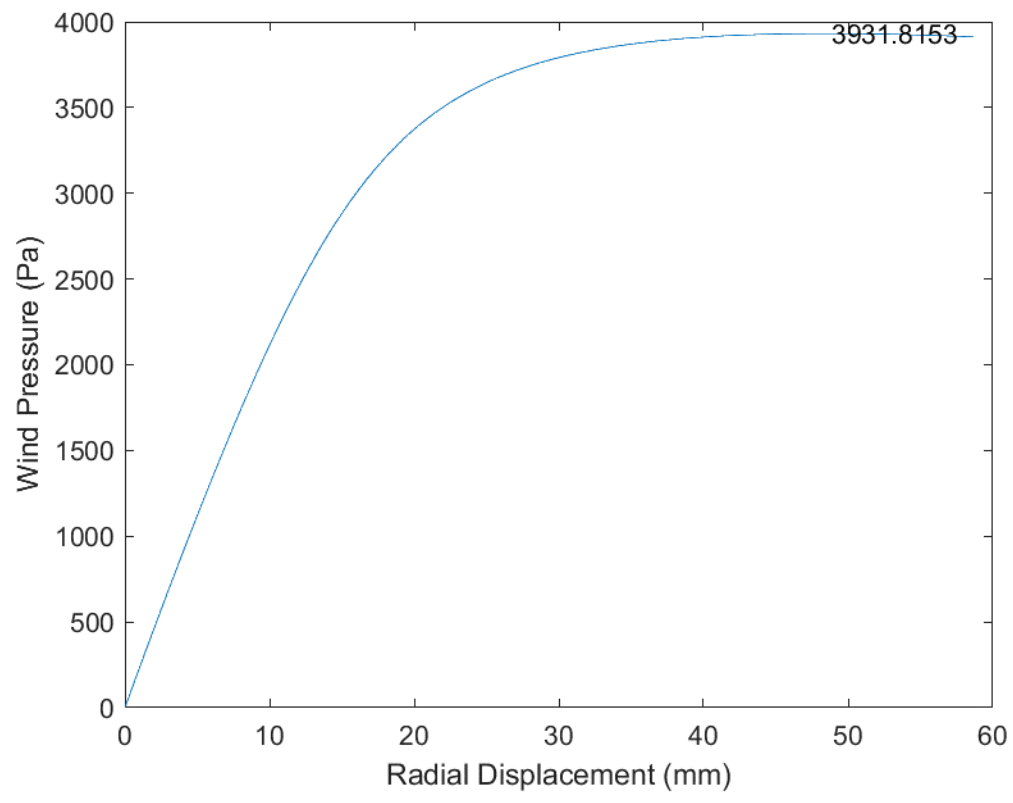


Fig. B.103 D54_H15_S36_R00_W00_V00_CL03_CD03_WT05_ST03

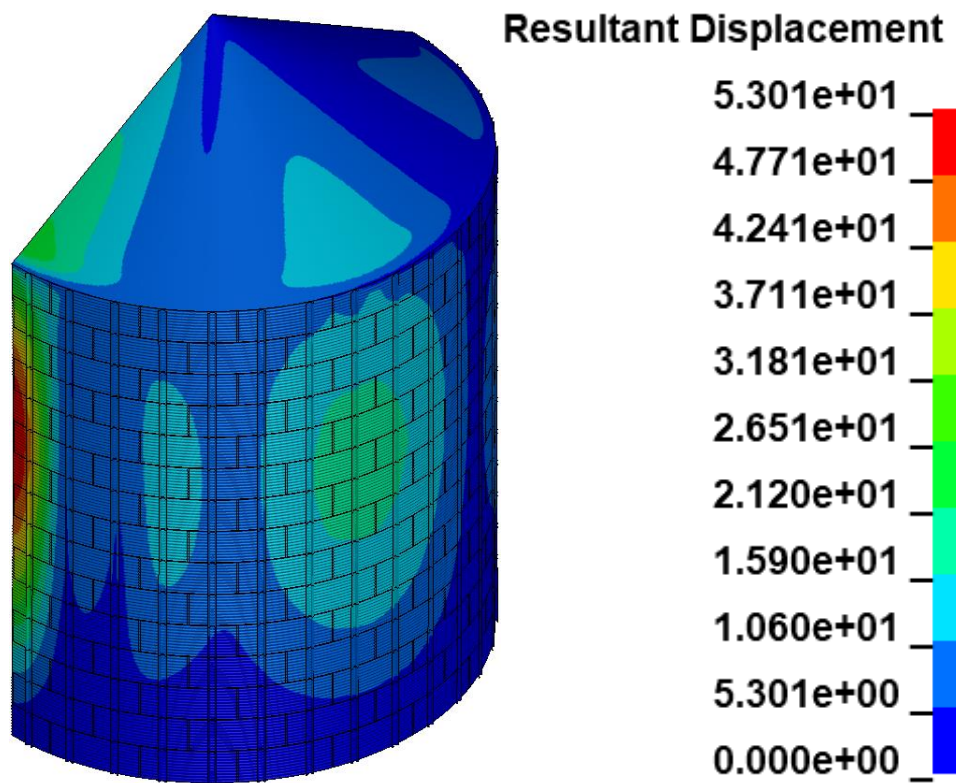
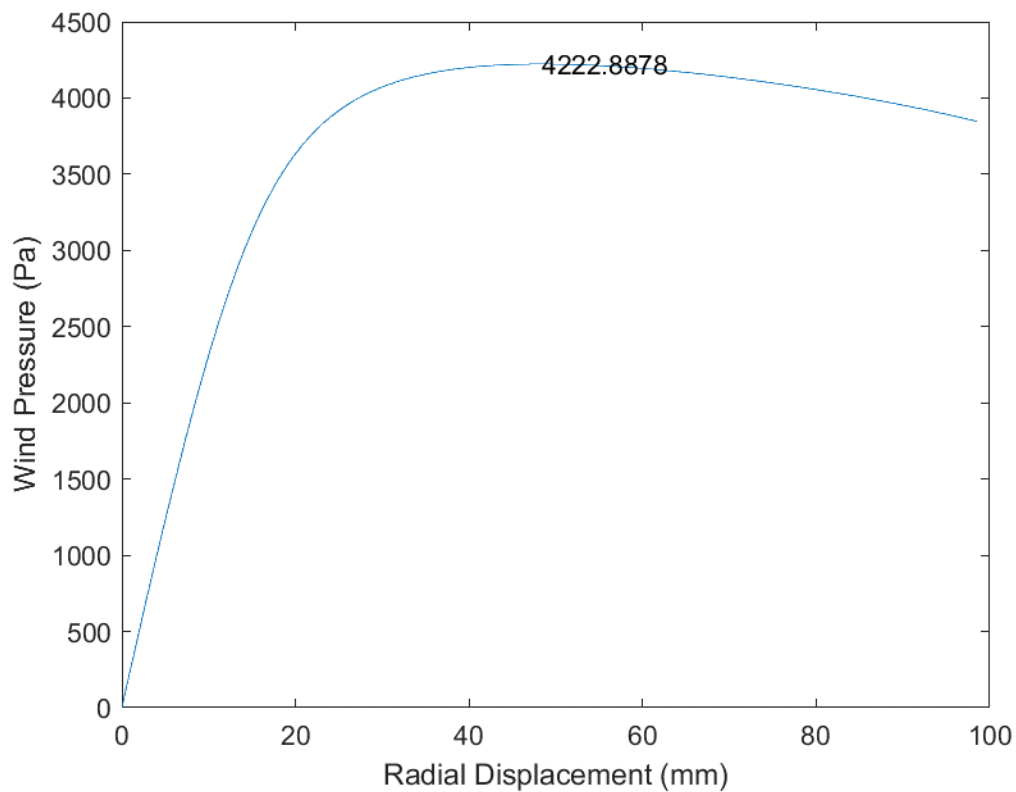


Fig. B.104 D54_H15_S36_R00_W00_V00_CL03_CD03_WT05_ST04

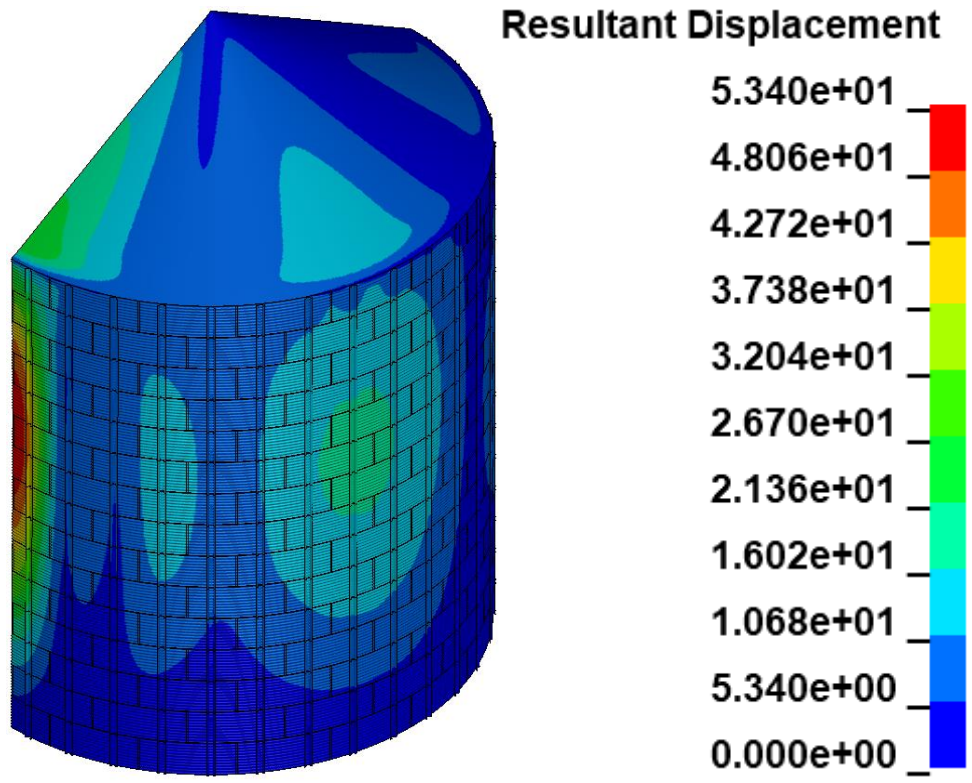
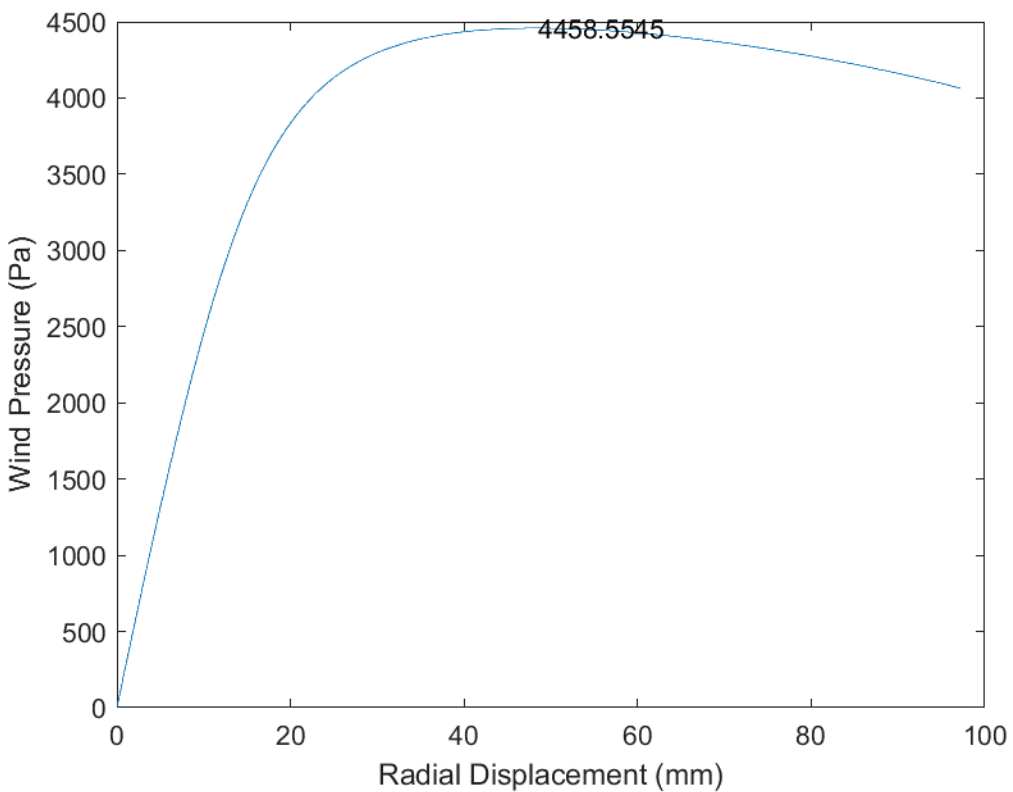


Fig. B.105 D54_H15_S36_R00_W00_V00_CL03_CD03_WT05_ST05

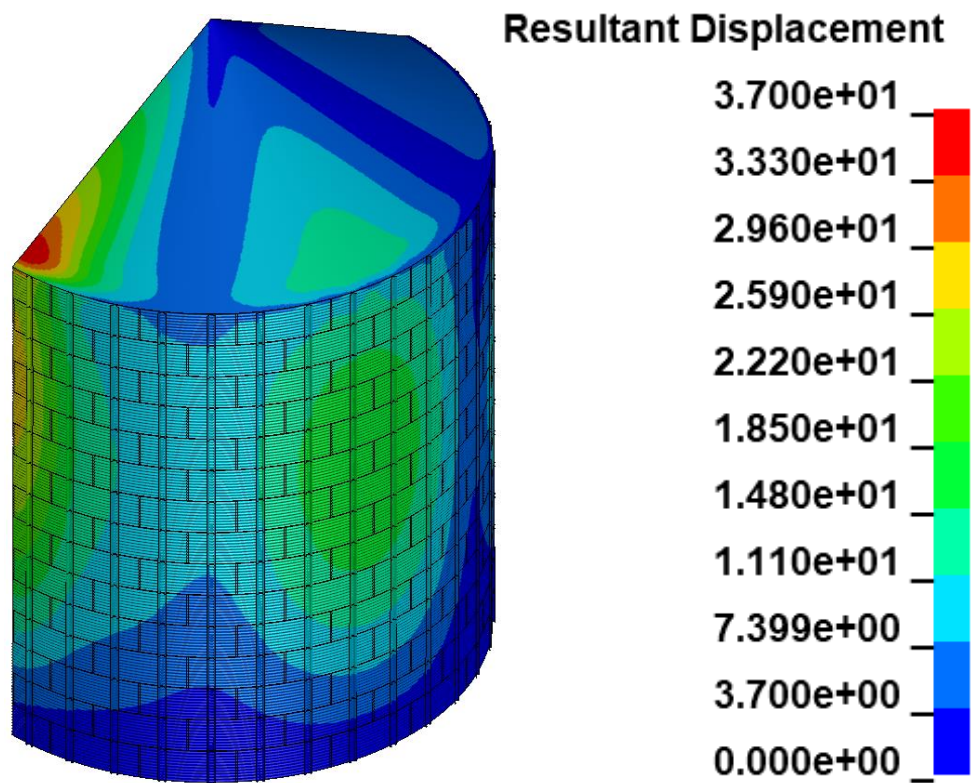
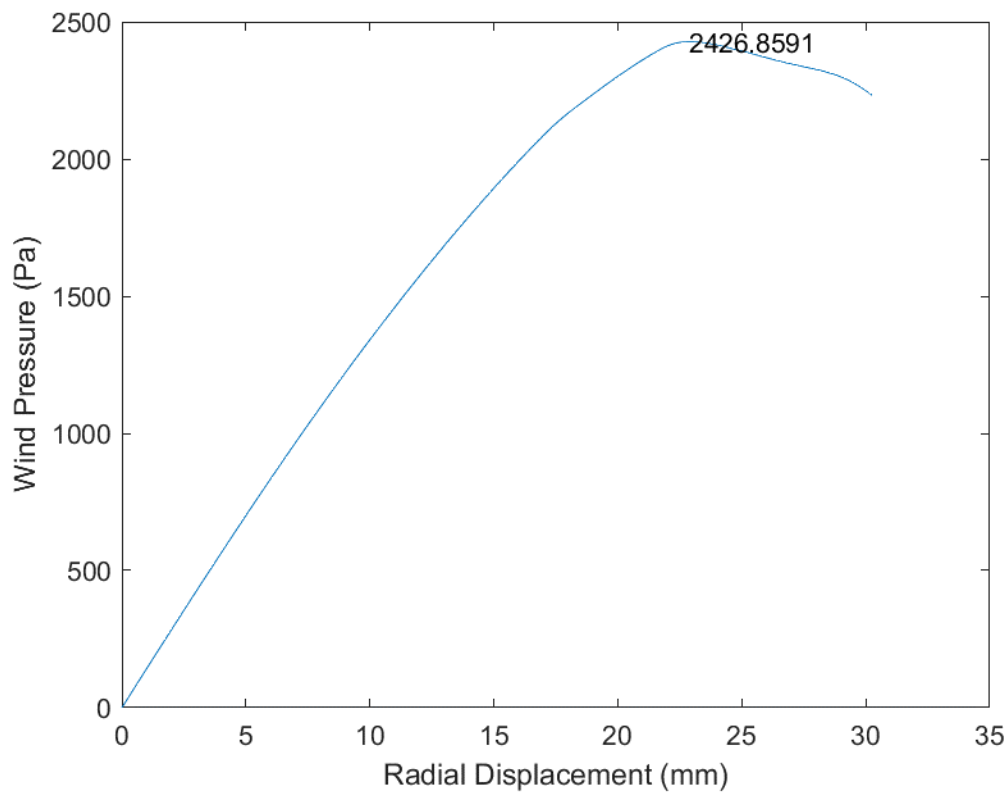


Fig. B.106 D54_H15_S36_R00_W00_V00_CL03_CD04_WT03_ST03

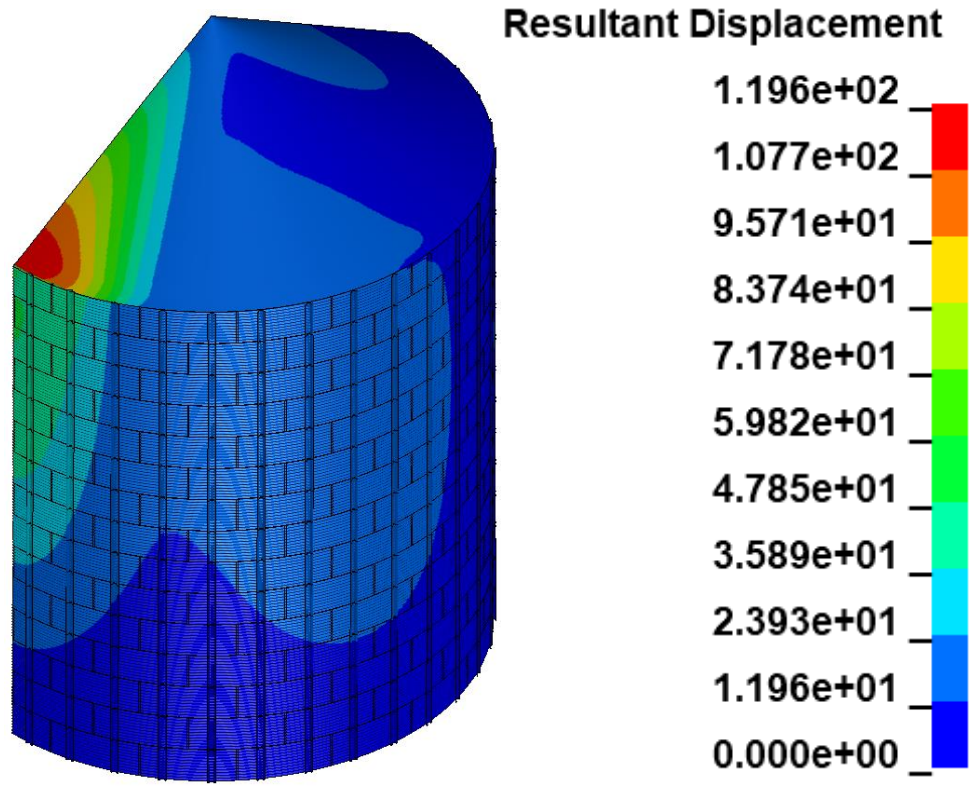
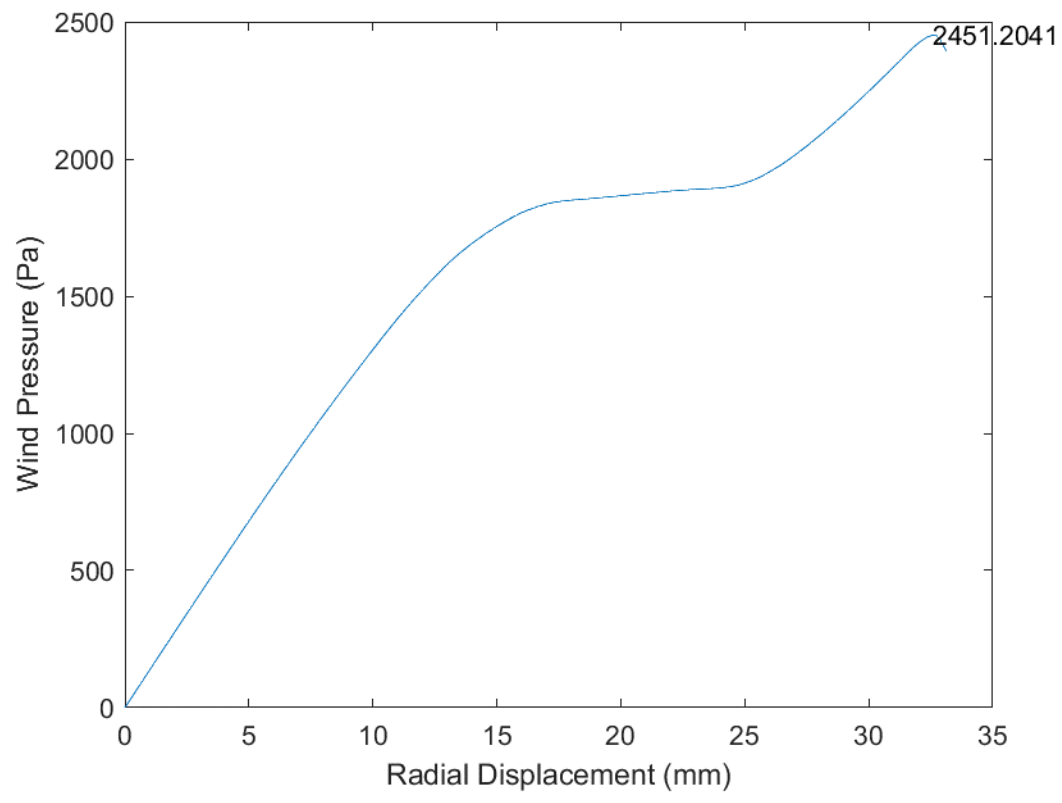


Fig. B.107 D54_H15_S36_R00_W00_V00_CL03_CD05_WT03_ST03

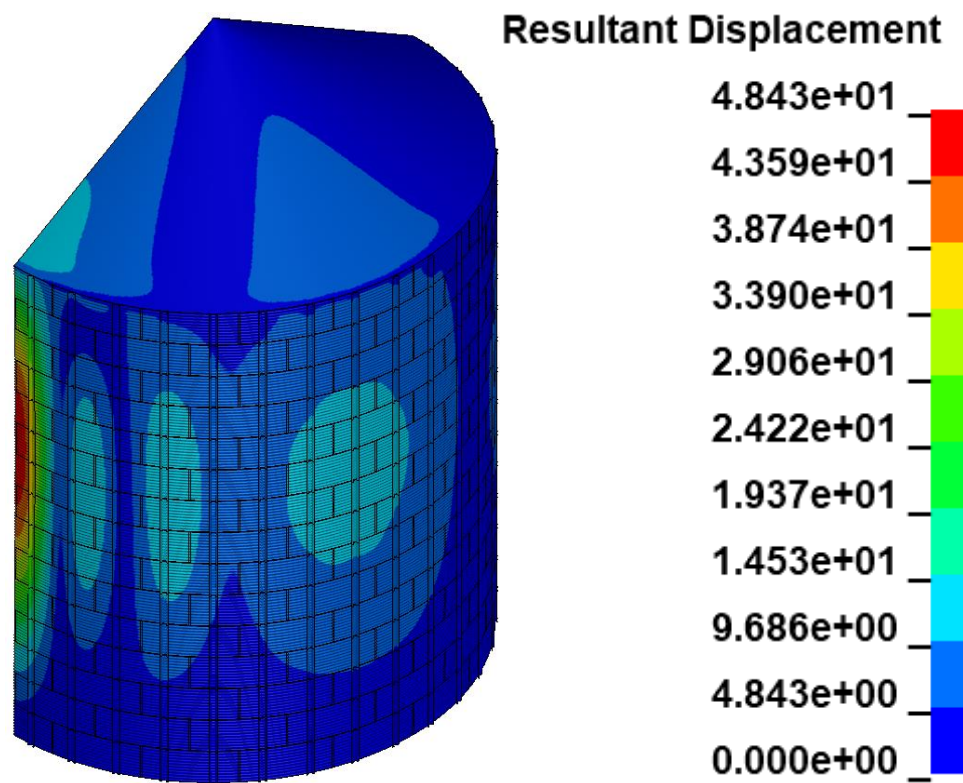
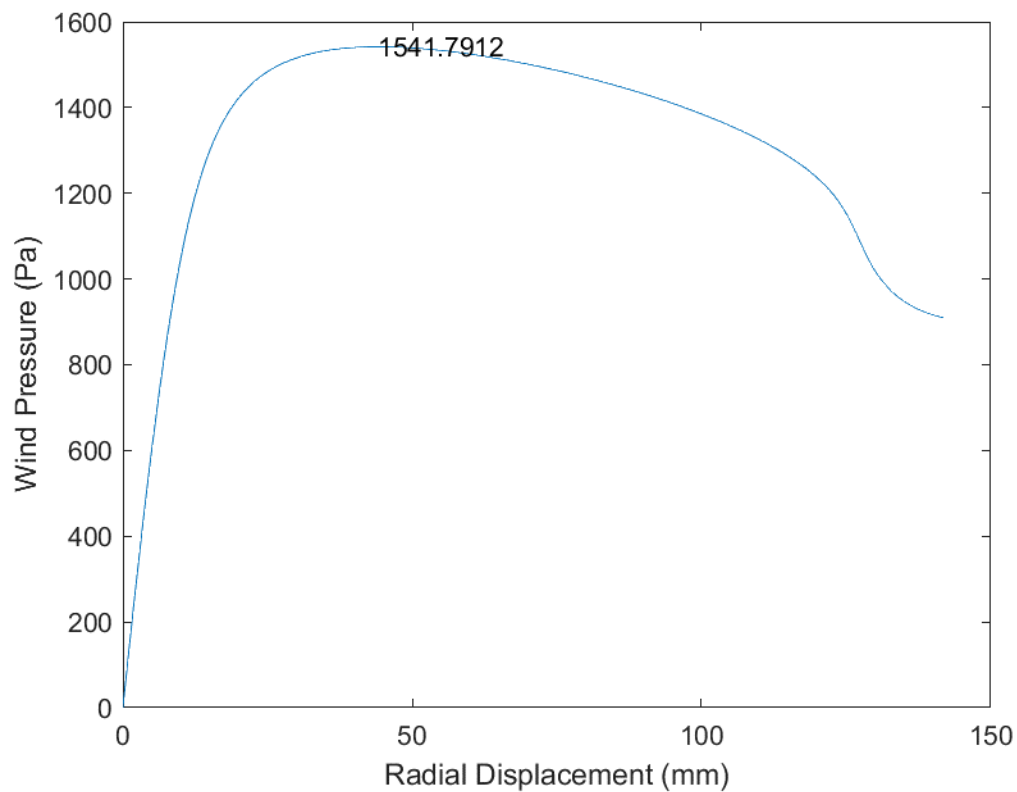


Fig. B.108 D54_H15_S36_R00_W00_V01_CL03_CD03_WT03_ST03

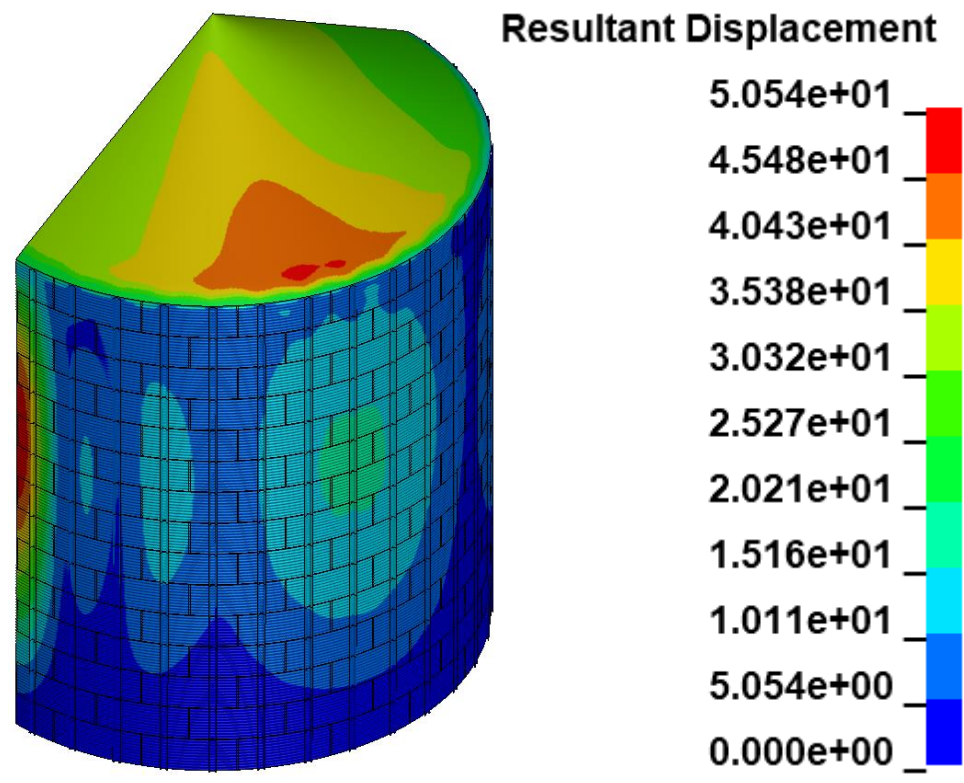
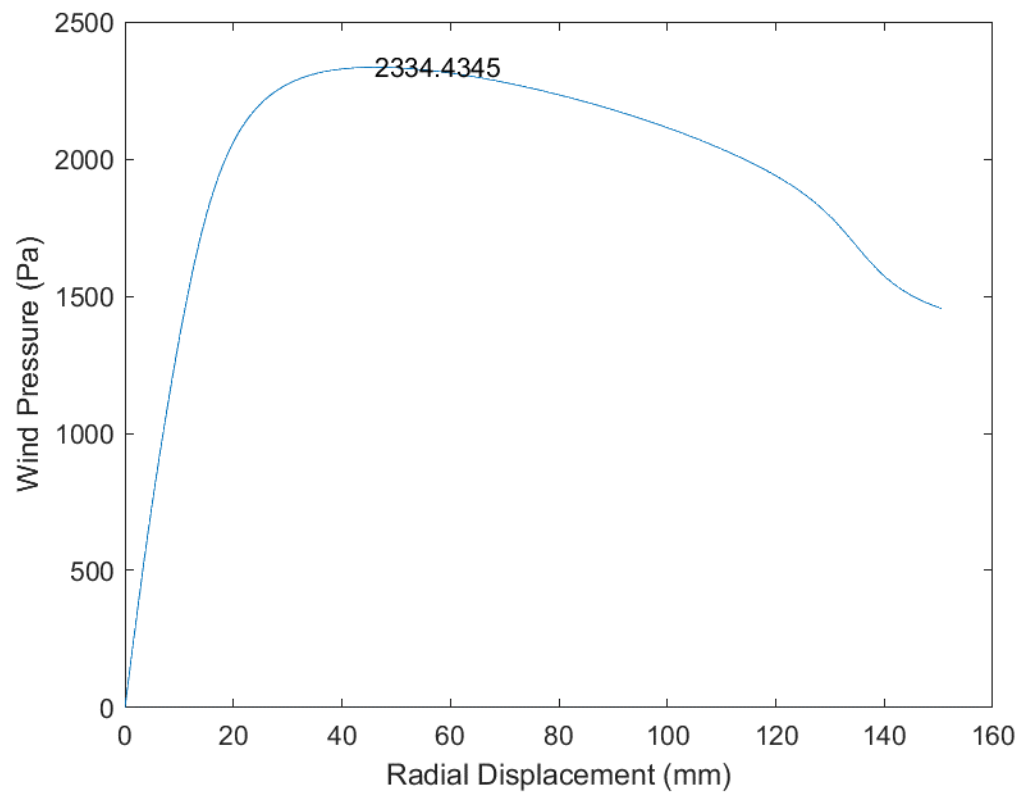


Fig. B.109 D54_H15_S36_R00_W01_V00_CL03_CD03_WT03_ST03

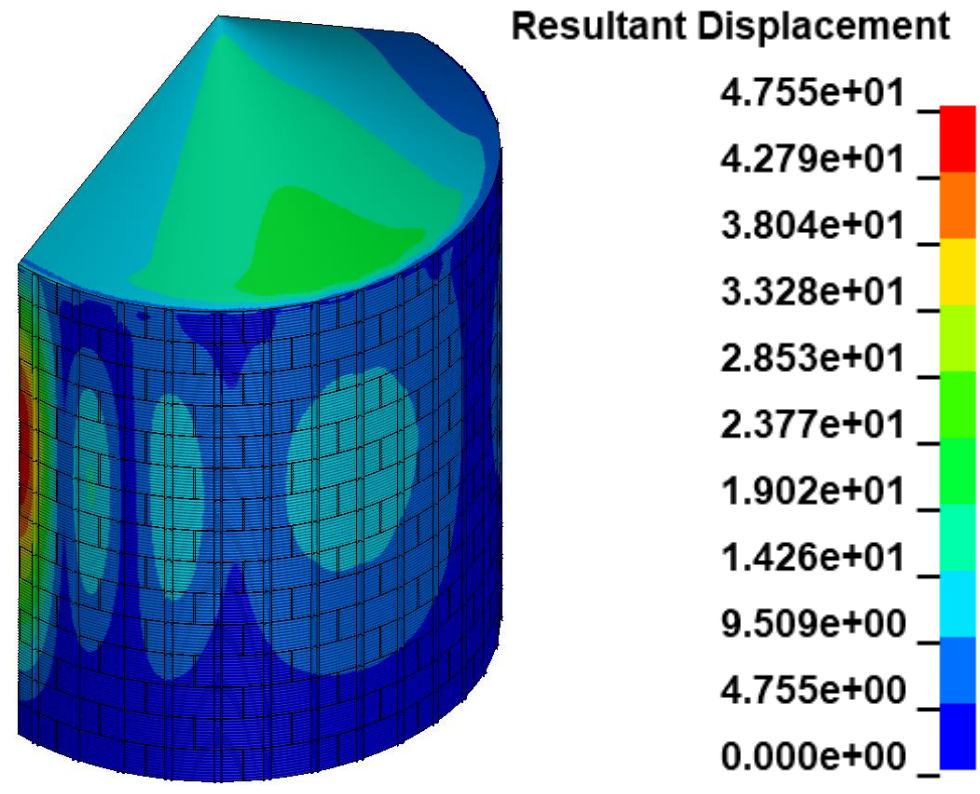
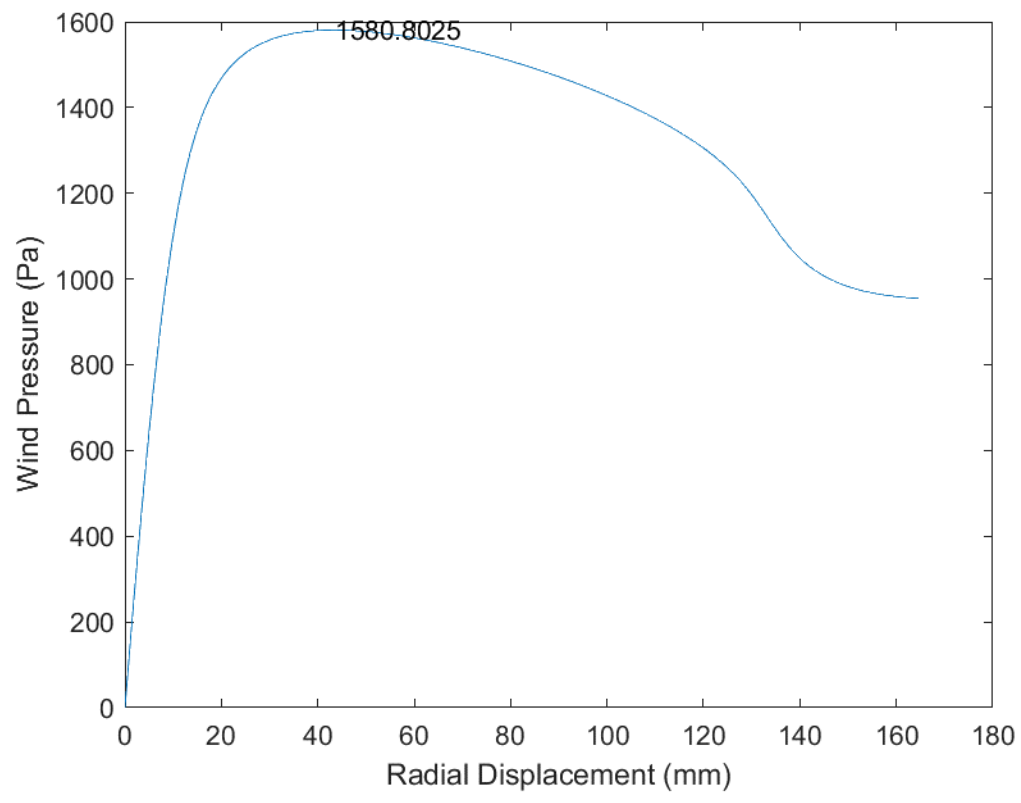


Fig. B.110 D54_H15_S36_R00_W01_V01_CL03_CD03_WT03_ST03

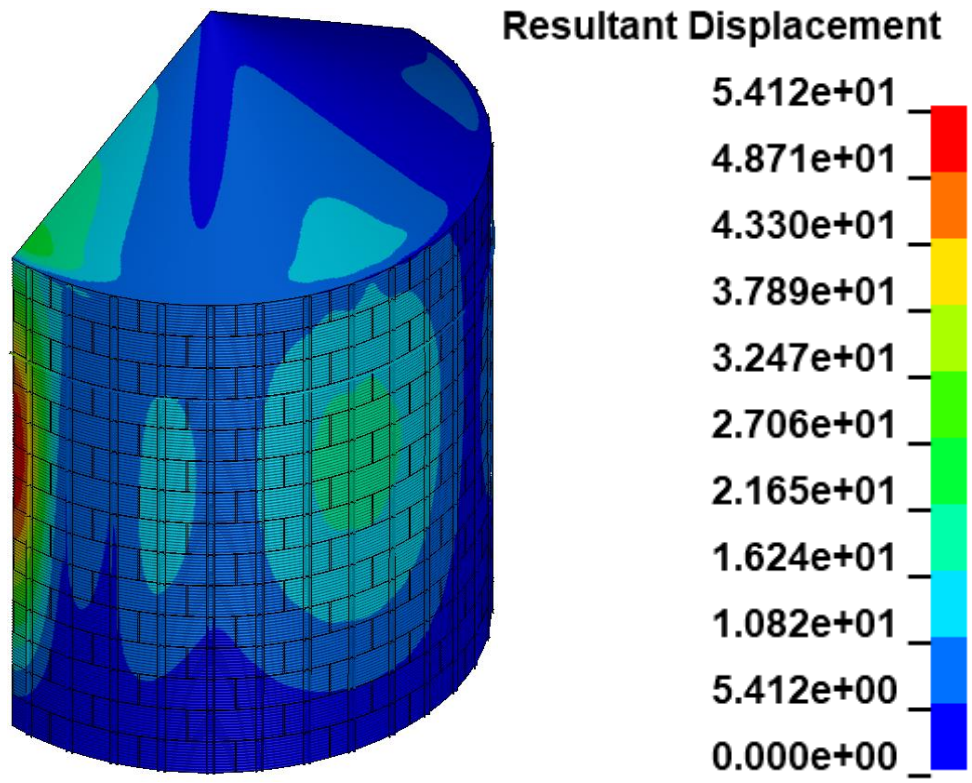
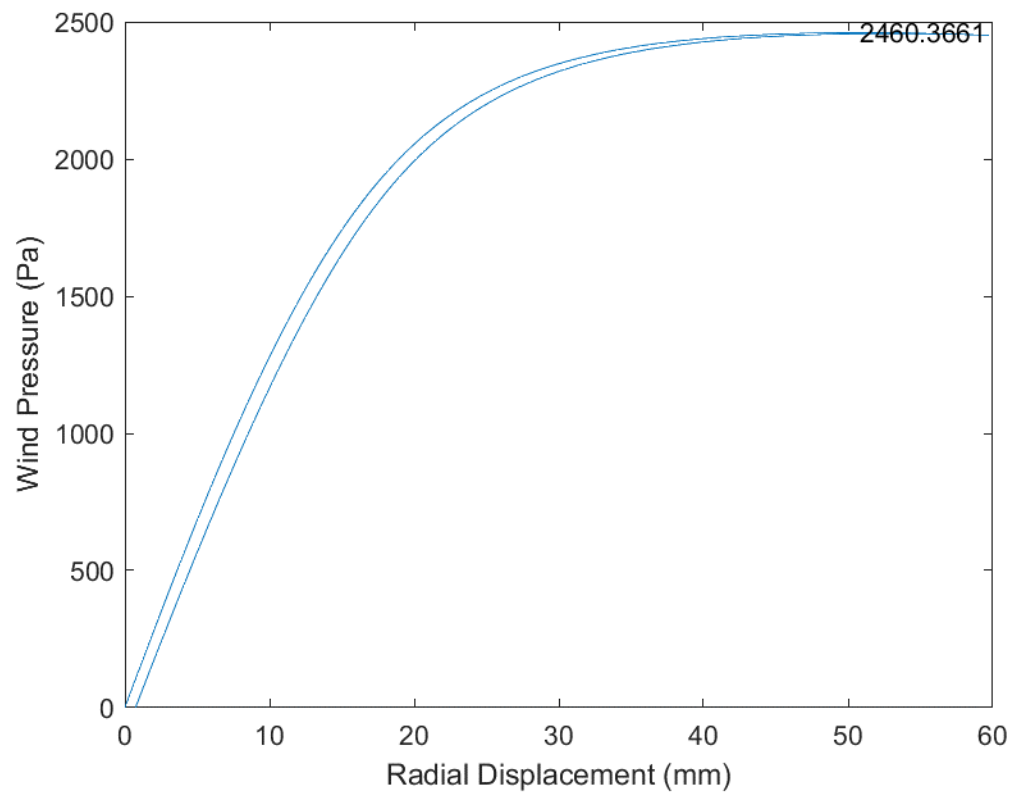


Fig. B.111 D54_H15_S36_R01_W00_V00_CL03_CD03_WT03_ST03

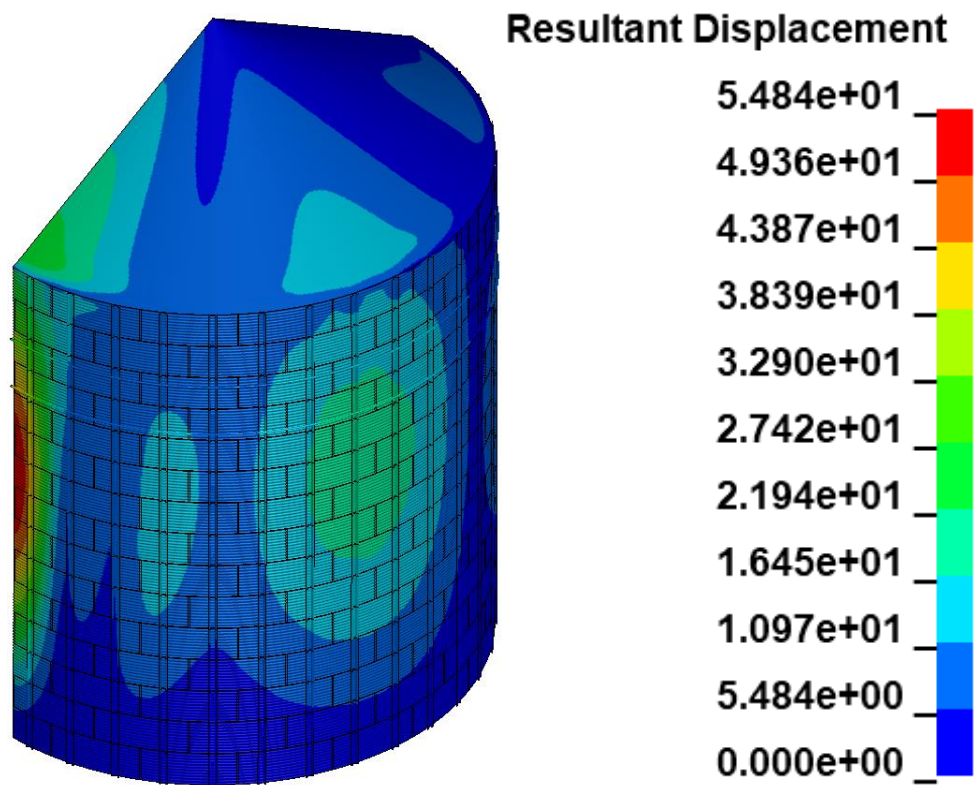
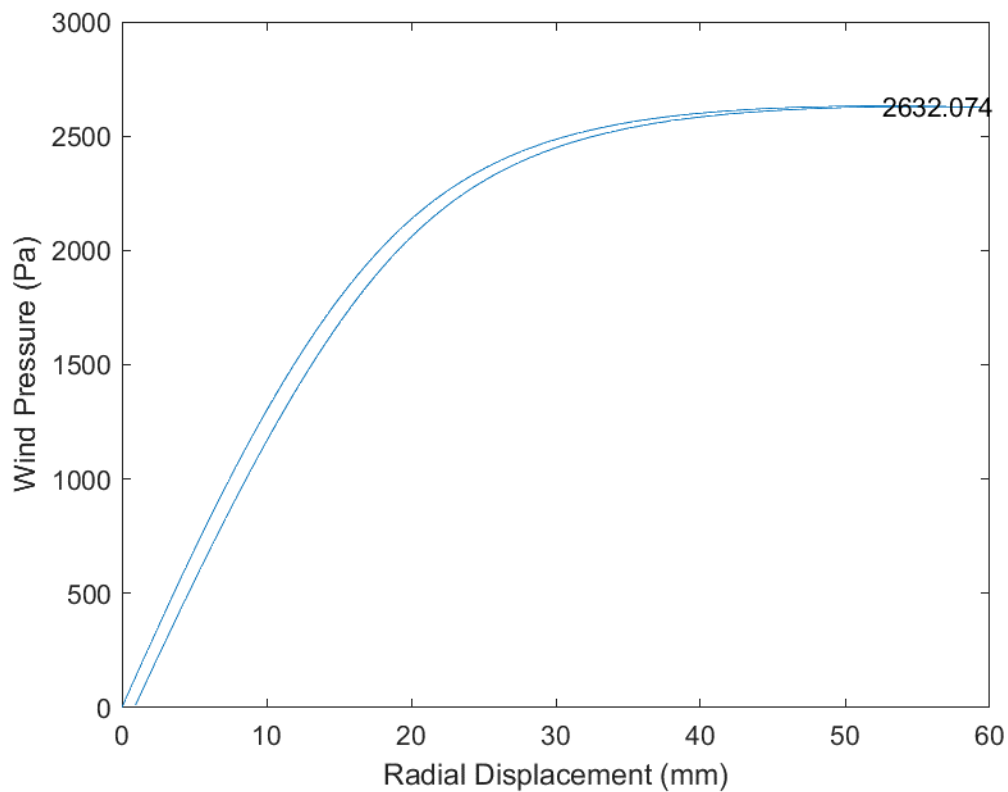


Fig. B.112 D54_H15_S36_R02_W00_V00_CL03_CD03_WT03_ST03

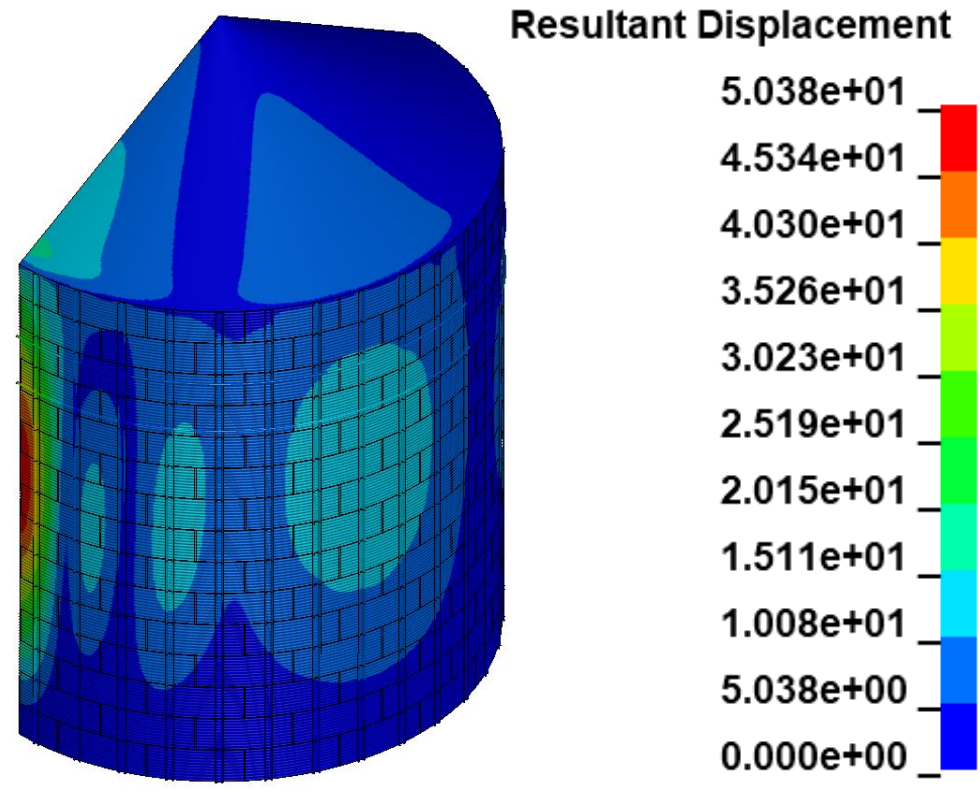
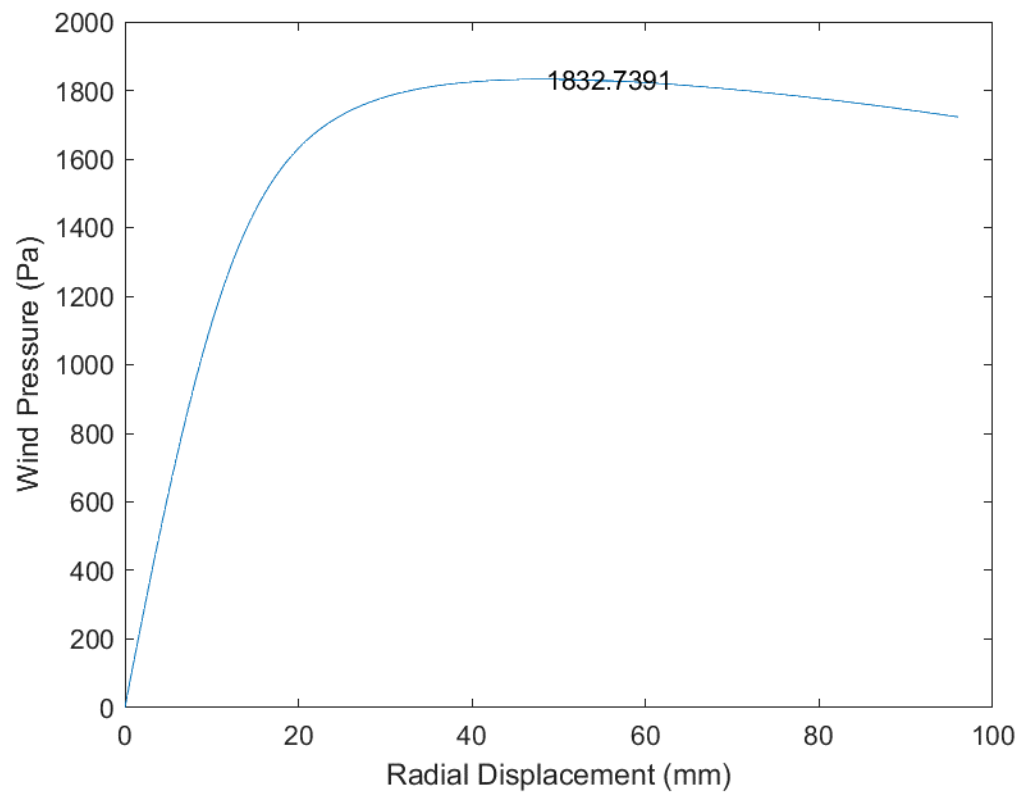


Fig. B.113 D54_H15_S36_R02_W00_V01_CL03_CD03_WT03_ST03

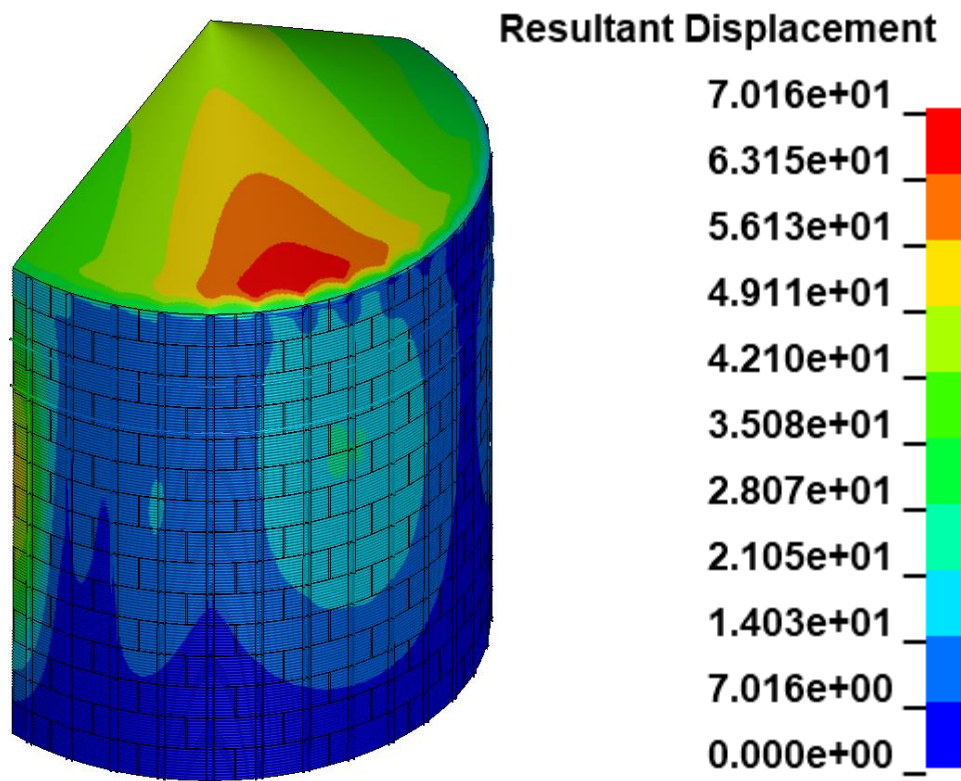
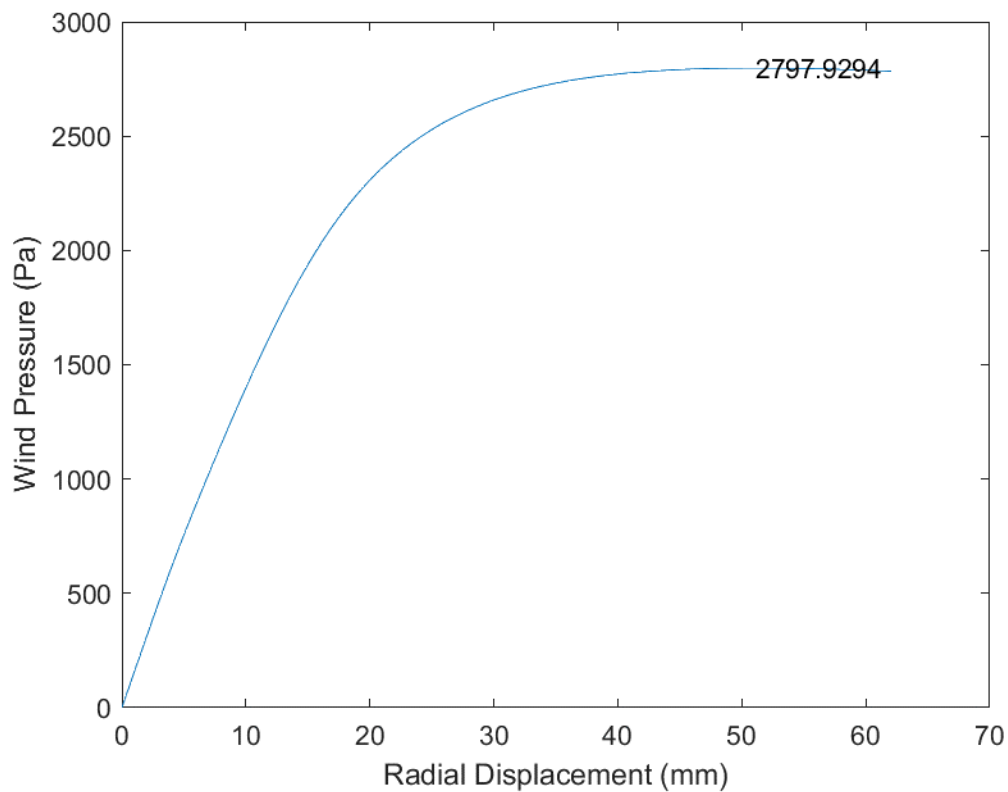


Fig. B.114 D54_H15_S36_R02_W01_V00_CL03_CD03_WT03_ST03

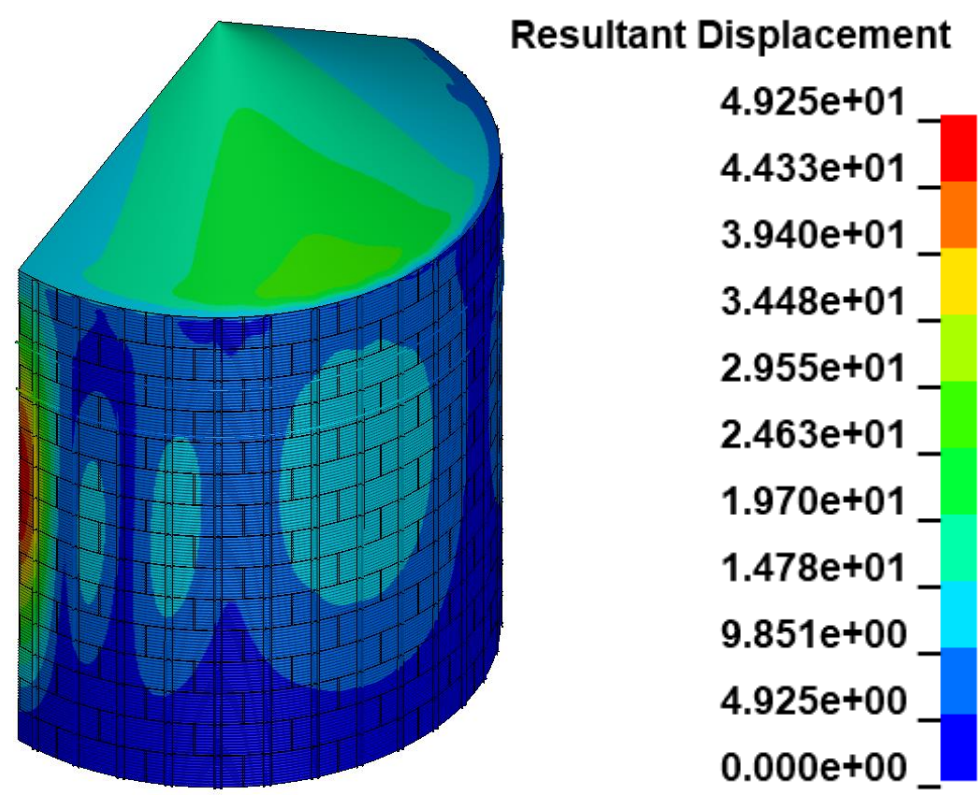
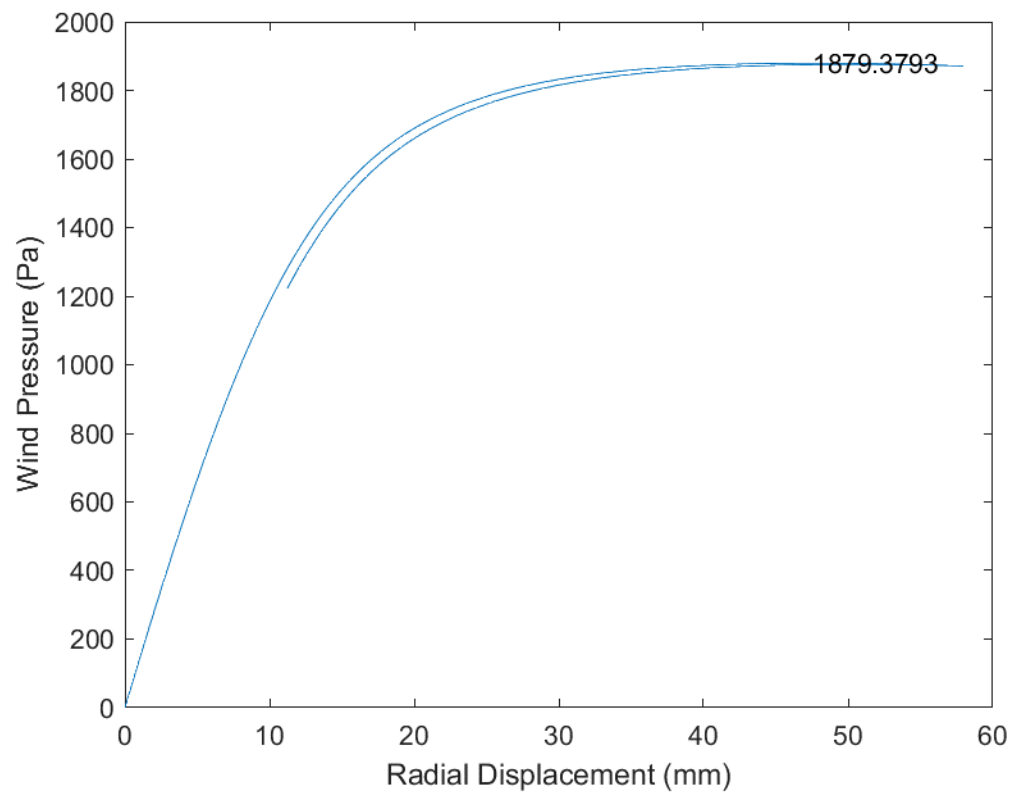


Fig. B.115 D54_H15_S36_R02_W01_V01_CL03_CD03_WT03_ST03

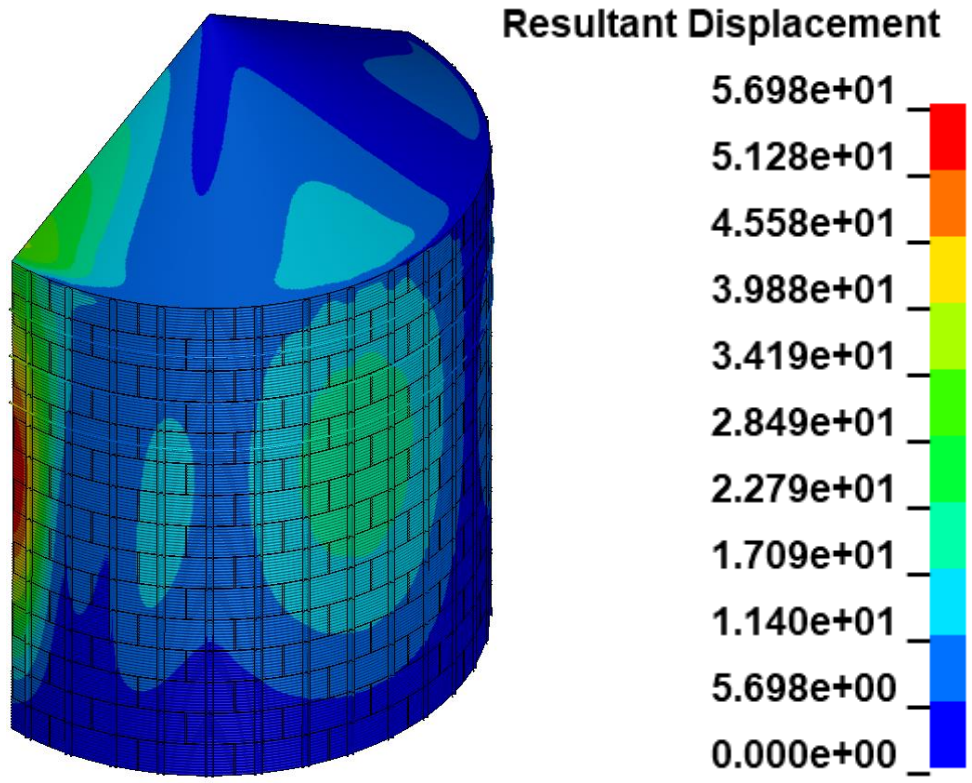
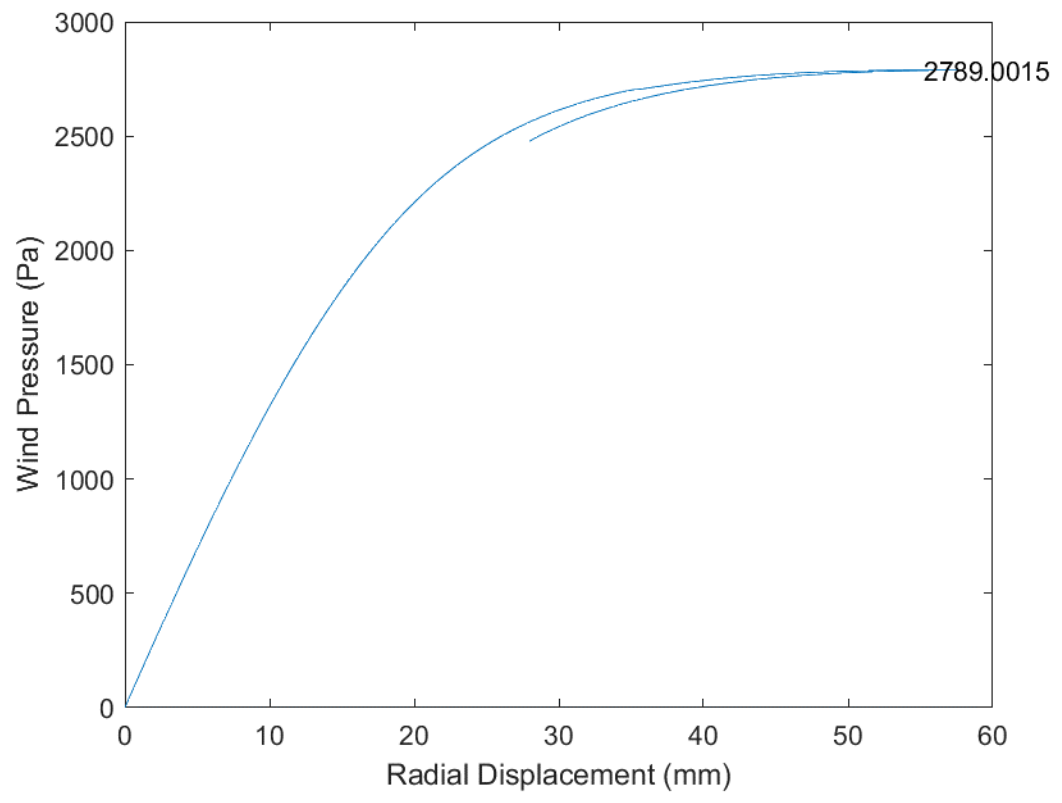


Fig. B.116 D54_H15_S36_R03_W00_V00_CL03_CD03_WT03_ST03

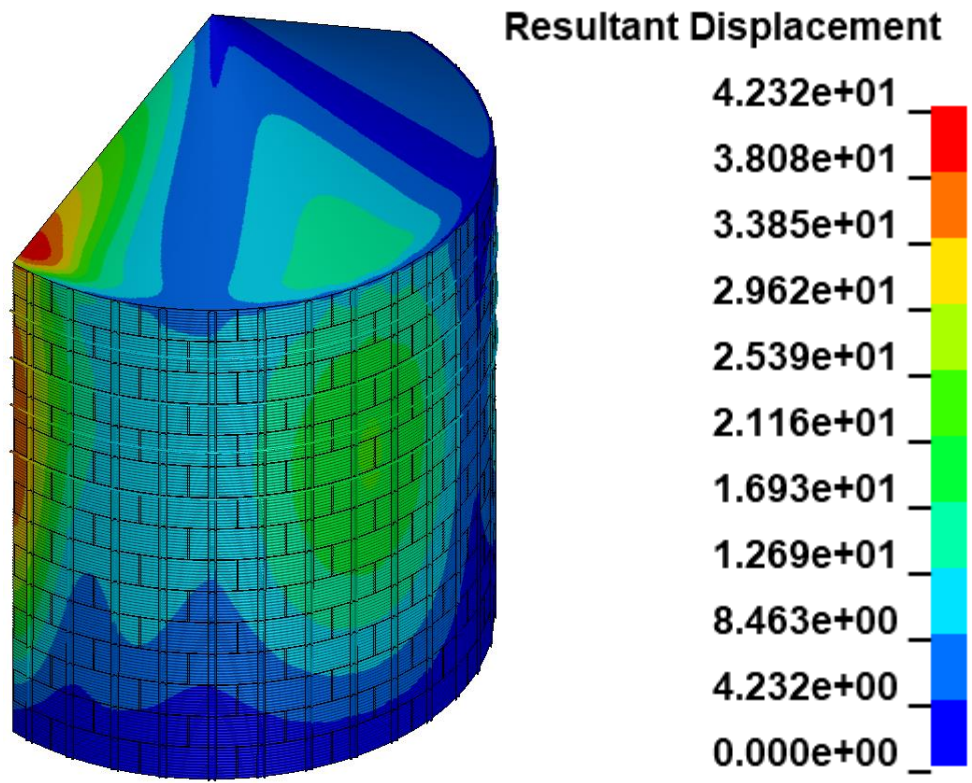
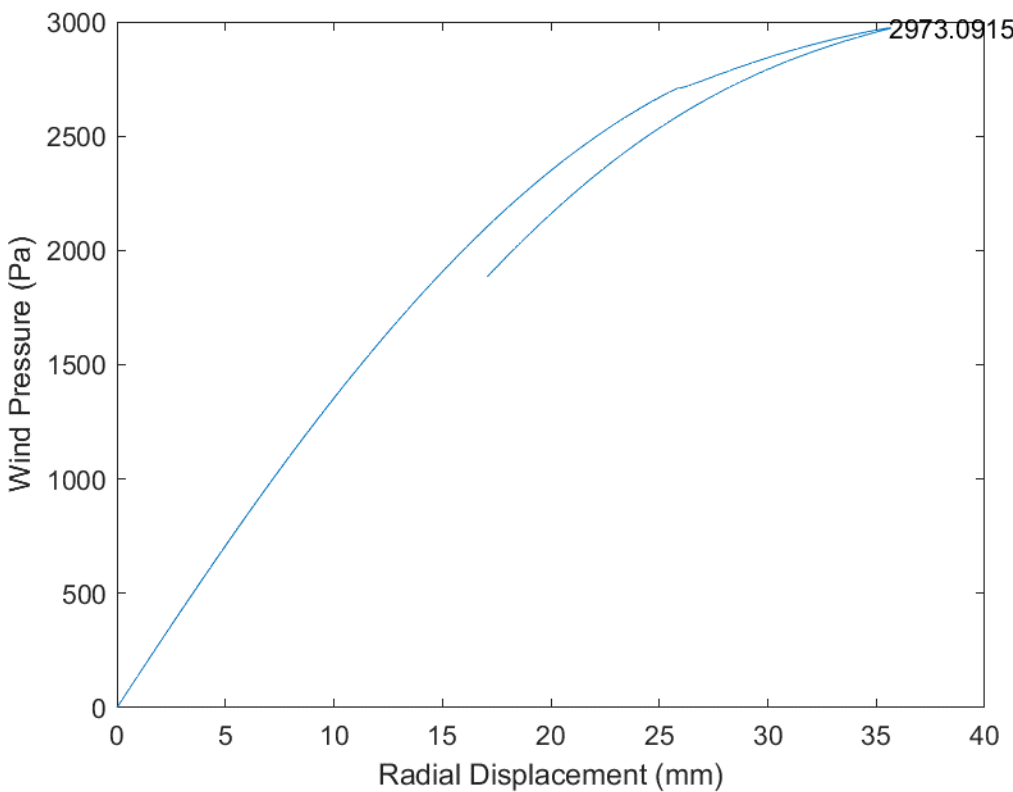


Fig. B.117 D54_H15_S36_R04_W00_V00_CL03_CD03_WT03_ST03

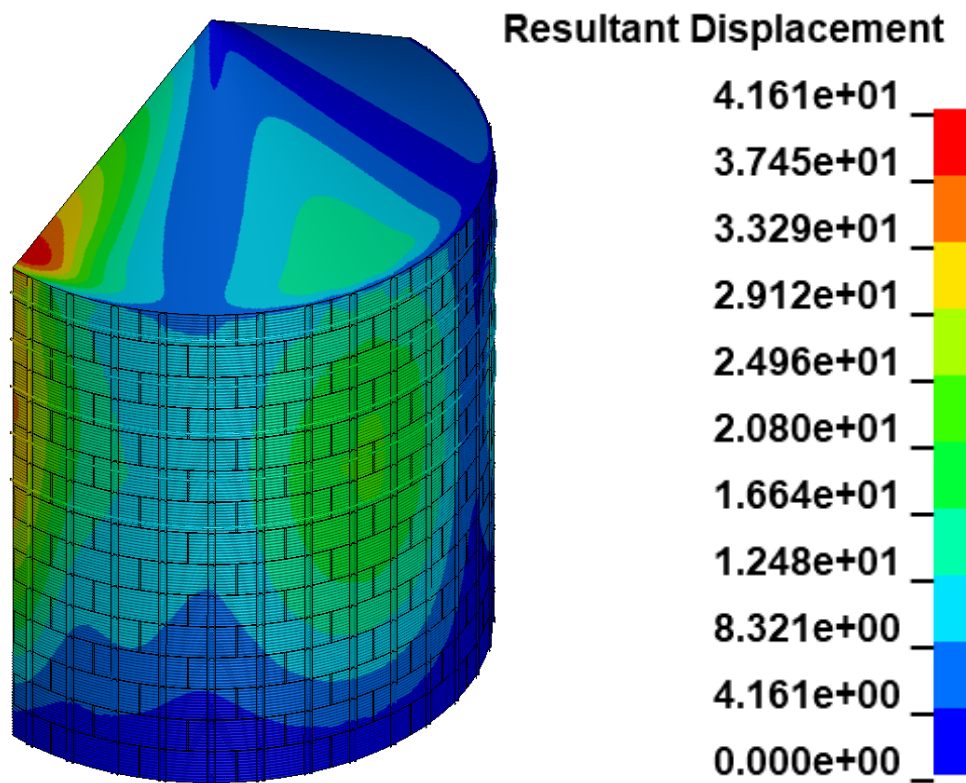
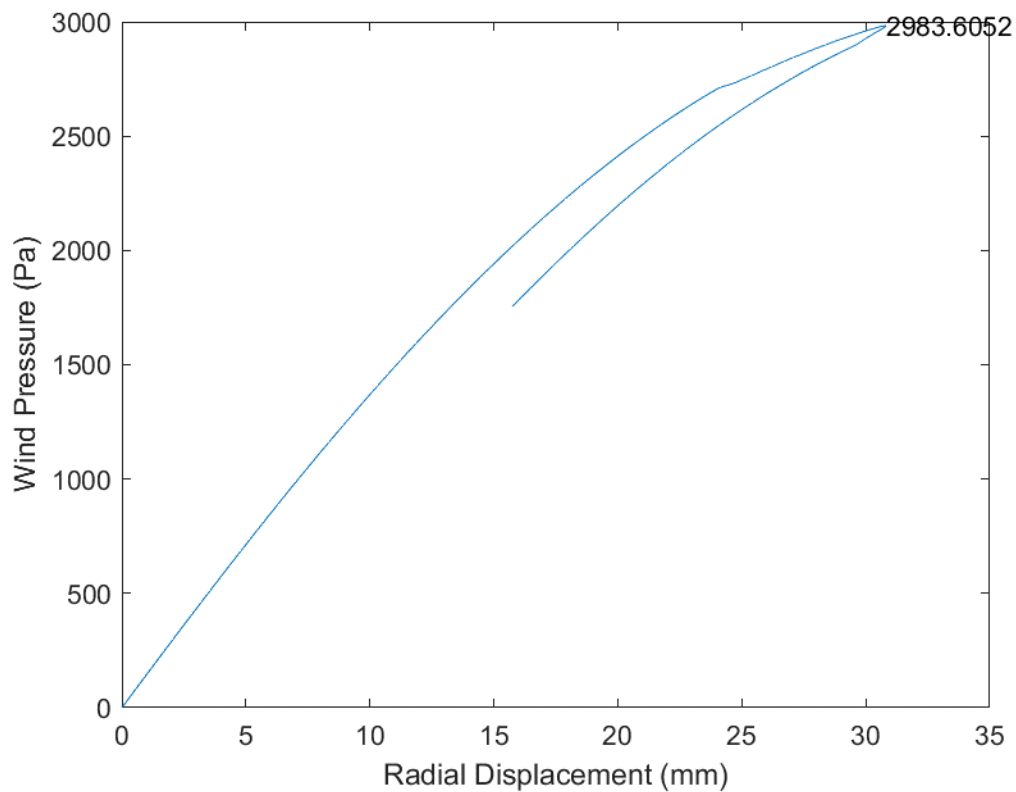


Fig. B.118 D54_H15_S36_R05_W00_V00_CL03_CD03_WT03_ST03

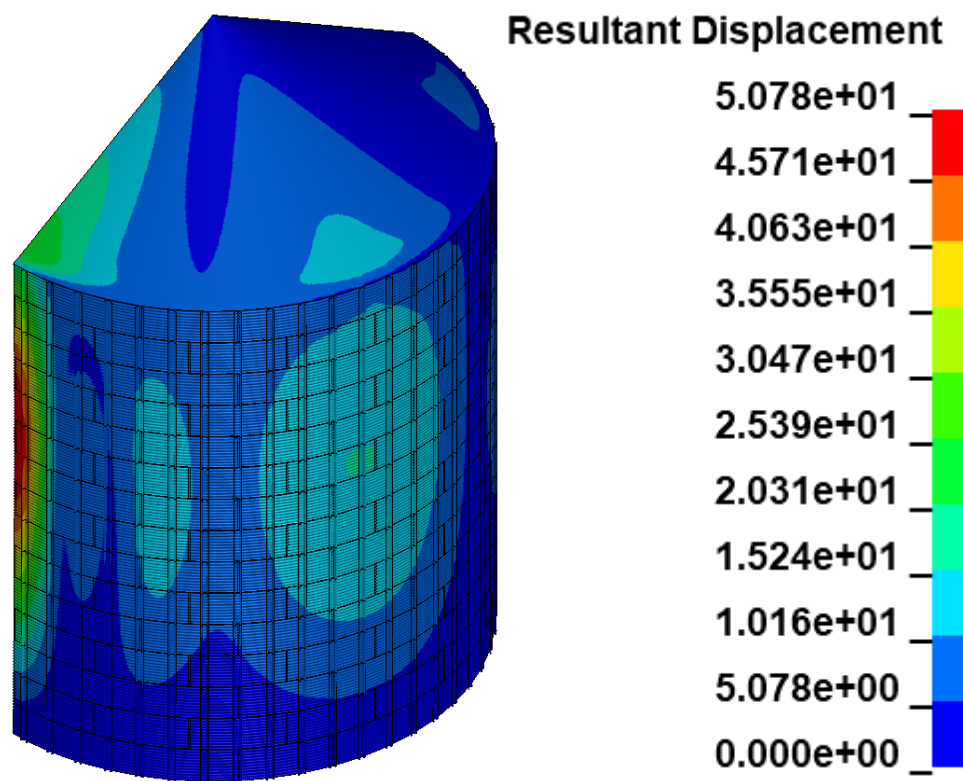
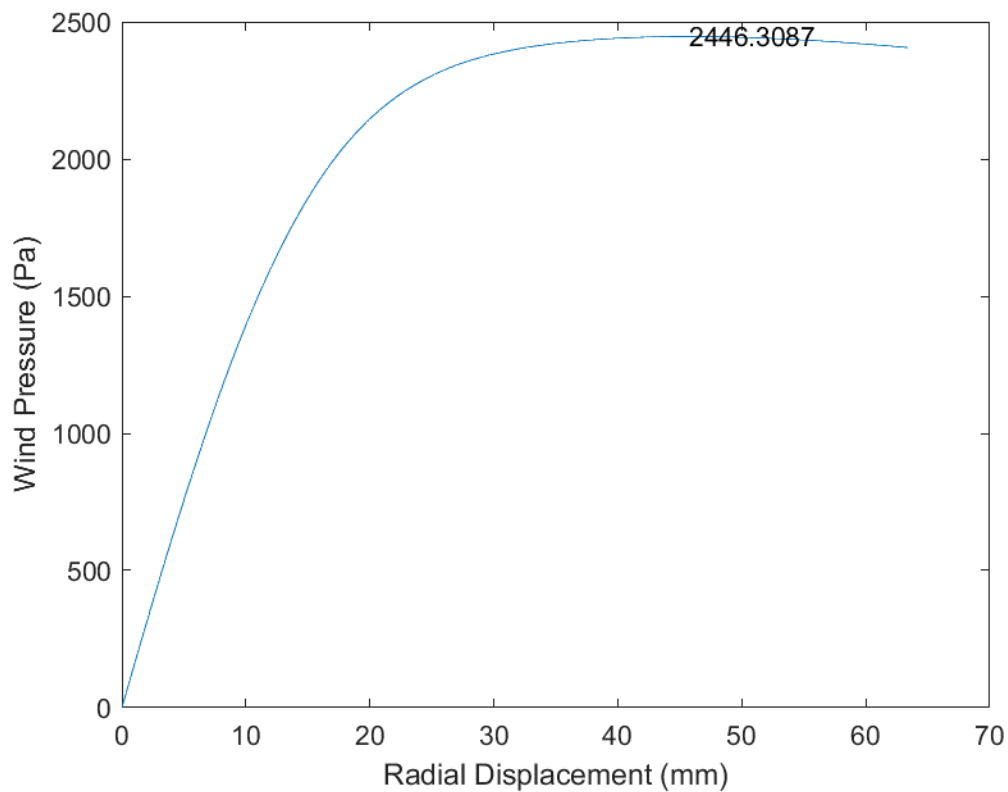


Fig. B.119 D54_H15_S54_R00_W00_V00_CL03_CD03_WT03_ST03

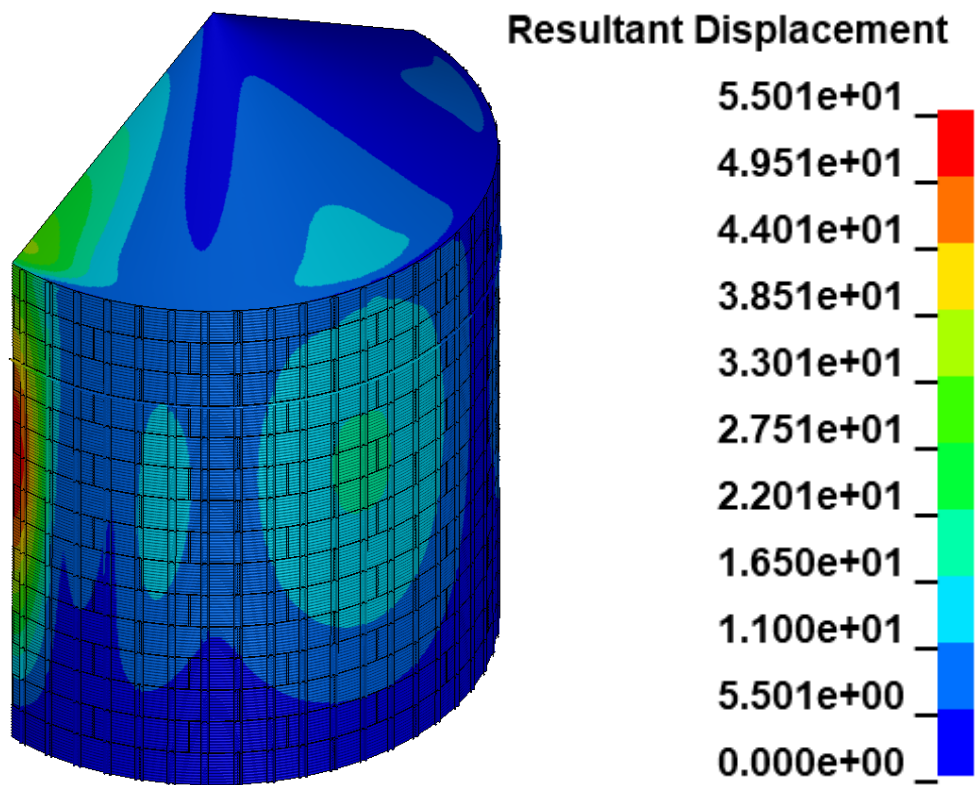
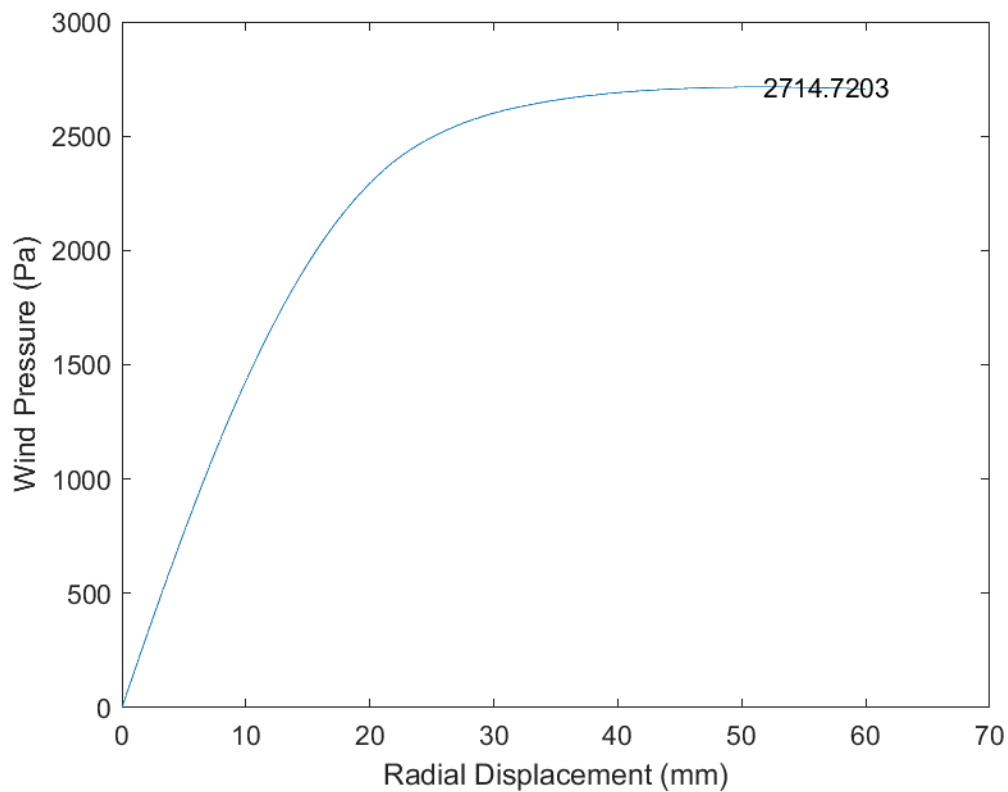


Fig. B.120 D54_H15_S54_R01_W00_V00_CL03_CD03_WT03_ST03

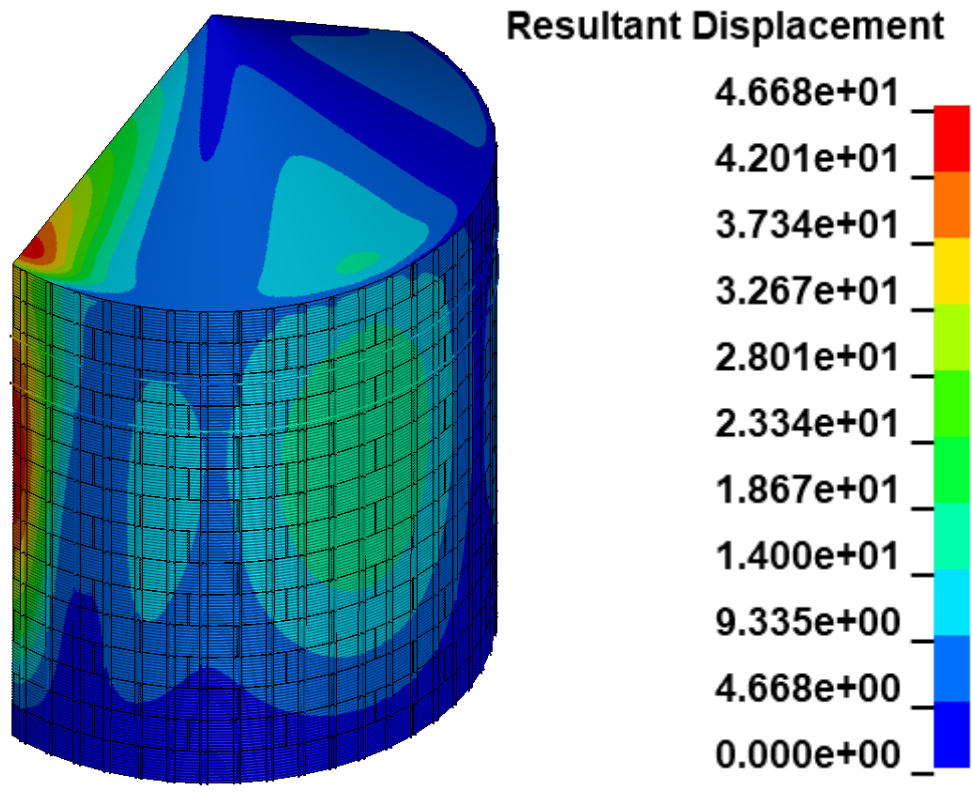
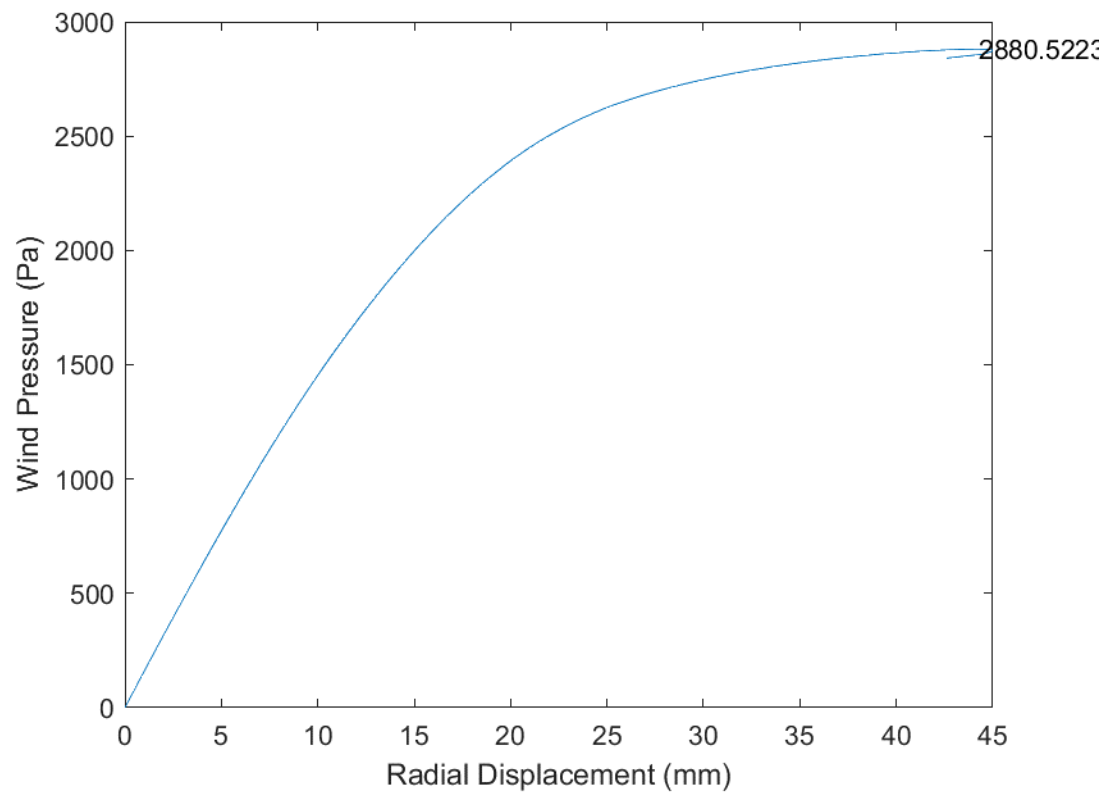


Fig. B.121 D54_H15_S54_R02_W00_V00_CL03_CD03_WT03_ST03

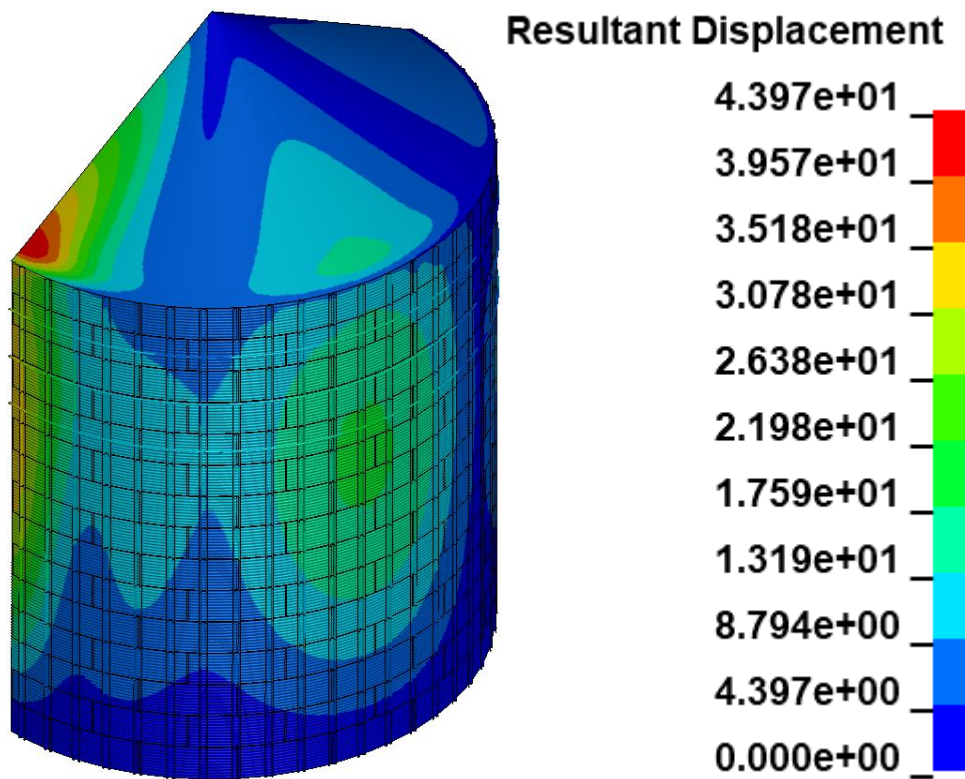
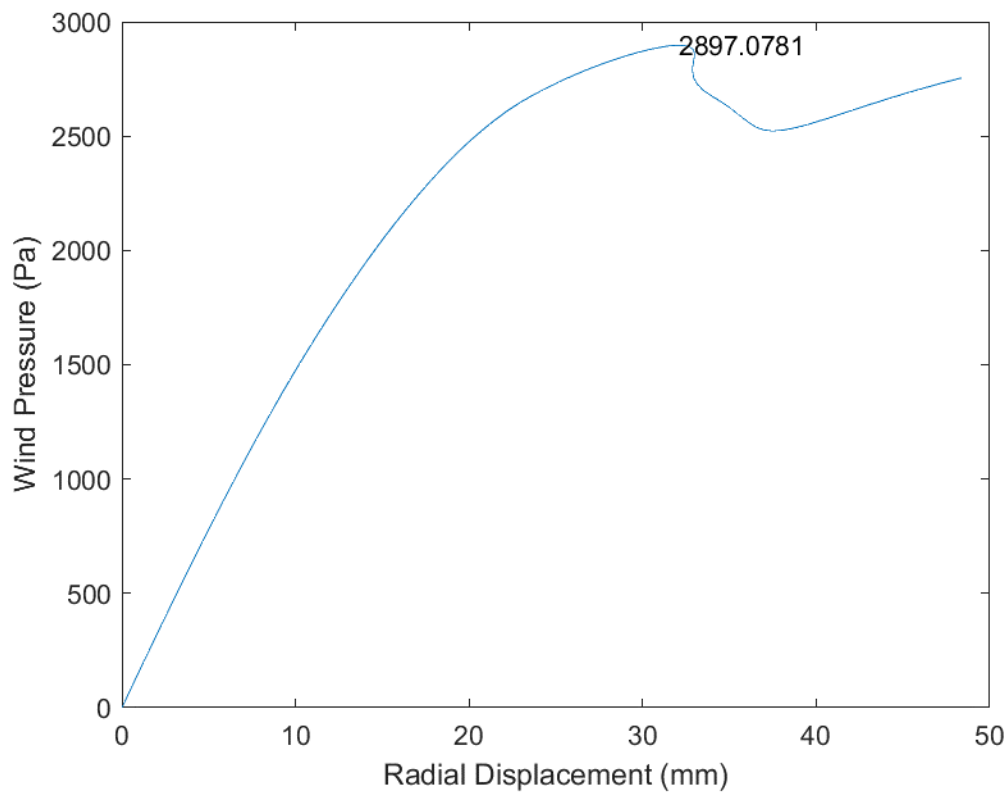


Fig. B.122 D54_H15_S54_R03_W00_V00_CL03_CD03_WT03_ST03

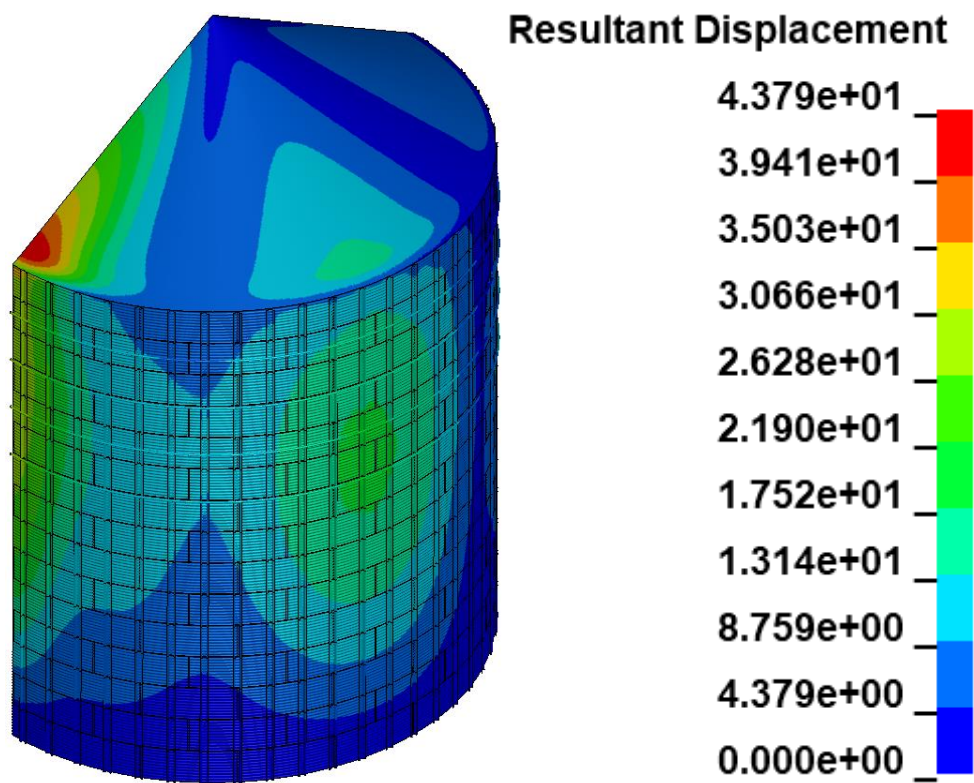
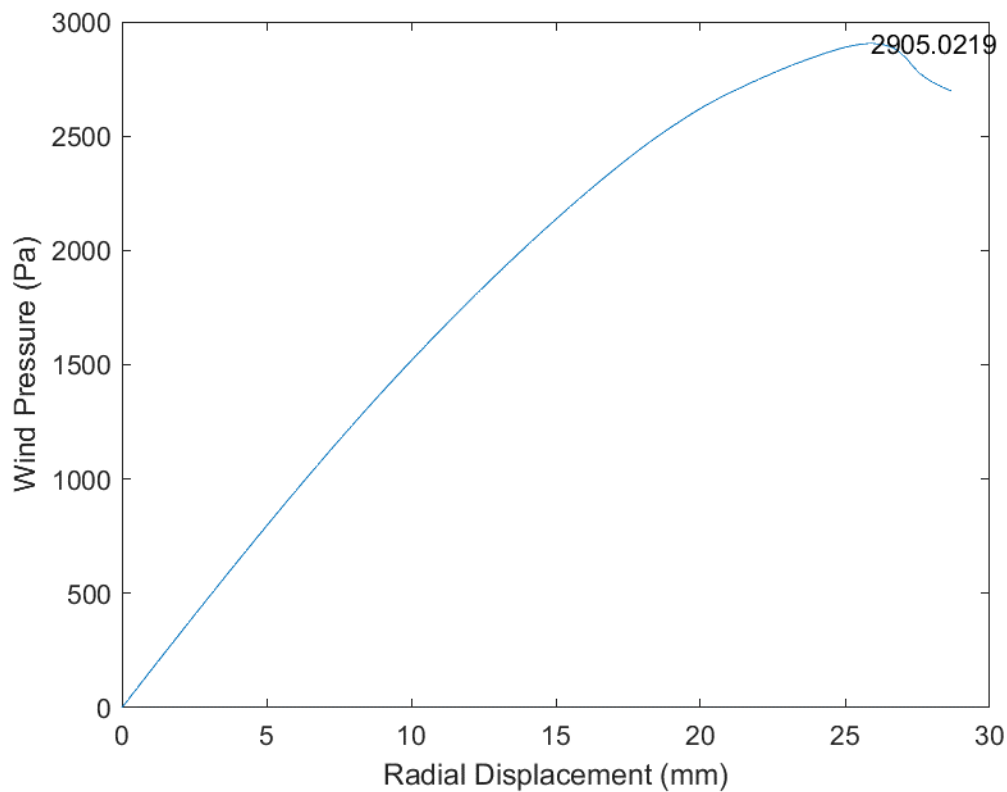


Fig. B.123 D54_H15_S54_R04_W00_V00_CL03_CD03_WT03_ST03

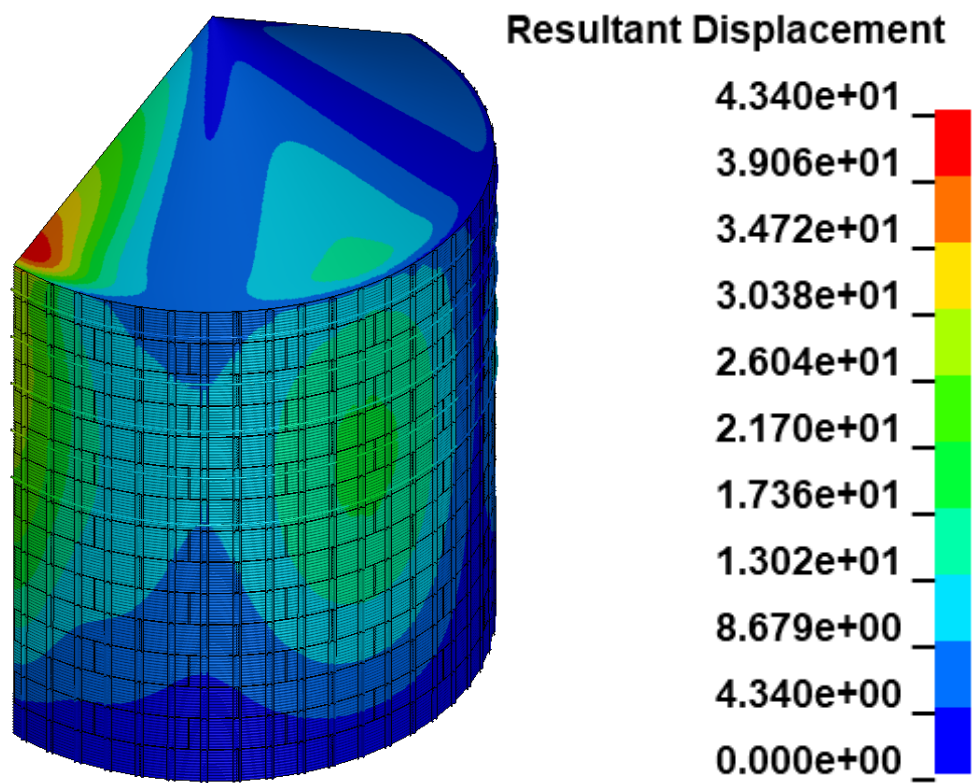
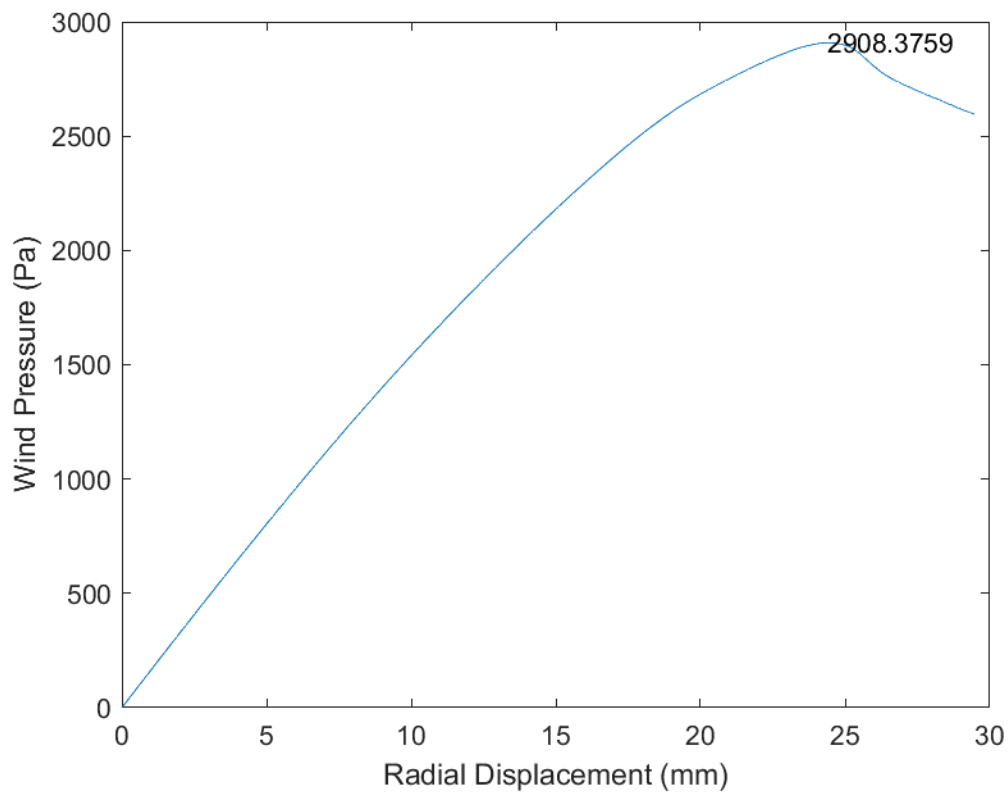


Fig. B.124 D54_H15_S54_R05_W00_V00_CL03_CD03_WT03_ST03

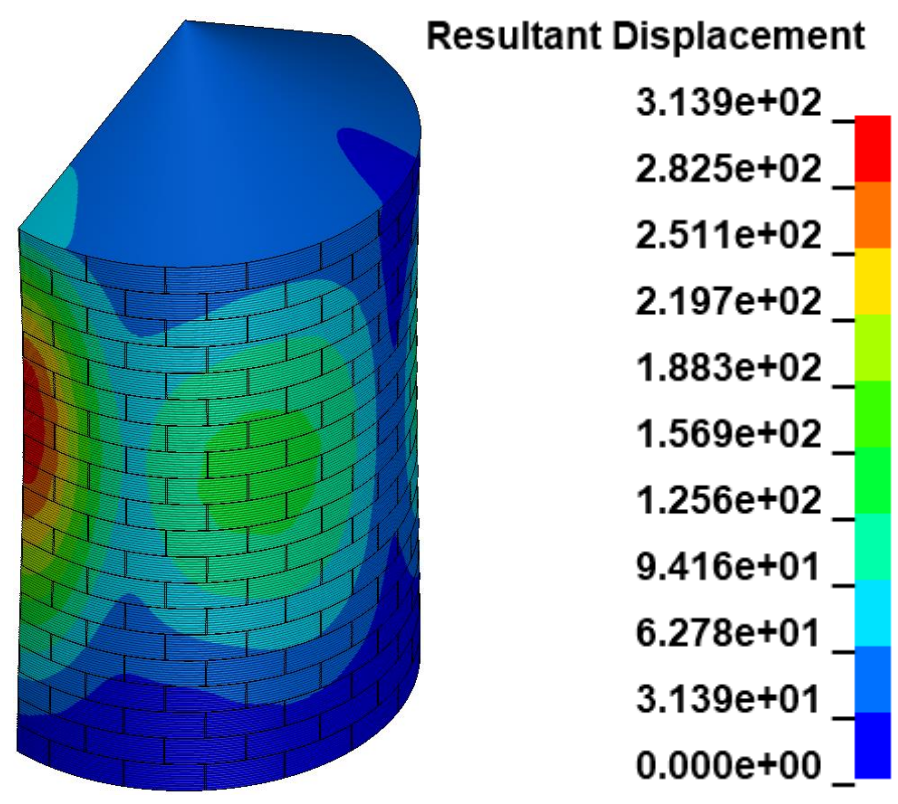
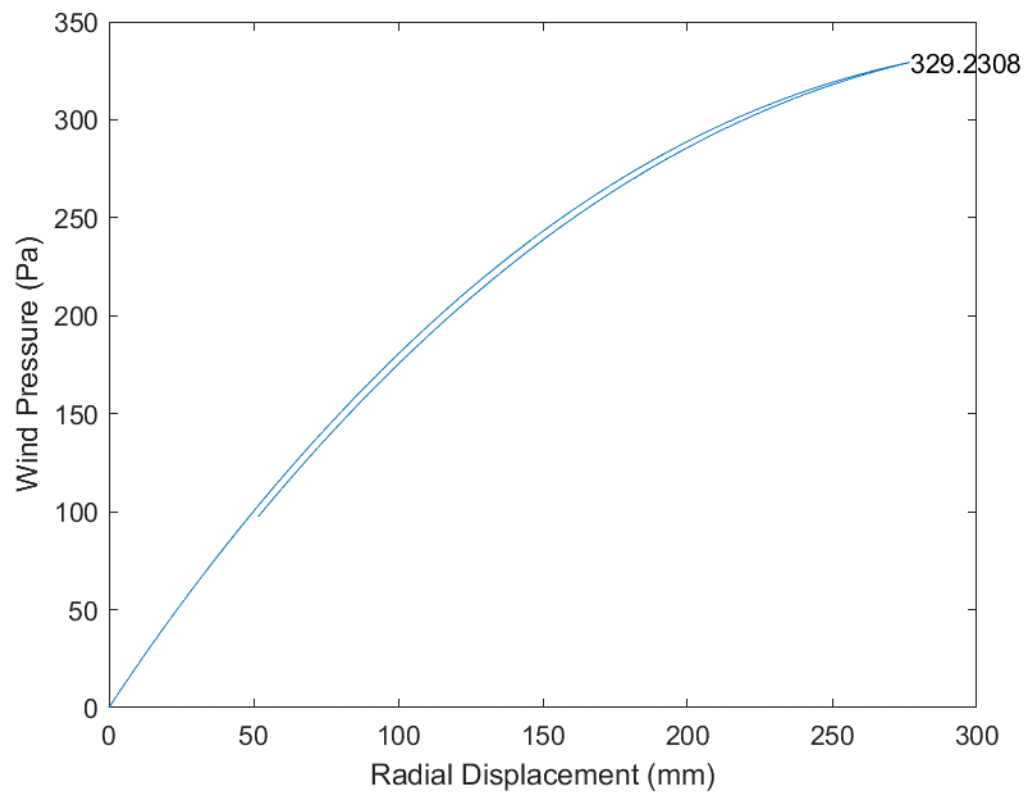


Fig. B.125 D54_H20_S00_R00_W00_V00_CL03_CD03_WT03_ST03

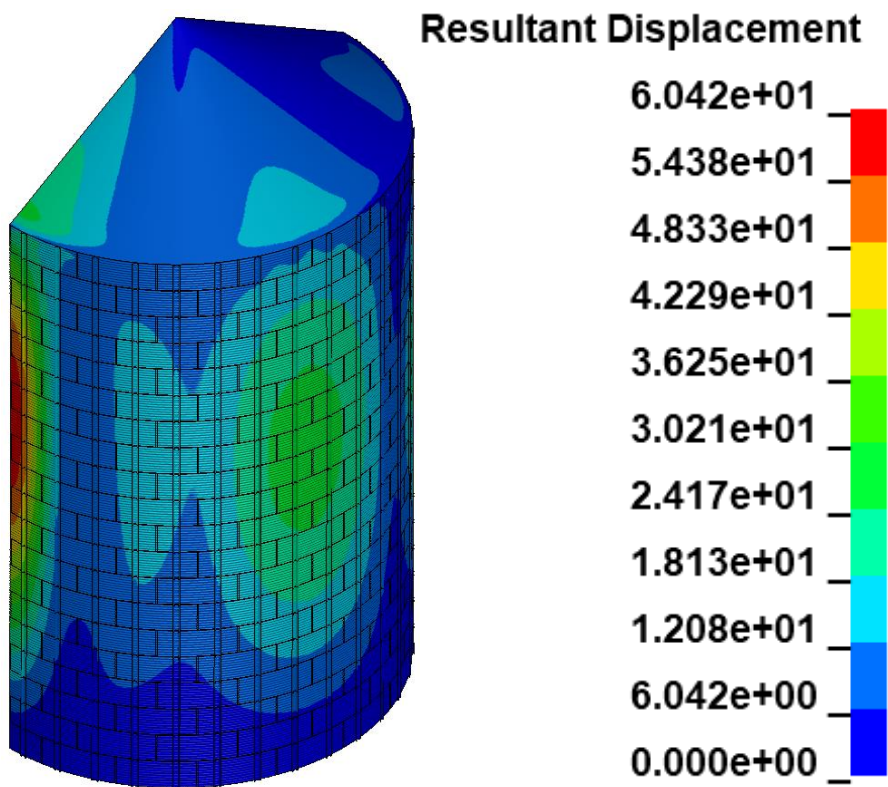
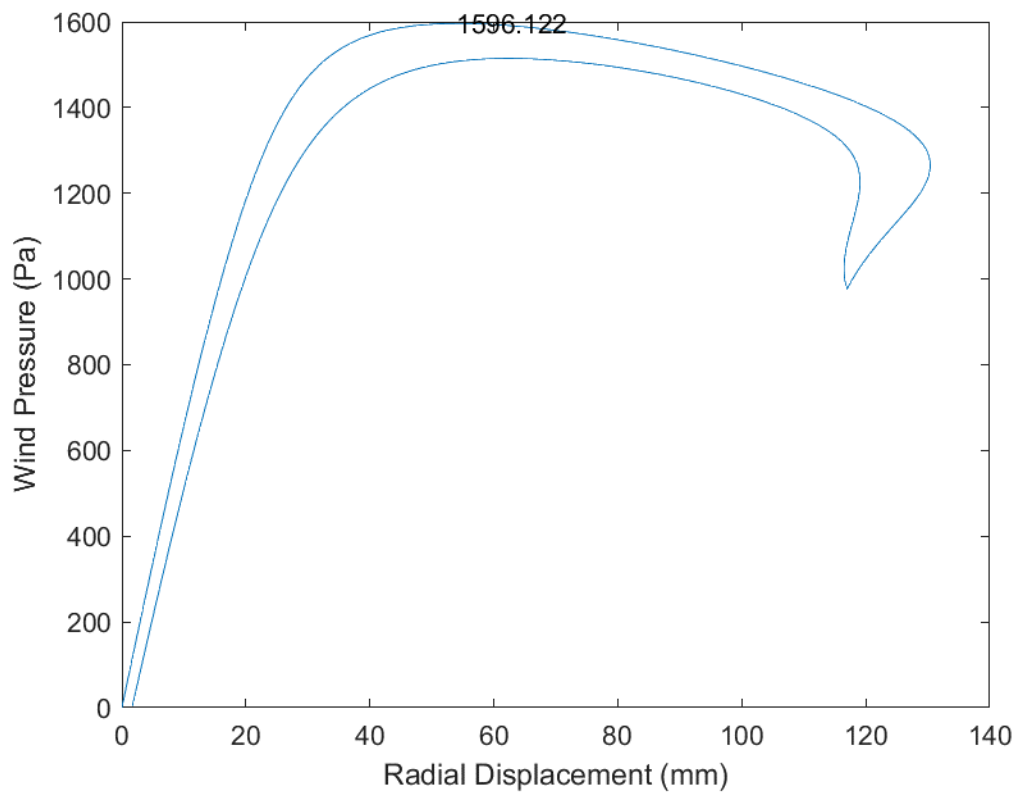


Fig. B.126 D54_H20_S36_R00_W00_V00_CL03_CD03_WT03_ST03

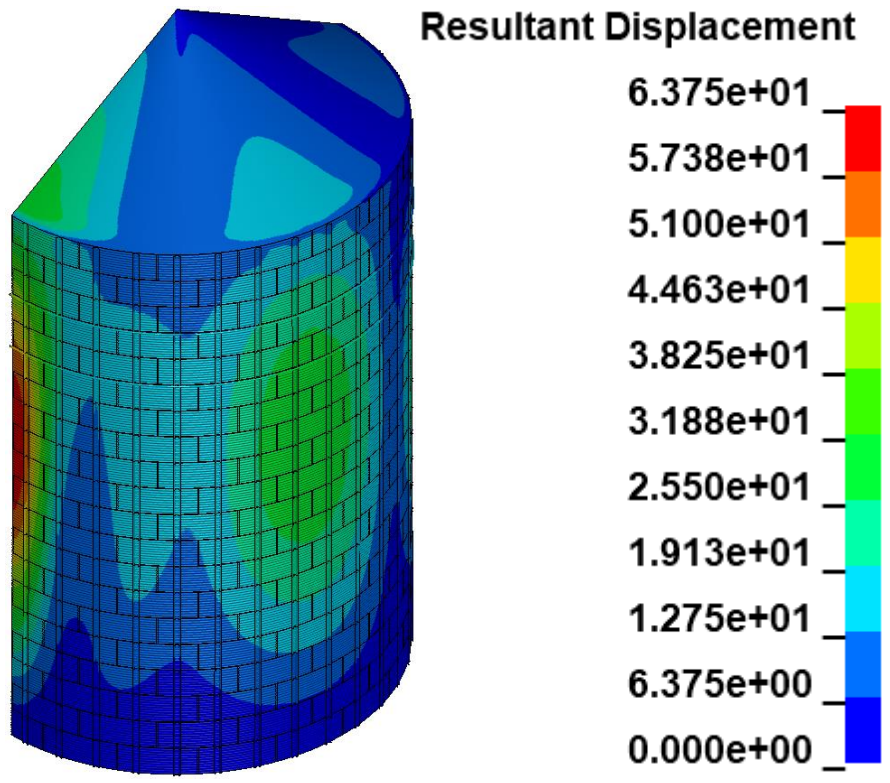
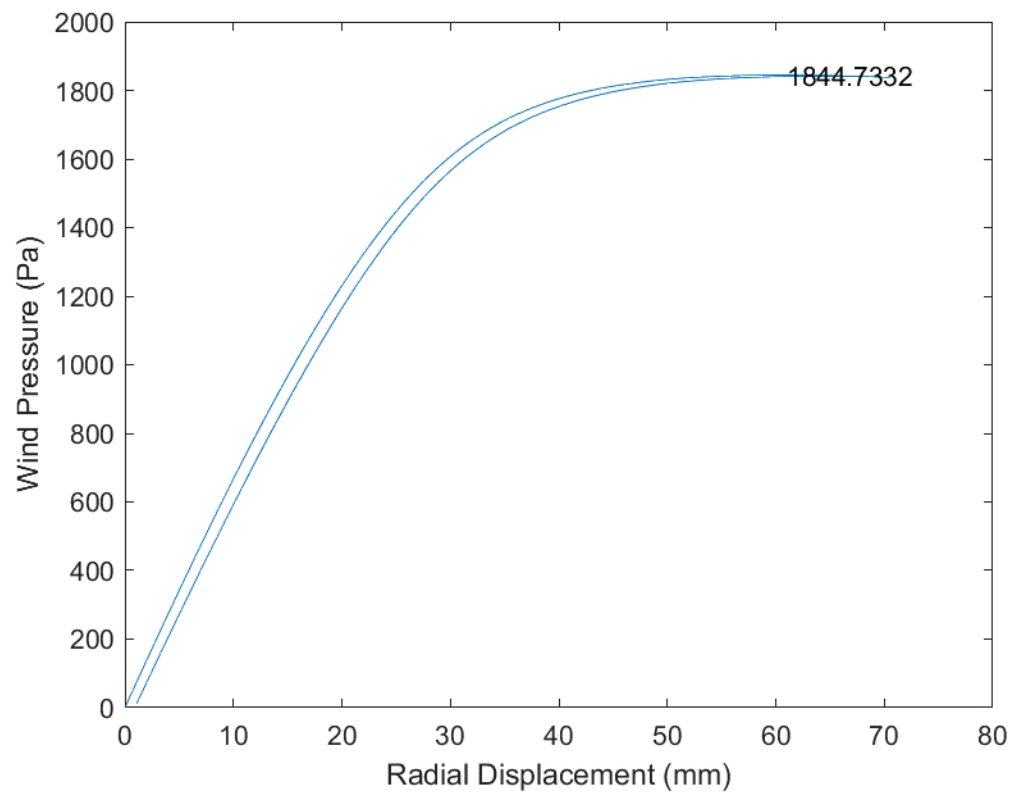


Fig. B.127 D54_H20_S36_R02_W00_V00_CL03_CD03_WT03_ST03

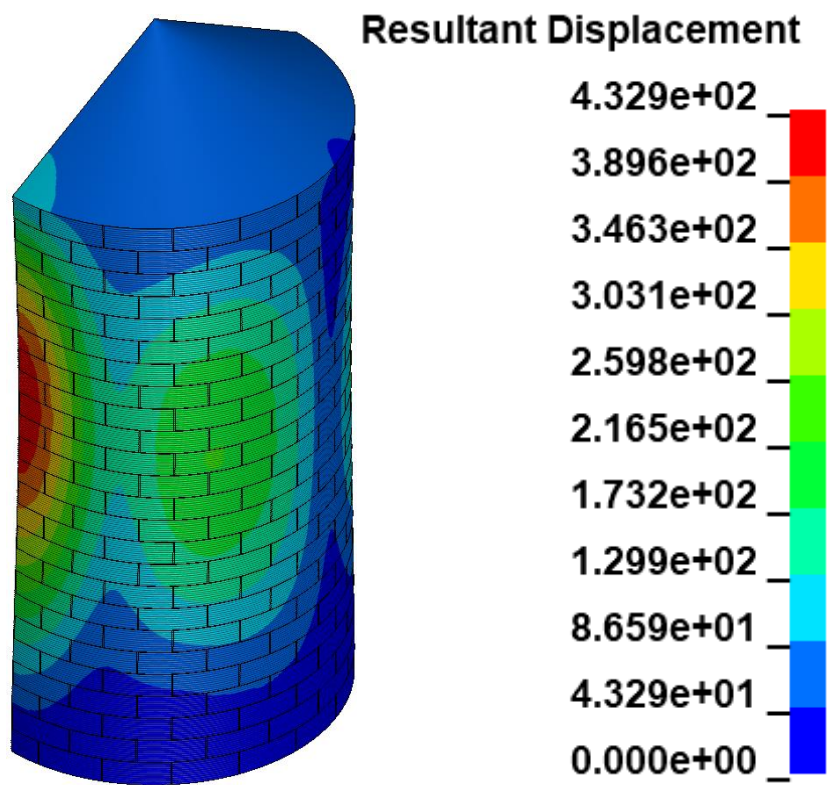
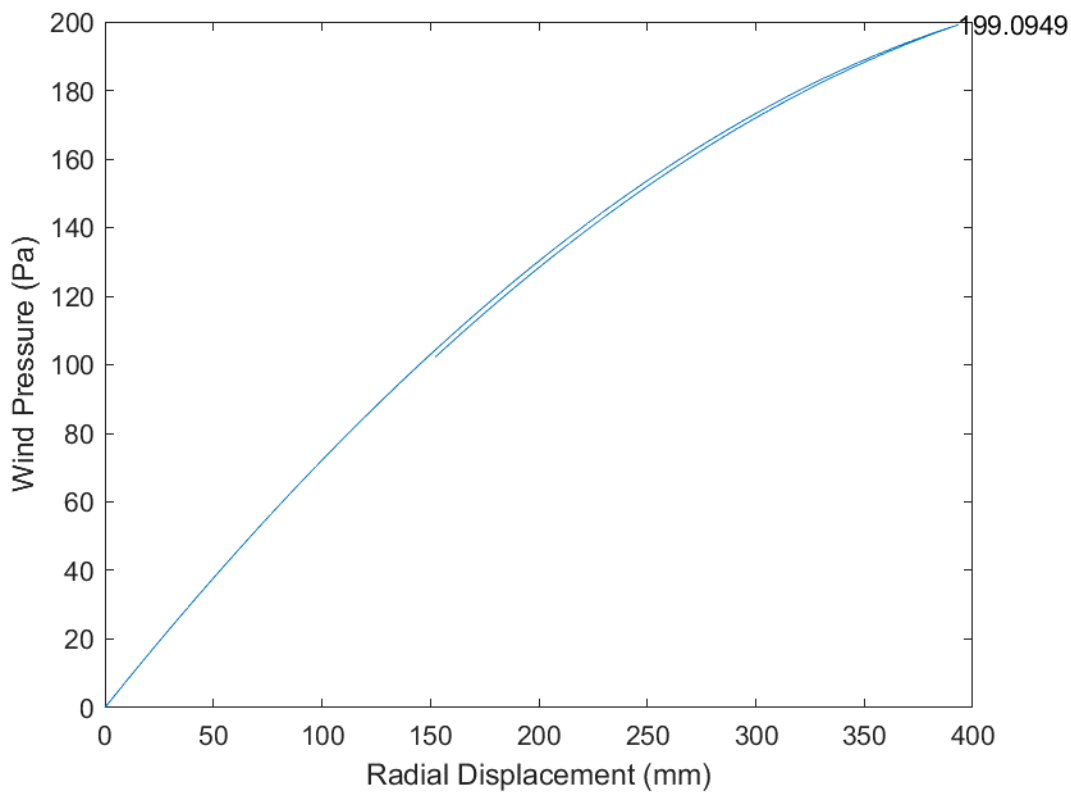


Fig. B.128 D54_H25_S00_R00_W00_V00_CL03_CD03_WT03_ST03

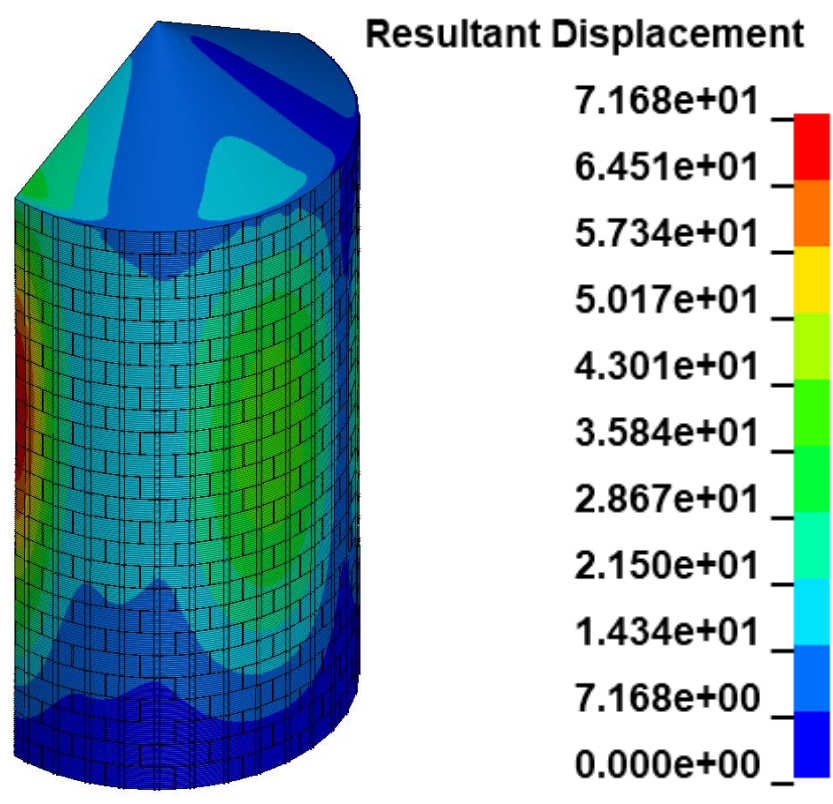
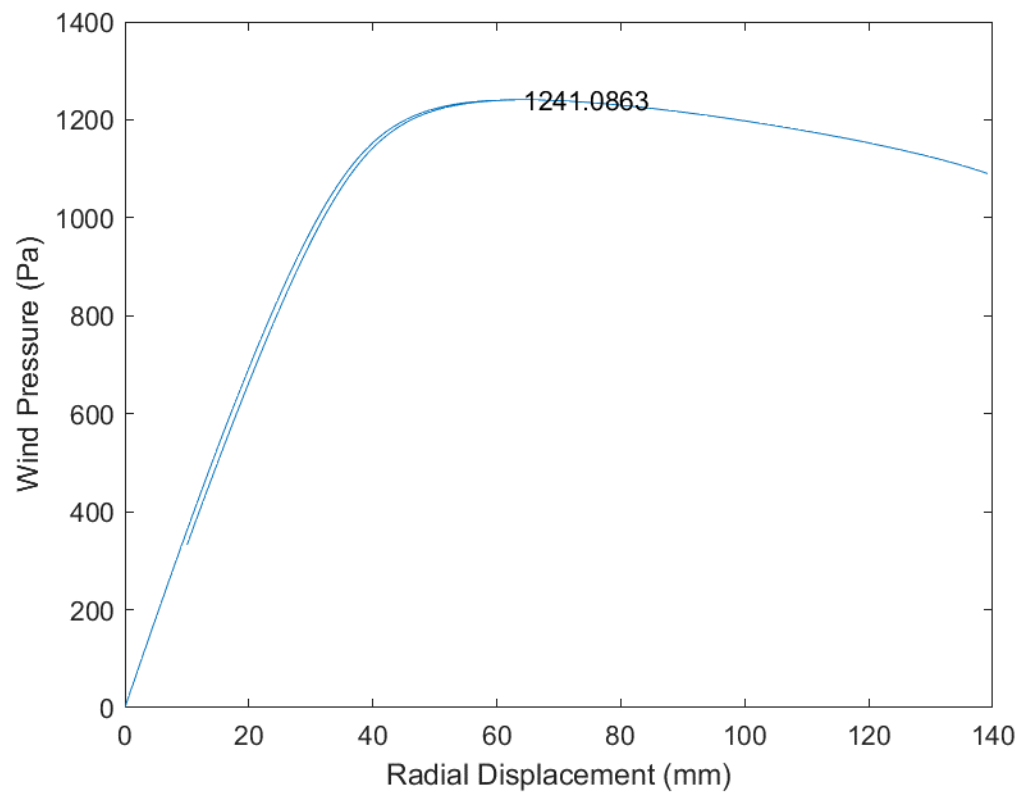


Fig. B.129 D54_H25_S36_R00_W00_V00_CL03_CD03_WT03_ST03

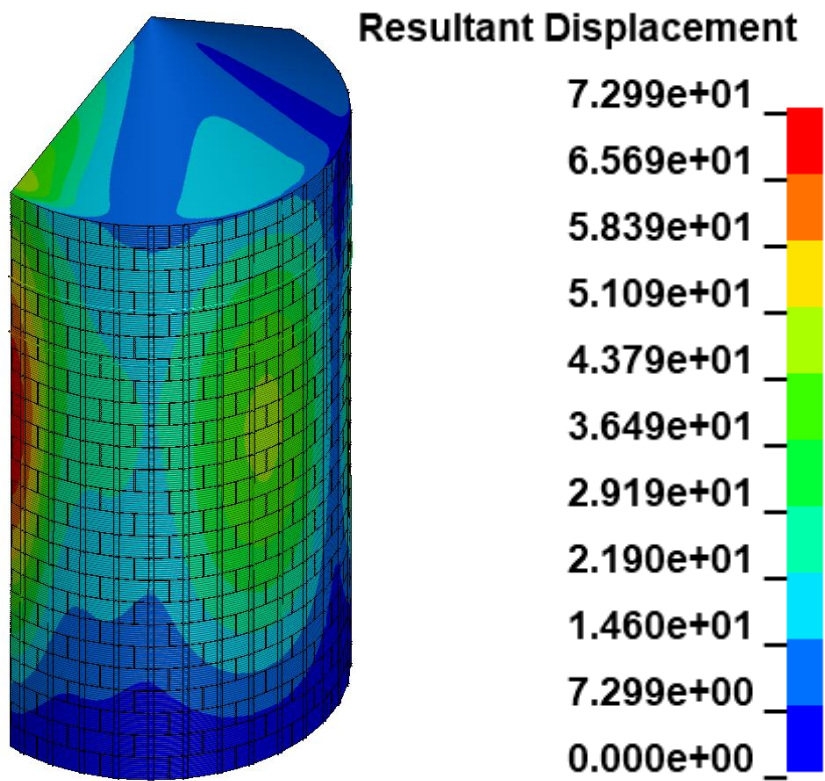
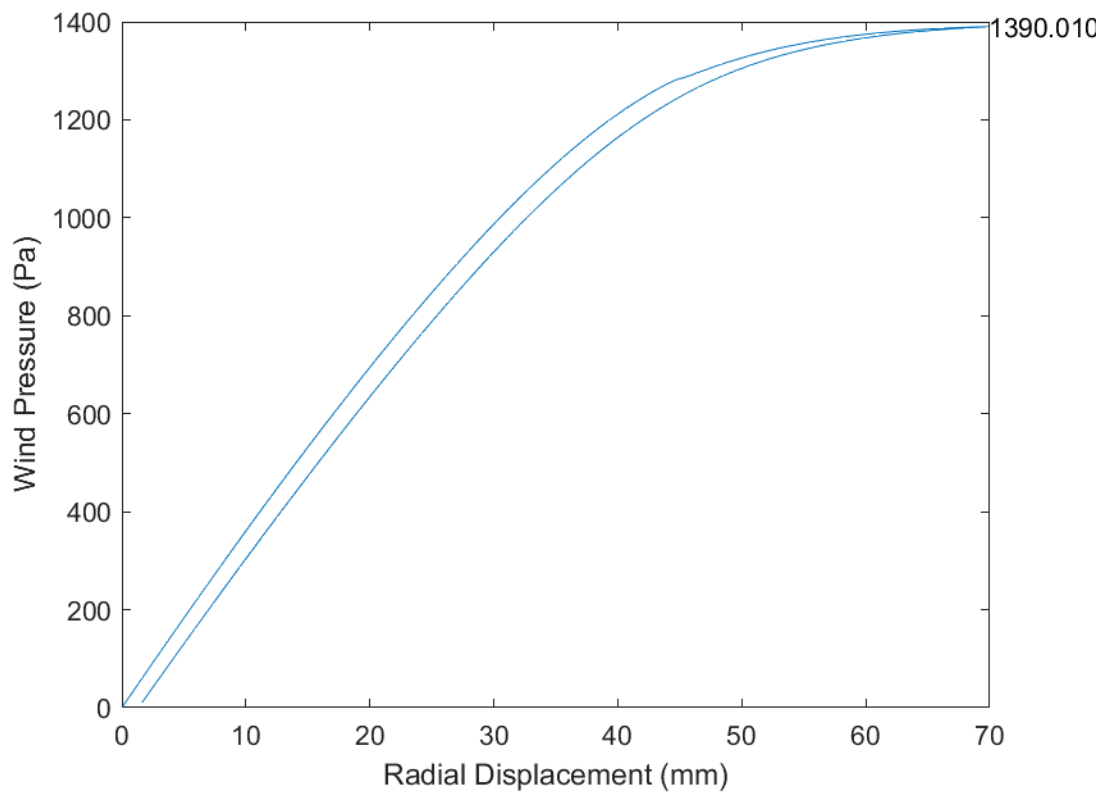


Fig. B.130 D54_H25_S36_R02_W00_V00_CL03_CD03_WT03_ST03

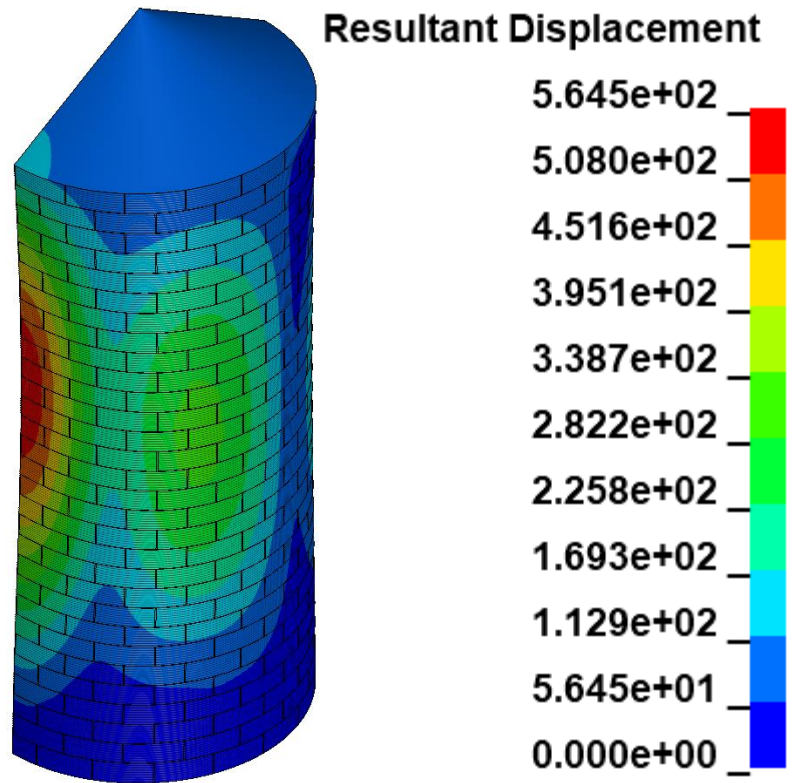
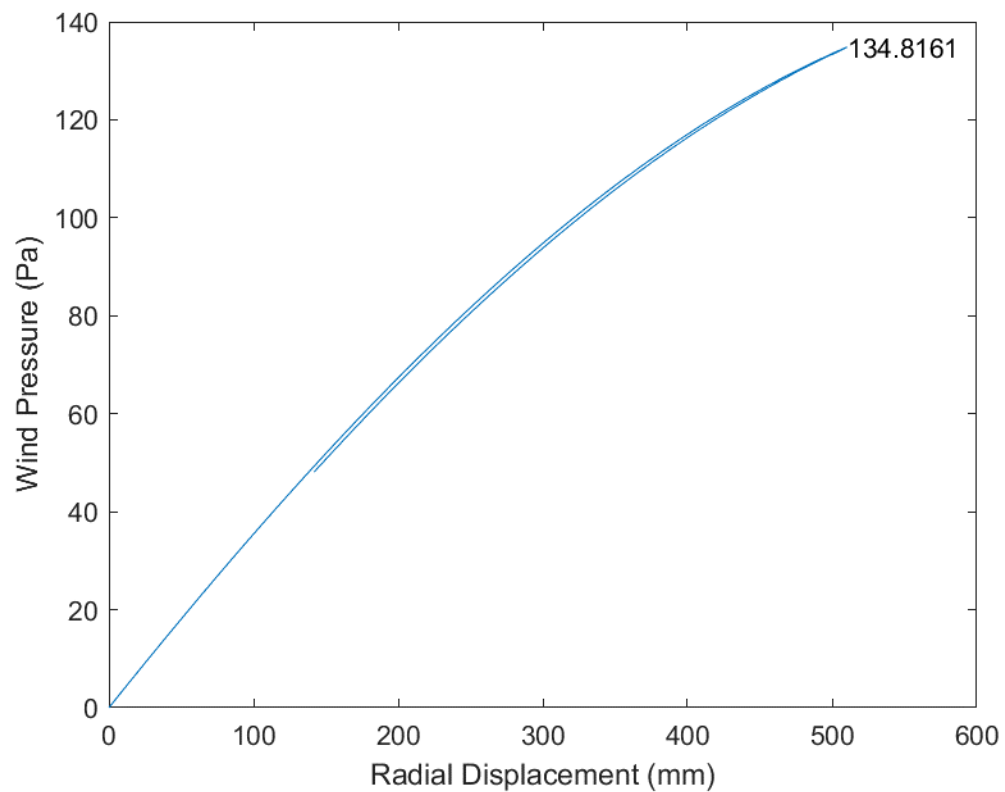


Fig. B.131 D54_H30_S00_R00_W00_V00_CL03_CD03_WT03_ST03

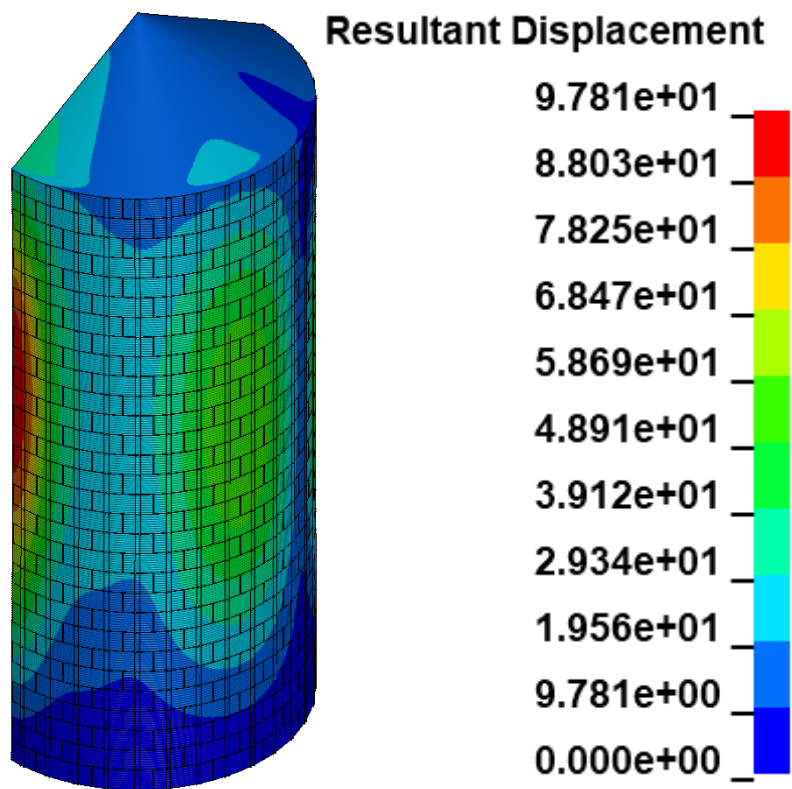
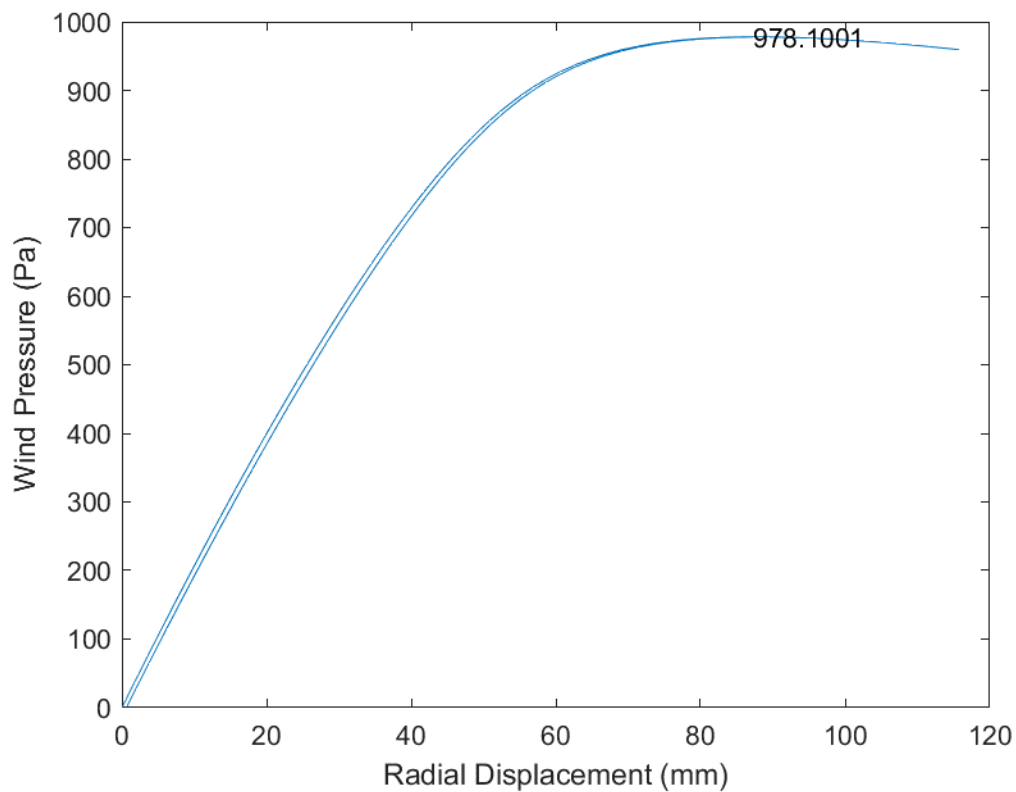


Fig. B.132 D54_H30_S36_R00_W00_V00_CL03_CD03_WT03_ST03

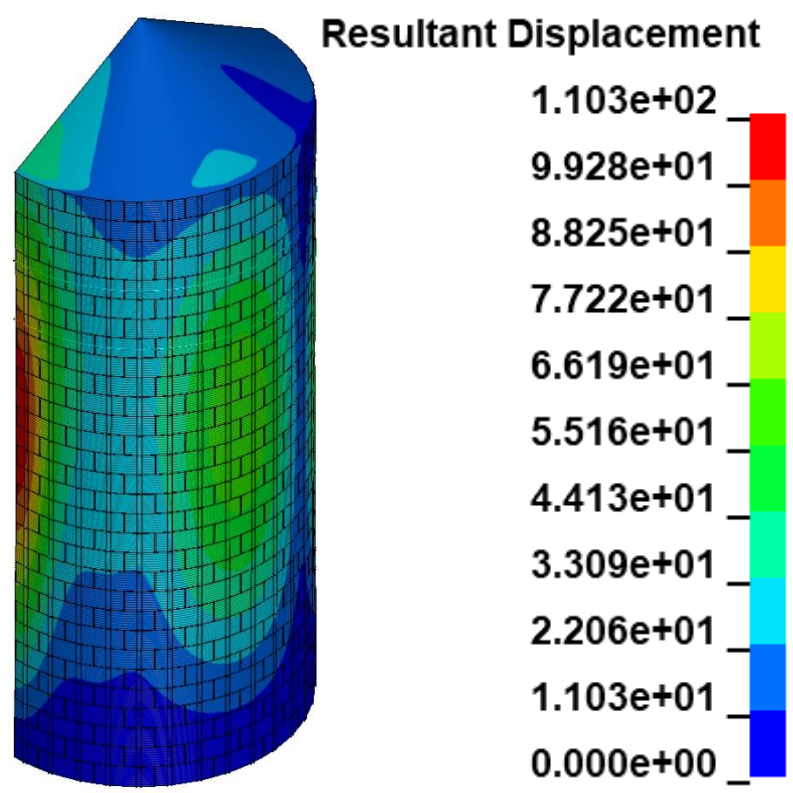
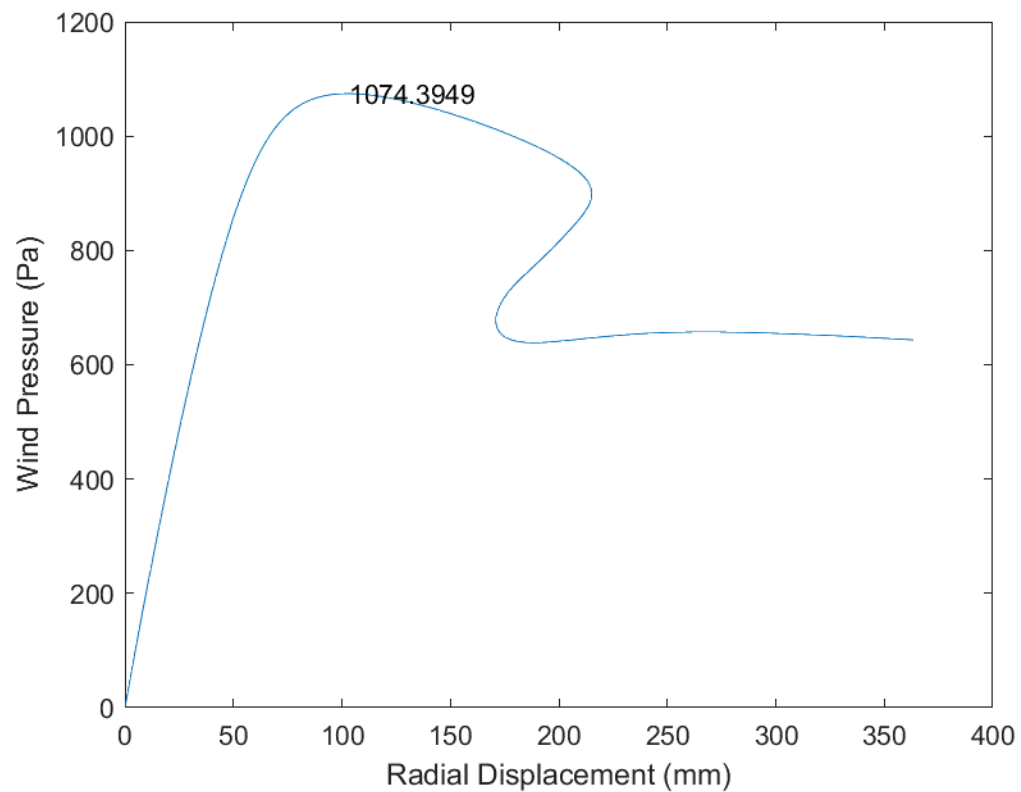


Fig. B.133 D54_H30_S36_R02_W00_V00_CL03_CD03_WT03_ST03

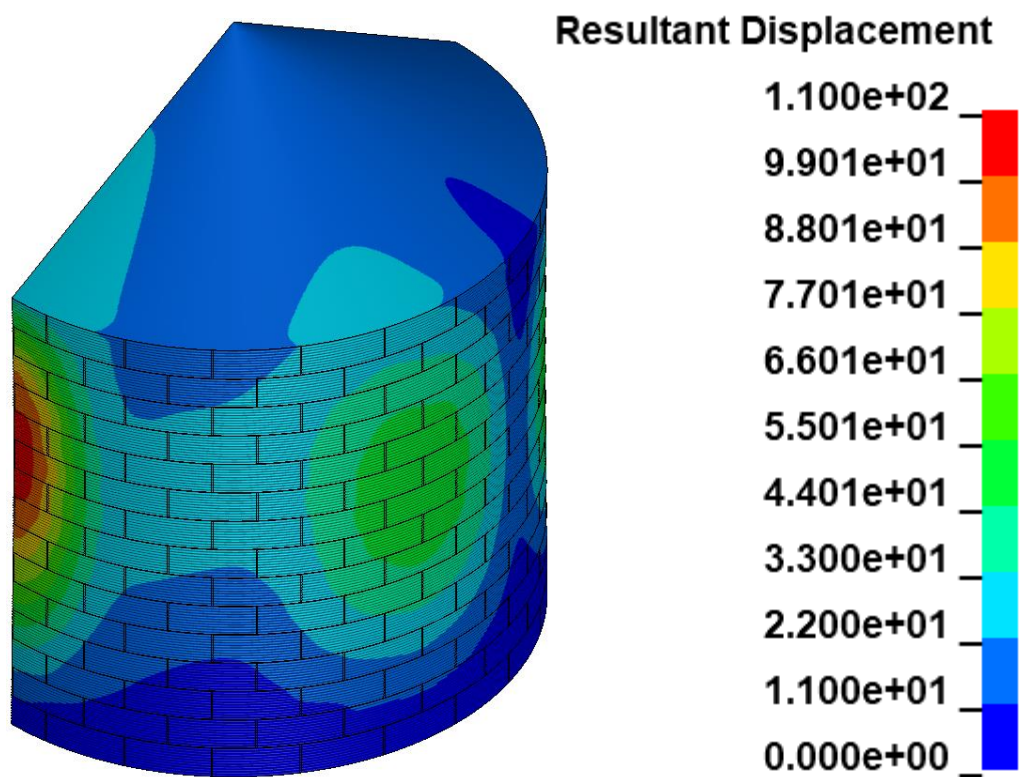
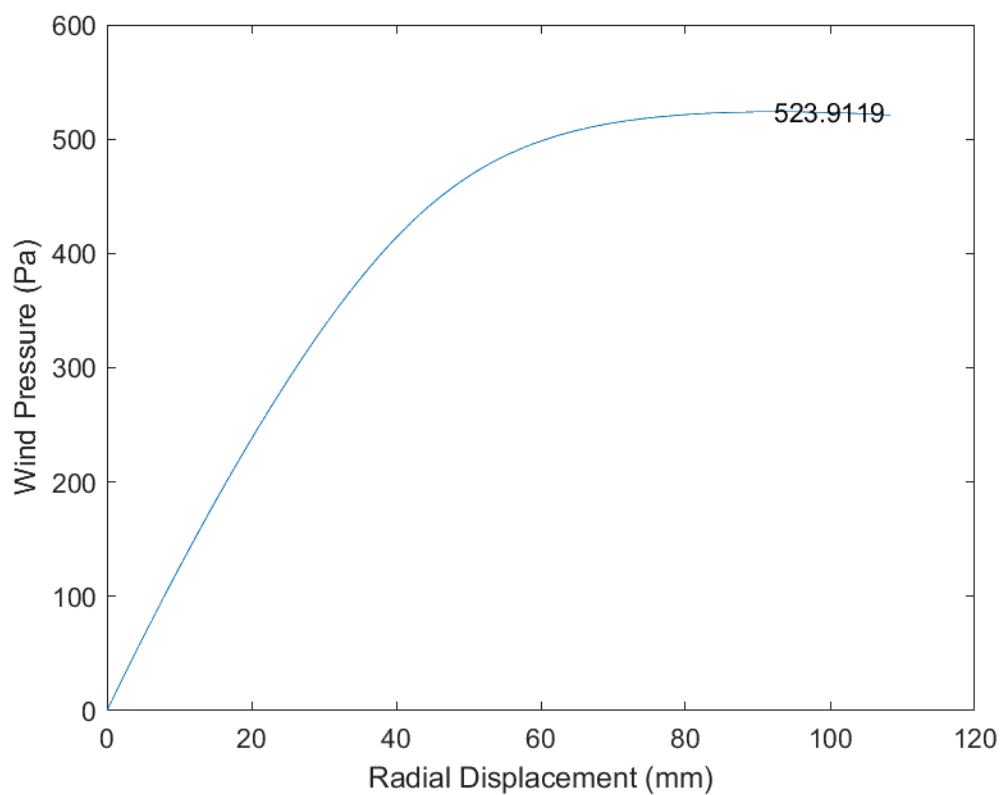


Fig. B.134 D66_H15_S00_R00_W00_V00_CL03_CD03_WT03_ST03

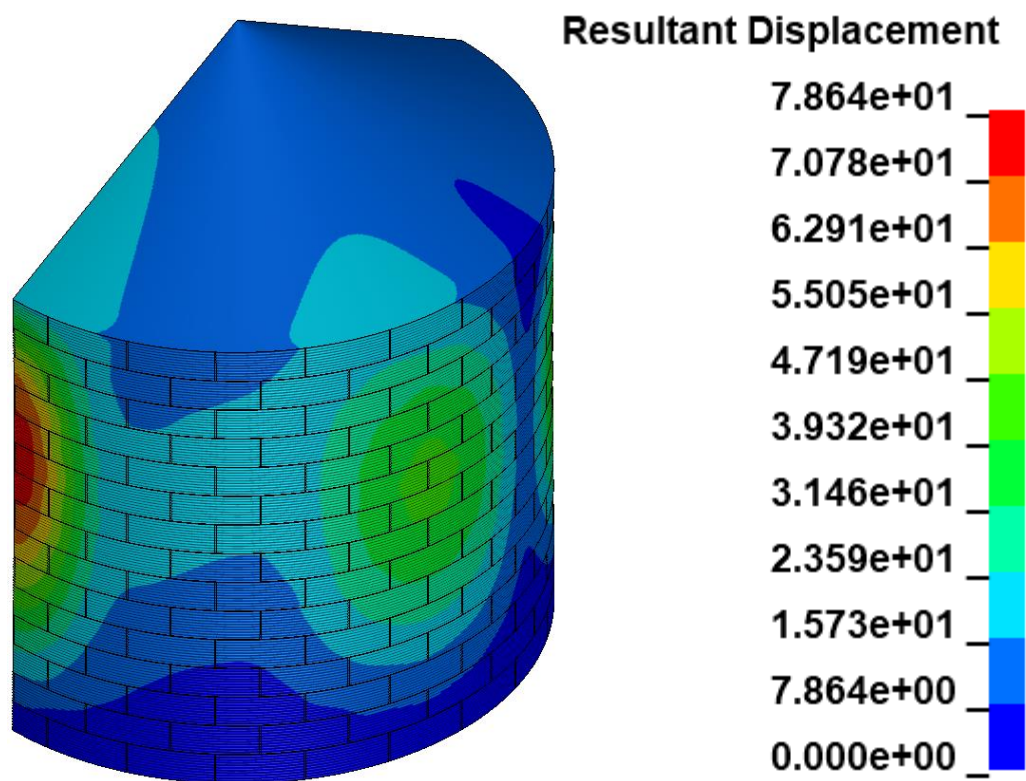
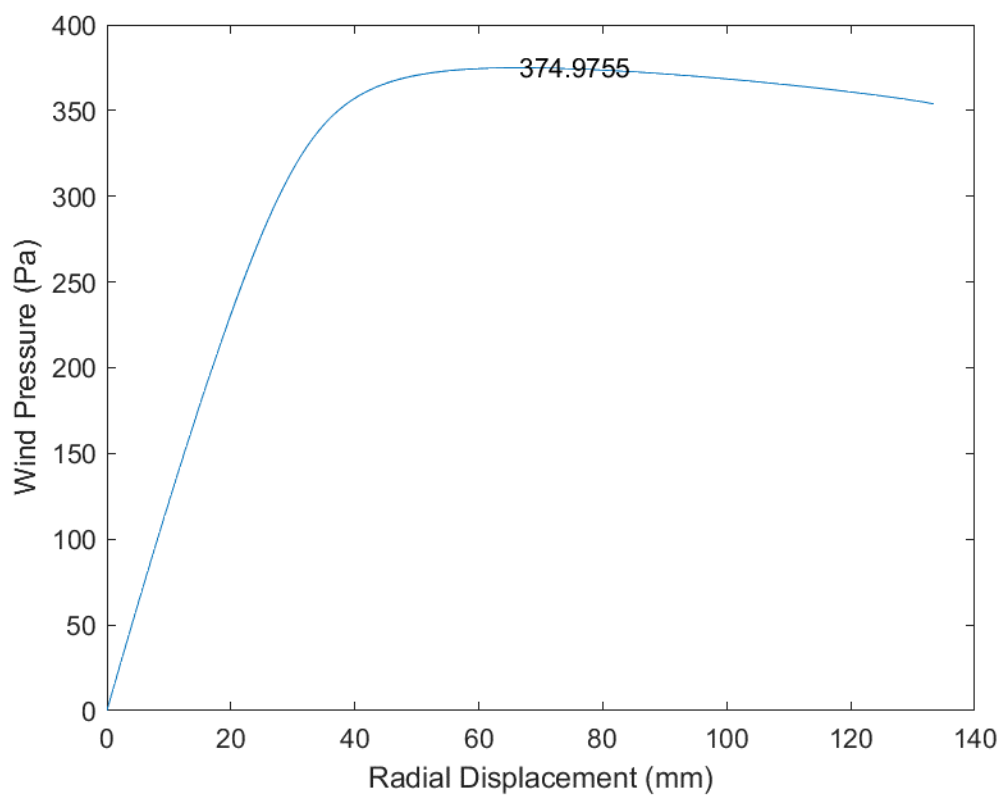


Fig. B.135 D66_H15_S00_R00_W00_V01_CL03_CD03_WT03_ST03

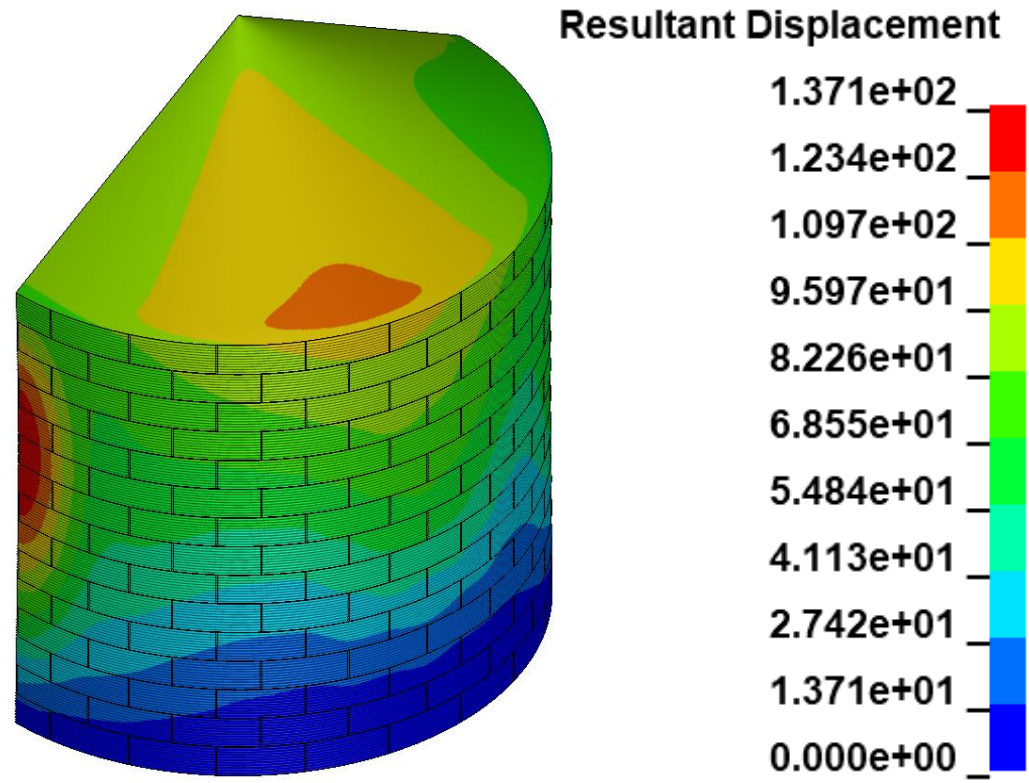
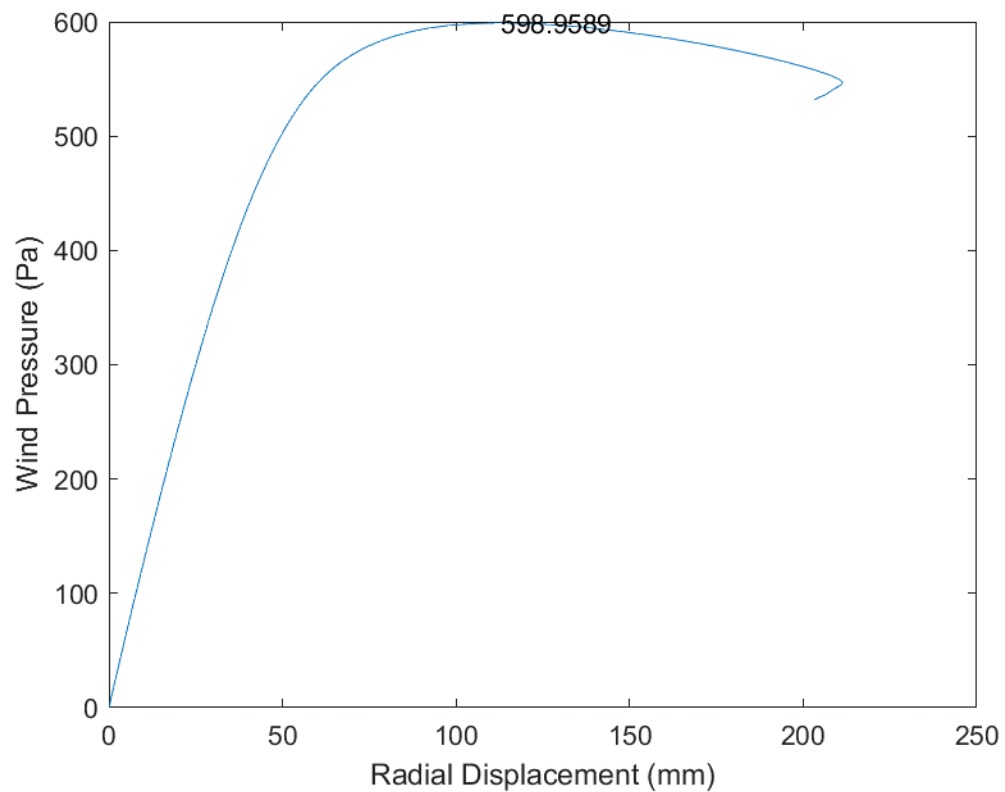


Fig. B.136 D66_H15_S00_R00_W01_V00_CL03_CD03_WT03_ST03

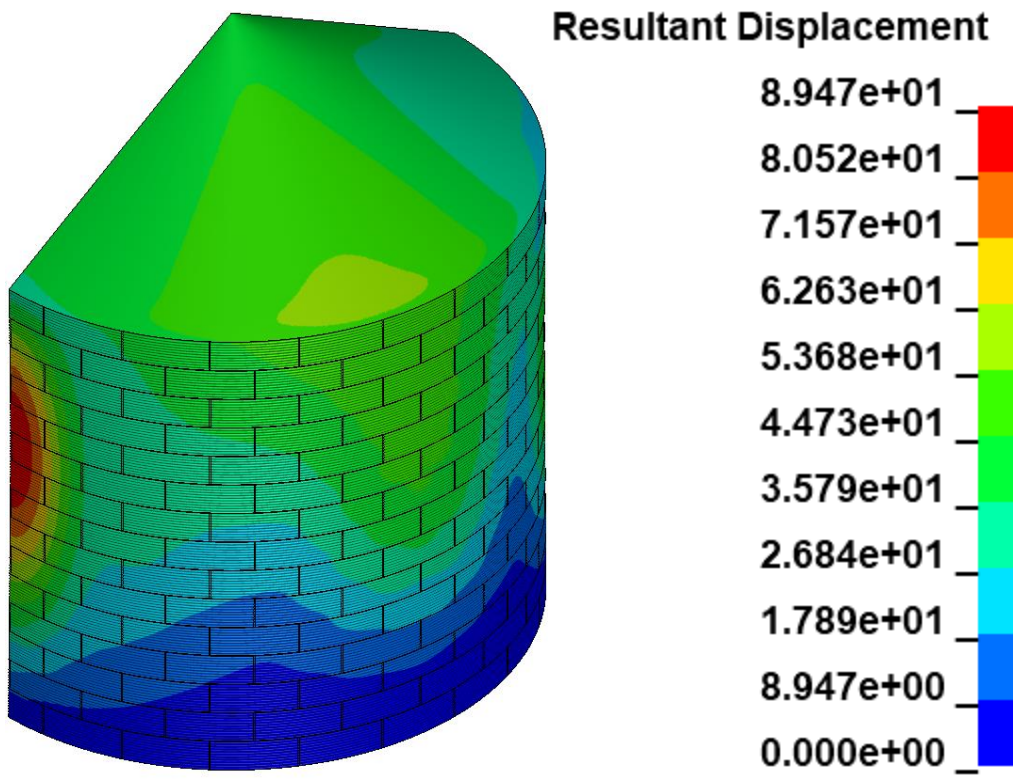
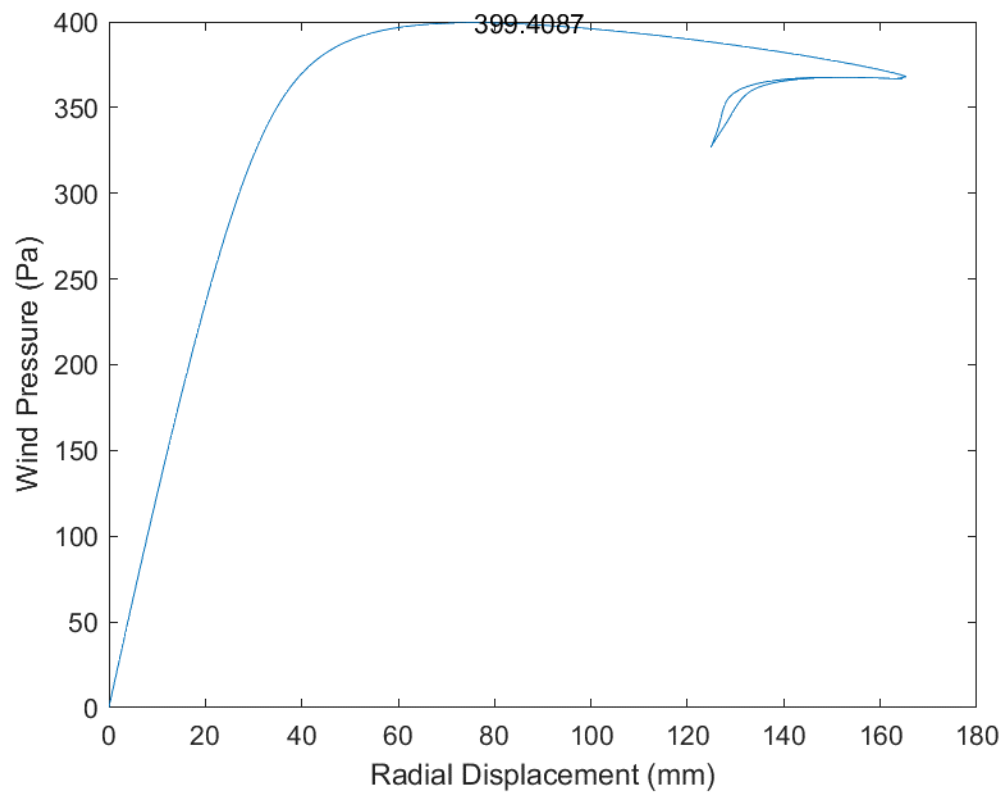


Fig. B.137 D66_H15_S00_R00_W01_V01_CL03_CD03_WT03_ST03

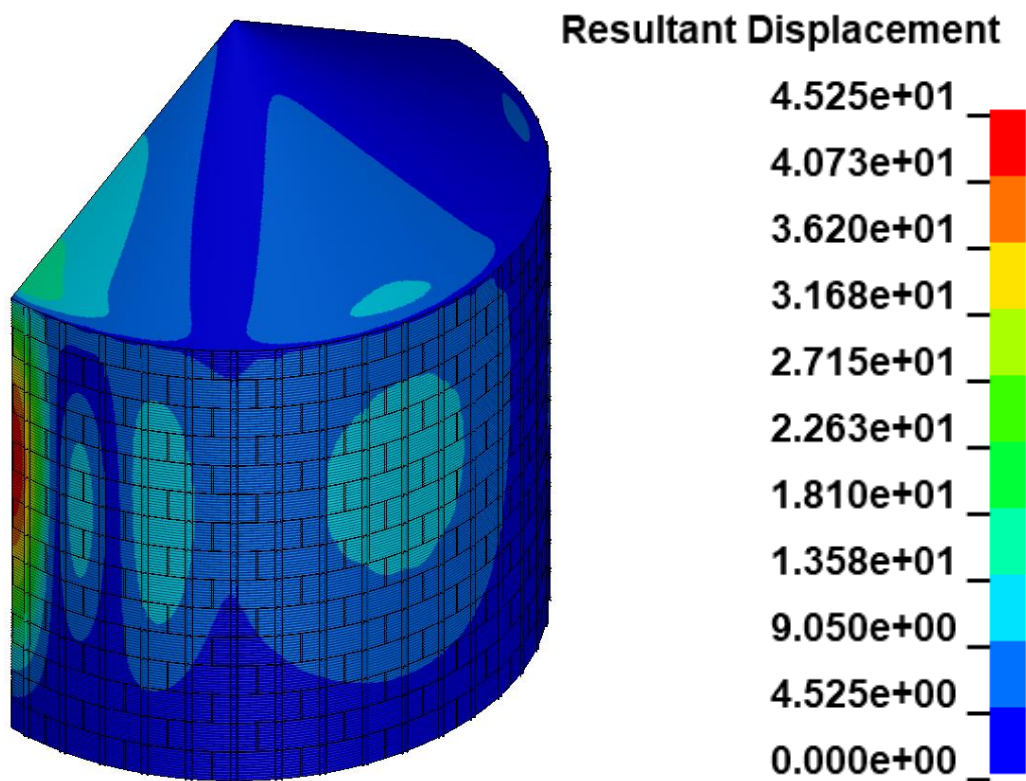
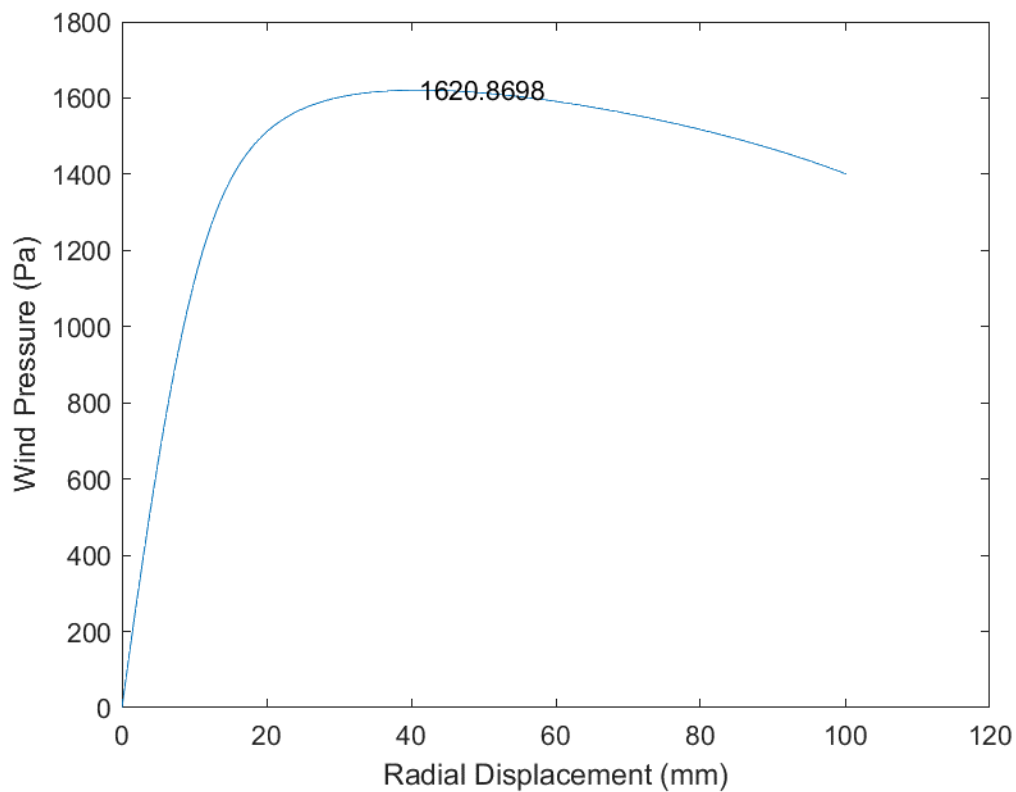


Fig. B.138 D66_H15_S44_R00_W00_V00_CL03_CD03_WT03_ST03

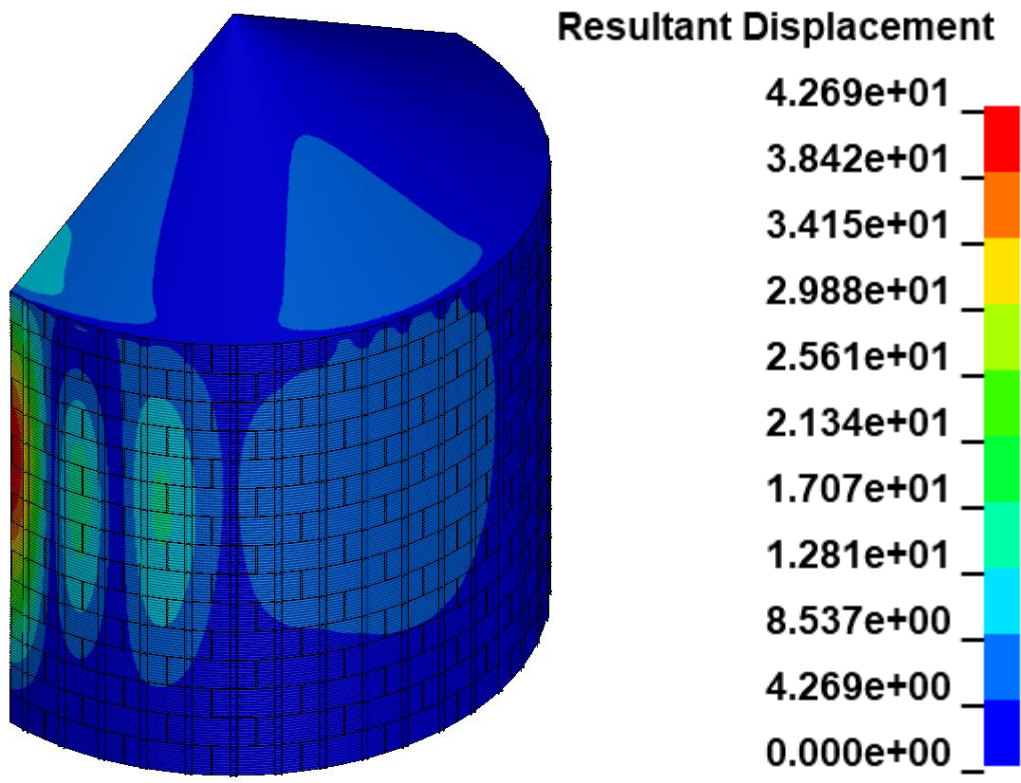
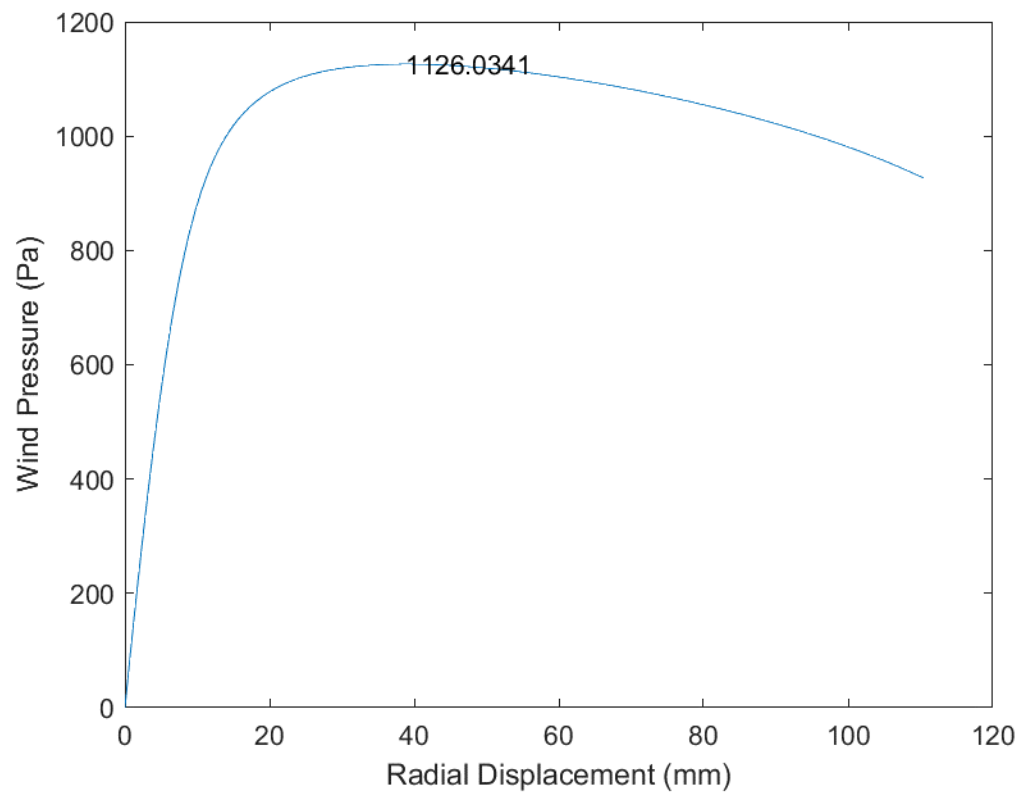


Fig. B.139 D66_H15_S44_R00_W00_V01_CL03_CD03_WT03_ST03

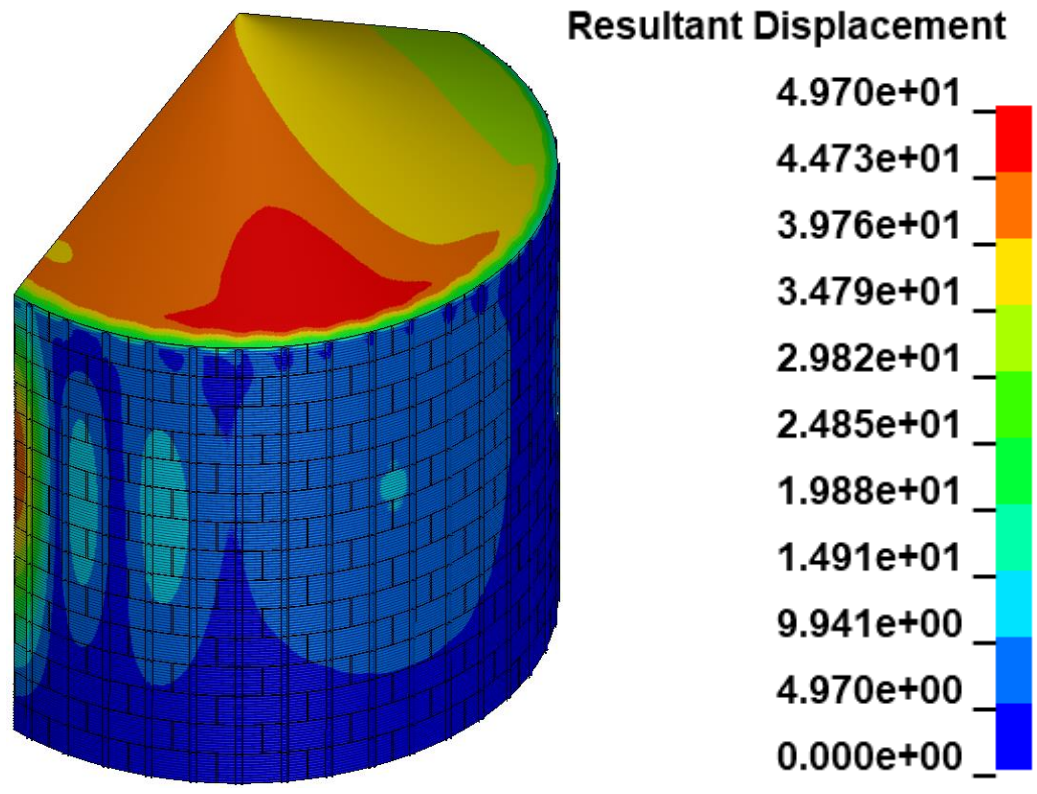
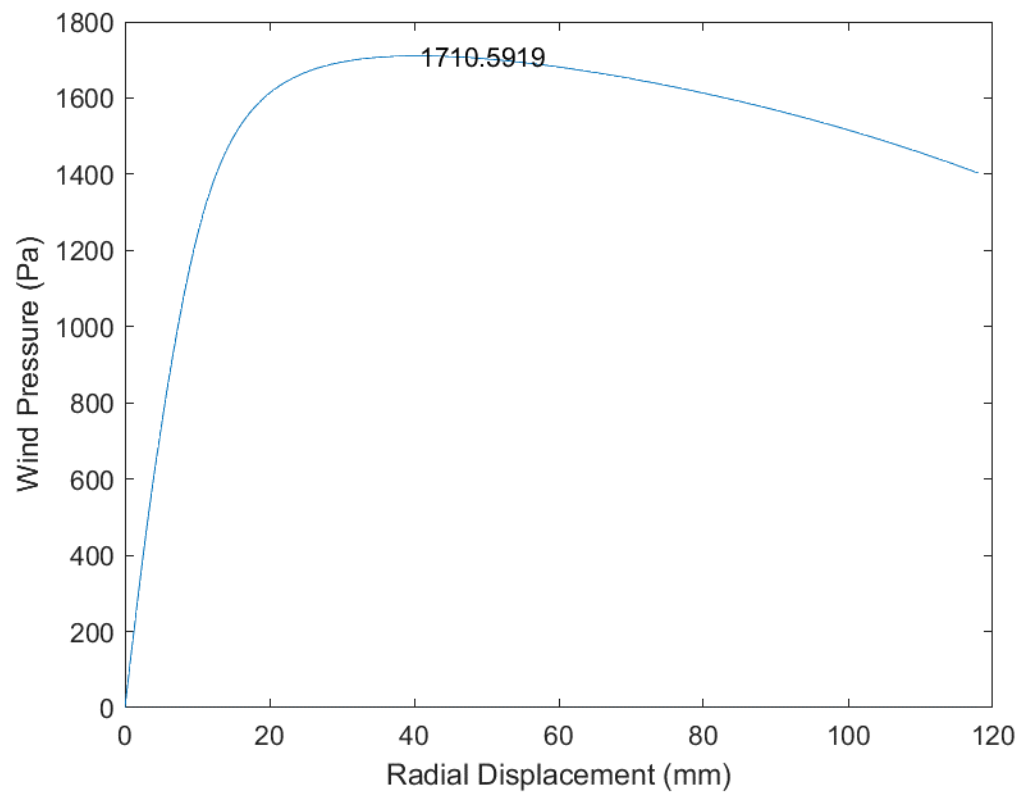


Fig. B.140 D66_H15_S44_R00_W01_V00_CL03_CD03_WT03_ST03

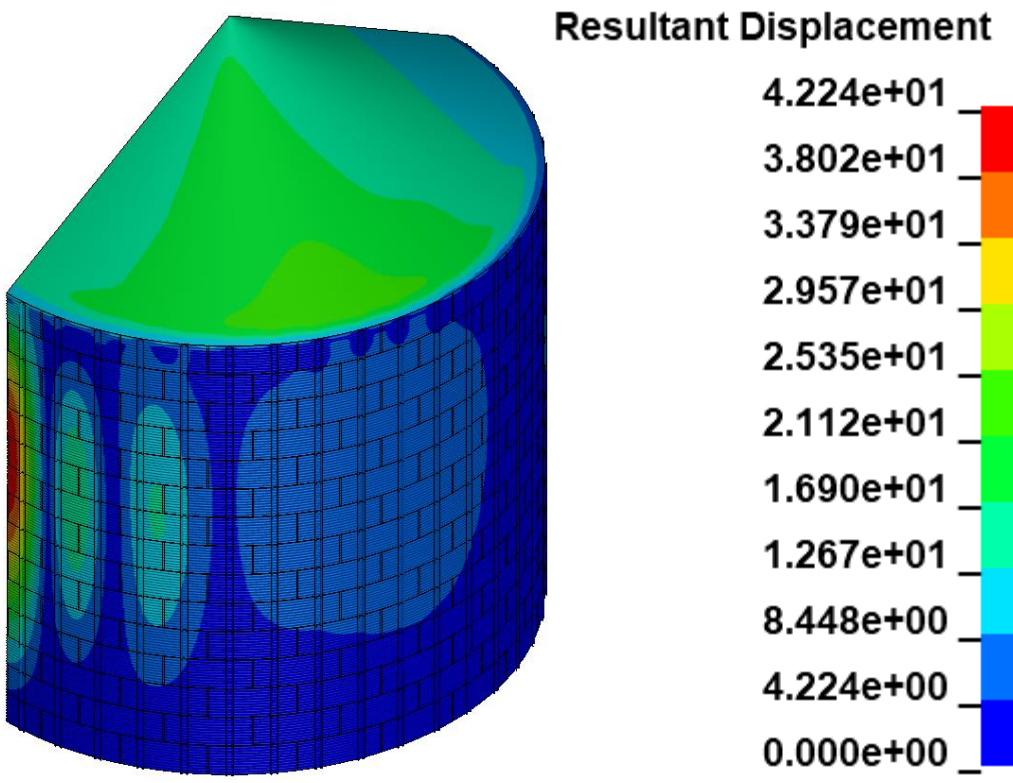
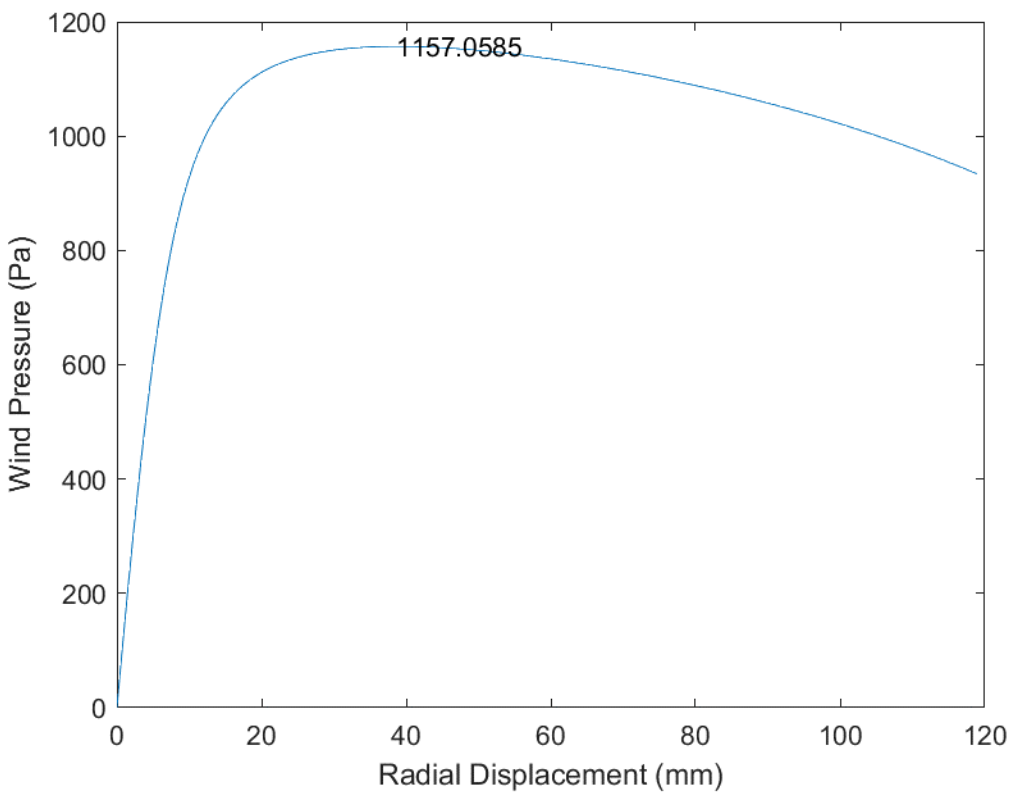


Fig. B.141 D66_H15_S44_R00_W01_V01_CL03_CD03_WT03_ST03

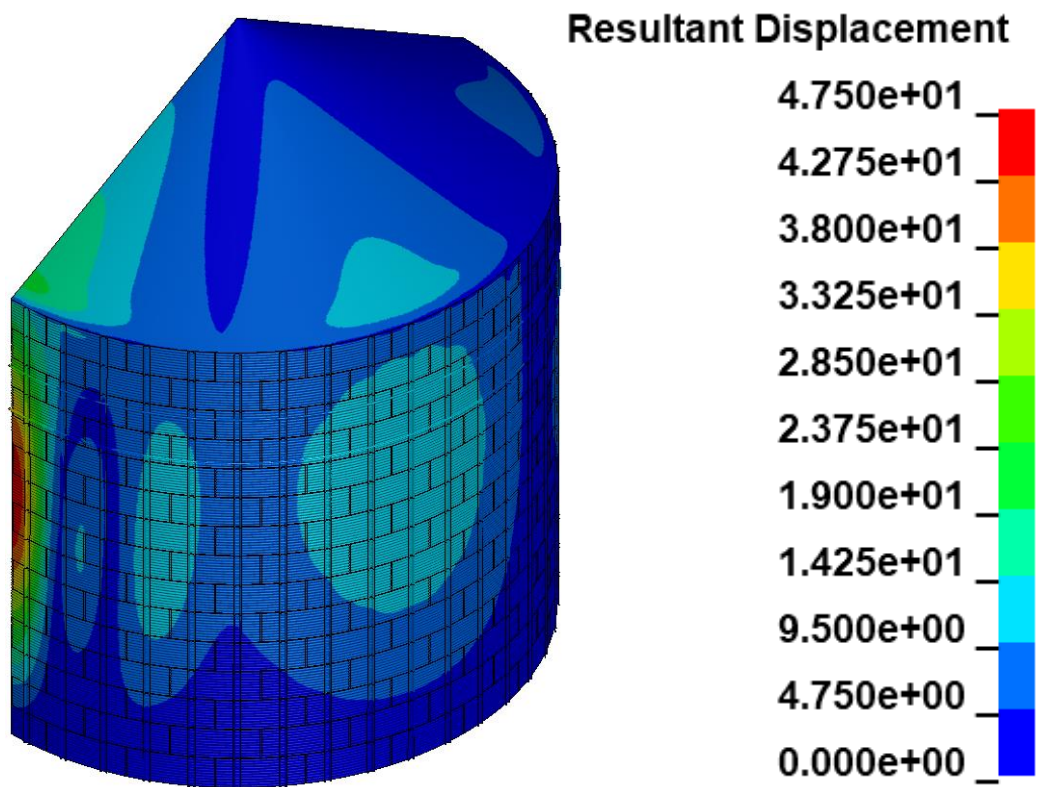
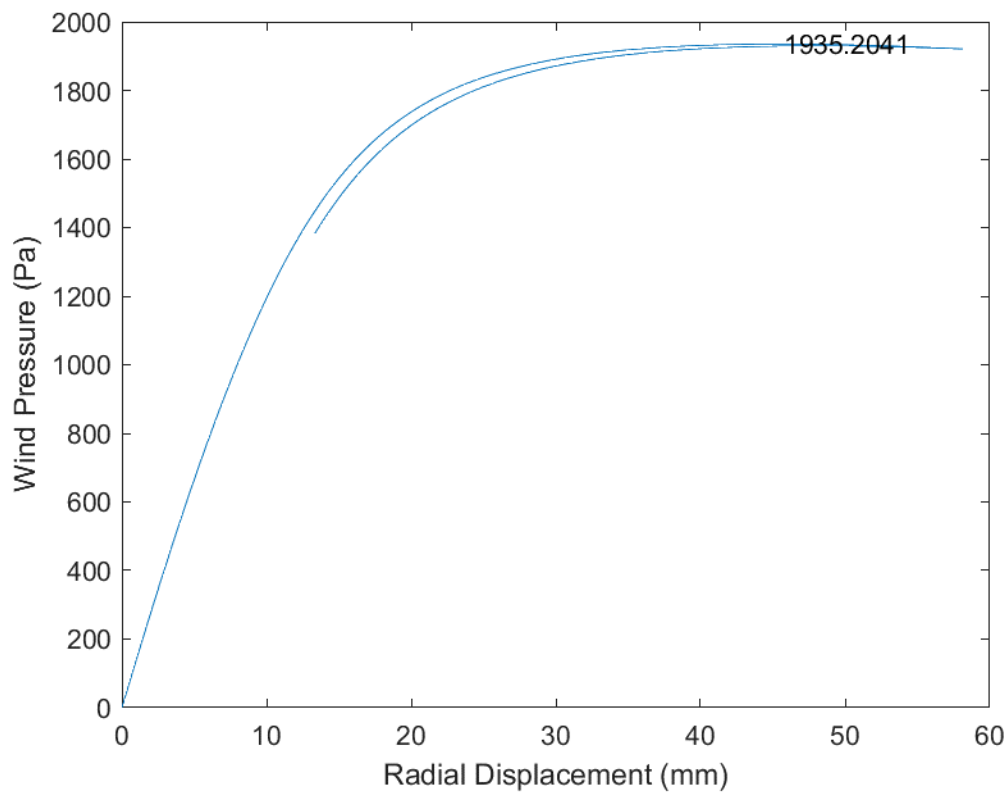


Fig. B.142 D66_H15_S44_R02_W00_V00_CL03_CD03_WT03_ST03

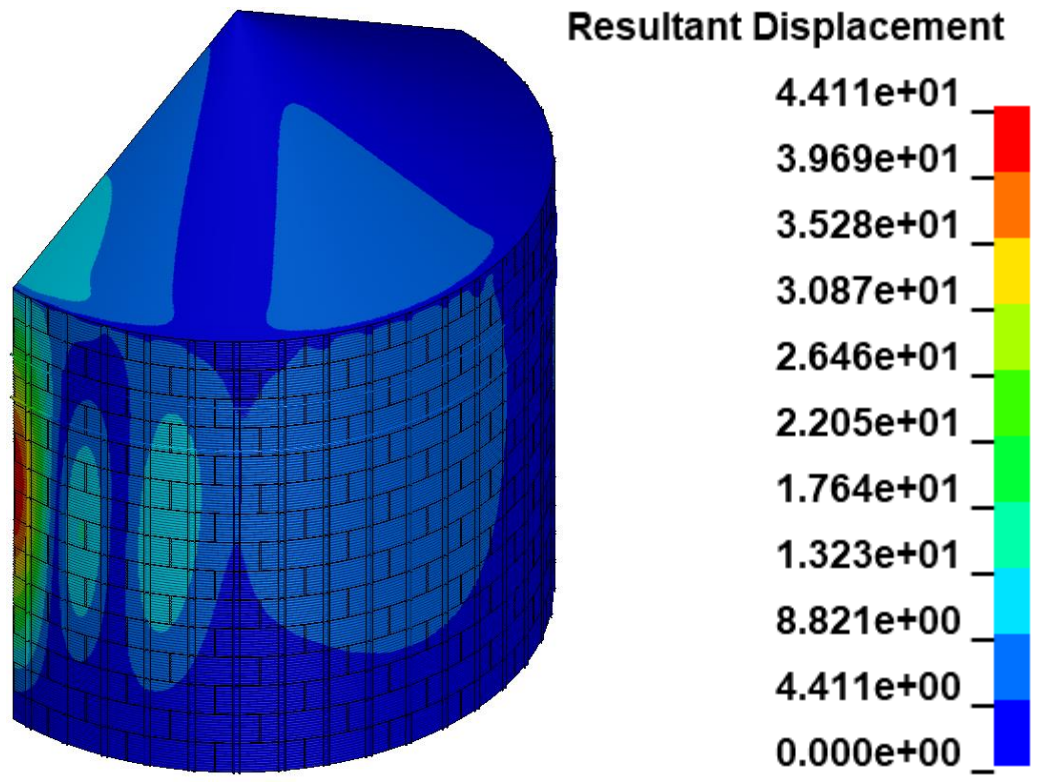
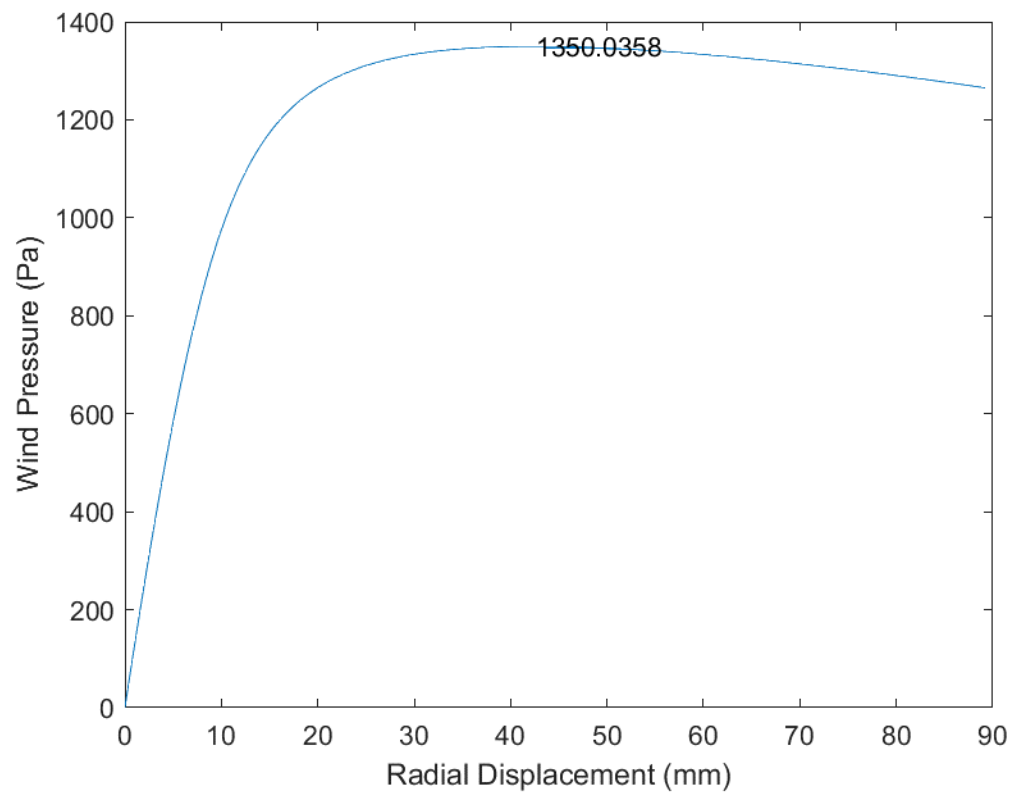


Fig. B.143 D66_H15_S44_R02_W00_V01_CL03_CD03_WT03_ST03

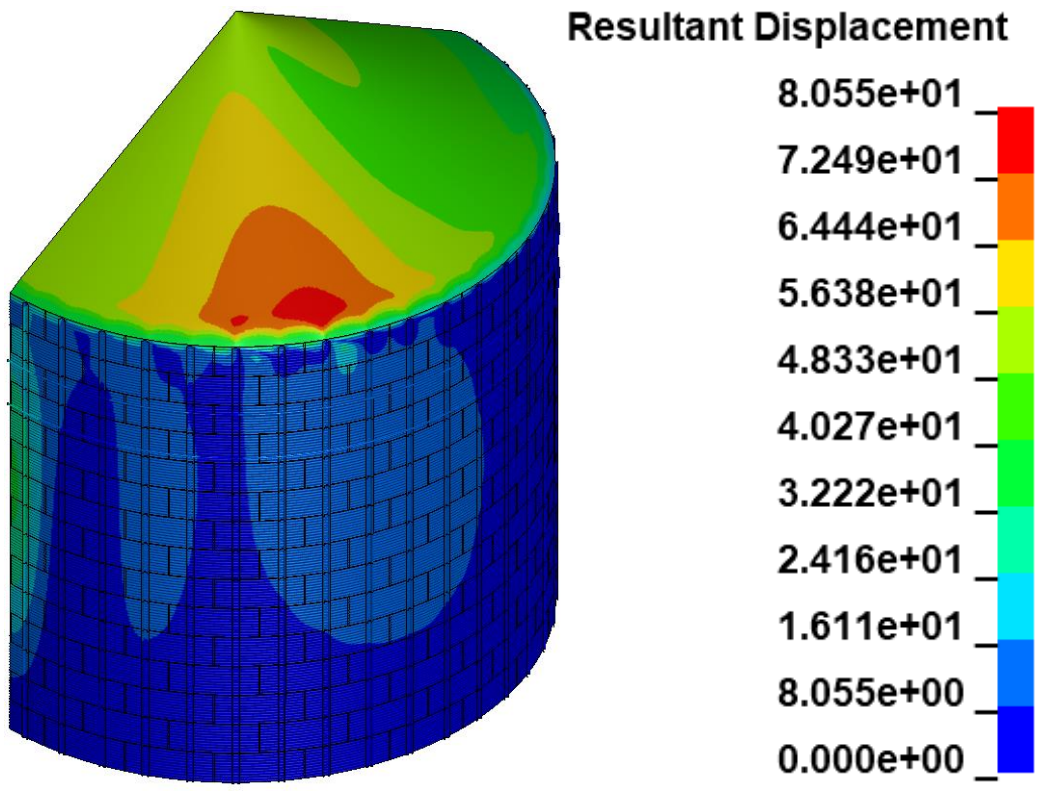
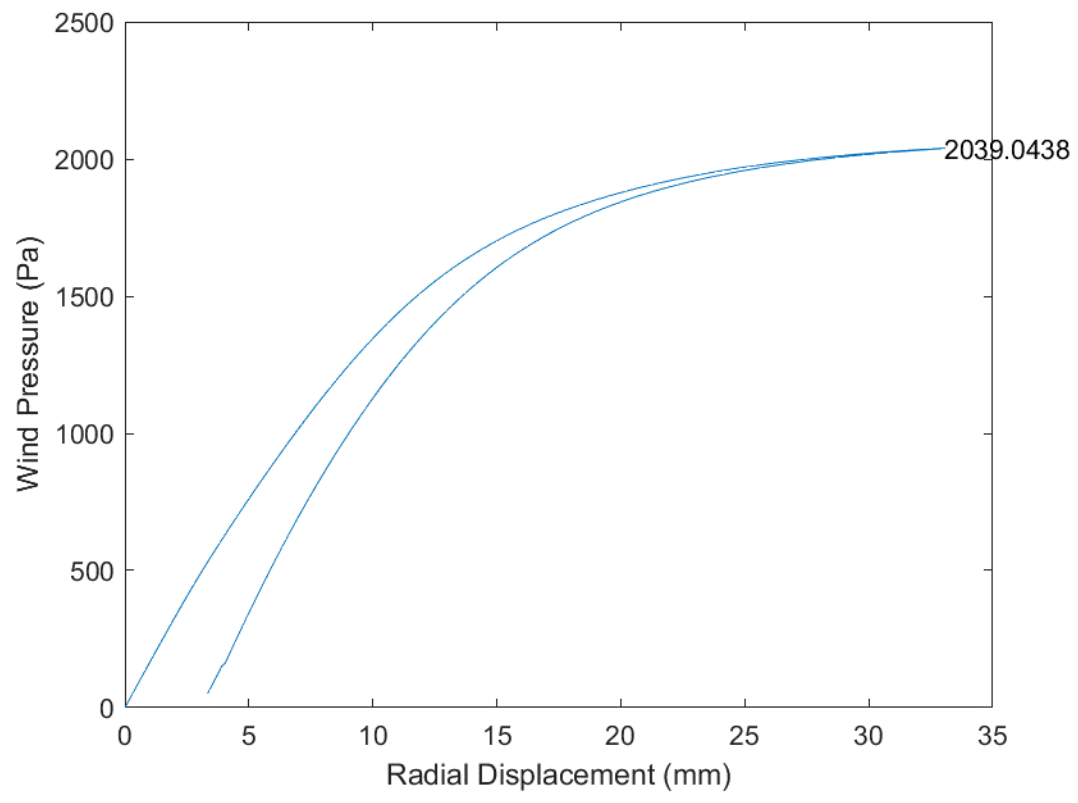


Fig. B.144 D66_H15_S44_R02_W01_V00_CL03_CD03_WT03_ST03

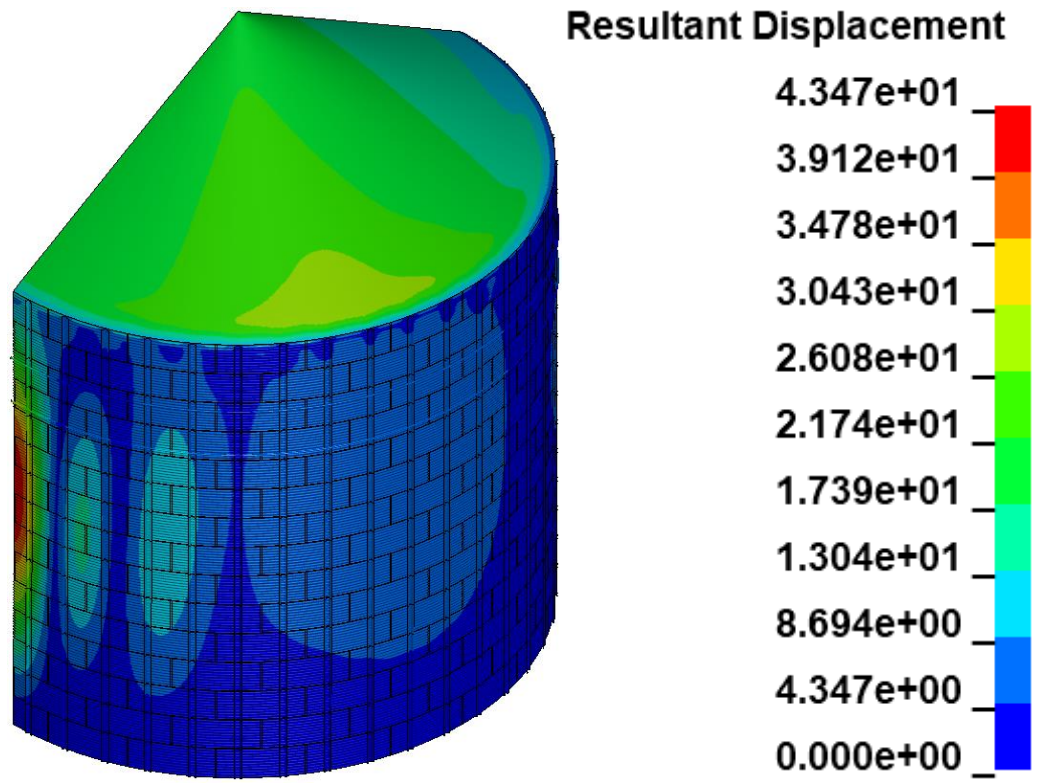
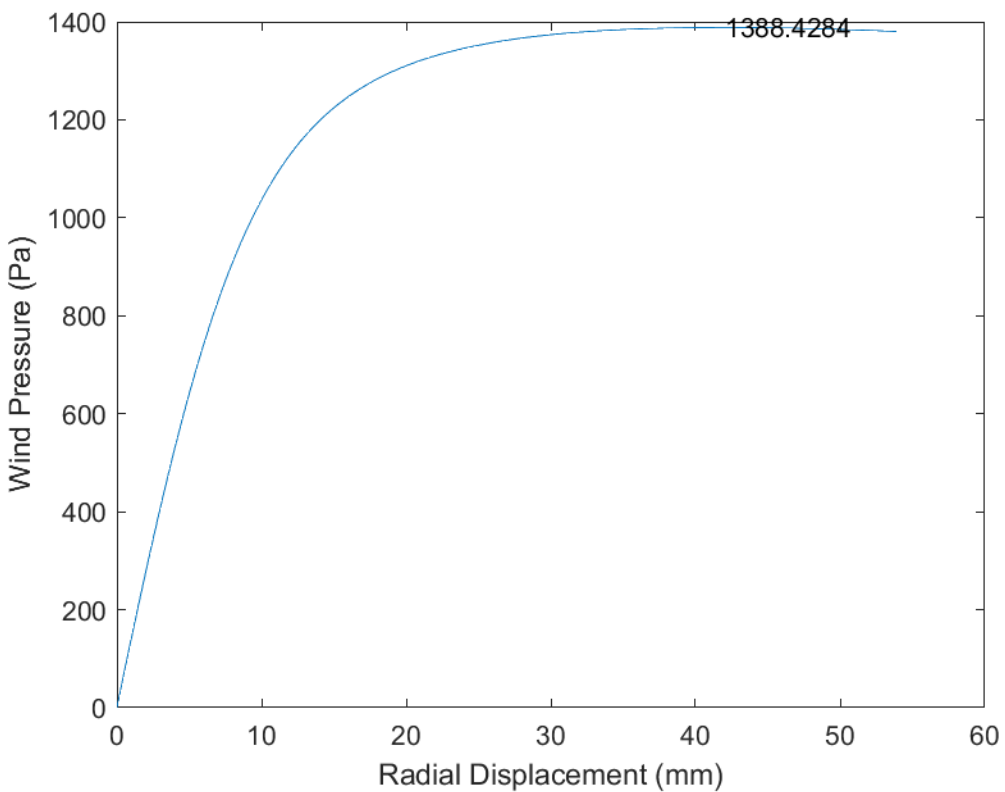


Fig. B.145 D66_H15_S44_R02_W01_V01_CL03_CD03_WT03_ST03

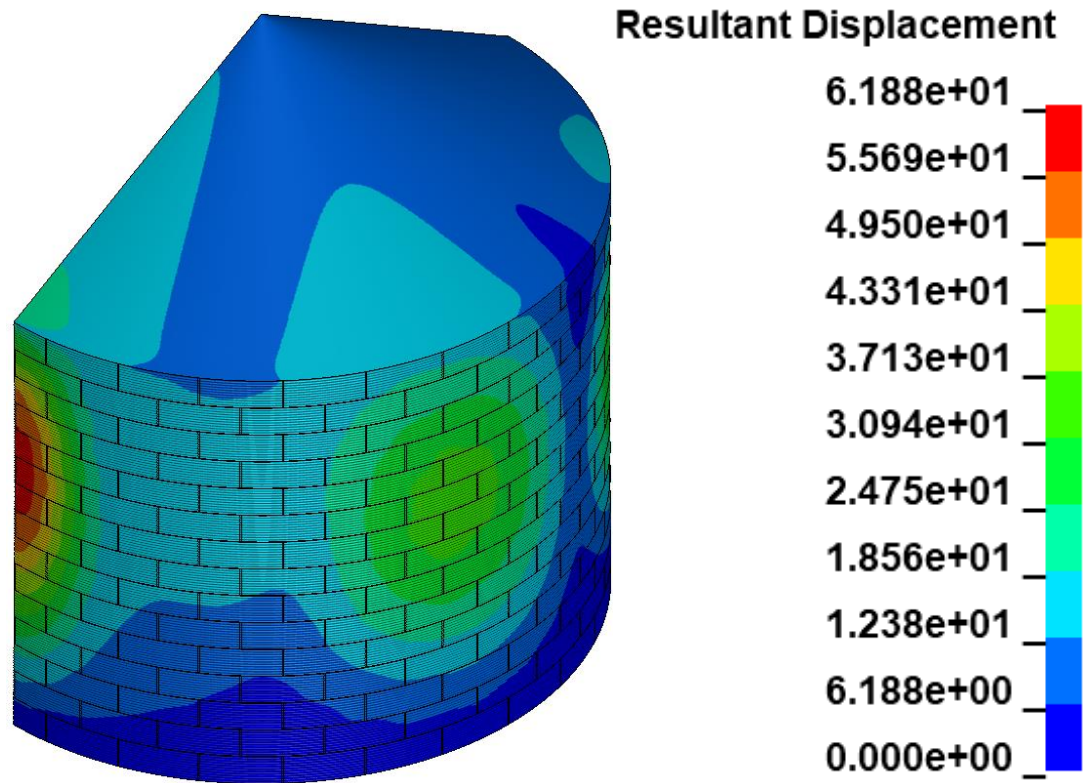
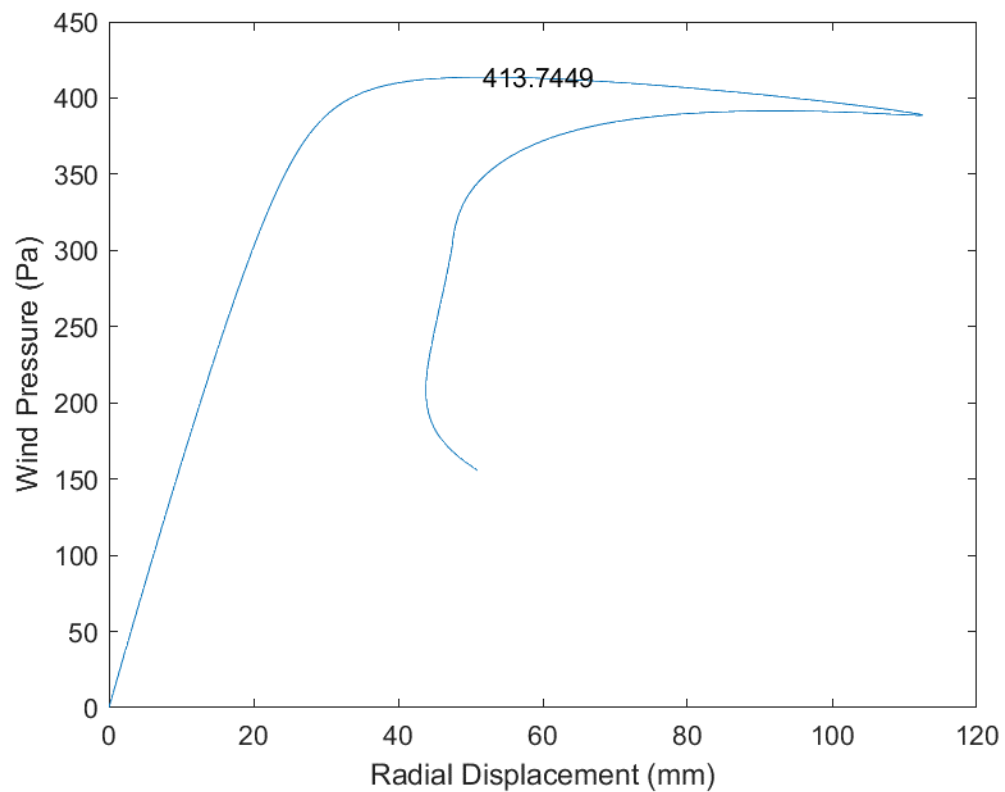


Fig. B.146 D78_H15_S00_R00_W00_V00_CL03_CD03_WT03_ST03

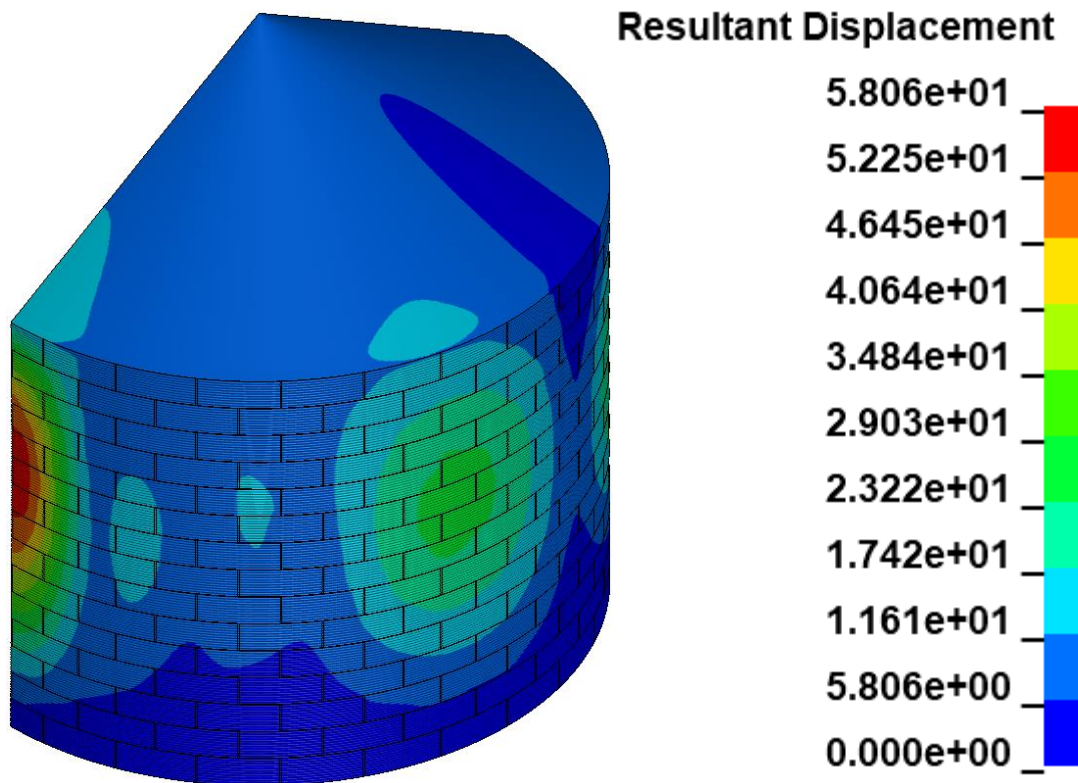
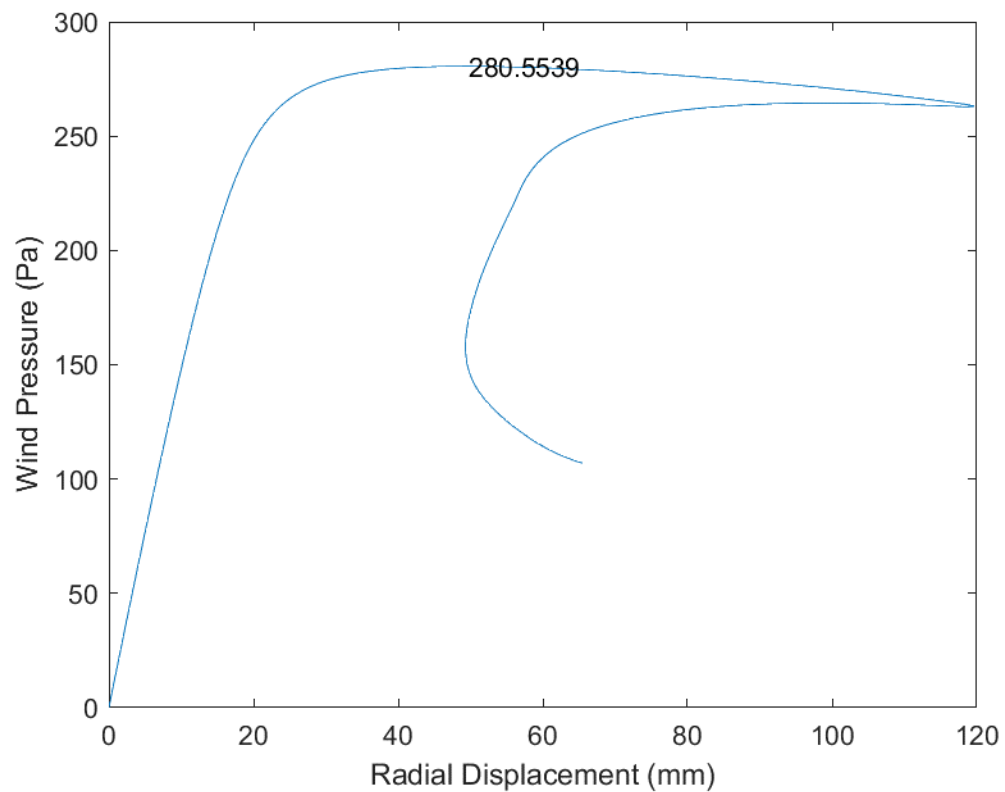


Fig. B.147 D78_H15_S00_R00_W00_V01_CL03_CD03_WT03_ST03

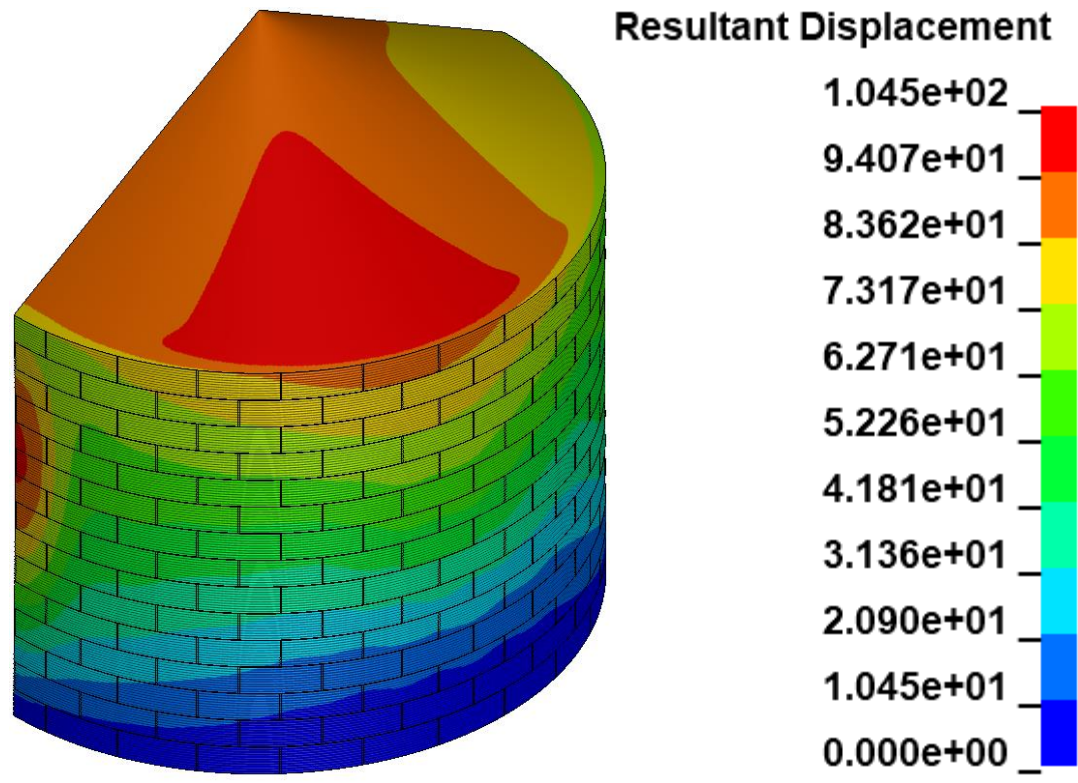
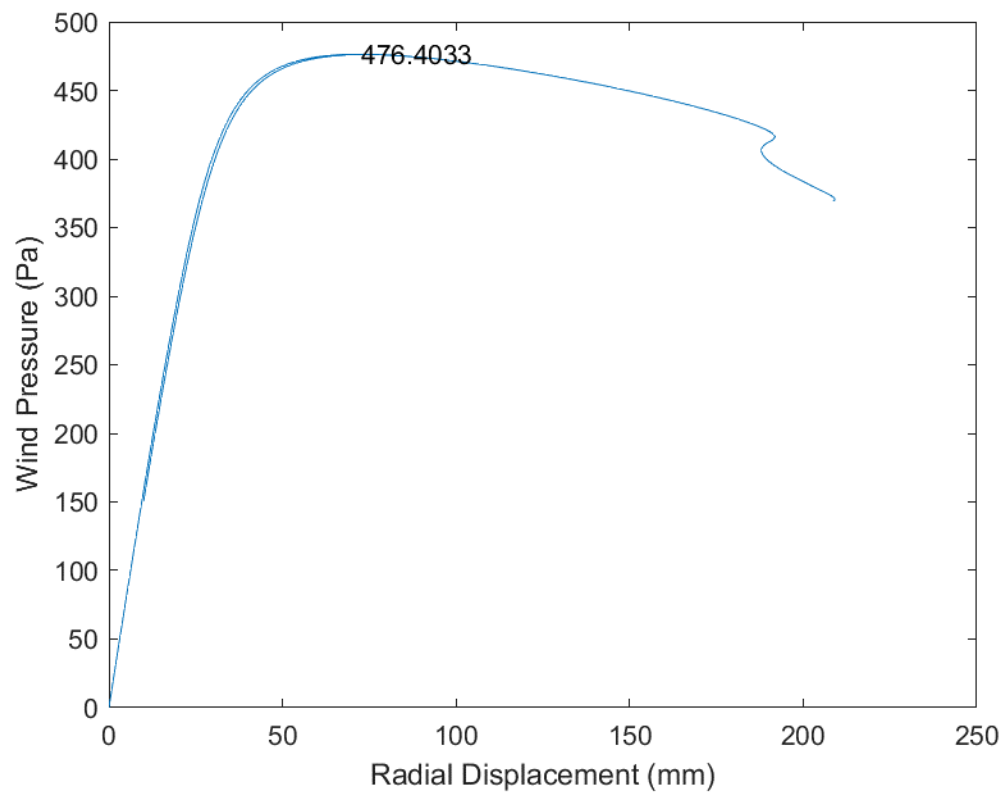


Fig. B.148 D78_H15_S00_R00_W01_V00_CL03_CD03_WT03_ST03

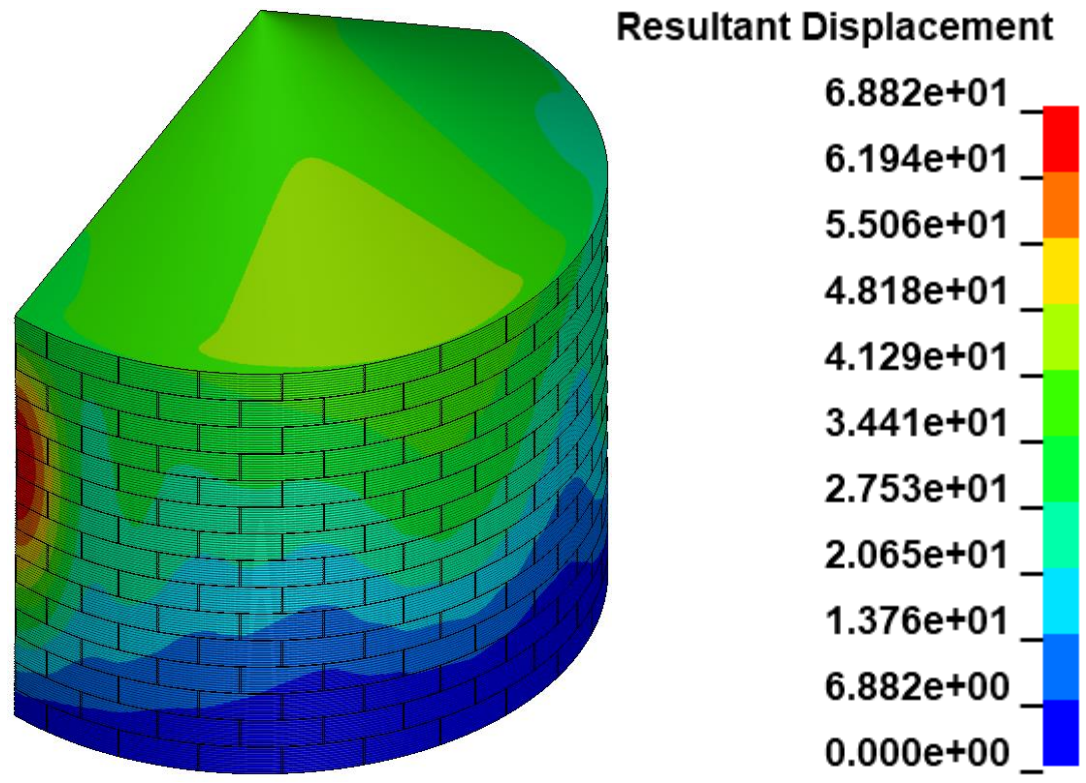
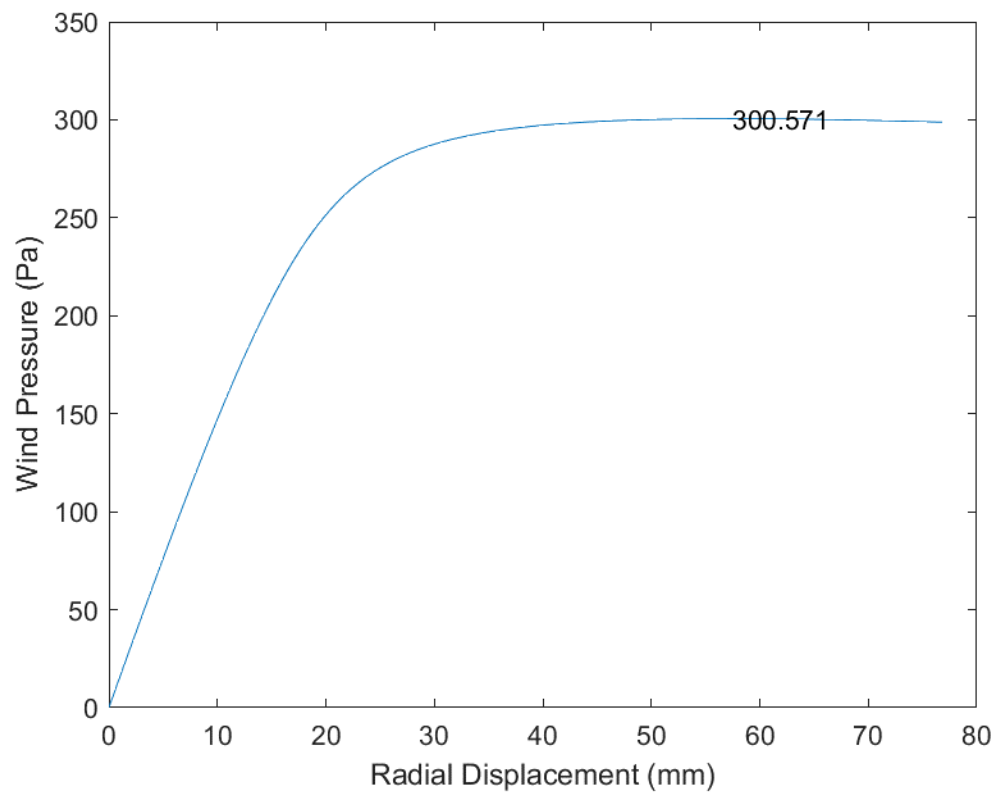


Fig. B.149 D78_H15_S00_R00_W01_V01_CL03_CD03_WT03_ST03

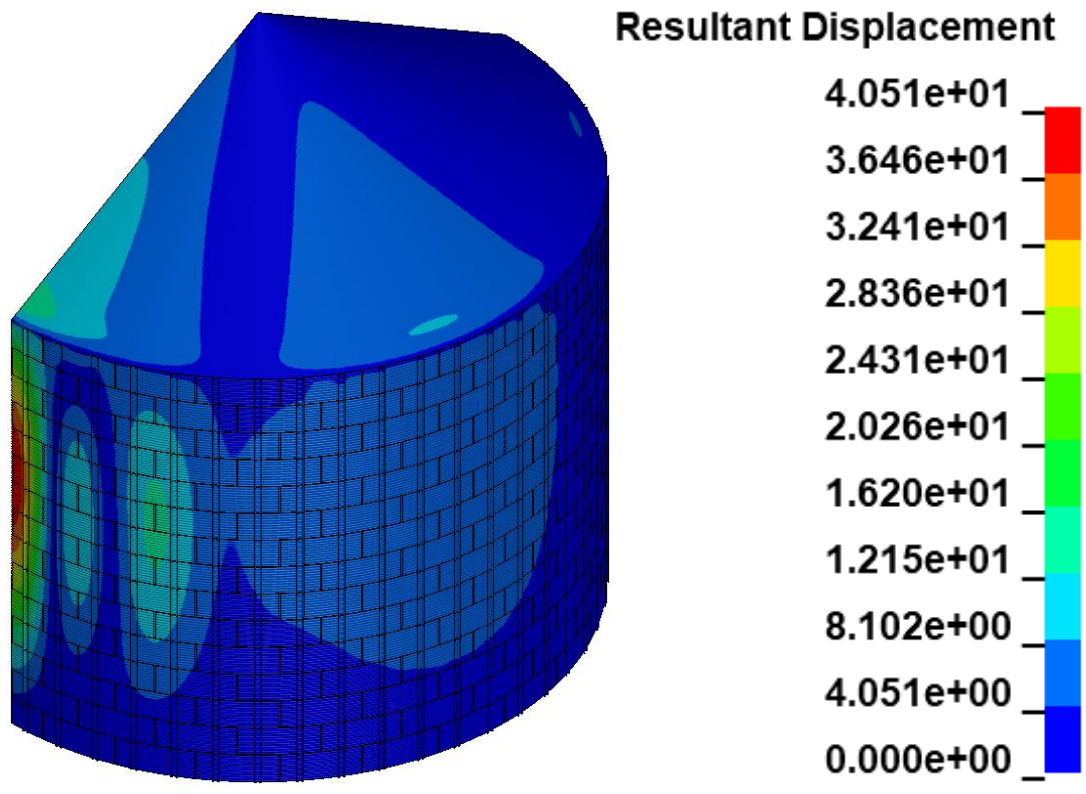
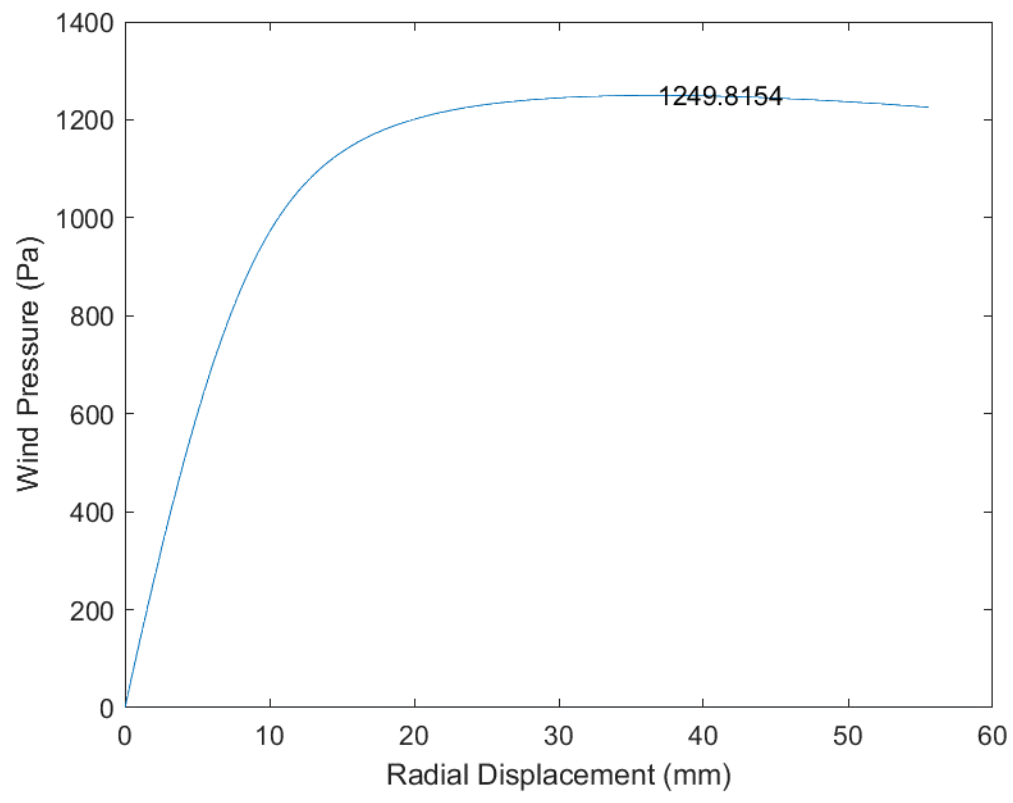


Fig. B.150 D78_H15_S52_R00_W00_V00_CL03_CD03_WT03_ST03

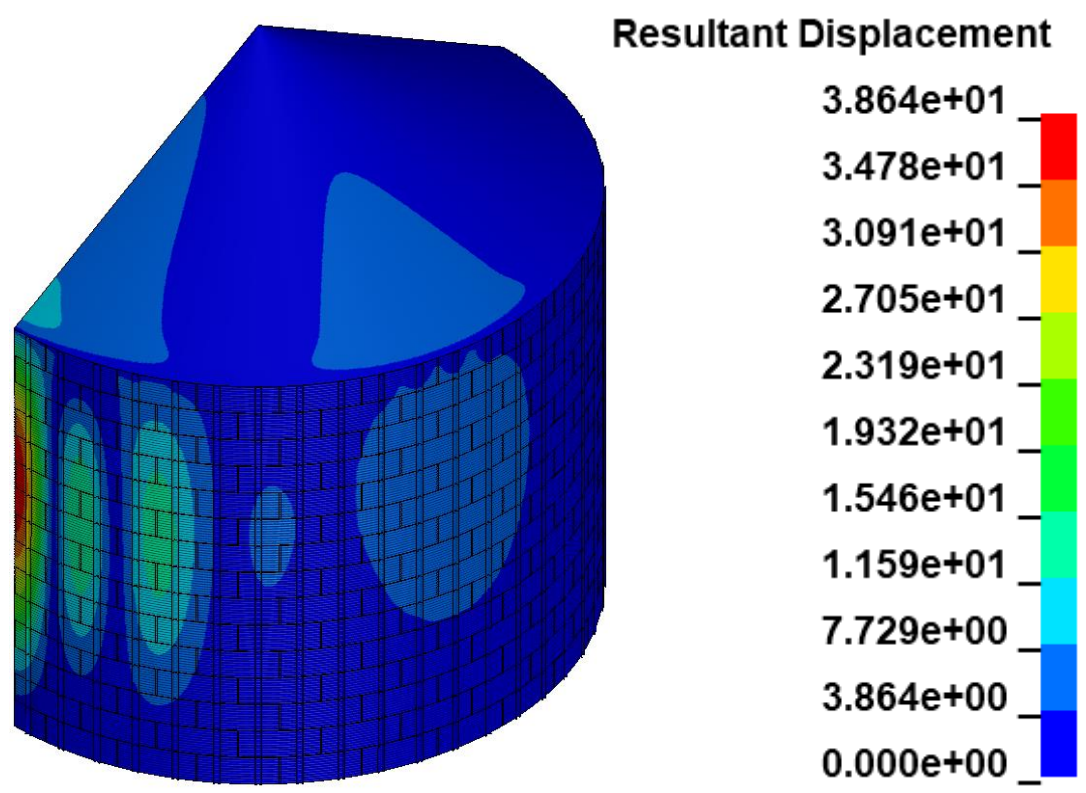
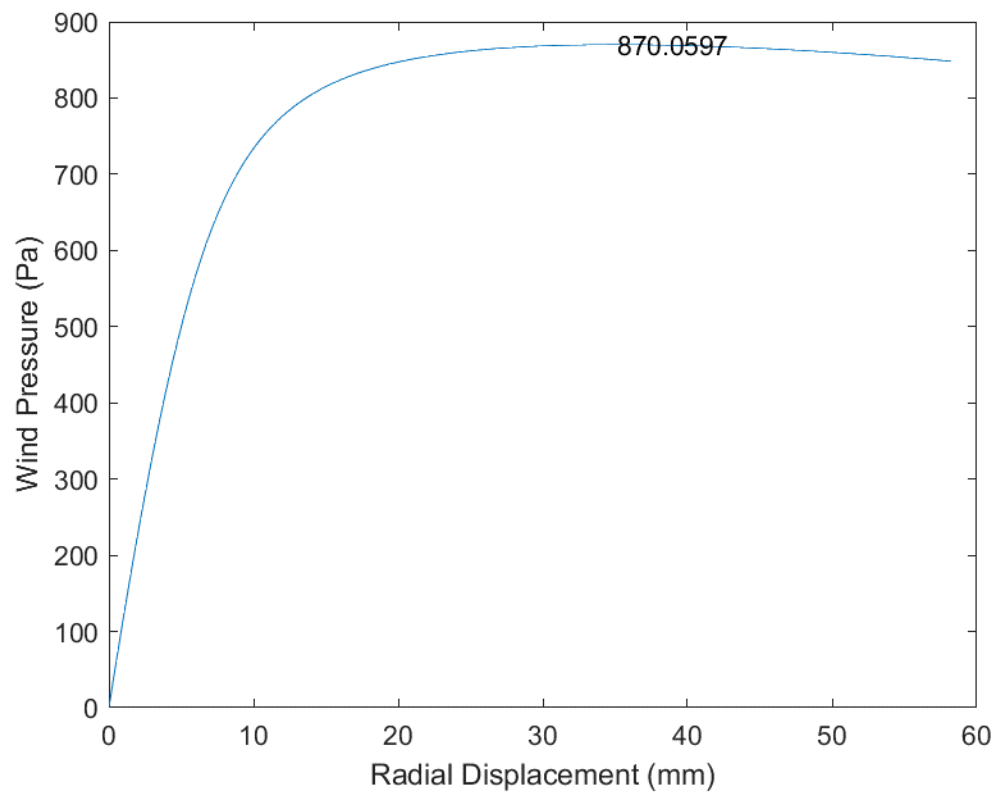


Fig. B.151 D78_H15_S52_R00_W00_V01_CL03_CD03_WT03_ST03

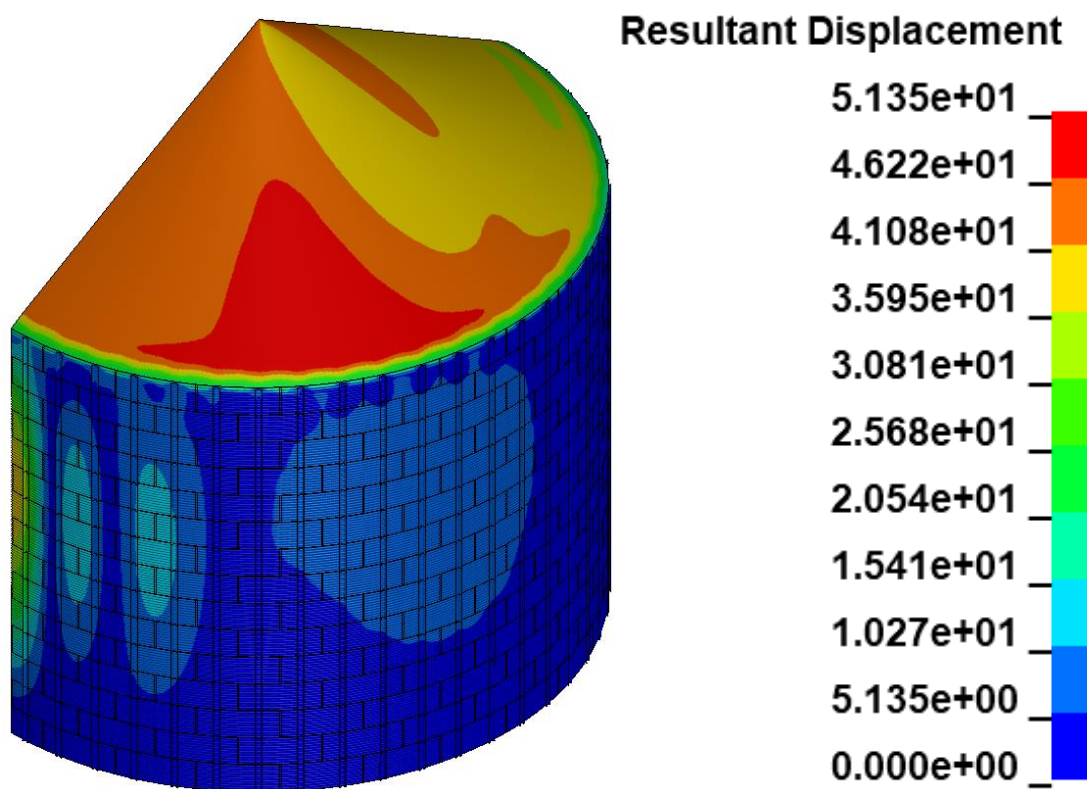
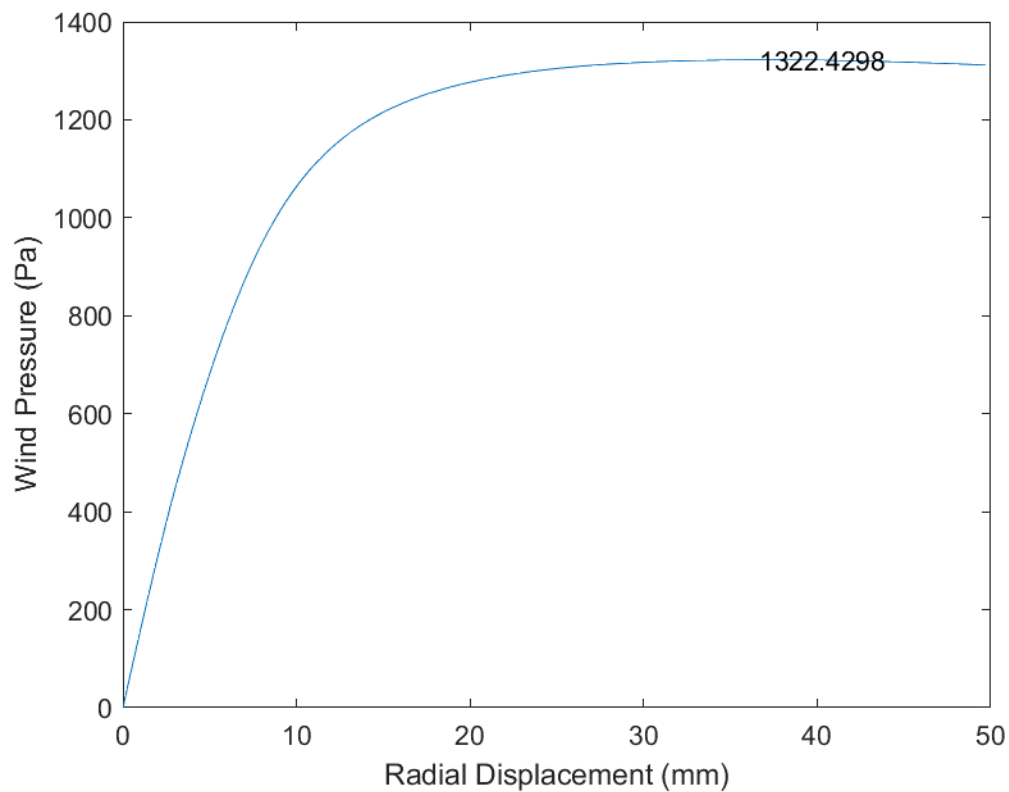


Fig. B.152 D78_H15_S52_R00_W01_V00_CL03_CD03_WT03_ST03

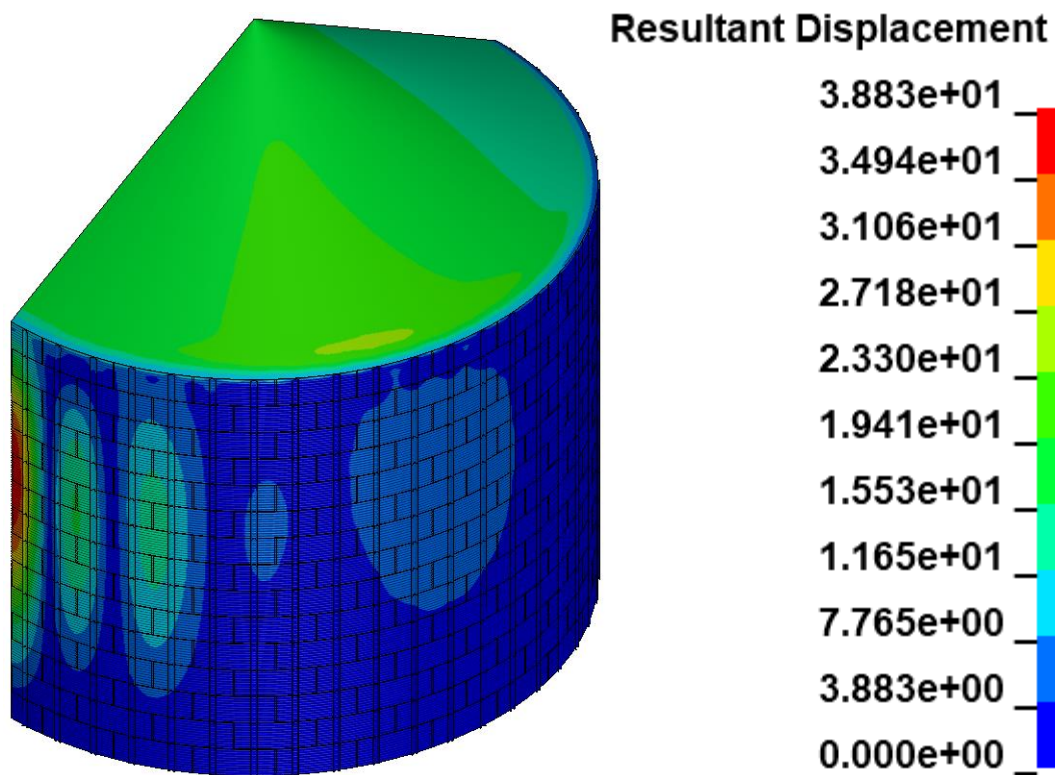
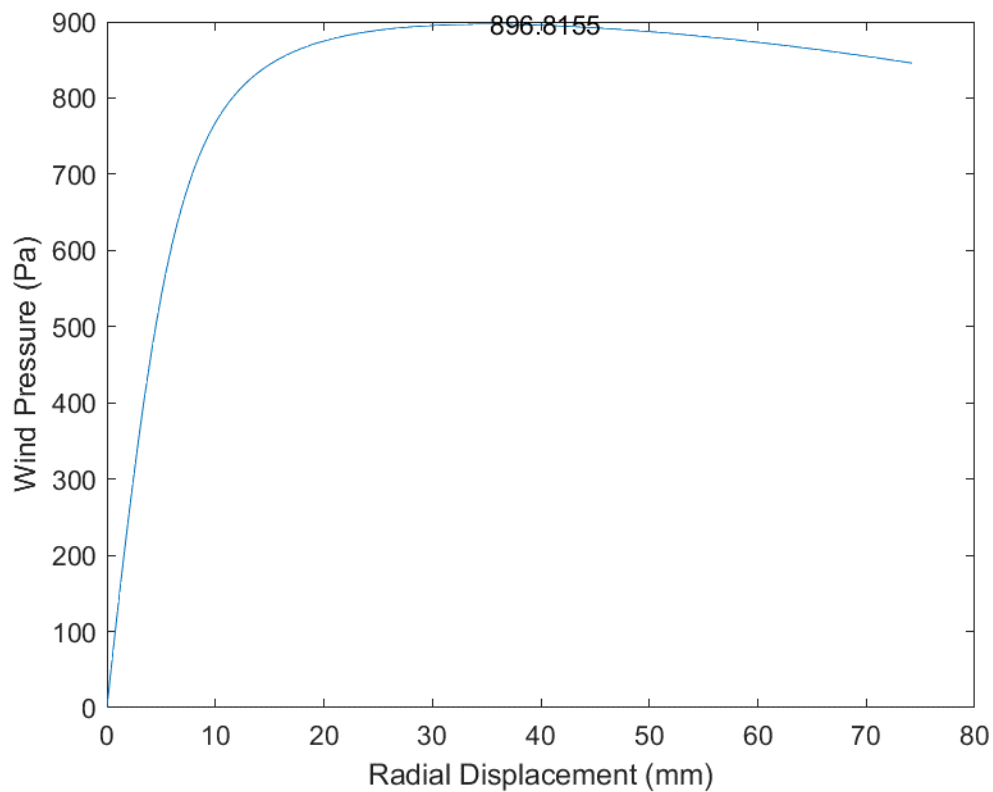


Fig. B.153 D78_H15_S52_R00_W01_V01_CL03_CD03_WT03_ST03

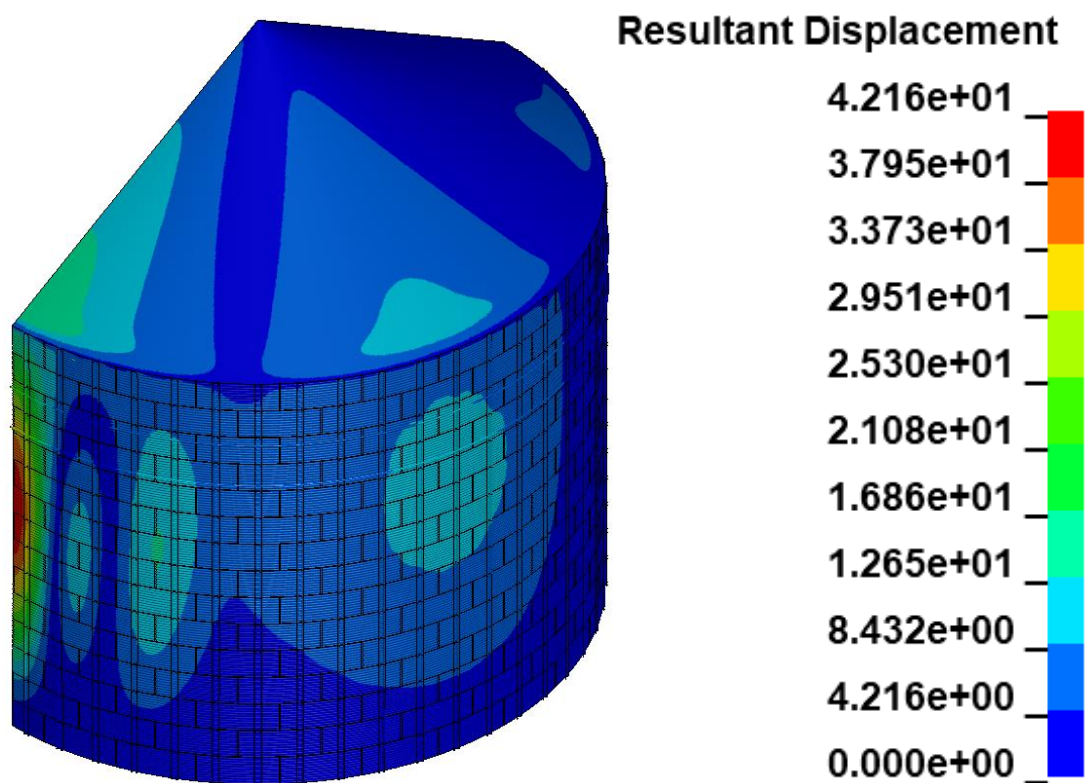
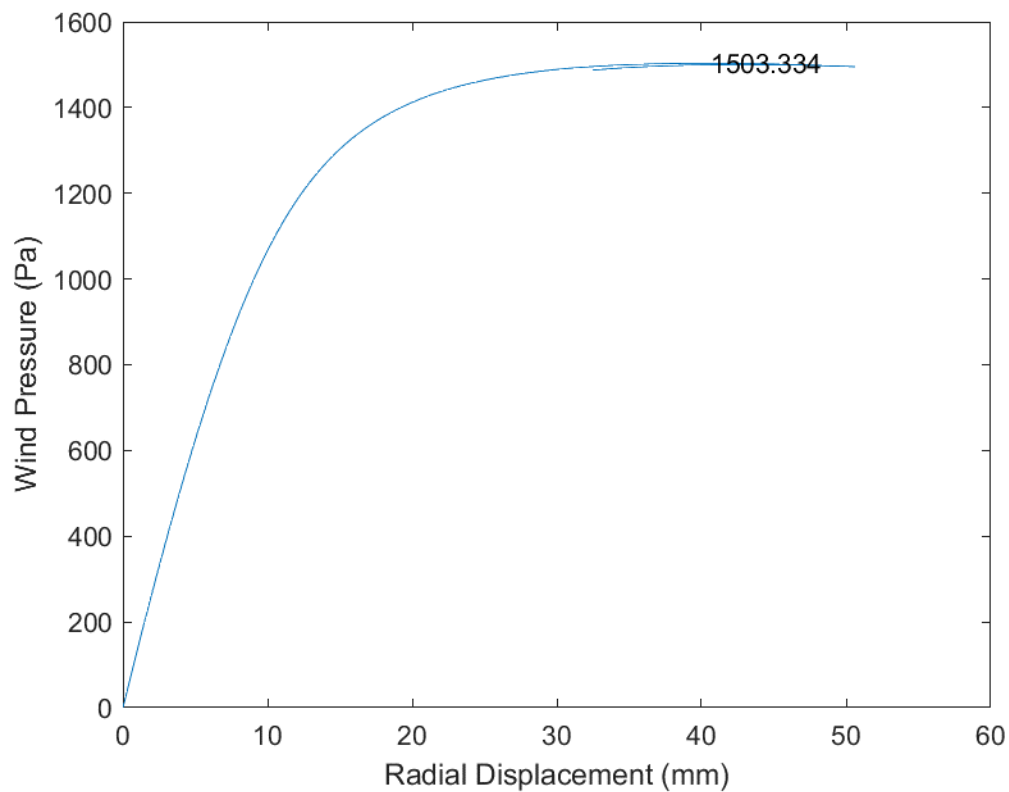


Fig. B.154 D78_H15_S52_R02_W00_V00_CL03_CD03_WT03_ST03

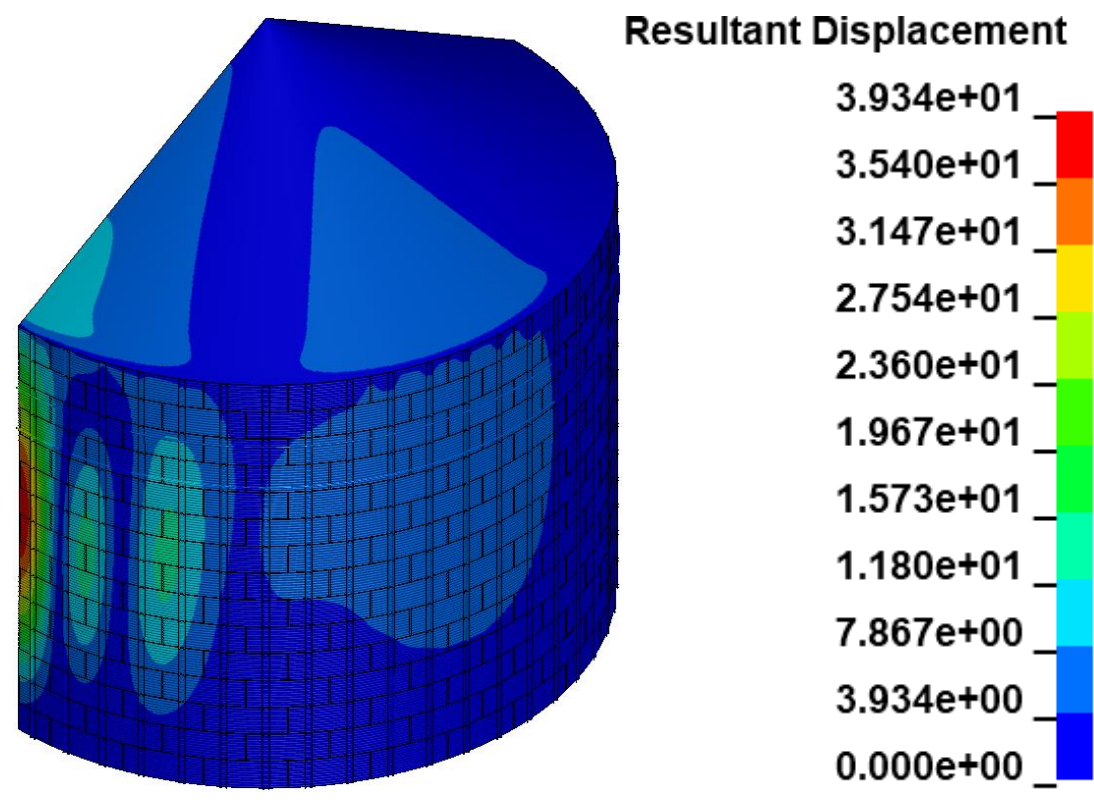
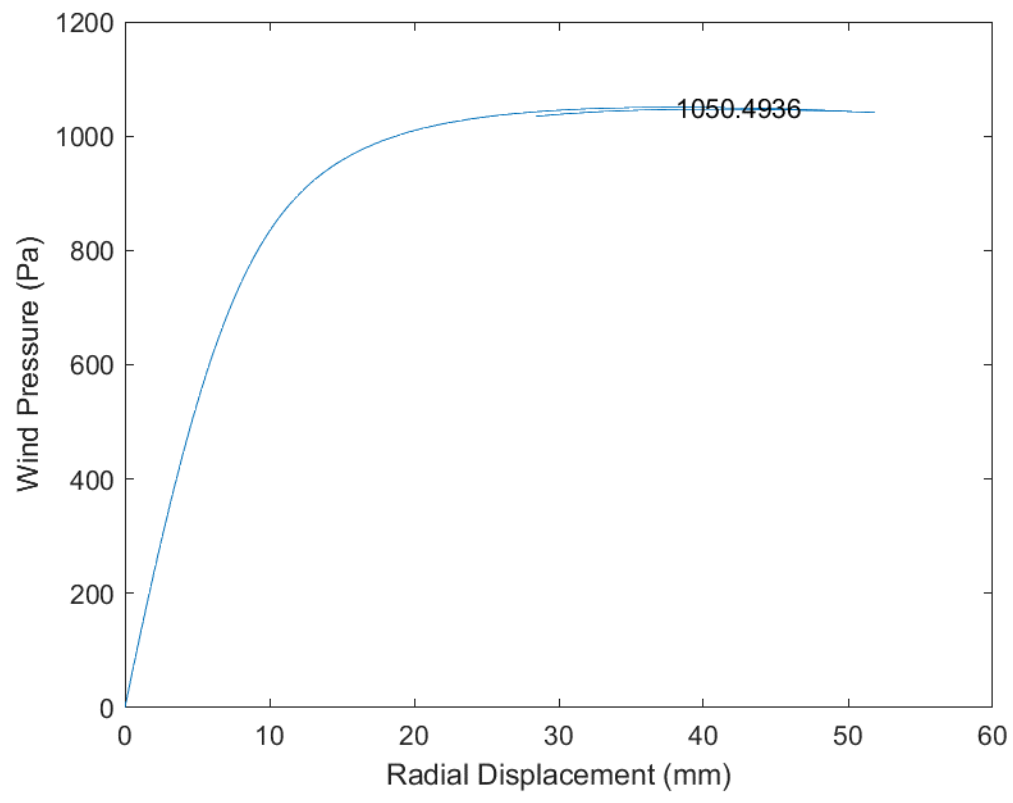


Fig. B.155 D78_H15_S52_R02_W00_V01_CL03_CD03_WT03_ST03

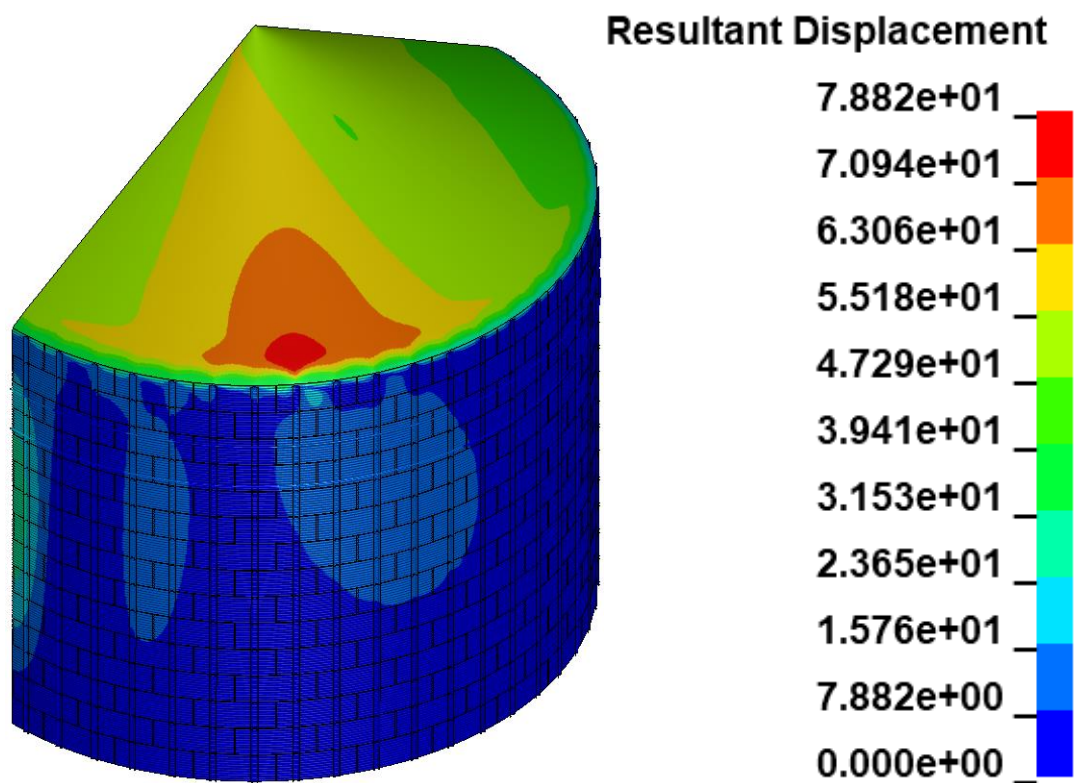
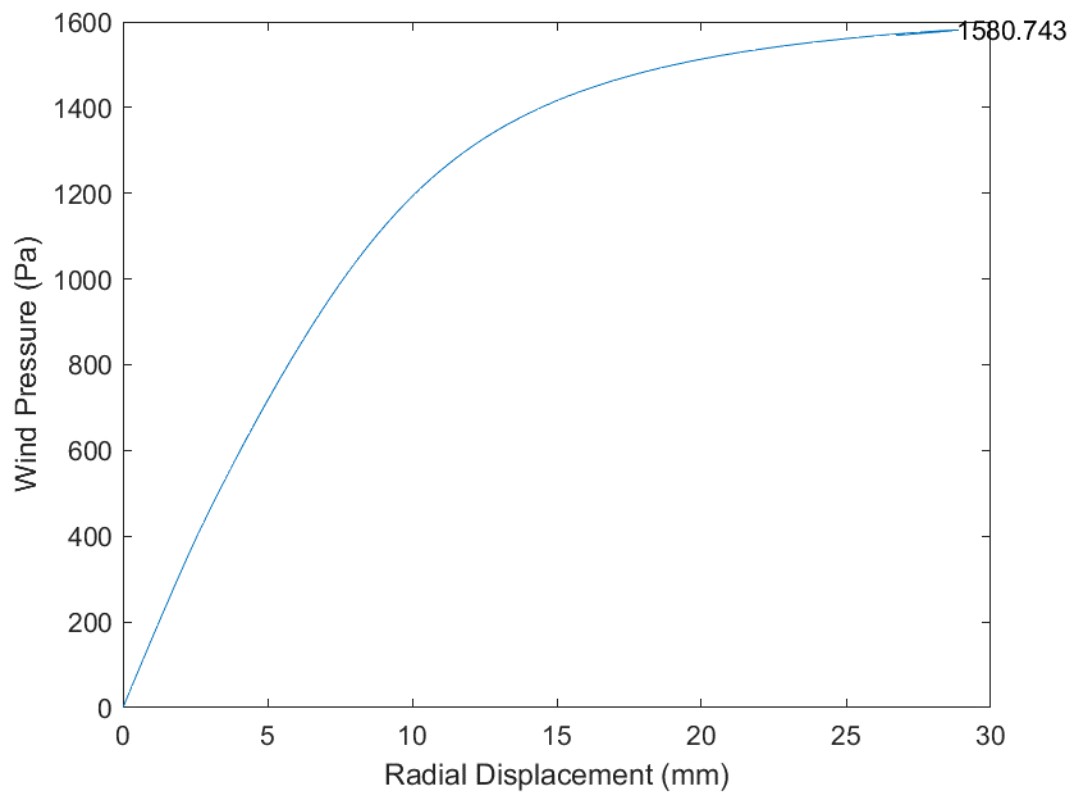


Fig. B.156 D78_H15_S52_R02_W01_V00_CL03_CD03_WT03_ST03

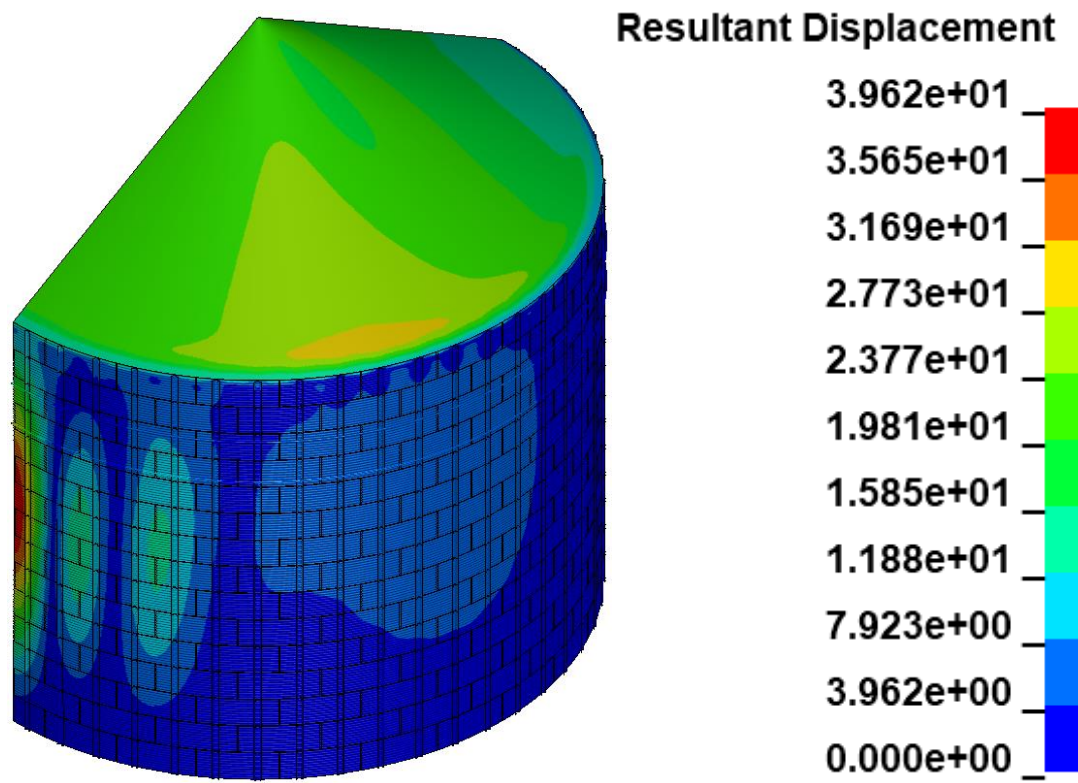
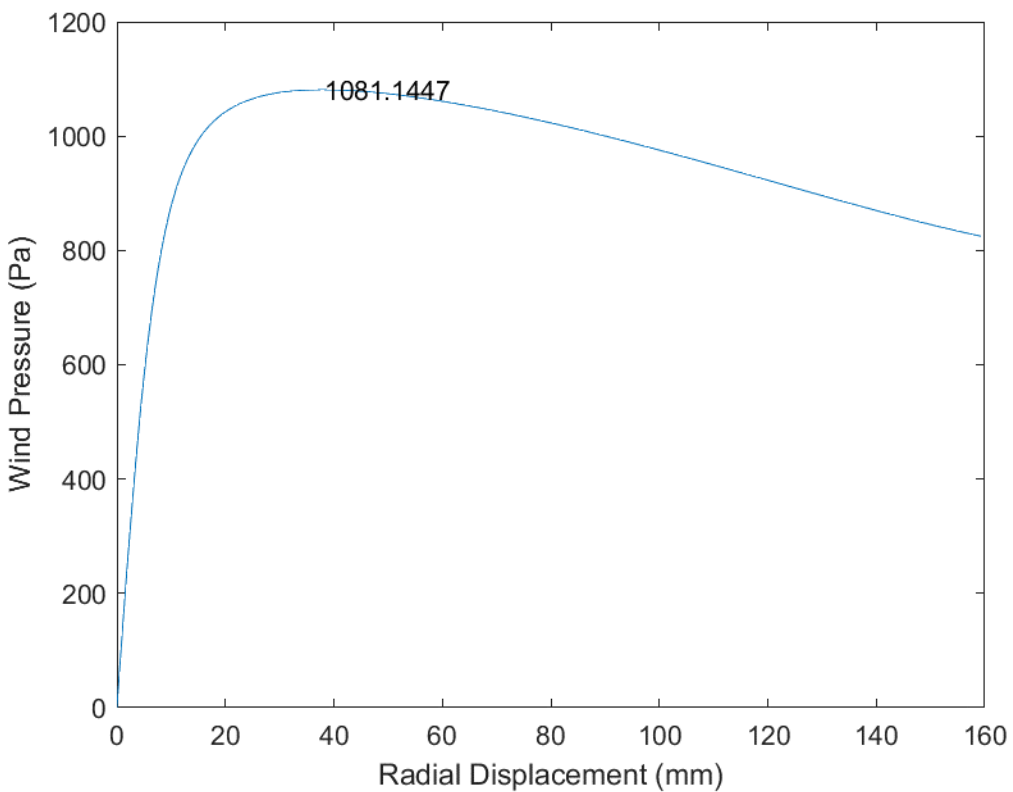


Fig. B.157 D78_H15_S52_R02_W01_V01_CL03_CD03_WT03_ST03

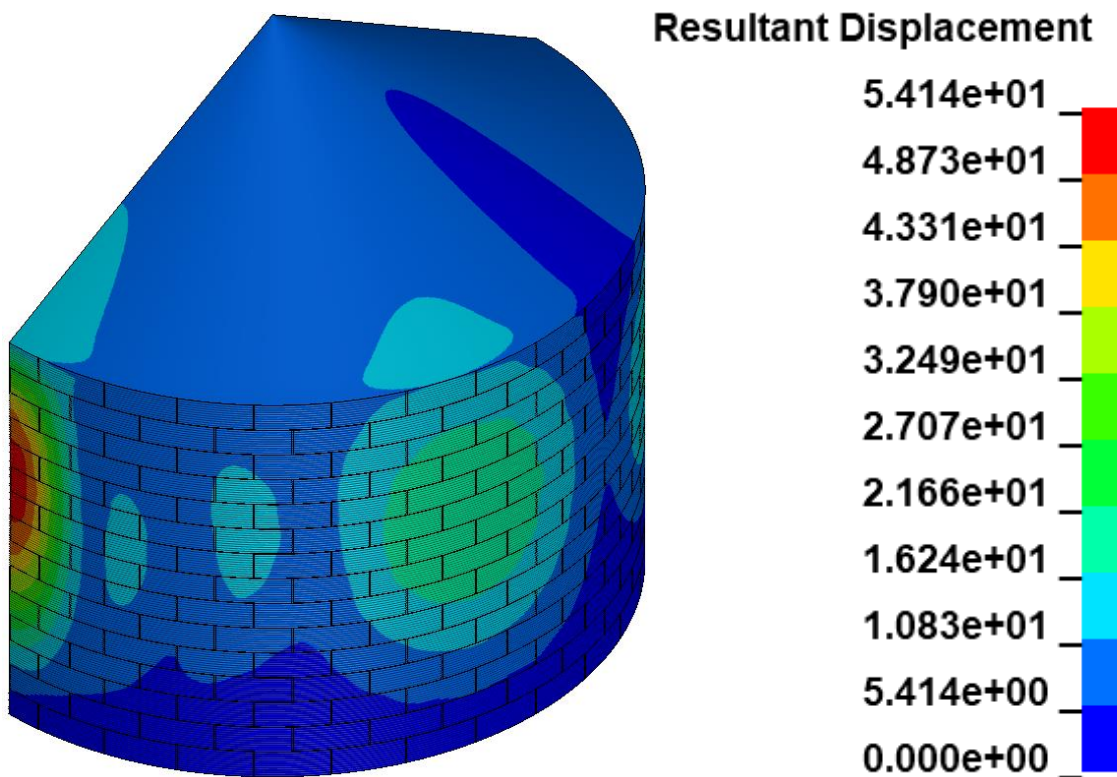
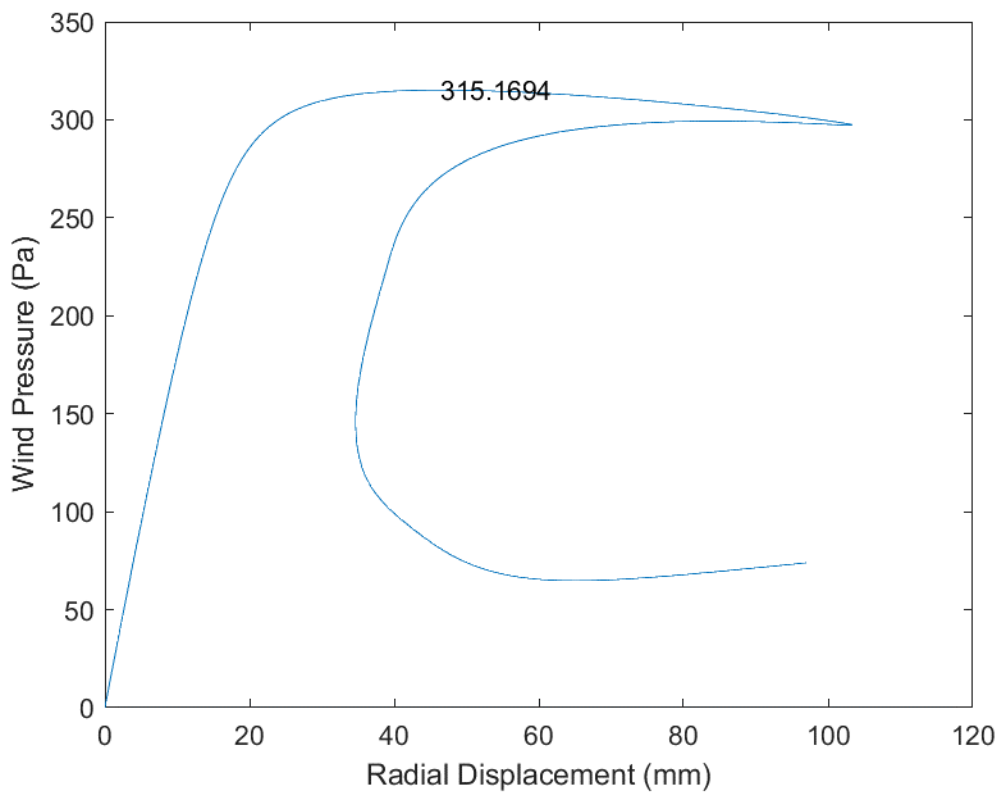


Fig. B.158 D90_H15_S00_R00_W00_V00_CL03_CD03_WT03_ST03

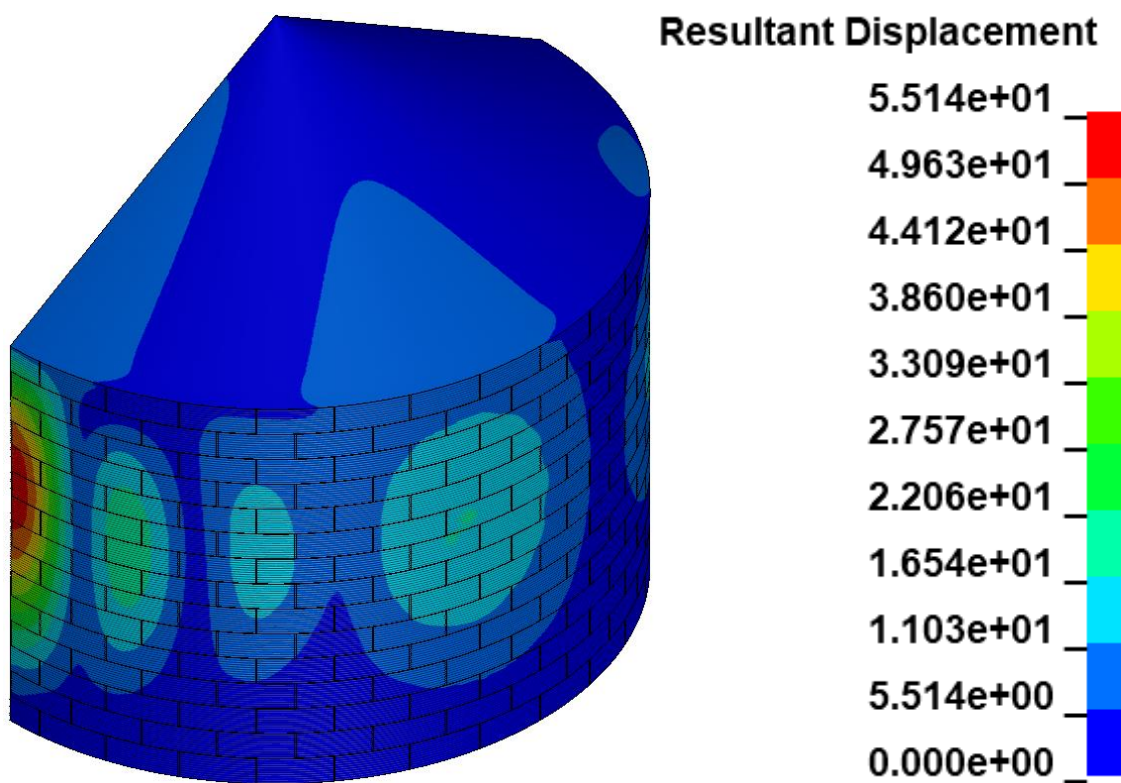
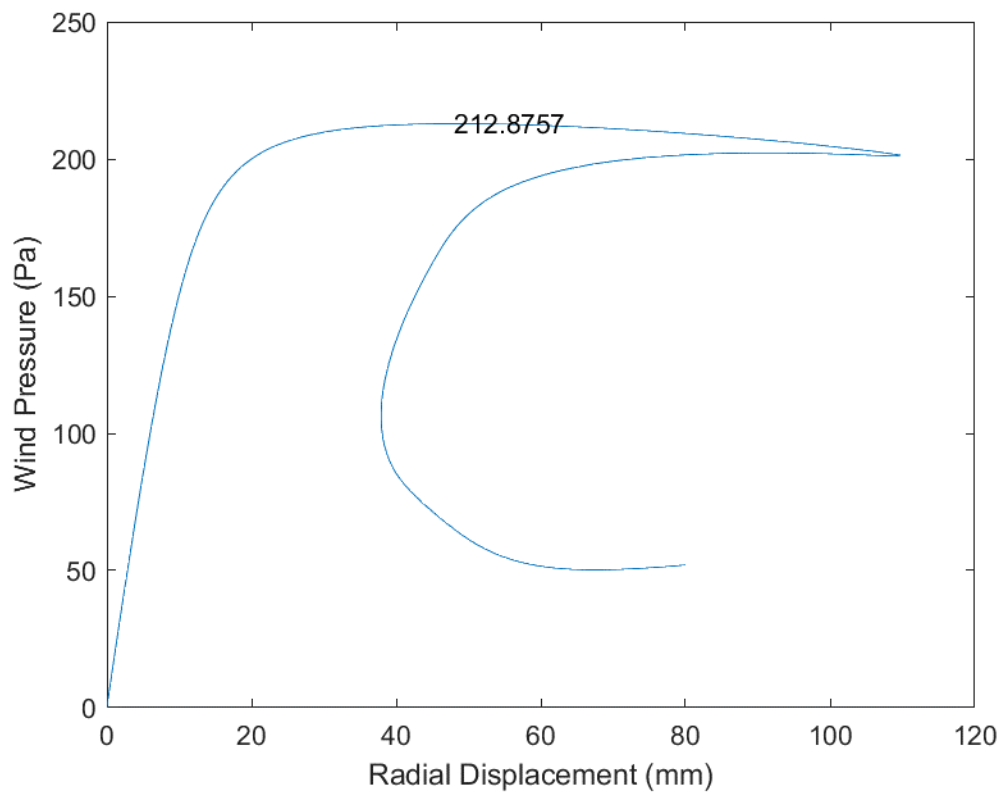


Fig. B.159 D90_H15_S00_R00_W00_V01_CL03_CD03_WT03_ST03

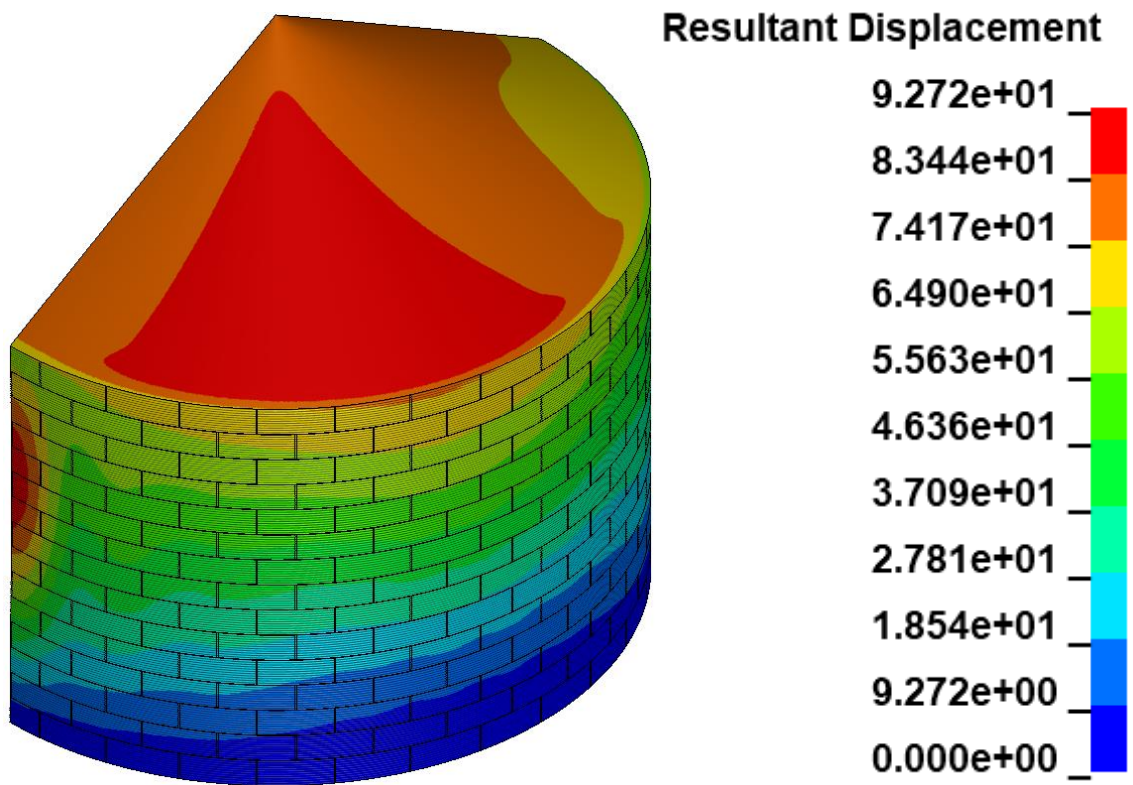
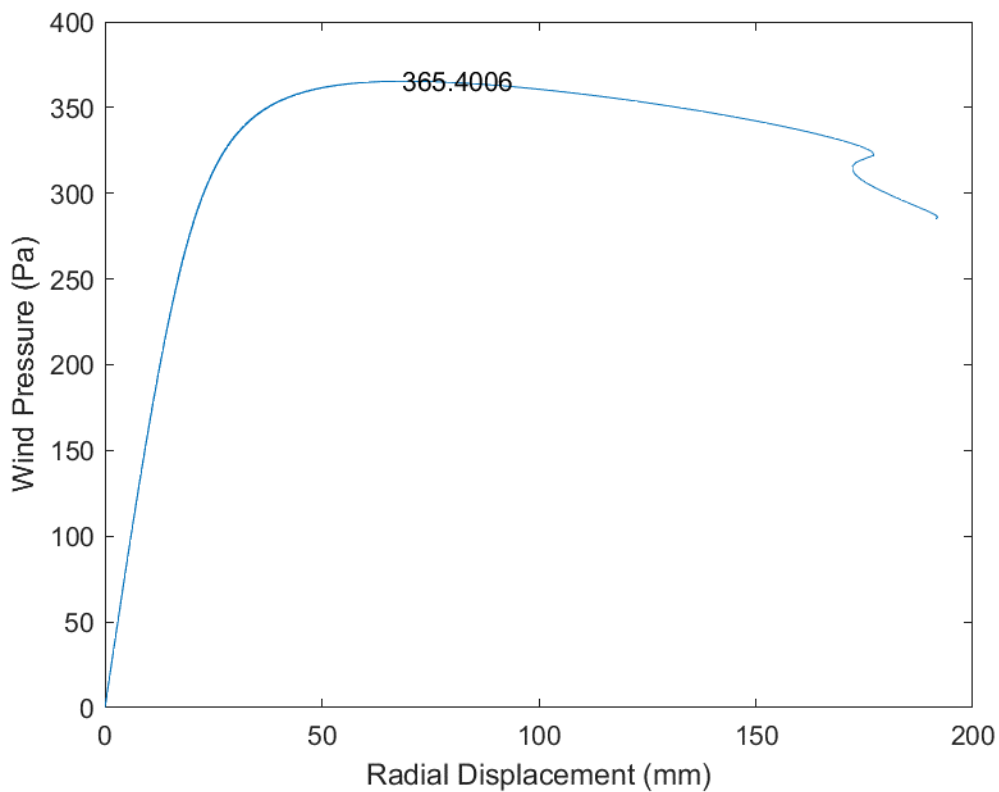


Fig. B.160 D90_H15_S00_R00_W01_V00_CL03_CD03_WT03_ST03

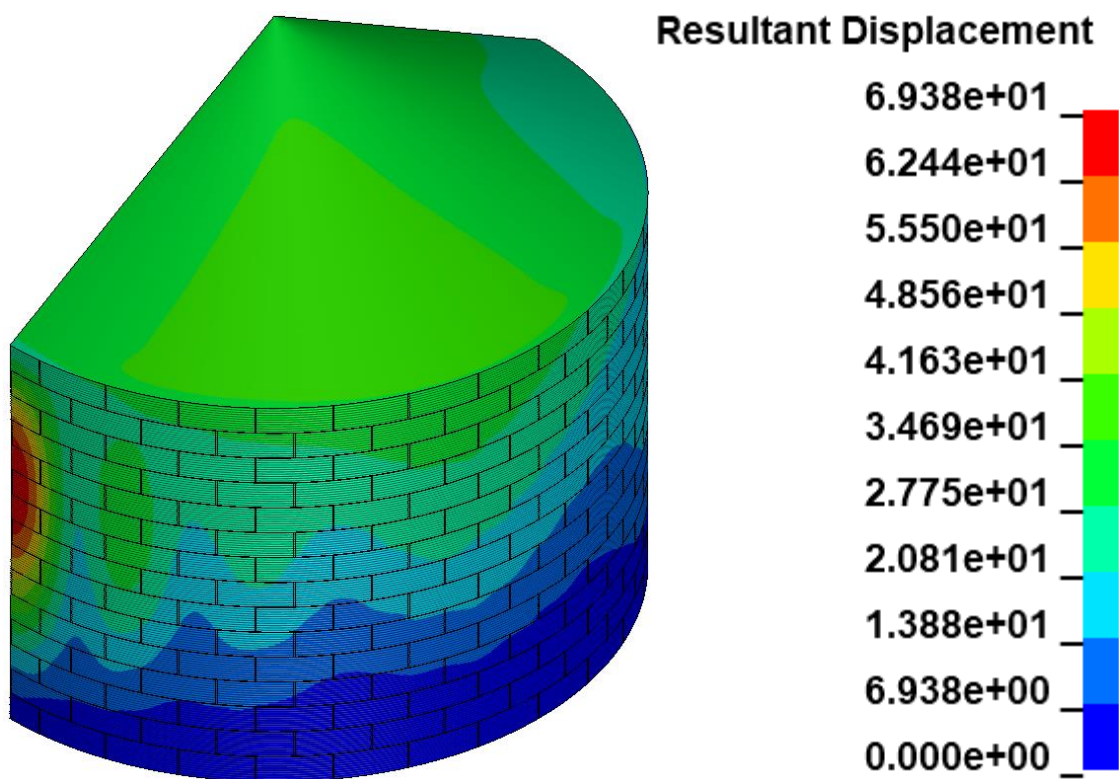
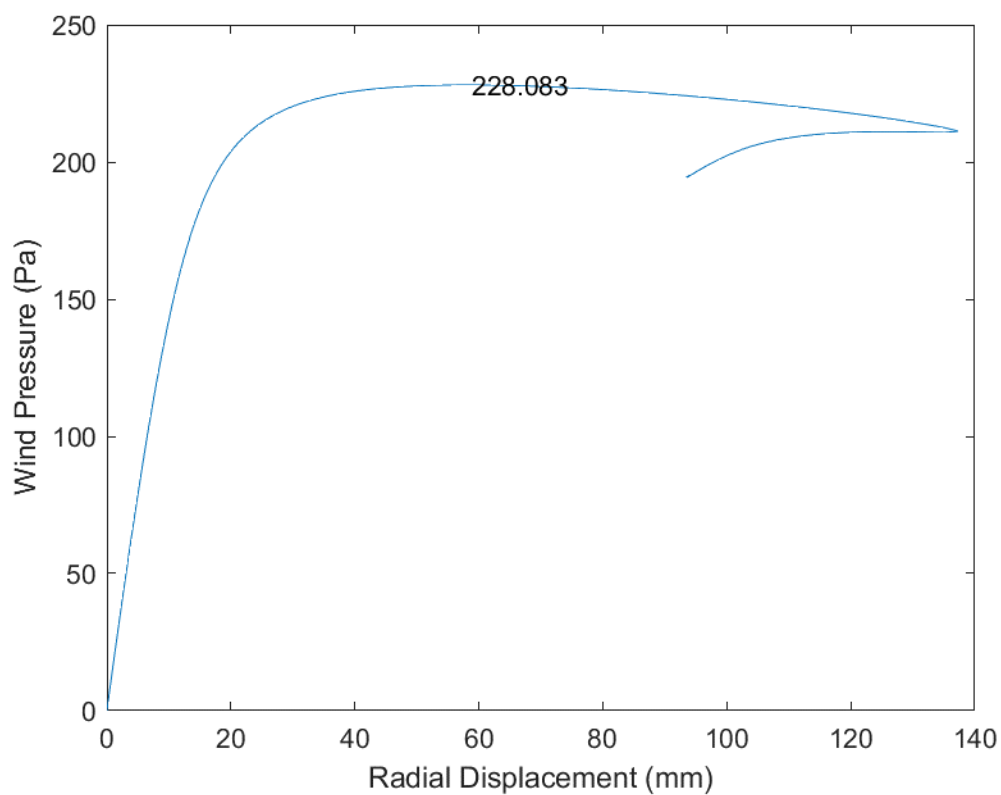


Fig. B.161 D90_H15_S00_R00_W01_V01_CL03_CD03_WT03_ST03

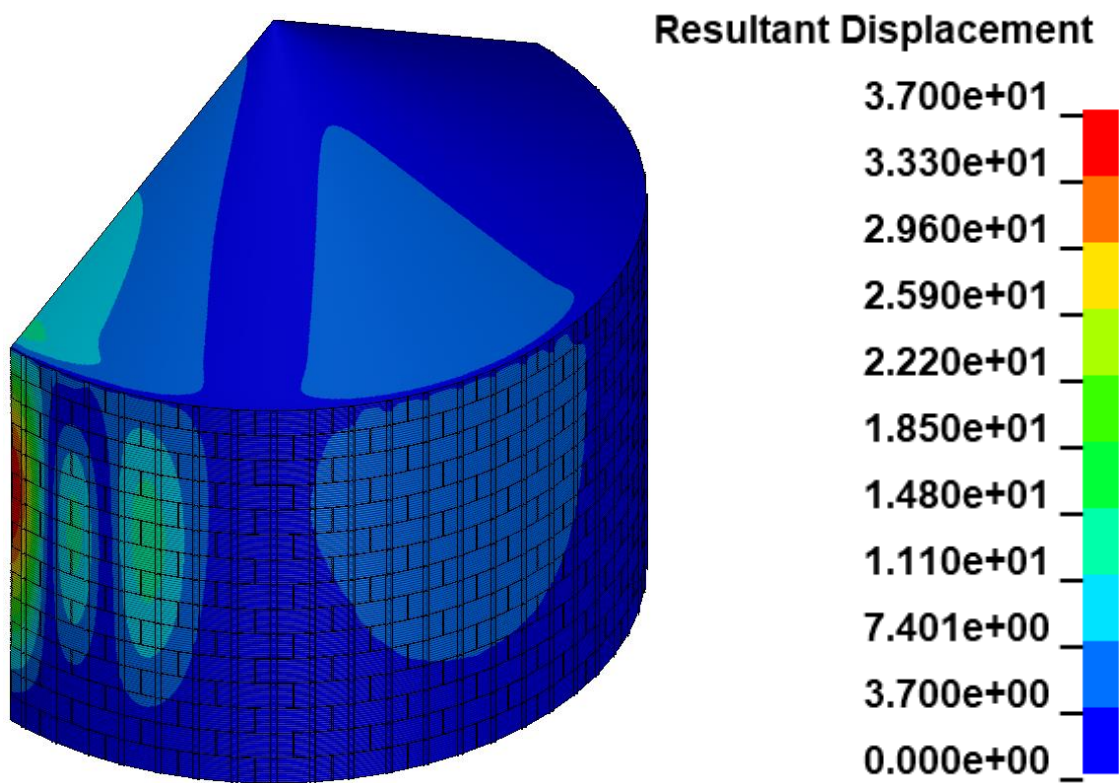
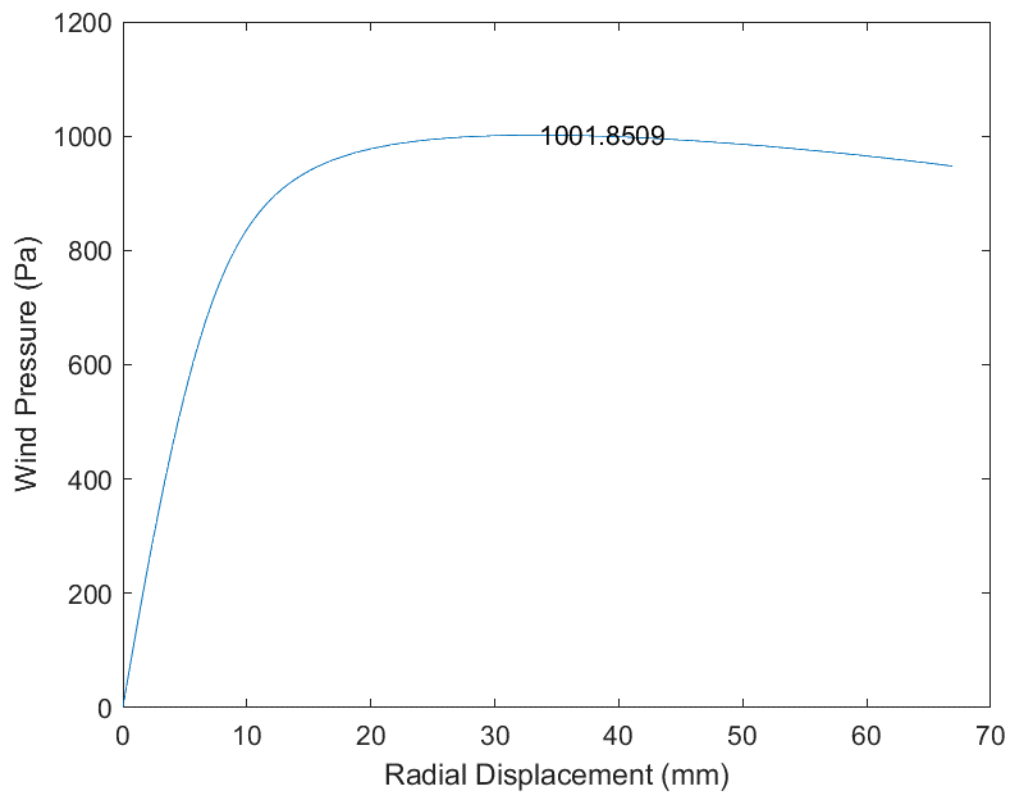


Fig. B.162 D90_H15_S60_R00_W00_V00_CL03_CD03_WT03_ST03

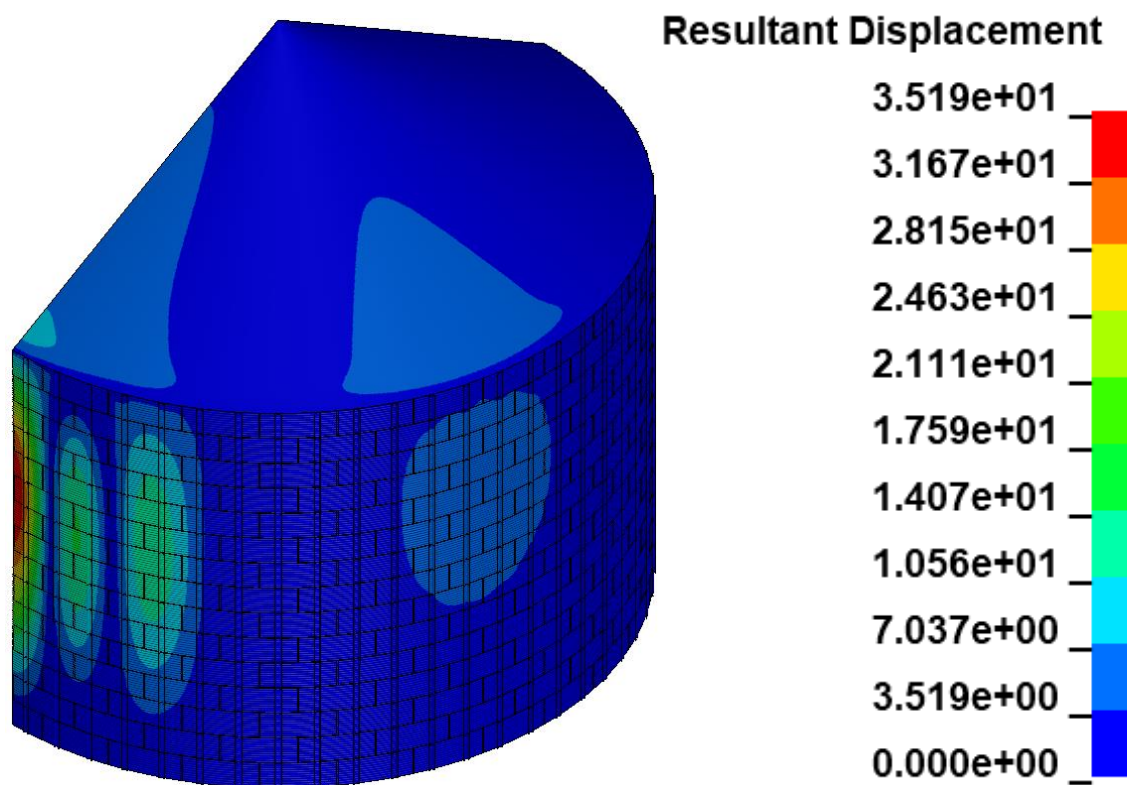
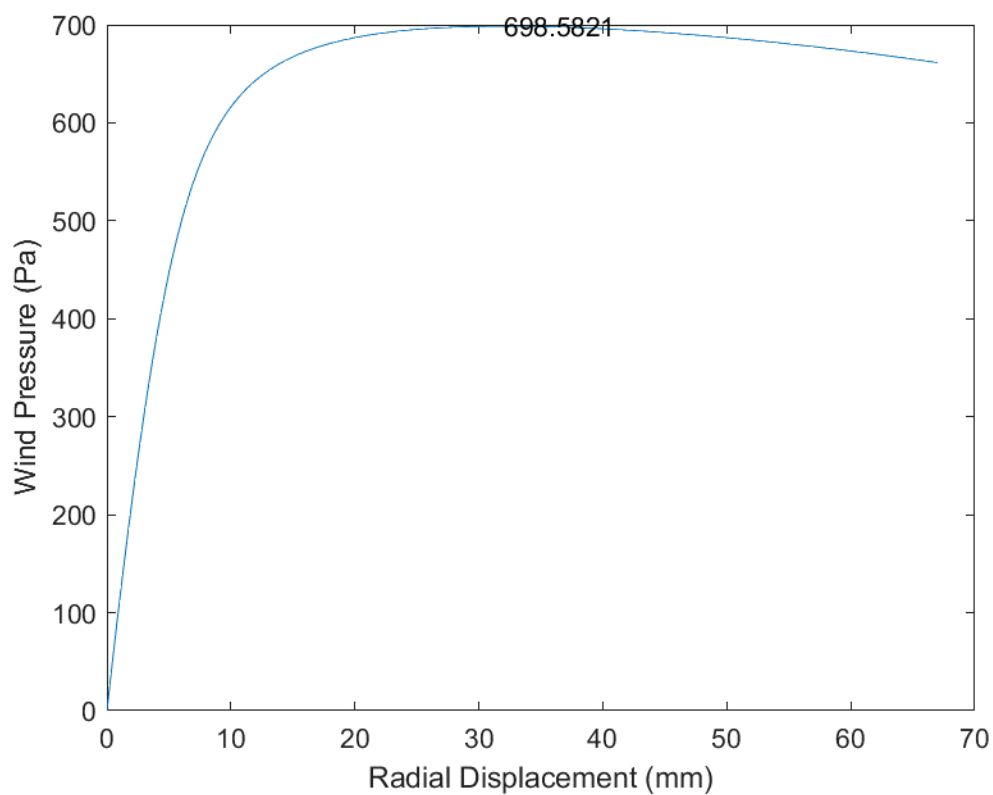


Fig. B.163 D90_H15_S60_R00_W00_V01_CL03_CD03_WT03_ST03

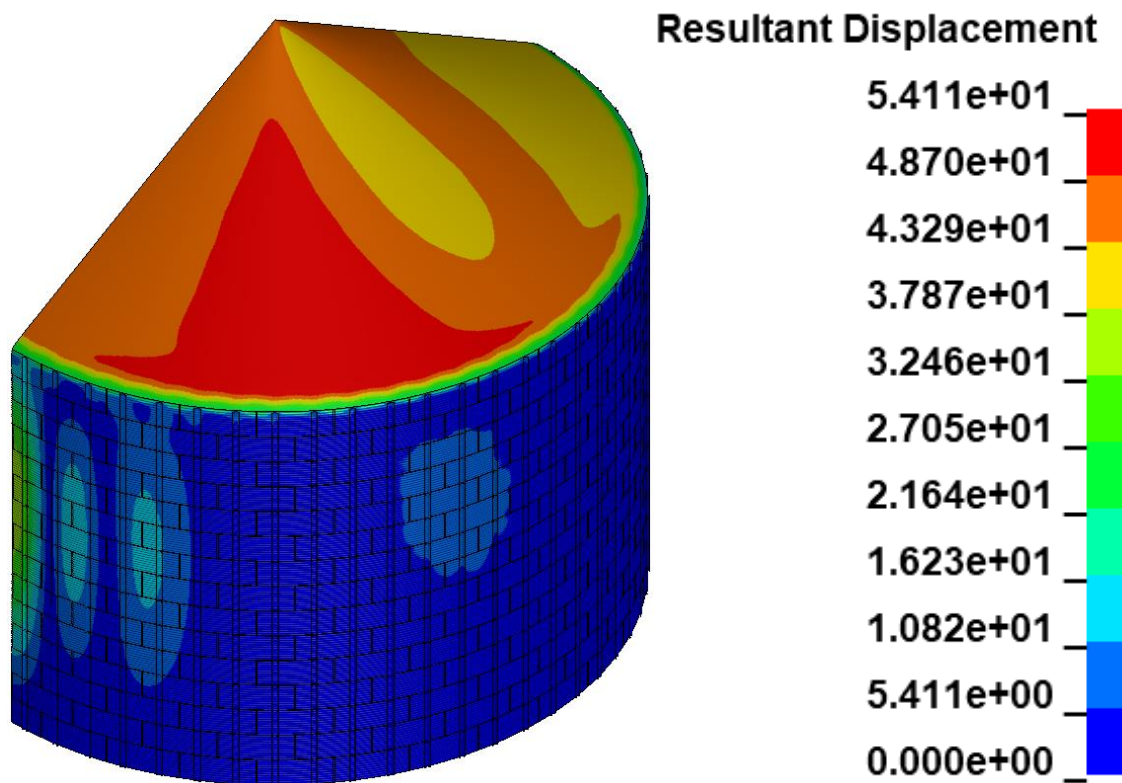
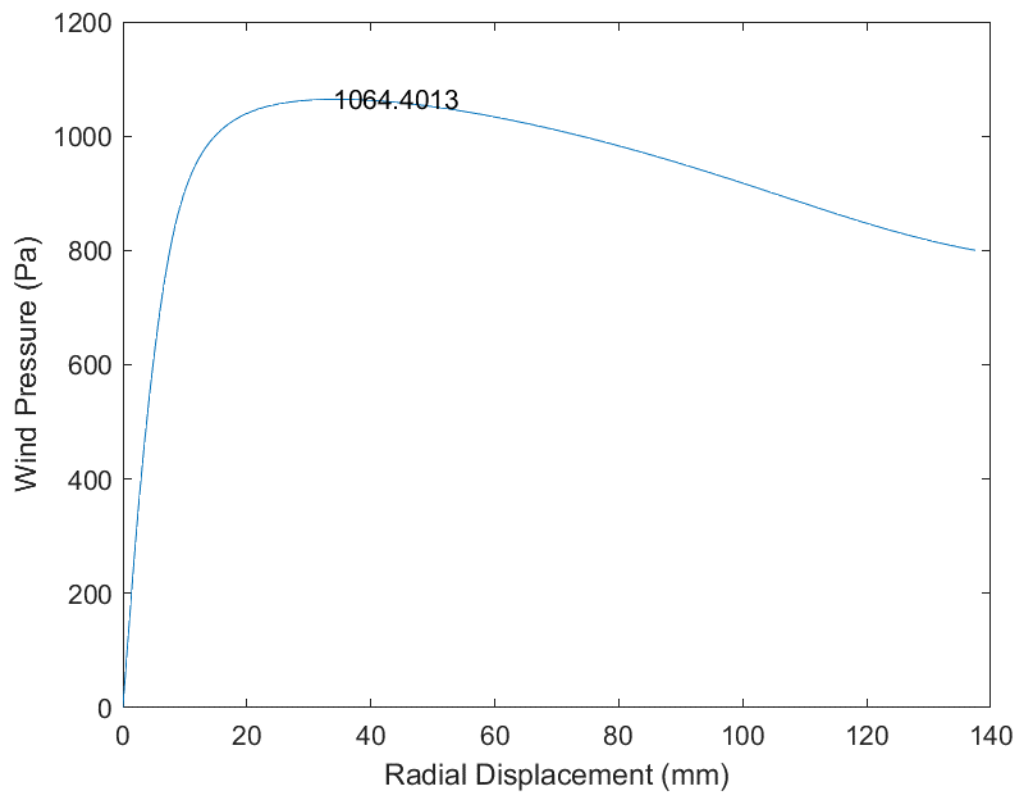


Fig. B.164 D90_H15_S60_R00_W01_V00_CL03_CD03_WT03_ST03

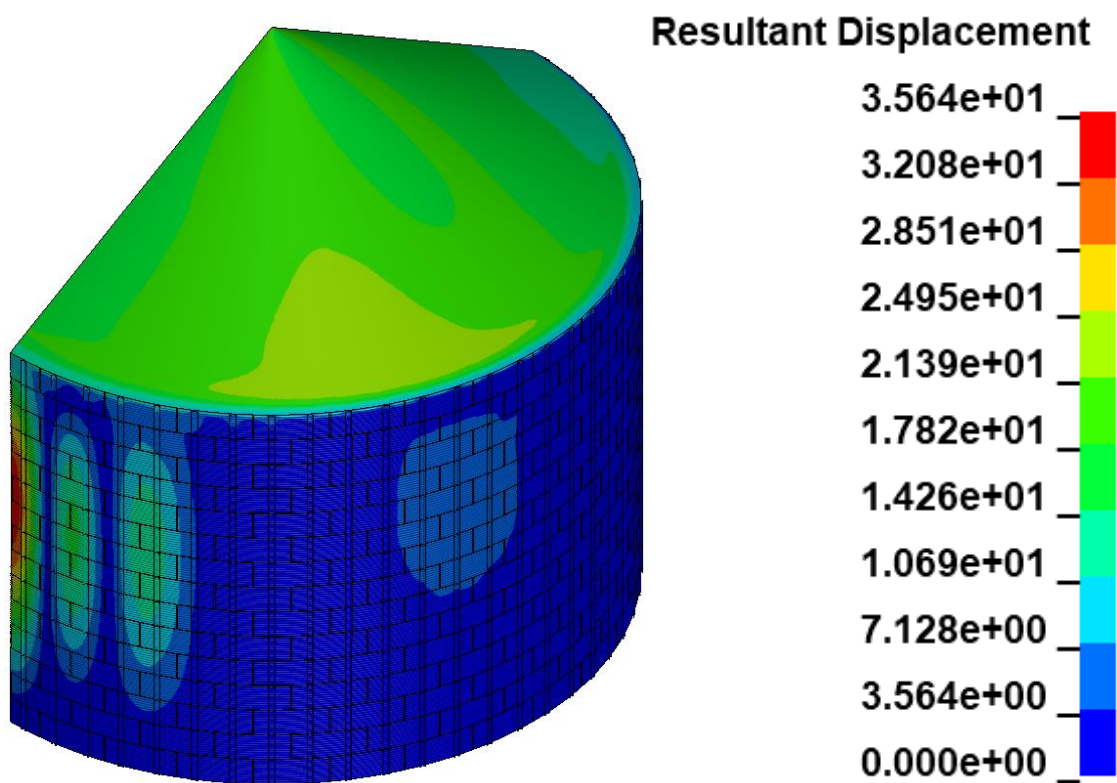
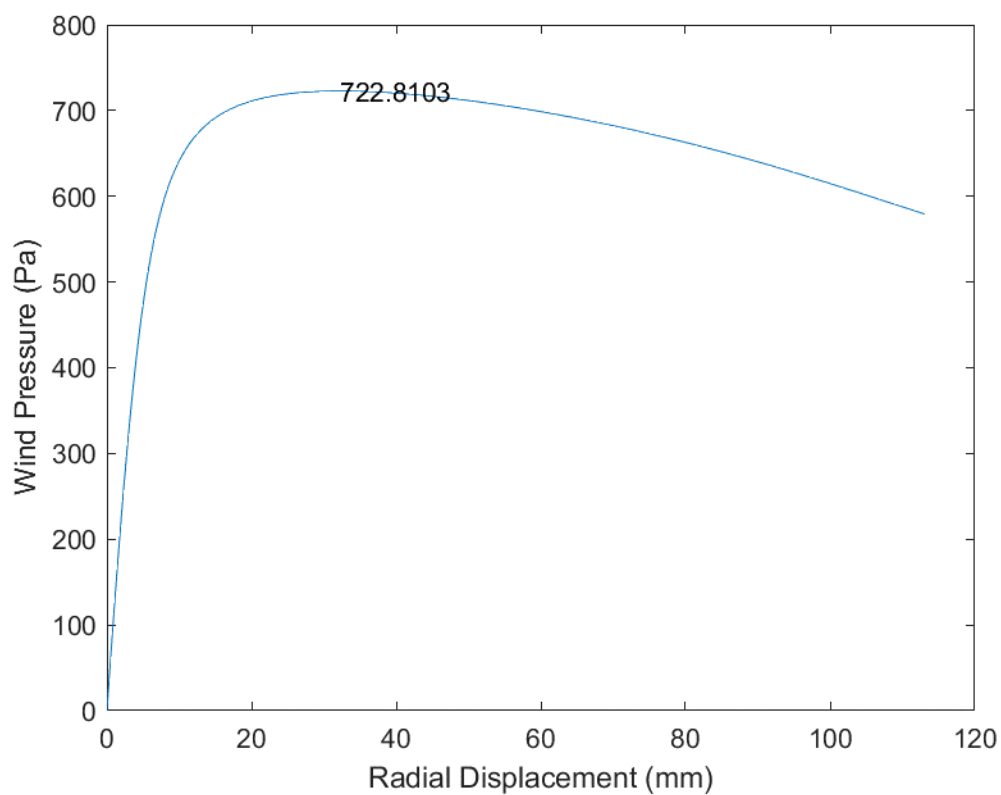


Fig. B.165 D90_H15_S60_R00_W01_V01_CL03_CD03_WT03_ST03

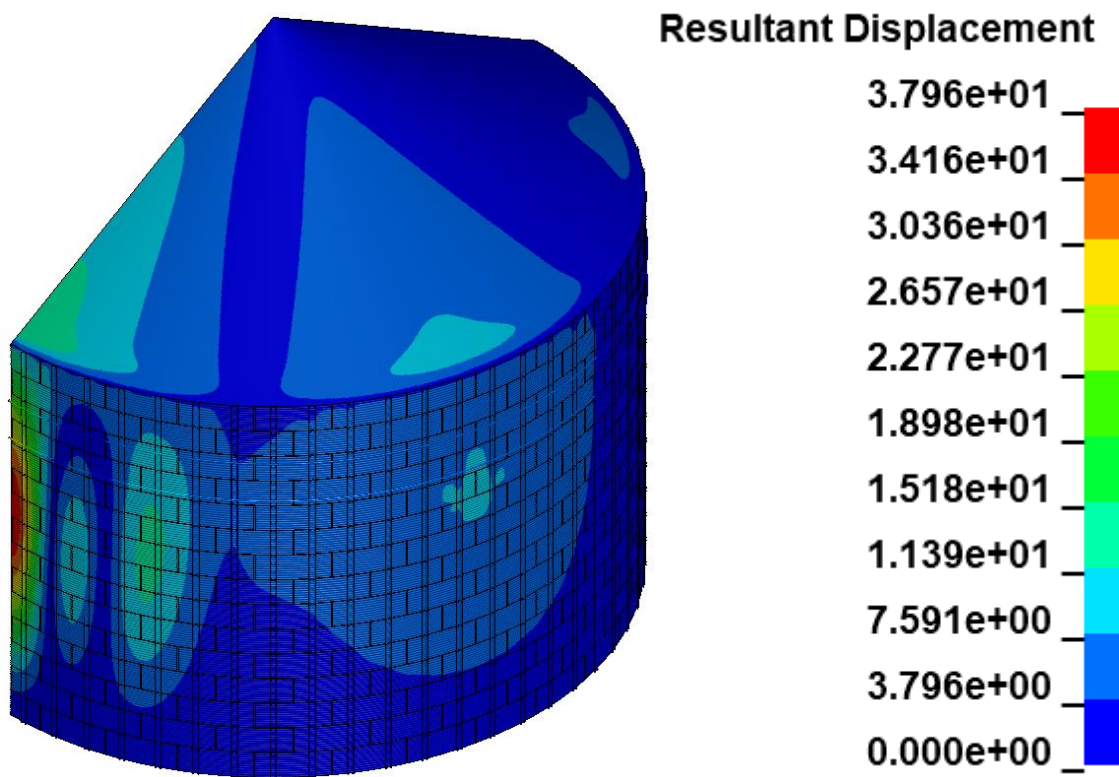
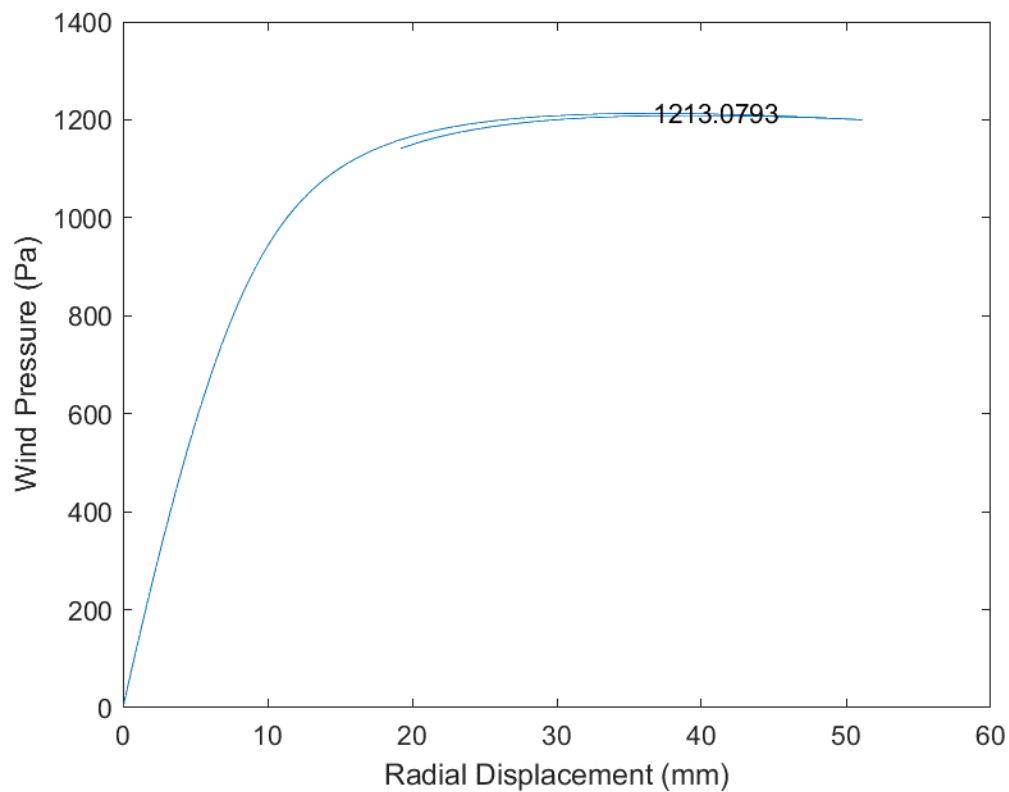


Fig. B.166 D90_H15_S60_R02_W00_V00_CL03_CD03_WT03_ST03

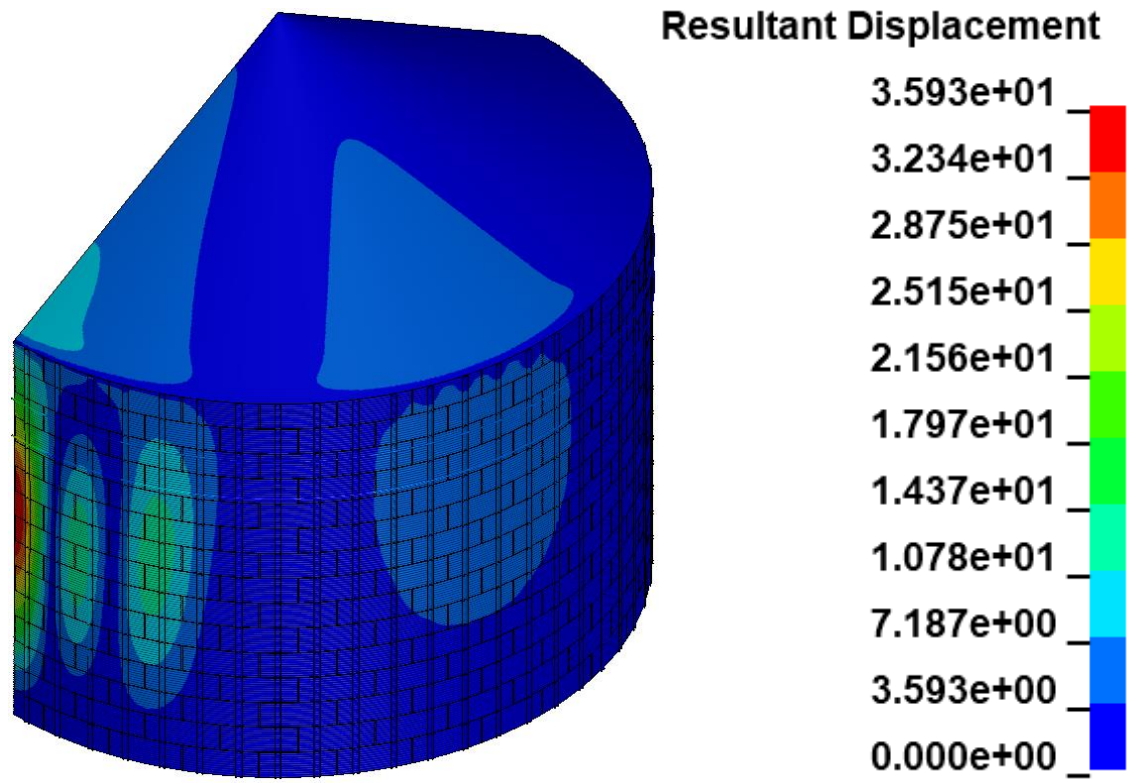
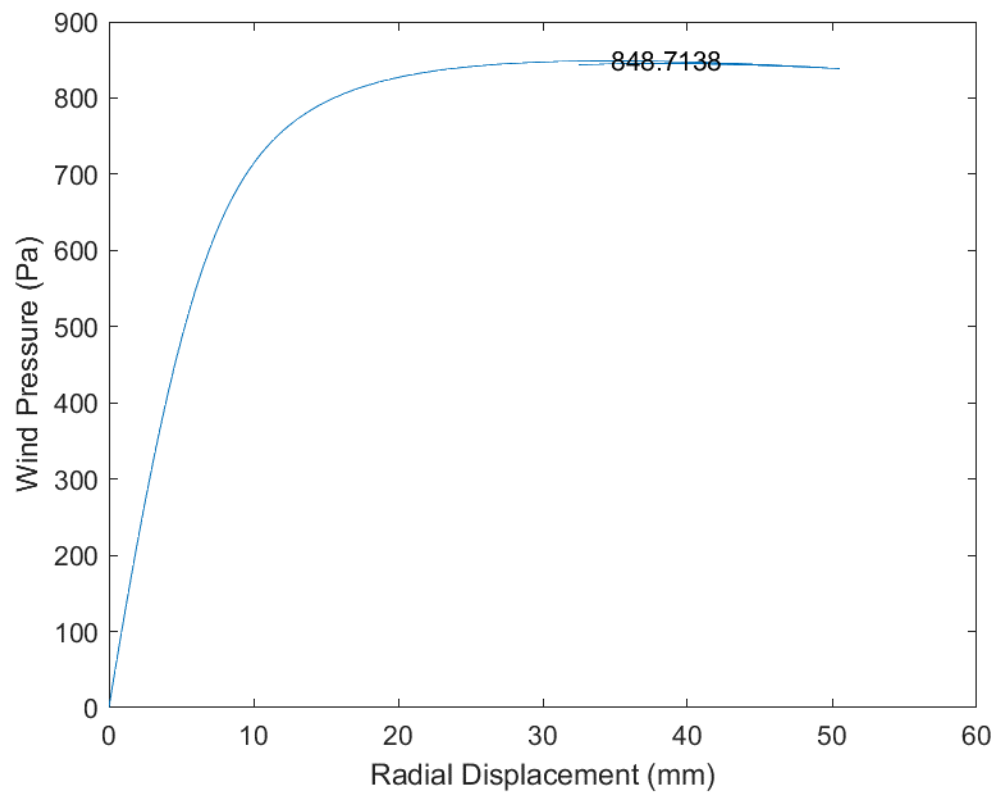


Fig. B.167 D90_H15_S60_R02_W00_V01_CL03_CD03_WT03_ST03

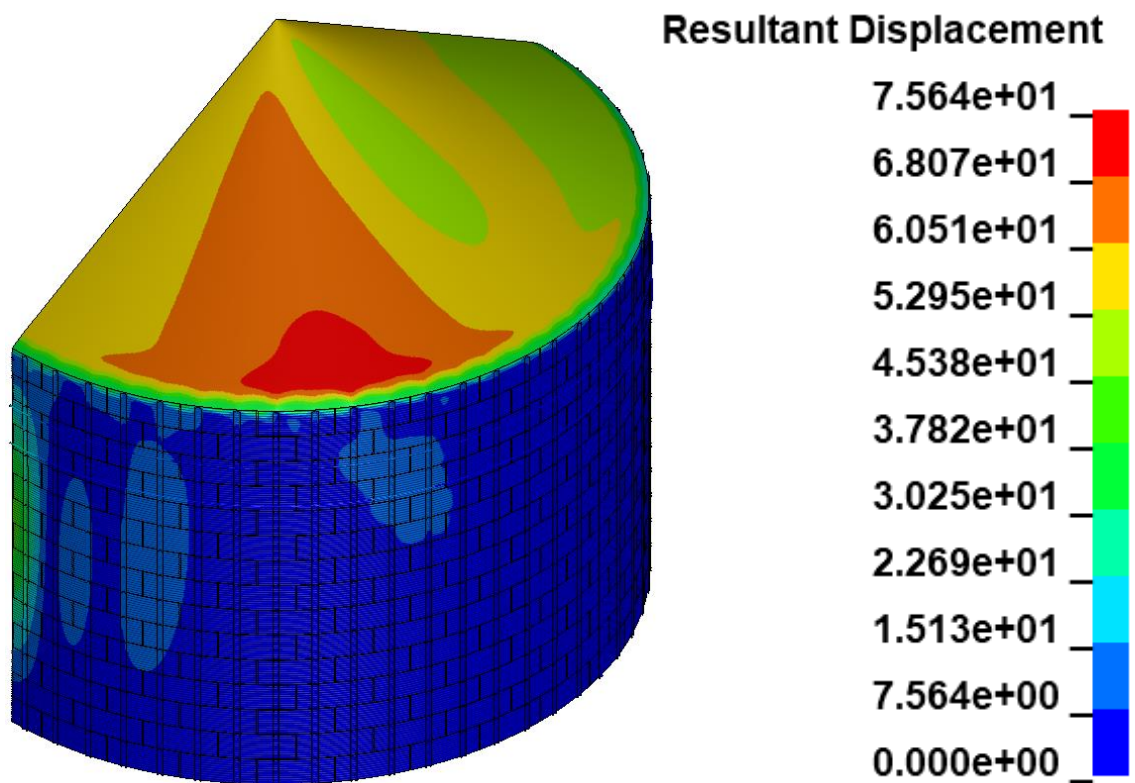
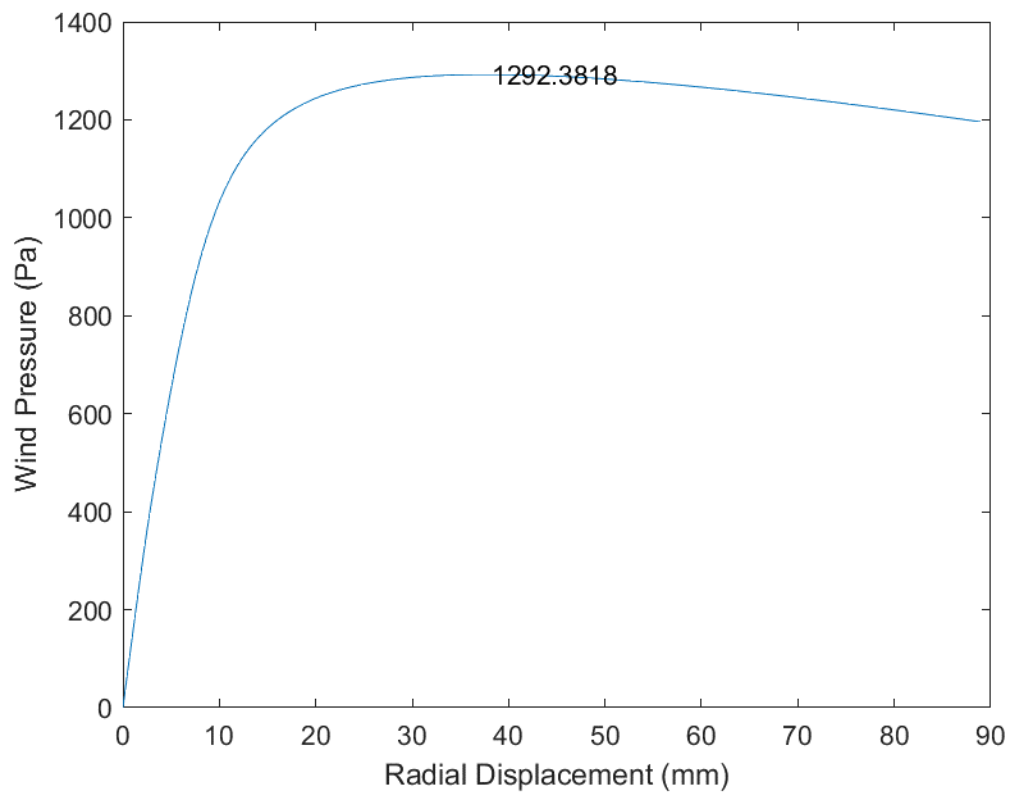


Fig. B.168 D90_H15_S60_R02_W01_V00_CL03_CD03_WT03_ST03

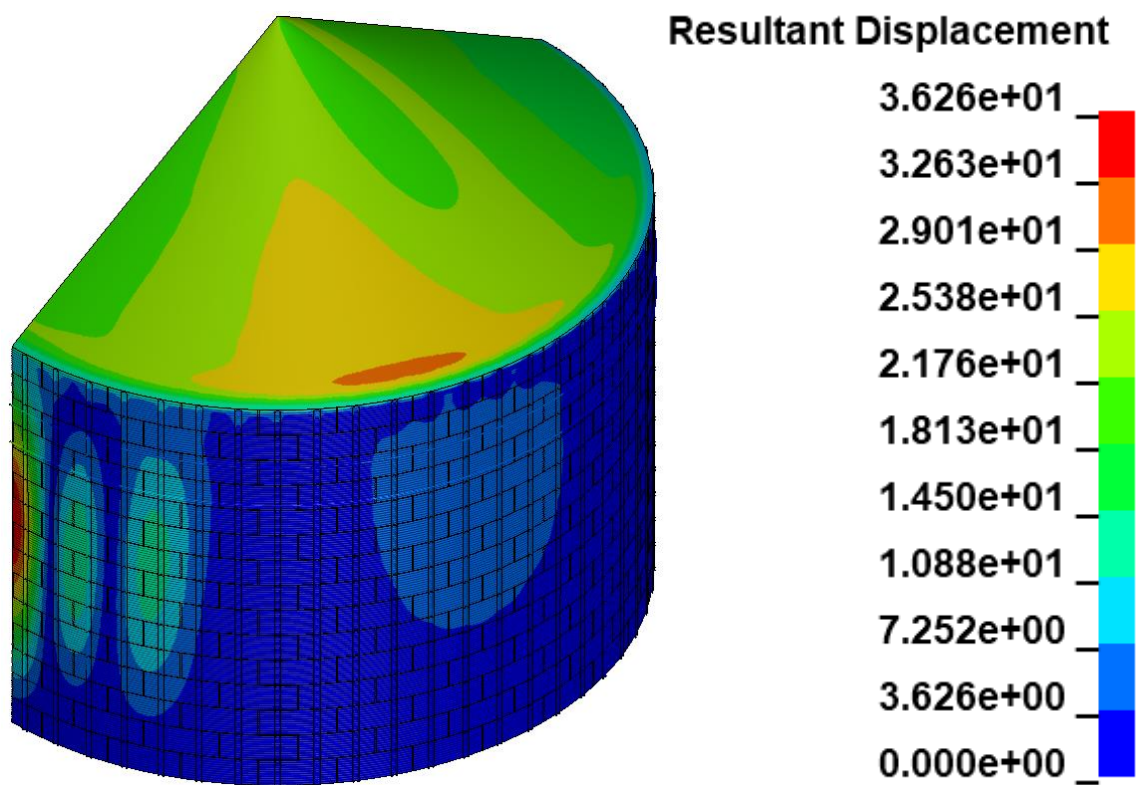
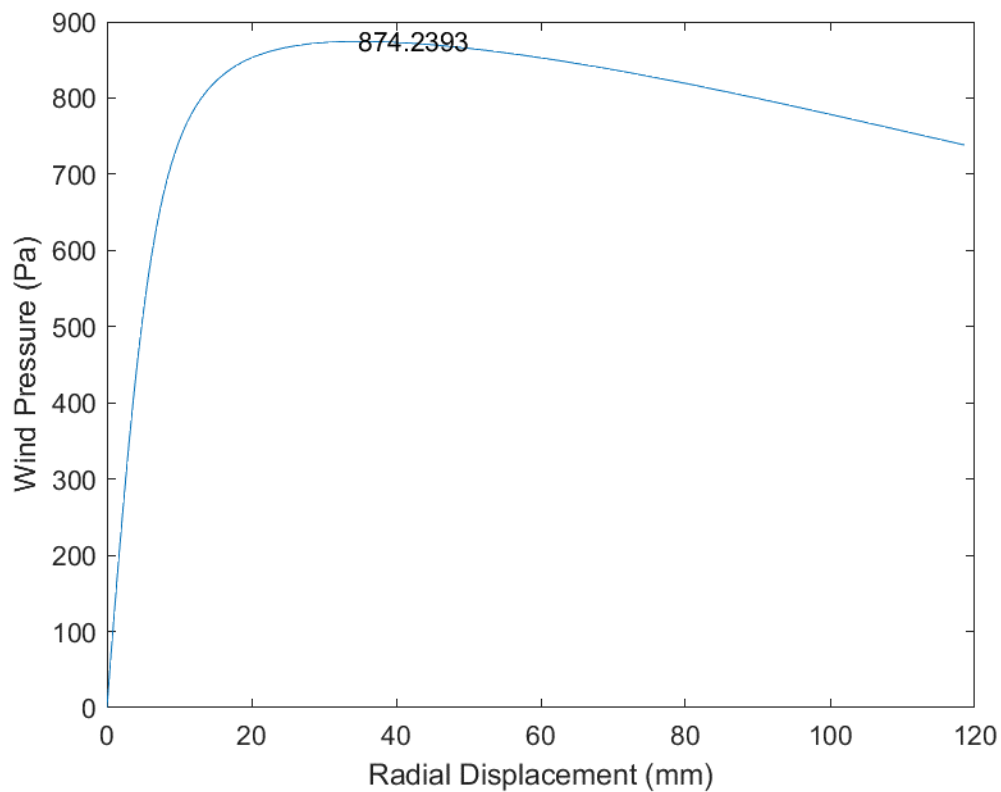


Fig. B.169 D90_H15_S60_R02_W01_V01_CL03_CD03_WT03_ST03

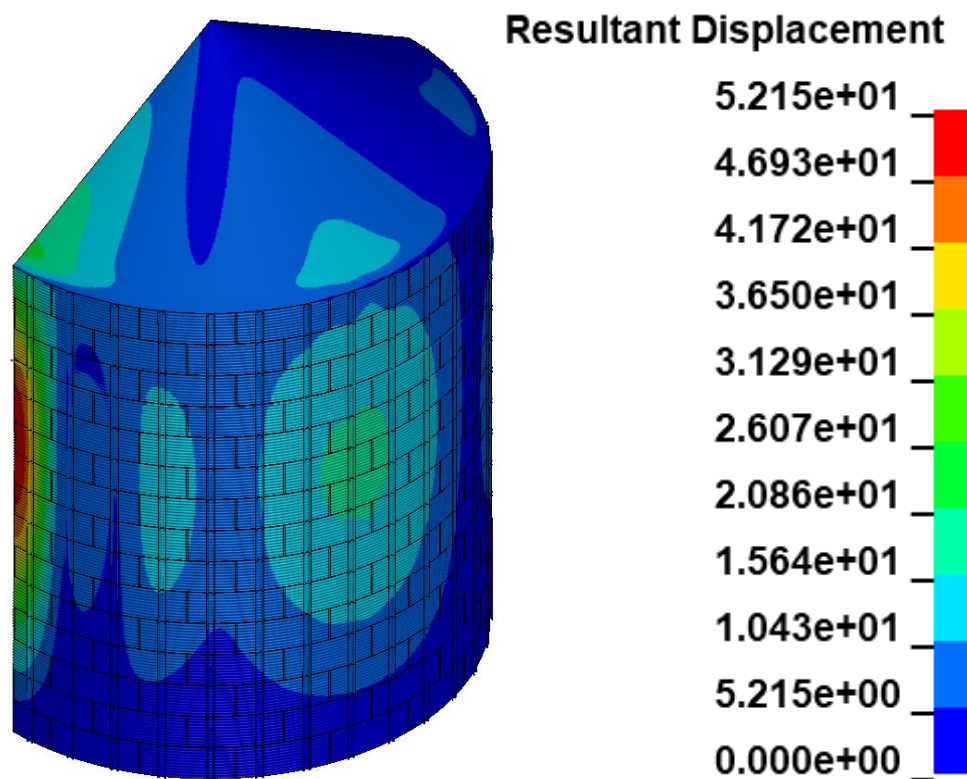
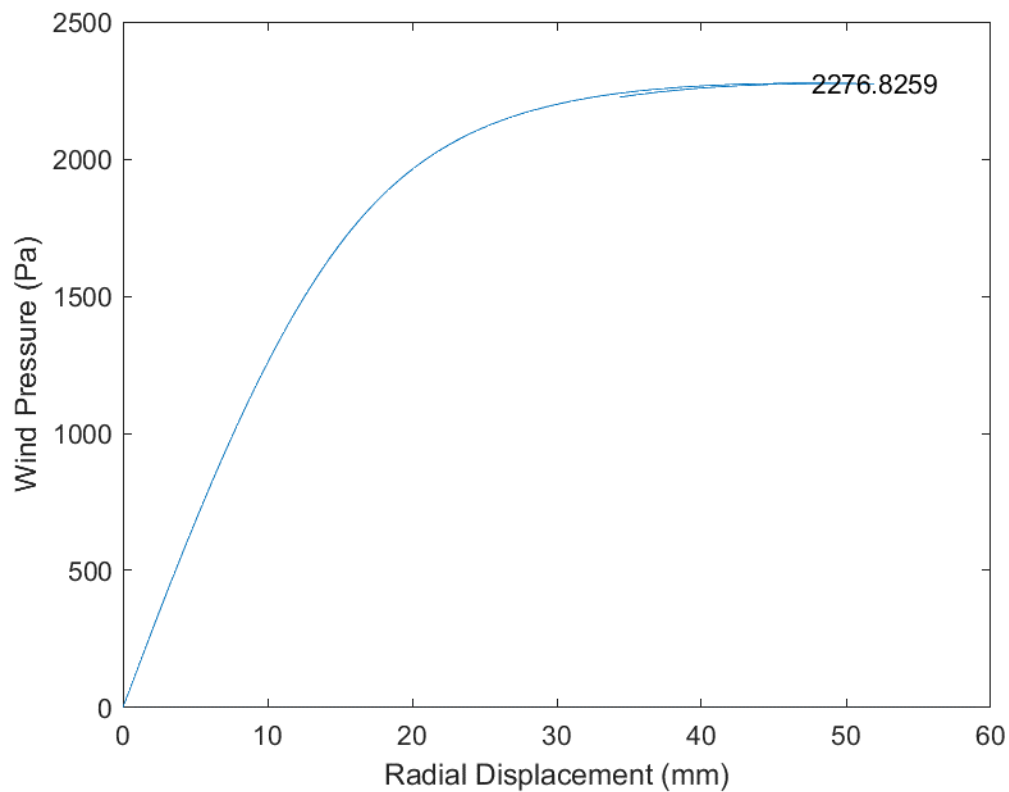


Fig. B.170 D54_H15_S36_R01_W00_V00_CL03_CD03_WT03_ST03, Light Rings

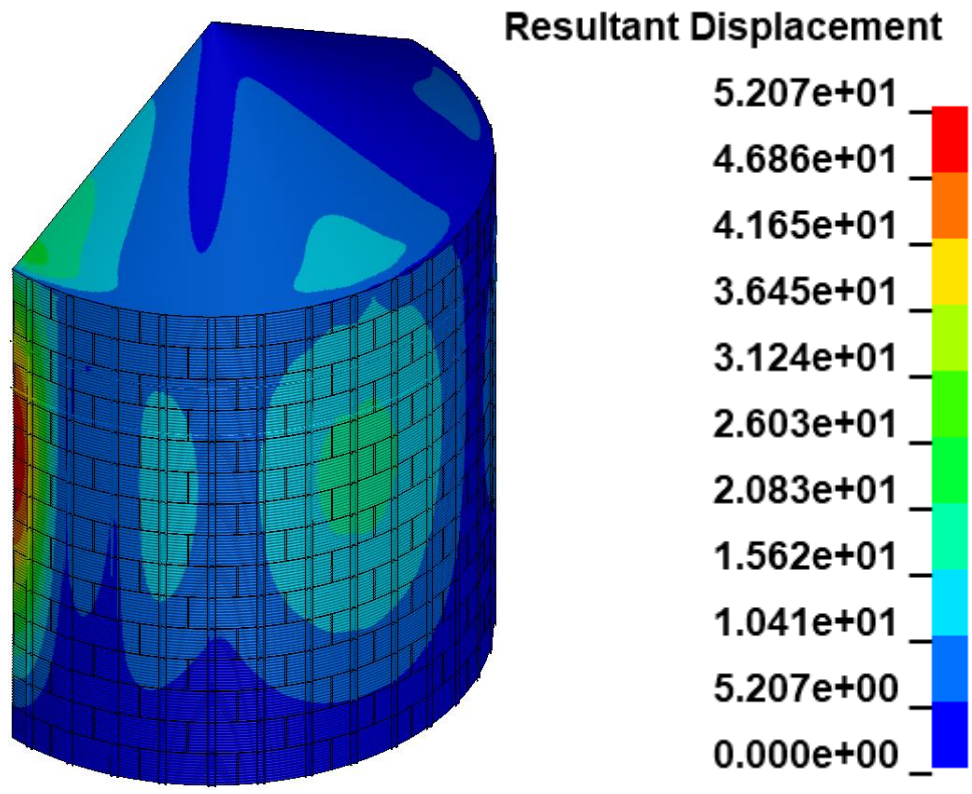
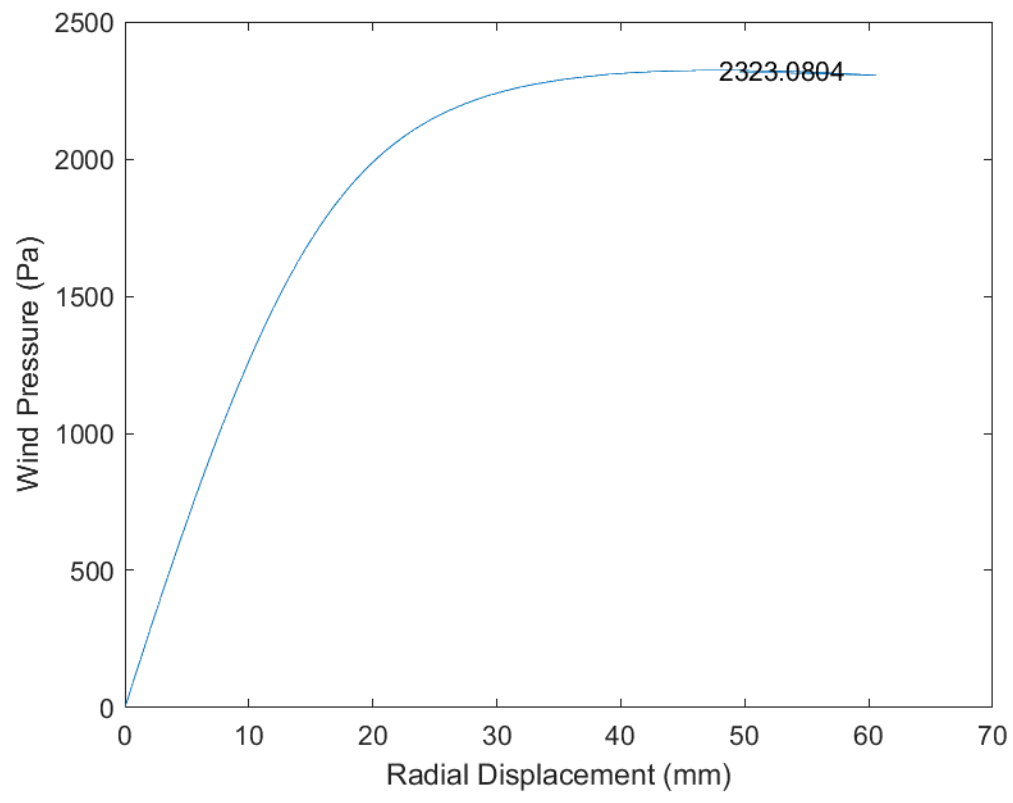


Fig. B.171 D54_H15_S36_R02_W00_V00_CL03_CD03_WT03_ST03, Light Rings

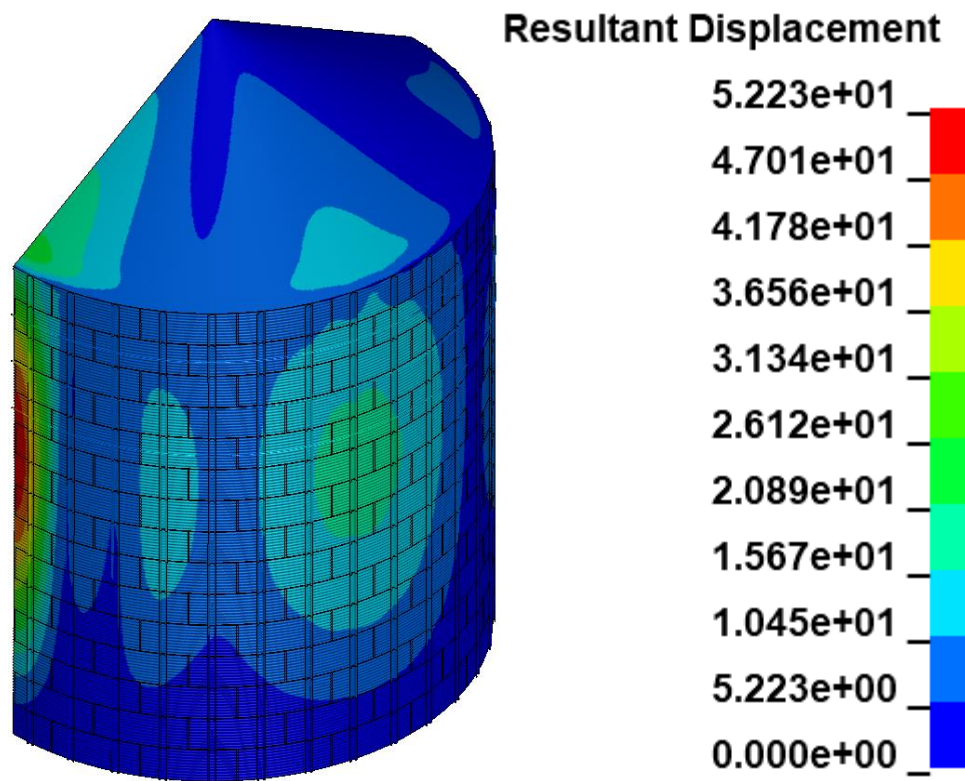
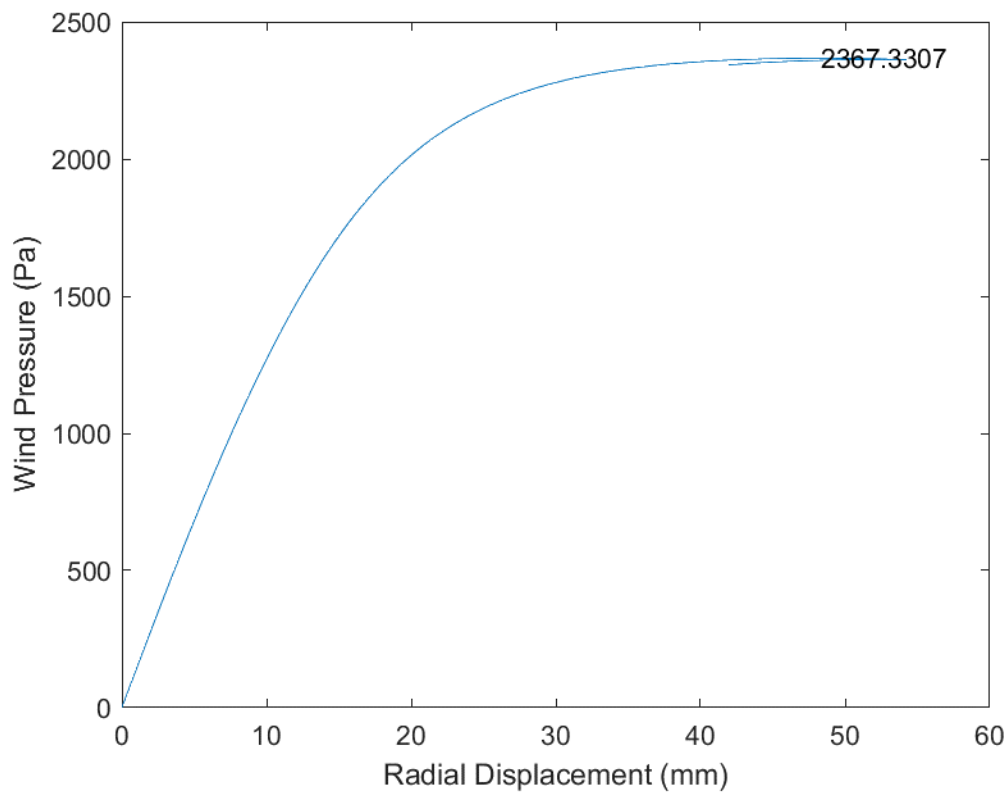


Fig. B.172 D54_H15_S36_R03_W00_V00_CL03_CD03_WT03_ST03, Light Rings

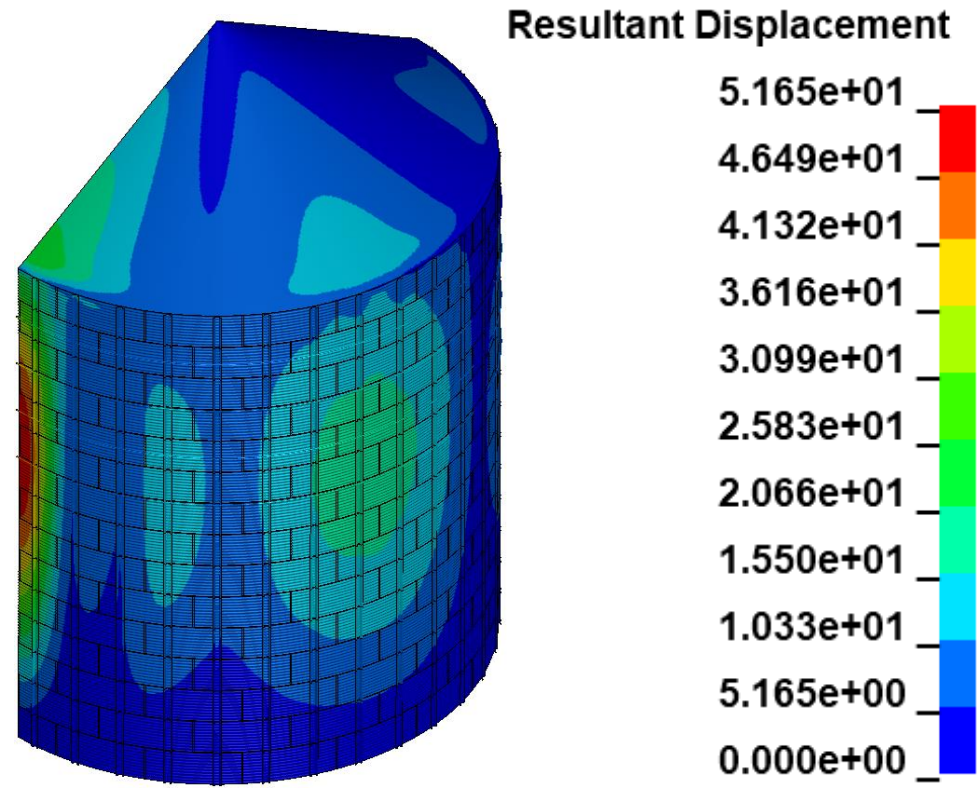
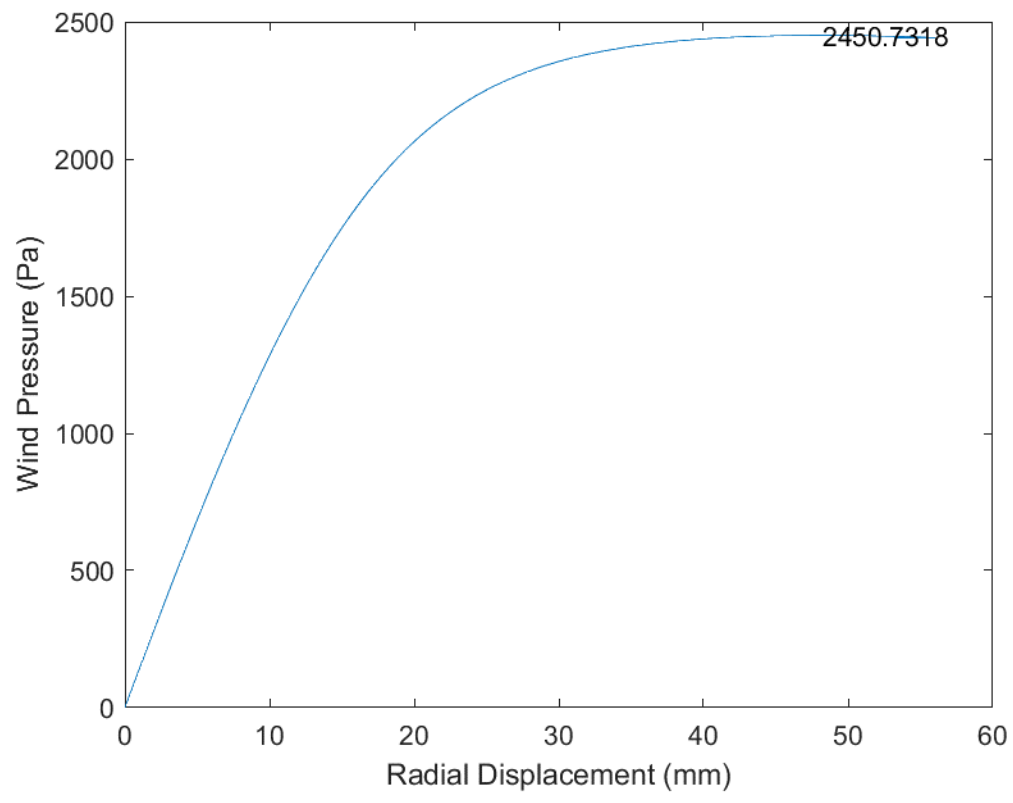


Fig. B.173 D54_H15_S36_R04_W00_V00_CL03_CD03_WT03_ST03, Light Rings

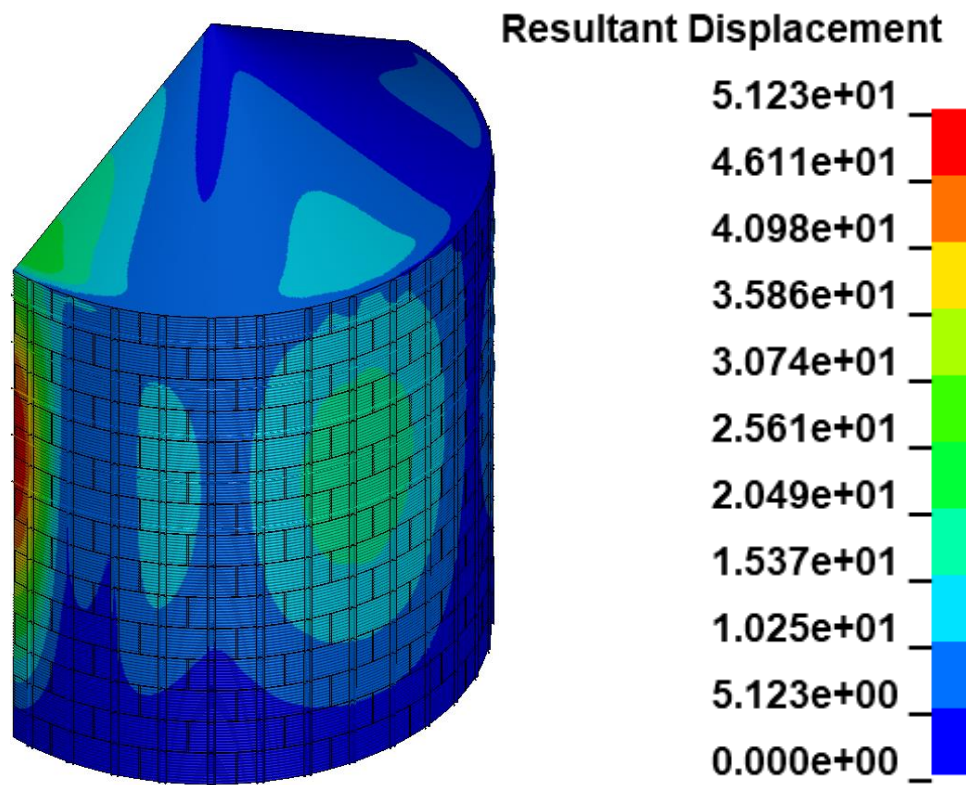
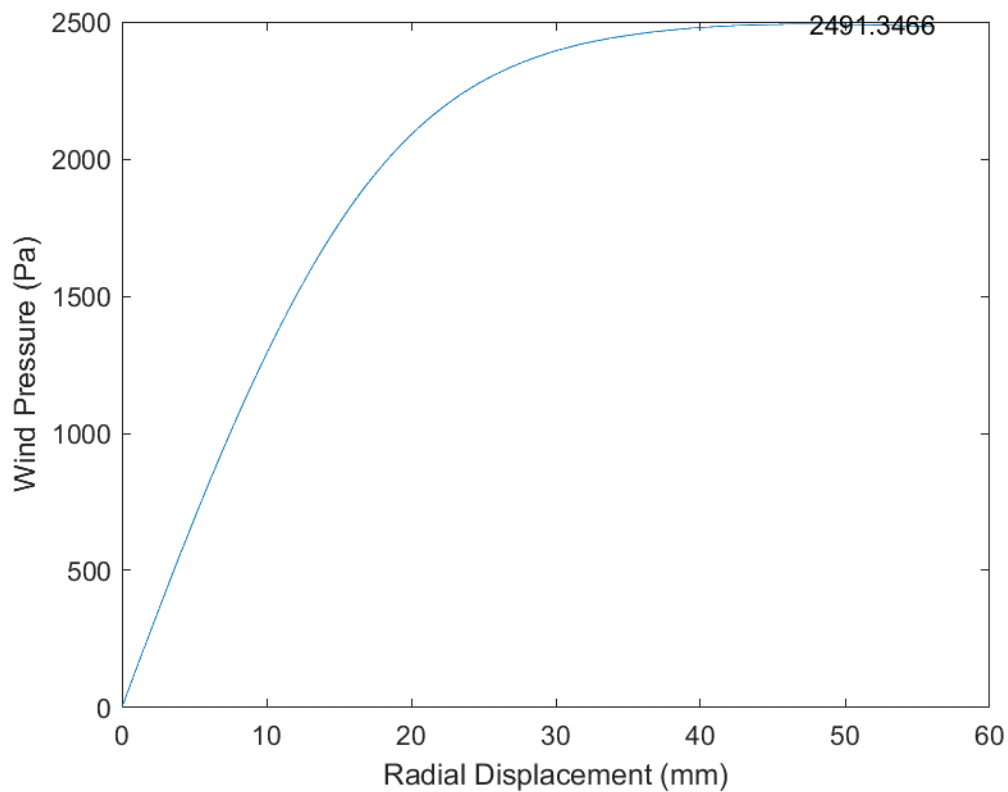


Fig. B.174 D54_H15_S36_R05_W00_V00_CL03_CD03_WT03_ST03, Light Rings

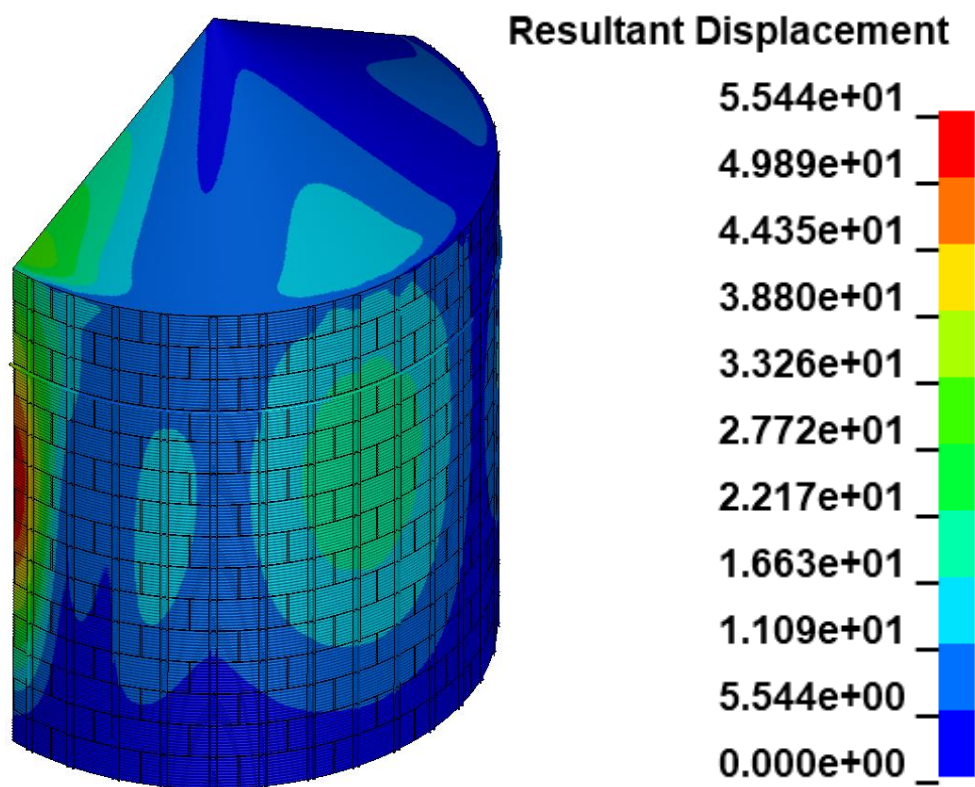
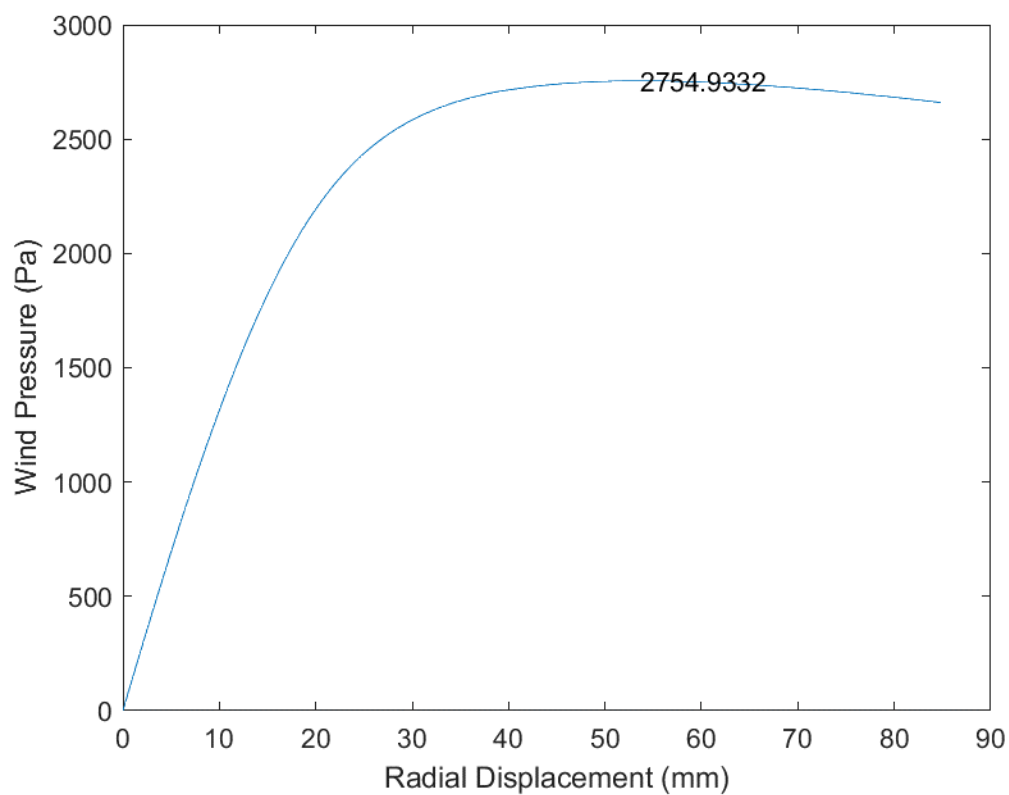


Fig. B.175 D54_H15_S36_R01_W00_V00_CL03_CD03_WT03_ST03, Heavy Rings

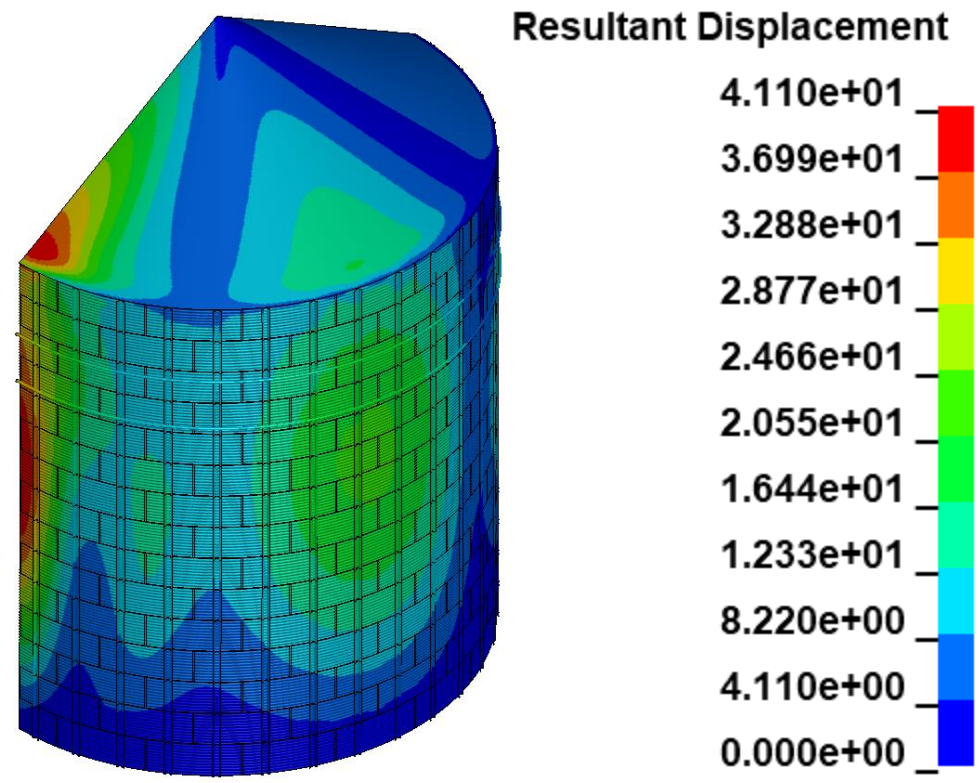
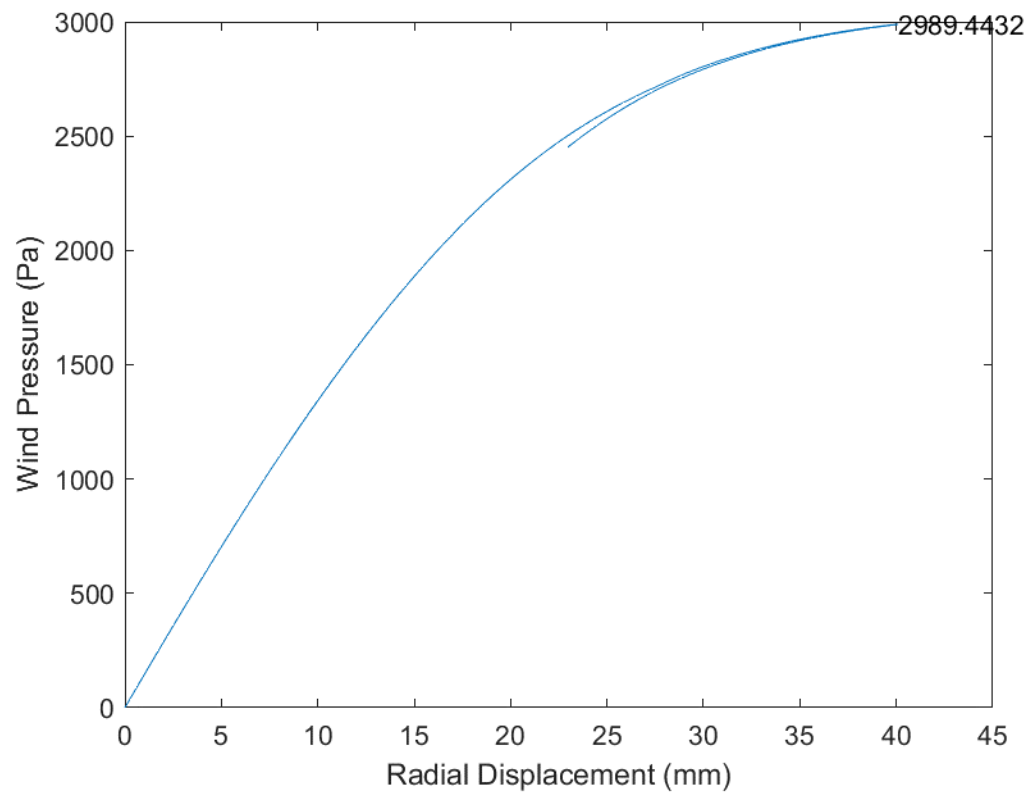


Fig. B.176 D54_H15_S36_R02_W00_V00_CL03_CD03_WT03_ST03, Heavy Rings

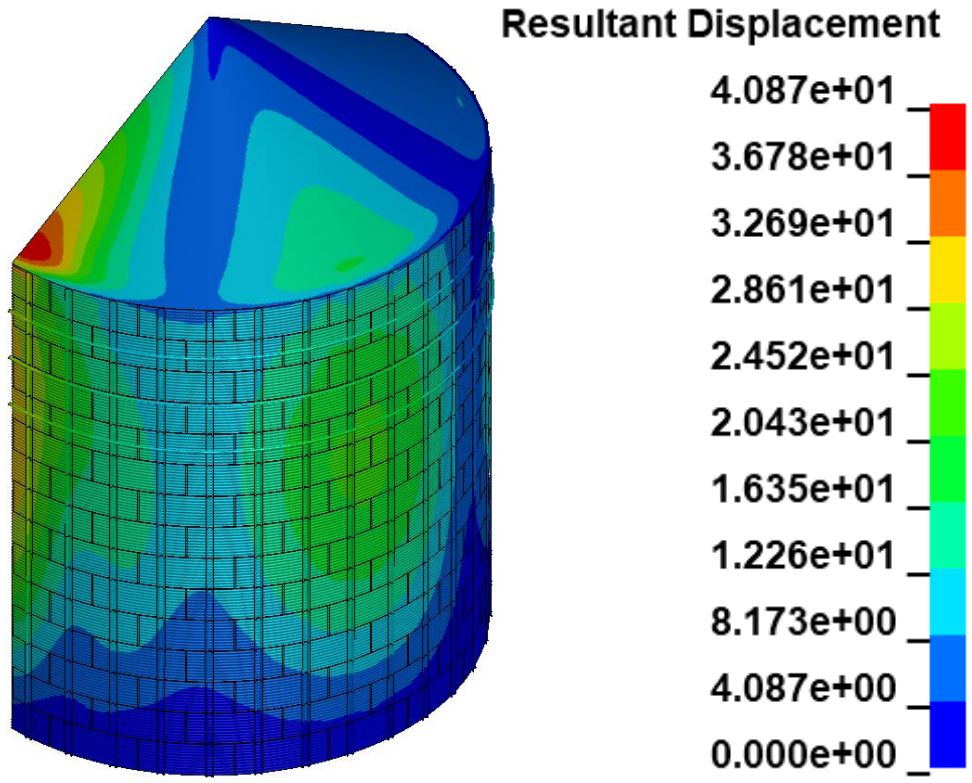
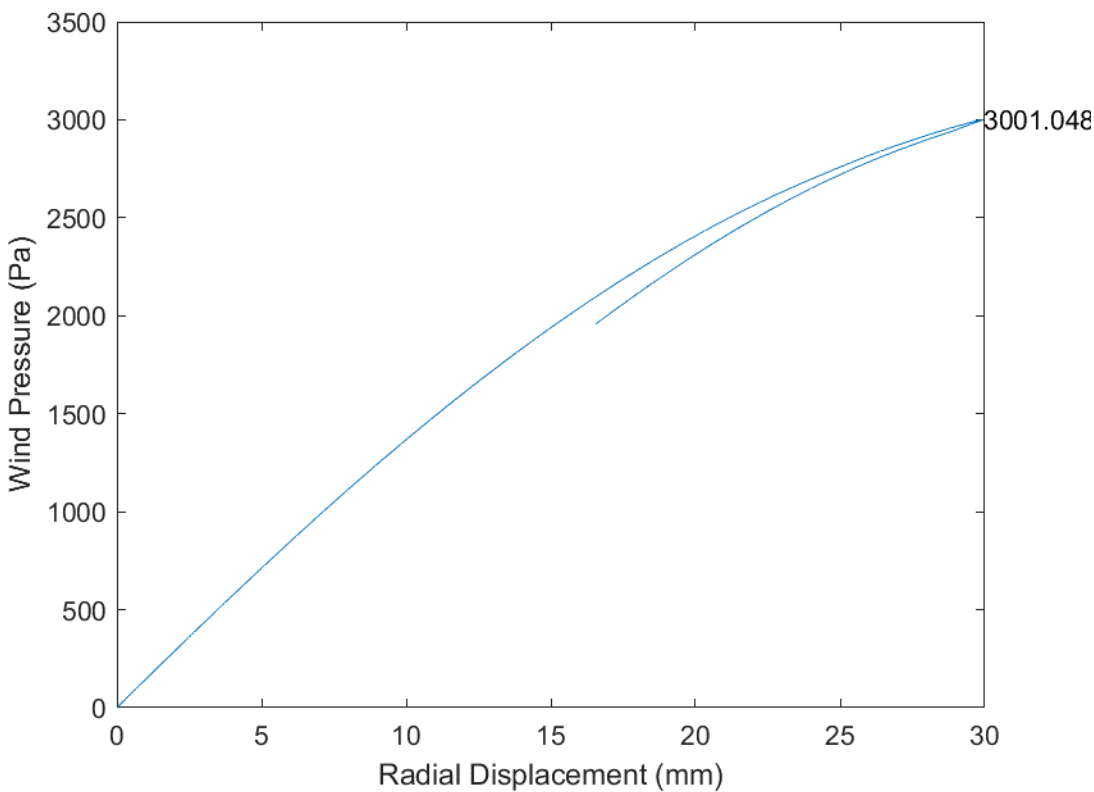


Fig. B.177 D54_H15_S36_R03_W00_V00_CL03_CD03_WT03_ST03, Heavy Rings

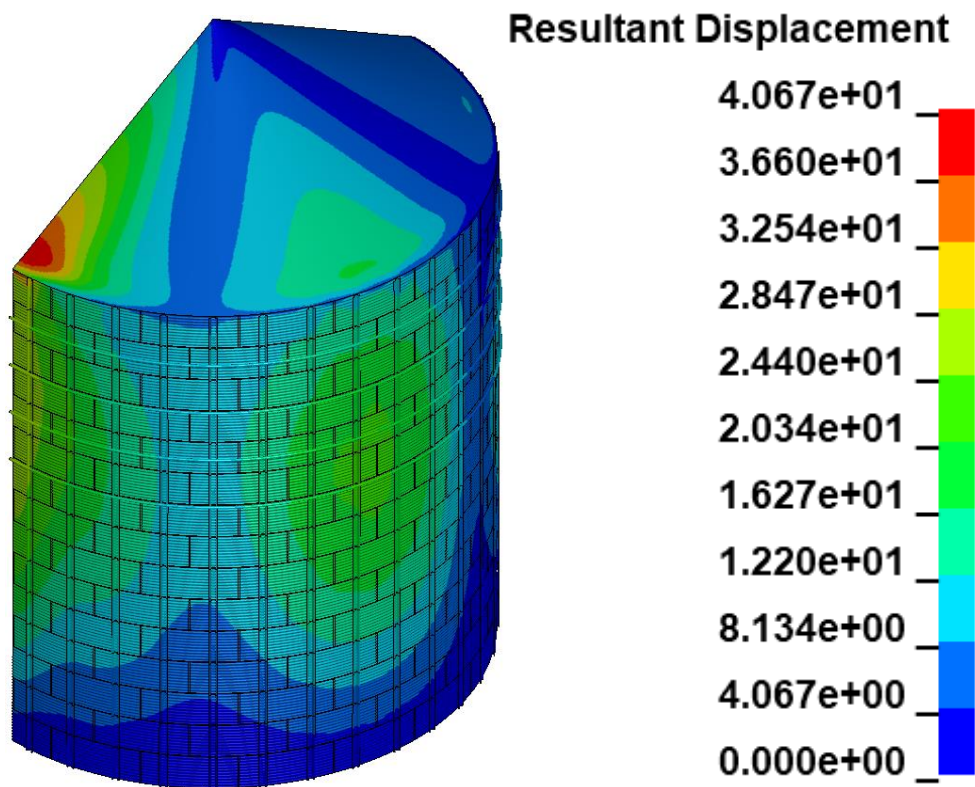
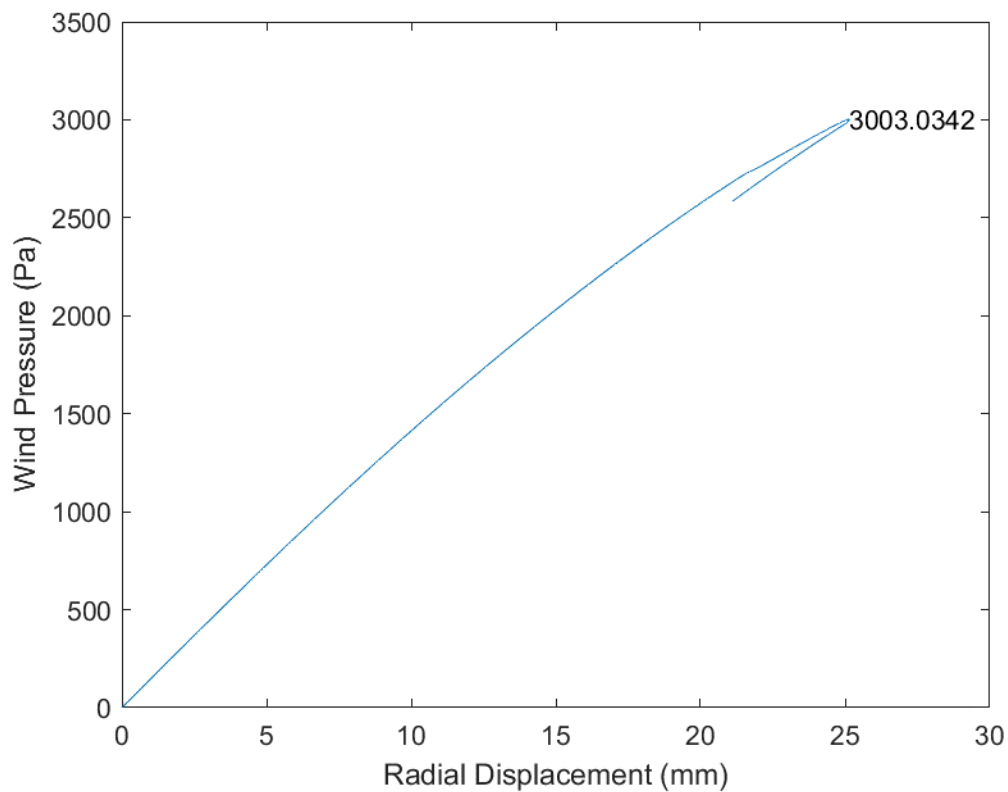


Fig. B.178 D54_H15_S36_R04_W00_V00_CL03_CD03_WT03_ST03, Heavy Rings

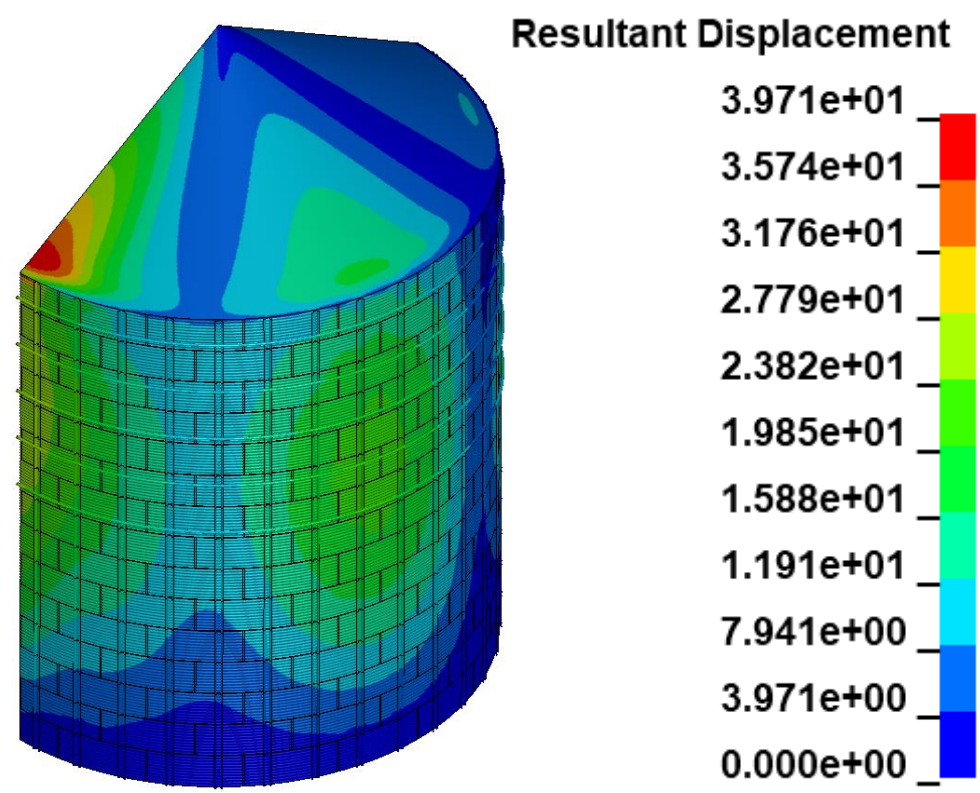
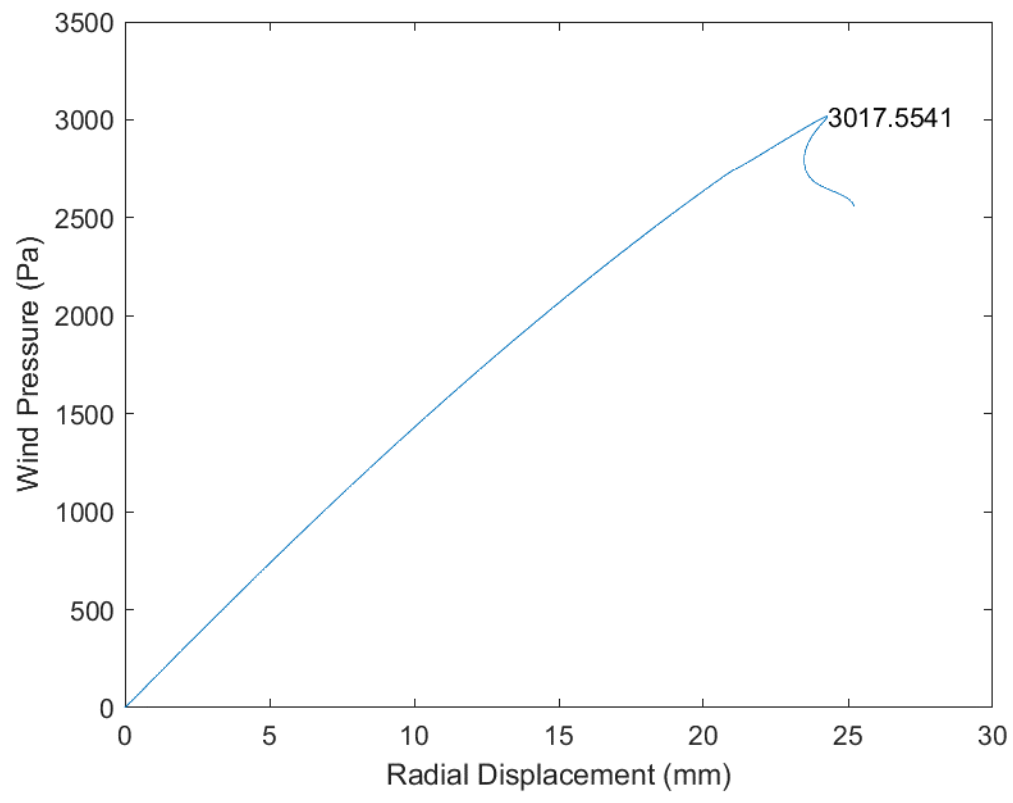


Fig. B.179 D54_H15_S36_R05_W00_V00_CL03_CD03_WT03_ST03, Heavy Rings